

# RoMANS

## Rocky Mountain Atmospheric Nitrogen and Sulfur Study

### Volume 2

Chapter 5. Source Apportionment to Aerosol Species  
Concentrations and Dry and Wet Deposition

Chapter 6. Summary and Conceptual Model  
Reference List

CD of electronic draft files on back cover

March 2009

ISSN 0737-5352-84





## RoMANS

# Rocky Mountain Atmospheric Nitrogen and Sulfur Study Report

March 2009

### Principal Investigators:

William C. Malm<sup>1</sup>  
Jeffrey L. Collett, Jr.<sup>2</sup>

### Authors:

Michael G. Barna<sup>1</sup>  
Kristi A. Gebhart<sup>1</sup>  
Bret A. Schichtel<sup>1</sup>

### Contributors:

Katie Beem<sup>2</sup>  
Christian M. Carrico<sup>2</sup>  
Derek E. Day<sup>3</sup>  
Jenny L. Hand<sup>3</sup>  
Sonia M. Kreidenweis<sup>2</sup>  
Taehyoung Lee<sup>2</sup>  
Ezra Levin<sup>2</sup>  
Charles McDade<sup>4</sup>

Gavin R. McMeeking<sup>2</sup>  
John V. Molenaar<sup>5</sup>  
Suresh Raja<sup>2</sup>  
Marco A. Rodriguez<sup>3</sup>  
Florian Schwandner<sup>2</sup>  
Amy P. Sullivan<sup>2</sup>  
Courtney Taylor<sup>2</sup>

<sup>1</sup>National Park Service  
CSU/CIRA

Fort Collins, Colorado 80523-1375

<sup>2</sup>Department of Atmospheric Science  
Colorado State University  
Fort Collins, Colorado 80523-1371

<sup>3</sup>Cooperative Institute for Research in the Atmosphere (CIRA)  
Colorado State University  
Fort Collins, Colorado 80523-1375

<sup>4</sup>Crocker Nuclear Laboratory  
University of California  
Davis, California 95616-8569

<sup>5</sup>Air Resource Specialists  
Fort Collins, Colorado 80525

### Disclaimer

The assumptions, findings, conclusions, judgments, and views presented herein are those of the authors and should not be interpreted as necessarily representing National Park Service policies.



## Chapter 5. Source Apportionment to Aerosol Species Concentrations and Dry and Wet Deposition

### 5.1. SOURCE ATTRIBUTION APPROACH

Apportionment of source emissions to haze and/or ecosystem effects at some predetermined receptor site is a difficult but necessary requirement if the goal is to reduce emissions and thereby have some sort of predictable positive outcome (e.g., reduced haze or moderation of deleterious ecosystem effects). However, apportionment of emissions to haze can be quite a different problem than apportionment to ecosystem effects. Haze is caused by particles that are typically composed of molecules that have at least two chemical constituents such as ammonium and nitrate ions. The precursor gas to ammonium is ammonia while for nitrate it is nitrogen oxides. Ammonia and nitrogen oxides are not typically emitted from the same sources or even from the same source regions. Anthropogenic ammonia is primarily emitted from agricultural activity such as fertilizer application and animal feedlots and secondarily from fertilizer application on lawns in urban areas and from mobile sources with catalytic converters. Nitrogen oxides emissions are primarily associated with mobile sources (urban areas) and large point sources such as electrical generating facilities. Without ammonia, nitrogen oxide emissions would most likely be deposited out as nitric acid, and without nitrogen oxide emissions, a larger fraction of ammonia would most likely deposit as ammonia. Therefore it is the combination of these two source types that is responsible for the resulting haze formed from their emissions.

On the other hand, regardless of the chemical form and phase of the nitrogen, it will ultimately be deposited onto terrestrial or aquatic surfaces. For instance, ammonia deposited to a terrestrial or aquatic ecosystem forms ammonium, which in turn is biologically converted to nitrate, and so forth. Here the apportionment problem is more straightforward in that controlling sources of ammonia or nitrogen oxides has a more direct link to the effect of concern. However, where these species are deposited depends on the chemical form and phase of the nitrogen. Gaseous ammonia and nitric acid have higher deposition rates and will deposit closer to the sources, while particulate nitrogen can be transported hundreds of kilometers before deposition.

Assessing changes in ambient concentrations of aerosol species and wet deposition as a function of changing ammonia, nitrogen oxides, and sulfur dioxide emissions is dependent on a number of chemical and physical mechanisms. For example, ammonia will increase particle mass by reacting with acidic sulfate aerosols, nitric acid, and organic acids. The equilibrium between ammonia and nitric acid and their reaction product, ammonium nitrate, is temperature and humidity dependent and can go from predominantly gases to particles with the diurnal shifts in temperature. The condensation of ammonia onto particles is dependent on the acidity of the particles and ambient relative humidity. These reactions do not necessarily take place at or near the sources of ammonia, nitrogen oxides, or sulfur dioxide but over the transport pathways from source to receptor. As an example, ammonium sulfate concentrations at RMNP may be a result of sulfur dioxide emissions in California being transported across ammonia sources in southern Idaho, where an acid sulfate aerosol becomes partially neutralized, and with additional transport over other ammonia sources such as the Front Range or northeastern Colorado, where the partially neutralized aerosol could become fully neutralized ammonium sulfate.

If chemical transport models were perfect, all apportionment problems could be addressed by modeling changing emission characteristics and observing how concentrations of species of interest at some predetermined receptor sites respond. A precise prediction of an aerosol species' concentration and deposition relies on accurately knowing emissions, wind and cloud fields, transport and dispersion characteristics, and chemical conversion and removal mechanisms along all transport pathways. However, many of these defining features are not known, especially for aerosols other than sulfates and ozone.

Therefore the strategy taken for apportioning various aerosol species concentrations and deposition to source emissions is a weight-of-evidence approach, comparing and contrasting results from multiple analyses. Spatial concentration gradients have already been presented in section 4.4, and cases in which spatial concentration gradients go from high to low, such as ammonia concentrations being highest in eastern Colorado and successively lower as one moves toward RMNP, suggest possible transport from the higher concentration area to the regions of lower concentration. Simple wind direction analysis has shown that when winds blow from the direction of known source regions, concentrations of all aerosol species tended to increase, in some cases dramatically (section 4.4).

In this chapter, the qualitative spatial gradient and wind direction analyses are built upon to develop quantitative estimates of the contributions from source regions within and outside of Colorado. This is done through a multistep process starting from a simple qualitative back trajectory analysis to a final quantitative hybrid-receptor modeling technique. Each successive analysis builds on the previous method, incorporating new data and/or more sophisticated statistical methods to refine the results. This process allows for a better understanding of the effects of the additional data and statistical methods, providing insights into the quality of the final results.

The first analysis is a simple back trajectory study to examine the association of high concentration and wet-deposition episodes with transport directions (section 5.3.2). This addresses the question "what high emissions areas did the back trajectories pass over before arriving in the receptor site?" For instance, what source regions do back trajectories that are associated with high particulate nitrate concentrations pass over before arriving at RMNP? Are high concentrations of ammonia associated with back trajectories that passed over areas with high rates of emissions of ammonia, or over monitoring sites that have measured high ambient levels of ammonia that may be indicative of a region of high ammonia emissions?

Next, a statistical analysis of all trajectories is presented in the form of residence time analysis (section 5.3.3). Do air masses that correspond to back trajectories of high concentrations of a species spend more time over known source areas of that species? This analysis is then extended into developing quantitative statistical relationships between source areas and measured concentrations. The analysis is known as trajectory mass balance (TrMB) and is presented in section 5.3.4.

The final apportionment method is a hybrid technique relying on modeled transport and dispersion of known emissions into RMNP, without accounting for chemical conversion or wet and dry deposition. This is a modeled analog of releasing a conservative tracer for every known source region. These modeled concentrations are then used in a receptor-type framework to

develop apportionment estimates of all measured aerosol species concentrations as well as wet deposition measurements. This analysis is presented in section 5.5.

The final section in this chapter presents the results of exercising the full, regional-scale, chemical transport model (Comprehensive Air quality Model with extensions—CAMx). Model predictions are compared to measurements both in space and time. However, because of limitations in modeled emission inventories and cloud processes, they are not used to estimate the relative contributions of various source regions to measured deposition and concentrations at this time. As the issues with the chemical transport modeling are better understood and resolved, these tools will be used to quantitatively examine the source-receptor relationship.

## 5.2. MESOSCALE METEOROLOGICAL MODELING

### 5.2.1. Modeling Protocol

The Pennsylvania State University/National Center for Atmospheric Research Fifth Generation Mesoscale Meteorological Model (MM5) (Grell et al., 1994) was used to generate hourly meteorological fields on three nested domains of 35 vertical layers and horizontal grid sizes of 36, 12, and 4 km. A map of the domain locations is shown in Figure 5.1, and Figure 5.2 illustrates the terrain resolution on the 36-km and 4-km domains over Colorado.

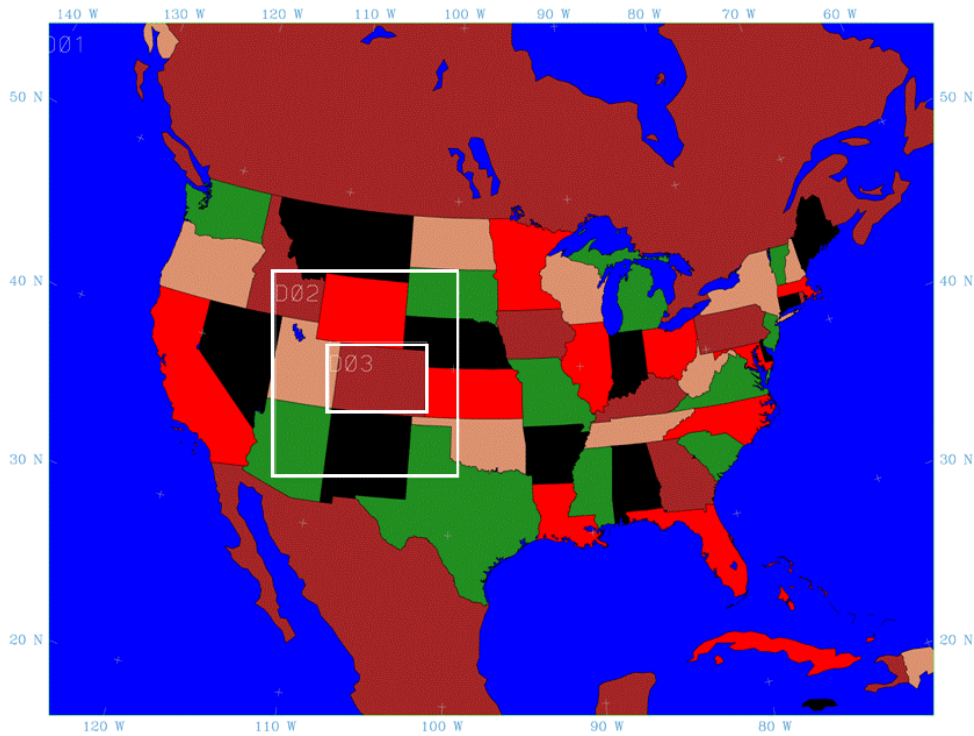


Figure 5.1. Three MM5 modeling domains. The 36-km domain is the entire map, 4-km domain covers most of Colorado, and the 12-km domain is intermediate.

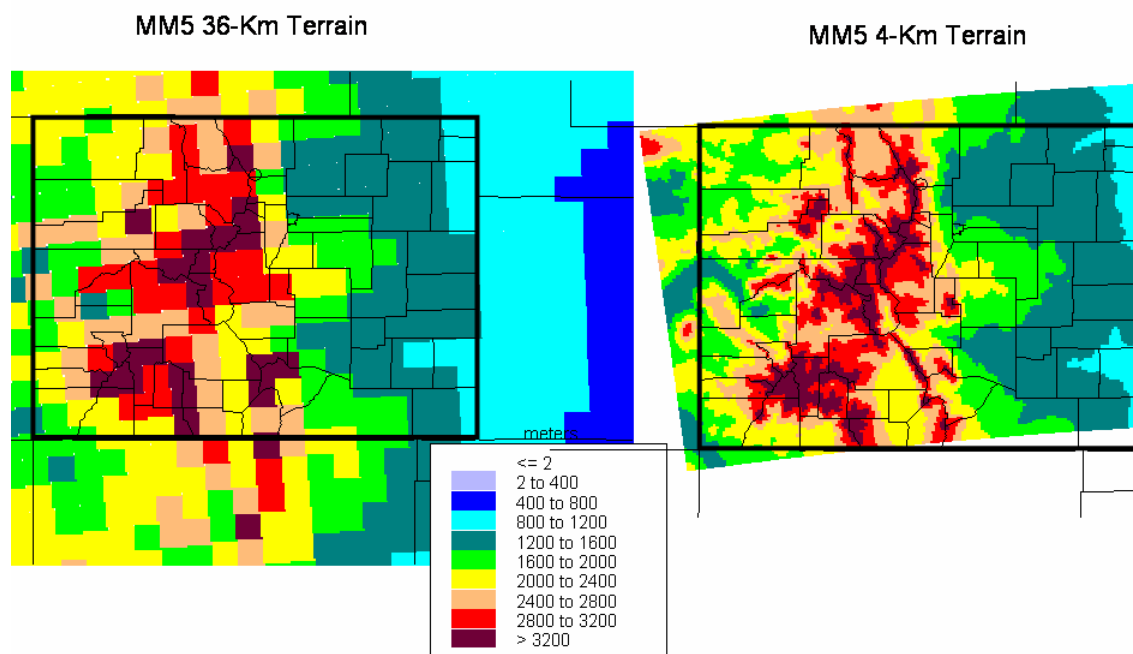


Figure 5.2. Gridded terrain over Colorado in the MM5 36 km (left) and 4 km (right) domains.

MM5 was initialized with the North American Regional Reanalysis (NARR) (Mesinger et al., 2006; North American Regional Reanalysis, 2007). These data were also used for analysis nudging on the coarse domain. Data used for observational data assimilation on the 4-km domain included surface and upper air observations obtained from the National Center for Atmospheric Research (NCAR) as well as meteorological data collected as part of RoMANS, including data from 10-m towers at the RoMANS core measurement site in RMNP, in Lyons, Colorado, and at Gore Pass, a radar wind profiler in Estes Park, Colorado, and a SODAR in Granby, Colorado, during the spring field study. The RoMANS data are discussed in Chapter 3. Major physics options used in MM5 were Reisner 2 microphysics (Reisner et al., 1998), the Kain-Fritsch 2 cumulus parameterization (Kain and Fritsch, 1993; Kain, 2004) on the two coarse domains, the Noah land surface model (Ek et al., 2003), and the MRF planetary boundary layer scheme (Hong and Pan, 1996). Further details of the mesoscale meteorological modeling are summarized in Table 5.1 and discussed in Appendix 2.

**Table 5.1.** MM5 modeling choices.

Parameter	Choice	Reasoning
Horizontal grids	<p>Domain 1: Lambert Conformal map projection, center -97 deg longitude, 40 deg latitude, true latitudes 33 and 45 deg latitude, dimensions 165 (east-west) by 129 (north-south), grid size 36 km.</p> <p>Domain 2: dimensions 103 (east-west) by 115 (north-south), grid size 12 km</p> <p>Domain 3: dimensions 163 (east-west) by 118 (north-south), grid size 4 km</p>	The national Regional Planning Organizations (RPO) grid was used for the outer domain to leverage work done for 2002, especially on the emissions inventory. The fine scale grid covers most of Colorado and the intermediate domain was offset slightly to the west to capture more complex terrain. The domains were as large as possible within the memory constraints of available computing hardware.
Vertical levels	<p>35 full sigma levels plus the surface (sigma = 1), with more near the surface: 1, 0.9975, .995, .99, .985, .98, .97, .96, .95, .94, .93, .92, .91, .90, .88, .86, .84, .82, .80, .77, .74, .70, .65, .60, .55, .50, .45, .40, .35, .30, .25, .20, .15, .10, .05, 0.0</p> <p>Reference state pressure at atmosphere top = 100 hPa</p> <p>Reference state pressure at surface = 1000 hPa</p>	Used national RPO 34 levels plus an additional layer at 0.9975 with a middle height of 10 m to match RoMANS 10-m tower data.
Reference state temperatures	<p>Reference state surface temperature = 280 K</p> <p>Stratosphere temperature = 210 K</p>	MM5 manual recommends $T_{s0} = 270, 280, 290,$ and $300$ K for polar, midlatitude winter, midlatitude summer, and tropical atmospheres, respectively. WRAP used 275 K but this seems a bit cold. They also used no isothermal layer for the stratosphere.
Forecast length	<p>Each forecast was for 3.5 days with the first 12 hrs discarded as spinup.</p> <p>The first forecast started 13 Dec 2005 at 0Z and the last started 29 Dec 2006 0Z.</p>	Typically air quality applications use 4-6 day forecasts. The MM5 Manual recommends minimum forecasts of at least 24 hrs, discarding a 12-hr spinup time, due to issues with skin temperature, Colle et al. (1999, 2000) say 12 hrs needed for spin up, but the best precipitation forecast is at 18-36 hrs.
Surface and land use data	24 USGS categories	Commonly used protocol Morris et al., 2006, consistency with land surface model.
Nest interaction	One-way nesting.	More flexibility to use domains independently.
Four Dimensional Data Assimilation (FDDA) Options		
Grid 4DDA run	Domain 1 only for winds, temperature, and mixing ratio.	Commonly used protocol.
Observational nudging	Domain 3 only for winds, temperature, and mixing ratio. Coefficient = $4e-4$	Commonly used protocol.
Analysis data for lateral boundary conditions, initial conditions and analysis nudging	North American Regional Reanalysis (NARR)	Recommended by scientists at Colorado State University. NARR is consistent with the Eta/NAM forecast model and includes extensive observational nudging. Horizontal grid scale is 32 km with data updated every 3 hrs.

Parameter	Choice	Reasoning
Observational data for nudging	NCAR DS353.4 – ADP Upper air obs NCAR DS464.0 – ADP surface obs ROMANS 10-m tower data at the core site, Gore Pass, and Lyons. SODAR data in Granby during spring, radar profiler data in Estes Park during both field campaigns.	
Physics options:		
Microphysics (Explicit moisture schemes)	Reisner 2 – Based on mixed-phase scheme, includes super cooled water, graupel & ice number concentrations. Used by FSL and RUC	Previous studies
Cumulus parameterization	Kain-Fritsch2 – on domains 1 and 2, None – on domain 3 (4 Km)	ENVIRON Gorge: Kain-Fritsch2 on 36 & 12 km, none on 4 km.
Planetary boundary layer (PBL) scheme	Medium Range Forecast (MRF)	Suitable for high resolution, popular & efficient. Can be used with LSM. WRAP and ENVIRON. Gorge used Pleim-Chang. Gorge study report says PBLs were too low with this scheme. Only Eta and MRF work with Noah Land Surface Model. Eta – Used in Eta/NAM model. May get too warm and moist.
Thermal roughness	Zilitinkevich	Needed for MRF boundary layer scheme. Used by Eta Model MM5 manual says use one of 2 options of which this is more expensive, but may be better
Radiation	Rapid Radiative Transfer Model (RRTM)	Consistency with WRAP. Commonly used scheme. New highly accurate and efficient. Takes into account water vapor, O <sub>3</sub> , CO <sub>2</sub> . Interacts with cloud and precip fields.
Shallow convection	No	Consistency with WRAP
Horizontal Temperature diffusion	Offsets effect of coordinate slope over topography	Model default
Varying sea sfc temp	Yes	Consistency with WRAP.
Surface scheme	Noah Land-Surface Model	Consistency with NARR data used for initial and boundary conditions and analysis nudging. Predicts soil moisture and temperatures in four layers, canopy moisture, water-equivalent snow depth, surface and underground runoff.

### 5.2.2. Comparison of Modeled to Measured Meteorology

An independent quality assurance evaluation of the RoMANS MM5 modeling output was conducted by the URS Corporation. Their complete report is included as Appendix 2. The major findings of that evaluation include the following:

- A review of the scripts used to run the programs of the MM5 modeling system were in good order without any errors that may have adversely affected the modeling.
- MM5 slightly overpredicted wind speed during the winter (December through early March) on the 4-km domain but underpredicted during the remaining months, with the gross error being larger during the winter.

- Wind directions tended to be most accurate when the winds were from the west or south. The agreement was less good with the more infrequent winds from the east (upslope), especially in areas of complex terrain. Overall, the model did a good job of predicting measured wind directions.
- Wind speed and wind direction predictions were better on the 12-km and 36-km domains than on the 4-km domain.
- The model had a warm bias for most of the year. The gross error for temperature is smaller during the spring and summer months. There was better model performance for the two coarser domains than on the 4-km domain. Predicted temperatures agreed better on the plains than in the mountains, and the model underpredicted some daily high temperatures in the mountains during the winter months.
- Predicted humidity agreed well with observations across the entire 4-km domain.
- The model did well in predicting where rain occurred, but generally overpredicted rainfall quantities. There was better agreement during the cooler months than in the summer when convection dominates.

While additional refinement of the MM5 modeling could potentially improve model performance, resources and time are limited. The 4-km dataset was deemed acceptable for use in air quality studies focused on Colorado.

In addition to the independent evaluation, other assessments of the MM5 output were conducted. These are summarized below.

#### **5.2.2.1. Precipitation**

MM5 precipitation estimates often overpredict measured precipitation. For example, Colle et al. (1999) found that during the cool season in the Pacific Northwest, MM5 overpredicted precipitation on steep windward slopes and underpredicted in the lee of the mountains and that a 36-km horizontal resolution was significantly better than 12-km. Colle et al. (2000) found, however, that increasing the resolution to 4 km produced further improvements only for heavy precipitation events. Fernandez et al. (2007) reported noticeable precipitation errors over mountainous areas and unrealistically high summer precipitation. Grubisic et al. (2005) tested four different microphysics schemes and found that all overpredicted precipitation in the Sierra Nevada mountains and that increasing the horizontal resolution did not increase the skill in forecasting orographic precipitation. Therefore, it was expected that the MM5 modeling for RoMANS would probably also overpredict precipitation.

Some preliminary assessments of the RoMANS MM5 precipitation are discussed below and in the URS report in Appendix 2. Additionally, as part of RoMANS, all available measured precipitation data for 2006 for the state of Colorado were archived but have not yet been analyzed. Future evaluation of these data, especially for possible spatial and temporal biases in the MM5 precipitation output, could potentially lead to better understanding of when, where, and why MM5 predicts precipitation poorly. This could lead to different modeling protocols or use of different input data to improve the precipitation calculations for this and future air quality studies in the Rocky Mountains.

## DRAFT

At this time, the RoMANS MM5 precipitation estimates have been compared to two sets of measured data, the hourly measured values at the RoMANS core site as described in Chapter 3 and from the National Weather Service Climate Prediction Center (CPC) (Higgins, 1996) daily gridded values. While generally thought of as measured precipitation, the CPC values are on a 0.25 by 0.25 degree grid for 10-60 deg N and 140-60 deg W for which there are not measured values in every grid cell. CPC precipitation amounts are interpolated from measurements collected at more than 8000 stations in the United States and Mexico, using a modified Cressman scheme. Data from the following sources are included

- World Meteorological Organization (WMO),
- Global Telecommunications System (GTS) sites,
- SHEF (Standard Hydrologic Exchange Format) - from National Weather Service River Forecast Centers,
- Hydrometeorological Automated Data System (HADS),
- SNOTEL (SNOWpack TELEmetry) dataset,
- Mexican National Weather Service.

In remote, mountainous regions, there are probably not enough measured precipitation values included in the CPC analysis to truly capture the actual inhomogeneous precipitation patterns in complex terrain. This is especially true during the summer when small-scale convective storms are more frequent than in other seasons.

Figures 5.3 and 5.4 show the daily measured, CPC, and MM5 4-km domain precipitation amounts at the RoMANS core site for spring and summer, respectively. Tables 5.2 and 5.3 give the summary statistics for the daily and hourly precipitation estimates, and Tables 5.4 and 5.5 show the correlations between the various estimates of daily and hourly precipitation at the core site.

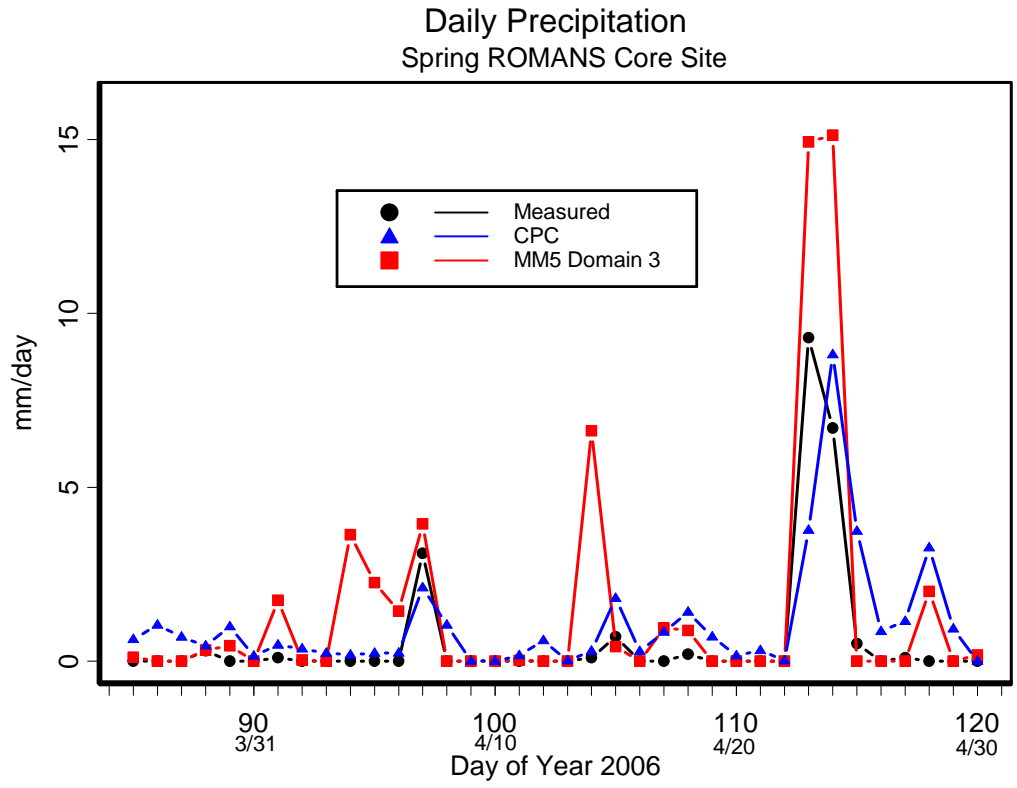


Figure 5.3. Daily precipitation totals at the RoMANS core site during the spring study as measured, estimated by CPC, and estimated by MM5 on the 4-km domain.

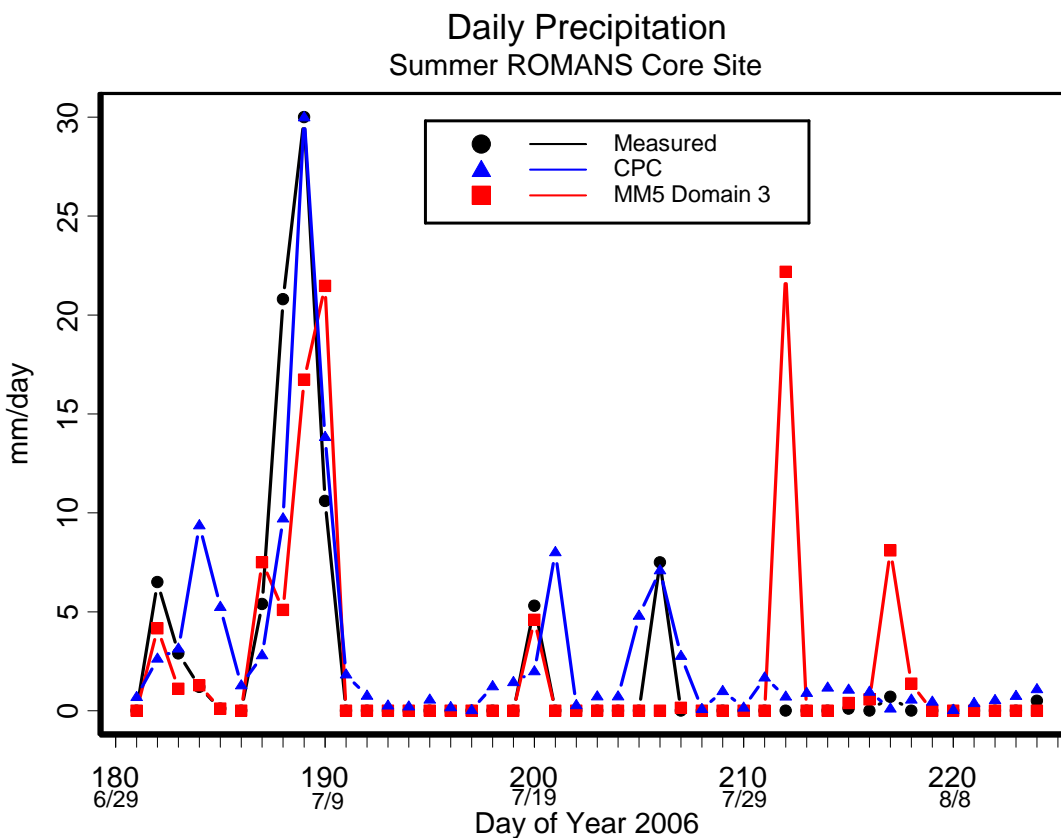


Figure 5.4. Daily precipitation totals at the RoMANS core site during the summer study as measured, estimated by CPC, and estimated by MM5 on the 4-km domain.

**Table 5.2.** Summary statistics for 24-hr-averaged measured and calculated precipitation (mm) at the RoMANS core site during the spring and summer studies.

	Season	N > 0	N	Mean	Median	Stand. Dev.	Max	Total
<b>Measured</b>	Spring	10	36	0.59	0.00	1.92	9.3	21.1
<b>CPC</b>	Spring	34	36	1.05	0.53	1.66	8.8	37.9
<b>MM5 4 km</b>	Spring	20	36	1.53	0.011	3.61	15.1	55.0
<b>MM5 12 km</b>	Spring	19	36	1.31	0.009	3.21	14.5	47.1
<b>MM5 36 km</b>	Spring	29	36	3.27	1.23	4.41	19.3	117.6
<b>Measured</b>	Summer	13	44	2.08	0.00	5.75	30.0	91.6
<b>CPC</b>	Summer	44	44	2.80	0.97	5.18	30.0	123.2
<b>MM5 4 km</b>	Summer	16	44	2.15	0.14	5.33	22.2	94.8
<b>MM5 12 km</b>	Summer	17	44	1.68	0.00	4.44	21.9	74.0
<b>MM5 36 km</b>	Summer	30	44	2.35	0.00	5.21	26.3	103.2

**Table 5.3.** Summary statistics for 1-hr-averaged measured and calculated precipitation (mm) at the RoMANS core site during the spring and summer studies.

	Season	N > 0	N	Mean	Median	Stand. Dev.	Max	Total
<b>Measured</b>	Spring	37	840	0.025	0.000	0.197	4.2	21.1
<b>MM5 4 km</b>	Spring	201	840	0.066	0.000	0.347	4.5	55.0
<b>MM5 12 km</b>	Spring	191	840	0.056	0.000	0.297	3.9	47.1
<b>MM5 36 km</b>	Spring	401	840	0.140	0.000	0.348	3.0	117.6
<b>Measured</b>	Summer	60	1032	0.089	0.000	0.500	7.5	91.6
<b>MM5 4 km</b>	Summer	83	1032	0.092	0.000	0.431	6.5	94.8
<b>MM5 12 km</b>	Summer	93	1032	0.072	0.000	0.469	7.7	74.0
<b>MM5 36 km</b>	Summer	206	1032	0.100	0.000	0.546	4.0	103.2

**Table 5.4.** Correlations between 24-hr precipitation estimates at the RoMANS core site for spring/summer.

	MM5 36 km	MM5 12 km	MM5 4 km	Measured	CPC
<b>MM5 36 km</b>	1 / 1	.576 / .858	.624 / .924	.440 / .420	.530 / .395
<b>MM5 12 km</b>	.576 / .858	1 / 1	.994 / .973	.920 / .566	.701 / .596
<b>MM5 4 km</b>	.624 / .924	.994 / .973	1 / 1	.911 / .562	.737 / .556
<b>Measured</b>	.440 / .420	.920 / .566	.911 / .562	1 / 1	.738 / .867
<b>CPC</b>	.530 / .395	.701 / .596	.737 / .556	.738 / .867	1 / 1

**Table 5.5.** Correlations between 1-hr precipitation estimates at the RoMANS core site for spring/summer.

	MM5 36 km	MM5 12 km	MM5 4 km	Measured
<b>MM5 36 km</b>	1 / 1	.484 / .491	.512 / .608	.215 / .209
<b>MM5 12 km</b>	.484 / .491	1 / 1	.966 /	.486 / .288
<b>MM5 4 km</b>	.512 / .608	.966 / .920	1 / 1	.468 / .302
<b>Measured</b>	.215 / .209	.486 / .288	.468 / .302	1 / 1

Compared to the measured values, the total precipitation amounts at the core site for each of the two RoMANS study periods were overpredicted by all three MM5 domains and CPC values except for the MM5 12-km predictions during the summer, which underpredicted the measurements. Likewise, the number of days and number of hours of measured precipitation was also overpredicted by all methods. The 24-hr-averaged, 12-km and 4-km MM5 precipitation forecasts correlated extremely well with the measured values at the core site during the spring, even better than did CPC. During the summer, CPC correlated better with the measurements than did MM5. The measured hourly amounts correlated approximately equally well with the 12-km and 4-km MM5 output. The correlation between the hourly measured and the hourly MM5 36-km values was significantly poorer than for the two higher resolution domains.

### 5.3. BACK TRAJECTORY ANALYSES FOR SPRING AND SUMMER

#### 5.3.1. Trajectory Model

The HYbrid Single-Particle Lagrangian Integrated Trajectory (HYSPLIT) model (Draxler and Hess, 1998) was developed by the NOAA Environmental Research Laboratories. It can compute a range of outputs from simple air parcel trajectories to dispersion and deposition simulations. For RoMANS, version 4.8r of the model was used in simple back trajectory mode. Default vertical motion, which was employed for RoMANS, is calculated using the input vertical velocity field. Required input is a gridded meteorological dataset on a polar, Lambert, or Mercator map projection with data at regular intervals. Back trajectory positions or “endpoints” are calculated hourly. For RoMANS, trajectories were calculated for up to 10 days backward in time, using the output from all three domains from the MM5 model and 1 deg gridded data from the Global Data Assimilation System (GDAS) for areas beyond the MM5 domains. Trajectories were started from heights of 100, 200, 500, and 1000 m above ground level (AGL).

The advection of a particle or puff is computed from the average of the three-dimensional velocity vectors at the initial position and at the first guess of the next position. Velocity vectors are linearly interpolated in both space and time. Trajectories terminate if they exit the model top (specified as 10 km AGL for RoMANS), but advection continues along the surface if trajectories intersect the ground.

#### 5.3.2. Discussion of Trajectories and Meteorology during Episodes

Following is a summary of the meteorology and transport during particulate and wet deposition episodes during both RoMANS field campaigns. Included for each episode are plots of the 1-minute meteorological data measured at the core measurement site, plots of the hourly upper-air winds by time and by height as measured by the radar profiler at Estes Park and as predicted by the mesoscale meteorological model at Estes Park, 5-day-long back trajectories arriving at the core site, and contour plots of the CPC- and MM5-predicted precipitation. For clarity, only the trajectories started at 100 m are included. There were no episodes when the higher trajectories were dramatically different.

##### 5.3.2.1. Particulate Episodes

###### 5.3.2.1.1. *April 20–23, 2006 (Julian Days 110–113) – Particulate Episode*

The suite of meteorological and trajectory data for April 20, 2006, is presented in Figures 5.5–5.8. Figures 5.9–5.12 show the same data for April 21, Figures 5.13–5.16 for April 22, and Figures 5.17–5.20 for April 23. There was no measured precipitation at the core site during these days. As shown, on April 20 the 10-m winds at the core site were northwesterly at 0–3 m/sec during the morning and nighttime hours and were southeasterly at 2–6 m/sec during midday. Temperatures ranged from about -4 to 8 deg C and RH was 40–60% at night and below 30% during midday. The Estes Park profiler showed easterly winds in a layer up to about 2000 m AGL during most of the day from about 9:00 am until about 8:00 pm, with an elevated layer of easterlies during 6:00–9:00 am. MM5 captured the timing and depth of the easterlies quite well. Back trajectories show a Front Range influence, with trajectories then continuing to the north across Wyoming with some then turning east and some west.

## DRAFT

On April 21, 10-m winds were mostly northerly, tending to be northwesterly during the nighttime hours, with somewhat more northeasterly flow during midday. Wind speeds were steadier than on the April 20, mostly staying in the 2–6 m/sec range all day. Temperatures were warmer and RH was somewhat lower than the previous day, with temperatures ranging from 0 to above 10 C, and RH of 10–60%. Back trajectories and upper-air winds were mostly westerly, though there were some near-surface easterly winds during 5:00–7:00 pm.

Back trajectories on April 22 were very similar to those on April 21. The 10-m wind speeds were 0–3 m/sec at night and up to about 7 m/sec during midday. Wind directions were mostly northwesterly at night and predominantly southerly but with variable directions during the day. Temperatures got up to about 15 C and RH was around 10% during midday. The profiler showed a shallow layer of easterly winds during the evening hours.

Back trajectories on April 23 were similar to those on April 20. Ten-meter winds at the core site were northerly until about 8:00 am when they switched to southerly for the remainder of the day, being southwesterly until about 11:00 am and then southeasterly for the remainder of the day. RH was less than 20% in the late morning and then rose steadily to more than 80% by the end of the day and the temperature dropped to about 0 C. The coldest temperature of the day was at midnight on the 24<sup>th</sup>. Midday temperatures were as high as 15 C. The profiler in Estes Park showed westerly winds at all levels until noon when the winds up to about 2000 m switched to easterly. When observational nudging was used in MM5, it was able to capture the timing of this directional switch quite well on all domains. Without the observational nudging, however, the directional change was captured on the 4-km domain but was late by about 2 hours. Precipitation began at about midnight on April 24. See the section on April 24–25 in the discussion of the wet deposition episodes for the meteorology on the following 2 days.

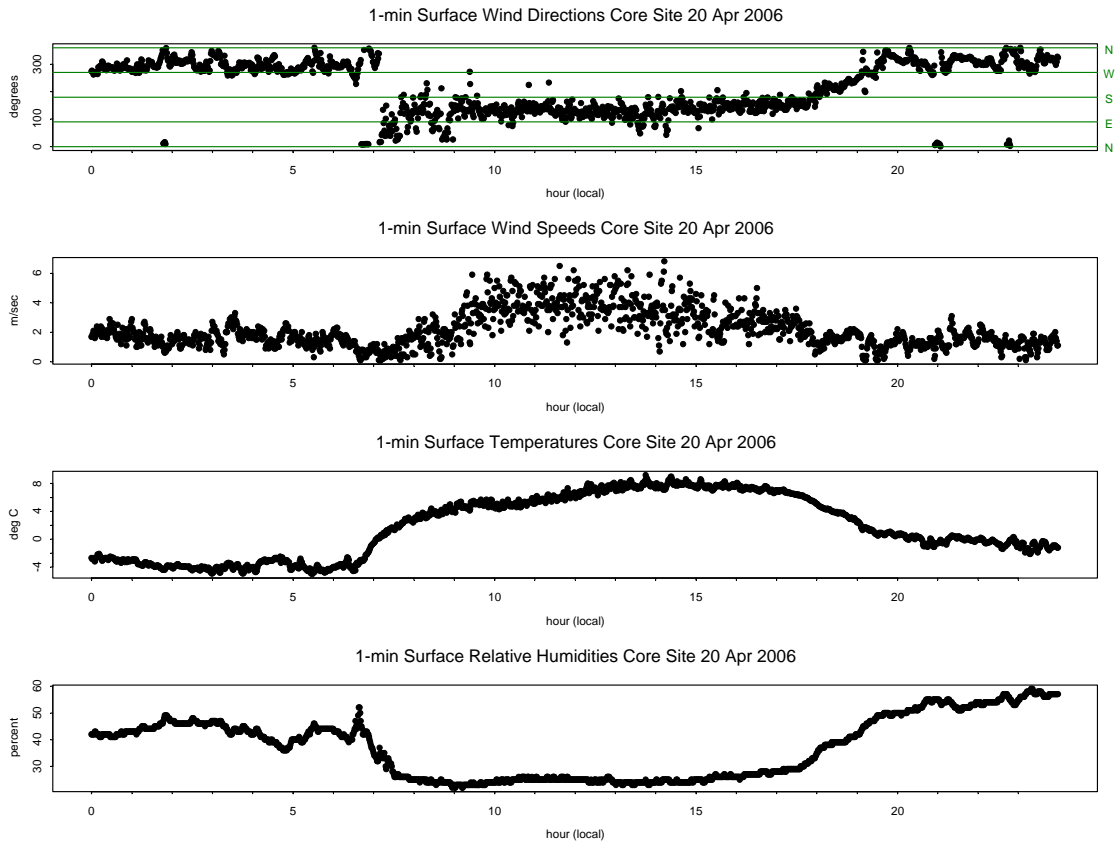


Figure 5.5. Measured wind direction, wind speed, temperature, and relative humidity at the RoMANS core measurement site on April 20, 2006 (Julian Day (JD) = 110).

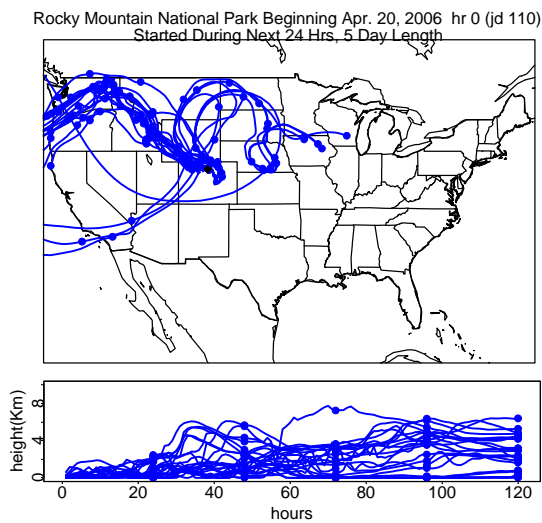


Figure 5.6. Back trajectories started at 100 m AGL at the RoMANS core measurement site on April 20, 2006 (JD = 110). Trajectories were tracked hourly for 5 days.

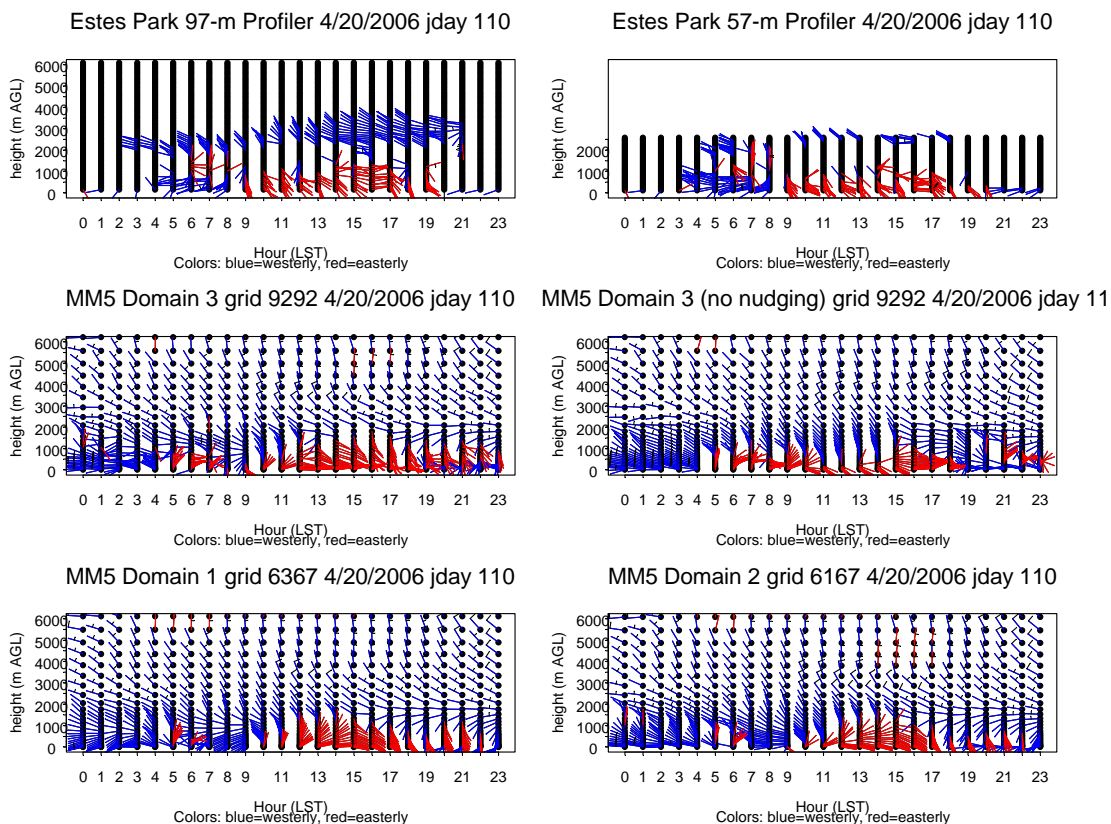


Figure 5.7. Horizontal winds by height above ground and by hour at Estes Park, Colorado, on April 20, 2006 (JD = 110), as measured by the two modes of the radar wind profiler and as calculated by MM5 on Domain 1 (36 km), Domain 2 (12 km), and Domain 3 (4 km). Domain 3 results are shown with and without observational nudging. Each long barb is 10 m/sec; short barbs are 5 m/sec. Stems are red for easterly winds and blue for westerly.

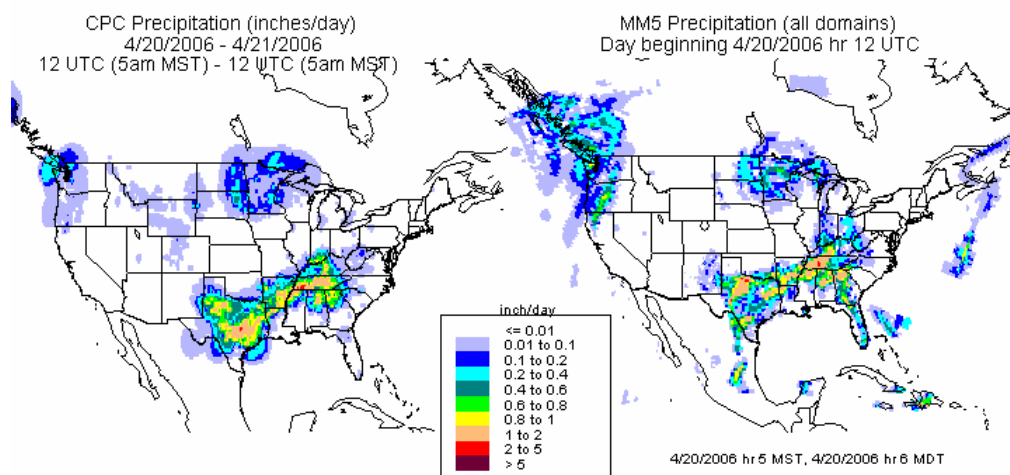


Figure 5.8. Contours of CPC (left) and MM5 (right) 24-hr precipitation totals beginning April 20, 2006, 12:00 UTC (5:00 am MST).

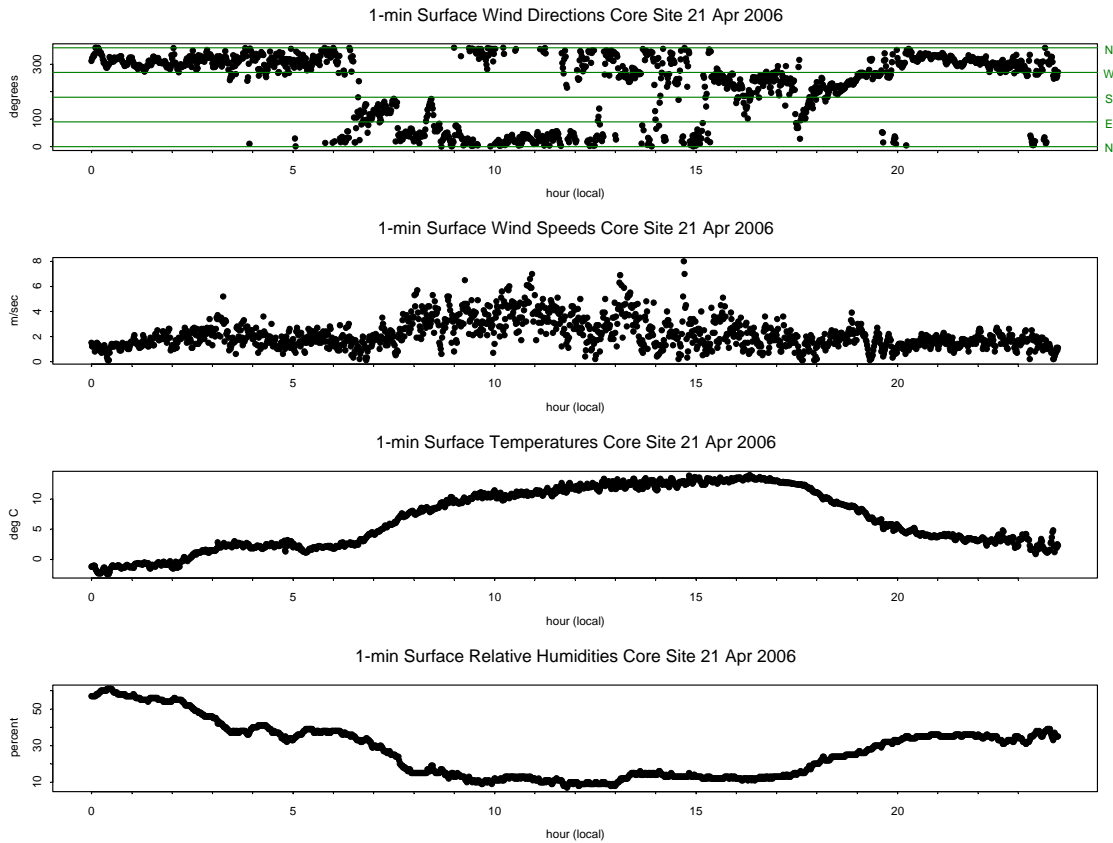


Figure 5.9. Measured wind direction, wind speed, temperature, and relative humidity at the RoMANS core measurement site on April 21, 2006 (JD = 111).

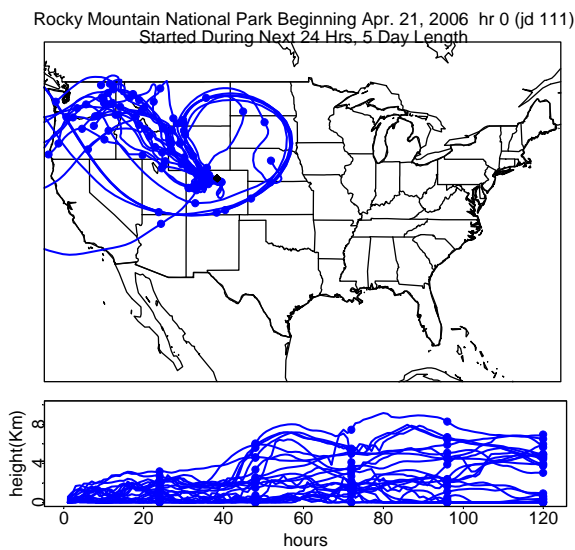


Figure 5.10. Back trajectories started at 100 m AGL at the RoMANS core measurement site on April 21, 2006 (JD = 111). Trajectories were tracked hourly for 5 days.

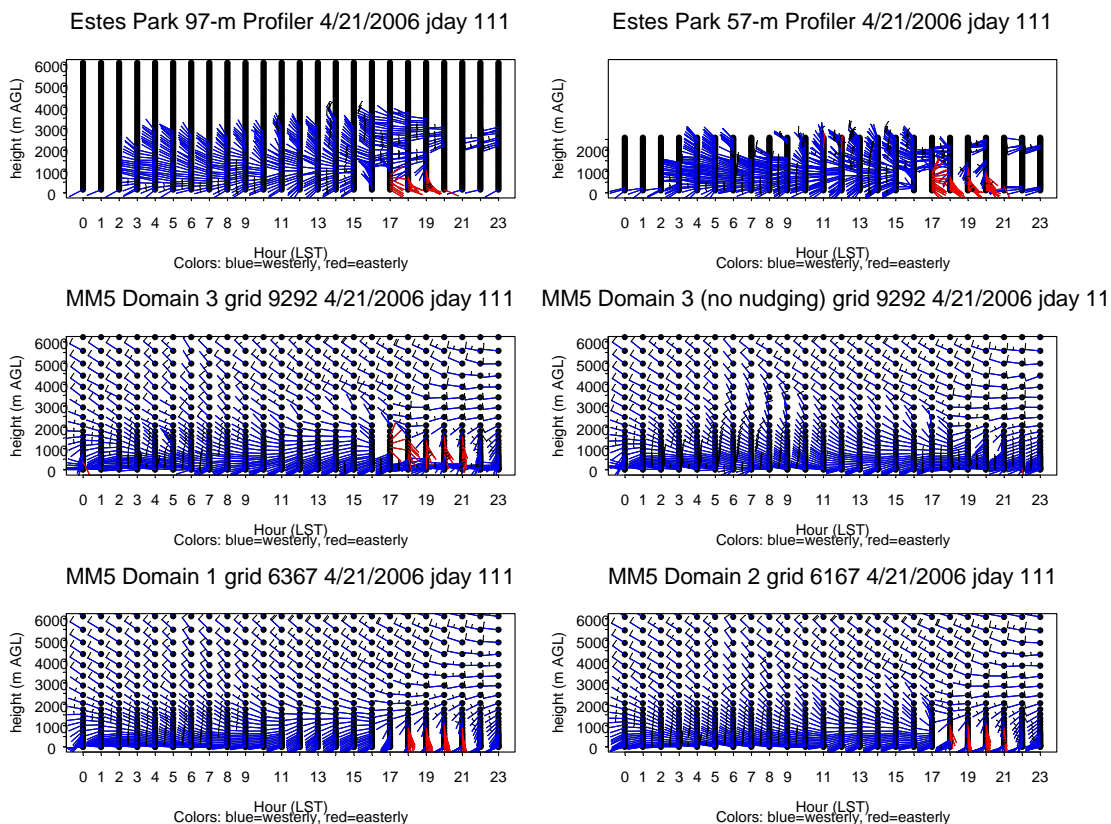


Figure 5.11. Horizontal winds by height above ground and by hour at Estes Park, Colorado, on April 21, 2006 (JD = 111), as measured by the two modes of the radar wind profiler and as calculated by MM5 on Domain 1 (36 km), Domain 2 (12 km), and Domain 3 (4 km). Domain 3 results are shown with and without observational nudging. Each long barb is 10 m/sec; short barbs are 5 m/sec. Stems are red for easterly winds and blue for westerly.

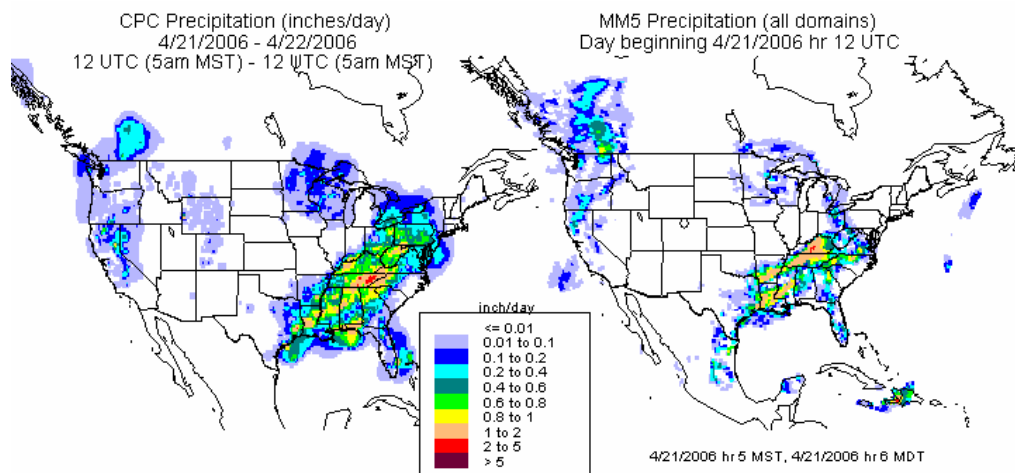


Figure 5.12. Contours of CPC (left) and MM5 (right) 24-hr precipitation totals beginning April 21, 2006, 12:00 UTC (5:00 am MST).

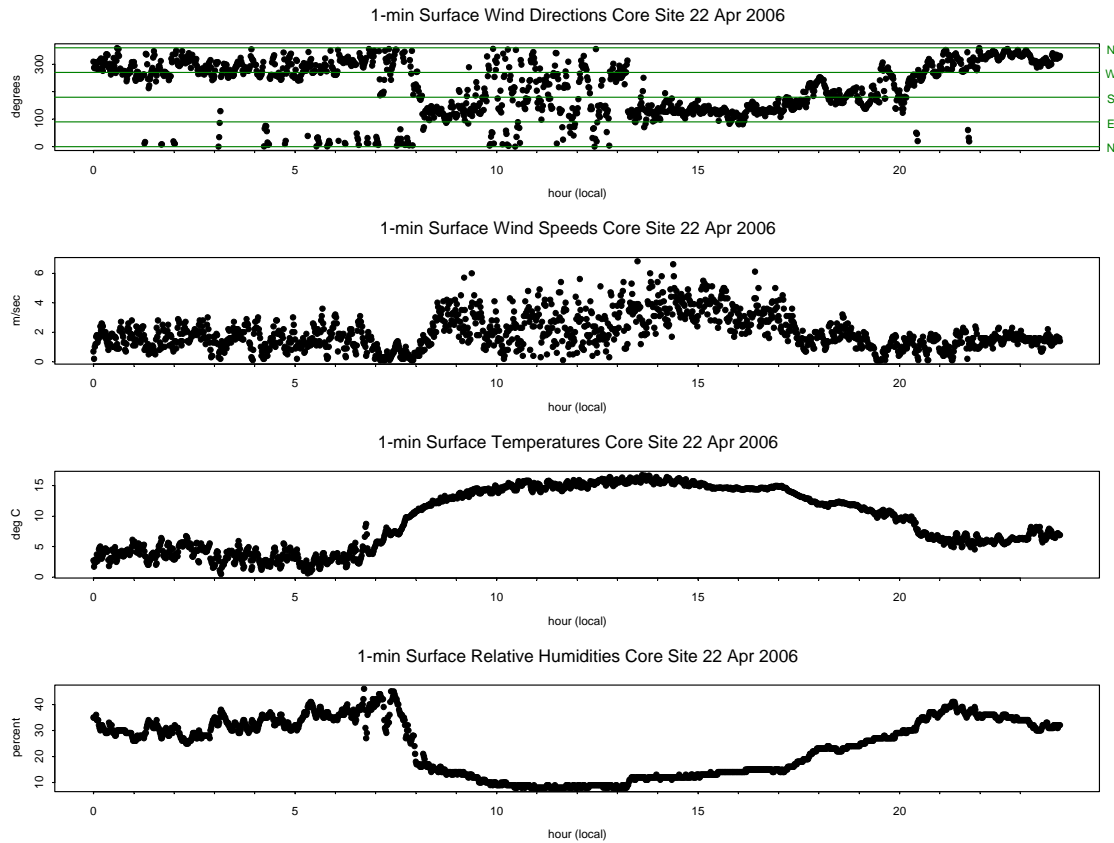


Figure 5.13. Measured wind direction, wind speed, temperature, and relative humidity at the ROMANS core measurement site on April 22, 2006 (JD = 112).

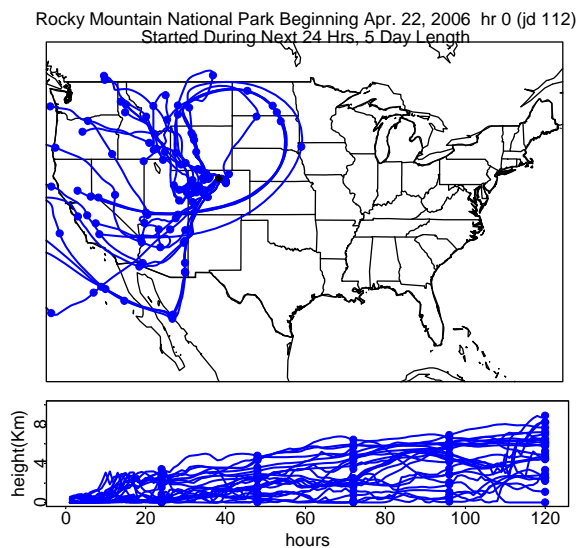


Figure 5.14. Back trajectories started at 100 m AGL at the RoMANS core measurement site on April 22, 2006 (JD = 112). Trajectories were tracked hourly for 5 days.

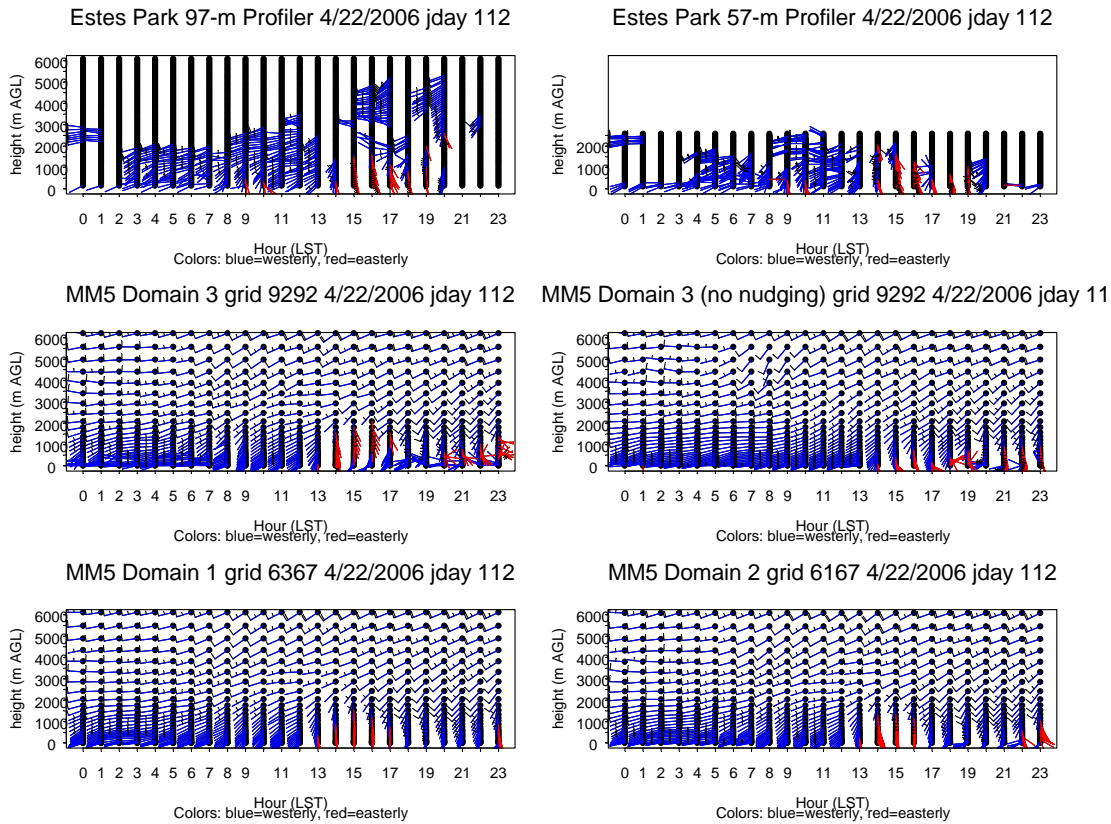


Figure 5.15. Horizontal winds by height above ground and by hour at Estes Park, Colorado, on April 22, 2006 (JD = 112), as measured by the two modes of the radar wind profiler and as calculated by MM5 on Domain 1 (36 km), Domain 2 (12 km), and Domain 3 (4 km). Domain 3 results are shown with and without observational nudging. Each long barb is 10 m/sec, short barbs are 5 m/sec. Stems are red for easterly winds and blue for westerly.

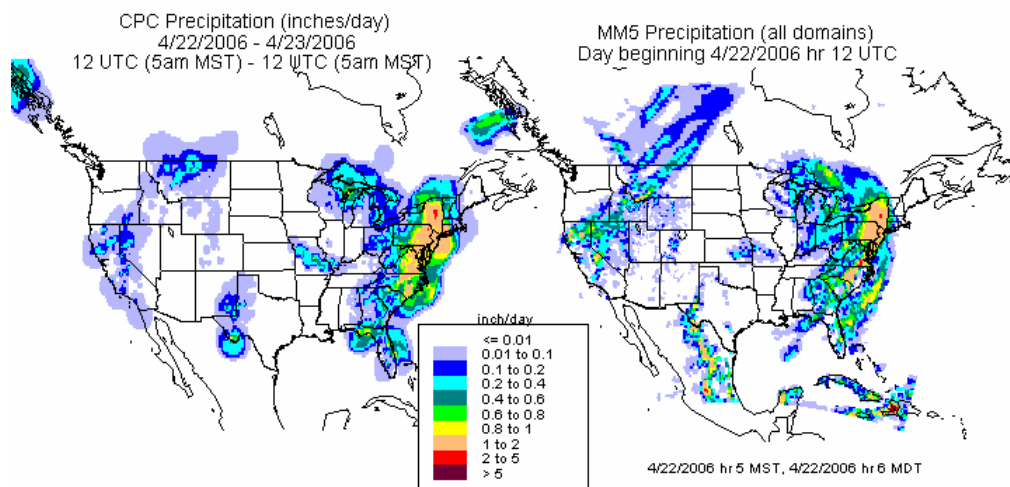


Figure 5.16. Contours of CPC (left) and MM5 (right) 24-hr precipitation totals beginning April 22, 2006, 12:00 UTC (5:00 am MST).

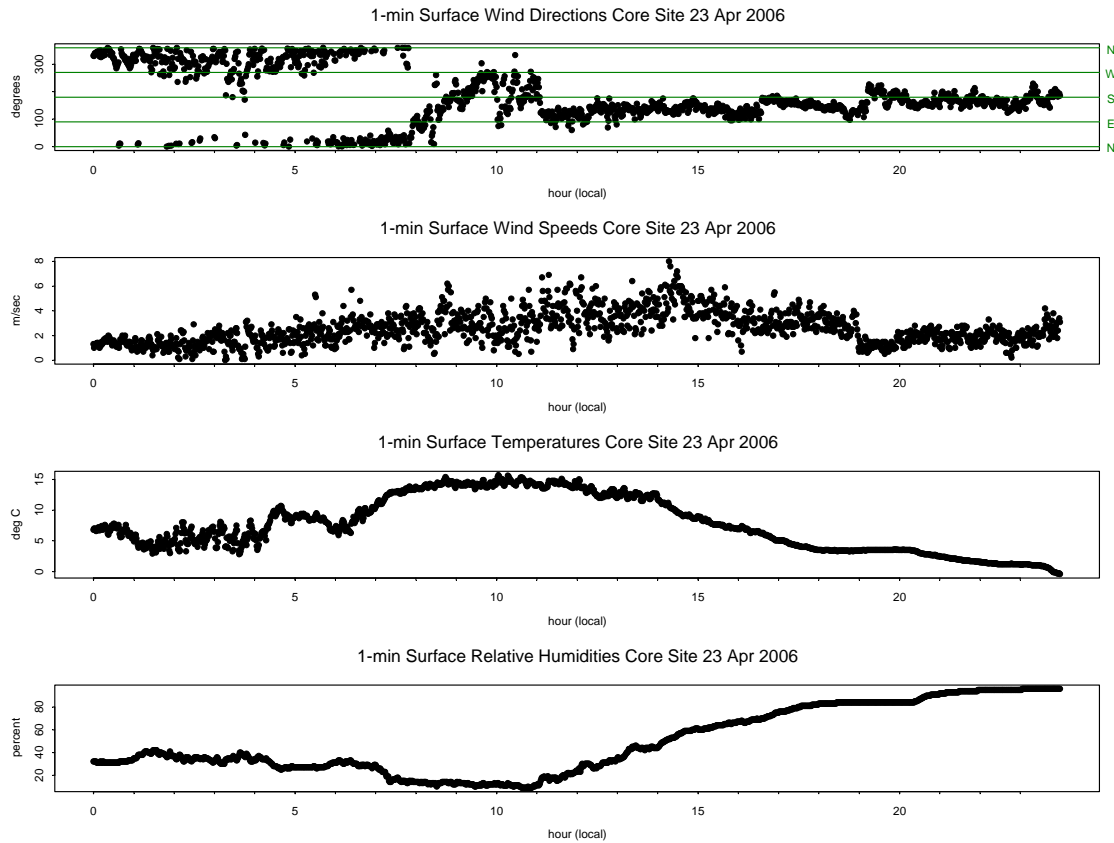


Figure 5.17. Measured wind direction, wind speed, temperature, and relative humidity at the RoMANS core measurement site on April 23, 2006 (JD = 113).

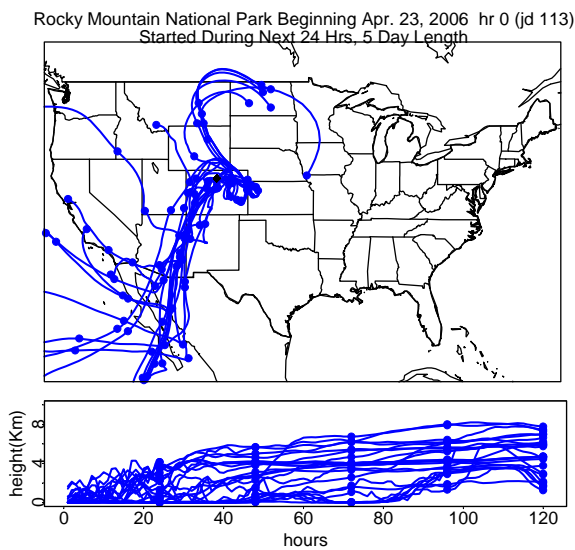


Figure 5.18. Back trajectories started at 100 m AGL at the RoMANS core measurement site on April 23, 2006 (JD = 113). Trajectories were tracked hourly for 5 days.

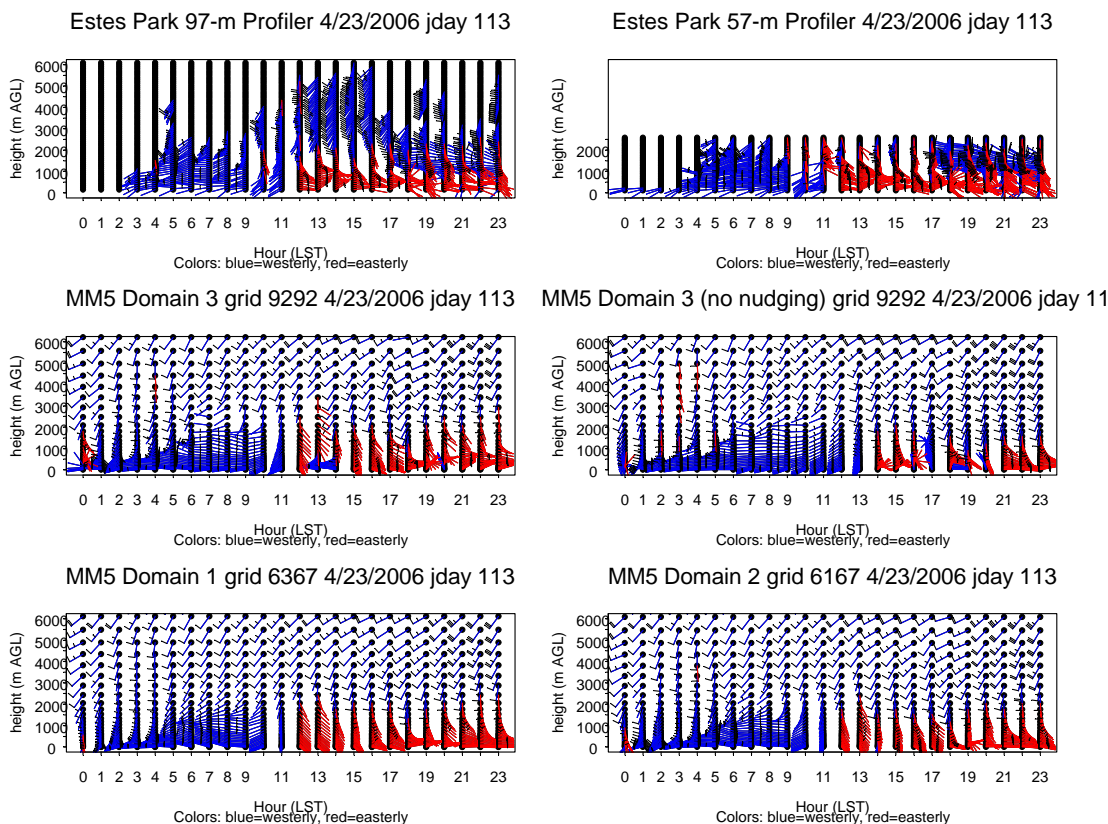


Figure 5.19. Horizontal winds by height above ground and by hour at Estes Park, Colorado, on April 23, 2006 (JD = 113), as measured by the two modes of the radar wind profiler and as calculated by MM5 on Domain 1 (36 km), Domain 2 (12 km), and Domain 3 (4 km). Domain 3 results are shown with and without observational nudging. Each long barb is 10 m/sec; short barbs are 5 m/sec. Stems are red for easterly winds and blue for westerly.

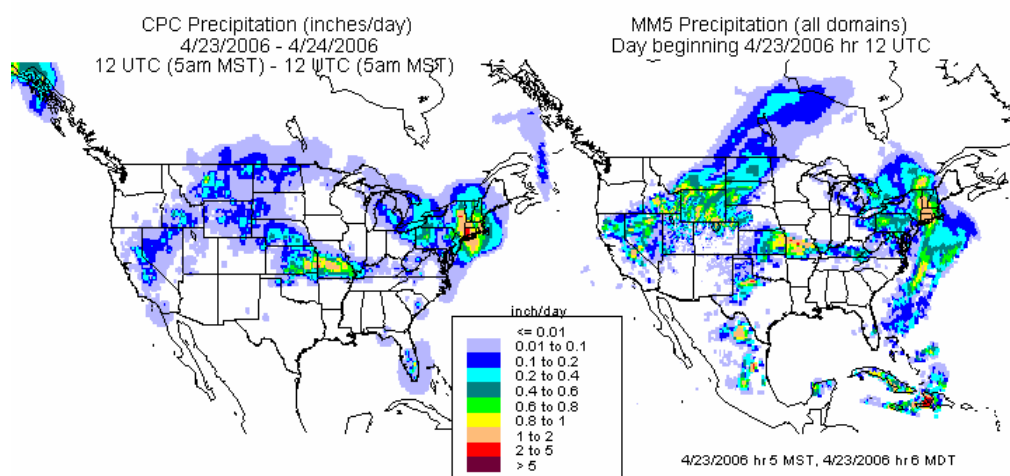


Figure 5.20. Contours of CPC (left) and MM5 (right) 24-hr precipitation totals beginning April 23, 2006, 12:00 UTC (5:00 am MST).

**5.3.2.1.2. July 22–23, 2006 (Julian Days 203–204) – Particulate Episode**

The suite of meteorological data for July 22 and July 23 is presented in Figures 5.21–24 and 5.25–28, respectively. There was no measured precipitation at the core site on July 22, though there was some light precipitation on the afternoon of July 23 during hours 24, 17, and 18, totaling 1.2 mm.

On July 22, the 10-m wind speeds at the core site ranged from less than 1 m/sec around the times of sunrise and sunset to nearly 6 m/sec during midafternoon. Wind directions at the core site were northwesterly until about 6:00 am and after 8:00 pm, southeasterly between 11:00 am and 6:00 pm, northerly between 8:00 am and 10:00 am, and transitioning from northerly to southeasterly during 6:00–9:00 am. Temperatures ranged from 7 to 20 C and RH from 30% to 90%. Back trajectories arrived from the north, across eastern Wyoming, after having crossed Montana and other northern tier states to the west. There was also some transport from the east, particularly Nebraska and eastern South Dakota. The Estes Park profiler showed near-surface easterly wind for most of the day, but during the early morning hours there was a very shallow layer of westerly winds at the surface, below the easterly layer. MM5 did not capture these early morning easterly winds but did correctly have easterly winds in the surface layer between 7:00 am and 9:00 pm.

On July 23, the core site 10-m winds were northerly, mostly northwesterly, before 7:00 am and after 5:00 pm. Wind directions were more northeasterly during most of the remainder of the day except between noon and 3:00 pm when southeasterly winds predominated. Temperatures ranged from less than 10 to about 25 C and RH from 20% to 80%. Back trajectories on July 23 were very similar to those on July 22, but with less transport from the east. At Estes Park, the profiler showed mostly westerly winds, except for a shallow layer of easterly winds between 9:00 am and 2:00 pm and again during the 4:00–5:00 pm hour. The MM5 model was about an hour late in starting the easterly flow and only the nudged 4-km domain showed the 4:00–5:00 pm easterlies.

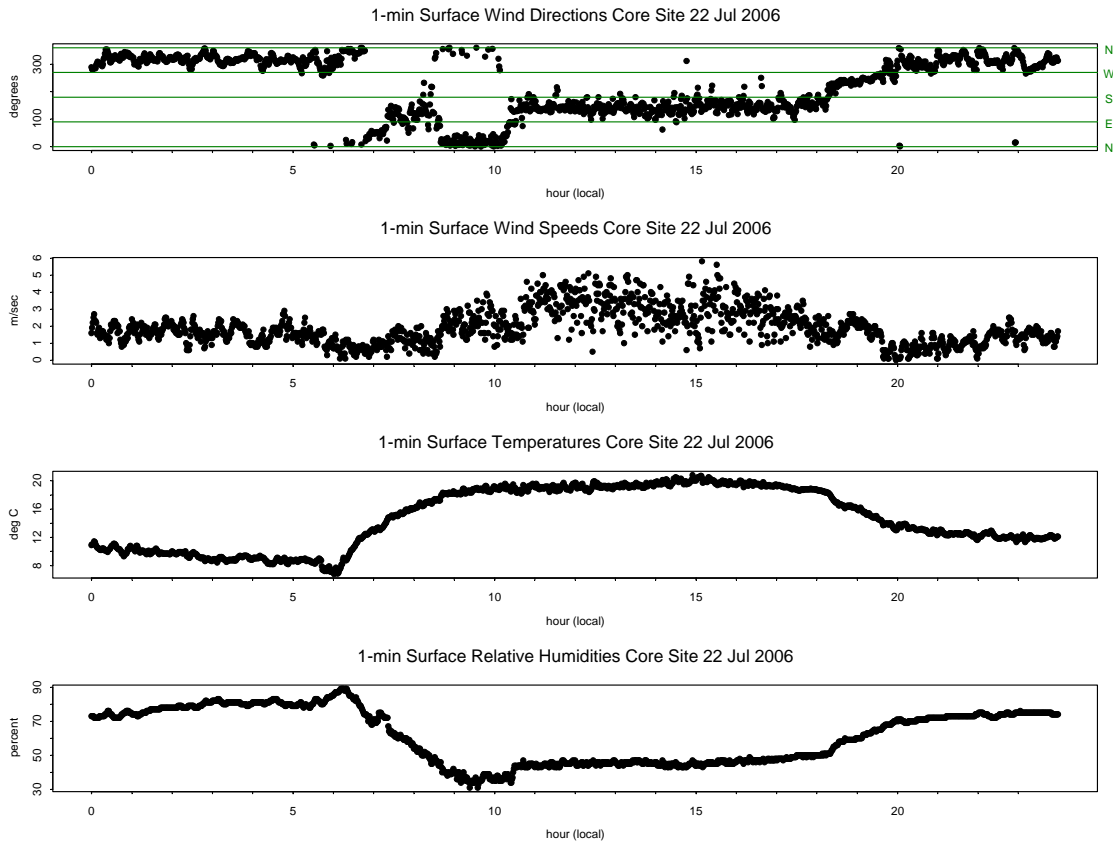


Figure 5.21. Measured wind direction, wind speed, temperature, and relative humidity at the RoMANS core measurement site on July 22, 2006 (JD = 203).

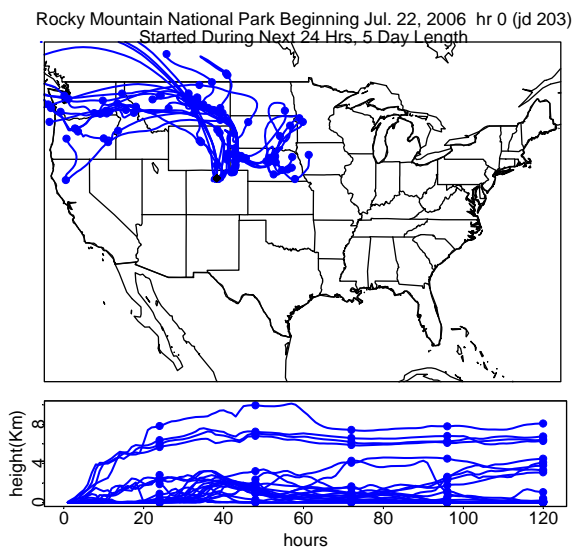


Figure 5.22. Back trajectories started at 100 m AGL at the RoMANS core measurement site on July 22, 2006 (JD = 203). Trajectories were tracked hourly for 5 days.

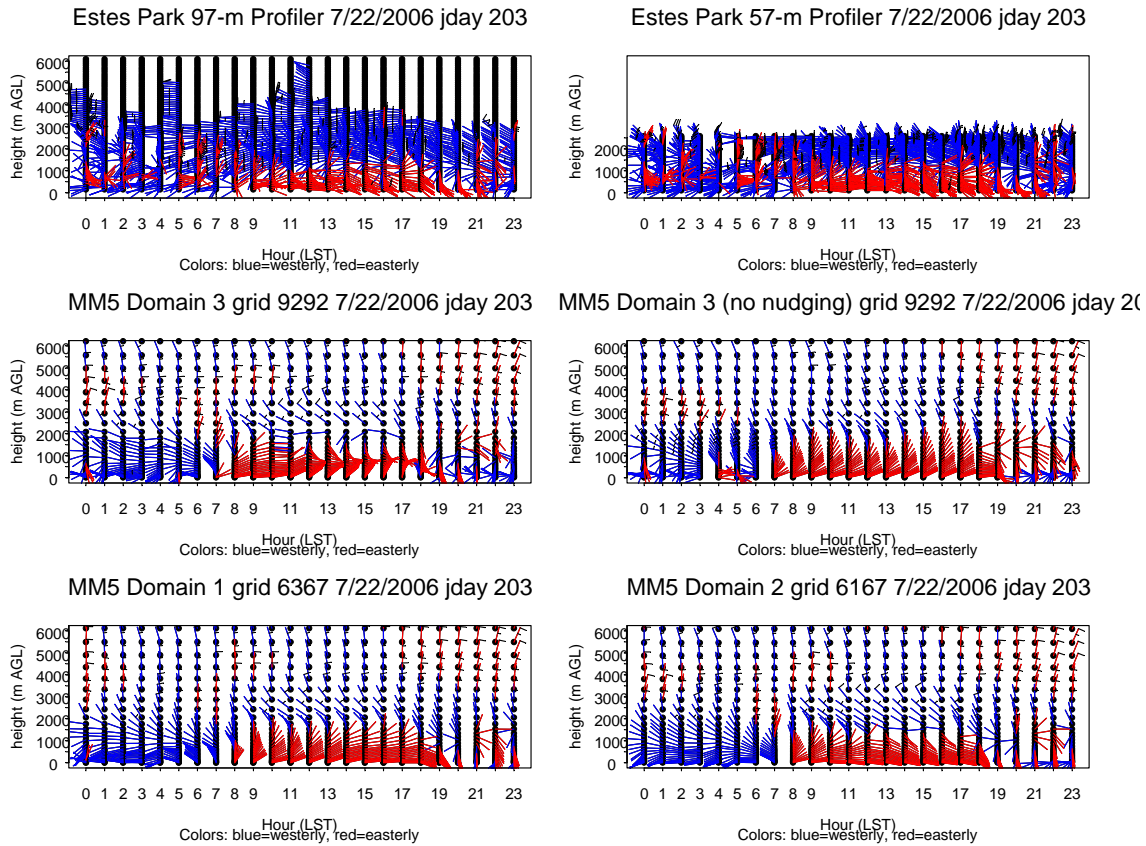


Figure 5.23. Horizontal winds by height above ground and by hour at Estes Park, Colorado, on July 22, 2006 (JD = 203), as measured by the two modes of the radar wind profiler and as calculated by MM5 on Domain 1 (36 km), Domain 2 (12 km), and Domain 3 (4 km). Domain 3 results are shown with and without observational nudging. Each long barb is 10 m/sec; short barbs are 5 m/sec. Stems are red for easterly winds and blue for westerly.

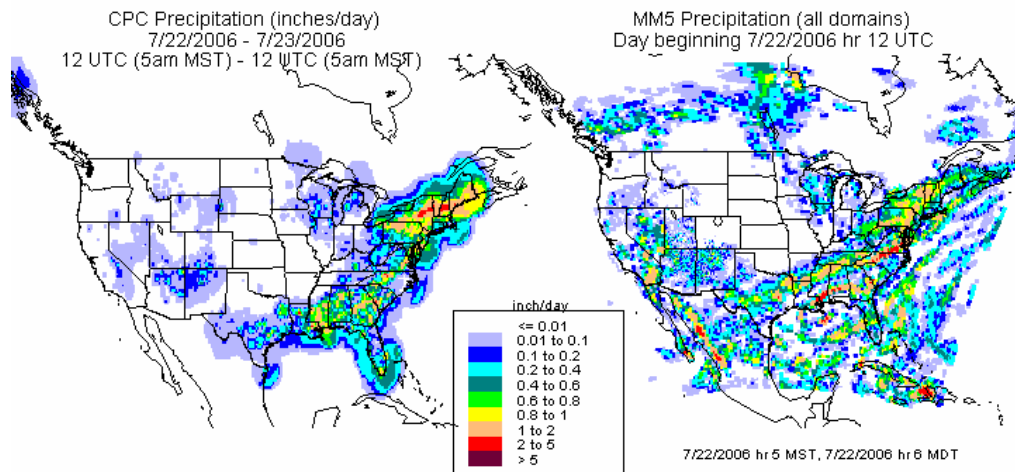


Figure 5.24. Contours of CPC (left) and MM5 (right) 24-hr precipitation totals beginning July 22, 2006, 12:00 UTC (5:00 am MST, 6:00 am MDT).

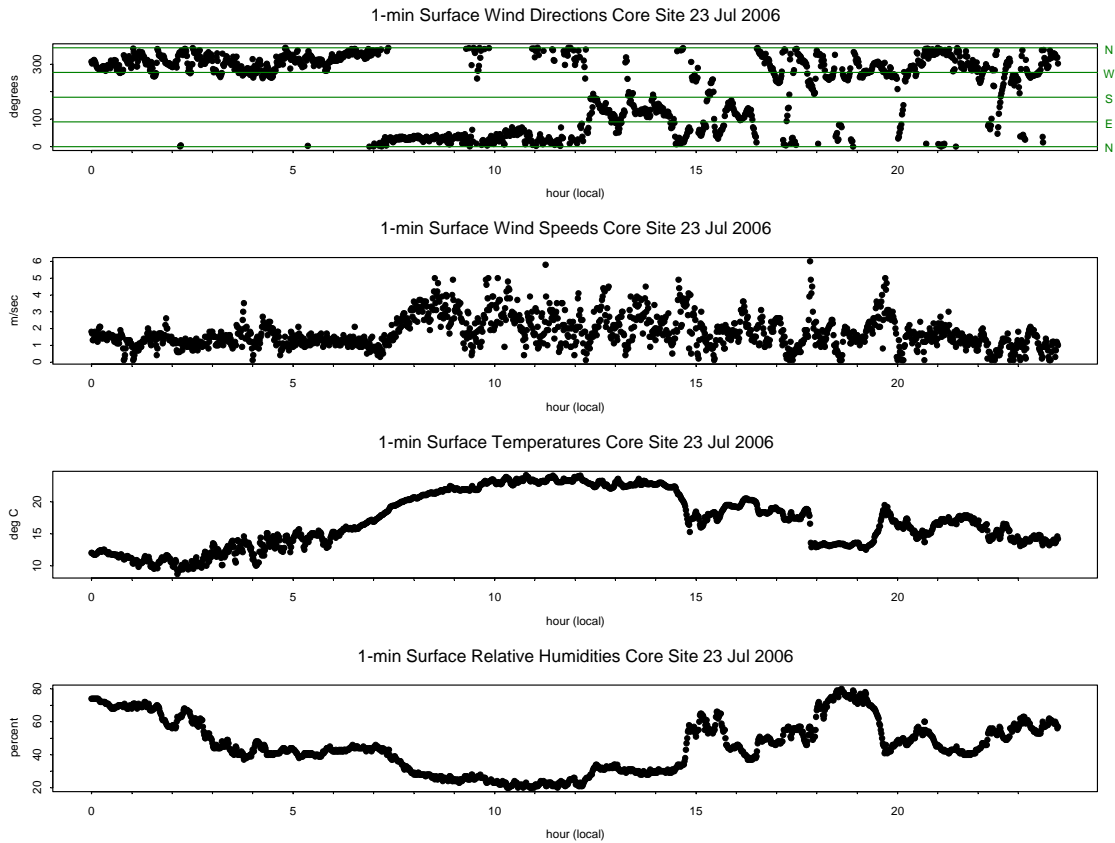


Figure 5.25. Measured wind direction, wind speed, temperature, and relative humidity at the RoMANS core measurement site on July 23, 2006 (JD = 204).

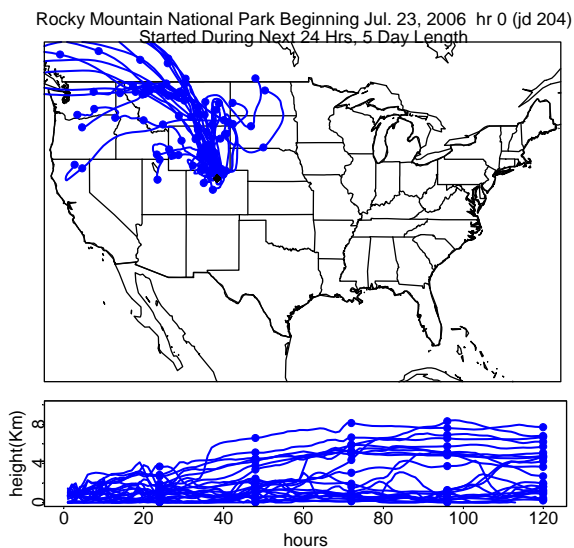


Figure 5.26. Back trajectories started at 100 m AGL at the RoMANS core measurement site on July 23, 2006 (JD = 204). Trajectories were tracked hourly for 5 days.

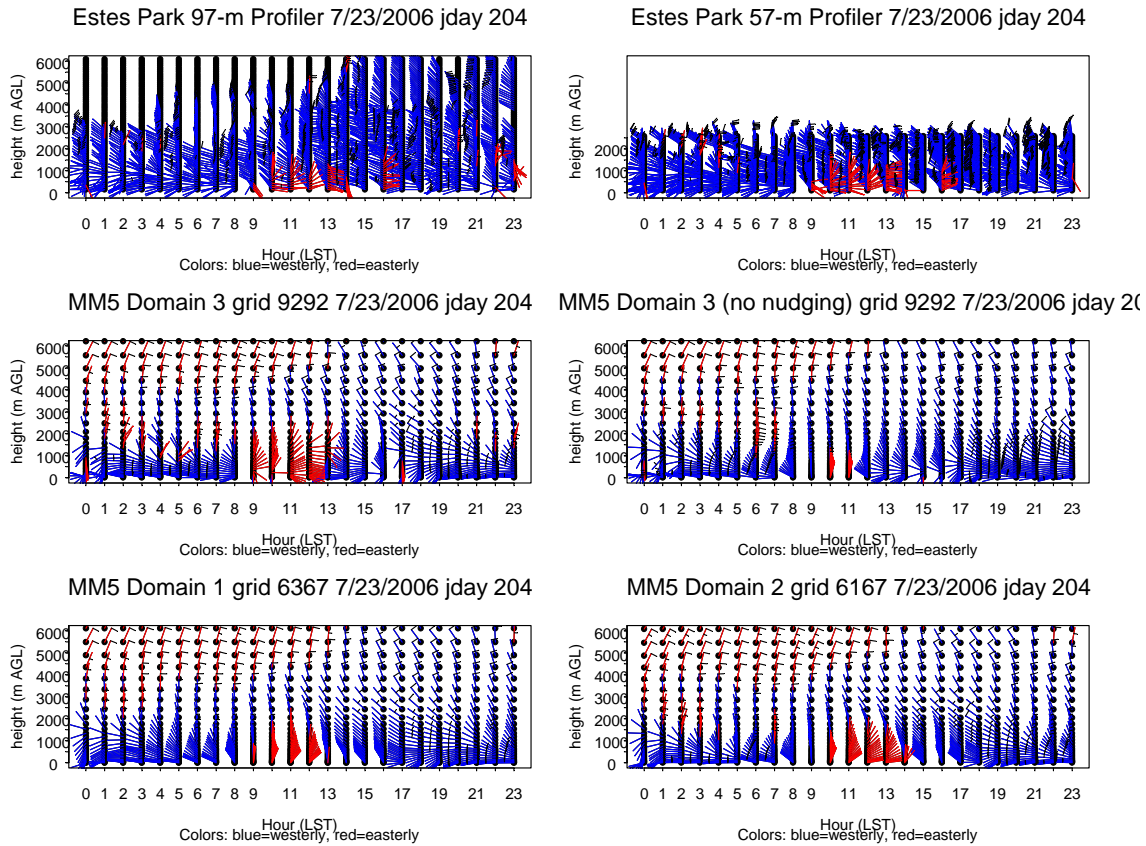


Figure 5.27. Horizontal winds by height above ground and by hour at Estes Park, Colorado, on July 23, 2006 (JD = 204), as measured by the two modes of the radar wind profiler and as calculated by MM5 on Domain 1 (36 km), Domain 2 (12 km), and Domain 3 (4 km). Domain 3 results are shown with and without observational nudging. Each long barb is 10 m/sec; short barbs are 5 m/sec. Stems are red for easterly winds and blue for westerly.

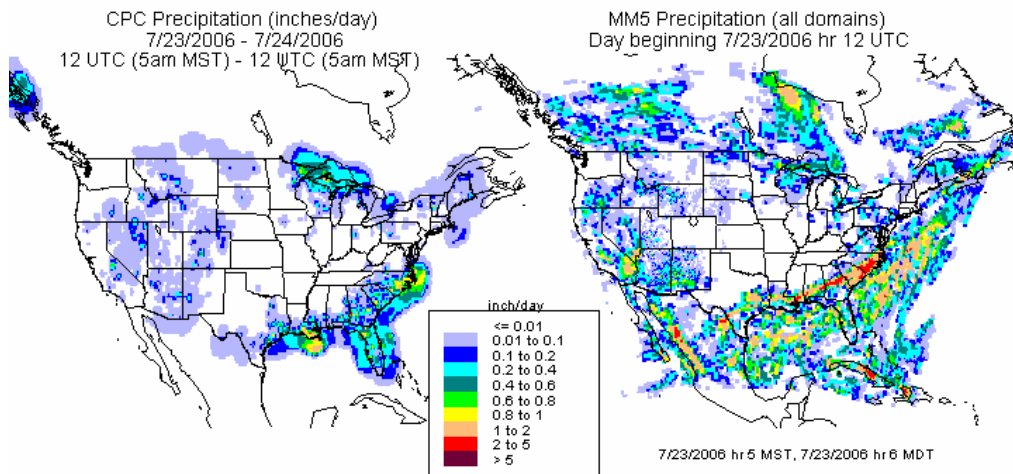


Figure 5.28. Contours of CPC (left) and MM5 (right) 24-hr precipitation totals beginning July 23, 2006, 12:00 UTC (5:00 am MST, 6:00 am MDT).

### 5.3.2.1.3. July 31, 2006 (Julian Day 212) – Particulate Episode

Meteorology at the core site and in Estes Park for July 31 is shown in Figures 5.29–5.32. There was a small amount of measured precipitation at the core site, a daily total of 0.3 mm, which fell at about 9:50 and 10:50 am. The times of the precipitation coincide with the brief peaks in RH and wind speed and slight drops in temperature, which can be seen in the time lines. There was more precipitation on the following day (2.3 mm on August 1).

The 10-m winds at the core site were northerly, mostly northwesterly until 9:00 am and from 7:00 pm until the end of the day, and mostly southerly during the remaining hours. Wind speeds were light, ranging mostly from 0 to 5 m/sec. The coldest temperature of the day was 10 C at midnight. The maximum temperature was 22 C between 8:00 and 9:00 am. RH ranged from 30% at 5:00 pm to nearly 70% at midnight. Back trajectories showed a strong Front Range and eastern Colorado influence, with older air masses being mostly from western Colorado, southern Wyoming, and Utah. Some also arrived from Nebraska and South Dakota. The Estes Park profiler had easterly winds from the surface to as high as 2500 m from 10:00 am until the end of the day. MM5 did a poor job of reproducing the Estes Park winds on the 4-km domain on this day. The 12-km and 36-km domains did somewhat better but started the easterly flow an hour late and all domains erroneously showed westerly winds near the surface.

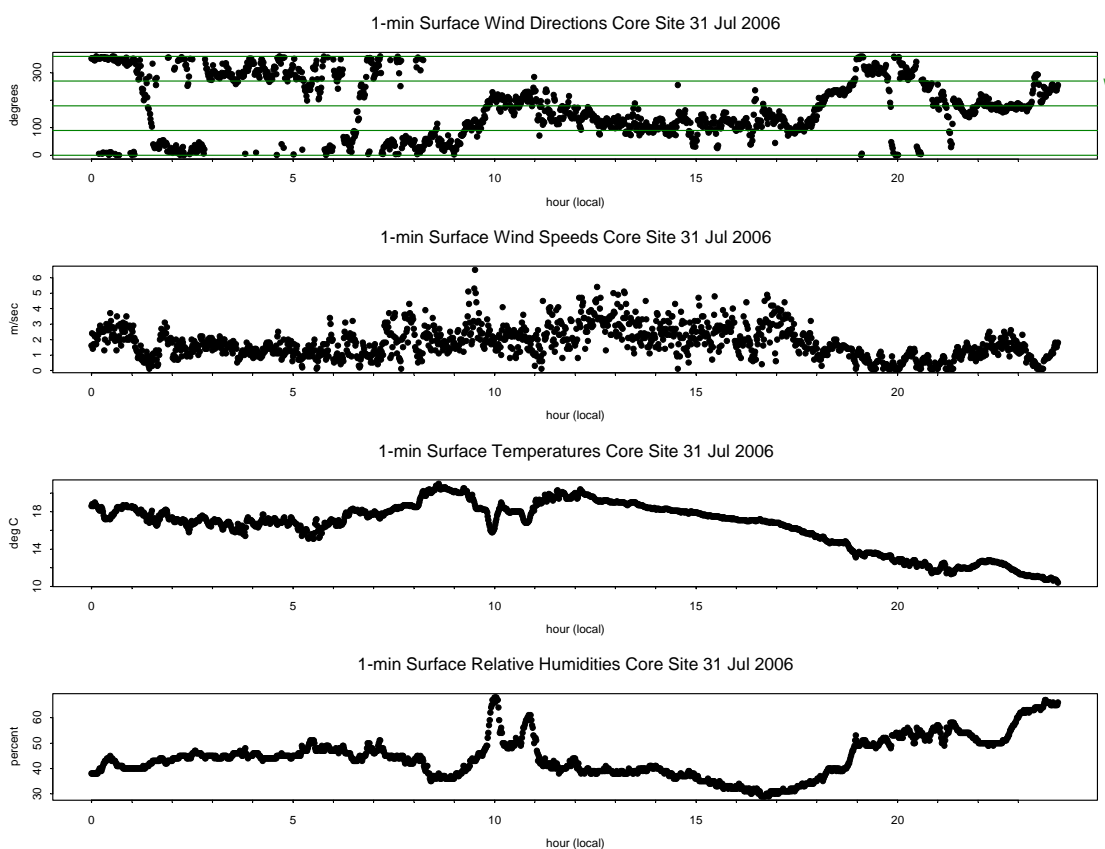


Figure 5.29. Measured wind direction, wind speed, temperature, and relative humidity at the RoMANS core measurement site on July 31, 2006 (JD = 212).

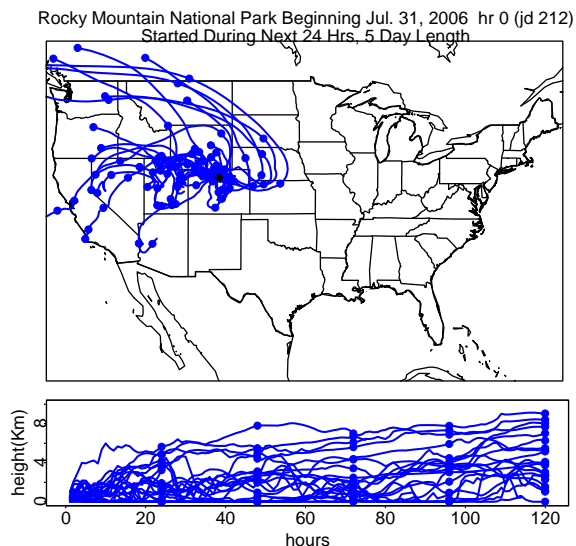


Figure 5.30. Back trajectories started at 100 m AGL at the RoMANS core measurement site on July 31, 2006 (JD = 212). Trajectories were tracked hourly for days.

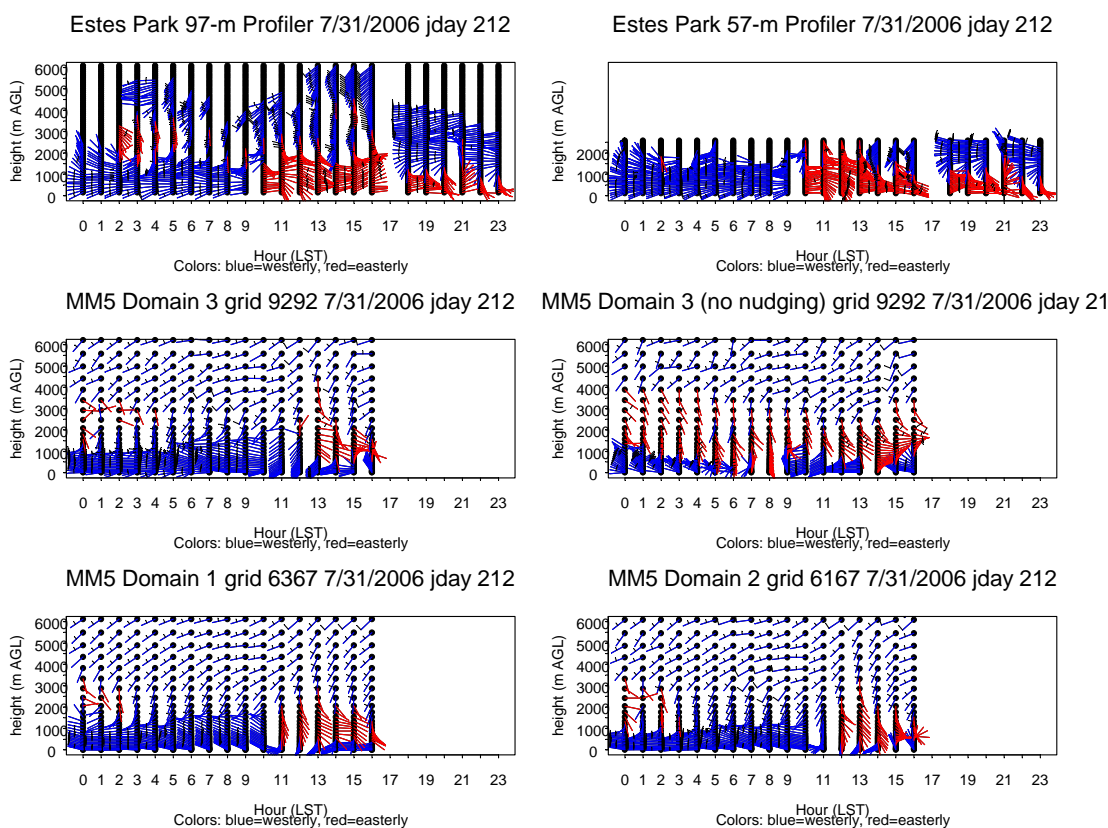


Figure 5.31. Horizontal winds by height above ground and by hour at Estes Park, Colorado, on July 31, 2006 (JD = 212), as measured by the two modes of the radar wind profiler and as calculated by MM5 on Domain 1 (36 km), Domain 2 (12 km), and Domain 3 (4 km). Domain 3 results are shown with and without observational nudging. Each long barb is 10 m/sec; short barbs are 5 m/sec. Stems are red for easterly winds and blue for westerly.

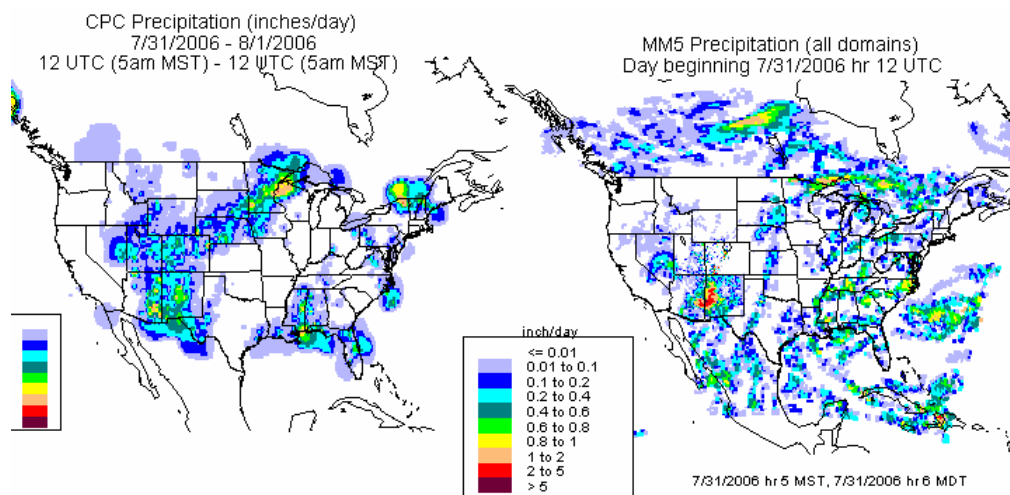


Figure 5.32. Contours of CPC (left) and MM5 (right) 24-hr precipitation totals beginning July 31, 2006, 12:00 UTC (5:00 am MST, 6:00 am MDT).

### 5.3.2.2. Wet Episodes

#### 5.3.2.2.1. April 7, 2006 (Julian Day 97) – Wet Episode

The meteorological data for April 7 are shown in Figures 5.33–5.36. The daily total measured precipitation was 3.1 mm, which fell mostly between 7:00 am and shortly after noon. The 10-m winds at the core site were northwesterly at 2–10 m/sec during hours 0:00–9:00. Then the speed slowed to 2–5 m/sec with mostly northeasterly winds until hour 15 (3:00 pm). For the remainder of the day, the wind directions made a slow transition from northeasterly, through easterly, southerly, westerly, and back to northwesterly with wind speeds of 1–4 m/sec. Temperatures generally fluctuated between about -2 to 2 C until about 6:00 pm when there was a gradual decline to approximately -6 C at midnight. Relative humidity ranged from 50% to more than 80%, with the highest values between 9:00 am and noon and again at the end of the day.

Back trajectories were mostly from the northeast, with transport from Wyoming, South Dakota, Minnesota, Iowa, Missouri, and Arkansas in one pathway (arriving during 6:00–9:00 am), and from noon to 11:00 pm the trajectories all arrived from across South Dakota, Minnesota, and Canada and were associated with high wind speeds. In the early morning from midnight to 5:00 am, the transport was from northern Utah, Nevada, and California.

The radar profiler in Estes Park measured easterly winds during all hours of the day but in a gradually lower layer as the day progressed. Between midnight and 5:00 am, the bottom of the easterly layer was at about 3000 m AGL with westerly winds below that. By noon, nearly all winds from the surface to the top of the measurements were easterly. MM5 captured these features quite well, both in depth and in timing.

Both CPC and MM5 showed precipitation across northern Colorado. In general, MM5 daily totals were lower than CPC across much of the country.

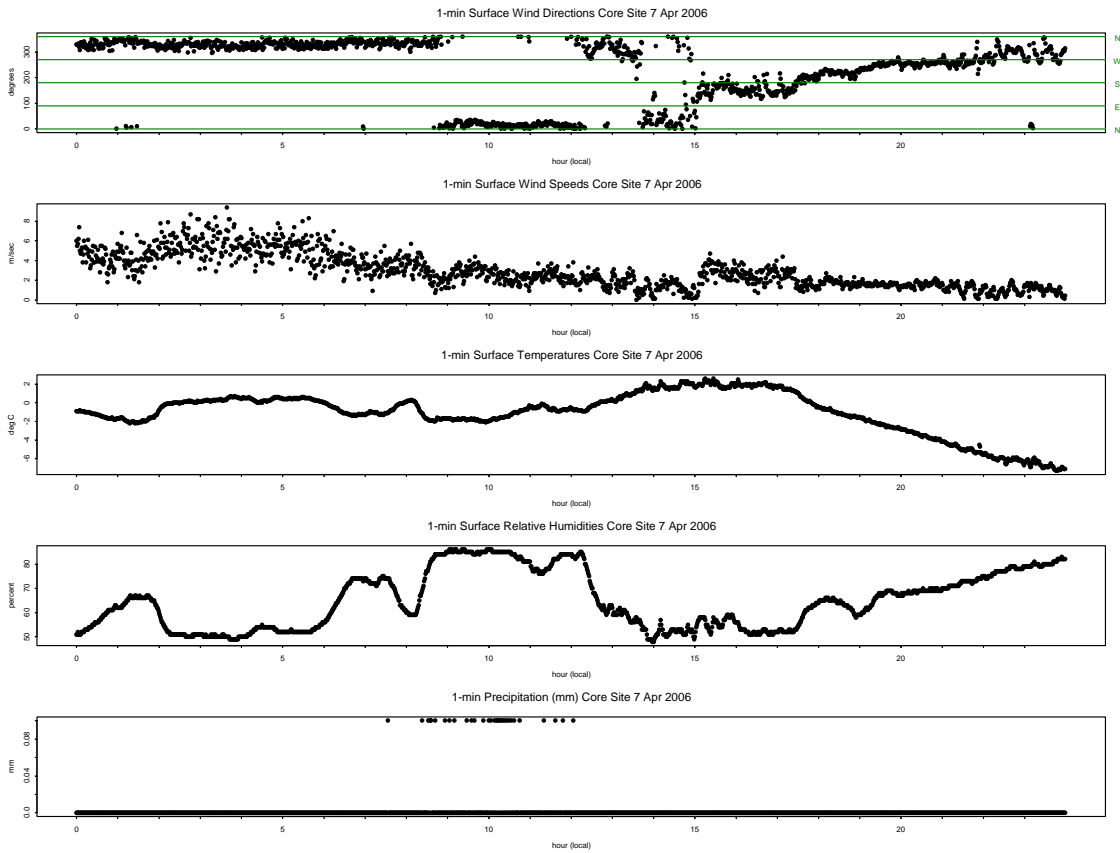


Figure 5.33. Measured wind direction, wind speed, temperature, relative humidity, and precipitation at the RoMANS core measurement site on April 7, 2006 (JD = 97).

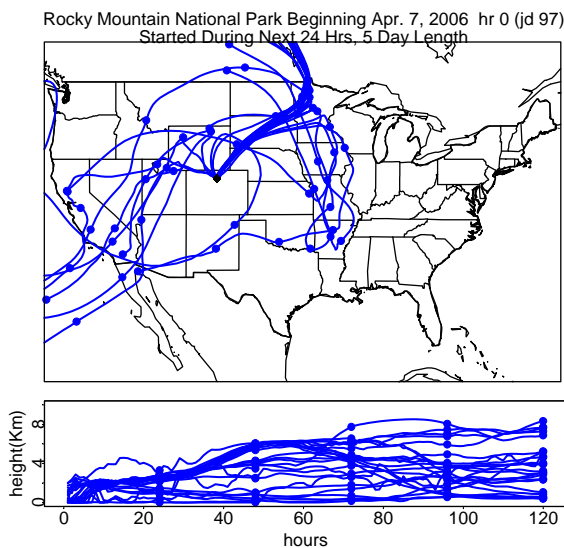


Figure 5.34. Back trajectories started at 100 m AGL at the RoMANS core measurement site on April 7, 2006 (JD = 97). Trajectories were tracked hourly for 5 days.

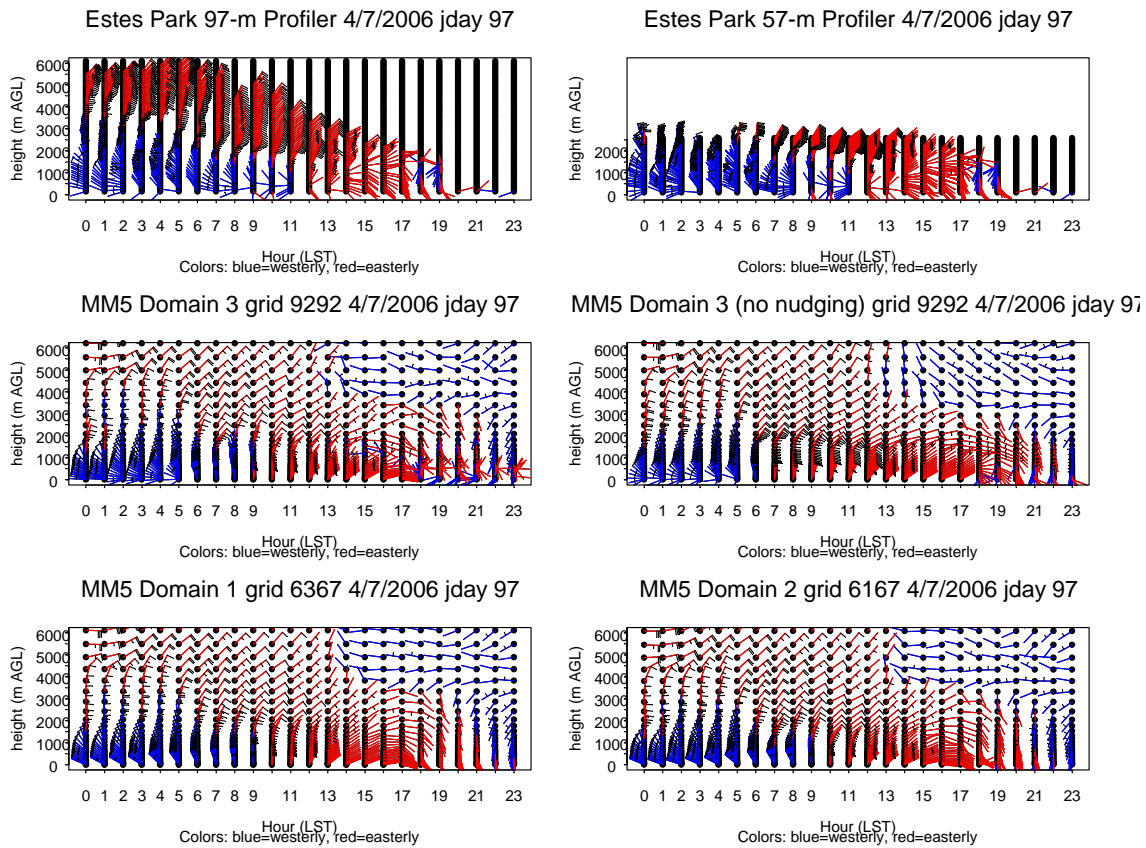


Figure 5.35. Horizontal winds by height above ground and by hour at Estes Park, Colorado, on April 7, 2006 (JD = 97), as measured by the two modes of the radar wind profiler and as calculated by MM5 on Domain 1 (36 km), Domain 2 (12 km), and Domain 3 (4 km). Domain 3 results are shown with and without observational nudging. Each long barb is 10 m/sec; short barbs are 5 m/sec. Stems are red for easterly winds and blue for westerly.

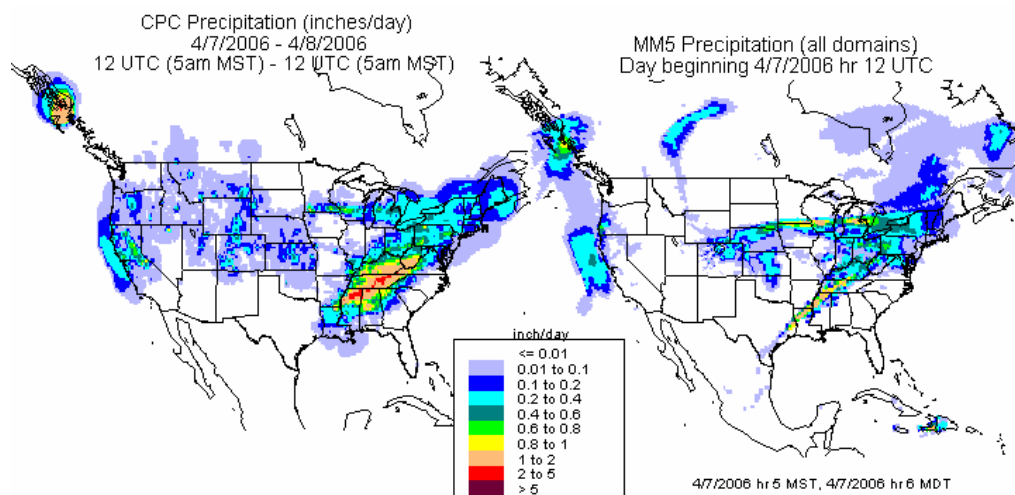


Figure 5.36. Contours of CPC (left) and MM5 (right) 24-hr precipitation totals beginning April 7, 2006, 12:00 UTC (5:00 am MST, 6:00 am MDT).

### 5.3.2.2.2. April 18, 2006 (Julian Day 108) – Wet Episode

Core site meteorology, 5-day back trajectories arriving at the core site, upper-air winds at Estes Park, and precipitation contours for April 18 are shown in Figures 5.37–5.40. The total 24-hr precipitation at the core site was 2.4 mm. This fell mostly just before 10:00 am, with a smaller amount of precipitation measured during the 2:00–3:00 pm hour. The 10-m winds at the core site were mostly northwesterly with wind speeds of 2–10 m/sec for the entire day. Wind speeds were somewhat slower, 0–5 m/sec after 5:00 pm. Temperatures were relatively cold, ranging from -7 to -1 C. RH ranged from 30% at 11:00 am and again at 2:00 pm to 80% just before 3:00 pm.

Back trajectories were all westerly. Trajectories arrived after passing over Wyoming, Montana, Oregon, Nevada, northern California, and parts of surrounding states. The Estes Park profiler showed all westerly winds for the day and MM5 agreed. The CPC and MM5 precipitation patterns were quite similar across the country, though MM5 overpredicted the amounts in east Texas. Both CPC and MM5 showed precipitation in north-central and northwestern Colorado.

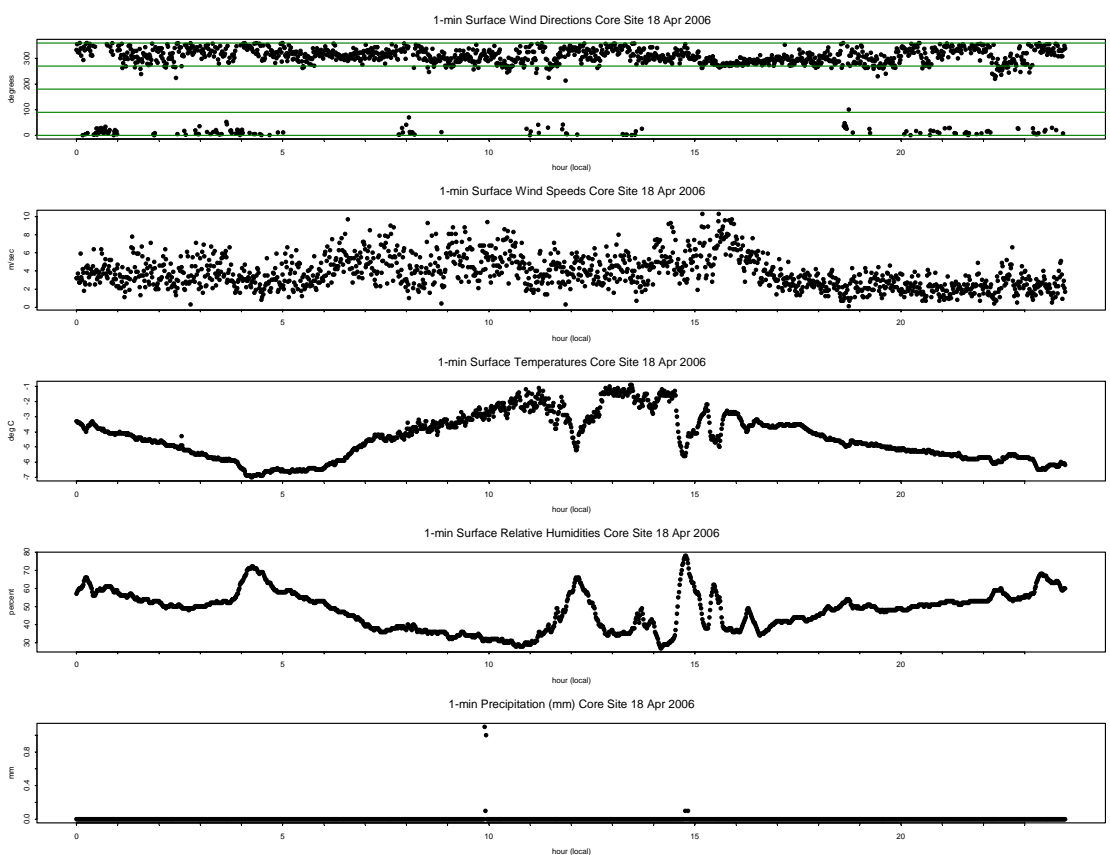


Figure 5.37. Measured wind direction, wind speed, temperature, and relative humidity, and precipitation at the RoMANS core measurement site on April 18, 2006 (JD = 108).

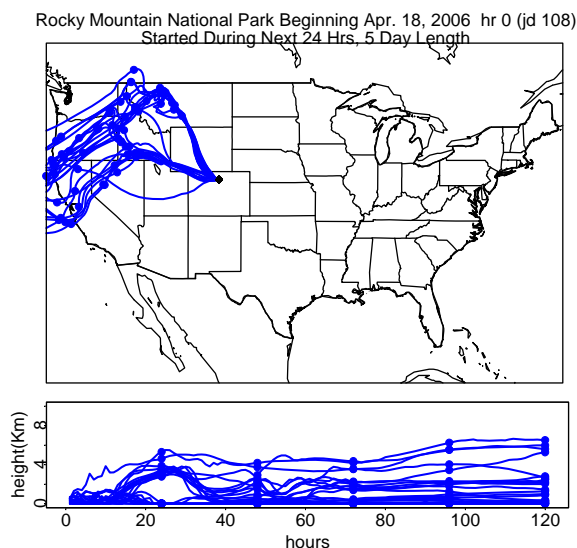


Figure 5.38. Back trajectories started at 100 m AGL at the RoMANS core measurement site on April 18, 2006 (JD = 108). Trajectories were tracked hourly for 5 days.

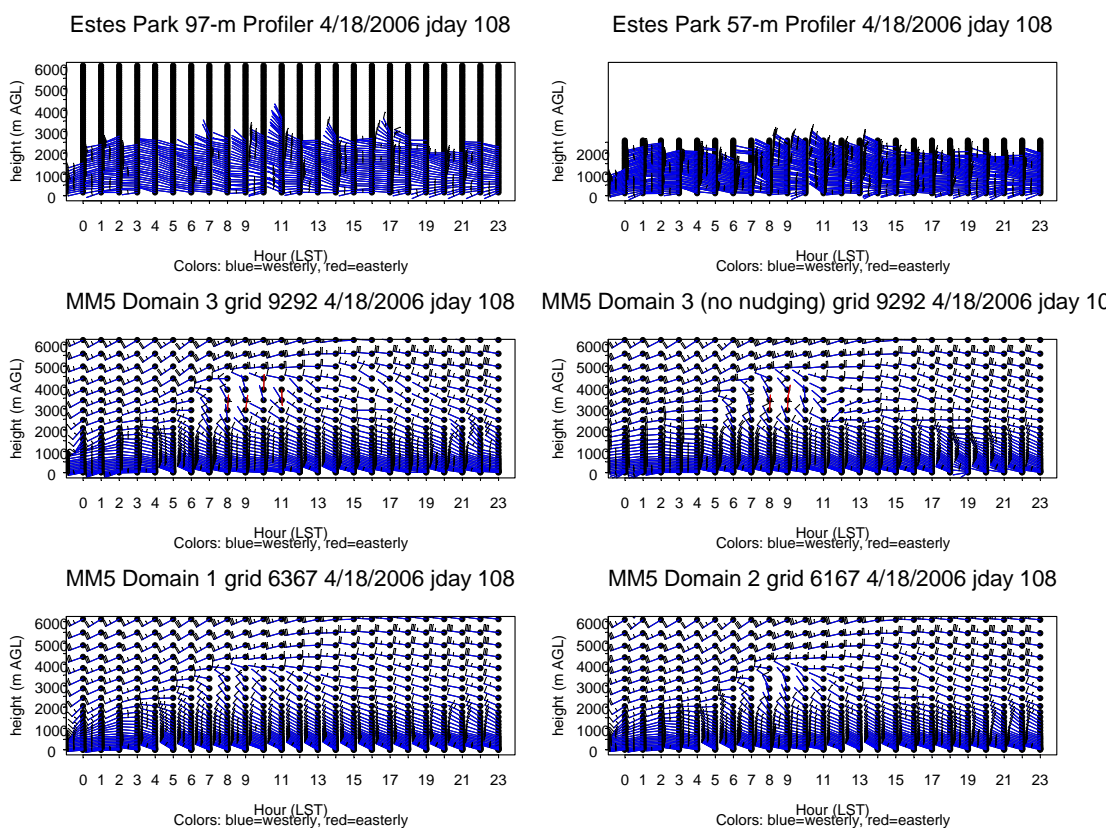


Figure 5.39. Horizontal winds by height above ground and by hour at Estes Park, Colorado, on April 18, 2006 (JD = 108), as measured by the two modes of the radar wind profiler and as calculated by MM5 on Domain 1 (36 km), Domain 2 (12 km), and Domain 3 (4 km). Domain 3 results are shown with and without observational nudging. Each long barb is 10 m/sec; short barbs are 5 m/sec. Stems are red for easterly winds and blue for westerly.

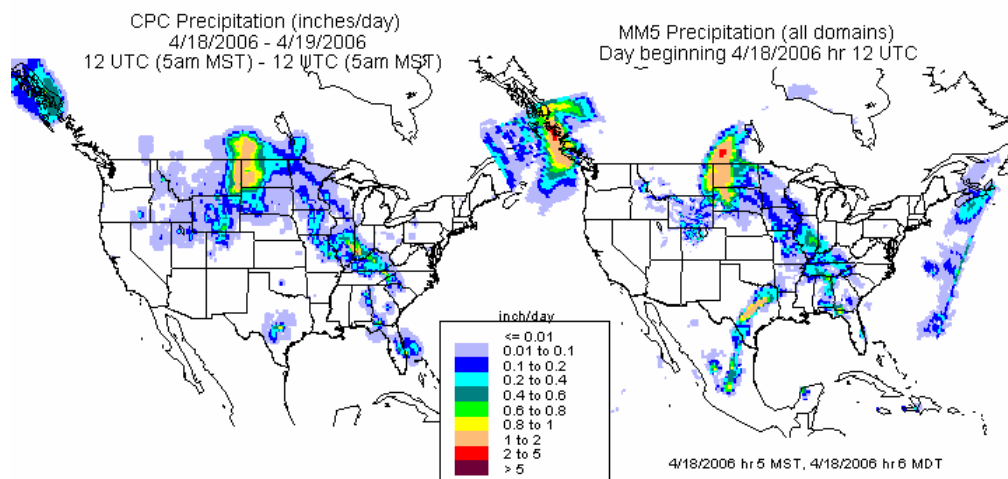


Figure 5.40. Contours of CPC (left) and MM5 (right) 24-hr precipitation totals beginning April 18, 2006, 12:00 UTC (5:00 am MST, 6:00 am MDT).

### 5.3.2.2.3. *April 24–25, 2006 (Julian Days 114–115) – Wet Episode*

Core site meteorology, back trajectories, Estes Park upper-air winds, and precipitation contours for April 24 are shown in Figures 5.41–5.44 and Figures 5.45–5.48 for April 25. As shown, on April 24, the 10-m wind directions at the core site were from the southeast nearly the entire day, except between 10:00 and 11:00 pm when they were briefly from the northwest. However, the speeds during that hour were very light, making the direction uncertain. Wind speeds ranged from 0 to 5 m/sec throughout the day. Temperatures declined steadily throughout the day from about -3 C at midnight on April 24 to -8 C at midnight on April 25. RH was high, ranging from 87% to 96%. The precipitation total at the core site for the day was 14.7 mm, which fell mostly between midnight and 6:00 am, though there were also periods of precipitation between noon and 4:00 pm and again between 8:00 pm and the end of the day.

The April 24 back trajectories show air masses arriving from the northeast, primarily from northeastern Colorado, Nebraska, and the Dakotas. Upper-air winds at Estes Park on April 24 had an easterly component at the surface all day long. MM5 also captured the easterly flow, except at around 1:00 am to 2:00 am, depending on the domain. The 4-km MM5 domain more accurately showed the elevated layer of easterly winds that occurred from 3:00 pm through the end of the day than did the 12-km and 36-km domains.

The precipitation contours on April 24 for both CPC and MM5 show precipitation in northern Colorado and in the surrounding states to the north and east. MM5 has higher precipitation amounts in the western Dakotas and in central Texas than does CPC.

On April 25, the temperatures at the core site began to warm, staying between -10 and -8 C until about 6:00 am, warming to about -4 C by 1:00 pm, and then remaining between -4 and -2 C for the rest of the day. RH was still relatively high, staying between 80% and 95% for most of the day. Precipitation fell before 2:00 am, between 7:00 and 8:00 am, and at about 10:00 am. The daily total at the core site was 2.3 mm. The 10-m winds at the core site were mostly southeasterly until about 5:00 pm and then northerly after that. Wind speeds ranged from 0 to 4 m/sec. Back trajectories arrived from the northeast until 3:00 am, and then arrived from the

southwest for the remainder of the day. The radar profiler in Estes Park showed easterly winds in a shallow layer near the surface for the entire day, with westerly winds all day above 1000 m AGL. The 4-km MM5 winds were very similar, but the 12-km and 36-km MM5 winds were uniformly westerly. The precipitation contours show the storm moving eastward but still some light precipitation in Colorado. The CPC amounts across Colorado as a whole are higher than MM5.

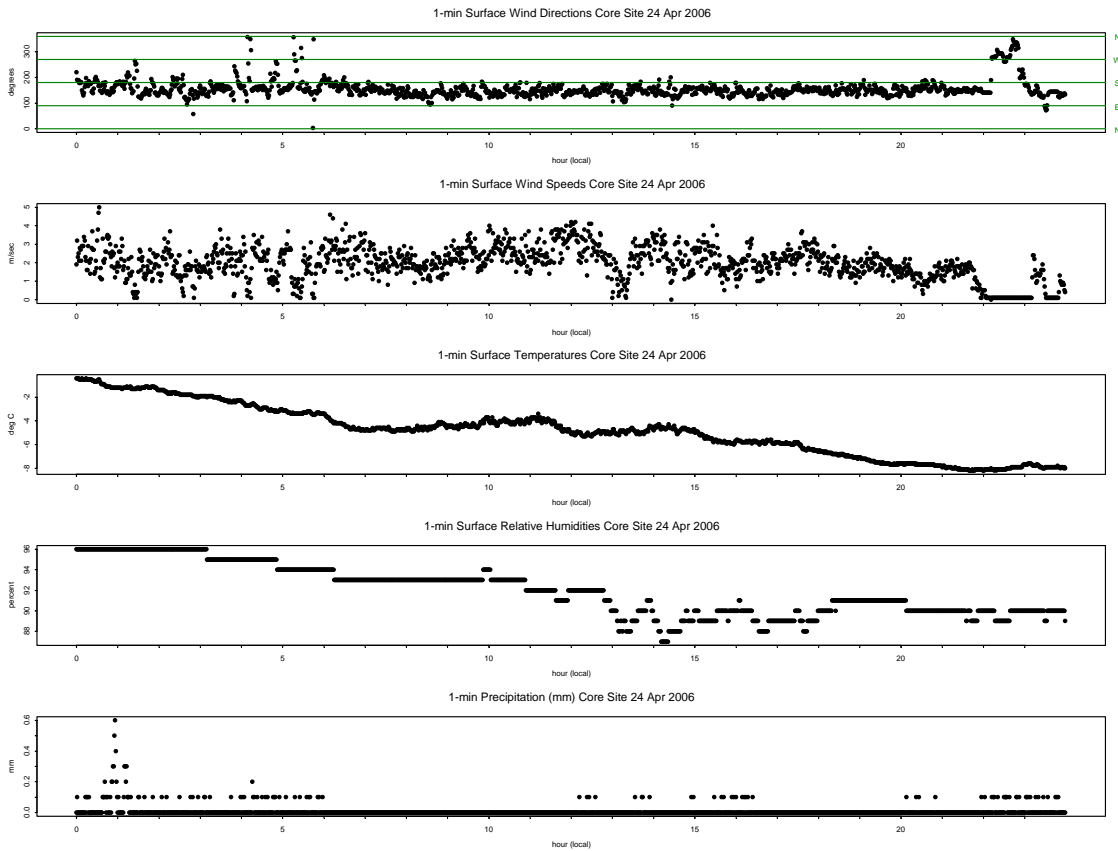


Figure 5.41. Measured wind direction, wind speed, temperature, and relative humidity, and precipitation at the RoMANS core measurement site on April 24, 2006 (JD = 114).

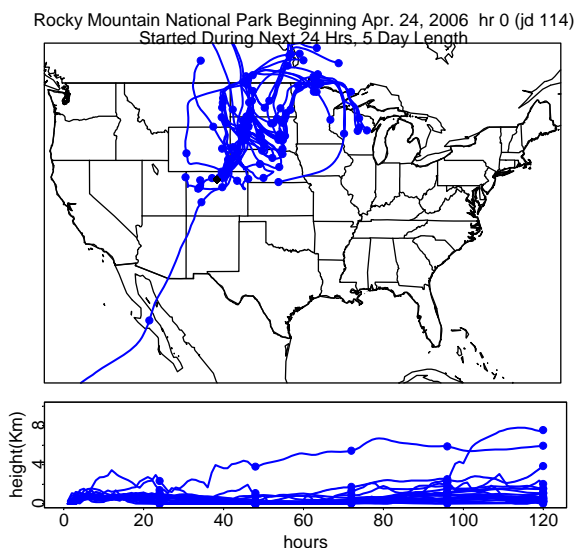


Figure 5.42. Back trajectories started at 100 m AGL at the RoMANS core measurement site on April 24, 2006 (JD = 114). Trajectories were tracked hourly for 5 days.

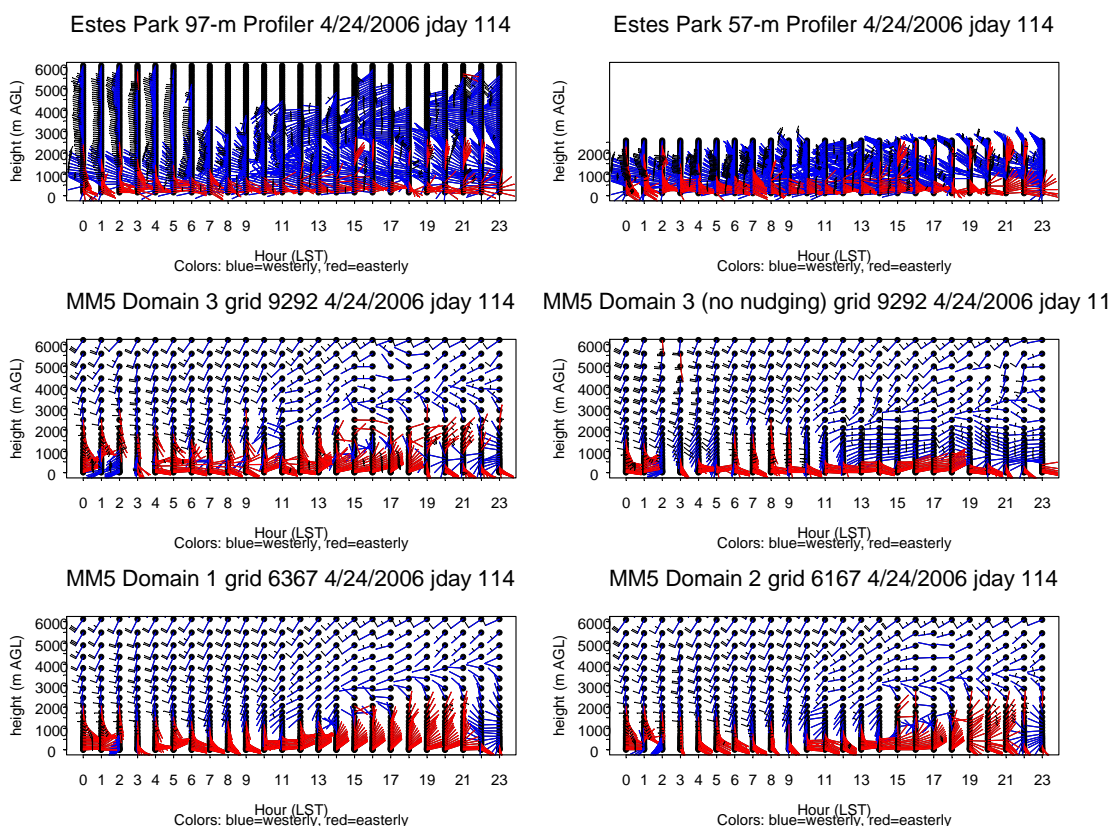


Figure 5.43. Horizontal winds by height above ground and by hour at Estes Park, Colorado, on April 24, 2006 (JD = 110), as measured by the two modes of the radar wind profiler and as calculated by MM5 on Domain 1 (36 km), Domain 2 (12 km), and Domain 3 (4 km). Domain 3 results are shown with and without observational nudging. Each long barb is 10 m/sec; short barbs are 5 m/sec. Stems are red for easterly winds and blue for westerly.

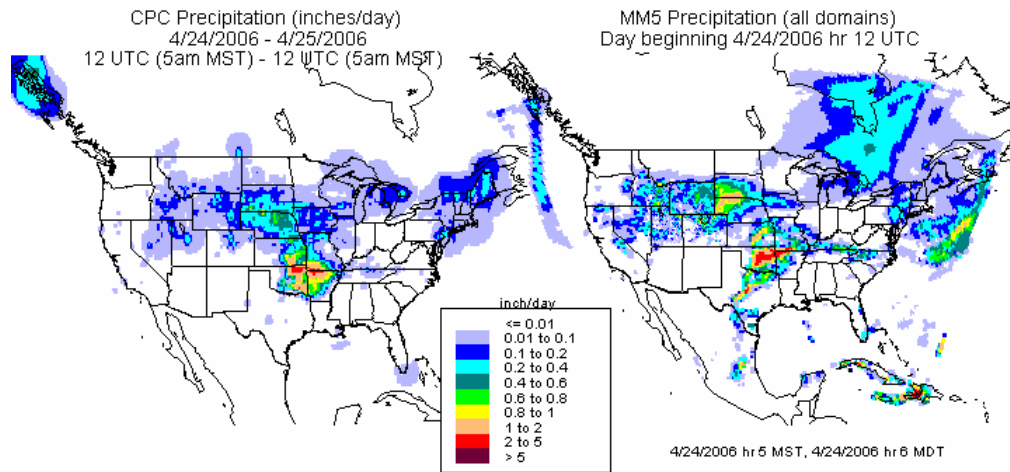


Figure 5.44. Contours of CPC (left) and MM5 (right) 24-hr precipitation totals beginning April 24, 2006, 12:00 UTC (5:00 am MST, 6:00 am MDT).

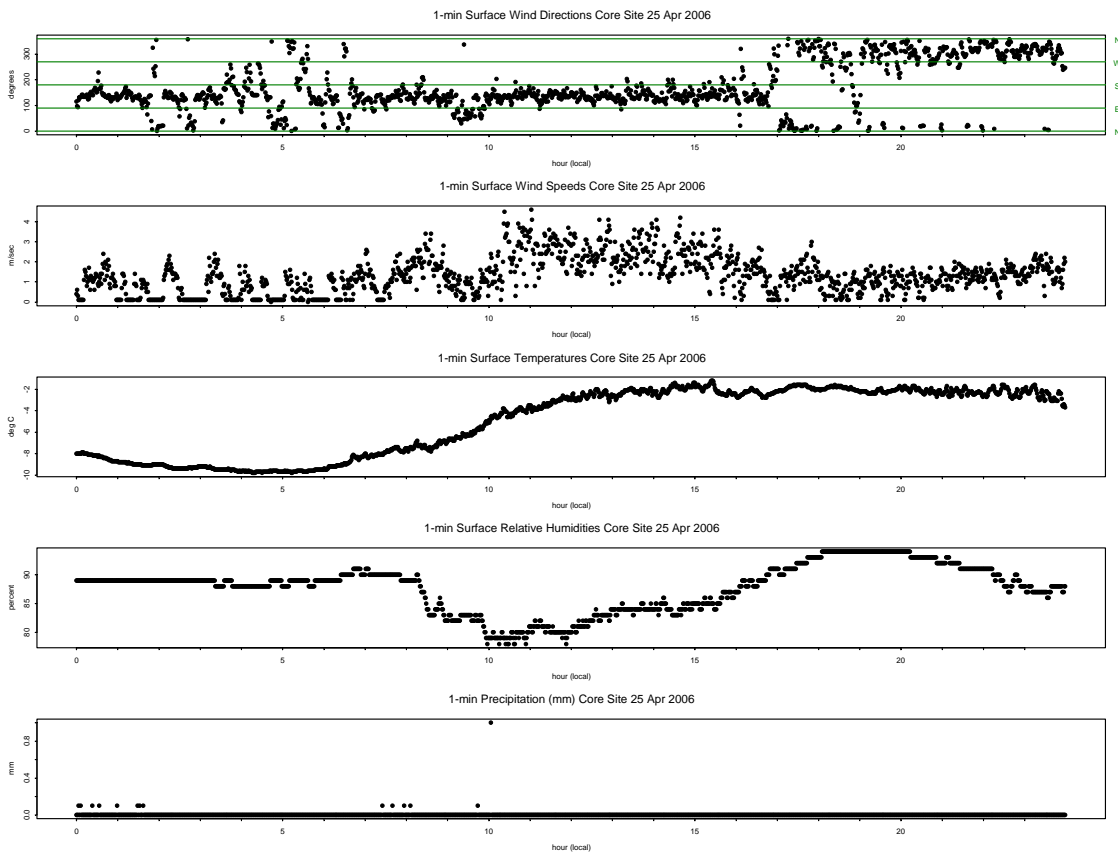


Figure 5.45. Measured wind direction, wind speed, temperature, and relative humidity, and precipitation at the RoMANS core measurement site on April 25, 2006 (JD = 115).

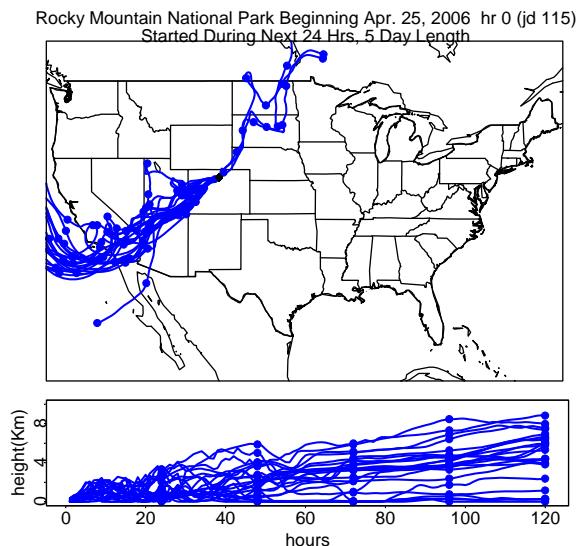


Figure 5.46. Back trajectories started at 100 m AGL at the RoMANS core measurement site on April 25, 2006 (JD = 115). Trajectories were tracked hourly for 5 days.

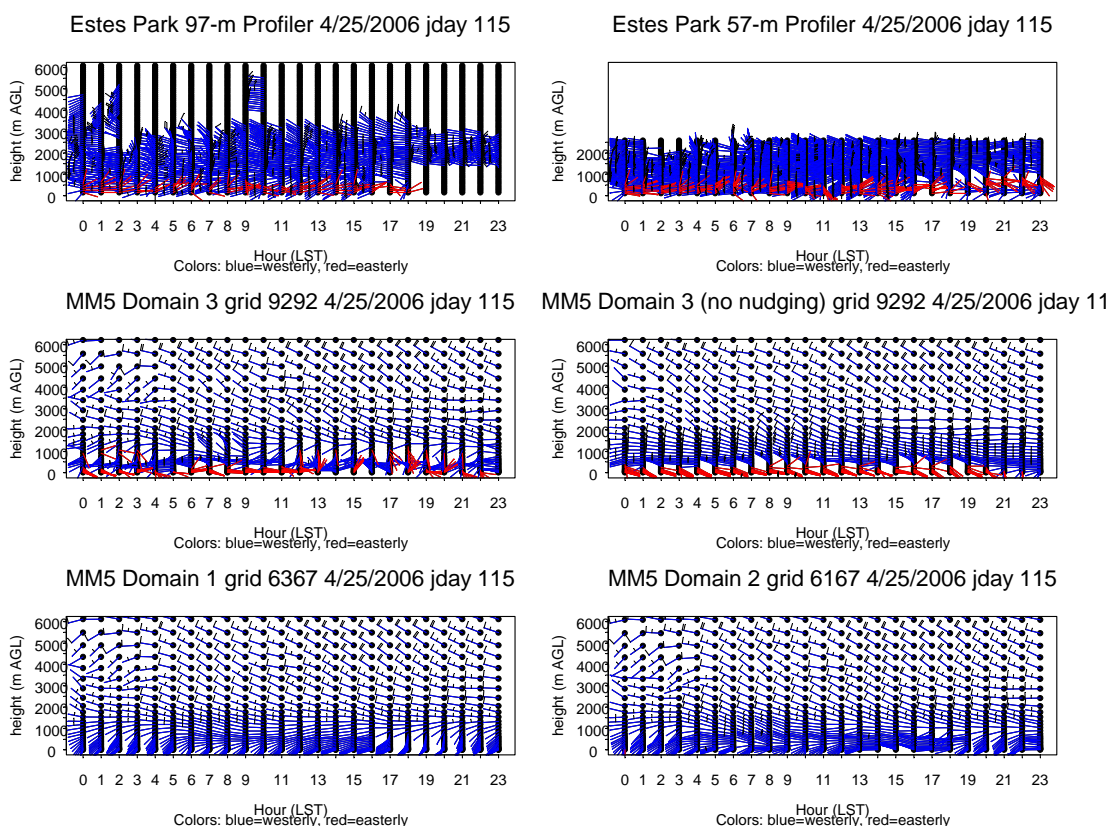


Figure 5.47. Horizontal winds by height above ground and by hour at Estes Park, Colorado, on April 25, 2006 (JD = 111), as measured by the two modes of the radar wind profiler and as calculated by MM5 on Domain 1 (36 km), Domain 2 (12 km), and Domain 3 (4 km). Domain 3 results are shown with and without observational nudging. Each long barb is 10 m/sec; short barbs are 5 m/sec. Stems are red for easterly winds and blue for westerly.

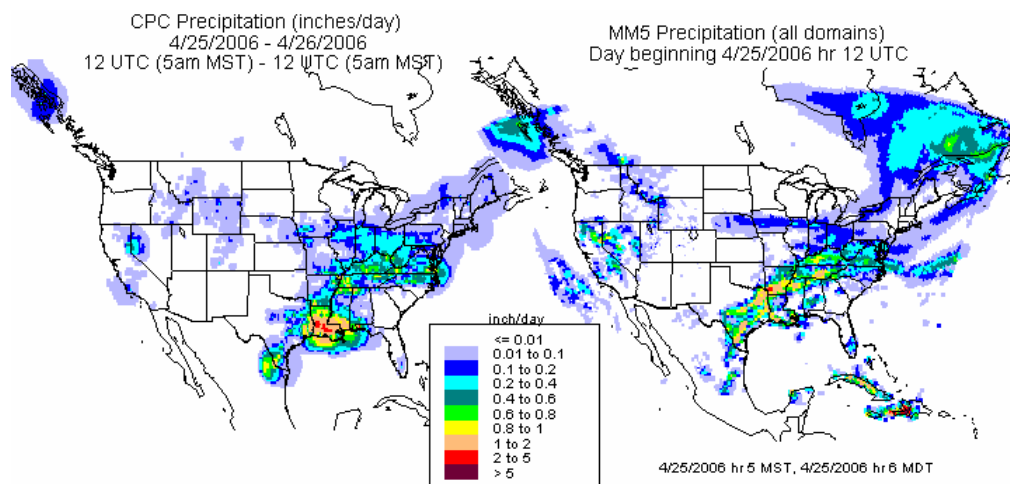


Figure 5.48. Contours of CPC (left) and MM5 (right) 24-hr precipitation totals beginning April 25, 2006, 12:00 UTC (5:00 am MST, 6:00 am MDT).

#### 5.3.2.2.4. July 7–9, 2006 (Julian Days 188–190) – Wet Episode

Core site meteorology, back trajectories, upper-air winds at Estes Park, and precipitation contours for July 7 are shown in Figures 5.49–5.52. Similar graphs for July 8 and July 9 are in Figures 5.53–5.56 and Figures 5.57–5.60, respectively. Total rainfall for the 3 days measured at the core site was 66 mm, 23 mm on July 7, 27 mm on July 8, and 16 mm on July 9.

The 10-m winds at the core site on July 7 were northerly, mostly northwesterly, except during 9:00 am through 3:00 pm when they were southeasterly from 9:00 to 11:00 am, and mostly northeasterly from 11:00 am to 3:00 pm. Wind speeds were generally below 3 m/sec, except during 5:00 am to 1:00 pm when they were variable but as high as 7 m/sec. This is also evident in the radar profiler data where the near-surface winds are from the west for most hours. However, above ~500 m the winds are mostly from the east. MM5 was late in starting the easterly flow on the 4- and 12-km domains and never had easterly flow at the surface on the 36-km domain. MM5 had fewer levels at all hours with winds from the east. This is reflected in the back trajectories in which they arrived from the west during all hours, having crossed western Colorado, Arizona, western Mexico, and parts of Utah. Temperatures ranged from 8 to 20 C and RH from 40% to more than 90%, being above 90% from 5:00 pm until the end of the day. The precipitation fell mostly between the hours of 2:00 to 11:00 pm. CPC precipitation contours had precipitation throughout Colorado, while MM5 had precipitation mostly in western Colorado and much less precipitation throughout the Four Corners states than did CPC.

On July 8, precipitation fell mostly from 9:00 am and later and was heaviest during noon to 1:00 pm, and 9:00 to 10:00 pm. RH was above 90% all day and temperatures ranged from 8 to 11 C, with the minimum at midnight on July 9. Wind speeds at the core site 10-m tower were less than 3 m/sec all day except for a brief period of winds up to about 4 m/sec at about 10:00 am. Wind directions were northwesterly before 6:00 am and between 4:00 and 7:00 pm. Southerly winds predominated between 6:00 and 7:00 am, from noon to 4:00 pm, and from 7:00 pm until the end of the day. Back trajectories were from the north-northeast over much of Wyoming and also crossed northwestern Colorado, northeastern Colorado, Utah, Arizona, southern Nevada, and southern California. Easterly winds on the Estes Park profiler were above about 1500 m AGL

early in the day with easterly winds at or near ground level during 7:00–9:00 am and 11:00 am to 3:00 pm and on and off after that. MM5 matched the 7:00 am time for easterly winds at the surface but in general had more easterlies than were measured on the profiler. However, wind speeds were generally low, making the directions somewhat uncertain. Both MM5 and CPC showed precipitation over Colorado and surrounding states, with a similar spatial pattern.

On July 9 the 10-m wind directions at the core site were northerly all day except during 6:00–10:00 pm when they were southerly. Wind speeds were 0–4 m/sec all day. The temperature and RH were fairly constant. Temperature ranged from 7 to 9 C and RH from 86% to 97%. Light precipitation fell during most of the day, with heaviest amounts around 11:00 am and 2:00 pm. Back trajectories were predominantly from the northeast and north, crossing northeastern Colorado, western Nebraska, western South Dakota, Wyoming, and then parts of southern Idaho, northern Utah, Nevada, and California. The Estes Park radar profiler had easterly winds at or near the surface mostly during 8:00 am to 2:00 pm. All three MM5 domains were an hour or two early in starting easterly winds near the surface and had easterly winds through a greater depth than was measured. Both CPC and MM5 precipitation contours show rain over all of Colorado and surrounding states.

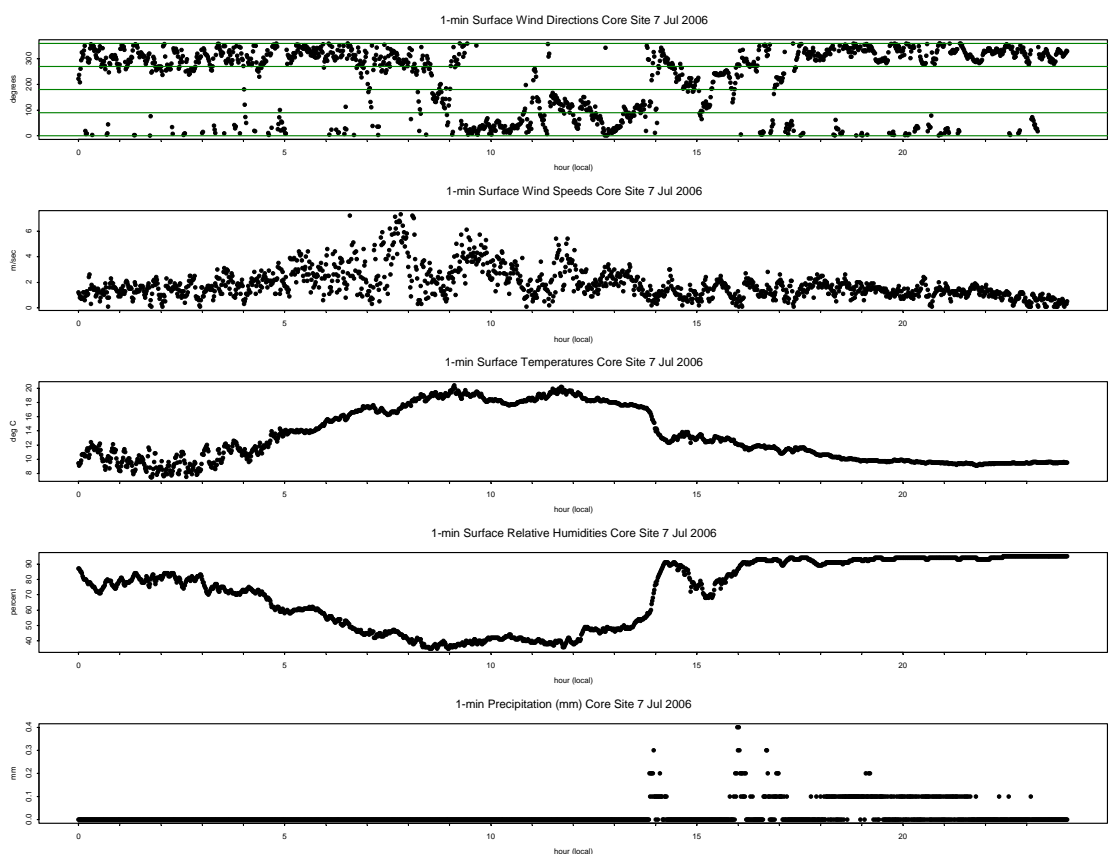


Figure 5.49. Measured wind direction, wind speed, temperature, and relative humidity, and precipitation at the RoMANS core measurement site on July 7, 2006 (JD = 188).

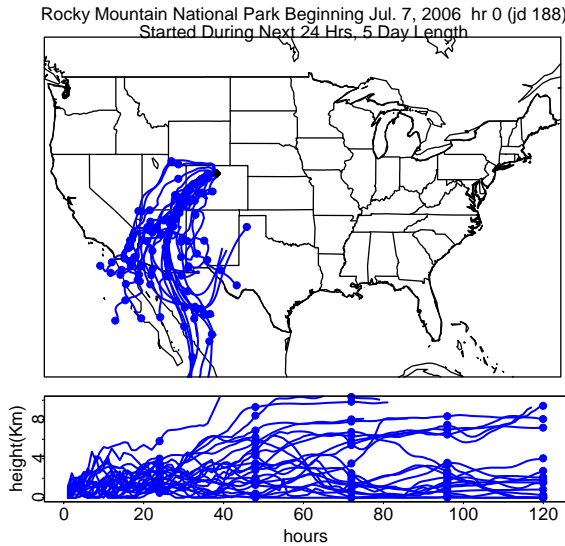


Figure 5.50. Back trajectories started at 100 m AGL at the RoMANS core measurement site on July 7, 2006 (JD = 188). Trajectories were tracked hourly for 5 days.

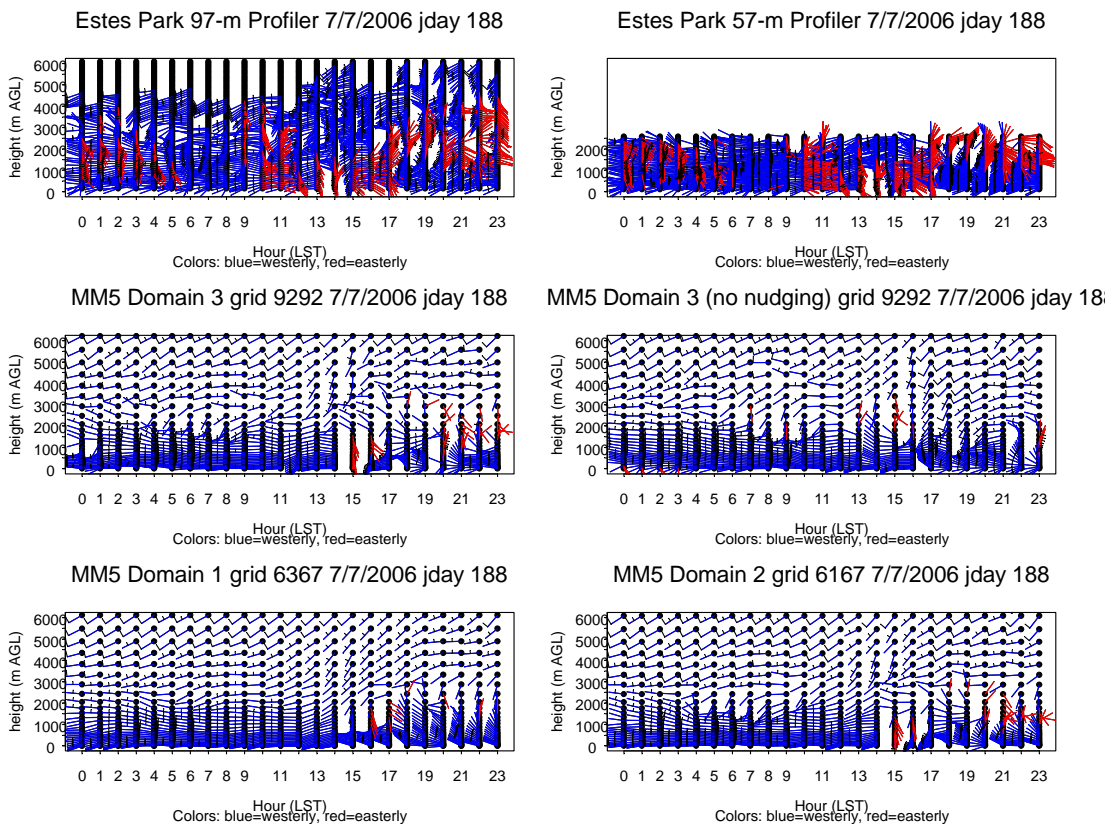


Figure 5.51. Horizontal winds by height above ground and by hour at Estes Park, Colorado, on July 8, 2006 (JD = 188), as measured by the two modes of the radar wind profiler and as calculated by MM5 on Domain 1 (36 km), Domain 2 (12 km), and Domain 3 (4 km). Domain 3 results are shown with and without observational nudging. Each long barb is 10 m/sec; short barbs are 5 m/sec. Stems are red for easterly winds and blue for westerly.

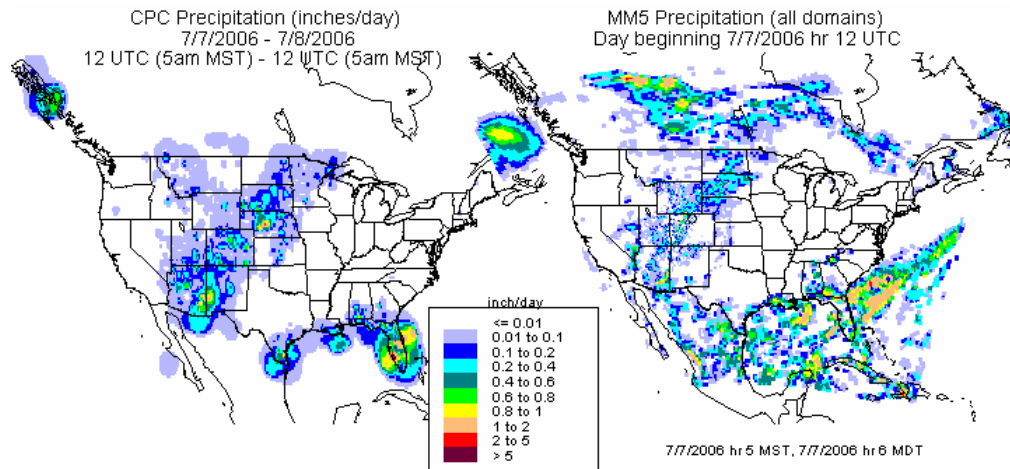


Figure 5.52. Contours of CPC (left) and MM5 (right) 24-hr precipitation totals beginning July 7, 2006, 12:00 UTC (5:00 am MST, 6:00 am MDT).

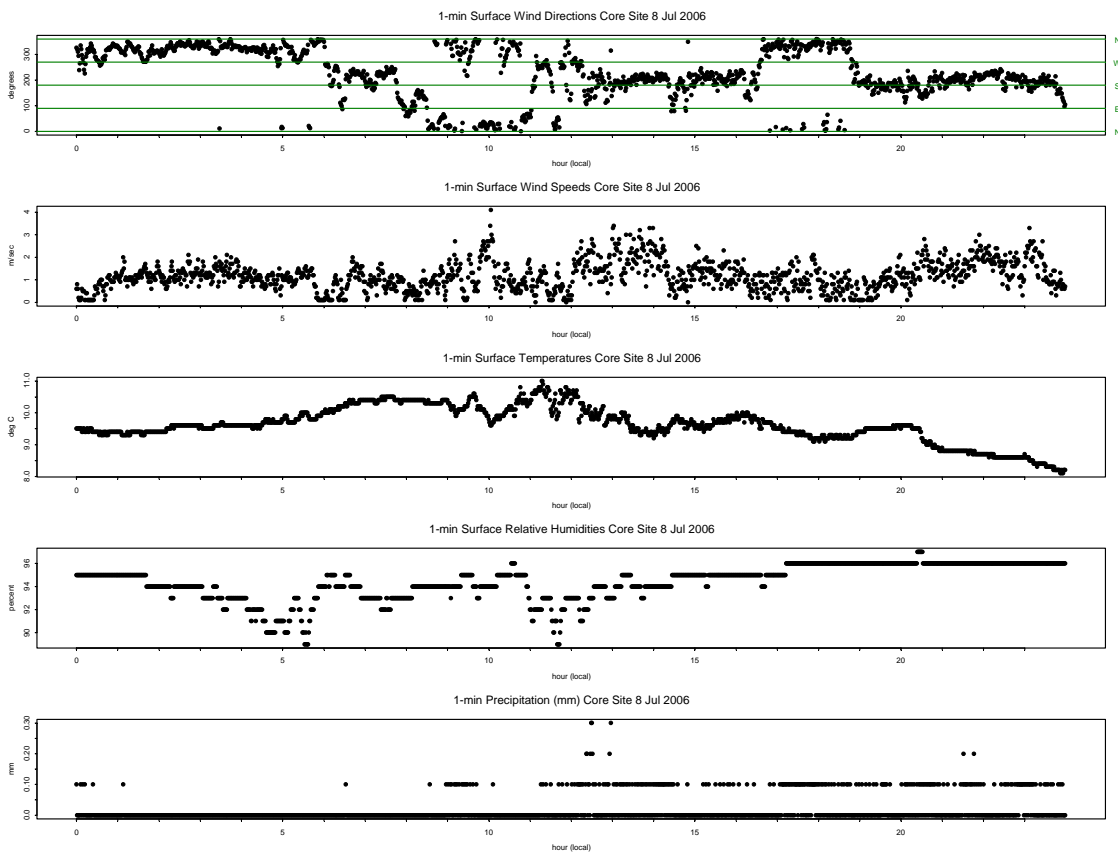


Figure 5.53. Measured wind direction, wind speed, temperature, and relative humidity, and precipitation at the RoMANS core measurement site on July 8, 2006 (JD = 189).

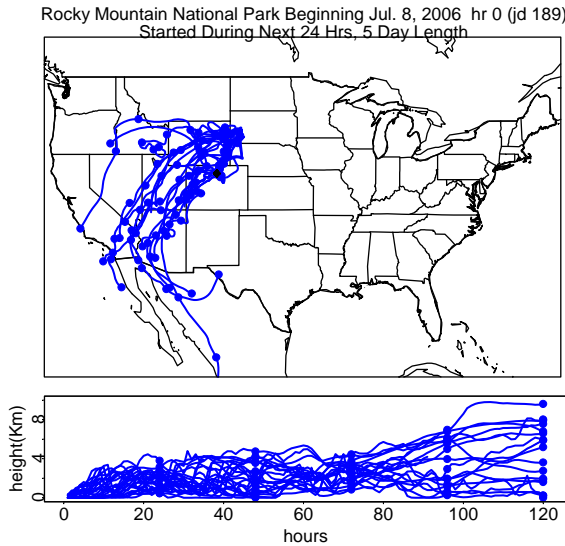


Figure 5.54. Back trajectories started at 100 m AGL at the RoMANS core measurement site on July 8, 2006 (JD = 189). Trajectories were tracked hourly for 5 days.

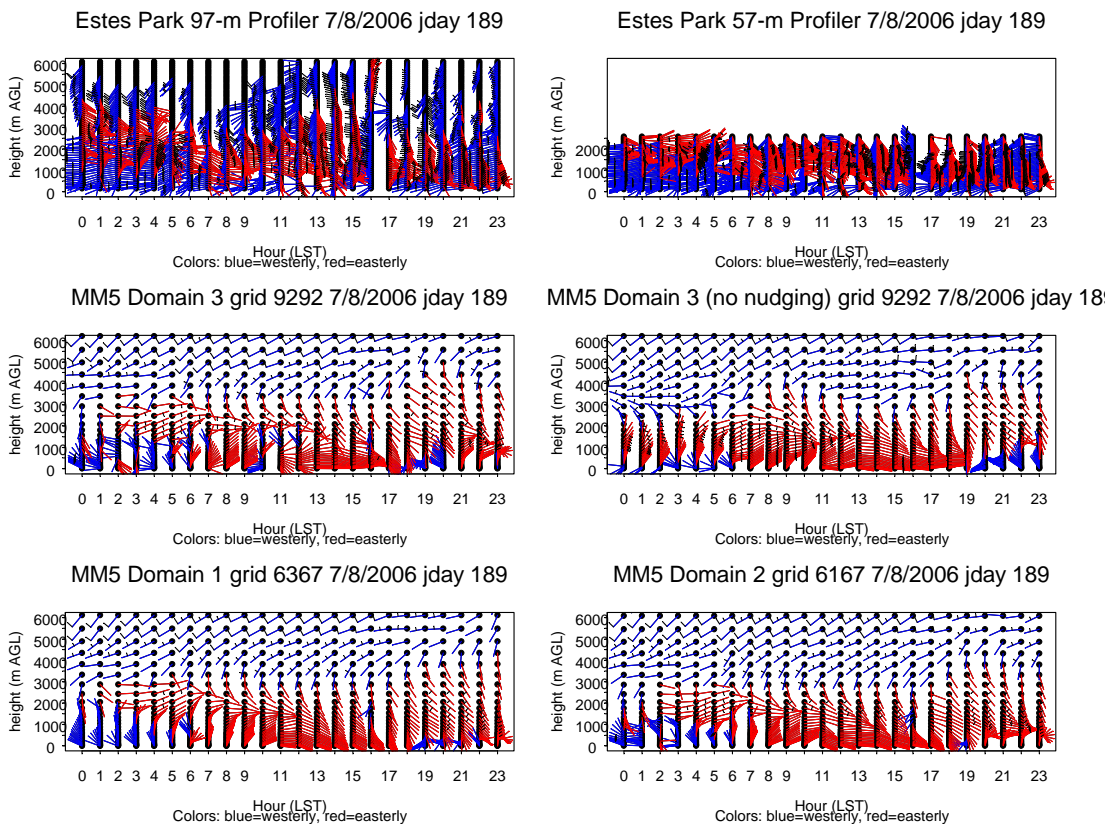


Figure 5.55. Horizontal winds by height above ground and by hour at Estes Park, Colorado, on July 8, 2006 (JD = 189), as measured by the two modes of the radar wind profiler and as calculated by MM5 on Domain 1 (36 km), Domain 2 (12 km), and Domain 3 (4 km). Domain 3 results are shown with and without observational nudging. Each long barb is 10 m/sec; short barbs are 5 m/sec. Stems are red for easterly winds and blue for westerly.

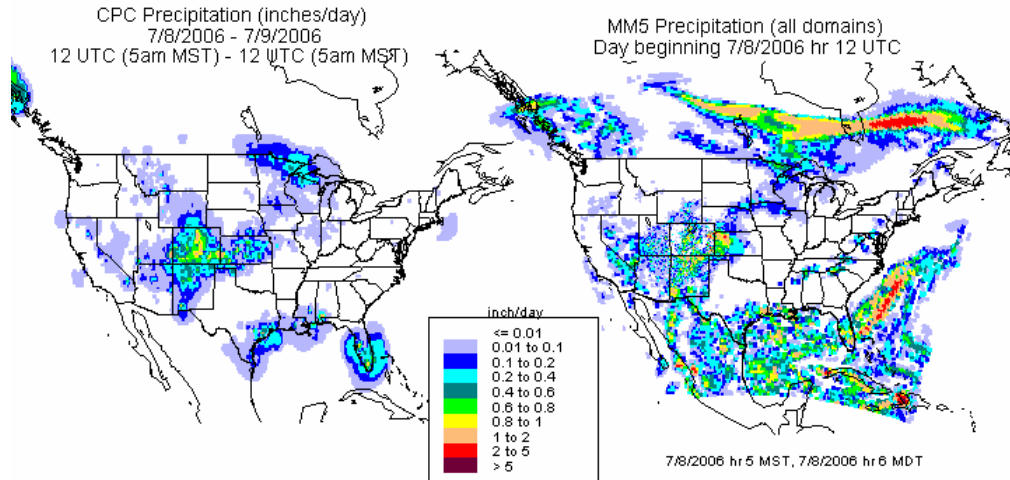


Figure 5.56. Contours of CPC (left) and MM5 (right) 24-hr precipitation totals beginning July 8, 2006, 12:00 UTC (5:00 am MST, 6:00 am MDT).

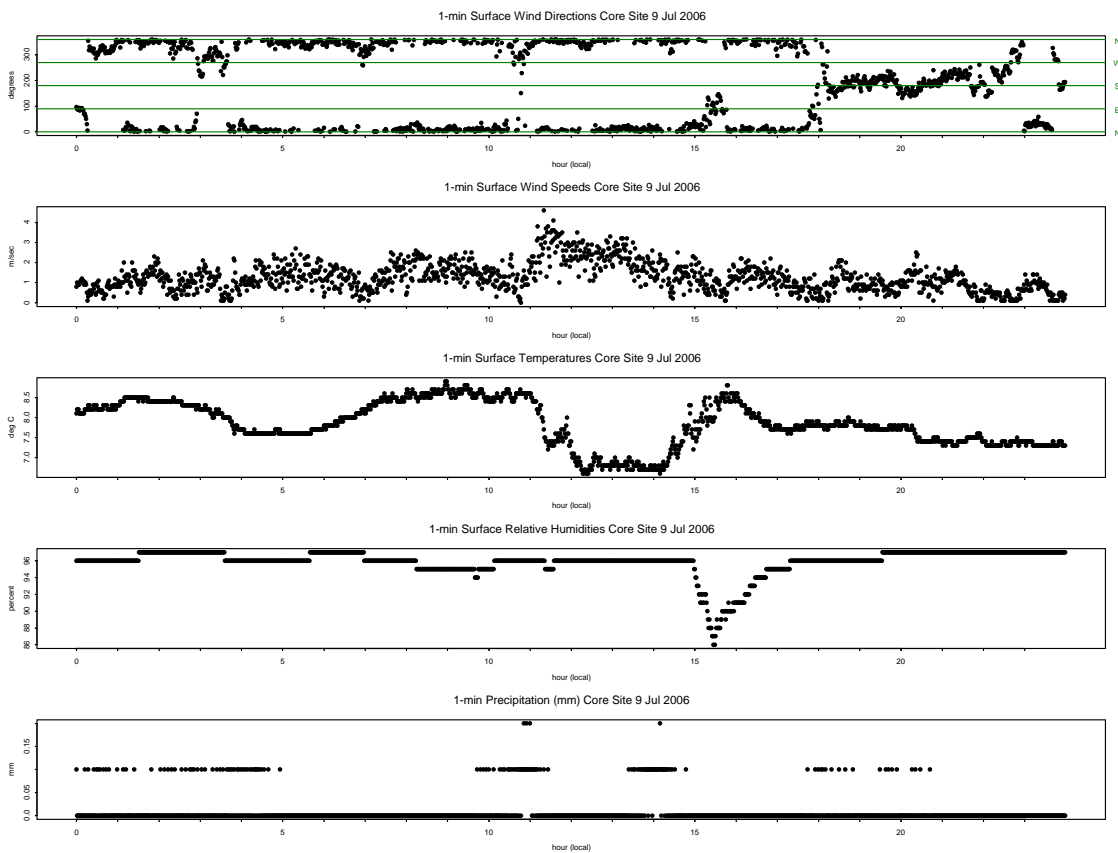


Figure 5.57. Measured wind direction, wind speed, temperature, and relative humidity, and precipitation at the RoMANS core measurement site on July 9, 2006 (JD = 190).

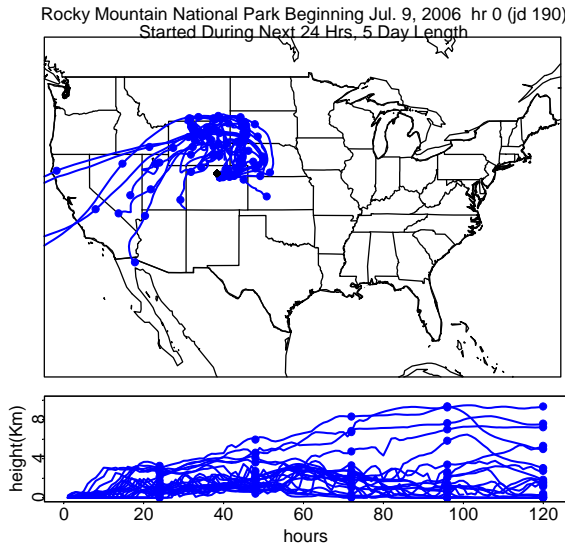


Figure 5.58. Back trajectories started at 100 m AGL at the RoMANS core measurement site on July 9, 2006 (JD = 190). Trajectories were tracked hourly for 5 days.

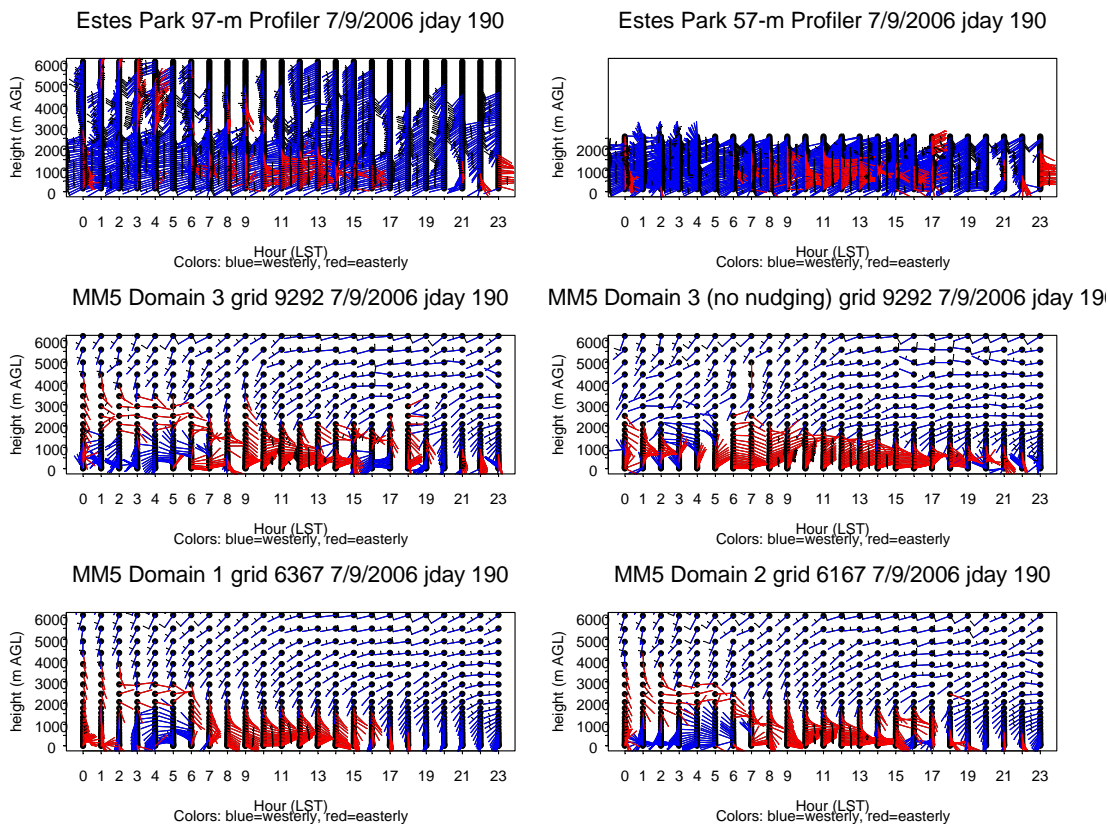


Figure 5.59. Horizontal winds by height above ground and by hour at Estes Park, Colorado, on July 9, 2006 (JD = 190), as measured by the two modes of the radar wind profiler and as calculated by MM5 on Domain 1 (36 km), Domain 2 (12 km), and Domain 3 (4 km). Domain 3 results are shown with and without observational nudging. Each long barb is 10 m/sec; short barbs are 5 m/sec. Stems are red for easterly winds and blue for westerly.

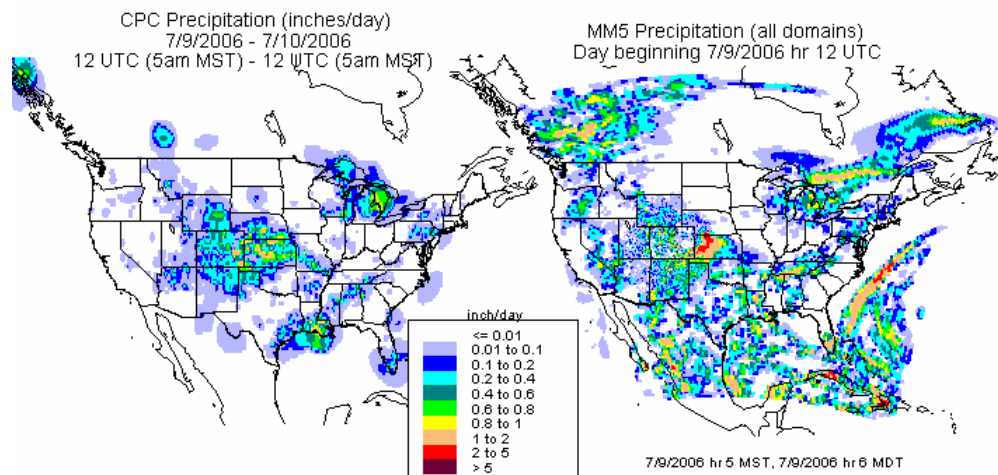


Figure 5.60. Contours of CPC (left) and MM5 (right) 24-hr precipitation totals beginning July 9, 2006, 12:00 UTC (5:00 am MST, 6:00 am MDT).

#### 5.3.2.2.5. July 15, 2006 (Julian Day 196) – Wet Episode

Core site meteorology, back trajectories, upper-air winds at Estes Park, and precipitation contours for July 15 are shown in Figures 5.61–5.64. The total measured precipitation for July 15 was 0.6 mm, which fell between 4:00 and 5:00 pm. MM5 did not capture this light precipitation event. The 10-m wind directions at the core site were northwesterly most of the day, except between 7:00 and 8:00 am and between 1:00 and 4:00 pm when they were more likely to be northeasterly to southeasterly. Wind speeds were mostly between 0 and 2 m/sec before 8:00 am and after 5:00 pm, but during midday speeds were higher, mostly 2–7 m/sec. Temperatures ranged from 12 to 26 C, with a typical diurnal cycle of the minimum at about the time of sunrise and maximum in late afternoon. RH ranged from 10% to 50%. The peak RH was around the time of the precipitation in late afternoon. The 5-day back trajectories arrived from northeastern Colorado, western Colorado, Utah, Nevada, California, and northwestern Arizona. The radar wind profiler in Estes Park showed easterly winds near the surface between 3:00 am and 3:00 pm, with an elevated layer of easterly winds from 3:00 pm until the end of the day. None of the MM5 domains replicated this pattern. All three domains showed uniformly westerly winds, except for a layer above 4000 m AGL during the morning hours. The CPC precipitation had light precipitation in Colorado, but MM5 did not. There was no measured precipitation at the core site on the following day, July 16.

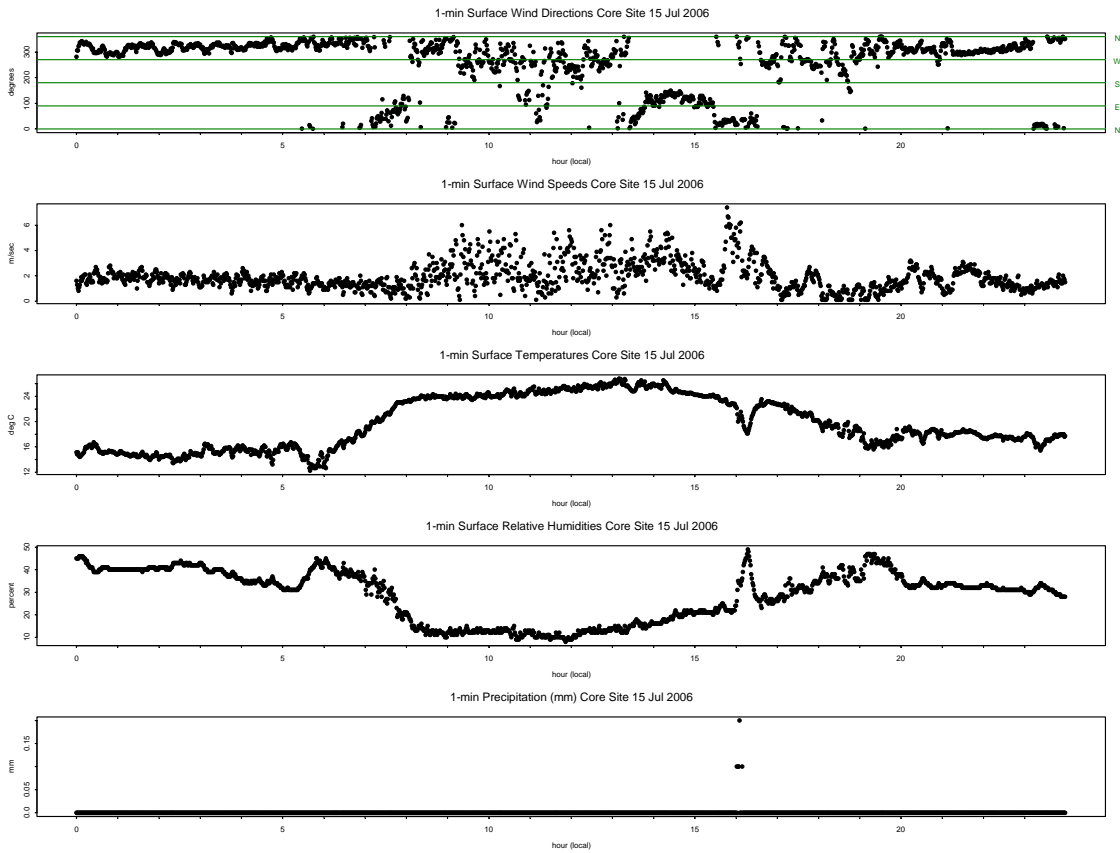


Figure 5.61. Measured wind direction, wind speed, temperature, and relative humidity, and precipitation at the RoMANS core measurement site on July 15, 2006 (JD = 196).

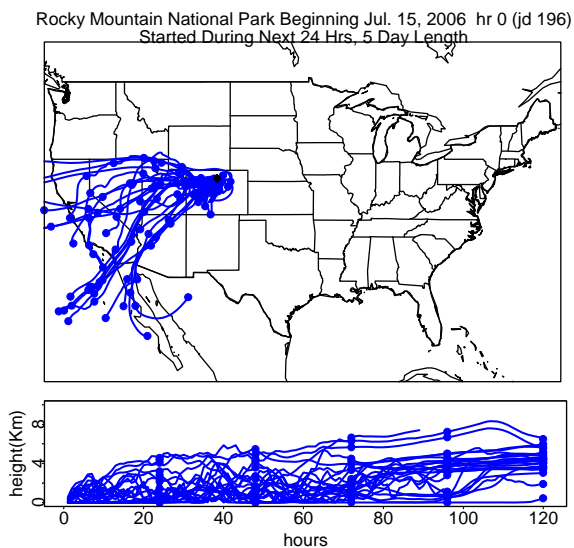


Figure 5.62. Back trajectories started at 100 m AGL at the RoMANS core measurement site on July 15, 2006 (JD = 196). Trajectories were tracked hourly for 5 days.

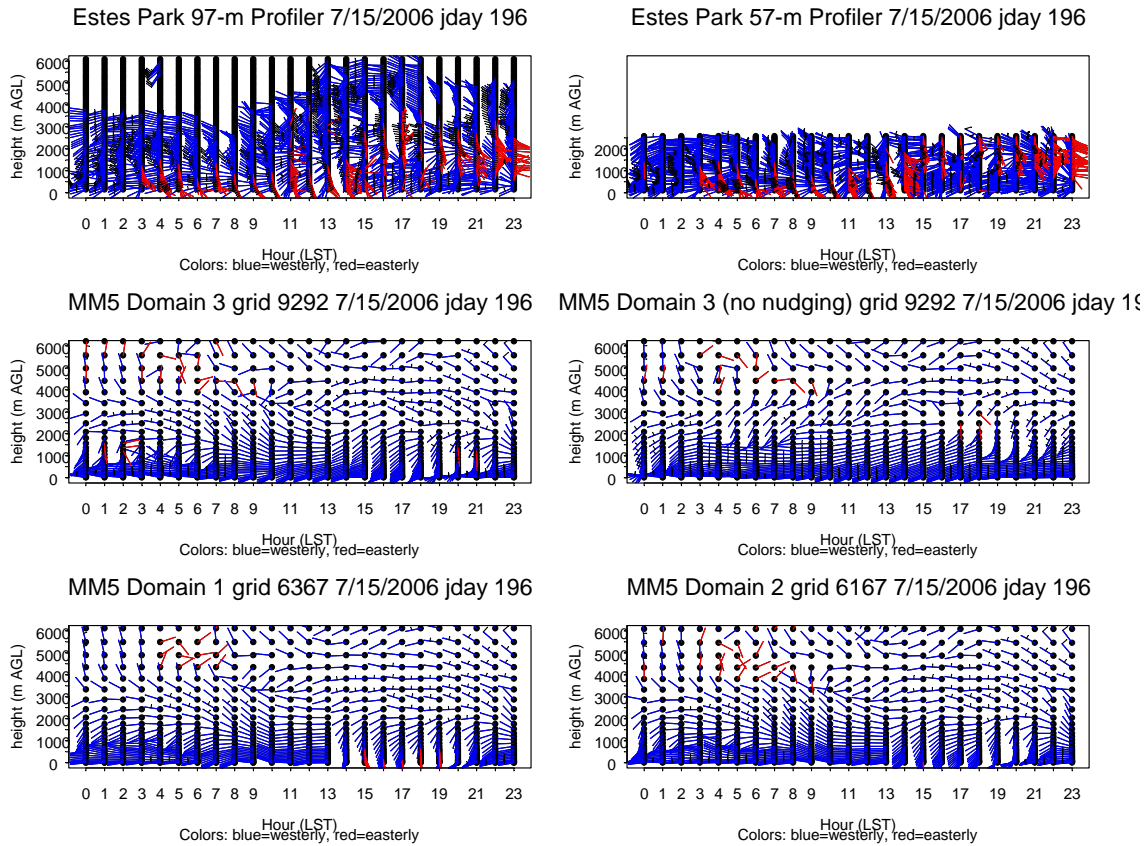


Figure 5.63. Horizontal winds by height above ground and by hour at Estes Park, Colorado, on July 15, 2006 (JD = 196) as measured by the two modes of the radar wind profiler and as calculated by MM5 on Domain 1 (36 km), Domain 2 (12 km), and Domain 3 (4 km). Domain 3 results are shown with and without observational nudging. Each long barb is 10 m/sec; short barbs are 5 m/sec. Stems are red for easterly winds and blue for westerly.

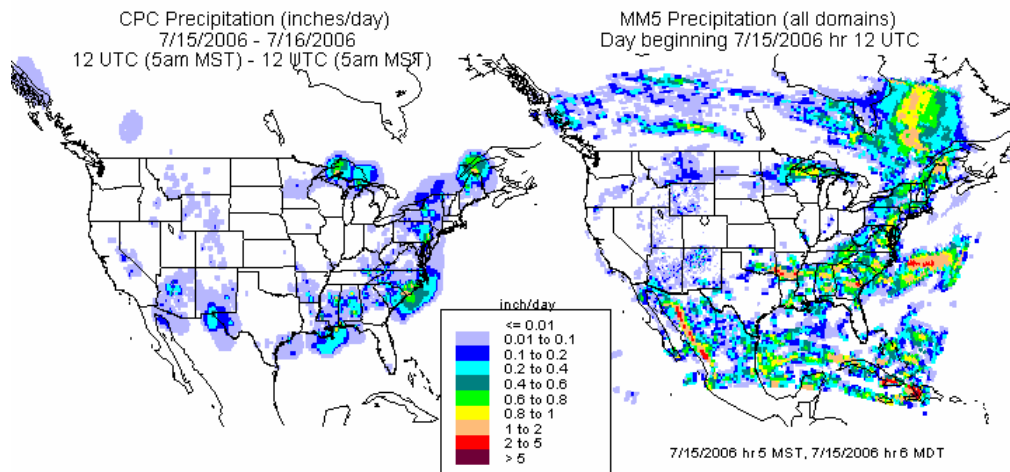


Figure 5.64. Contours of CPC (left) and MM5 (right) 24-hr precipitation totals beginning July 15, 2006, 12:00 UTC (5:00 am MST, 6:00 am MDT).

**5.3.2.2.6. July 19–20, 2006 (Julian Days 200–201) – Wet Episode**

The core site meteorology and back trajectories, the upper air winds at Estes Park, and contours of the precipitation on July 19 are shown in Figures 5.65–5.68. Similar graphs for July 20 are in Figures 5.69–5.72.

The 10-m wind directions at the core site on July 19 were predominantly northwesterly, except during 11:00 am to 1:00 pm when they were mostly northeasterly. Wind speeds ranged from 0 to 7 m/sec on both days, but were generally below 3 m/sec after 3:00 pm on July 19 until 7:00 am on July 20. Temperatures rose gradually from about 15 C at midnight on July 19 to about 25 C at noon, then fell to about 20 C an hour later, and then fell sharply to 10 C by 2:00 pm on July 19. After 2:00 pm on July 19 the temperature remained mostly below 15 C until 7:00 am on July 20. The maximum temperature on July 20 was 22 C between noon and 1:00 pm. The RH on July 19 was fairly constant between 30% and 40% until it rose rapidly to more than 80% between 1:00 and 2:00 pm on July 19. From then until 7:00 am on July 20, the RH was between 60% and 80%. There was a period of lower RH from 8:00 am until 1:00 pm on July 20 when RH was between 30% and 50%, then it was between 60% and 90% for the rest of July 20. The total precipitation on July 19 was 5.3 mm that fell between 1:00 and 3:00 pm. July 20 had 2.1 mm of precipitation that fell between 1:00 and 2:00 pm and between 6:00 and 7:00 pm.

The back trajectories arriving at the core site on July 19 arrived from the west, including areas in western Colorado, Arizona, New Mexico, Utah, Nevada, and southern California. On July 20, the trajectories originated west of RMNP but circulated around RMNP, finally arriving from the southeast.

The easterly winds measured by the profiler on July 19 were slightly above the surface during most of the day. The layer of easterly winds deepened from less than 500 m to more than 3000 m between 11:00 am and 1:00 pm. MM5 showed mostly westerly winds all day on July 19 and at all levels except at 1:00 pm on the 4-km and 12-km domains and between 10:00 and 11:00 pm on all domains, and it also showed an elevated layer of easterly winds between 1:00 and 5:00 pm, though the depth of the layer in MM5 was less than observed by the profiler. On July 20 the profiler showed a layer of easterly winds from about 500 to about 2000 m AGL between midnight and 8:00 am. Between 10:00 am and 7:00 pm there was a shallower layer of easterly winds between the surface and up to as high as 1000 m. MM5 captured the early morning elevated easterly winds but not those later in the day, except between 1:00 and 2:00 pm, when it matched the profiler quite well.

Both CPC and MM5 precipitation contours showed rain over most of Colorado and in the states to the west and south on July 19. On July 20 the CPC precipitation data were similar to July 19 for Colorado and the other Four Corners states, but MM5 had no precipitation for most of Colorado.

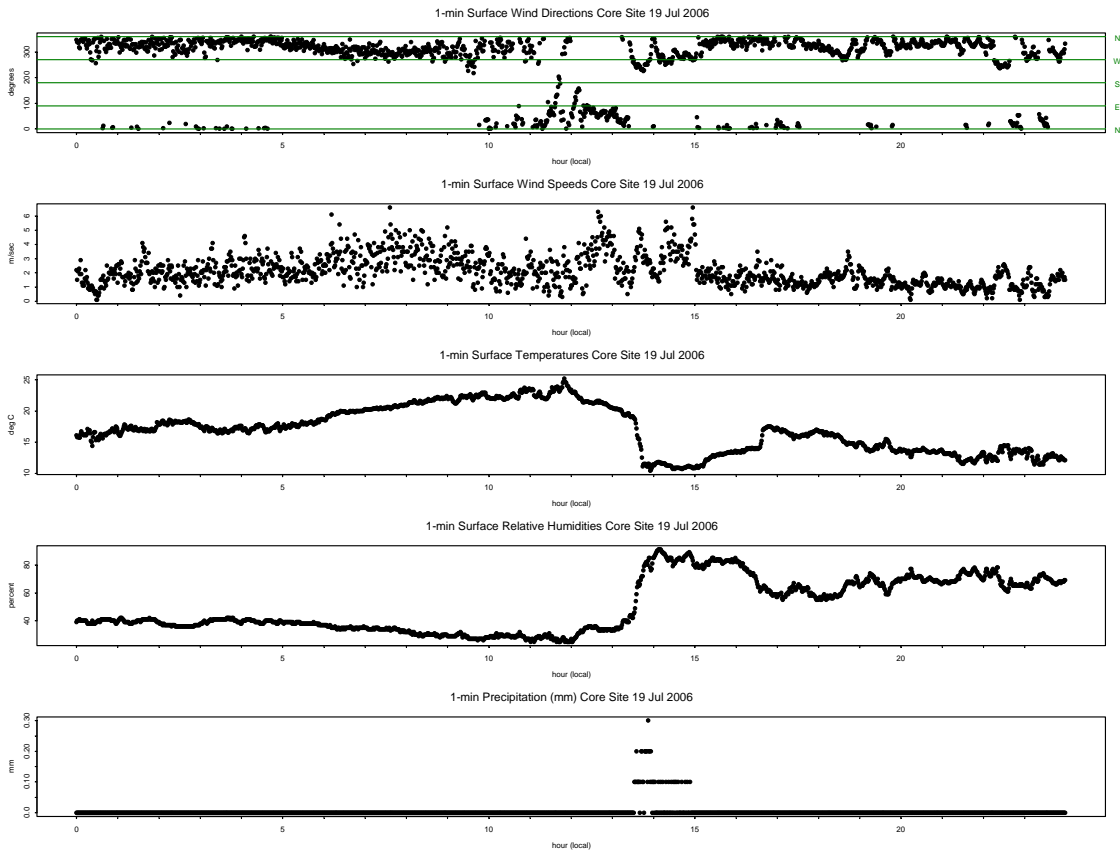


Figure 5.65. Measured wind direction, wind speed, temperature, relative humidity, and precipitation at the RoMANS core measurement site on July 19, 2006 (JD = 196).

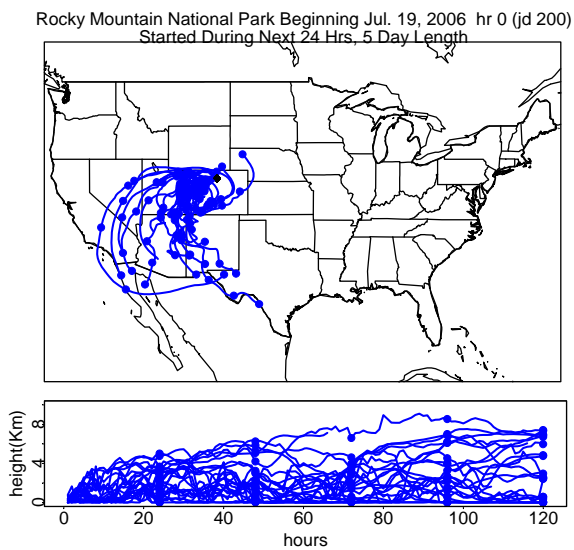


Figure 5.66. Back trajectories started at 100 m AGL at the RoMANS core measurement site on July 19, 2006 (JD = 200). Trajectories were tracked hourly for 5 days.

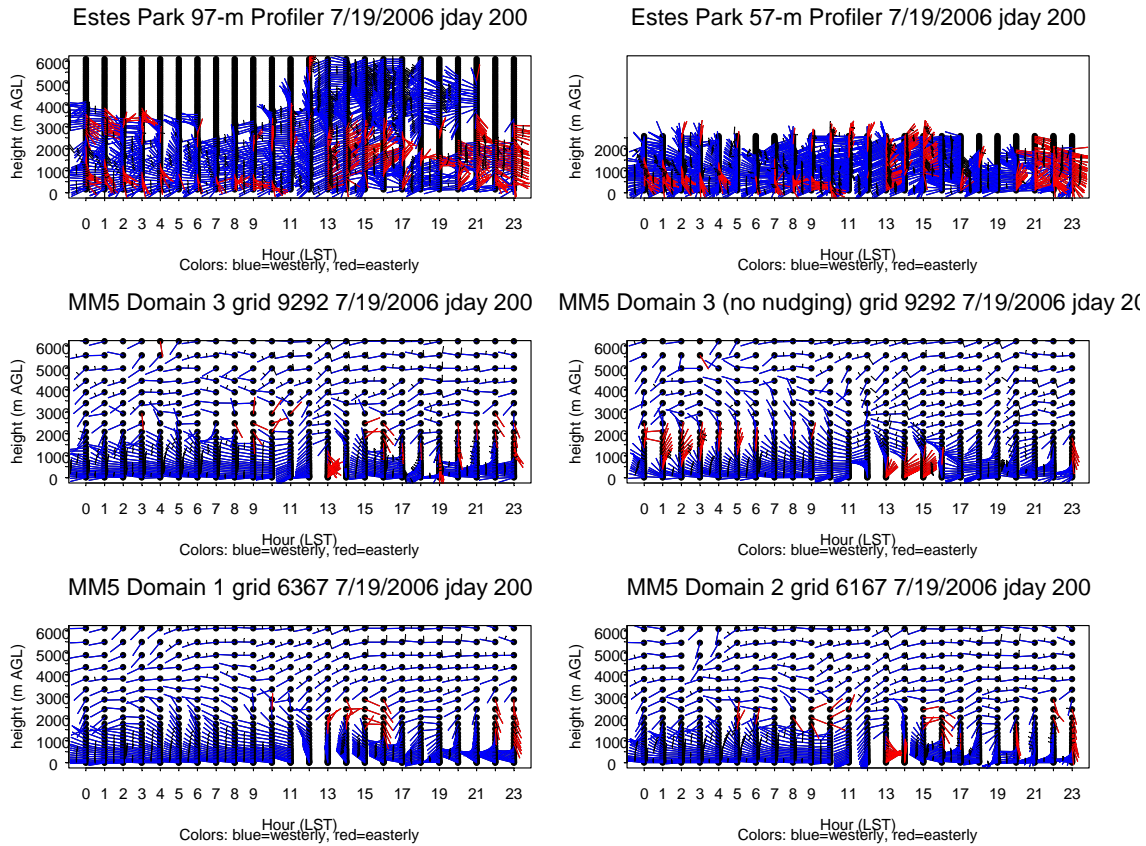


Figure 5.67. Horizontal winds by height above ground and by hour at Estes Park, Colorado, on July 19, 2006 (JD = 200), as measured by the two modes of the radar wind profiler and as calculated by MM5 on Domain 1 (36 km), Domain 2 (12 km), and Domain 3 (4 km). Domain 3 results are shown with and without observational nudging. Each long barb is 10 m/sec; short barbs are 5 m/sec. Stems are red for easterly winds and blue for westerly.

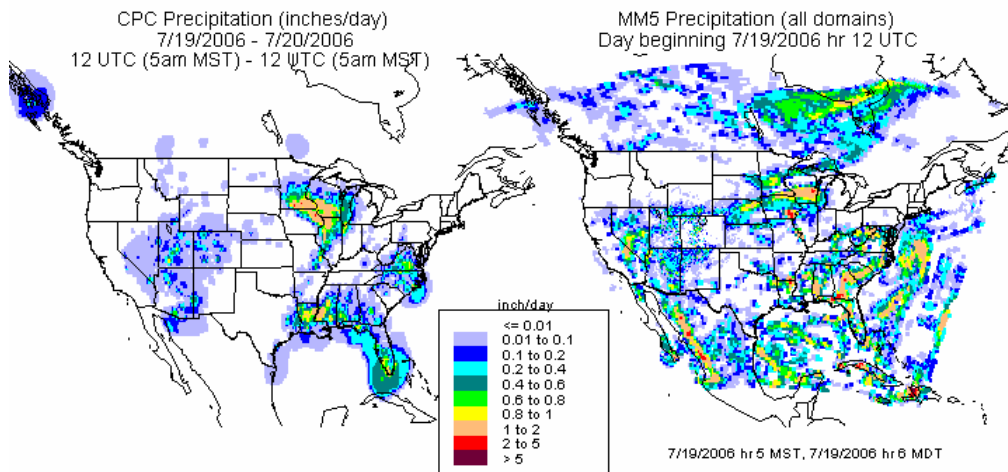


Figure 5.68. Contours of CPC (left) and MM5 (right) 24-hr precipitation totals beginning July 19, 2006, 12:00 UTC (5:00 am MST, 6:00 am MDT).

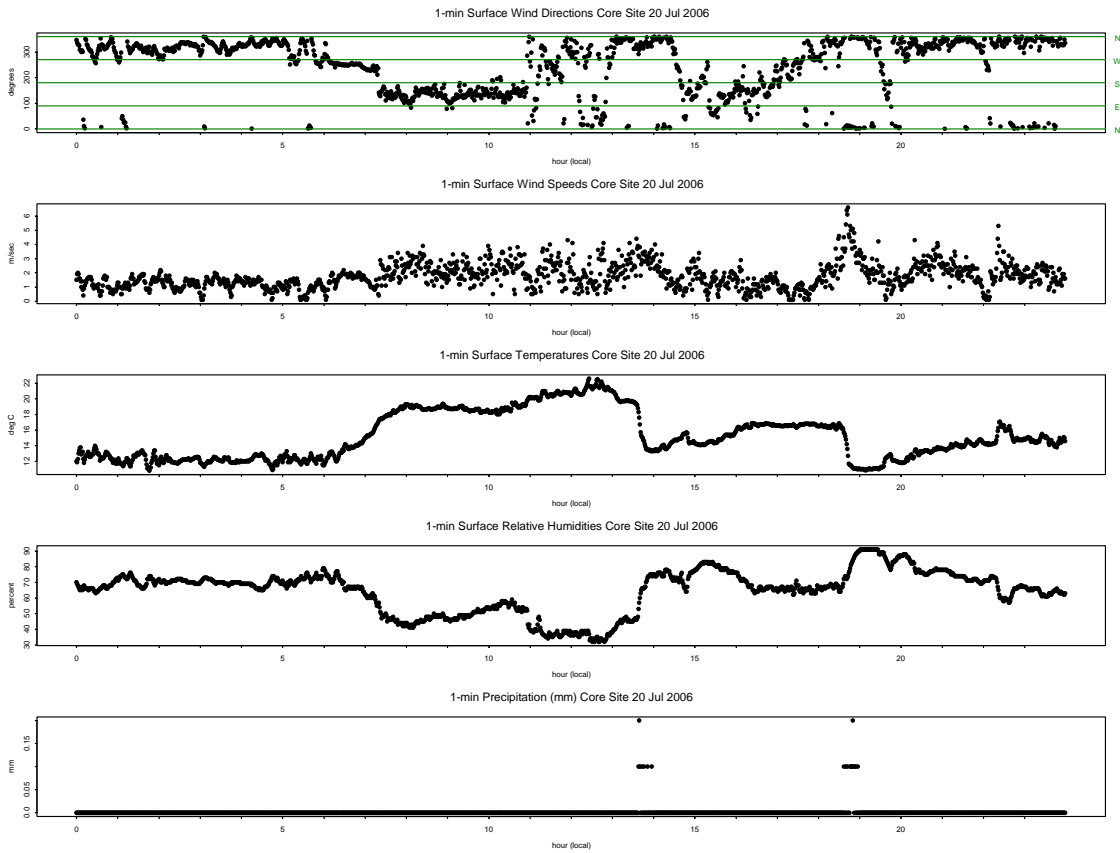


Figure 5.69. Measured wind direction, wind speed, temperature, relative humidity, and precipitation at the RoMANS core measurement site on July 20, 2006 (JD = 201).

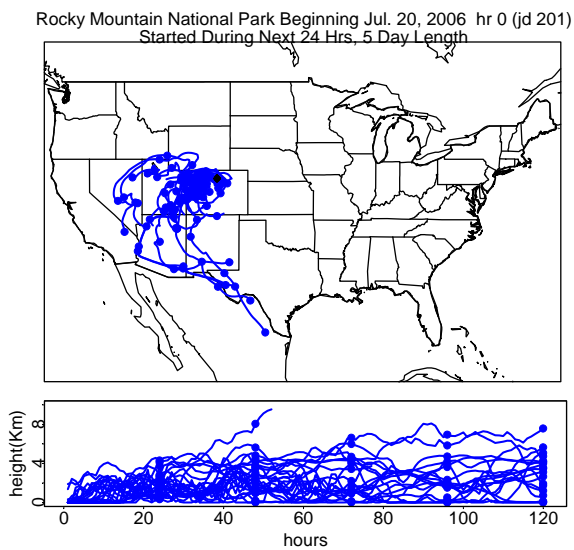


Figure 5.70. Back trajectories started at 100 m AGL at the RoMANS core measurement site on July 20, 2006 (JD = 201). Trajectories were tracked hourly for 5 days.

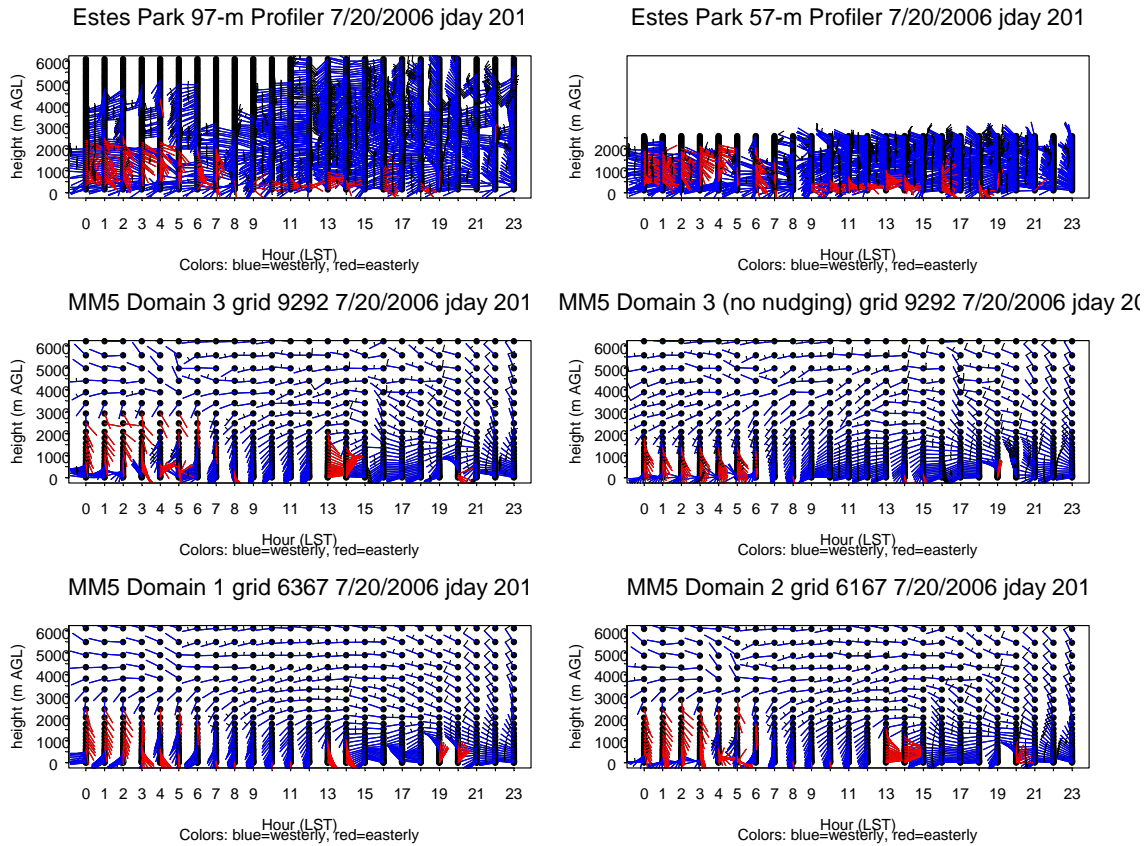


Figure 5.71. Horizontal winds by height above ground and by hour at Estes Park, Colorado, on July 20, 2006 (JD = 201), as measured by the two modes of the radar wind profiler and as calculated by MM5 on Domain 1 (36 km), Domain 2 (12 km), and Domain 3 (4 km). Domain 3 results are shown with and without observational nudging. Each long barb is 10 m/sec; short barbs are 5 m/sec. Stems are red for easterly winds and blue for westerly.

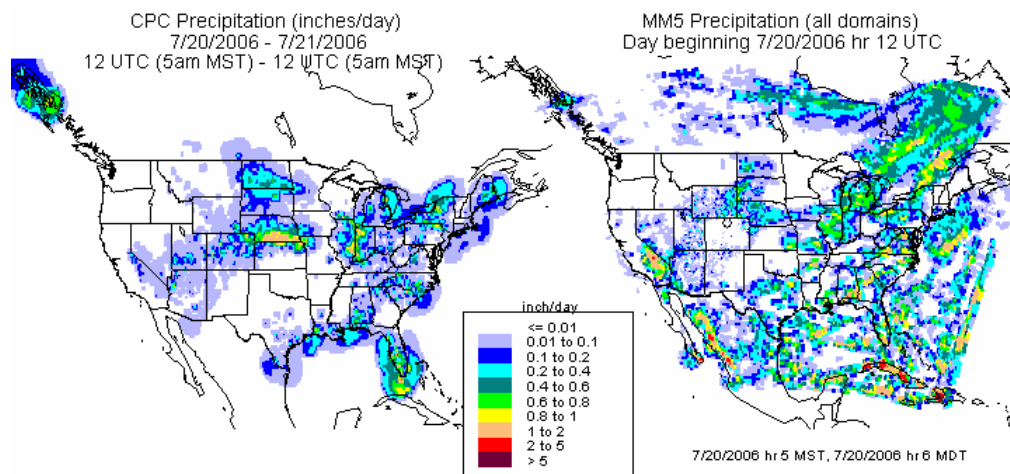


Figure 5.72. Contours of CPC (left) and MM5 (right) 24-hr precipitation totals beginning July 20, 2006, 12:00 UTC (5:00 am MST, 6:00 am MDT).

**5.3.2.2.7. July 25, 2006 (Julian Day 206) – Wet Episode**

Figures 5.73–5.76 show the core site meteorology, the HYSPLIT back trajectories, the upper-air winds at Estes Park, and the precipitation contours, respectively, for July 25.

The 10-m winds at the core site on July 25 were mostly northerly, fluctuating between northwesterly and northeasterly, except for a few short time periods of southeasterly winds. The longest period of southeasterlies was between noon and 2:00 pm. Wind speeds were between 0 and 7 m/sec. Between midnight and 4:00 pm the temperature was between 12 and 22 C. It then fell to about 12 C by 5:00 pm and remained between 10 and 12 C for the remainder of the day. The RH was between 40% and 70% until 4:00 pm when it rose rapidly to 90% and remained between 80% and 90% for the rest of the day. Precipitation totaling 10.3 mm for the day fell between mostly between 4:00 and 6:00 pm.

Back trajectories were from the west, arriving mostly from northwestern Colorado, Utah, western Wyoming, western Montana, and Idaho.

The measured easterly upper-air winds were not well matched by MM5 on this day. The Estes Park profiler showed a layer of easterly winds at or just above the surface for most of the day, but MM5 had mostly westerly winds at all levels. The 4-km domain had easterlies up to about 2000 m AGL at 3:00 pm and matched a few of the elevated layers of easterly winds during some other hours. The 12-km domain had a surface-based layer of easterlies at noon and again at 3:00–4:00 pm.

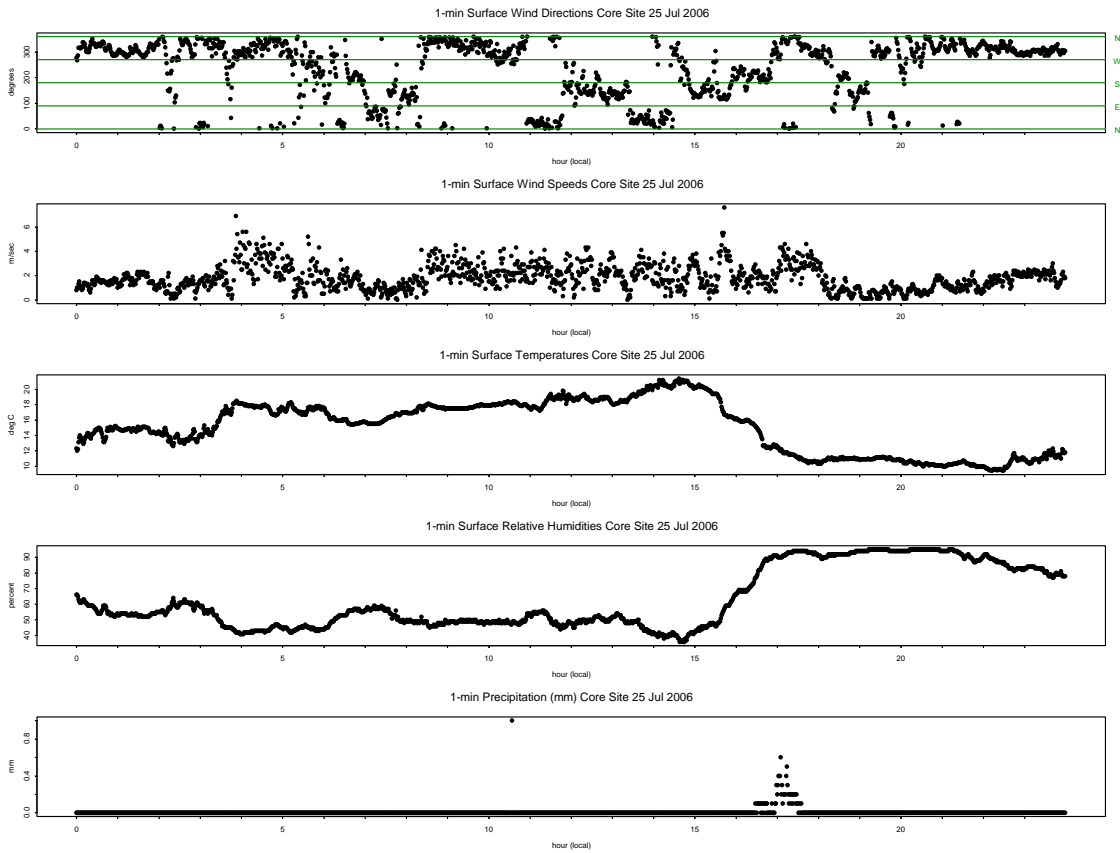


Figure 5.73. Measured wind direction, wind speed, temperature, relative humidity, and precipitation at the RoMANS core measurement site on July 25, 2006 (JD = 206).

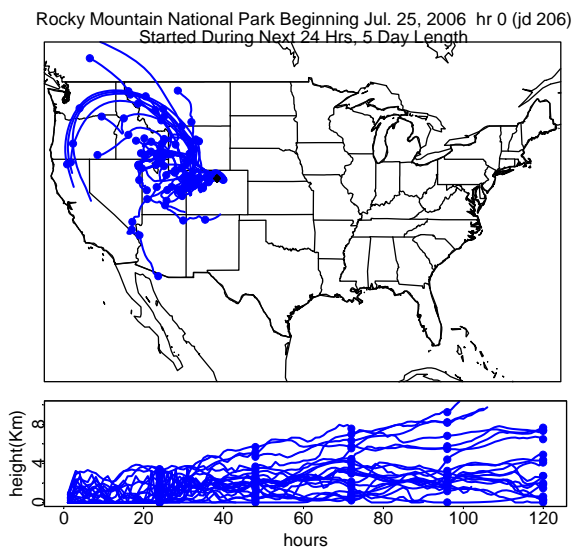


Figure 5.74. Back trajectories started at 100 m AGL at the RoMANS core measurement site on July 25, 2006 (JD = 206). Trajectories were tracked hourly for 5 days.

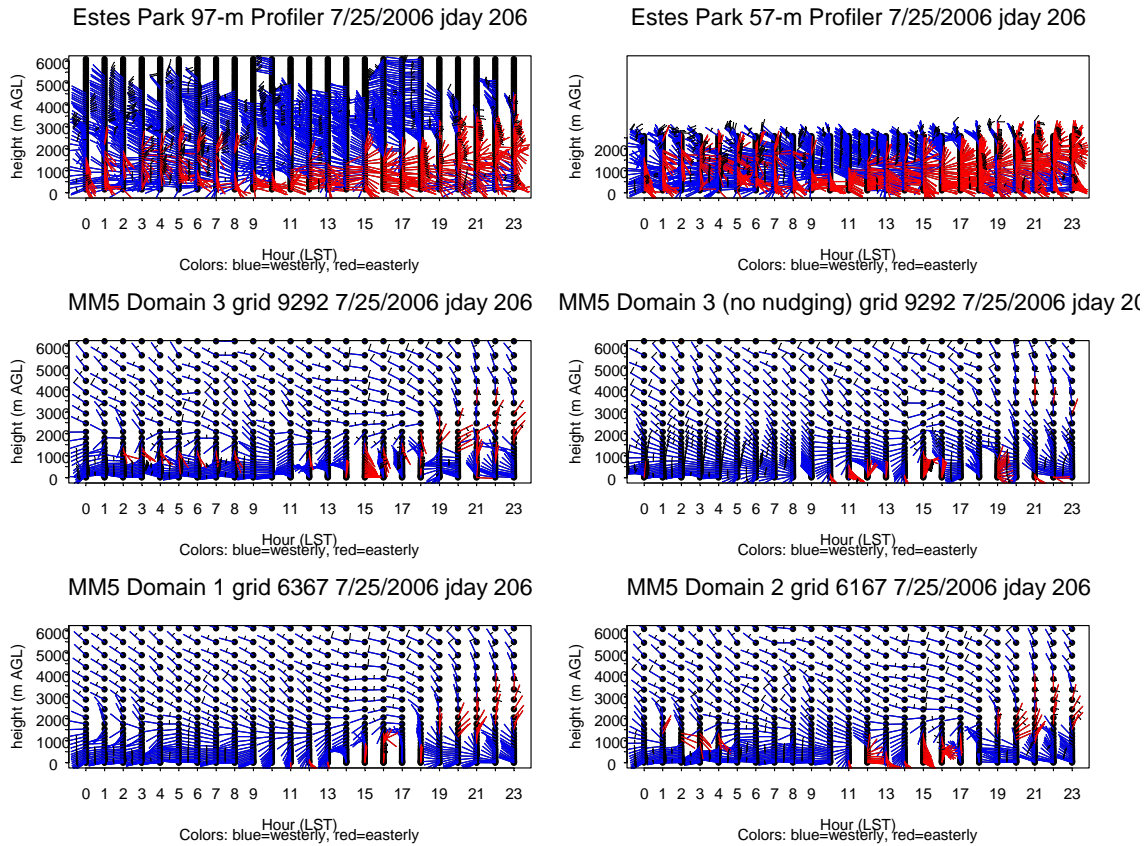


Figure 5.75. Horizontal winds by height above ground and by hour at Estes Park, Colorado, on July 25, 2006 (JD = 206), as measured by the two modes of the radar wind profiler and as calculated by MM5 on Domain 1 (36 km), Domain 2 (12 km), and Domain 3 (4 km). Domain 3 results are shown with and without observational nudging. Each long barb is 10 m/sec; short barbs are 5 m/sec. Stems are red for easterly winds and blue for westerly.

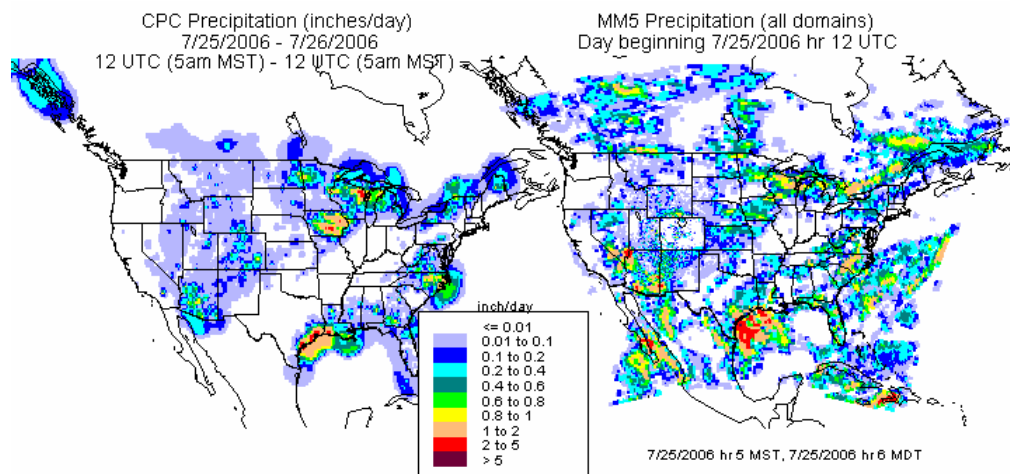


Figure 5.76. Contours of CPC (left) and MM5 (right) 24-hr precipitation totals beginning July 25, 2006, 12:00 UTC (5:00 am MST, 6:00 am MDT).

In summary, most episodes of relatively high measured wet deposition and ambient particulate concentrations were associated with easterly transport in the lowest km of the atmosphere. The modeled wind field generated by MM5 generally captured this easterly transport, though there were some events when the depth or the timing of the easterly flow was miscalculated. Precipitation was predicted better during the spring than during the summer episodes.

### 5.3.3. Statistical Back Trajectory Analyses

A back trajectory identifies the centerline of the pathway an air mass took en route to the receptor. Meteorological parameters such as precipitation, mixing height, and wind speed along the trajectory can also be examined so that a comprehensive air mass history is available for analysis. The assumption is that sources, or lack of sources, along the pathway and near the receptor are responsible for the receptor's air quality. These are powerful techniques that potentially link source regions to the receptor concentrations. However, individual air mass histories can have large errors (Kahl and Samson, 1986; Kahl et al., 1989; Rolph and Draxler, 1990; Stohl, 1998; Gebhart et al., 2005). In fact, different model assumptions or wind fields can generate air mass trajectories that are 180 degrees out of phase. The large uncertainty in individual trajectories can be reduced through ensemble techniques that aggregate large numbers of air mass histories. These techniques then identify typical transport pathways and their associated characteristics for specified conditions of interest. Several of these techniques are described below.

#### 5.3.3.1. Residence Time

The residence time analysis (Ashbaugh et al., 1985; Poirot and Wishinski, 1986) aggregates trajectories by counting the number of hours each air mass resided within each grid cell over a specified domain. This is approximated by the number of hourly trajectory segment endpoints in the cell. These grid cell residence times are then normalized by the total number of hours, resulting in a probability field identifying the regions in which air masses most frequently resided en route to the receptor.

The overall residence time (ORT) for each grid cell is defined as

$$\text{Equation 5.1. } ORT_{i,j} = \frac{1}{N} \sum_{t=1}^T n_{i,j,t}$$

where  $n$  is the number of back trajectory segment endpoints in the grid cell at longitude  $I$  and latitude  $j$  before the trajectory arrived at the receptor during measurement period  $t$ .  $N$  is the total number of endpoints for all time periods and  $T$  is the total number of time periods. A trajectory segment endpoint is the position of the air mass at a specific time prior to impacting the receptor. Air mass positions were calculated hourly for up to 10 days back in time. High (HRT) and low (LRT) concentration or deposition residence times are similar, except only trajectories that arrived at the receptor when the concentration or deposition was greater than or less than, respectively, a selected value are considered. The definitions of high and low are arbitrary, but are often the highest and lowest 10–20% of the measurements. HRT and LRT are calculated by

DRAFT

$$\text{Equation 5.2. } HRT_{i,j} = \frac{1}{H} \sum_{t=1}^T h_{i,j,t}$$

$$\text{Equation 5.3. } LRT_{i,j} = \frac{1}{L} \sum_{t=1}^T l_{i,j,t}$$

where H and L are the total number of trajectory endpoints arriving during high- and low-concentration or deposition time periods and h and l are the number of trajectory segment endpoints in each grid cell for these times.

### 5.3.3.1.1. *Source Contribution Function (Distance-Weighted Residence Time)*

The overall source contribution function (OSC) is the overall residence time (ORT) normalized by an equal probability surface (EPS). The EPS is defined as an idealized ORT that would exist if all air masses arrived at the receptor following a straight trajectory with constant speed and equal probability from all directions. Residence time fields always have a peak at the receptor because all trajectories originate there. The source contribution function is the residence time with this central tendency removed. It is always proportional to the residence time multiplied by the distance of the grid cell from the receptor. For relative comparisons between grid cells, the proportionality constant is irrelevant, and in many applications it has been set to 1/rmax, where rmax is the maximum distance from the receptor to any trajectory. However, the proportionality constant can be derived with a smaller radius if desired.

OSC is defined as

$$\text{Equation 5.4. } OSC_{i,j} = \frac{ORT_{i,j}}{EPS_{i,j}}$$

where ORT is the overall residence time and EPS is calculated by

$$\text{Equation 5.5. } EPS_{i,j} = \frac{1}{r_{i,j}} \frac{A_{i,j}}{2 \pi R_{norm}}$$

where  $r_{i,j}$  is the distance from the receptor to the center of the grid cell.  $A_{i,j}$  is the area of the grid cell. In a grid system based on degrees of latitude and longitude, each grid cell does not have the same area, with cells to the north being smaller than those to the south. However, in practice, correcting for this effect rarely produces a noticeable change in the overall pattern. Grid cell area in square km for a 1 deg by 1 deg grid cell is calculated by

$$\text{Equation 5.6. } A_{i,j} = \Delta X \Delta Y \\ = (1^\circ Lat)^2 (111.1 \text{ Km}/^\circ Lat)^2 \text{Cos}(Lat).$$

$R_{norm}$  is the “normalization radius” or radius of the area in which the EPS integrates to 1, so  $(2 \pi R_{norm})$  is the total area in which the EPS is defined and is somewhat arbitrary. Because the

EPS is 0 beyond  $R_{norm}$ , OSC is undefined when  $r_{i,j}$  is greater than  $R_{norm}$ . As an example,  $R_{norm}$  here is calculated such that the ratio of  $R_{norm}$  to the total number of endpoints is equal to the ratio of radius to endpoints in the central 9 grid cells. Thus  $R_{norm}$  is calculated by solving

$$\text{Equation 5.7. } \frac{R_{norm}}{N} = \frac{R_{cent}}{N_{cent}}$$

where

$$\text{Equation 5.8. } N_{cent} = \sum_{i=iorg-1}^{iorg+1} \sum_{j=jorg-1}^{jorg+1} n_{i,j}$$

and  $iorg$  and  $jorg$  are the  $i$  and  $j$  coordinates of the grid cell containing the receptor (the origin).  $R_{cent}$  is calculated by solving for it in the following relationship:

$$\text{Equation 5.9. } \pi R_{cent}^2 = \sum_{i=iorg-1}^{iorg+1} \sum_{j=jorg-1}^{jorg+1} A_{i,j}$$

The functional equations for the overall high concentration and low concentration source contribution functions are then

$$\text{Equation 5.10. } \begin{aligned} OSC_{i,j} &= \frac{2 \pi R_{norm} r_{i,j}}{N A_{i,j}} \sum_{t=1}^T n_{i,j,t} \\ HSC_{i,j} &= \frac{2 \pi R_{norm} r_{i,j}}{H A_{i,j}} \sum_{t=1}^T h_{i,j,t} \\ LSC_{i,j} &= \frac{2 \pi R_{norm} r_{i,j}}{L A_{i,j}} \sum_{t=1}^T l_{i,j,t} \end{aligned}$$

$H$  and  $L$  are similar to  $N$  except they are the total number of back trajectory endpoints associated with high and low concentrations or deposition fluxes, respectively.

The source contribution function provides a formal means of limiting the extent that is considered in the analysis of the distance an air mass will travel. However, if this cut-off is ignored, then the source contribution function is proportional to multiplying the residence time probability by the distance between the receptor and grid cell. In practice, Equation 5.10 is reduced to the residence time multiplied by the distance to the grid cell:

$$\text{Equation 5.11. } \begin{aligned} OSC_{i,j} &= r_{i,j} ORT_{i,j} \\ HSC_{i,j} &= r_{i,j} HRT_{i,j} \\ LSC_{i,j} &= r_{i,j} LRT_{i,j} \end{aligned}$$

### 5.3.3.2. Conditional Probability

Conditional probability is the probability that, if an air mass passed through a grid cell, it arrived at the receptor when the concentration satisfied a given condition. The selected condition is usually the measurement of a high or low concentration or deposition. The high concentration and low conditional probabilities are calculated by

$$HCP_{i,j} = \frac{HRT_{i,j}}{ORT_{i,j}} * \frac{H}{N} = \sum_{t=1}^T h_{i,j,t} / \sum_{t=1}^T n_{i,j,t}$$

Equation 5.12.

$$LCP_{i,j} = \frac{LRT_{i,j}}{ORT_{i,j}} * \frac{L}{N} = \sum_{t=1}^T l_{i,j,t} / \sum_{t=1}^T n_{i,j,t}$$

where all variables are as defined in the residence time equations.

Grid cells that have few total endpoints may not have statistically significant conditional probabilities and are usually not reported. An extreme example is a grid cell with only one endpoint. The only possible values for the conditional probability are then 0 or 1. These are usually at the edges of the domain.

#### 5.3.3.2.1. Incremental Probability

The incremental probability identifies regions that are more or less likely to be traversed when the receptor concentrations satisfy a given condition compared to an average day (Poirot et al., 2001; Schichtel et al., 2006). For example, the high and low incremental probabilities are the difference between the high or low residence time probability and the overall residence time probability:

$$\begin{aligned} \text{Equation 5.13. } \quad HIP_{i,j} &= HRT_{i,j} - ORT_{i,j} \\ LIP_{i,j} &= LRT_{i,j} - ORT_{i,j} \end{aligned}$$

The high incremental probability (HIP) field differs from the high conditional probability (HCP) field because the HIP metric is determined by subtraction (the extent to which the high day probability is greater than the average day), while the HCP metric is determined by division (the fraction of total trajectory segment endpoints passing over a cell that results in high concentration days). Thus, the HCP indicates the potential for a location to contribute if that area is upwind of the receptor, while the HIP reflects the most probable upwind locations if the receptor concentration is high.

### 5.3.3.3. Specifics of the RoMANS Trajectory Analyses

The dates included in the residence time analyses were March 27 to April 30, 2006, for the spring RoMANS campaign and July 7 to August 11, 2006, for the summer campaign. For ambient concentrations and wet deposition rates, the cutoff values for the “high” and “low”

values were the 90<sup>th</sup> and 10<sup>th</sup> percentiles, respectively, for each campaign. Residence time analysis was also conducted for the precipitation rates. More than 90% of the hours had no precipitation, so low was defined as no precipitation and high as any measurable amount. Table 5.6 shows the values used for each species for each campaign. All analyses were first completed with a 0.5 or 0.2 deg grid cell size for the entire North American domain, using 5-day-long trajectories and then repeated with a 0.1 deg grid size for latitudes 36–42 deg N and longitudes 110–101 deg W. The smaller domain includes the state of Colorado with a surrounding 1 deg buffer. All concentrations are hourly values measured at the RoMANS core site. Measurement methods are described in Chapter 2 and discussions of measured values are in Chapters 3 and 4. Trajectories were started at 100, 200, 500, and 1000 m AGL.

For ammonia concentrations on the smaller domain, only trajectories of 1 day in length and endpoints less than 1 km in height were included in order to eliminate endpoints that were unlikely to be in contact with ground-based sources of ammonia and to eliminate endpoints that were so far back in time that the ammonia would likely have been depleted or nearly depleted by deposition before the air mass arrived at RMNP. Similar refinements for the remaining species may also help improve the meaningfulness of these analyses for other species. These have not yet been completed. Deposition data could also be analyzed.

**Table 5.6.** Cutoff values for “high” and “low” for each species and season used in the RoMANS back trajectory analyses.

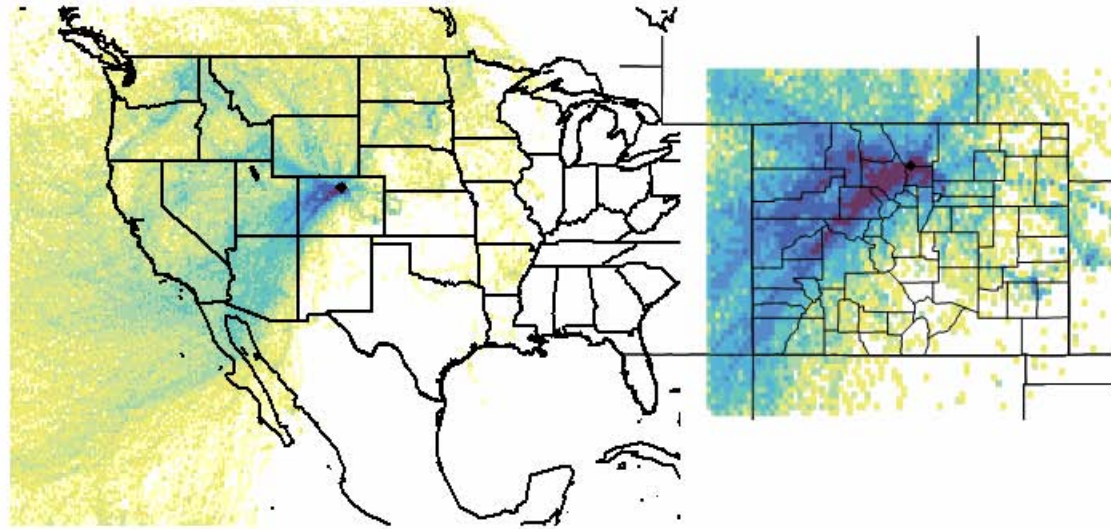
	Spring		Summer	
	Maximum low	Minimum high	Maximum low	Minimum high
<b>NO (ppb)</b>	0.009	0.627	-0.061	0.308
<b>NO<sub>2</sub> (ppb)</b>	0.548	2.970	0.993	2.779
<b>O<sub>3</sub> (ppb)</b>	37.51	61.59	27.96	62.71
<b>NH<sub>3</sub> (µg/m<sup>3</sup>)</b>	0.115	0.268	0.177	0.687
<b>SO<sub>4</sub>(µg/m<sup>3</sup>)</b>	0.128	0.726	0.410	0.923
<b>NH<sub>4</sub>(µg/m<sup>3</sup>)</b>	0.075	0.749	0.162	0.538
<b>Coarse mass (µg/m<sup>3</sup>)</b>	0.184	2.088	1.92	7.71
<b>POM (µg/m<sup>3</sup>)</b>	0.340	4.99	1.94	12.03
<b>NO<sub>3</sub> (µg/m<sup>3</sup>)</b>	0.056	1.454	0.0008	0.277
<b>Precipitation (mm)</b>	0.01	0.1	0.01	0.1
<b>SO<sub>2</sub> (µg/m<sup>3</sup>)</b>	-0.008	0.233	0.315	0.352

#### 5.3.3.4. Results of Statistical Trajectory Analyses during RoMANS

The overall residence times, showing areas from which air masses were most likely to reside during the 5 days prior to arriving at RMNP during the spring (top) and summer (bottom) RoMANS studies are shown in Figure 5.77. The left side shows the ORT for the coarse grid over the entire domain and the right side shows results limited to endpoints that fell within the fine grid within 1 degree of latitude or longitude of Colorado. The maps showing only Colorado have a different total number of endpoints (N in the denominator) and the grid sizes are also different, so the results for the smaller domain are not simply the same as zooming in on the larger domain, though, as expected, the patterns are very similar. The predominant wind direction during both seasons was westerly, with air masses more likely to arrive from the southwest or northwest than from due west. Both seasons included some transport from the east, especially northeastern Colorado. Spring included air masses arriving from the Dakotas,

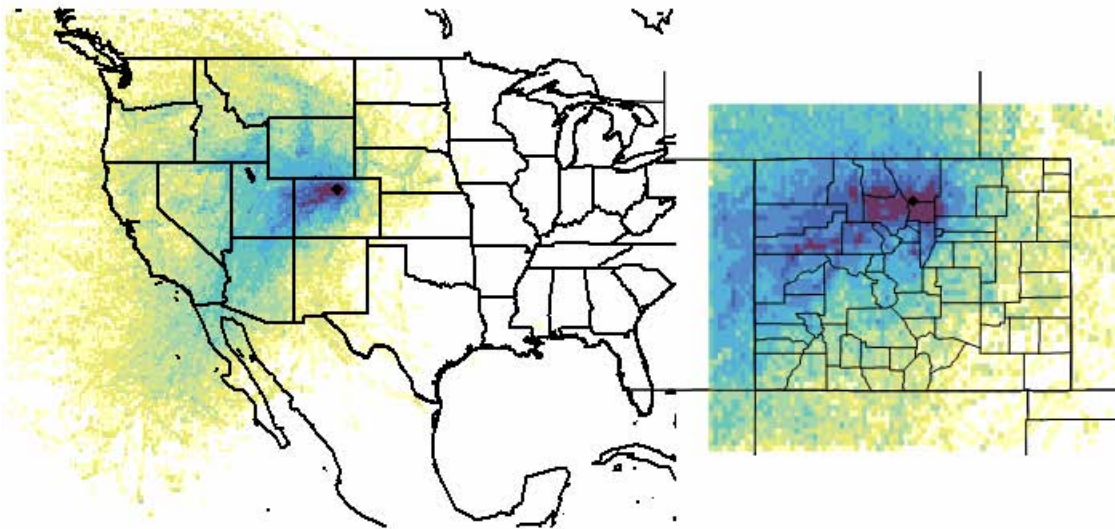
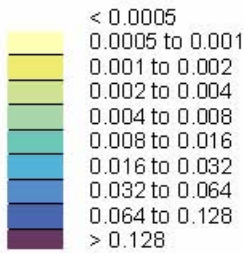
Nebraska, Minnesota, and Iowa, while summer easterlies were more southerly, with transport from Nebraska and South Dakota as well as eastern Colorado.

While all the types of trajectory analyses discussed in the methodology section were completed for all species for both seasons, in the interests of space, only the results of the high-concentration incremental probability are shown. These results are able to concisely illustrate both areas that were more likely (dark) and less likely (light) than average to be upwind on high concentration days. Figures 5.78–5.82 show the results for nitrogen-containing airborne concentrations,  $\text{NH}_3$ ,  $\text{NH}_4$ ,  $\text{NO}_3$ ,  $\text{NO}_2$ , and  $\text{NO}$ , respectively, measured at the core site. The top half of each figure has results for the spring RoMANS period, March 27 to April 30; the bottom half has the summer results, July 7 to August 11. The left side shows the entire domain of 10–70 deg N and 140–60 deg W, with a grid size of 0.2 deg latitude. The right side of each figure shows results limited to endpoints that fell within 1 deg of latitude or longitude of Colorado, 36–42 deg N and 110–101 deg W, with a 0.1 deg latitude grid size. In each case, 5-day-long trajectories were used. The total number of endpoints is approximately 145,000 for the full domain and 20,000 for the Colorado domain. In order to best illustrate the spatial patterns, a different contour interval was used for the finer Colorado domain than for the coarser national domain.



### Spring Overall Residence Time

Percent of Endpoints



### Summer Overall Residence Time

Figure 5.77. Overall residence time (ORT) for spring and summer RoMANS periods, showing areas that were most likely to be upwind of RMNP during each study period.

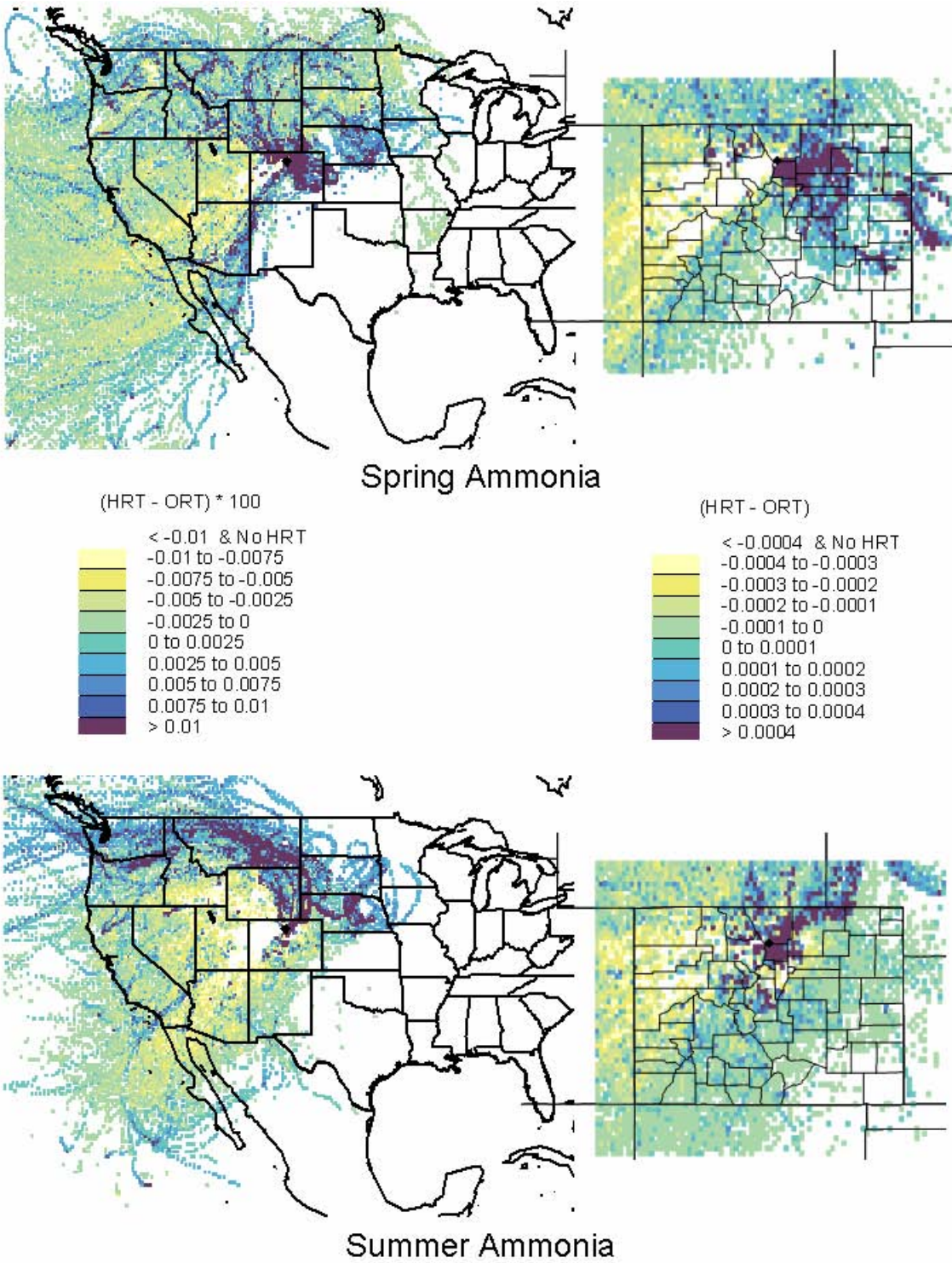


Figure 5.78. High concentration incremental probability for ammonia measured at the core site during spring (top) and summer (bottom).

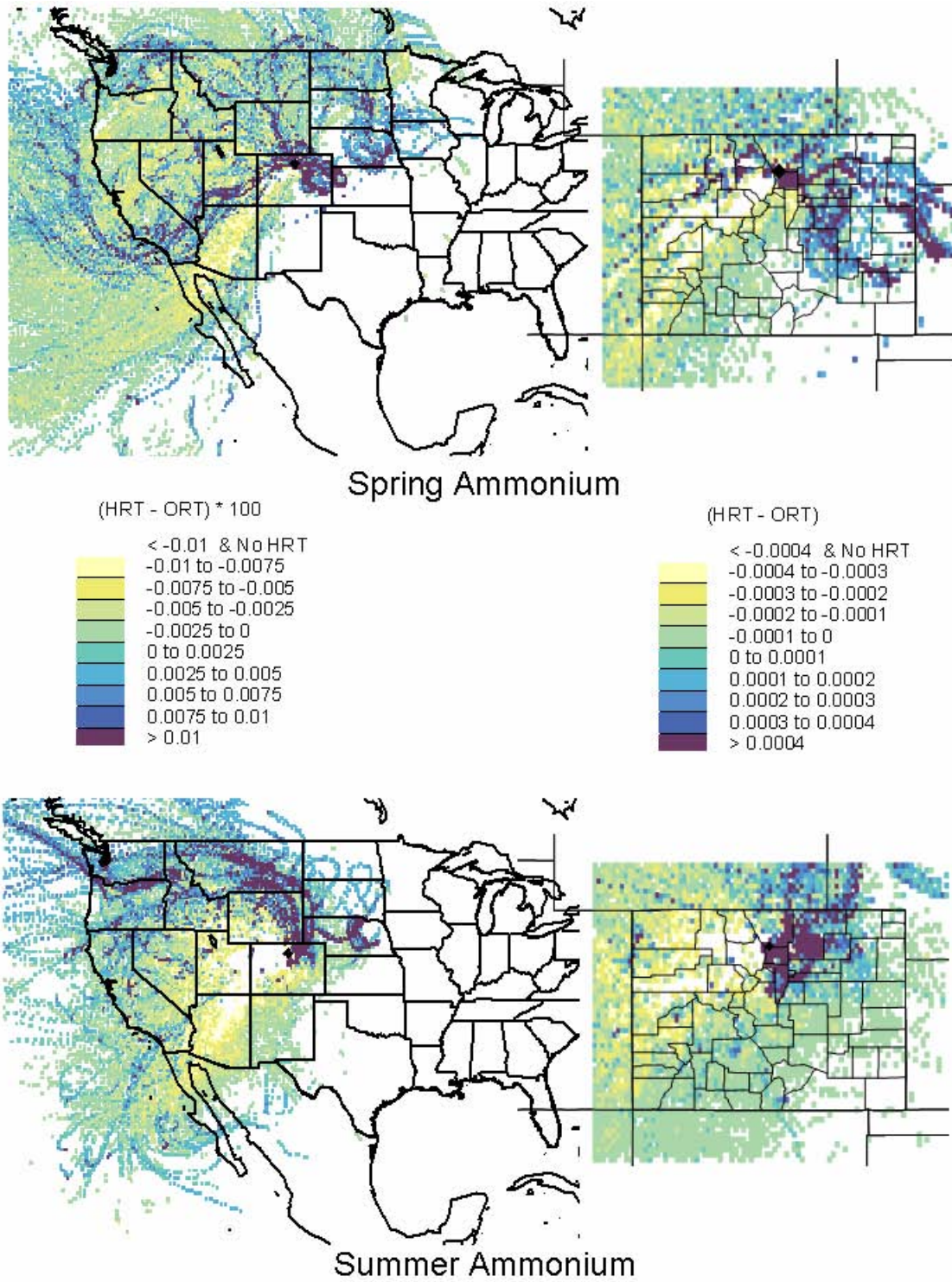


Figure 5.79. High concentration incremental probability for ammonium measured at the core site during spring (top) and summer (bottom).

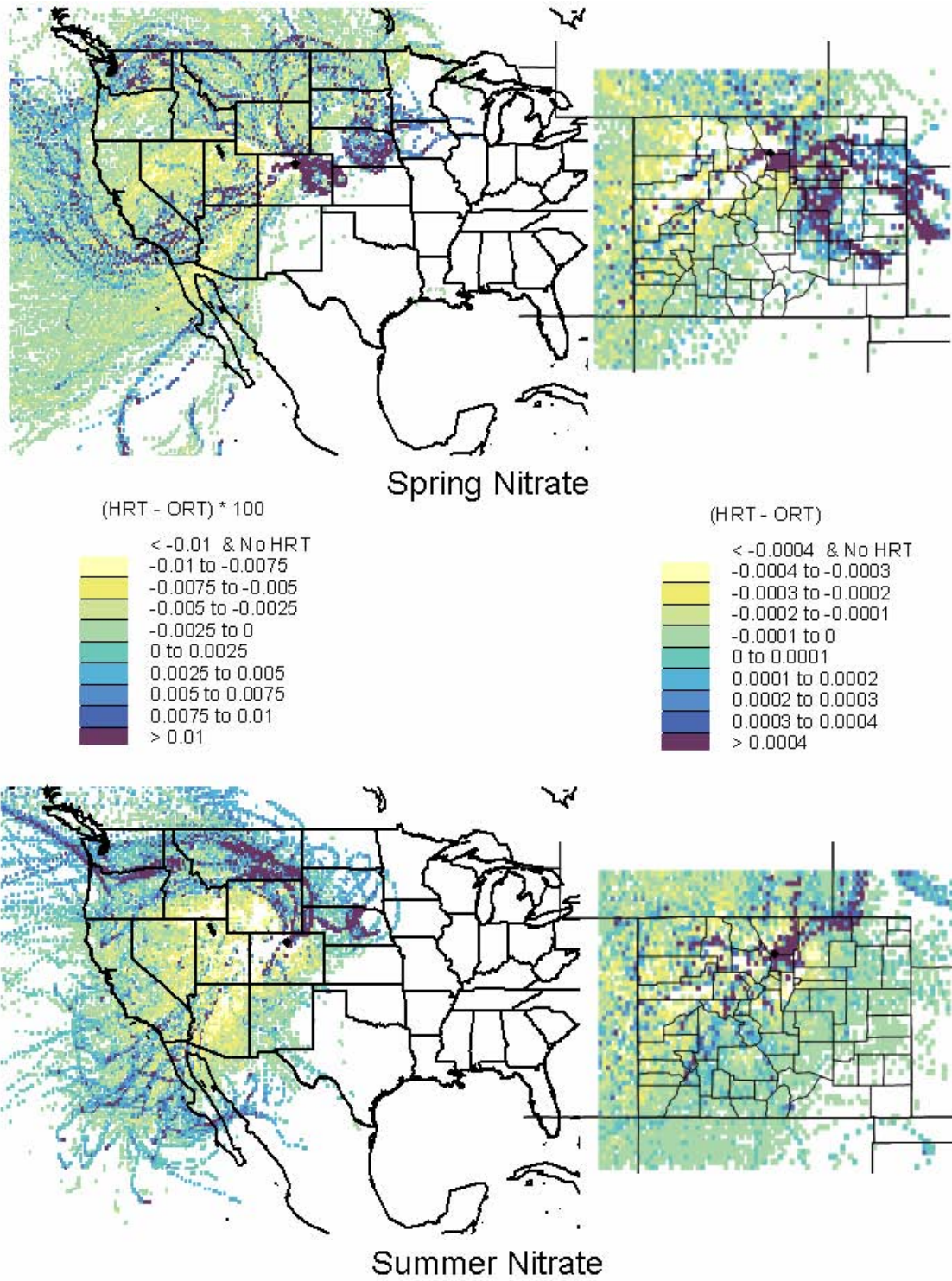


Figure 5.80. High concentration incremental probability for nitrate measured at the core site during spring (top) and summer (bottom).

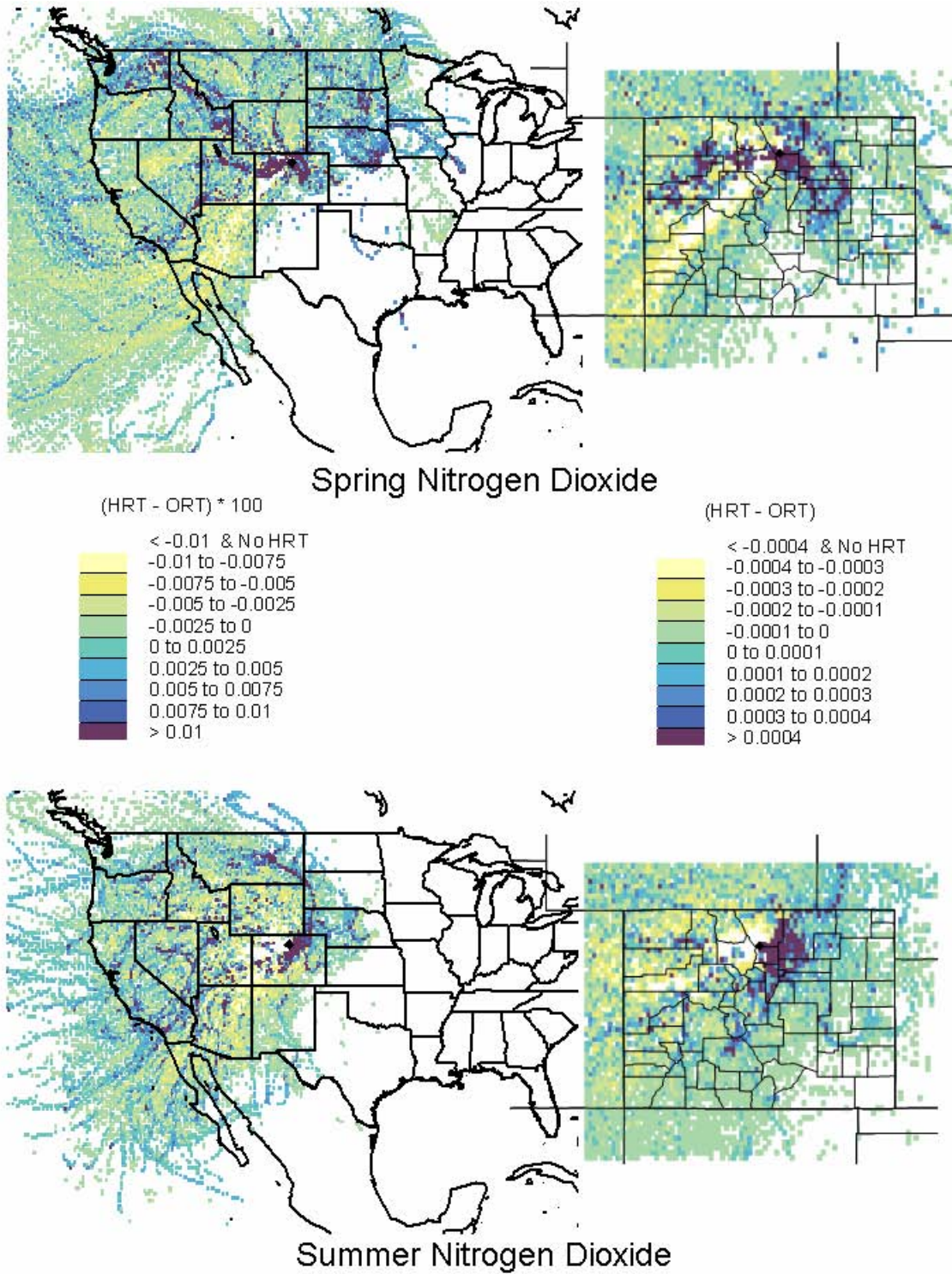


Figure 5.81. High concentration incremental probability for NO<sub>2</sub> measured at the core site during spring (top) and summer (bottom).

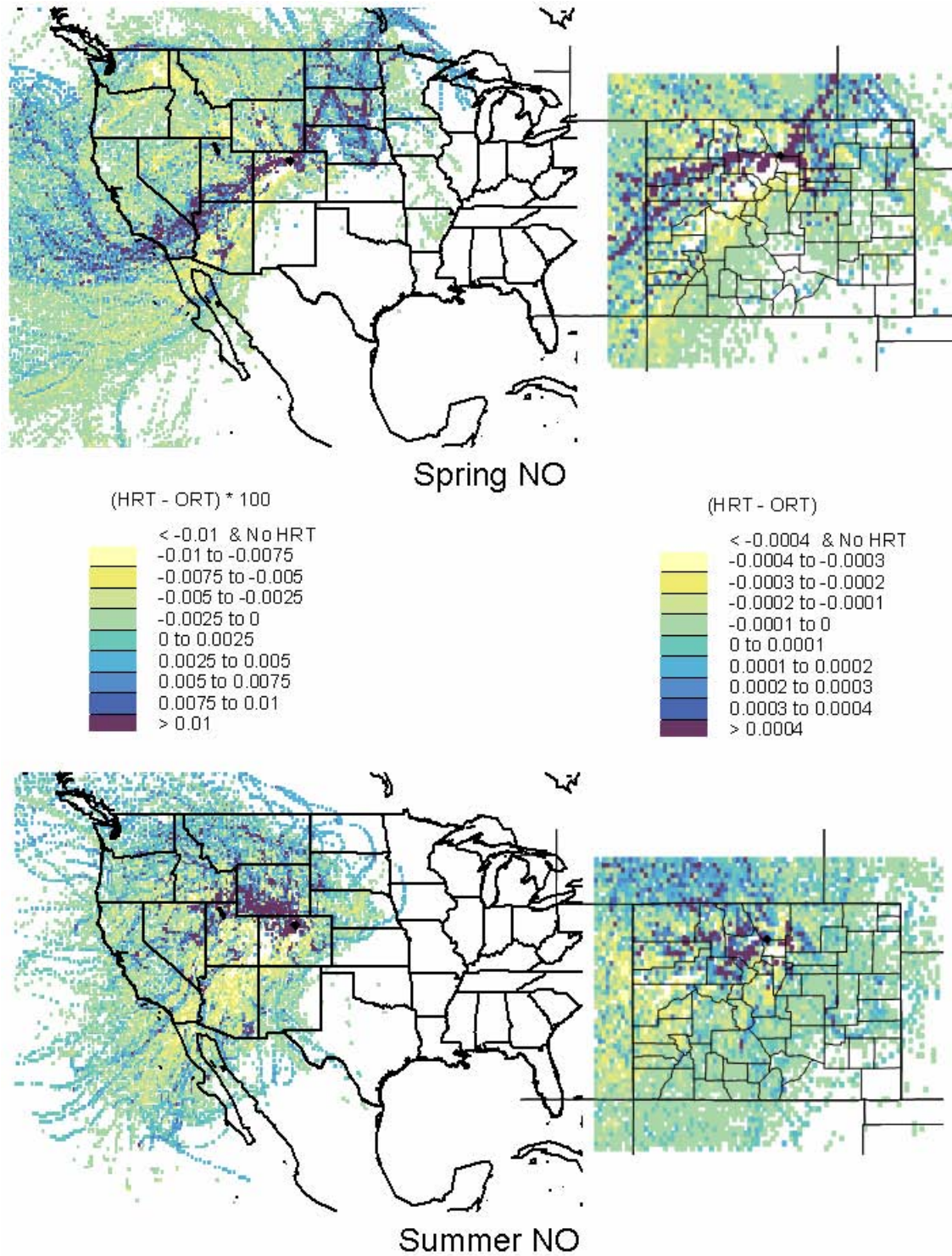


Figure 5.82. High concentration incremental probability for NO measured at the core site during spring (top) and summer (bottom).

The results for each species are unique from the others. Most show that high concentrations are associated with transport through northeastern Colorado, especially during the spring. An exception is NO, for which high concentrations are more likely to result from transport through northwestern Colorado during both spring and summer and southwestern Wyoming during the summer. The transport patterns associated with high NO concentrations are indicative of sources that are relatively close, such as within northern Colorado. During high ammonia and ammonium concentrations, the prior air mass transport is more likely than average to reside east of RMNP over the Front Range urban corridor and agricultural areas to its east. Both areas are known sources of ammonia. The back trajectories associated with high-NO<sub>2</sub> periods also preferably traverse the high-NO<sub>x</sub>-emission Front Range region, but unlike ammonia and ammonium do not extend much into the agricultural regions. Coal-fired power plants are also a large emitter of NO<sub>x</sub>. As shown in Figure 5.89, many of these power plants reside in the envelope of high incremental probabilities from the Craig and Hayden plants in northwestern Colorado to those near Colorado Springs.

Transport patterns associated with high particulate NO<sub>3</sub> during the summer indicate influence from sources along an extended transport pathway from Oregon and Washington, through Montana and eastern Wyoming, and then northeastern Colorado and the Front Range. During the spring, the scale of transport is reduced, with the highest incremental probabilities in eastern Colorado and Nebraska. Particulate nitrate is a secondary species formed primarily from NO<sub>x</sub> emissions. As would be expected, the residence time analysis shows more distant scales of transport for the nitrate compared to NO<sub>2</sub> from both the spring and summer periods.

The next group of figures shows results of the same analysis for the remaining analyzed species, SO<sub>2</sub>, SO<sub>4</sub>, O<sub>3</sub>, POM, coarse mass, and precipitation. These are shown in Figures 5.83–5.88. Results for coarse mass, sulfur dioxide, and sulfate are similar to those for nitrate, indicating sources to the north and west as well as in eastern Colorado, while transport patterns associated with high ozone show many similarities to those for high NO and NO<sub>2</sub>.

High concentrations of POM during the spring were associated with transport from northeastern Colorado and west of RMNP. During the summer, the incremental residence time analysis indicates the potential of contributions from more distant sources to RMNP. This includes the northwestern United States where a number of wildfires occurred during the summer months (Figure 5.90) and northwestern Nebraska where a large wildfire occurred near the end of July. This summertime transport pathway from the northwest through northeastern Colorado and to RMNP is common among many of the pollutants, including ammonia, ammonium, sulfate, and nitrate. Biomass burning is a known source of all of these pollutants and may be contributing to these concentrations. However, this transport pathway traverses agricultural, urban, and point sources that are also large sources of these pollutants. This method is insufficient to separate potential contributions from these different sources.

As shown in Figure 5.88, precipitation in RMNP during both the spring and summer preferentially occurred with air mass transport from the east-northeast. These were upslope events that brought lower-lying air from the plains and foothills into the mountains.

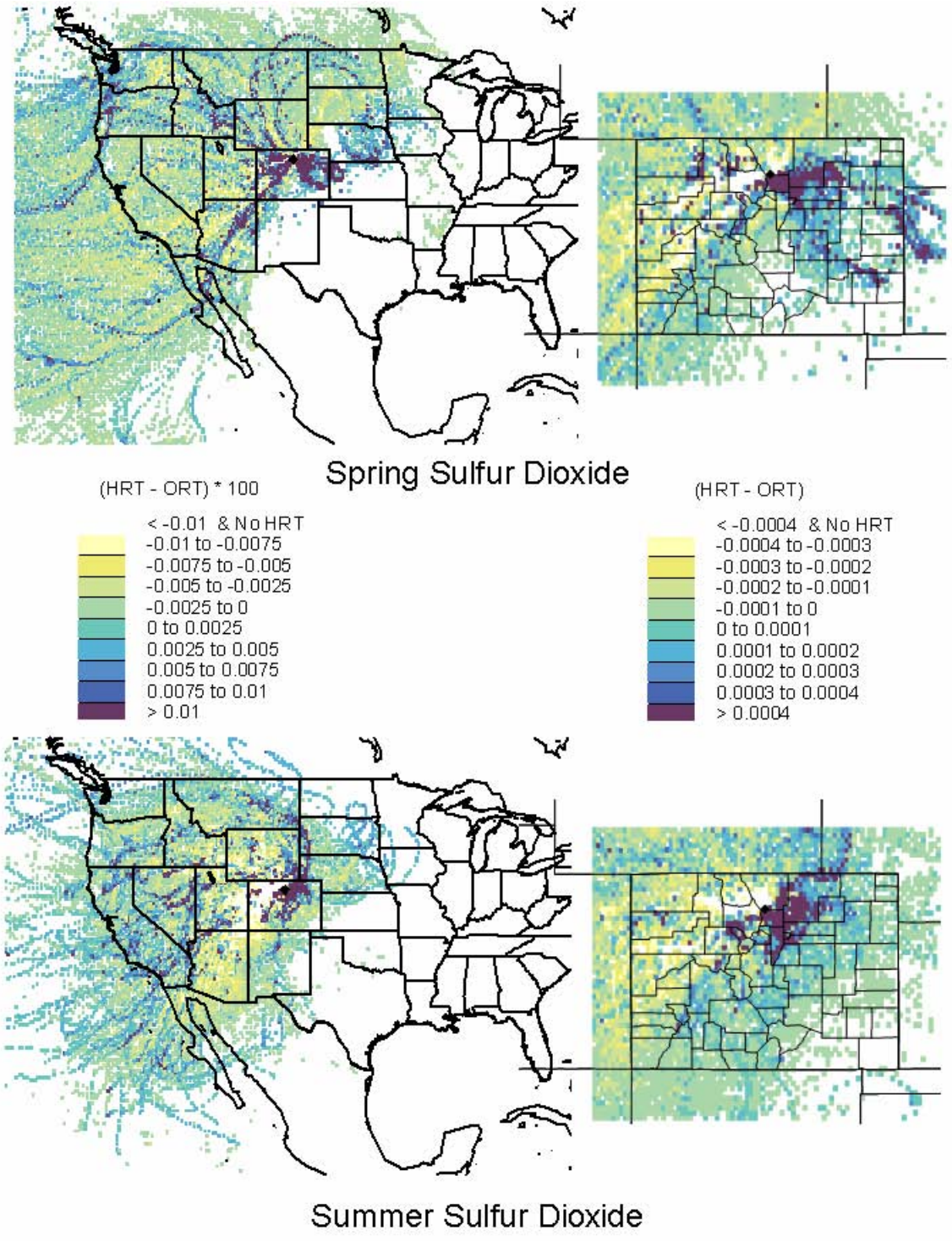


Figure 5.83. High concentration incremental probability for SO<sub>2</sub> measured at the core site during spring (top) and summer (bottom).

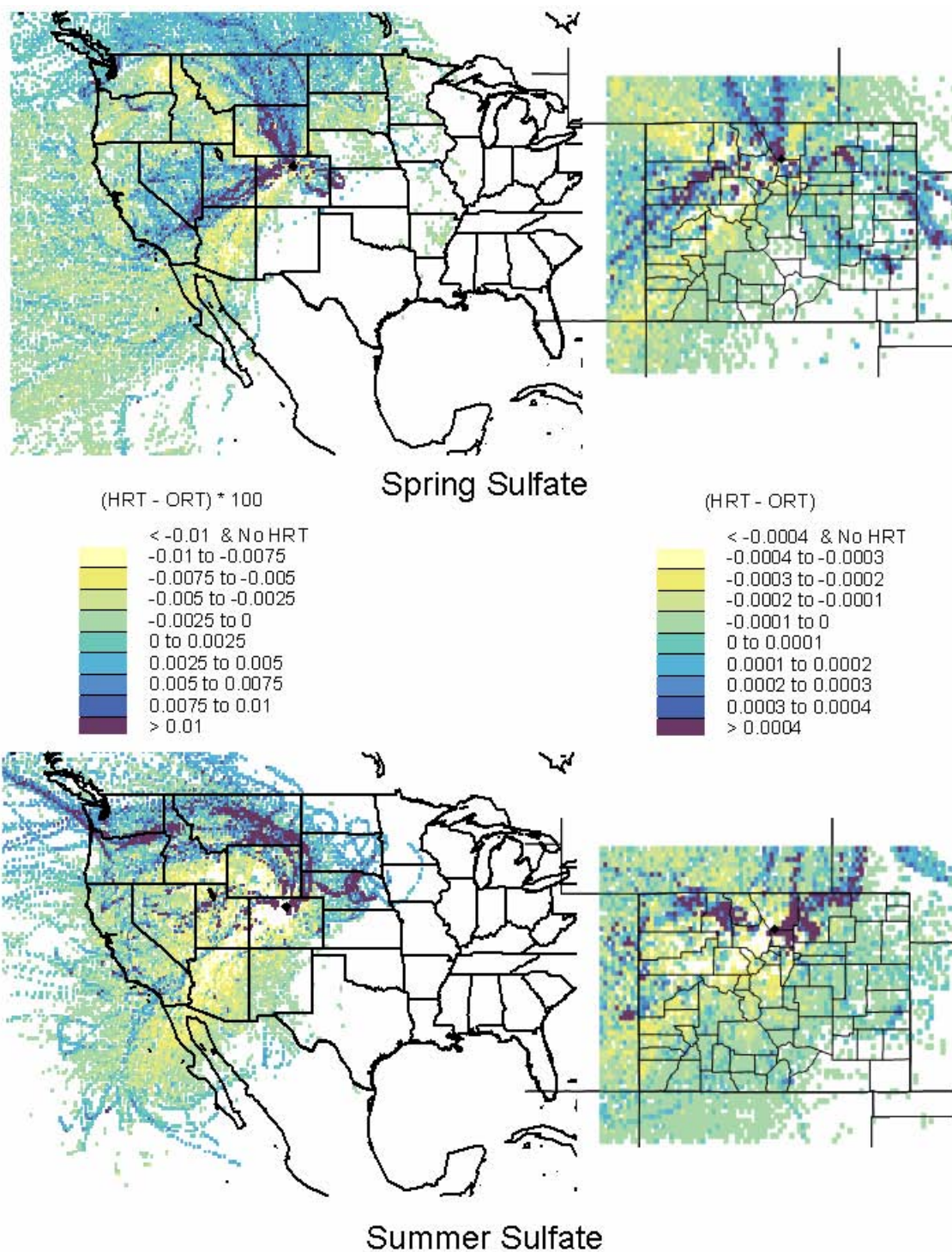


Figure 5.84. High concentration incremental probability for SO<sub>4</sub> measured at the core site during spring (top) and summer (bottom).

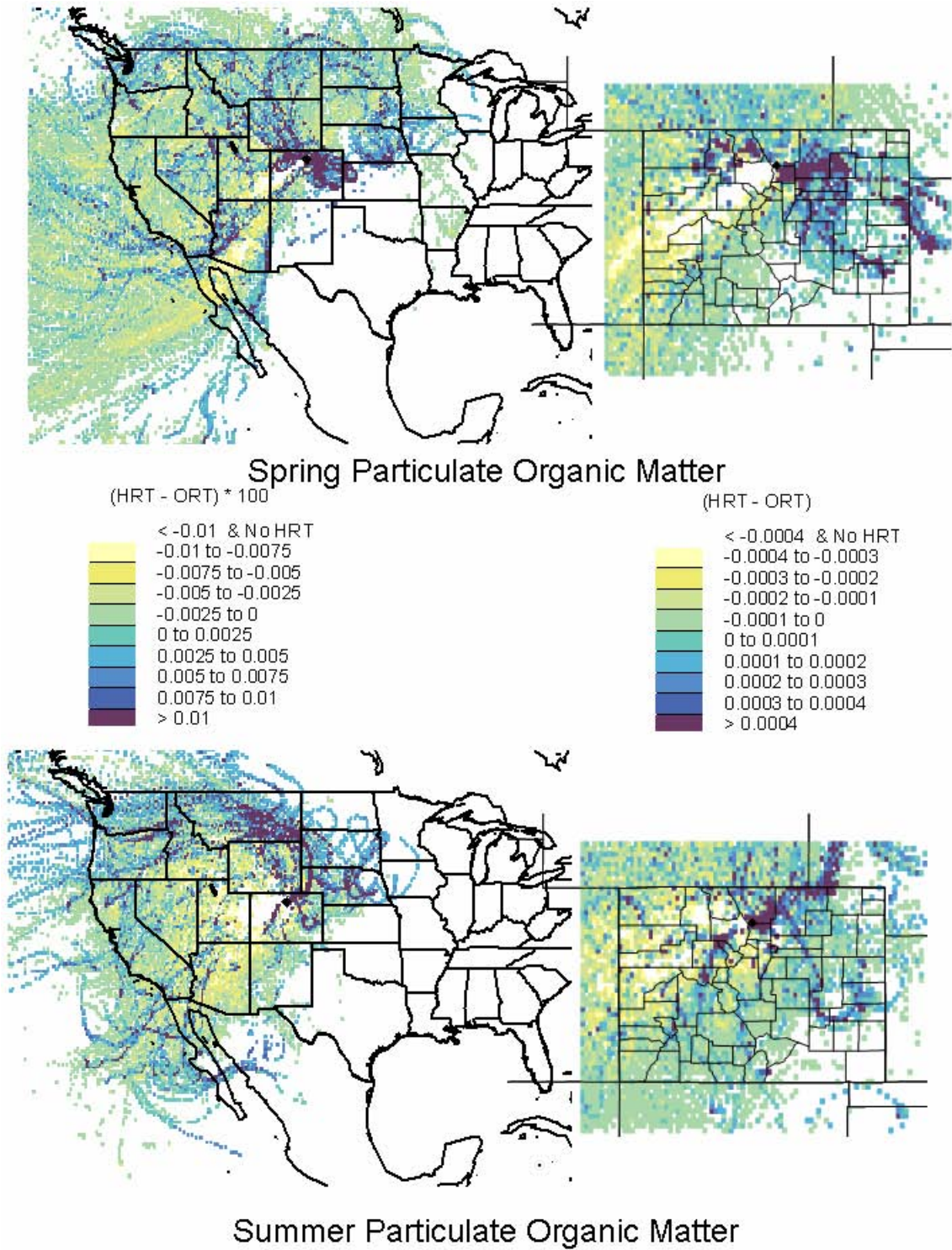


Figure 5.85. High concentration incremental probability for particulate organic matter (POM) measured at the core site during spring (top) and summer (bottom).

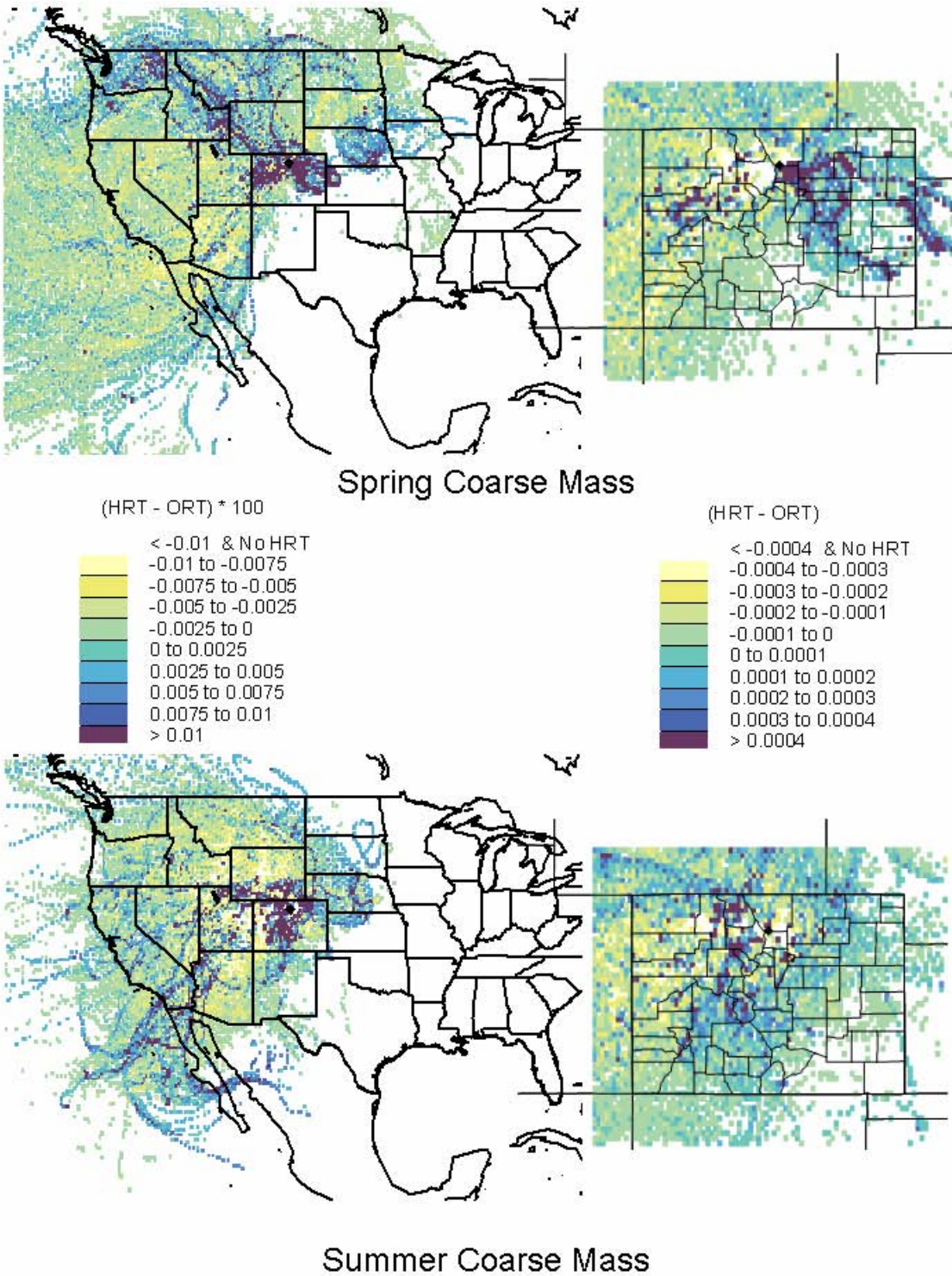


Figure 5.86. High concentration incremental probability for coarse mass measured at the core site during spring (top) and summer (bottom).

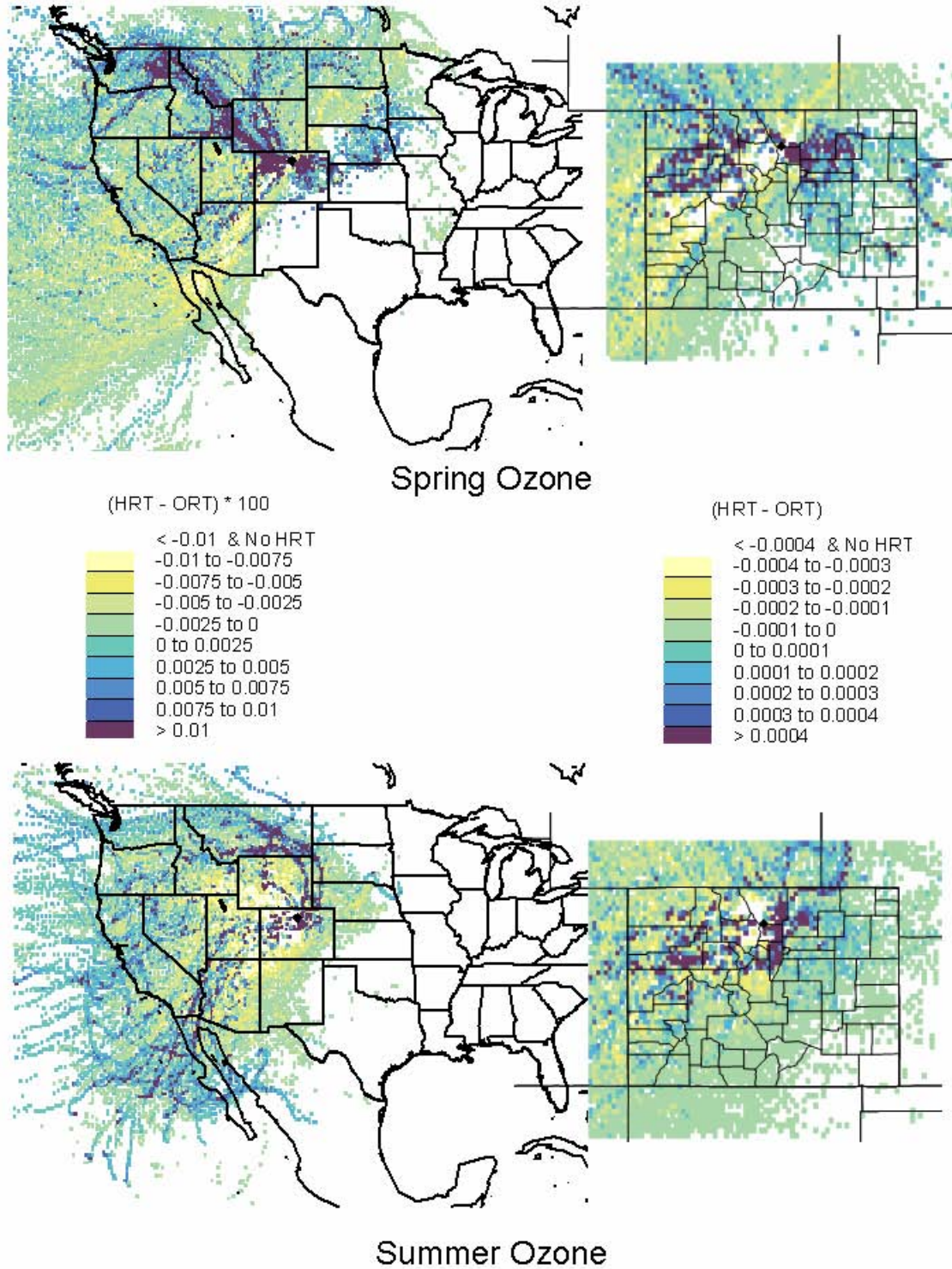
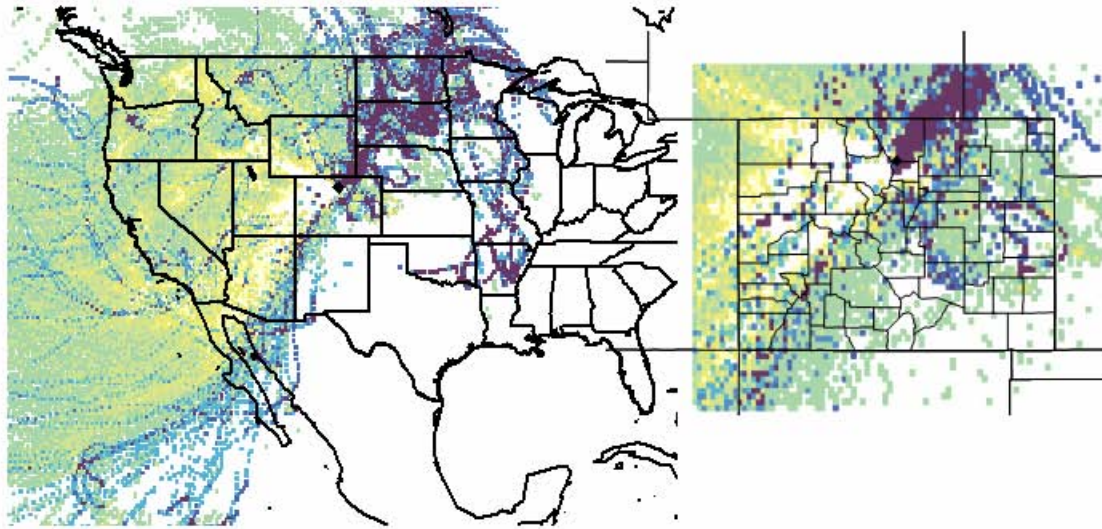
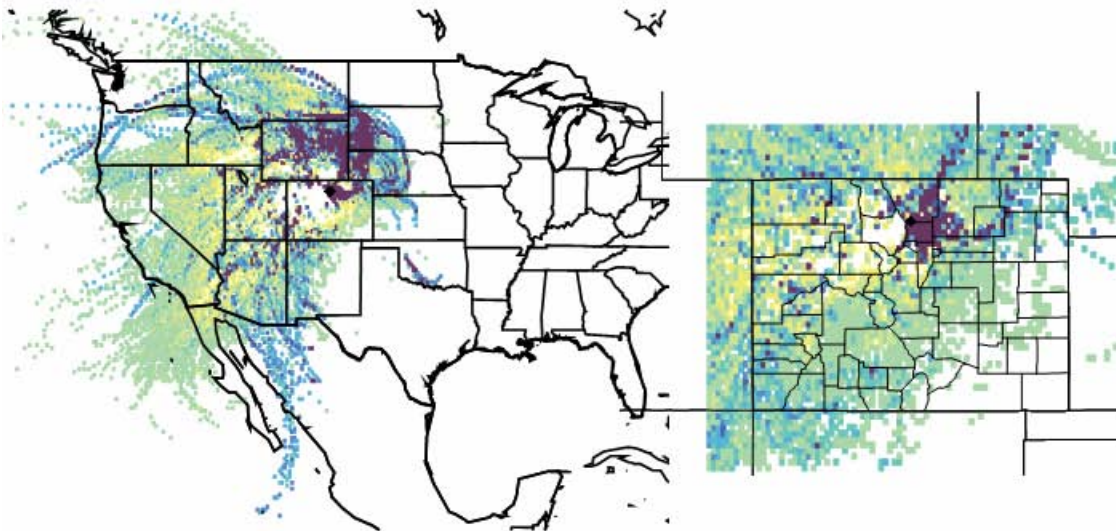
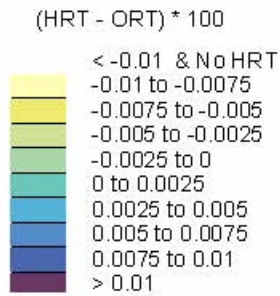


Figure 5.87. High concentration incremental probability for O<sub>3</sub> measured at the core site during spring (top) and summer (bottom).



Spring Precipitation



Summer Precipitation

Figure 5.88. High concentration incremental probability for precipitation measured at the core site during spring (top) and summer (bottom).

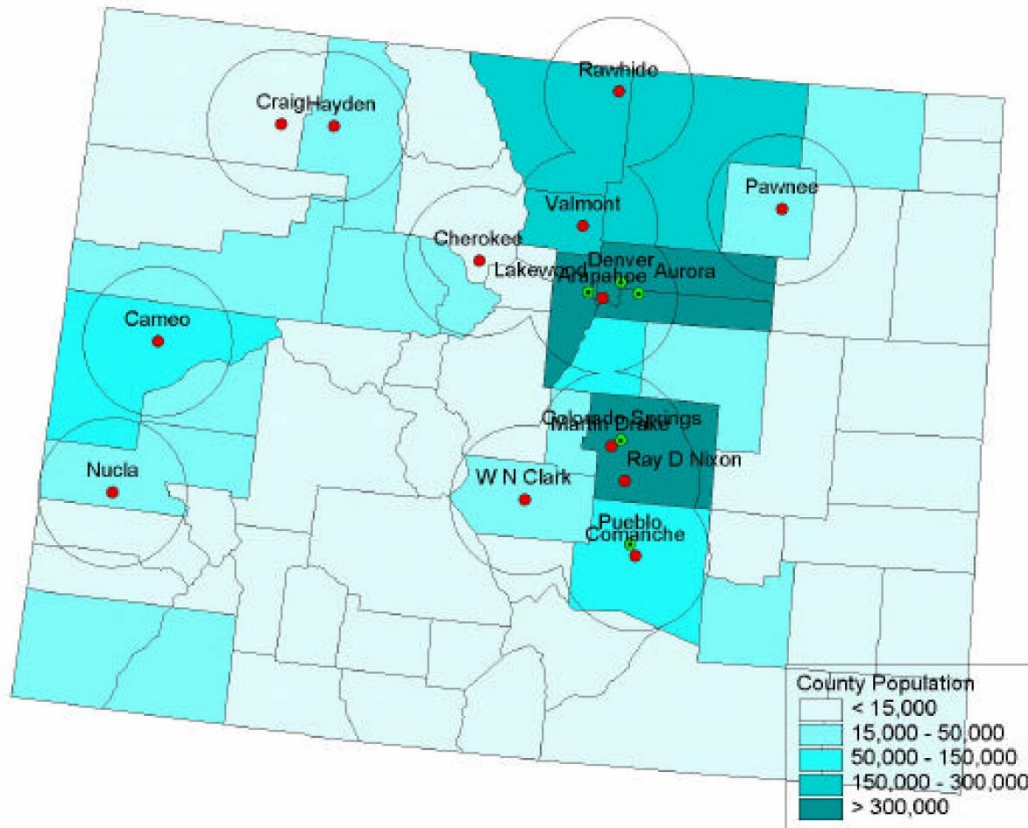


Figure 5.89. Location of Colorado coal-fired power plants (red dots) in the year 2000. The green dots represent the major urban centers.

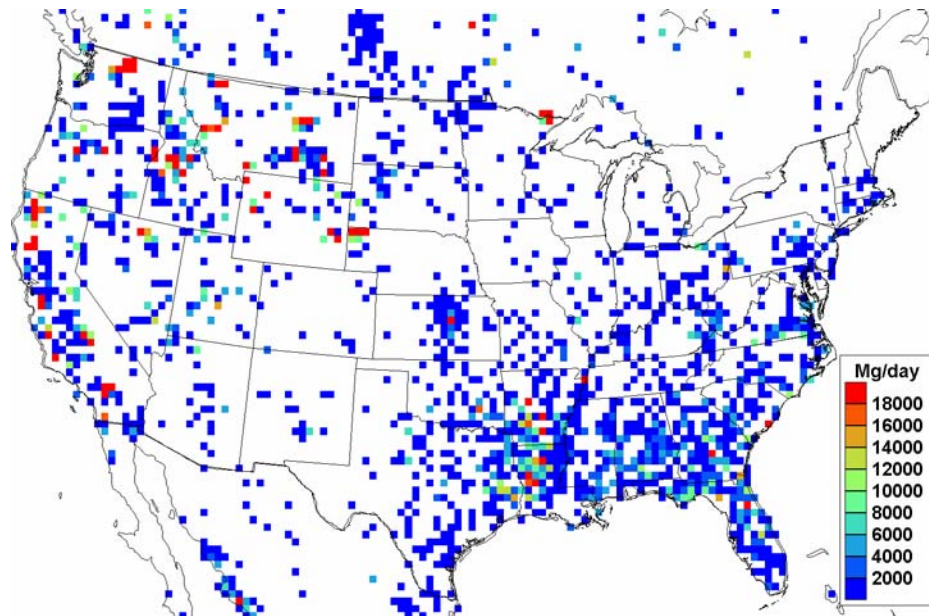


Figure 5.90. Average PM<sub>2.5</sub> emissions from biomass burning during July 7 to August 11, 2006, as estimated from a MODIS retrieval algorithm (Wiedinmyer et al., 2006).

### 5.3.4. Trajectory Mass Balance

The Trajectory Mass Balance (TrMB) Model (Pitchford and Pitchford, 1985; Iyer et al., 1987; Gebhart et al., 1988; Malm et al., 1989; Gebhart and Malm, 1989, 1994; Malm, 1992; Gebhart et al., 1993; Gebhart et al., 2006) is a special case of the general mass balance equation (Iyer et al., 1987; Malm et al., 1989) in which measured concentrations at a receptor are assumed to be linearly related to the frequency of air mass transport from a source area to the receptor by the following relationship:

$$\text{Equation 5.14. } C_{it} = \sum_{j=1}^J Q_{ijt} T_{ijt} N_{jt}$$

The subscripts i, j, and t refer to chemical species, source area, and time, respectively. C is the measured concentration, Q is the emission rate, T is a factor to account for chemical transformation, deposition, and diffusion, and N is the number of back trajectory endpoints. An endpoint is defined as the calculated position of an air parcel that eventually will arrive at the receptor. Endpoints are calculated hourly for up to 10 days back in time. In this application the only variables used explicitly are C, the hourly concentrations measured at the receptor, and N, the number of back trajectory endpoints in each source area for each day. Trajectory lengths were limited to 1–5 days and the lowest 1–3 km, depending on species. The remaining term, QT, called the “transfer coefficients,” is estimated by ordinary least squares (OLS) regression for each source, such that Equation 5.14 simplifies to Equation 5.15 where

$$\text{Equation 5.15. } C_t = \bar{a}_0 + \sum_{j=1}^J \bar{a}_j N_{jt} + \text{error}_t$$

The subscript i has been dropped for simplicity since we are now dealing with a single, measured species. The species concentrations at the receptor per endpoint in the source region are  $a = QT$  and are the regression coefficients with units of concentration per endpoint. These are estimates of the average relationship between air mass residence time in the source area and measured values at the receptor. The intercept was fixed at 0, forcing all identified source areas to account for the measured concentrations. Although emissions and precipitation data are available for RoMANS, they have not been included in the modeling. Note that whenever a quantity is replaced by its average, the error increases.

The error, as shown in Equation 5.16, is due to the deviations of the unknown terms from the mean plus measurement error:

$$\text{Equation 5.16. } \text{error}_t = \sum_{j=1}^J (a_{jt} - \bar{a}_j) N_{jt} + \text{measurement error}$$

TrMB source areas are chosen based on several criteria. First, areas are chosen based on interest in the attributions from the area, e.g., separating the influence of sources in Colorado from sources outside the state. Second, sources near the receptor can be smaller than sources farther away, due to the inherent error in trajectory endpoint locations as the time from the receptor increases and because emissions from more distant sources have usually experienced more

dispersion than emissions from closer areas. Third, model performance is better if the source areas have significant emissions of the pollutant of interest and if all or most trajectories passing through the source region would be expected to have similar exposure to emissions, dispersion, and transformation en route to the receptor. Finally, to avoid collinearities between source regions, the timing and number of trajectories passing through each region should be reasonably independent from other regions. It is often difficult to choose areas that simultaneously satisfy all criteria. For this assessment, three sets of source areas, one for ammonia and ammonium shown in Figure 5.91, one for nitrate, shown in Figure 5.92, and one for sulfur dioxide and sulfate, shown in Figure 5.93, were chosen.

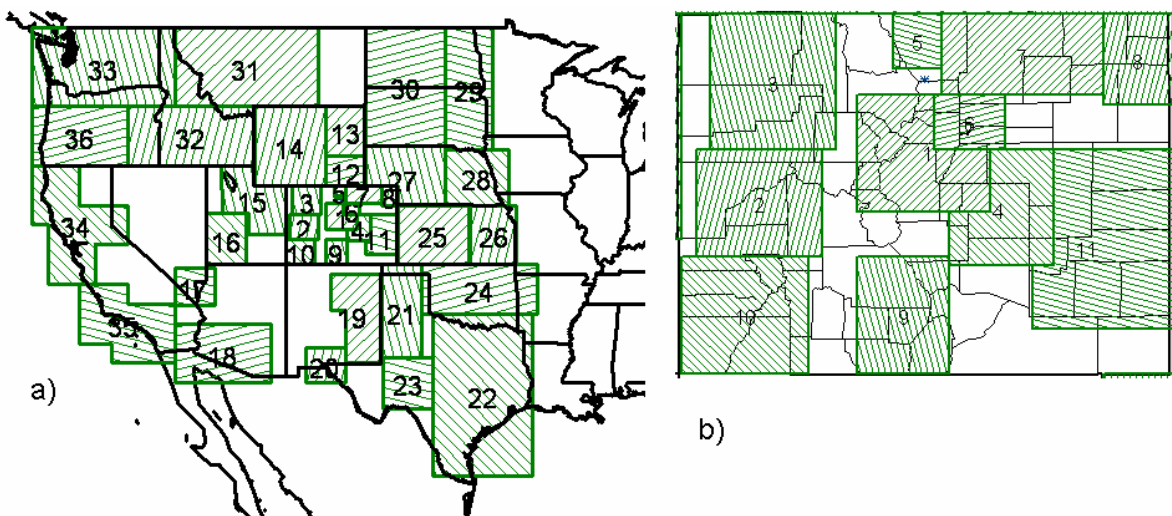


Figure 5.91. Maps of source areas used for TrMB analyses for ammonia and ammonium concentrations. The western United States is shown in a) and the state of Colorado is shown in b).

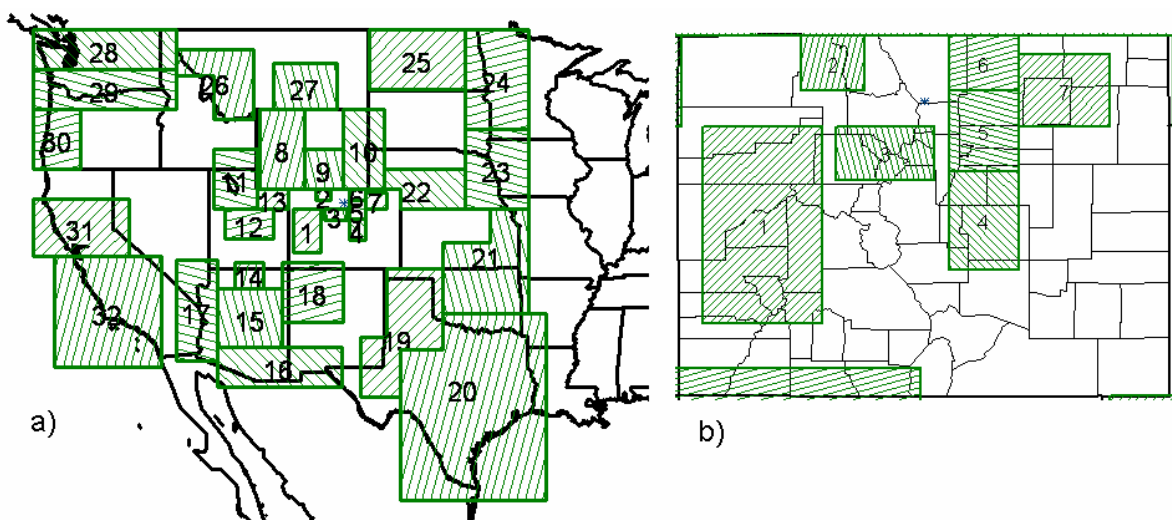


Figure 5.92. Maps of source areas used for TrMB analyses for nitrate concentrations. The western United States is shown in a) and the state of Colorado is shown in b).

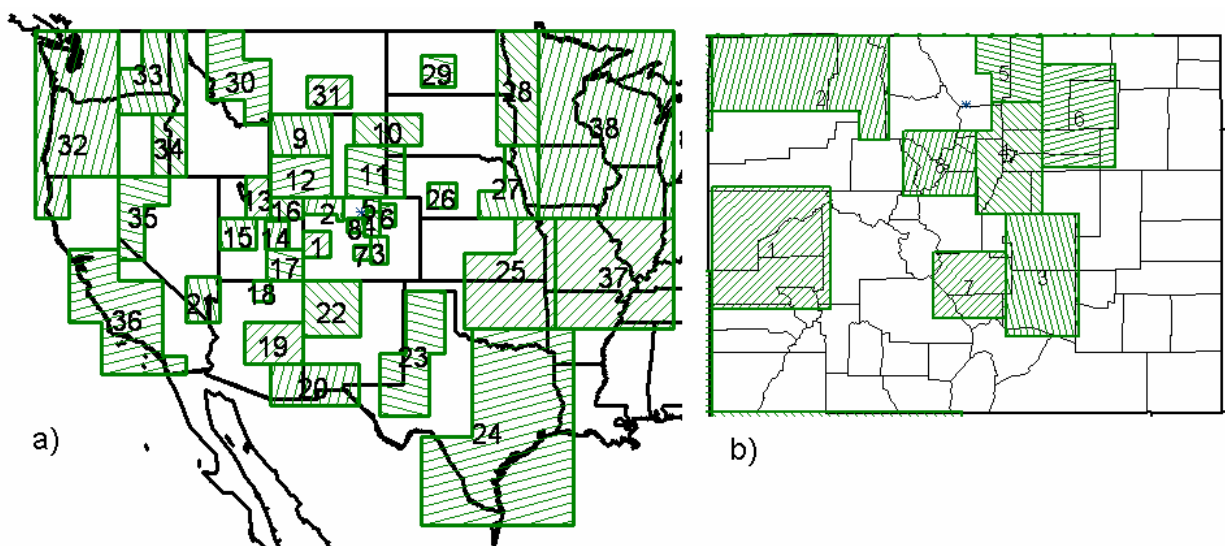


Figure 5.93. Maps of source areas used for TrMB analyses for sulfur dioxide and sulfate concentrations. The western United States is shown in a) and the state of Colorado is shown in b).

Collinearities between source areas were investigated using the variance inflation factor (VIF) (Belsley et al., 1980):

$$\text{Equation 5.17. } VIF_j = \frac{1}{1 - R_j^2}$$

where  $R_j^2$  is the multiple correlation coefficient of the endpoints in source area  $j$ , regressed on the endpoints in the remaining source areas. A high value indicates that the endpoints in a single source region could be nearly explained by a linear combination of the endpoints in the remaining source regions. A VIF greater than 10 is considered to have strong collinearity. Another indication of collinearities between source areas is the correlation matrix of the endpoints, although correlations can only reveal collinearities between pairs of source areas, e.g., source 1 with source 2, and not cases where two or more source areas could be linearly combined to predict another. A further indication of collinearities is large standard errors for the regression coefficients.

An assumption of TrMB is that errors in trajectories are random; however, there can be regionally and seasonally dependent biases in trajectories that would lead to large errors in the mean TrMB source attributions. TrMB is more sensitive to errors of trajectory placement on high concentration days than on low concentration days. Furthermore, source attributions for individual observations can be very inaccurate even when the study-long mean attributions are predicted accurately. TrMB is also not able to estimate attributions from sources very near the receptor and therefore it is not possible to estimate the influence of emissions within the park itself or from very nearby, such as from Estes Park. However, despite these caveats, TrMB has proven useful in previous studies, especially when used as part of a comprehensive assessment involving several source apportionment techniques (Gebhart et al., 2006).

The detailed results of the TrMB analyses for ambient concentrations of ammonia, ammonium, nitrate, sulfur dioxide, and sulfate measured at the RoMANS core site are shown in Tables 5.7–5.16. Spring is defined as March 27 to April 30, 2006, and summer is July 7 to August 11, 2006. These tables show the regression coefficient and standard error, T statistic, P value, VIF, total number of back trajectory endpoints, mean predicted concentration, mean percent attribution, relative percent attribution, and number of hours when a back trajectory arrived from each source areas. The relative percent attributions are calculated by setting negative attributions to 0 and then normalizing all positive values to a sum of 100%. The reported uncertainties for these values are based only on the standard error of the regression coefficient. The captions for Tables 5.7–5.16 also give additional details about each model run including the trajectory start heights, endpoint heights, and trajectory lengths and some aggregated statistics including the mean observed and modeled concentrations and the  $R^2$  between hourly observed and modeled values. Trajectory lengths were limited to 3 days for ammonia because ammonia deposits and reacts quickly and has a shorter lifetime in the atmosphere than other species such as sulfate. Similarly, because ammonia is emitted near the ground, as opposed to being emitted from elevated stacks, only trajectory endpoints that were within 1 km of the ground were considered likely to have picked up emissions.

Table 5.17 summarizes all the TrMB results for all species and both seasons. Because the source areas for each species are different, the smaller source regions were grouped into larger areas for comparison across species. Figures 5.94 and 5.95 show the fractions of each species estimated by TrMB to have arrived from areas within and outside Colorado for spring and summer, respectively. Figures 5.96 and 5.97 are similar but show results for the same aggregated areas as in Table 5.17.

TrMB estimates that during both spring and summer, most of the ammonia (71% spring and 67% summer) and approximately half the ammonium and half the sulfur dioxide were from within Colorado, while only 15–25% of the nitrate and 19–27% of the sulfate were from Colorado. The fractions from within the state did not vary substantially between the seasons, except that there were smaller fractions of nitrate and sulfate from within the state during the summer.

The areas of Colorado that contributed the most varied by species and season. The largest contribution to summer ammonia was from northeastern Colorado (31%), with western Colorado and the Front Range contributing 21% and 6%, respectively. During the spring, western Colorado was estimated to contribute 22% of the ammonia, while northeastern Colorado (16%) and the Front Range (19%) contributed slightly less. Western Colorado had the largest in-state contribution to both sulfur dioxide and sulfate during both seasons, but during the summer season, TrMB estimates that more sulfate came from Wyoming than from western Colorado. The Colorado Front Range was the largest source of nitrate during the spring (18%), but during the summer, when concentrations were very low, TrMB estimated that the largest fractions arrived from Wyoming (22%) and Utah (15%), with western Colorado (13%) being a larger source during this time than the Front Range (2%).

**Table 5.7.** Results of TrMB source apportionment analyses for spring ammonia. Trajectory start heights were 50 and 100 m. Trajectories were limited to 100 m above ground and 3 days in length. See Figure 5.89 for a map of source areas. Areas without trajectory endpoints are not shown in the table. N = 437 hours,  $R^2 = 0.515$ , mean observed =  $0.191 \mu\text{g}/\text{m}^3$ , mean predicted =  $0.136 \mu\text{g}/\text{m}^3$ . Source areas 12 and 13 were combined due to collinearity.

Source Area	Coef.±SE	T	P	VIF	Total Ends	Mean Pred conc ( $\mu\text{g}/\text{m}^3$ )	% Pred Conc	Rel. % ± unc	No. hrs hit
1 CO Ski Country	0.012 ±0.002	6.740	0.000	1.1	881	0.024	21	18 ±3	164
2 CO Mesa, Delta, Montrose	0.007 ±0.002	3.660	0.000	1.1	770	0.012	17	9 ±2	145
3 CO Craig	0.005 ±0.001	3.920	0.000	1.1	1161	0.013	16	10 ±2	163
4 CO Springs, Pueblo	0.053 ±0.01	5.160	0.000	1.7	52	0.006	1	5 ±1	10
5 CO N Larimer	0.062 ±0.016	3.760	0.000	1.1	43	0.006	4	4 ±1	25
6 CO Denver	0.009 ±0.003	3.160	0.000	1.3	330	0.007	3	5 ±2	44
7 CO Weld, Morgan	0.014 ±0.001	10.430	0.000	1.5	675	0.022	7	16 ±2	67
8 CO Sterling	-0.005 ±0.009	-0.510	0.610	1.8	36	0.000	0	0 ±1	3
9 CO Alamosa	0.012 ±0.012	1.000	0.320	1.0	17	0.000	0	0 ±0	2
10 CO Cortez, Durango	0.017 ±0.007	2.350	0.020	1.1	112	0.004	4	3 ±1	39
11 CO La Junta, Hugo	0.006 ±0.005	1.270	0.200	2.4	90	0.001	0	1 ±1	6
<b>Total From Colorado</b>								<b>71%</b>	
12 & 13 WY East	0.005 ±0.002	2.260	0.020	1.0	114	0.001	1	1 ±0	17
14 WY West	0.004 ±0.001	3.230	0.000	1.2	620	0.006	5	4 ±1	51
15 UT Northeast	0.005 ±0.003	1.810	0.070	1.4	463	0.005	7	4 ±2	67
16 UT Southwest	0.003 ±0.008	0.320	0.750	1.4	73	0.000	1	0 ±1	12
17 NV Las Vegas	0.002 ±0.006	0.370	0.710	1.2	80	0.000	1	0 ±1	14
18 AZ South	0.007 ±0.002	3.480	0.000	1.0	297	0.005	4	4 ±1	25
19 NM East	0.052 ±0.053	0.990	0.320	1.0	4	0.000	0	0 ±0	2
25 KS West	0.006 ±0.002	2.530	0.010	2.8	256	0.004	1	3 ±1	7
27 NE West	0.008 ±0.003	3.120	0.000	2.3	241	0.005	1	3 ±1	12
28 NE East	0.001 ±0.004	0.300	0.770	1.5	77	0.000	0	0 ±1	5
29 ND SD East	0.002 ±0.002	0.820	0.410	1.0	153	0.001	1	0 ±1	7
30 ND SD West	0.003	2.700	0.010	1.1	410	0.003	1	2 ±1	13

Source Area	Coef.±SE	T	P	VIF	Total Ends	Mean Pred conc (µg/m <sup>3</sup> )	% Pred Conc	Rel. % ± unc	No. hrs hit
	±0.001								
31 MT	0.004 ±0.003	1.640	0.100	1.2	186	0.002	1	1 ±1	20
32 ID South	0.001 ±0.001	1.060	0.290	1.3	508	0.001	2	1 ±1	31
33 WA	0.003 ±0.001	2.760	0.010	1.2	561	0.004	3	3 ±1	22
34 CA North	-0.001 ±0.003	-0.250	0.800	1.2	144	0.000	0	0 ±1	16
35 CA South	-0.003 ±0.004	-0.660	0.510	1.2	103	-0.001	-2	0 ±1	10
36 OR	0.006 ±0.004	1.660	0.100	1.1	61	0.001	0	1 ±0	6

**Table 5.8.** Results of TrMB source apportionment analyses for summer ammonia. Trajectory start heights were 50 and 100m. Trajectories were limited to 100 m above ground and 3 days in length. See Figure 5.89 for a map of source areas. Areas with no trajectory endpoints are not shown in the table. N = 607 hours, R<sup>2</sup> = 0.301, mean observed = 0.447 µg/m<sup>3</sup>, mean predicted = 0.309 µg/m<sup>3</sup>.

Source Area	Coef.±SE	T	P	VIF	Total Ends	Mean Pred conc (µg/m <sup>3</sup> )	% Pred Conc	Rel. % ± unc	No. hrs hit
1 CO Ski Country	0.012 ±0.002	5.38	0.00	1.1	1667	0.032	14	10 ±2	194
2 CO Mesa, Delta, Montrose	0.014 ±0.004	3.83	0.00	1.1	872	0.020	9	6 ±2	124
3 CO Craig	0.009 ±0.002	5.34	0.00	1.1	2903	0.043	22	14 ±3	278
4 CO Springs, Pueblo	-0.013 ±0.009	-1.35	0.18	2.5	194	-0.004	-2	0 ±1	17
5 CO N Larimer	0.035 ±0.018	1.94	0.05	1.1	144	0.008	4	3 ±1	59
6 CO Denver	0.002 ±0.002	0.67	0.51	1.2	1363	0.004	2	1 ±2	112
7 CO Weld, Morgan	0.014 ±0.001	10.62	0.00	1.5	3939	0.092	21	29 ±3	180
9 CO Alamosa	0.046 ±0.018	2.60	0.01	1.0	85	0.006	2	2 ±1	21
10 CO Cortez, Durango	0.005 ±0.007	0.79	0.43	1.0	207	0.002	1	1 ±1	29
11 CO La Junta, Hugo	0.012 ±0.014	0.84	0.40	2.5	97	0.002	0	1 ±1	6
<b>Total From Colorado</b>								<b>67%</b>	
12 WY Southeast	0.137 ±0.013	10.52	0.00	1.6	153	0.034	3	11 ±1	23
13 WY Northeast	0.006 ±0.029	0.20	0.84	2.1	36	0.000	0	0 ±1	5
14 WY West	0.008 ±0.002	3.95	0.00	1.0	1335	0.017	6	5 ±1	92
15 UT Northeast	0.006 ±0.002	3.48	0.00	1.1	1615	0.017	8	5 ±2	125

Source Area	Coef.±SE	T	P	VIF	Total Ends	Mean Pred conc (µg/m <sup>3</sup> )	% Pred Conc	Rel. % ± unc	No. hrs hit
16 UT Southwest	0.012 ±0.006	1.90	0.06	1.1	252	0.005	2	2 ±1	25
17 NV Las Vegas	0.031 ±0.03	1.01	0.32	1.1	28	0.001	0	0 ±0	7
18 AZ South	0.018 ±0.013	1.40	0.16	1.0	30	0.001	0	0 ±0	1
20 NM Las Cruces, Juarez	0.03 ±0.063	0.47	0.64	1.0	6	0.000	0	0 ±0	1
27 NE West	0.013 ±0.004	3.47	0.00	1.5	344	0.007	1	2 ±1	19
28 NE East	-0.018 ±0.075	-0.24	0.81	1.4	6	0.000	0	0 ±0	1
30 ND SD West	-0.009 ±0.011	-0.84	0.40	1.7	51	-0.001	0	0 ±0	5
31 MT	0.038 ±0.008	4.69	0.00	1.1	129	0.008	1	3 ±1	9
32 ID South	0.007 ±0.003	1.90	0.06	1.1	636	0.007	4	2 ±1	43
33 WA	0.074 ±0.015	5.03	0.00	1.0	44	0.005	1	2 ±0	4
34 CA North	0.041 ±0.042	0.96	0.34	1.0	9	0.001	0	0 ±0	1

**Table 5.9.** Results of TrMB source apportionment analyses for spring ammonium. Trajectory start heights were 50, 100, 200, 500, and 1000 m. Trajectories were limited to 1000m above ground and 5 days in length. See Figure 5.89 for a map of source areas. Areas with no trajectory endpoints are not shown in the table. N = 607 hours, R<sup>2</sup> = 0.290, mean observed = 0.273 µg/m<sup>3</sup>, mean predicted = 0.203 µg/m<sup>3</sup>.

Source Area	Coef.±SE	T	P	VIF	Total Ends	Mean Pred conc (µg/m <sup>3</sup> )	% Pred Conc	Rel % ± unc	No. hrs hit
1 CO Ski Country	0.004 ±0.001	4.59	0.00	1.4	6670	0.034	19	14 ±4	444
2 CO Mesa, Delta, Montrose	0.002 ±0.001	2.01	0.05	1.6	6616	0.014	10	6 ±4	400
3 CO Craig	0.001 ±0	2.40	0.02	1.3	8757	0.014	11	6 ±3	477
4 CO Springs, Pueblo	0.011 ±0.004	2.97	0.00	3.1	453	0.007	1	3 ±1	25
5 CO N Larimer	0.016 ±0.003	5.38	0.00	1.4	811	0.018	7	7 ±2	131
6 CO Denver	-0.001 ±0.001	-0.99	0.32	1.6	1470	-0.003	4	0 ±1	63
7 CO Weld, Morgan	0.004 ±0.001	3.70	0.00	2.8	3048	0.015	1	6 ±2	105
8 CO Sterling	0.01 ±0.007	1.35	0.18	4.9	224	0.003	0	1 ±1	12
9 CO Alamosa	0.001 ±0.004	0.24	0.81	1	137	0.000	0	0 ±0	8
10 CO Cortez, Durango	0.004 ±0.002	2.46	0.01	1.4	2066	0.013	9	5 ±3	253
11 CO La Junta,	0.003	1.15	0.25	6	545	0.002	0	1 ±1	11

## DRAFT

Source Area	Coef.±SE	T	P	VIF	Total Ends	Mean Pred conc (µg/m <sup>3</sup> )	% Pred Conc	Rel % ± unc	No. hrs hit
Hugo	±0.003								
<b>Total From Colorado</b>								<b>50%</b>	
12 WY Southeast	0.02 ±0.003	5.98	0.00	4.3	1019	0.028	1	12 ±2	91
13 WY Northeast	-0.013 ±0.004	- 2.87	0.00	4.8	478	-0.009	0	0 ±1	34
14 WY West	0.001 ±0.001	2.06	0.04	1.6	5512	0.009	5	4 ±2	205
15 UT Northeast	0.003 ±0.001	2.99	0.00	1.5	3652	0.016	7	6 ±3	257
16 UT Southwest	0.002 ±0.003	0.89	0.38	1.8	1070	0.004	1	1 ±2	141
17 NV Las Vegas	0.007 ±0.002	2.72	0.01	1.6	1144	0.011	4	4 ±2	138
18 AZ South	0 ±0	0.62	0.54	1.2	4677	0.002	1	1 ±2	183
19 NM East	0.003 ±0.028	0.10	0.92	6.7	35	0.000	0	0 ±1	4
20 NM Las Cruces, Juarez	-0.005 ±0.007	- 0.73	0.47	1.1	66	0.000	0	0 ±0	4
21 TX Panhandle	-0.005 ±0.04	- 0.13	0.89	6.7	16	0.000	0	0 ±0	1
22 TX East	0.002 ±0.004	0.43	0.67	4.9	232	0.001	0	0 ±1	5
24 OK	0 ±0.006	- 0.05	0.96	4.8	156	0.000	0	0 ±1	8
25 KS West	0.003 ±0.002	1.08	0.28	8.7	799	0.003	0	1 ±1	15
26 KS East	-0.001 ±0.006	- 0.18	0.86	1	83	0.000	0	0 ±0	6
27 NE West	-0.007 ±0.002	- 3.40	0.00	4.6	1147	-0.011	4	0 ±2	43
28 NE East	0.01 ±0.002	6.76	0.00	2	691	0.010	2	4 ±1	19
29 ND SD East	-0.001 ±0.001	- 1.90	0.06	3	2308	-0.005	0	0 ±1	34
30 ND SD West	0.001 ±0.001	0.77	0.44	3.2	3470	0.002	-1	1 ±2	49
31 MT	0.005 ±0.001	4.44	0.00	1.9	2659	0.018	8	7 ±2	117
32 ID South	-0.001 ±0.001	- 1.75	0.08	1.6	5059	-0.007	-2	0 ±2	164
33 WA	-0.001 ±0.001	- 1.20	0.23	3.8	6318	-0.007	-4	0 ±3	119
34 CA North	0.002 ±0.001	2.53	0.01	1.4	2418	0.008	5	3 ±2	152
35 CA South	0.003 ±0.001	3.29	0.00	1.2	2461	0.011	4	4 ±2	145
36 OR	0 ±0.001	0.15	0.88	2.9	2785	0.001	0	0 ±2	100

**Table 5.10.** Results of TrMB source apportionment analyses for summer ammonium. Trajectory start heights were 50, 100, 200, 500, and 1000 m. Trajectories were limited to 1000m in height and 5 days in length. See Figure 5.89 for a map of source areas. Areas with no trajectory endpoints are not shown in the table. N = 715 hours,  $R^2 = 0.07$ , mean observed =  $0.336 \mu\text{g}/\text{m}^3$ , mean predicted =  $0.281 \mu\text{g}/\text{m}^3$ .

Source Area	Coef.±SE	T	P	VIF	Total Ends	Mean Pred conc ( $\mu\text{g}/\text{m}^3$ )	% Pred Conc	Rel % ± unc	No. hrs hit
1 CO Ski Country	0.002±0	6.39	0.00	1.2	9637	0.032	13	11±2	442
2 CO Mesa, Delta, Montrose	0.001±0.001	1.66	0.10	1.6	7297	0.009	4	3±2	348
3 CO Craig	0.002±0	5.79	0.00	1.6	17616	0.042	16	15±3	518
4 CO Springs, Pueblo	- 0.001±0.001	- 0.72	0.47	2.4	931	-0.001	0	0±1	50
5 CO N Larimer	0.006±0.001	4.50	0.00	1.2	2213	0.019	7	7±2	301
6 CO Denver	0±0.001	0.83	0.41	1.6	4729	0.003	1	1±1	202
7 CO Weld, Morgan	0.002±0	6.07	0.00	1.6	12645	0.028	9	10±2	267
8 CO Sterling	0.008±0.02 0±0.002	0.40 -	0.69 0.94	1.2 1.1	25 678	0.000 0.000	0 0	0±0 0±1	9 70
9 CO Alamosa		0.08							
10 CO Cortez, Durango	0.004±0.001	3.54	0.00	1.3	1909	0.011	4	4±1	184
11 CO La Junta, Hugo	0±0.002	0.19	0.85	2.7	411	0.000	0	0±0	20
<b>Total From Colorado</b>								<b>51%</b>	
12 WY Southeast	0.004±0.002	2.07	0.04	1.7	1406	0.007	2	2±1	166
13 WY Northeast	0.003±0.002	1.50	0.13	1.9	998	0.004	1	1±1	83
14 WY West	0.001±0	2.93	0.00	1.5	11322	0.013	4	5±2	352
15 UT Northeast	0.002±0	7.07	0.00	1.4	12226	0.037	13	13±2	460
16 UT Southwest	0±0.001	0.11	0.91	1.6	3648	0.000	0	0±2	287
17 NV Las Vegas	0.001±0.001	0.86	0.39	1.4	1717	0.003	1	1±1	184
18 AZ South	0.004±0.001	4.59	0.00	1.1	2073	0.012	6	4±1	165
19 NM East	0.001±0.003	0.39	0.70	1.1	319	0.001	0	0±0	34
20 NM Las Cruces, Juarez	0.003±0.002	1.38	0.17	1.0	354	0.001	1	1±0	27
21 TX Panhandle	- 0.009±0.011	- 0.80	0.43	5.9	71	-0.001	-1	0±0	4
22 TX East	-0.01±0.019	- 0.54	0.59	1.3	12	0.000	0	0±0	1
23 TX SW	0.008±0.011	0.68	0.50	3.5	84	0.001	0	0±0	9
24 OK	0.036±0.116	0.31	0.76	3.1	3	0.000	0	0±0	1
25 KS West	0.004±0.005	0.73	0.47	1.8	90	0.000	0	0±0	7
27 NE West	0.001±0.001	2.21	0.03	2.2	2127	0.004	1	1±1	54
28 NE East	0±0.002	- 0.22	0.83	3.7	576	0.000	0	0±0	12
29 ND SD East	0.002±0.003	0.64	0.52	2.9	307	0.001	0	0±0	16
30 ND SD West	0.002±0.001	1.52	0.13	1.5	1129	0.003	1	1±1	51
31 MT	0.001±0	4.03	0.00	1.5	5278	0.009	2	3±1	106
32 ID South	0.001±0	4.10	0.00	1.2	7753	0.013	4	4±1	208
33 WA	0.004±0	8.19	0.00	1.3	2382	0.013	3	5±1	66
34 CA North	0.005±0.001	5.95	0.00	1.1	1656	0.012	3	4±1	86
35 CA South	0.002±0.001	2.73	0.01	1.2	1616	0.005	2	2±1	97

DRAFT

Source Area	Coef.±SE	T	P	VIF	Total Ends	Mean Pred conc (µg/m <sup>3</sup> )	% Pred Conc	Rel % ± unc	No. hrs hit
36 OR	0.001±0.001	0.70	0.49	1.2	1069	0.001	0	0±1	44

**Table 5.11.** Results of TrMB source apportionment analyses for spring nitrate. Trajectory start heights were 50, 100, 200, 500, and 1000 m. Trajectories were limited to 5 days in length and 3000m in height. See Figure 5.90 for a map of source areas. Areas with no trajectory endpoints are not shown in the table. N = 343 hours, R<sup>2</sup> = 0.464, mean observed = 0.466 µg/m<sup>3</sup>, mean predicted = 0.425 µg/m<sup>3</sup>.

Source Area	Coef.±SE	T	P	VIF	Total Ends	Mean Pred conc (µg/m <sup>3</sup> )	% Pred Conc	Relative % ± unc	No. hrs hit
1 CO Mesa, Delta, Montrose	0.001±0.001	0.56	0.58	2.1	8409	0.018	2	3±8	226
2 CO Craig	- 0.002±0.004	- 0.39	0.69	3.2	1846	-0.009	0	0±6	107
3 CO Ski Country	0±0.002	0.13	0.89	1.5	4072	0.003	3	1±6	198
4 CO Springs, Pueblo	0.034±0.011	2.99	0.00	2.8	362	0.036	4	7±3	32
5 CO Denver	0.007±0.003	2.86	0.00	3.2	2166	0.045	6	8±4	55
6 CO N Front Range	0.008±0.009	0.84	0.40	3.6	744	0.017	3	3±5	60
7 CO Weld, Morgan	0.008±0.005	1.59	0.11	2.7	571	0.013	1	2±2	24
Total From Colorado								25%	
8 WY West	- 0.008±0.003	- 2.51	0.01	4	3456	-0.080	-6	0±8	114
9 WY South	0.006±0.004	1.61	0.11	3.7	2588	0.045	9	8±7	128
10 WY East	0.003±0.003	0.77	0.44	3.7	1949	0.014	3	3±5	78
11 UT SLC	0.002±0.003	0.54	0.59	2.5	2434	0.013	-1	2±6	109
12 UT Central	0.008±0.004	1.89	0.06	1.6	1274	0.032	7	6±4	93
13 UT NE	- 0.008±0.008	- 0.96	0.34	1.6	571	-0.013	55	0±3	75
14 AZ NGS	0.006±0.007	0.92	0.36	1.8	935	0.017	16	3±5	126
15 AZ Central	- 0.002±0.002	- 1.44	0.15	1.5	3329	-0.023	-30	0±4	151
16 AZ NM South	0.001±0.003	0.32	0.75	2	1317	0.004	3	1±3	62
17 NV CA AZ Las Vegas	0.006±0.002	2.91	0.00	2.2	4090	0.076	22	14±6	157
18 NM 4 Corners	0.003±0.005	0.61	0.54	2.2	1225	0.010	9	2±4	99
19 TX Panhandle	- 0.014±0.028	- 0.50	0.62	1.1	21	-0.001	-1	0±0	2
21 OK KS East	- 0.144±0.582	- 0.25	0.80	1.2	1	0.000	0	0±0	1
22 NE South	0.001±0.005	0.12	0.91	2.4	489	0.001	0	0±2	14
23 NE IA Border	0.031±0.005	6.86	0.00	2.1	439	0.040	2	7±1	19
24 ND SD MN Border	0.001±0.002	0.74	0.46	1.5	1596	0.006	1	1±2	34
25 ND	0.003±0.002	1.33	0.19	1.8	1480	0.012	1	2±2	53
26 MT West	0.006±0.004	1.33	0.19	3.3	1573	0.027	0	5±5	69
27 MT South	0.007±0.006	1.16	0.25	2.6	848	0.018	9	3±4	52

Source Area	Coef.±SE	T	P	VIF	Total Ends	Mean Pred conc (µg/m <sup>3</sup> )	% Pred Conc	Relative % ± unc	No. hrs hit
28 WA North	0.001±0.002	0.58	0.57	2.5	2301	0.009	4	2±4	62
29 WA OR	0.001±0.002	-	0.66	2.7	2696	-0.007	-4	0±4	68
30 OR Coast	0.01±0.006	1.67	0.10	2.2	653	0.019	6	4±3	40
31 CA North	0.005±0.003	1.59	0.11	1.6	1717	0.024	-38	4±4	96
32 CA South	0.002±0.001	1.71	0.09	1.6	5869	0.038	12	7±6	155

**Table 5.12.** Results of TrMB source apportionment analyses for summer nitrate. Trajectory start heights were 50, 100, 200, 500, and 1000 m. Trajectories were limited to 5 days in length and 3000m in height. See Figure 5.90 for a map of source areas. Areas with no trajectory endpoints are not shown in the table. N = 425 hours, R<sup>2</sup> = 0.108, mean observed = 0.227 µg/m<sup>3</sup>, mean predicted = 0.202 µg/m<sup>3</sup>.

Source Area	Coef.±SE	T	P	VIF	Total Ends	Mean Pred conc (µg/m <sup>3</sup> )	% Pred Conc	Relative % ± unc	No. hours hit
1 CO Mesa, Delta, Montrose	0.001±0	1.81	0.07	1.4	14325	0.022	17	9±6	284
2 CO Craig	0±0.001	0.00	1.00	1.2	4099	0.000	0	0±5	255
3 CO Ski Country	0.001±0.001	0.95	0.34	1.2	7522	0.010	8	4±5	271
4 CO Springs, Pueblo	0.002±0.003	0.91	0.36	1.4	688	0.004	3	2±2	64
5 CO Denver	0±0.001	-	0.86	2.2	6830	-0.002	-2	0±5	153
6 CO N Front Range	0.001±0.001	-	0.55	1.7	2619	-0.005	-5	0±4	127
7 CO Weld, Morgan	0.002±0.004	-	0.68	1.4	446	-0.002	-2	0±2	41
<b>Total From Colorado</b>								<b>15%</b>	
8 WY West	0±0.001	-	0.94	2.2	7883	-0.001	-1	0±7	235
9 WY South	0.001±0.001	1.31	0.19	2	6199	0.017	14	7±6	219
10 WY East	0.004±0.001	3.70	0.00	2.6	3890	0.035	16	15±5	137
11 UT SLC	0.001±0.001	1.43	0.15	1.3	5813	0.015	9	6±5	213
12 UT Central	0.001±0.001	-	0.64	1.5	4610	-0.006	-5	0±6	236
13 UT NE	0.003±0.001	1.97	0.05	1.4	3123	0.021	11	9±5	220
14 AZ NGS	0.004±0.002	2.17	0.03	1.8	2422	0.025	15	10±6	180
15 AZ Central	0±0.001	0.38	0.70	1.9	4297	0.003	2	1±4	154
16 AZ NM South	0.001±0.002	-	0.50	1.4	1332	-0.003	-3	0±3	56
17 NV CA AZ Las Vegas	0.002±0.001	1.86	0.06	1.4	5794	0.023	11	10±6	213
18 NM 4 Corners	0.001±0.001	-	0.45	1.2	1848	-0.004	-5	0±2	75
19 TX Panhandle	0.004±0.015	0.25	0.81	2	77	0.001	1	0±1	9
21 OK KS East	0.001±0.011	-	0.94	2	78	0.000	0	0±1	6
22 NE South	-	-	0.26	2.1	945	-0.004	-3	0±2	19

Source Area	Coef.±SE	T	P	VIF	Total Ends	Mean Pred conc (µg/m <sup>3</sup> )	% Pred Conc	Relative % ± unc	No. hours hit
	0.002±0.001	1.12							
23 NE IA Border	0.011±0.007	1.65	0.10	6.2	245	0.007	2	3±2	9
24 ND SD MN Border	-0.01±0.009	- 1.14	0.26	5.4	142	-0.003	-1	0±1	6
25 ND	- 0.011±0.008	- 1.25	0.21	1.3	127	-0.003	-2	0±1	14
26 MT West	0±0.001	- 0.31	0.76	1.8	2308	-0.002	-1	0±3	75
27 MT South	0.002±0.001	1.34	0.18	2.6	2377	0.011	5	5±4	75
28 WA North	0.001±0.004	0.33	0.74	1.8	356	0.001	0	1±2	24
29 WA OR	0.003±0.001	3.25	0.00	1.5	2180	0.015	4	6±2	57
30 OR Coast	- 0.001±0.004	- 0.29	0.77	1.3	473	-0.001	0	0±2	34
31 CA North	0.002±0.001	1.65	0.10	1.2	1762	0.008	4	4±3	72
32 CA South	0.002±0.001	2.91	0.00	1.3	3808	0.020	8	9±3	139

**Table 5.13.** Results of TrMB source apportionment analyses for spring sulfur dioxide. Trajectory start heights were 50, 100, 200, 500, and 1000 m. Trajectories were limited to 5 days in length and 3000 m in height. See Figure 5.91 for a map of source areas. Areas with no trajectory endpoints are not shown in the table. N = 595 hours, R<sup>2</sup> = 0.223, mean observed = 0.148 µg/m<sup>3</sup>, mean predicted = 0.126 µg/m<sup>3</sup>.

Source Area	Coef.±SE	T	P	VIF	Total Ends	Mean Pred conc (µg/m <sup>3</sup> )	% Pred Conc	Relative % ± unc	No. hours hit
1 CO Mesa, Delta, Montrose	0.002±0.001	3.29	0.00	1.8	7488	0.024	16	13±6	391
2 CO Craig	0.003±0.001	4.93	0.00	2.9	6376	0.037	50	20±6	333
3 CO Springs, Pueblo	0.007±0.003	1.99	0.05	1.8	287	0.003	1	2±1	25
4 CO Denver	0.002±0.001	2.51	0.01	1.6	2347	0.007	3	4±2	62
5 CO N Larimer	0±0.004	- 0.11	0.91	5.1	856	-0.001	-1	0±4	75
6 CO Weld, Morgan	0.002±0.001	1.70	0.09	2.6	952	0.003	2	2±1	39
7 CO Canon City	- 0.022±0.018	- 1.22	0.22	1.4	35	-0.001	-2	0±1	10
8 CO Ski Country	0.002±0.001	2.71	0.01	1.5	4537	0.018	14	10±5	356
<b>Total From Colorado</b>								<b>50%</b>	
9 WY NW	- 0.002±0.001	- 1.71	0.09	2.5	2060	-0.007	-17	0±3	125
10 WY NE	0±0.002	- 0.17	0.86	1.8	730	0.000	-1	0±2	54
11 WY SE	0±0.001	0.39	0.69	3.2	2694	0.001	4	1±3	108
12 WY SW	0.001±0.001	1.02	0.31	4.6	6047	0.010	14	5±7	196
13 UT SLC	0±0.002	0.18	0.86	1.8	1025	0.001	0	0±3	127
14 UT E Central	- 0.001±0.002	- 0.34	0.73	1.6	1264	-0.001	-2	0±3	135
15 UT West	0.006±0.003	2.11	0.04	1.8	878	0.008	7	4±3	118

Source Area	Coef.±SE	T	P	VIF	Total Ends	Mean Pred conc (µg/m <sup>3</sup> )	% Pred Conc	Relative % ± unc	No. hours hit
16 UT NE	- 0.002±0.002	- 0.81	0.42	1.6	797	-0.003	-2	0±3	119
17 UT SE	0±0.001	0.13	0.90	2.8	4719	0.001	2	1±7	328
18 AZ NGS	0.004±0.003	1.35	0.18	1.8	1137	0.007	7	4±4	205
19 AZ E Central	0.002±0.001	3.27	0.00	1.5	4680	0.014	11	8±3	249
20 AZ NM South	- 0.001±0.002	- 0.62	0.53	1.6	807	-0.001	-1	0±2	59
21 NV Las Vegas	- 0.001±0.001	- 0.54	0.59	1.6	2069	-0.002	-11	0±3	161
22 NM 4 Corners	0.002±0.001	1.53	0.13	1.8	1707	0.006	4	3±3	139
23 TX Panhandle	0.004±0.009	0.44	0.66	1.3	33	0.000	0	0±0	2
24 TX East	0.001±0.004	0.12	0.90	5.8	220	0.000	0	0±1	6
25 OK KS East	- 0.002±0.004	- 0.37	0.71	5.7	233	-0.001	-1	0±1	7
26 NE West	- 0.001±0.008	- 0.15	0.88	2.2	87	0.000	-1	0±1	9
27 NE IA Border	0.003±0.002	1.56	0.12	2.4	419	0.002	1	1±1	18
28 ND SD MN Border	0.001±0.001	0.46	0.64	2.3	1300	0.001	5	1±2	44
29 ND Central	0±0.002 0±0.001	0.18 -	0.86 0.64	1.5 2.3	436 2871	0.000 -0.002	1 -4	0±1 0±3	43 109
30 MT West		0.47							
31 MT South	0.002±0.005	0.43	0.67	1.5	164	0.001	4	0±1	25
32 WA OR West	0.003±0	9.01	0.00	1.8	6635	0.035	29	19±3	137
33 WA OR ID	- 0.003±0.001	- 5.23	0.00	3.1	5948	-0.026	-24	0±4	122
34 OR ID South	- 0.001±0.001	- 1.18	0.24	1.4	1500	-0.003	-12	0±2	94
35 NV CA	0.001±0.001	1.06	0.29	1.8	1794	0.004	7	2±3	104
36 CA South	- 0.001±0.001	- 1.49	0.14	1.7	5772	-0.008	-4	0±4	249
37 MO IL	0±0.001	0.08	0.94	2.8	523	0.000	0	0±1	6
38 MI MN IA IL	0±0.001	- 0.18	0.86	4.7	1243	-0.001	-2	0±2	40

**Table 5.14.** Results of TrMB source apportionment analyses for summer sulfur dioxide. Trajectory start heights were 50, 100, 200, 500, and 1000 m. Trajectories were limited to 5 days in length. See Figure 5.91 for a map of source areas. Areas with no trajectory endpoints are not shown in the table. N = 596 hours,  $R^2 = 0.135$ , mean observed =  $0.158 \mu\text{g}/\text{m}^3$ , mean predicted =  $0.147 \mu\text{g}/\text{m}^3$ .

Source Area	Coef.±SE	T	P	VIF	Total Ends	Mean Pred conc (µg/m <sup>3</sup> )	% Pred Conc	Relative % ± unc	No. hours hit
1 CO Mesa, Delta, Montrose	0±0	0.72	0.47	1.5	11135	0.003	4	2±3	430
2 CO Craig	0.001±0	3.84	0.00	1.3	15518	0.022	21	14±4	591

## DRAFT

Source Area	Coef.±SE	T	P	VIF	Total Ends	Mean Pred conc (ug/m <sup>3</sup> )	% Pred Conc	Relative % ± unc	No. hours hit
3 CO Springs, Pueblo	- 0.002±0.001	- 2.07	0.04	1.3	877	-0.003	-4	0±1	61
4 CO Denver	0.001±0	3.15	0.00	1.6	10082	0.011	6	7±3	284
5 CO N Larimer	0.002±0.001	3.42	0.00	1.6	4641	0.012	6	8±3	275
6 CO Weld, Morgan	0.002±0.001	2.49	0.01	1.8	2102	0.007	3	4±2	145
7 CO Canon City	0.003±0.001	1.91	0.06	1.2	969	0.003	3	2±1	92
8 CO Ski Country	0.001±0	4.74	0.00	1.2	9965	0.019	15	12±3	430
<b>Total From Colorado</b>								<b>49%</b>	
9 WY NW	0±0	- 0.16	0.87	1.6	6230	-0.001	-1	0±2	223
10 WY NE	- 0.002±0.001	- 1.49	0.14	2.7	1959	-0.004	-3	0±2	112
11 WY SE	0.002±0	4.63	0.00	2.2	9939	0.023	14	15±4	369
12 WY SW	0±0	0.40	0.69	2.1	14616	0.002	2	2±4	424
13 UT SLC	0±0.001	- 0.51	0.61	1.6	4282	-0.002	-2	0±3	304
14 UT E Central	- 0.001±0.001	- 0.96	0.34	1.5	4208	-0.003	-4	0±3	331
15 UT West	0.001±0.001	1.09	0.28	1.8	3821	0.005	4	3±3	324
16 UT NE	0±0.001	0.49	0.63	1.5	5346	0.002	2	1±3	377
17 UT SE	0±0	0.70	0.48	1.8	10130	0.004	5	3±4	438
18 AZ NGS	0.002±0.001	1.93	0.05	1.4	2466	0.007	7	4±2	258
19 AZ E Central	0.001±0	1.16	0.25	1.6	4075	0.003	3	2±2	185
20 AZ NM South	0±0.001	0.31	0.76	1.5	1965	0.001	1	0±2	94
21 NV Las Vegas	0.002±0.001	2.58	0.01	1.4	3587	0.008	6	5±2	275
22 NM 4 Corners	0±0	- 0.39	0.69	1.2	3497	-0.001	-2	0±2	151
23 TX Panhandle	- 0.001±0.002	- 0.29	0.77	1.2	416	0.000	-1	0±1	30
24 TX East	- 0.003±0.004	- 0.88	0.38	1.4	170	-0.001	0	0±1	14
25 OK KS East	- 0.001±0.002	- 0.48	0.63	1.4	257	0.000	0	0±0	6
26 NE West	- 0.003±0.002	- 1.39	0.16	1.7	508	-0.002	-2	0±1	33
27 NE IA Border	0.003±0.002	1.53	0.13	2.6	369	0.001	0	1±1	11
28 ND SD MN Border	0.004±0.006	0.56	0.58	7.5	163	0.001	0	0±1	9
29 ND Central	0.016±0.009	1.72	0.09	1.4	44	0.001	0	1±0	6
30 MT West	0±0.001	- 0.58	0.56	1.6	3217	-0.001	-1	0±2	145
31 MT South	0.002±0.001	1.69	0.09	1.8	1992	0.004	3	2±2	110
32 WA OR West	0.001±0.001	0.97	0.33	2.3	3462	0.003	2	2±2	111
33 WA OR ID	0±0.001	0.36	0.72	2	2485	0.001	1	0±1	91

Source Area	Coef.±SE	T	P	VIF	Total Ends	Mean Pred conc (µg/m <sup>3</sup> )	% Pred Conc	Relative % ± unc	No. hours hit
34 OR ID South	0±0.001	-0.23	0.82	1.6	2215	0.000	-1	0±2	134
35 NV CA	0.003±0.001	2.66	0.01	1.1	1606	0.005	3	3±1	127
36 CA South	0.001±0	3.42	0.00	1.3	4998	0.009	6	6±2	235
38 MI MN IA IL	-0.003±0.01	-0.25	0.80	7.4	60	0.000	0	0±1	2

**Table 5.15.** Results of TrMB source apportionment analyses for spring sulfate. Trajectory start heights were 50, 100, 200, 500, and 1000 m. Trajectories were limited to 5 days in length and 10 km in height. See Figure 5.91 for a map of source areas. Areas with no trajectory endpoints are not shown in the table. N = 687 hours, R<sup>2</sup> = 0.397, mean observed = 0.607 µg/m<sup>3</sup>, mean predicted = 0.542 µg/m<sup>3</sup>.

Source Area	Coef.±SE	T	P	VIF	Total Ends	Mean Pred conc (µg/m <sup>3</sup> )	% Pred Conc	Relative % ± unc	No. hours hit
1 CO Mesa, Delta, Montrose	0.001±0.001	1.05	0.3	1.8	8993	0.016	4	2±3	453
2 CO Craig	0.004±0.001	2.93	0	2.8	6989	0.043	13	6±3	372
3 CO Springs, Pueblo	0±0.008	0.03	0.98	2	274	0	0	0±1	30
4 CO Denver	0±0.002	-0.21	0.83	1.6	2233	-0.001	0	0±1	63
5 CO N Larimer	0.028±0.008	-3.52	0	4	757	-0.031	-6	0±2	79
6 CO Weld, Morgan	0.011±0.003	4.43	0	2.6	874	0.014	1	2±1	36
7 CO Canon City	0.052±0.035	-1.49	0.14	1.5	50	-0.004	0	0±0	15
8 CO Ski Country	0.009±0.002	4.29	0	1.5	4844	0.06	14	9±3	397
<b>Total From Colorado</b>								<b>19%</b>	
9 WY NW	0.008±0.002	3.84	0	2.2	2585	0.031	4	4±1	143
10 WY NE	0.001±0.006	-0.1	0.92	2.9	835	-0.001	0	0±1	81
11 WY SE	0.03±0.003	10.24	0	4.5	3029	0.132	15	19±2	139
12 WY SW	0.003±0.002	-1.78	0.08	4.8	6423	-0.033	-8	0±3	212
13 UT SLC	0.007±0.004	1.91	0.06	1.9	1507	0.016	4	2±2	159
14 UT E Central	0.002±0.003	0.78	0.44	1.8	2276	0.007	1	1±2	227
15 UT West	0.005±0.004	1.42	0.16	1.9	1714	0.014	2	2±2	181
16 UT NE	0.021±0.005	4.41	0	1.7	1116	0.034	9	5±1	147
17 UT SE	0.003±0.002	1.62	0.11	2.8	6372	0.032	8	5±4	403
18 AZ NGS	0.01±0.006	1.77	0.08	1.9	1478	0.021	5	3±2	259
19 AZ E Central	0.003±0.001	2.93	0	1.5	6662	0.027	9	4±2	289
20 AZ NM South	0.006±0.003	1.9	0.06	1.6	1094	0.01	3	1±1	83
21 NV Las Vegas	0.007±0.002	3.51	0	1.7	3923	0.038	7	6±2	274
22 NM 4	-	-0.61	0.54	1.7	2009	-0.004	-2	0±1	157

Source Area	Coef.±SE	T	P	VIF	Total Ends	Mean Pred conc (µg/m <sup>3</sup> )	% Pred Conc	Relative % ± unc	No. hours hit
Corners	0.002±0.003								
23 TX Panhandle	0±0.028	-0.01	0.99	1	15	0	0	0±0	1
24 TX East	0.012±0.008	1.51	0.13	7.5	271	0.005	-3	1±1	5
25 OK KS East	-	-1.79	0.07	6.2	237	-0.006	3	0±1	10
26 NE West	0.015±0.018	-0.85	0.4	2.3	76	-0.002	-1	0±0	9
27 NE IA Border	0±0.004	0.03	0.98	2.6	507	0	0	0±1	31
28 ND SD MN Border	0.008±0.002	3.22	0	2.5	1593	0.018	2	3±1	55
29 ND Central	0.005±0.005	-1.03	0.3	1.7	551	-0.004	-1	0±1	62
30 MT West	0.003±0.001	2	0.05	2.2	4039	0.017	4	3±2	134
31 MT South	0.04±0.006	6.53	0	2.1	759	0.045	5	6±1	86
32 WA OR West	0.003±0.001	3.32	0	2.8	7455	0.036	17	5±2	211
33 WA OR ID	-	-2.3	0.02	4.3	7567	-0.028	-15	0±2	151
34 OR ID South	0.004±0.002	-1.72	0.09	1.2	1762	-0.009	-8	0±1	127
35 NV CA	0.004±0.002	2.21	0.03	1.6	3464	0.019	4	3±2	201
36 CA South	0.003±0.001	3.39	0	1.6	12471	0.047	10	7±3	425
37 MO IL	0.015±0.007	2.09	0.04	6.6	281	0.006	-4	1±1	7
38 MI MN IA IL	-	-4.25	0	4	1390	-0.023	3	0±1	44

**Table 5.16.** Results of TrMB source apportionment analyses for summer sulfate. Trajectory start heights were 50, 100, 200, 500, and 1000 m. Trajectories were limited to 5 days in length and 10 km in height. See Figure 5.91 for a map of source areas. Areas with no trajectory endpoints are not shown in the table. N = 721 hours, R<sup>2</sup> = 0.111, mean observed = 0.666 µg/m<sup>3</sup>, mean predicted = 0.628 µg/m<sup>3</sup>.

Source Area	Coef.±SE	T	P	VIF	Total Ends	Mean Pred conc (µg/m <sup>3</sup> )	% Pred Conc	Relative % ± unc	No. hours hit
1 CO Mesa, Delta, Montrose	0.003±0	6.09	0	1.5	12712	0.047	8	7±1	434
2 CO Craig	0.004±0	9.54	0	1.4	16612	0.091	14	14±2	572
3 CO Springs, Pueblo	0±0.002	-	0.94	1.4	1222	0	0	0±0	92
4 CO Denver	0.001±0	2.21	0.03	1.6	10517	0.013	2	2±1	303
5 CO N Larimer	0.005±0.001	5.33	0	1.7	5233	0.036	5	6±1	302
6 CO Weld, Morgan	-	-	0.44	1.8	2582	-0.004	-1	0±1	163
7 CO Canon City	0.003±0.002	1.3	0.19	1.2	1201	0.004	1	1±1	108
8 CO Ski Country	0.002±0	5.22	0	1.3	10335	0.035	6	6±1	423
Total From Colorado								36%	

## DRAFT

Source Area	Coef.±SE	T	P	VIF	Total Ends	Mean Pred conc (µg/m <sup>3</sup> )	% Pred Conc	Relative % ± unc	No. hours hit
9 WY NW	0.001±0.001	1.46	0.15	1.8	6770	0.008	1	1±1	240
10 WY NE	0.004±0.002	1.92	0.06	2.8	2135	0.011	2	2±1	162
11 WY SE	0.002±0.001	3.51	0	2.5	12608	0.033	5	5±2	377
12 WY SW	0.001±0	1.42	0.16	2.3	15473	0.015	3	2±2	421
13 UT SLC	0.003±0.001	3.15	0	1.6	5193	0.022	3	3±1	375
14 UT E Central	0.002±0.001	2.1	0.04	1.5	5523	0.015	2	2±1	413
15 UT West	0.002±0.001	1.37	0.17	1.7	5485	0.013	2	2±1	385
16 UT NE	0.001±0.001	1.04	0.3	1.5	6825	0.008	1	1±1	411
17 UT SE	0.003±0.001	4.78	0	1.9	11930	0.048	8	8±2	446
18 AZ NGS	0.006±0.002	3.85	0	1.4	2844	0.024	4	4±1	282
19 AZ E Central	0.002±0.001	2.75	0.01	1.7	5701	0.013	2	2±1	220
20 AZ NM South	0.001±0.001	0.73	0.46	1.5	2717	0.003	0	0±1	119
21 NV Las Vegas	0.005±0.001	6	0	1.4	5388	0.038	6	6±1	364
22 NM 4 Corners	0±0.001	0.2	0.84	1.2	3904	0.001	0	0±1	174
23 TX Panhandle	0.002±0.005	0.47	0.64	1.2	277	0.001	0	0±0	31
24 TX East	0.003±0.004	0.86	0.39	1.2	274	0.001	0	0±0	22
25 OK KS East	0.005±0.012	0.39	0.7	1.1	26	0	0	0±0	3
26 NE West	0.002±0.003	0.61	0.54	1.6	562	0.001	0	0±0	53
27 NE IA Border	0.009±0.003	2.93	0	2.4	443	0.005	1	1±0	27
28 ND SD MN Border	0.02±0.01	2.08	0.04	7.4	166	0.005	1	1±0	10
29 ND Central	- 0.006±0.015	-0.4	0.69	1.5	50	0	0	0±0	10
30 MT West	0.001±0.001	1.6	0.11	1.9	4268	0.007	1	1±1	207
31 MT South	0.009±0.001	6.76	0	1.8	2537	0.032	4	5±1	170
32 WA OR West	0.002±0.001	2.84	0	2.7	6112	0.02	3	3±1	235
33 WA OR ID	0.004±0.001	3.97	0	2	3221	0.016	2	3±1	155
34 OR ID South	0.001±0.001	0.53	0.6	1.9	2912	0.002	0	0±1	173
35 NV CA	0.005±0.001	3.94	0	1.2	2514	0.017	3	3±1	197
36 CA South	0.004±0	8.22	0	1.4	9723	0.052	8	8±1	365
38 MI MN IA IL	- 0.041±0.016	-2.6	0.01	7.4	60	-0.003	0	0±0	2

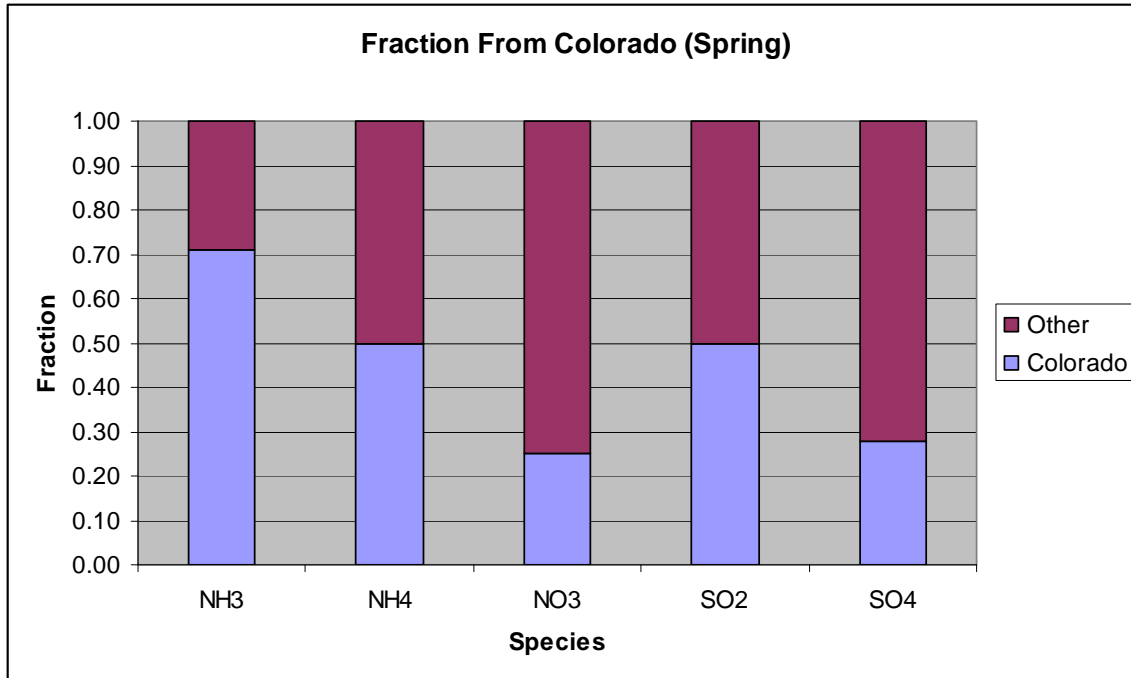


Figure 5.94. Spring TrMB modeled NH<sub>3</sub>, NH<sub>4</sub>, NO<sub>3</sub>, SO<sub>2</sub>, and SO<sub>4</sub> average fractional contributions from within and outside the state of Colorado.

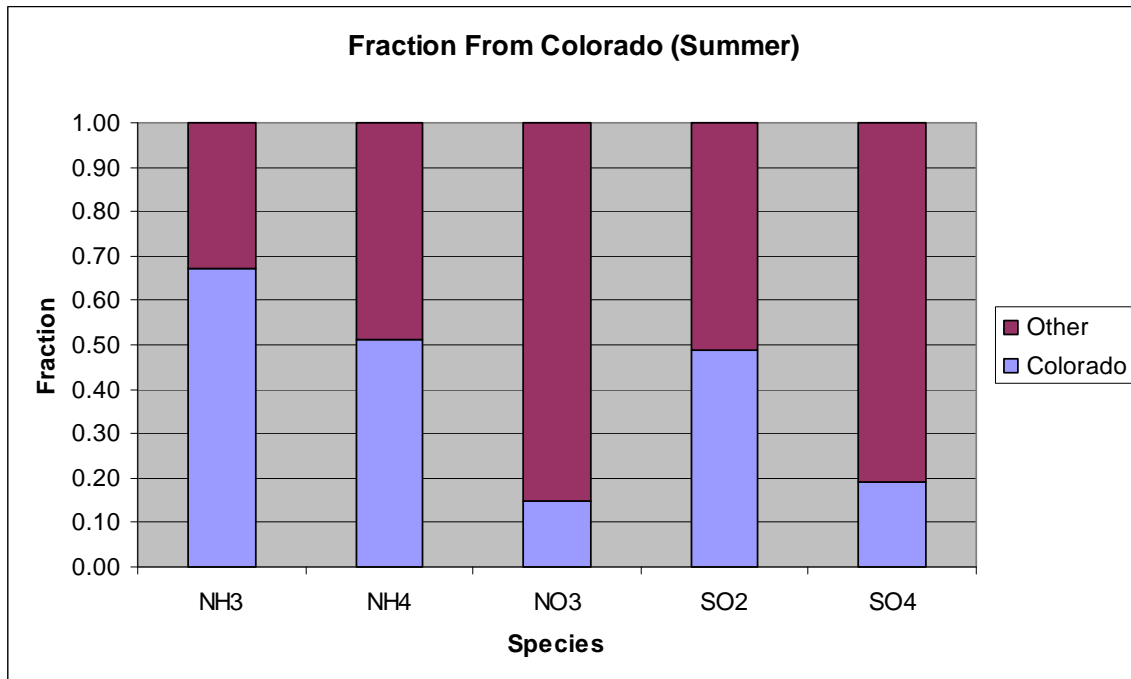


Figure 5.95. Summer TrMB modeled NH<sub>3</sub>, NH<sub>4</sub>, NO<sub>3</sub>, SO<sub>2</sub>, and SO<sub>4</sub> average fractional contributions from within and outside the state of Colorado.

**Table 5.17.** Percentage attributions to large source regions by TrMB for each season and species.

Source Area	Ammonia	Ammonium	Nitrate	Sulfur Dioxide	Sulfate
Season	Spring / Summer				
Front Range	19 / 6	10 / 7	18 / 2	6 / 15	0 / 8
NE CO	16 / 31	7 / 10	2 / 0	2 / 4	2 / 0
W CO	22 / 21	17 / 22	4 / 13	43 / 30	17 / 28
CA	0 / 0	4 / 2	7 / 9	0 / 6	7 / 8
WY	5 / 10	16 / 8	11 / 22	6 / 17	23 / 10
MT	1 / 0	0 / 4	5 / 6	0 / 2	9 / 6
ND, SD, NE, MN, IA	5 / 0	12 / 4	15 / 3	2 / 2	3 / 2
KS, OK, TX	3 / 7	1 / 1	0 / 0	0 / 0	2 / 0
AZ, NM	4 / 2	5 / 6	6 / 11	15 / 6	8 / 6
UT	4 / 2	7 / 13	8 / 15	5 / 7	15 / 16
ID, WA, OR	5 / 0	3 / 9	8 / 10	19 / 2	5 / 6
NV	0 / 0	4 / 1	14 / 10	2 / 8	9 / 9
Other	16 / 21	14 / 14	2 / 0	0 / 1	0 / 1

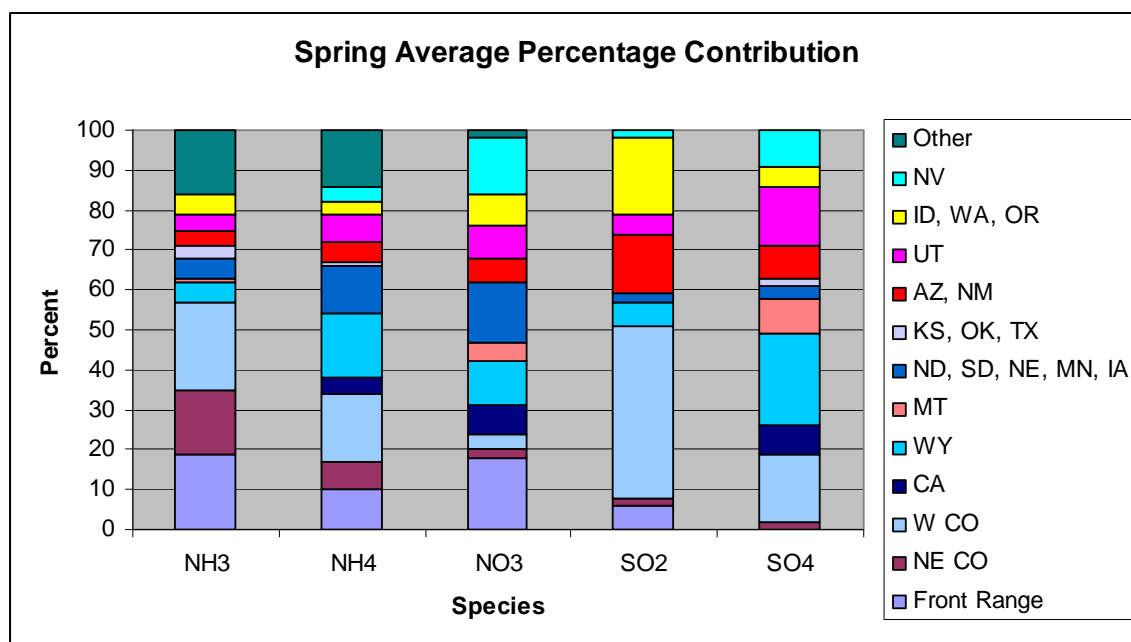


Figure 5.96. Spring TrMB modeled average percentage contribution for selected source areas.

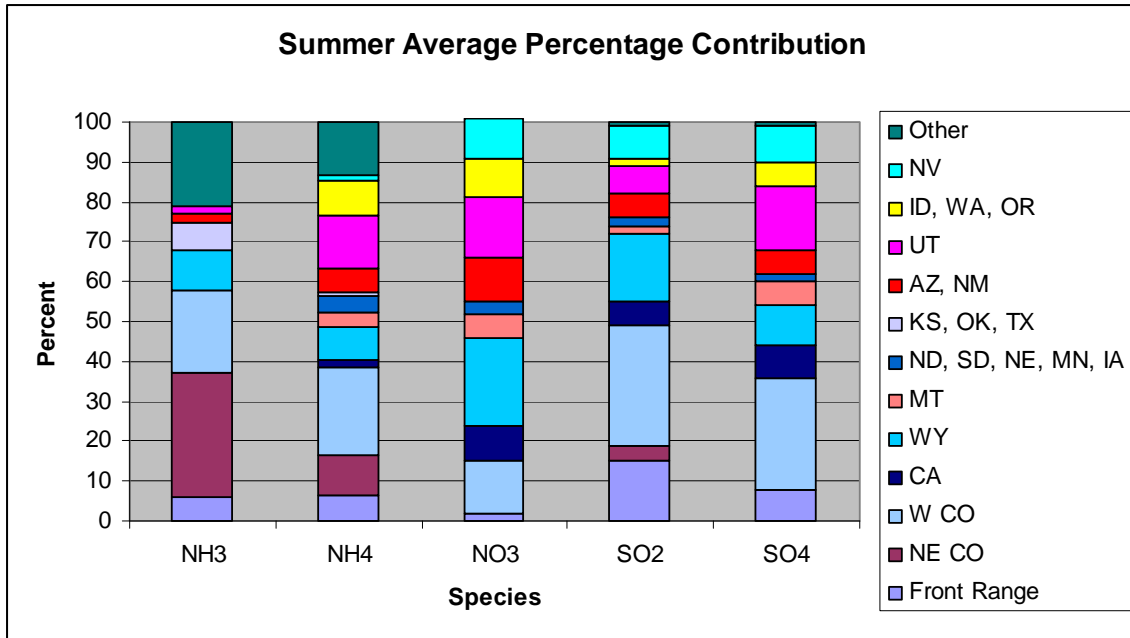


Figure 5.97. Summer TrMB modeled average percentage contribution for selected source areas.

## 5.4. EMISSION INVENTORY

### 5.4.1. Overview of Emission Inventories

An emission inventory, which defines the hourly flux of pollutants and pollutant precursors, is a key component of a chemical transport model (CTM). This study employed a detailed emission inventory developed by the WRAP (WRAP-RMC, 2005; IE, 2007). Emissions sources are typically divided into the following four categories:

- *Stationary Area Sources:* Sources that are treated as being spread over a spatial extent (usually a county or air district) and that are not movable. Because it is not possible to collect the emissions at each point of emission, they are estimated over larger regions. Examples of stationary area sources are residential heating and architectural coatings. Numerous sources such as dry cleaning facilities may be treated either as stationary area sources or as point sources.
- *Mobile Sources:* Vehicular sources that travel on roadways or off-road. These sources can be computed either as being spread over a spatial extent or as being assigned to a line location (called a link). Data in on-road inventories can be either emissions or activity data. Activity data consist of vehicle miles traveled (VMT) and, optionally, vehicle speed. MOBILE6 (U.S. EPA, 2003) is used to develop emission factors for mobile sources. Examples of on-road, mobile sources include light-duty gasoline vehicles and heavy-duty diesel vehicles.
- *Point Sources:* Sources that are identified by point locations, typically because they are regulated and their locations are available in regulatory reports. In addition, elevated point sources will have their emissions allocated vertically through the model layers, as opposed to being emitted into only the first model layer. Examples of point sources include electrical generating units (EGUs) and oil refineries.
- *Biogenic Emissions:* Emissions determined by vegetation type, which is defined by the Biogenic Emissions Landcover Database version 3 (BELD3) (U.S. EPA, 2007), and by meteorology. In addition to the anthropogenic sources listed above, vegetation can have an appreciable contribution to emissions, especially with respect to certain species of volatile organic compounds (VOCs).

Emission inventories are processed with the Sparse Matrix Operator Kernel Emissions (SMOKE) (IE, 2006) model. SMOKE is a highly optimized emissions processing system that prepares county-level or point emissions inventory data into gridded, hourly estimates of criteria and toxic pollutant fluxes formatted for input to a specific chemical mechanism within the CTM. In general, SMOKE requires an emissions inventory and temporal, spatial, and chemical allocation data to prepare emissions estimates for an air quality model. For some source categories, such as on-road mobile and stationary point sources, SMOKE also requires meteorology data to calculate emissions. SMOKE calculates biogenic emissions estimates with gridded land use, vegetative emissions factors, and meteorology data.

The emission inventory was calculated on a set of three nested Lambert-Conformal modeling domains that focus on central Colorado. The 3:1 nested domains consist of a continental U.S., 36-km domain, a 12-km domain focusing on states within the Intermountain West, and a 4-km domain covering most of the state of Colorado (Figure 5.98).

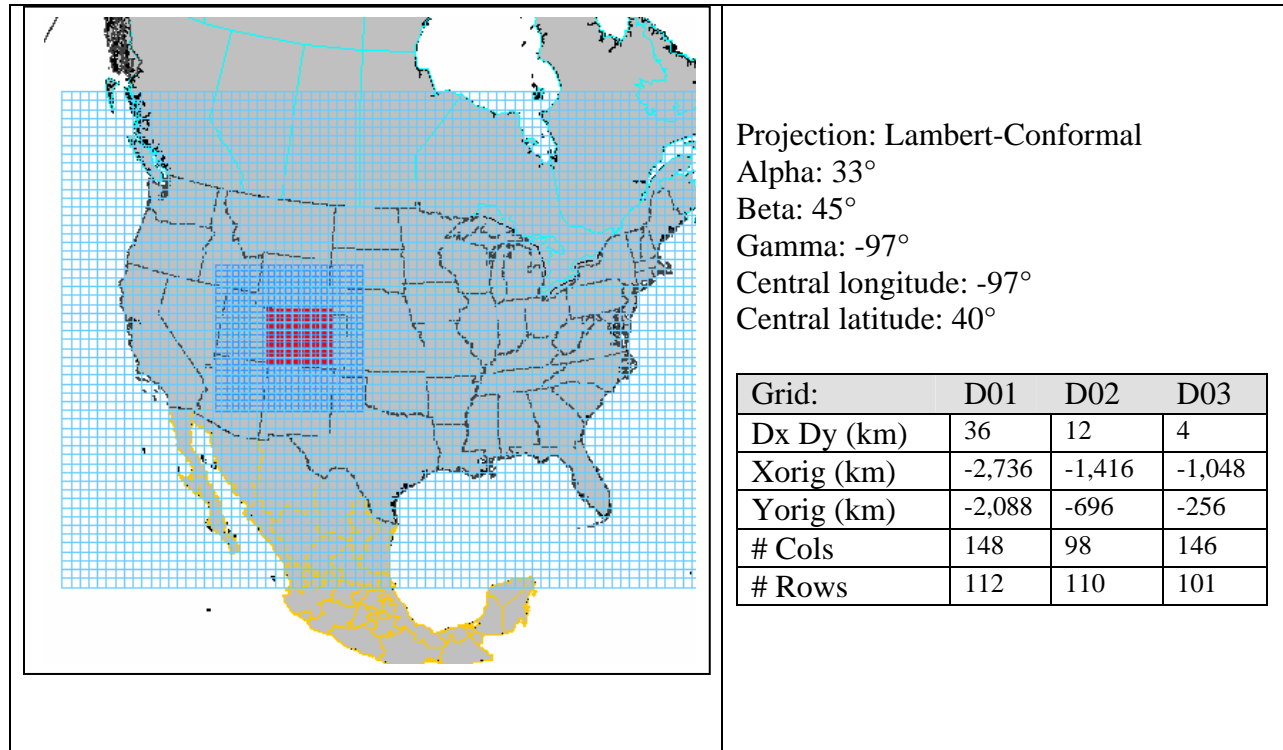


Figure 5.98. The nested 36/12/4-km domains.

#### 5.4.2. Emissions by Source Category

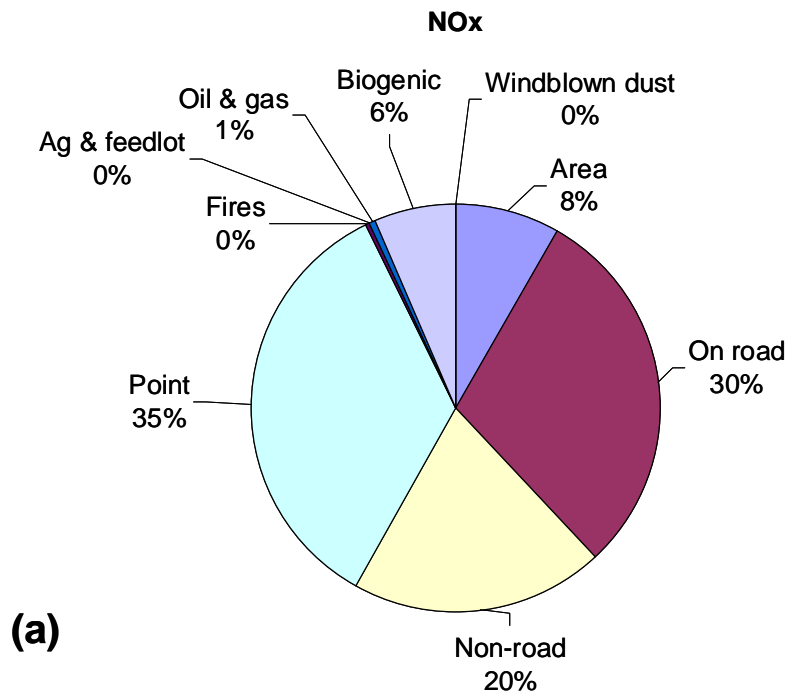
Emissions are calculated relative to 18 categories (Table 5.18), consisting primarily of the following source types: stationary area, on-road and off-road mobile, stationary point, oil and gas development, agricultural and feedlot operations, windblown dust, fires, and off-shore shipping. A summary of the annual average contribution from individual source categories for the United States and within Colorado are shown in Tables 5.19 and 5.20 and Figures 5.99 and 5.100, respectively. Of particular interest for this study are emissions of sulfur and nitrogen, with sulfur emitted in the form of SO<sub>2</sub> and nitrogen as either NO<sub>x</sub> or NH<sub>3</sub>. At the national scale (Table 5.19), mobile sources constitute half of the total NO<sub>x</sub> emissions, followed by point sources (35%), area sources (8%), and biogenic sources (6%). Within Colorado (Table 5.20), the contribution from mobile and point sources is similar (50% and 37%, respectively), followed by oil and gas development (7%), area sources (4%), biogenic sources (2%), and fires (1%). Ammonia emissions in the United States and within Colorado are dominated by agricultural and animal feedlot operations (64% and 86%, respectively), and point sources (primarily EGUs) are the most significant contributors to SO<sub>2</sub> emissions (88% in the United States and 90% within Colorado). The spatial distributions of SO<sub>2</sub>, NO<sub>x</sub>, and NH<sub>3</sub> are shown in Figure 5.101.

**Table 5.18.** Source categories and their associated pollutants in the emission inventory.

<b>Inventory Abbreviation</b>	<b>Spatial Coverage</b>	<b>Description</b>	<b>Inventory Pollutants</b>
ar	U.S., Canada, Mexico	Stationary area, including dust and county-level fires	CO, NO <sub>x</sub> , VOC, NH <sub>3</sub> , SO <sub>2</sub> , PM <sub>10</sub> , PM <sub>2.5</sub>
bg	North America and Caribbean	Biogenic, calculated with BEIS3.12 using BELD3 1-km land-use	VOC, NO <sub>x</sub>
mb	WRAP (without Colorado)	On-road mobile, county-level emissions	CO, NO <sub>x</sub> , VOC, NH <sub>3</sub> , SO <sub>2</sub> , PMC, PSO <sub>4</sub> , PNO <sub>3</sub> , PEC, POA
mbv	MWRPO, MANE-VU, VISTAS	On-road mobile, county-level activities and speeds, emissions calculated with MOBILE6	(same as “mb”)
mbv1	CENRAP	On-road mobile, county-level activities and speeds, emissions calculated with MOBILE6	(same as “mb”)
mbv2	CENRAP	On-road mobile, county-level activities and speeds, emissions calculated with MOBILE6	(same as “mb”)
mbvco	Colorado	On-road mobile, county-level activities and speeds, emissions calculated with MOBILE6	(same as “mb”)
nusm	Canada, Mexico	On-road mobile, county-level emissions	CO, NO <sub>x</sub> , VOC, NH <sub>3</sub> , SO <sub>2</sub> , PM <sub>10</sub> , PM <sub>2.5</sub>
nrm	WRAP, CENRAP, MWRPO	Non-road mobile, monthly and seasonal inventories	CO, NO <sub>x</sub> , VOC, NH <sub>3</sub> , SO <sub>2</sub> , PM <sub>10</sub> , PM <sub>2.5</sub>
nry	U.S., Canada, Mexico	Non-road mobile, annual inventories	CO, NO <sub>x</sub> , VOC, NH <sub>3</sub> , SO <sub>2</sub> , PM <sub>10</sub> , PM <sub>2.5</sub>
nwf	CENRAP, VISTAS	Point fires with precomputed plume rise	CO, NO <sub>x</sub> , VOC, NH <sub>3</sub> , SO <sub>2</sub> , PM <sub>10</sub> , PM <sub>2.5</sub>
wnwf	WRAP	Point fires with precomputed plume rise, does not include wildfires	CO, NO <sub>x</sub> , VOC, NH <sub>3</sub> , SO <sub>2</sub> , PM <sub>10</sub> , PM <sub>2.5</sub>
pt	U.S., Canada, Mexico	Stationary point, including Gulf of Mexico offshore	CO, NO <sub>x</sub> , VOC, NH <sub>3</sub> , SO <sub>2</sub> , PM <sub>10</sub> , PM <sub>2.5</sub>
pacmar	Pacific Ocean	Gridded commercial shipping lane emissions	CO, NO <sub>x</sub> , VOC, NH <sub>3</sub> , SO <sub>2</sub> , PM <sub>10</sub> , PM <sub>2.5</sub>
wbd	U.S., Canada, Mexico	Windblown dust	PM <sub>10</sub> , PM <sub>2.5</sub>
nh3	CENRAP, MWRPO	Agricultural NH <sub>3</sub>	NH <sub>3</sub>
nh3wrap	WRAP	Agricultural and animal NH <sub>3</sub>	NH <sub>3</sub>
wog	WRAP	Oil and gas	CO, NO <sub>x</sub> , VOC, NH <sub>3</sub> , SO <sub>2</sub> , PM <sub>10</sub> , PM <sub>2.5</sub>

**Table 5.19.** Annual emissions (tons per year) by source category within the contiguous United States.

U.S. Totals	CO	NO <sub>x</sub>	VOC	NH <sub>3</sub>	SO <sub>2</sub>	PM <sub>2.5</sub>	PMC
Area	9,284,652	1,668,722	7,771,707	974,489	1,215,341	2,143,278	6,432,855
On road	42,774,346	5,900,291	4,934,498	283,270	126,709	119,088	52,099
Non-road	24,004,625	4,013,060	3,042,086	4,919	407,981	319,281	24,762
Point	3,880,421	6,896,344	1,540,091	233,104	12,361,283	553,587	466,791
Fires	2,317,608	44,709	124,901	12,619	12,058	193,887	28,715
Ag & feedlot	0	0	0	2,715,473	0	0	0
Oil & gas	12,485	132,366	381,385	0	3,763	186	2
Biogenic	10,990,930	1,266,578	100,378,153	0	0	0	0
Windblown dust	0	0	0	0	0	1,010,240	3,581,761
<b>Total U.S.</b>	<b>93,265,068</b>	<b>19,922,068</b>	<b>118,172,822</b>	<b>4,223,872</b>	<b>14,127,134</b>	<b>4,339,547</b>	<b>10,586,986</b>



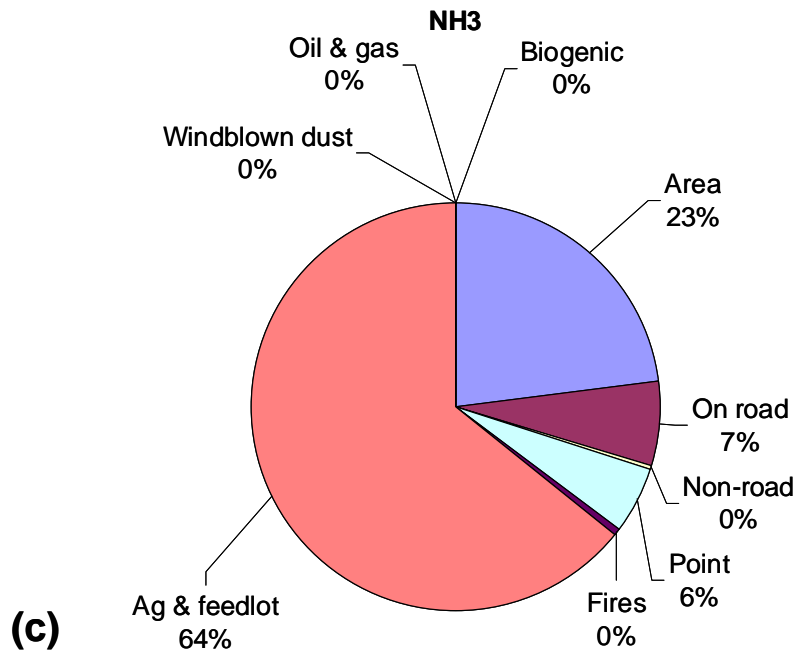
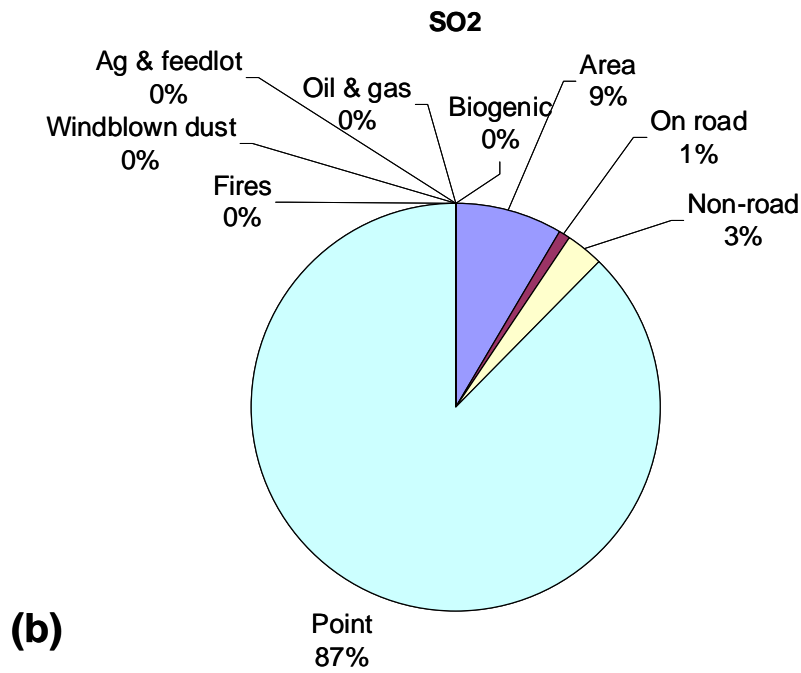
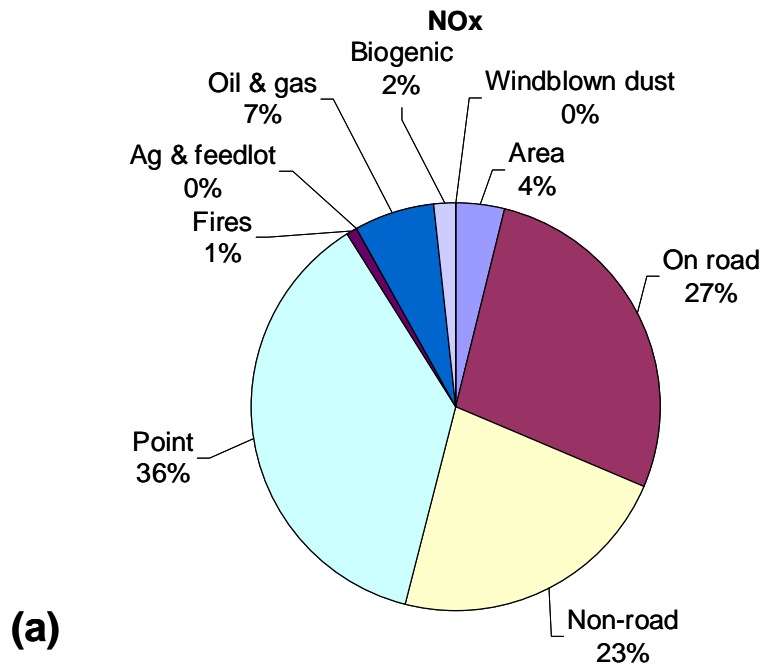


Figure 5.99. Relative contribution by source category to (a) NO<sub>x</sub>, (b) SO<sub>2</sub>, and (c) NH<sub>3</sub> emissions within the contiguous United States.

**Table 5.20.** Annual emissions (tons per year) by source category within Colorado.

Colorado Totals	CO	NO <sub>x</sub>	VOC	NH <sub>3</sub>	SO <sub>2</sub>	PM <sub>2.5</sub>	PMC
Area	82,138	11,543	95,902	1,278	6,248	24,714	55,459
On road	686,609	82,351	85,541	4,298	1,400	1,525	748
Non-road	487,556	68,162	42,188	49	2,535	467	284
Point	32,584	111,584	88,256	549	96,503	34	20,016
Fires	96,791	2,268	4,984	543	567	5,964	1,284
Ag & feedlot	0	0	0	33,226	0	0	0
Oil & gas	2,949	19,669	23,860	0	226	0	0
Biogenic	38,172	4,751	286,876	0	0	0	0
Windblown dust	0	0	0	0	0	0	0
<b>Total Colorado</b>	<b>1,426,800</b>	<b>300,327</b>	<b>627,607</b>	<b>38,741</b>	<b>107,479</b>	<b>32,704</b>	<b>77,790</b>



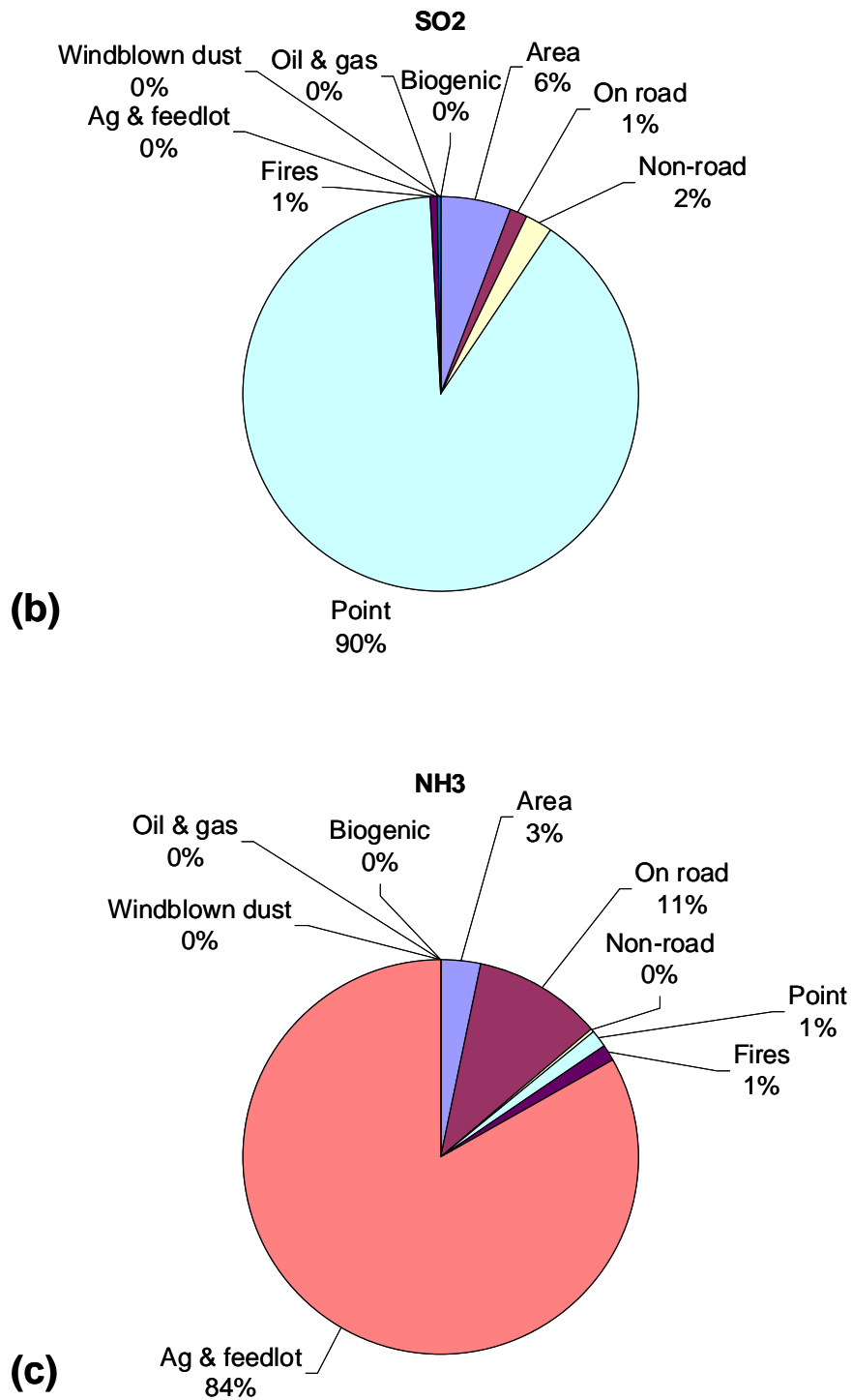
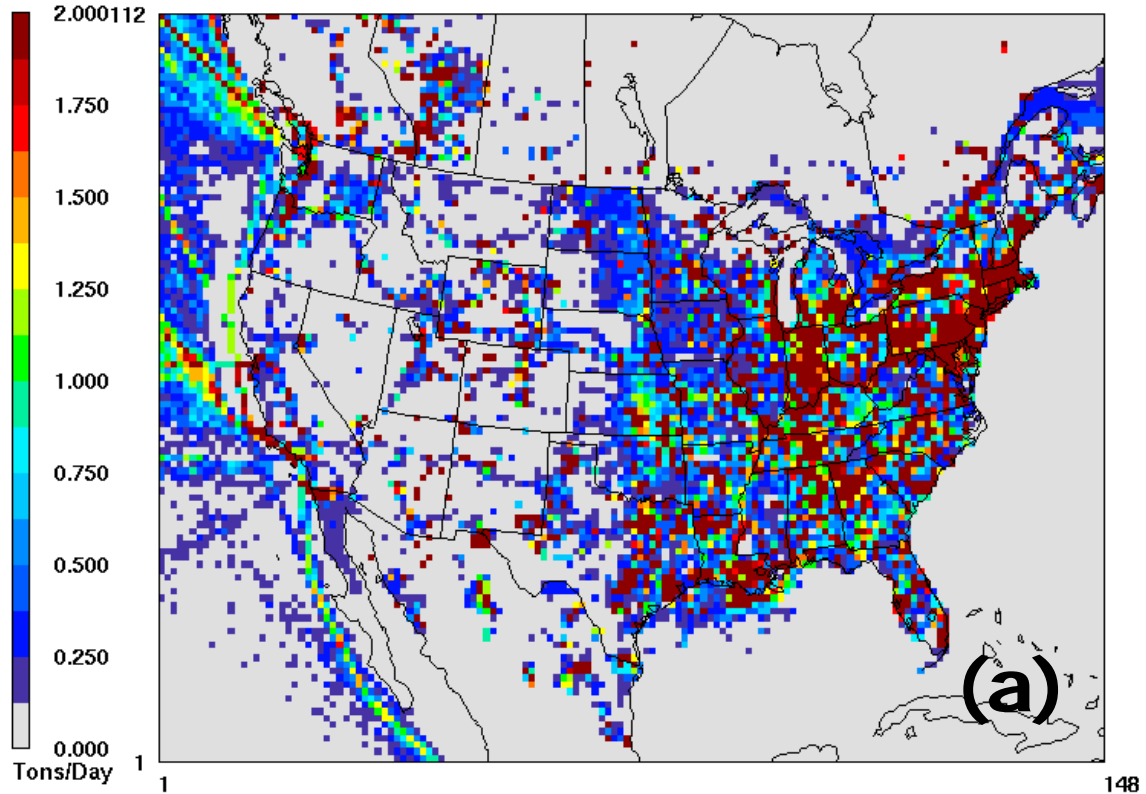
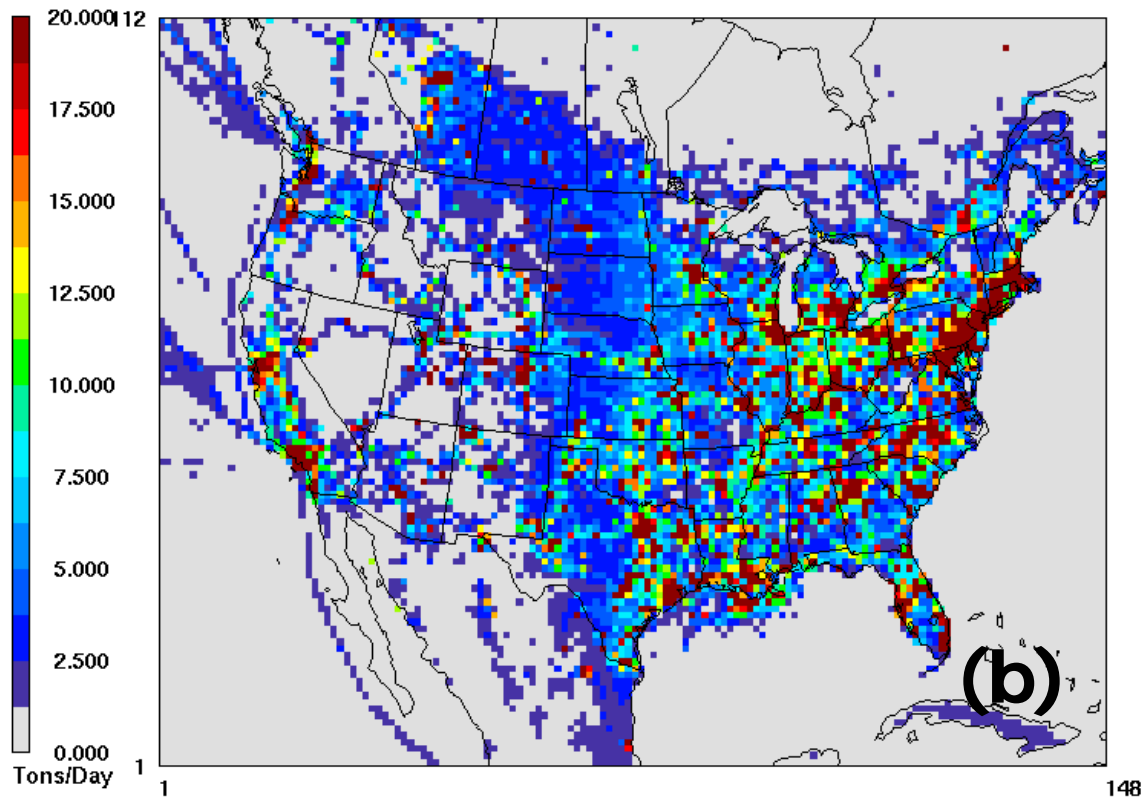


Figure 5.100. Relative contribution by source category to (a) NO<sub>x</sub>, (b) SO<sub>2</sub>, and (c) NH<sub>3</sub> emissions within Colorado.



148



148

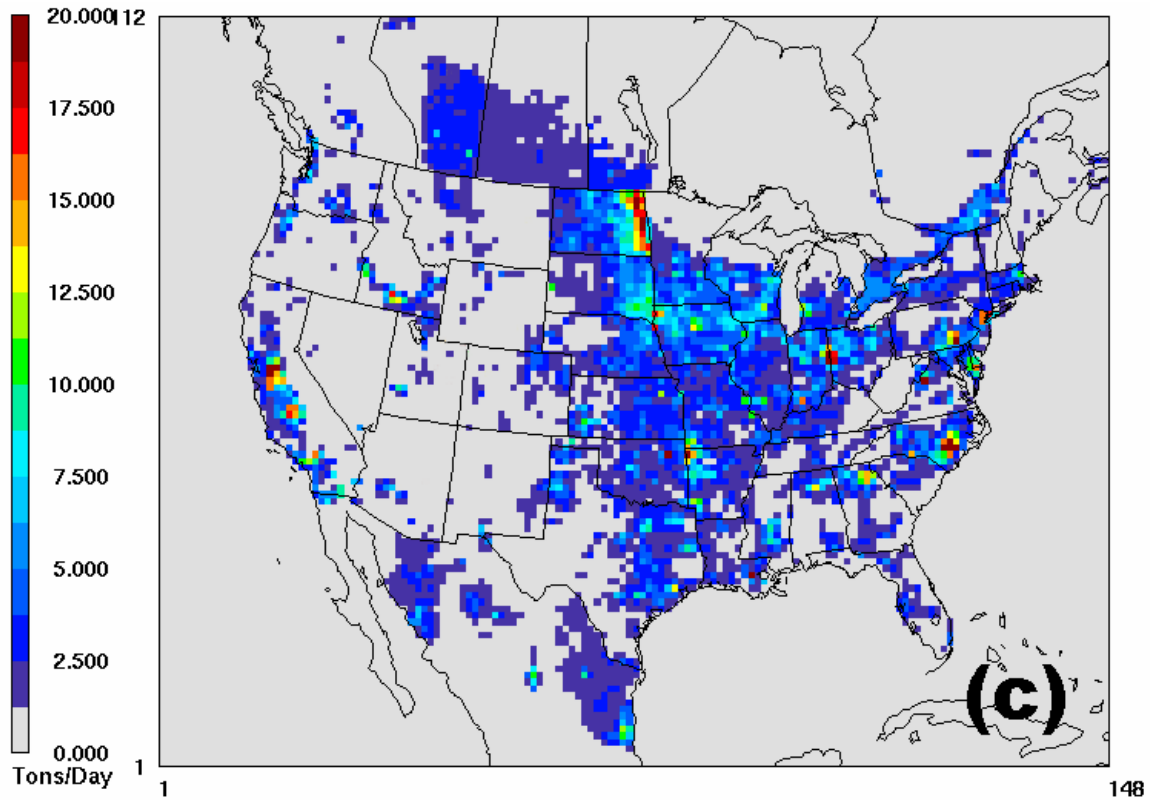


Figure 5.101. Spatial distribution of monthly (a)  $\text{SO}_2$ , (b)  $\text{NO}_x$ , and (c)  $\text{NH}_3$  emissions (tons/day).

## 5.5. HYBRID MODELING USING TRACER SIMULATIONS AND AMBIENT MONITORING DATA

The approach taken in this analysis, to apportion emission sources to measured concentrations of various aerosol species at a receptor site, combines modeled transport and dispersion of a conservative tracer released in proportion to emissions with receptor-oriented models to statistically account for removal and chemical processes. The average contribution of source regions throughout North America to the receptor concentration over a period of time will be assessed from these relationships. The goal of the analysis is to separate out the contributions from nearby local sources, sources along the Front Range, and other source regions east and west of the Continental Divide.

The tracer modeling system consists of three components: MM5 (Mesoscale Model 5) (Grell et al., 1994); a regional weather model, CAMx (Comprehensive Air Quality Model with extensions) (CAMx, 2007); a chemical transport model; and a detailed emission inventory (Adelman, 2007).

Tracer emissions are based on the ammonia, nitrogen oxide (NO<sub>x</sub>), and sulfur dioxide (SO<sub>2</sub>) emission inventories developed by the Western Regional Air Partnership (WRAP) and are updated to reflect the nested RoMANS model domains and time period (Mansell, 2005; Adelman, 2007). The major anthropogenic sources within the ammonia emission inventory are livestock operations, agricultural fertilizer applications, and mobile sources, while NO<sub>x</sub> emissions are about equally divided between mobile and point sources. Sulfur dioxide emissions are primarily associated with coal-fired power plants.

The tracer simulation was conducted using CAMx with the MM5 meteorology and ammonia, NO<sub>x</sub>, and SO<sub>2</sub> emissions as inputs. CAMx is an Eulerian grid air quality model that is often used to investigate regional air pollution. CAMx was modified to simulate an arbitrary number of conserved tracers, with no loss through chemical transformation or deposition. As shown in Figures 5.102–5.104, the inert tracer transport simulation was conducted for 94–100 different source regions throughout North America. The source regions were selected by centering them on high emission regions, based on the 2002 WRAP annual average NH<sub>3</sub>, NO<sub>x</sub>, and SO<sub>2</sub> inventories. Many areas with little or no emissions were excluded. The smallest source regions were selected near RMNP and they generally increased in size with distance from the park. Eight to ten source regions were selected within Colorado, including one at RMNP, the neighboring population center at Estes Park, Colorado, Denver, Colorado, as well the agricultural regions in northeastern Colorado.

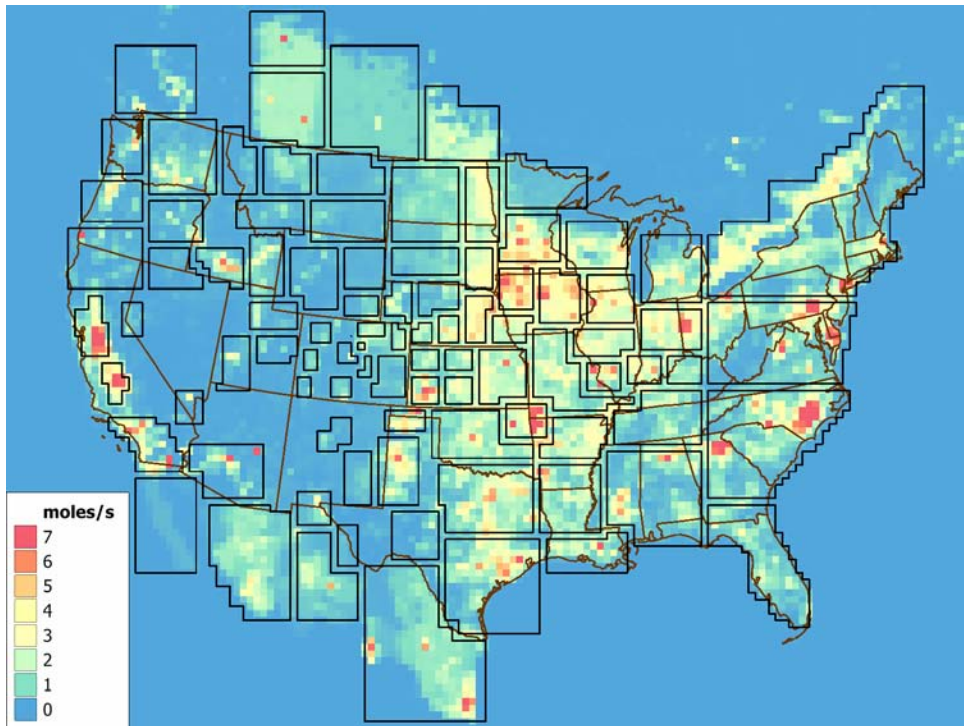


Figure 5.102. Source regions and average emission inventory for  $\text{NH}_3$  used in the conservative “tracer” analysis.

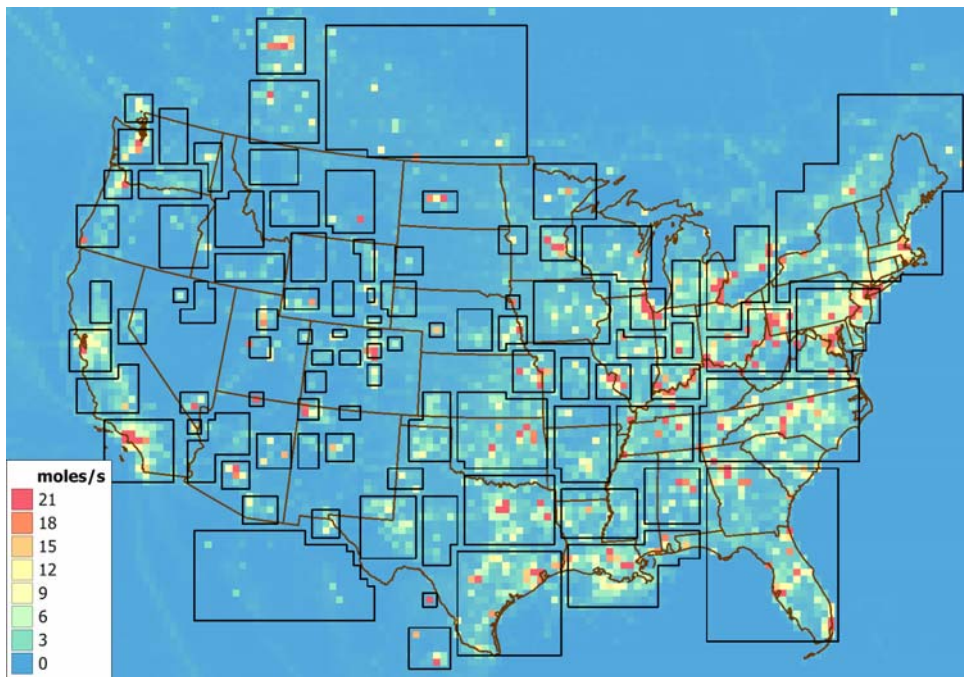


Figure 5.103. Source regions and average emission inventory for  $\text{NO}_x$  used in the conservative “tracer” analysis.

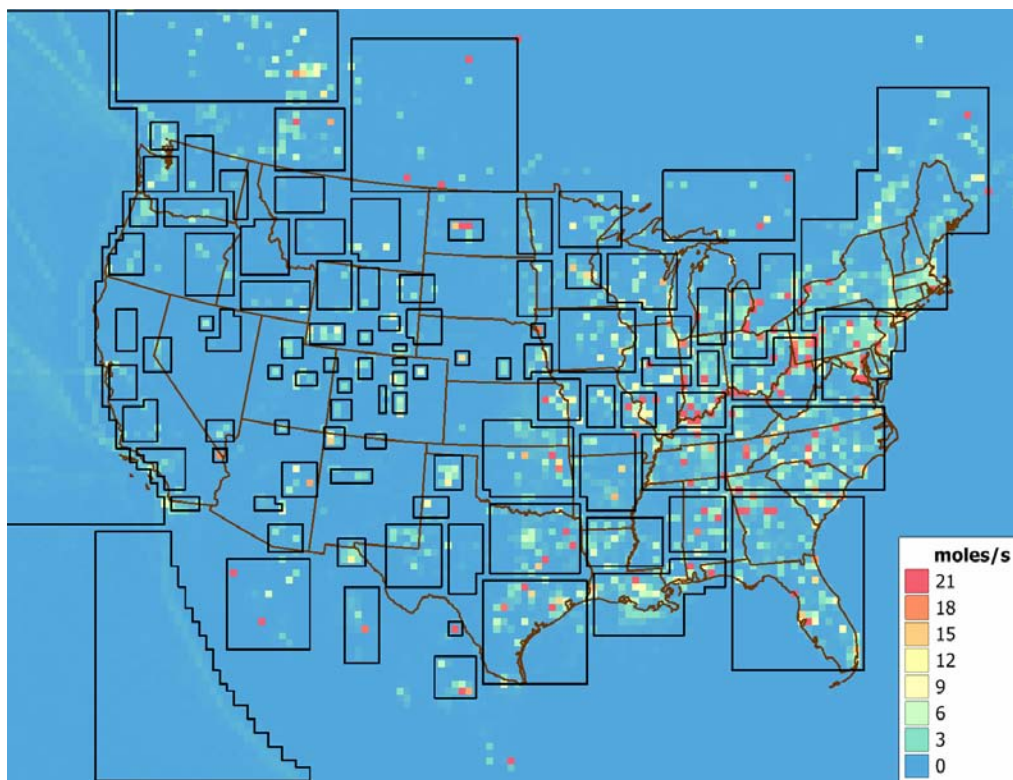


Figure 5.104. Source regions and average emission inventory for  $\text{SO}_2$  used in the conservative “tracer” analysis.

### 5.5.1. The Receptor Model

The starting point for any attribution analysis is the concentrations,  $C_{ki}$ , of modeled ammonia tracer for 1-hr time periods,  $k$ , for each of the source regions  $i$ . An analysis similar to the trajectory mass balance (TrMB) (section 5.3.4) can be exercised by looking at the relationship between  $C_{ki}$  and measured aerosol concentrations at a receptor site, in this case RMNP, using a statistical technique such as linear regression. For the most part the attributions are similar. For instance, the apportionment of ammonia during the spring time period using TrMB was 71%:29% for in state versus out of the state of Colorado, while using  $C_{ki}$  estimates the apportionment was 54%:46%. The TrMB apportionment for northeastern Colorado, western Colorado, and the Front Range using TrMB was 16%, 22%, and 19%, respectively, while using  $C_{ki}$  estimates it was 19%, 21%, and 6%, the 6% being only the Denver area while the whole Front Range was used in the TrMB analysis.

However, the  $C_{ki}$  concentrations between source regions can have high temporal collinearities causing instabilities in a regression analysis between ambient concentrations and  $C_{ki}$ . Contributions from some source areas may be erroneously inflated at the expense of others. Therefore an analysis was carried out that groups those source area  $C_{ki}$  values that are collinear into one variable, and it will be that variable that will be used in the regression model rather than individual  $C_{ki}$  concentrations.

It is assumed that the concentration of airborne aerosol species can be described by the sum of a number (hopefully, small) of source region vectors. The equation for this description is

$$\text{Equation 5.18. } C_{ki} = \sum_j a_{kj} S_{ji} + \varepsilon_{ik}$$

where

$k = 1 \dots m$ , the number of observations

$i = 1 \dots n$ , the number of sources contributing to the receptor

$j = 1 \dots N$ , the number of source region vectors

$C_{ki}$  = concentrations of ammonia from source  $i$  for time period  $k$

$a_{kj}$  = time weighting functions

$S_{ji}$  = source vectors

$\varepsilon_{ik}$  = error term including random and lack of fit error

The source vectors are essentially weighting factors that group together covarying source regions that on the average contribute to elevated concentrations of trace species under certain various, unique types of meteorological conditions.

When source vectors are unknown, it is sometimes possible to gain insight into source-receptor relationships through the use of a singular value decomposition (SVD) of  $C_{ki}$ :

$$\text{Equation 5.19. } C_{ki} = \sum_{j=1}^m u_{kj} s_j v_{ij} + \sum_{j=m}^n u_{kj} s_j v_{ij}$$

Comparison of equations 5.18 and 5.19 suggests

$$\text{Equation 5.20. } S_{ji} = v_{ji}$$

$$\text{Equation 5.21. } a_{kj} = u_{kj} s_j \cdot$$

and

$$\text{Equation 5.22. } \varepsilon_{ik} = \sum_{j=m}^n u_{kj} s_j v_{ij}$$

where

$s_j$  = the singular values and  $u_{kj}$

$v_{ji}$  = the eigenvectors

$m$  = the number unique eigenvectors

$\varepsilon_{ik}$  = error term.

Therefore the eigenvectors,  $v_{ji}$ , are the source vectors as derived from the modeled concentrations of ammonia at the receptor site over time. The source vectors,  $S_{ji}$ , are basic patterns found in the modeled dataset and are reflective of reoccurring meteorological patterns.

Similar eigenvector analyses have been used where  $C_{ki}$  are concentrations of a species of interest measured at a number of monitoring sites over time to estimate the relative contributions from

source regions to measured aerosol levels at the measurement sites. However, in this case the  $C_{ki}$  are modeled inert concentrations.

There are a variety of ways the SVD analysis can be used to approximately apportion the species of interest, in this case ammonia, to the various source regions. In the following analysis the eigenvectors are used to group various source regions into larger regions that represent transport from that larger region. These identified groups of source regions are then summed together for each time period (typically 1 hr) and treated as independent variables in a regression model where the dependent variables are the measured concentrations of the aerosol of interest and the averaged source regions are the independent variables:

$$\text{Equation 5.23. } (C)_k = \sum_j \alpha_{jk} \Phi_{jk}$$

where

$C_k$  = the measured aerosol concentrations

$\alpha_{jk}$  = the regression coefficients

$\Phi_{jk}$  = the average of modeled concentrations arriving at the receptor from sources areas grouped according to eigenvectors,  $v$ .

Other techniques, such as principle component or factor analysis, could be used to group together those source areas that covary with each other. However, all approaches to this covariance problem yield similar results.

### 5.5.2. The Data

Figures 5.105–5.110 are temporal plots of various gas, particle, and wet-deposited species that will be apportioned to the source areas defined in Figures 5.102–5.104. Figures 5.105 and 5.108 are temporal plots of particle ammonium ( $\text{NH}_4$ ), wet  $\text{NH}_4$ , and ammonia ( $\text{NH}_3$ ) concentrations for spring and summer, Figures 5.106 and 5.109 show time series of nitrogen oxides ( $\text{NO}_x$ ), nitric acid ( $\text{HNO}_3$ ), particle nitrate ( $\text{NO}_3$ ), and wet  $\text{NO}_3$  concentrations, while Figures 5.107 and 5.110 show sulfur dioxide ( $\text{SO}_2$ ), particle sulfate ( $\text{SO}_4$ ), and wet  $\text{SO}_4$  concentrations. Units are in  $\mu\text{g}/\text{m}^3$  for both gaseous and particle species, while wet concentrations are in  $\mu\text{eq}/\text{L}$ . Tables 5.21 and 5.22 are statistical summaries of these datasets.

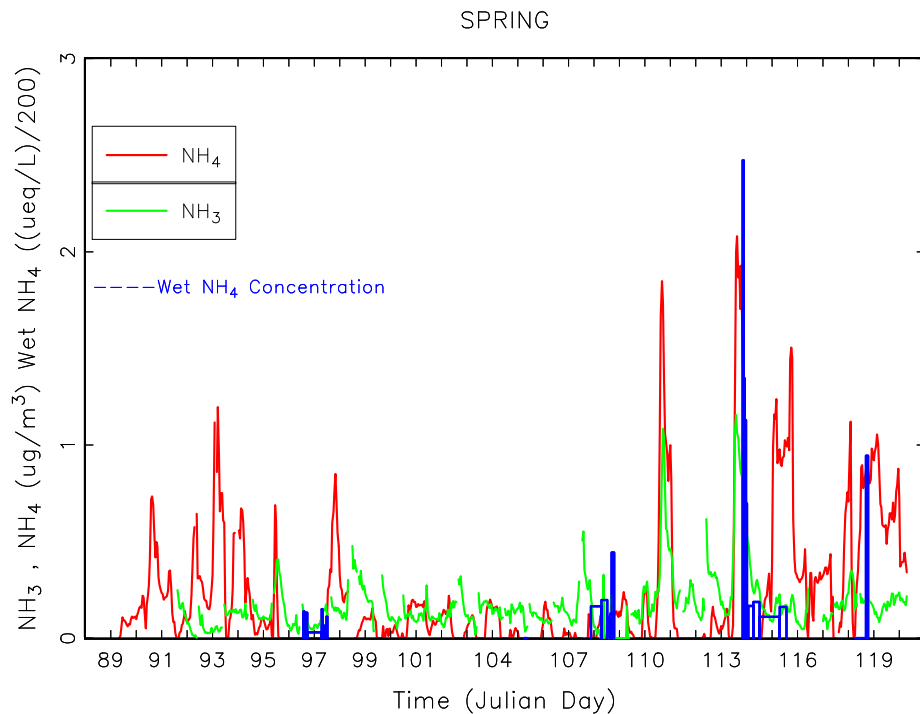


Figure 5.105. Time series of measured particle ammonium (NH<sub>4</sub>), ammonia (NH<sub>3</sub>), and wet-deposited ammonium (NH<sub>4</sub>) for the spring time period at the RMNP core site.

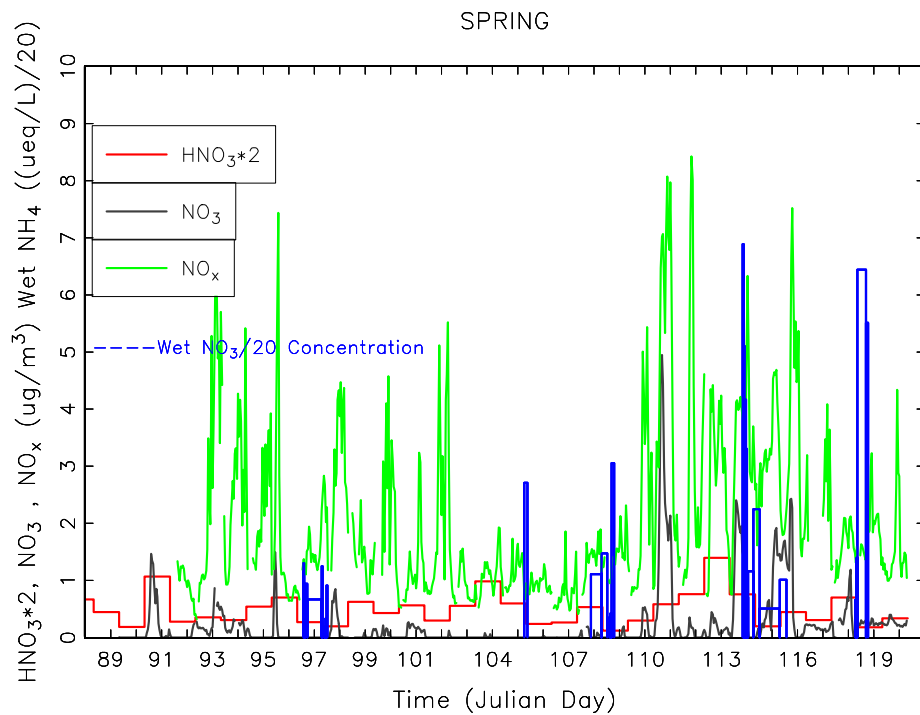


Figure 5.106. Time series of measured nitric acid (HNO<sub>3</sub>), nitrogen oxides (NO<sub>x</sub>), particle nitrate (NO<sub>3</sub>), and wet-deposited nitrate (NO<sub>3</sub>) for the spring time period at the RMNP core site.

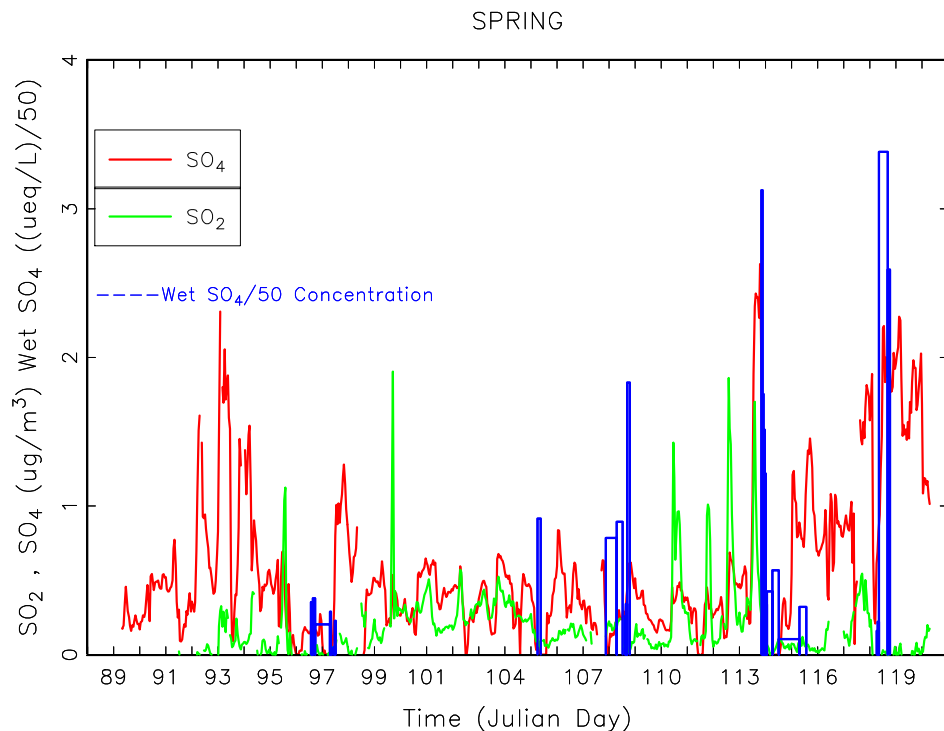


Figure 5.107. Time series of measured particle sulfate (SO<sub>4</sub>), sulfur dioxide (SO<sub>2</sub>), and wet-deposited sulfate (SO<sub>4</sub>) for the spring time period at the RMNP core site.

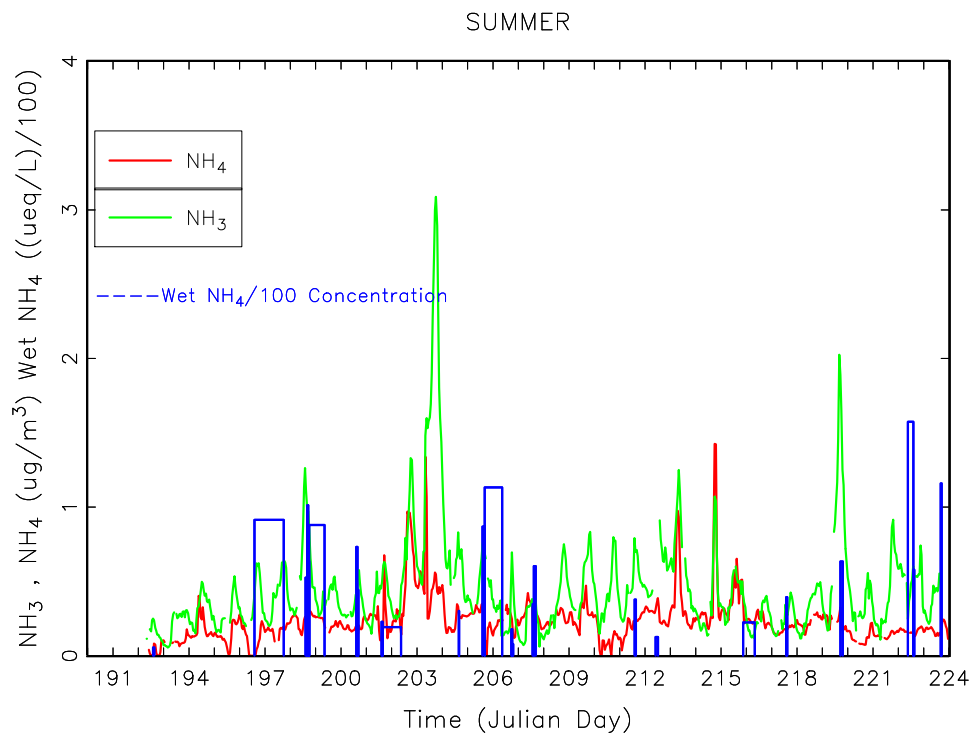


Figure 5.108. Time series of measured particle ammonium (NH<sub>4</sub>), ammonia (NH<sub>3</sub>), and wet-deposited ammonium (NH<sub>4</sub>) for the summer time period at the RMNP core site.

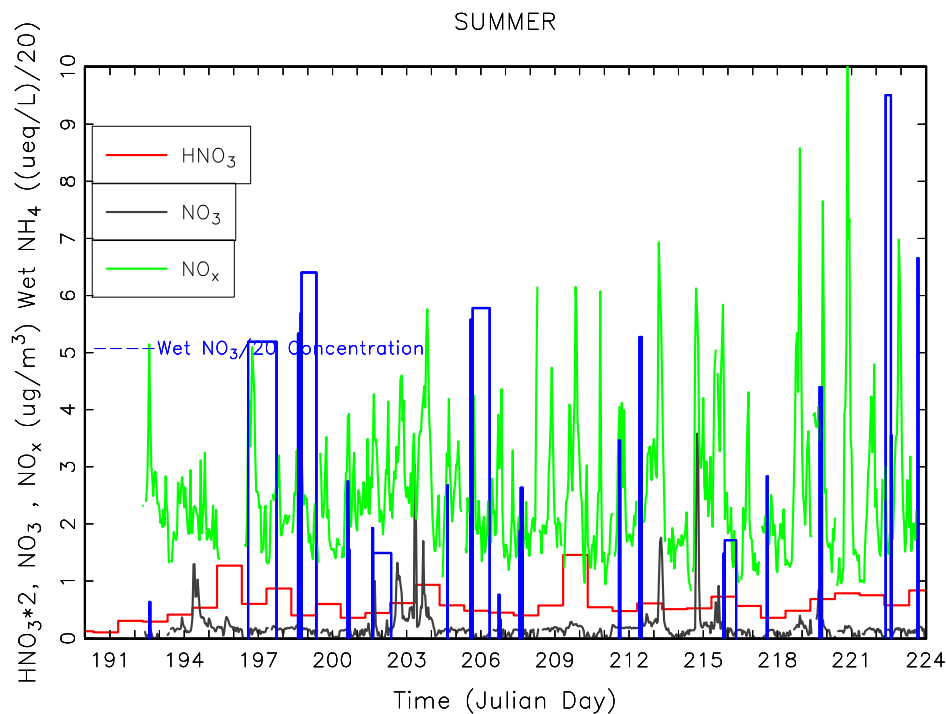


Figure 5.109. Time series of measured nitric acid ( $\text{HNO}_3$ ), nitrogen oxides ( $\text{NO}_x$ ), particle nitrate ( $\text{NO}_3$ ), and wet deposited nitrate ( $\text{NO}_3$ ) for the summer time period at the RMNP core site.

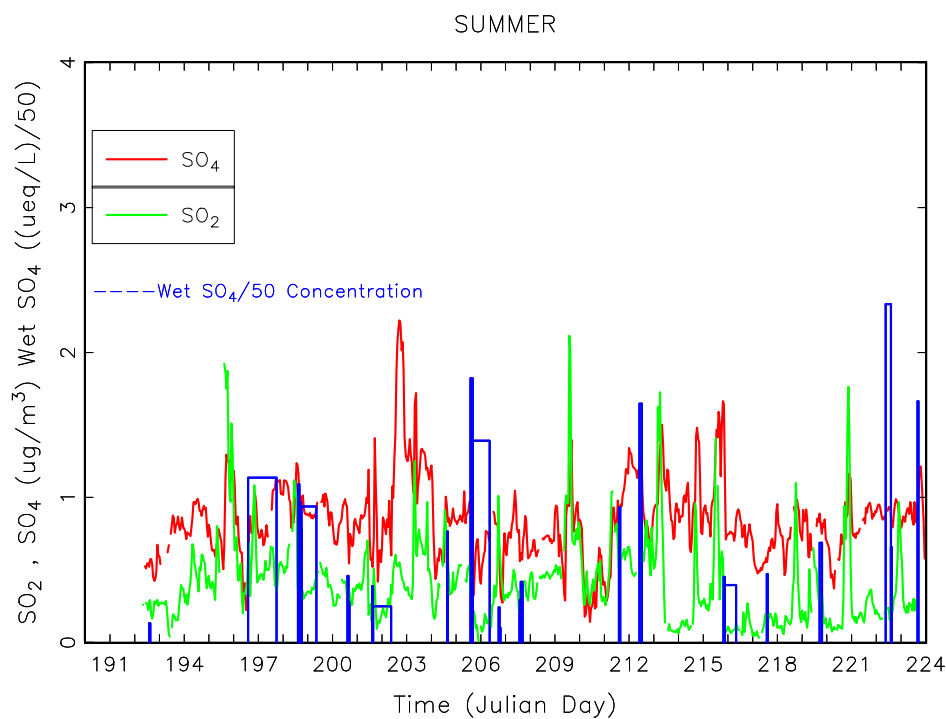


Figure 5.110. Time series of measured particle sulfate ( $\text{SO}_4$ ), sulfur dioxide ( $\text{SO}_2$ ), and wet-deposited sulfate ( $\text{SO}_4$ ) for the summer time period at the RMNP core site.

**Table 5.21.** Statistical summary of measured nitric acid, ammonia, sulfur dioxide, nitrogen oxides, particle ammonium, sulfate, and nitrate; wet-deposited ammonium, sulfate, and nitrate concentration; and wet-deposition flux of ammonium, sulfate, and nitrate for the spring time frame.

Variable	Mean	Std Dev	Minimum	Maximum	N
HNO <sub>3</sub> (µg/m <sup>3</sup> )	0.24	0.14	0.06	0.70	36
NH <sub>3</sub> (µg/m <sup>3</sup> )	0.17	0.15	0.00	1.16	624
SO <sub>2</sub> (µg/m <sup>3</sup> )	0.18	0.25	-0.13	1.91	624
NO <sub>x</sub> (µg/m <sup>3</sup> )	2.32	1.60	0.51	8.72	624
NH <sub>4</sub> (µg/m <sup>3</sup> )	0.23	0.35	0.00	2.08	728
SO <sub>4</sub> (µg/m <sup>3</sup> )	0.57	0.51	0.00	2.63	728
NO <sub>3</sub> (µg/m <sup>3</sup> )	0.22	0.52	0.00	4.95	728
Wet NH <sub>4</sub> (µeq/L)	63.58	105.69	0.00	494.56	30
Wet SO <sub>4</sub> (µeq/L)	38.48	45.74	0.00	169.21	30
Wet NO <sub>3</sub> (µeq/L)	37.91	38.17	1.72	137.76	30
Wet_NH <sub>4</sub> F (µeq/m <sup>2</sup> /hr)	225.96	499.73	0.00	2533.51	30
Wet_SO <sub>4</sub> F (µeq/m <sup>2</sup> /hr)	116.18	288.43	0.00	1537.64	30
Wet_NO <sub>3</sub> F (µeq/m <sup>2</sup> /hr)	104.89	217.72	0.44	1123.90	30

**Table 5.22.** Statistical summary of measured nitric acid, ammonia, sulfur dioxide, nitrogen oxides, particle ammonium, sulfate, and nitrate; wet-deposited ammonium, sulfate, and nitrate concentration; and wet-deposition flux of ammonium, sulfate, and nitrate for the summer time frame.

Variable	Mean	Std Dev	Minimum	Maximum	N
HNO <sub>3</sub> (µg/m <sup>3</sup> )	0.56	0.27	0.10	1.46	37
NH <sub>3</sub> (µg/m <sup>3</sup> )	0.45	0.36	0.06	3.09	691
SO <sub>2</sub> (µg/m <sup>3</sup> )	0.39	0.27	0.01	2.12	691
NO <sub>x</sub> (µg/m <sup>3</sup> )	2.50	1.18	0.84	11.64	694.00
NH <sub>4</sub> (µg/m <sup>3</sup> )	0.24	0.16	0.00	1.42	727
SO <sub>4</sub> (µg/m <sup>3</sup> )	0.84	0.28	0.14	2.22	727
NO <sub>3</sub> (µg/m <sup>3</sup> )	0.19	0.30	0.00	3.59	727
Wet NH <sub>4</sub> (µeq/L)	60.62	42.97	5.51	157.42	26
Wet SO <sub>4</sub> (µeq/L)	43.51	32.67	5.03	119.07	26
Wet NO <sub>3</sub> (µeq/L)	78.66	49.93	6.48	190.16	26
Wet_NH <sub>4</sub> F (µeq/m <sup>2</sup> /hr)	500.76	920.09	6.29	4431.82	26
Wet_SO <sub>4</sub> F (µeq/m <sup>2</sup> /hr)	348.78	529.88	5.29	2296.42	26
Wet_NO <sub>3</sub> F (µeq/m <sup>2</sup> /hr)	541.51	810.99	7.60	3323.76	26

The largest springtime episode for ammonia and particle ammonium occurred on April 23 (Julian Day (JD) = 113.5), when concentrations built up from near 0 to 1.16 and 2.1 µg/m<sup>3</sup>, respectively, in just a few hours (Figure 5.105). Five hrs later marked the start of a rain event, and 8 hrs later ammonium concentrations had decreased to near 0 and ammonia had also decreased substantially. The rain event lasted about 40 hrs; however, the concentrations of ammonium in the rain water were high for only about 3–4 hrs, indicating that concentrations of ambient gases and particles were scavenged out of the atmosphere in a very short time period. Particle nitrate (Figure 5.106) and sulfate (Figure 5.107) also reached near their highest levels during this time period, as did concentrations of these species in the rain water.

The spring time series shows that there are other time periods when gas- and particle-phase species are high, most notably starting on April 20 and 25 (JD = 110.5 and 115). Ammonium, nitrate, and sulfate are elevated on April 26 (JD = 117.75), while starting on April 27 (JD = 118.5) ammonium and sulfate are elevated for about 1½ days. Typically, monitoring periods corresponding to rain events have decreased ambient concentrations of aerosol levels.

Unlike the data from the one large spring meteorological event when all species concentrations were elevated, followed closely by a large wet deposition event, the summer data show that rain events were not related to the most elevated episodes of gas and particle species (Figures 5.108, 5.109, and 5.110). The largest concentrations of gas- and particle-phase aerosol species occurred over a time period from July 20 through July 22 (JD = 202.5 and 204), with very short events of a few hours occurring on July 31 and August 1 (JD = 213.25 and 214).

It also worth noting that when the gaseous precursors to the associated secondary species, such as SO<sub>2</sub> and SO<sub>4</sub>, are correlated, it is likely that the event or episode is more local in nature as opposed to events when the secondary species are elevated without commensurate increases in the primary gaseous precursors. Note that in most episodes identified above this is the case, suggesting that the elevated aerosol species are not associated with long-range transport. The two obvious exceptions are episodes starting on April 24, 25, and 26 (JD = 115, 117.75, and 118.5), when secondary species are elevated without NH<sub>3</sub> and SO<sub>2</sub> being elevated.

### 5.5.3. The Modeled Tracer Concentrations

The CAMx model was run without deposition and chemistry, as described in the previous section, with the 94, 95, and 100 source regions shown in Figures 5.102–5.104 for NH<sub>3</sub>, NO<sub>x</sub>, and SO<sub>2</sub>, respectively. These modeling results will be referred to as the tracer model (TM) runs. A first-order calculation of loss to deposition was estimated using  $C \cdot \exp(-kt)$  where C is the concentration without deposition,  $k = v_d/H$  where  $v_d$  is the deposition velocity and H is the scale height, and t is transport time. Transport time was estimated assuming an average transport velocity of 5 m/sec, and the deposition velocity used was 1, .3, and .2 cm/sec for NH<sub>3</sub>, SO<sub>2</sub>, and NO<sub>x</sub>, respectively.

Figures 5.111–5.116 are temporal plots of spring and summer measured and TM runs for NH<sub>3</sub>, NO<sub>x</sub>, and SO<sub>2</sub>. Because NH<sub>3</sub>, NO<sub>x</sub>, and SO<sub>2</sub> are not reduced due to chemical conversion to other species or by wet deposition, one would not expect the TM calculations to compare to measured ambient concentrations but to be substantially higher. On the other hand, if atmospheric transport and dispersion were realistically captured by the dispersion model, the timing between TM and measured values would be correlated.

Referring to Figures 5.111–5.116, notice that the timing between TM and measured values is indeed the same in many if not most cases, implying that the general transport patterns are being reproduced. The TM also captures the measured diurnal variability in summer ammonia concentrations that occurred on almost a daily basis.

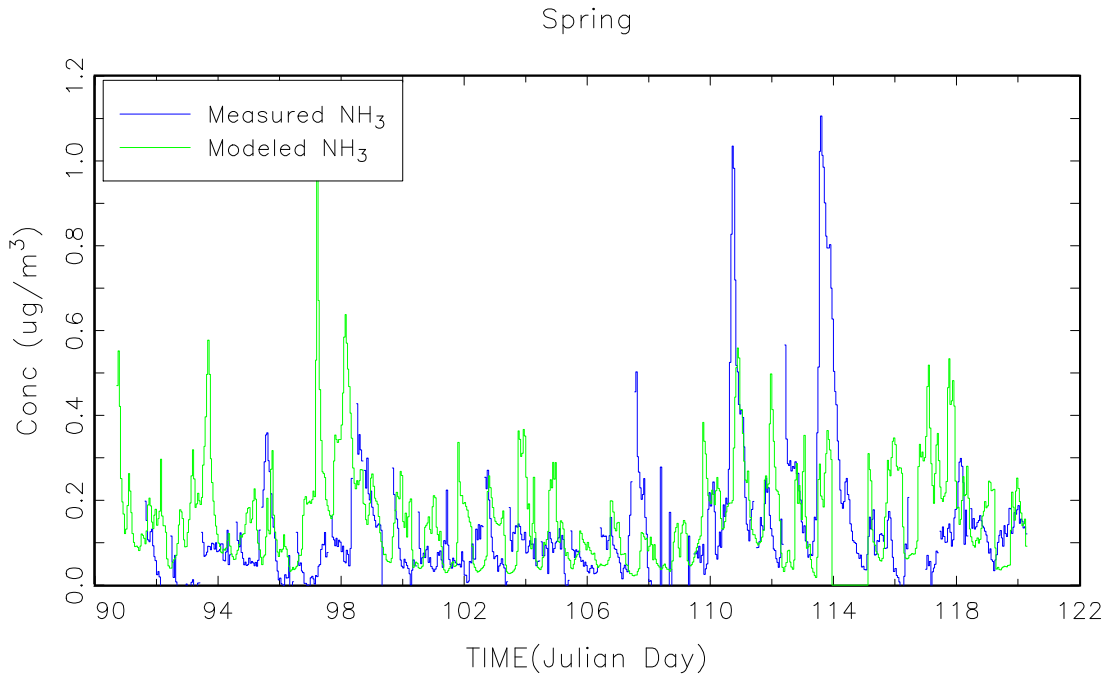


Figure 5.111. Measured and modeled tracer concentrations weighted to estimated ammonia emissions and first-order dry deposition for the spring time period.

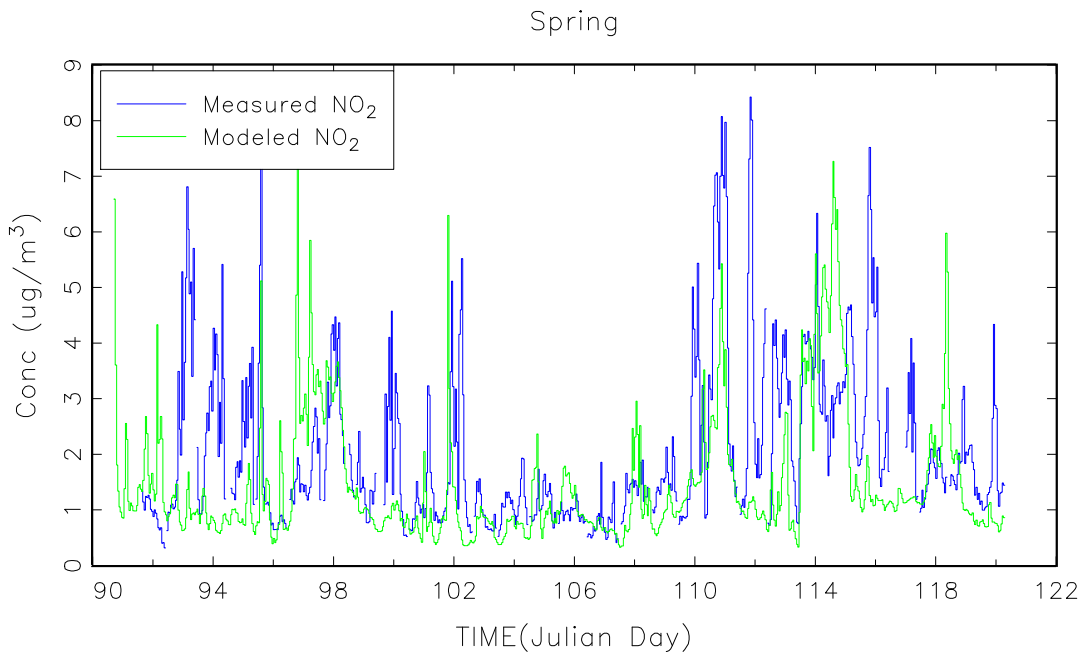


Figure 5.112. Measured and modeled tracer concentrations weighted to estimated nitrogen oxide emissions and first-order dry deposition for the spring time period.

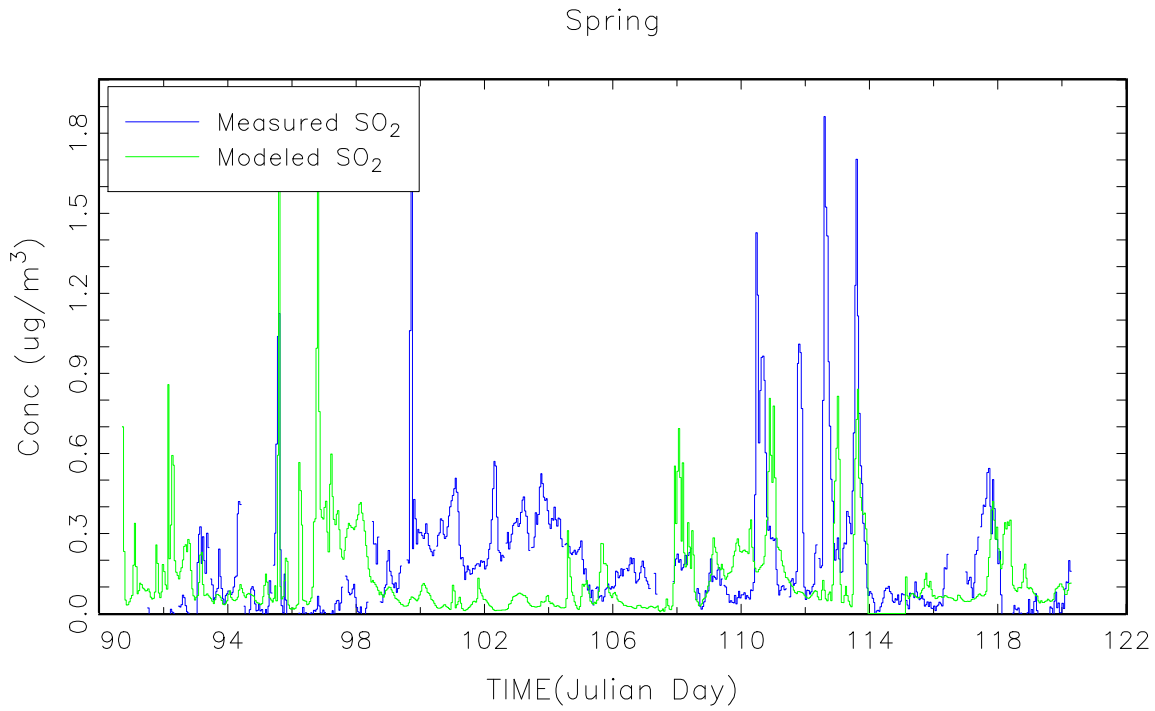


Figure 5.113. Measured and modeled tracer concentrations weighted to estimated ammonia emissions and first-order dry deposition for the spring time period.

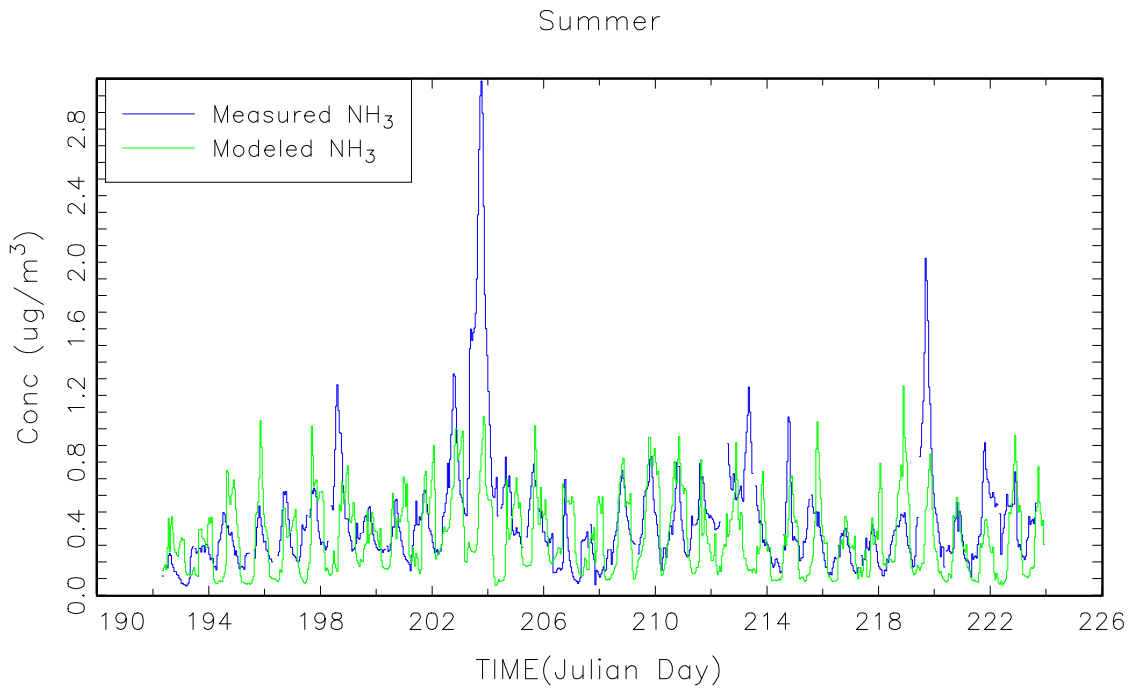


Figure 5.114. Measured and modeled tracer concentrations weighted to estimated ammonia emissions and first-order dry deposition for the summer time period.

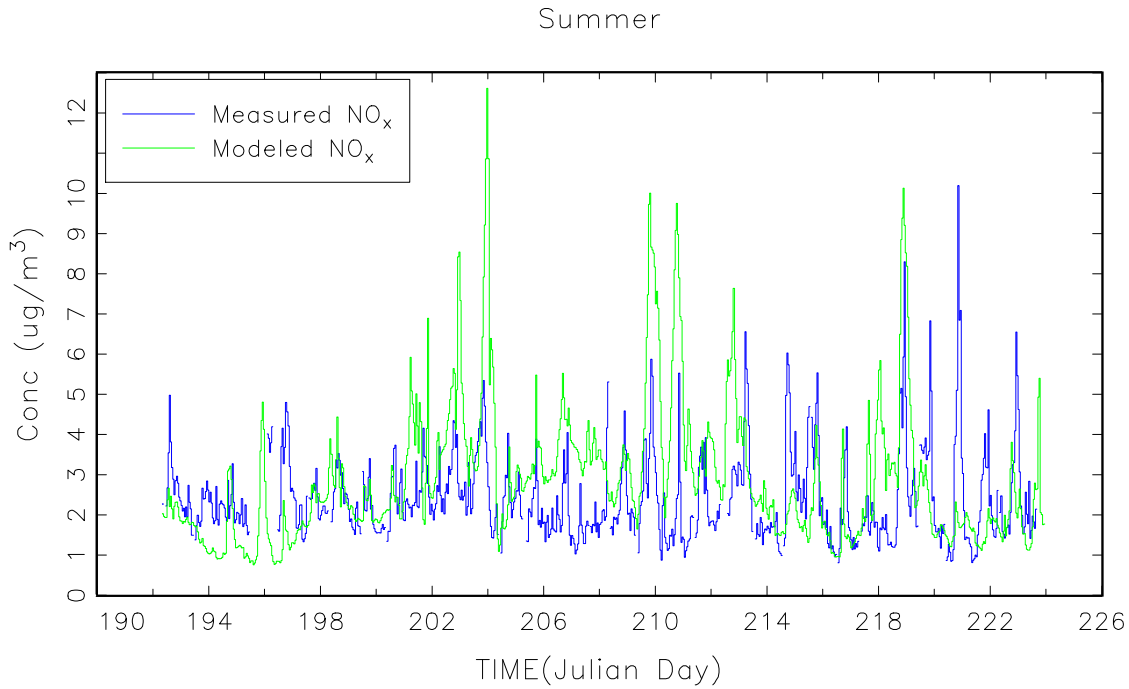


Figure 5.115. Measured and modeled tracer concentrations weighted to estimated nitrogen oxide emissions and first-order dry deposition for the summer time period.

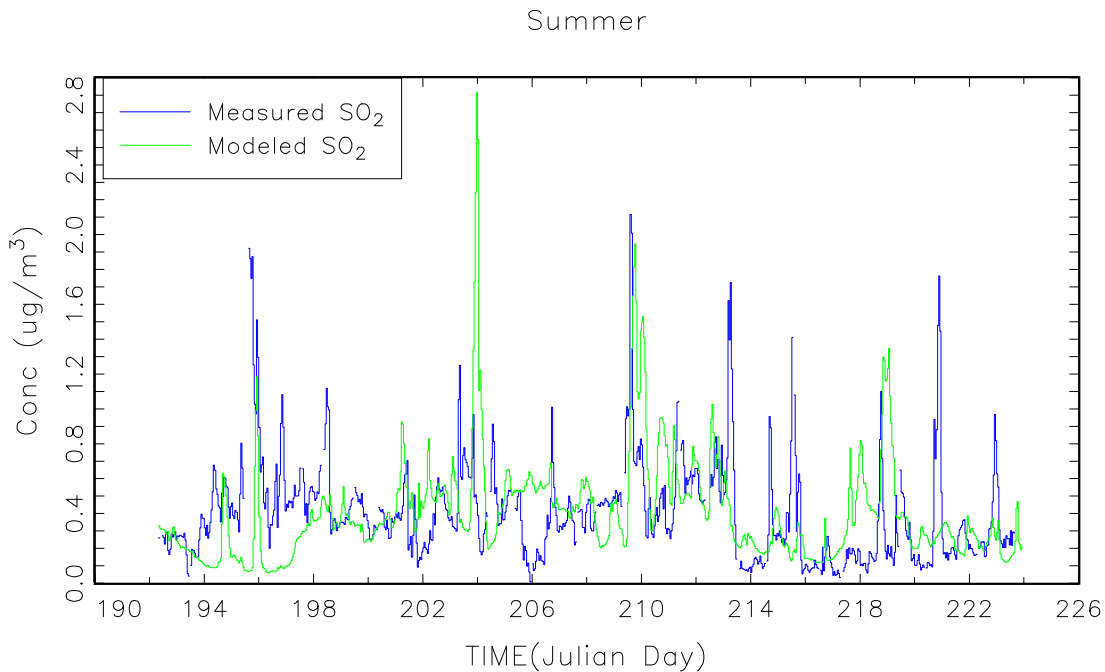


Figure 5.116. Measured and modeled tracer concentrations weighted to estimated ammonia emissions and first-order dry deposition for the summer time period.

#### 5.5.4. Apportionment of Aerosols to their Respective Source Regions

The goal of the eigenvector analysis is to identify those groups of source regions that transport to the receptor site during the same time periods. Therefore the modeled concentrations for each source area are normalized to the mean concentration for that site:

$$\text{Equation 5.24. } Z_{kj} = C_{kj} / \overline{C}_j$$

where

as before, k = a time index while j refers to a source region.

##### 5.5.4.1. Spring and Summer Monitoring Time Frame

The first eight spatial eigenvectors corresponding to NH<sub>3</sub>, NO<sub>x</sub>, and SO<sub>2</sub> emissions for the spring time period explain over 80% of the variance for each of the above species and were used in the analysis. The first ten eigenvectors were used for the summer time frame.

For the regression model represented by Equation 5.23, the spring time period source groupings associated with three eigenvectors corresponded to three regions loaded into the model for NH<sub>3</sub> in a statistically significant way. These source regions, labeled as Regions 6, 14, and 15 are shown in Figures 5.117–5.119. Note that the size of the circles does not represent the relative contribution of each source area to modeled concentrations, because the individual TM concentrations for each source region have been normalized to that source area's mean concentration. The figures only show which source regions transported emissions to the receptor site during a specific time period. Regions 14 and 15 as well as Region 7 were found to be statistically significant for NH<sub>4</sub>. Groupings for other source regions were found to be not statistically significant.

Spring Region 6 shows transport from the south with contributions from northeastern Colorado, while Region 14 represents transport from the northerly direction. Region 15 corresponds to a more local transport pattern with the highest-weighted source areas in the state of Colorado. Similar plots are shown in Figures 5.120–5.141 for spring NO<sub>x</sub>/HNO<sub>3</sub>/NO<sub>3</sub> and SO<sub>2</sub>/SO<sub>4</sub> and summer NH<sub>3</sub>/NH<sub>4</sub>, NO<sub>x</sub>/HNO<sub>3</sub>/NO<sub>3</sub> and SO<sub>2</sub>/SO<sub>4</sub> eigenvectors.

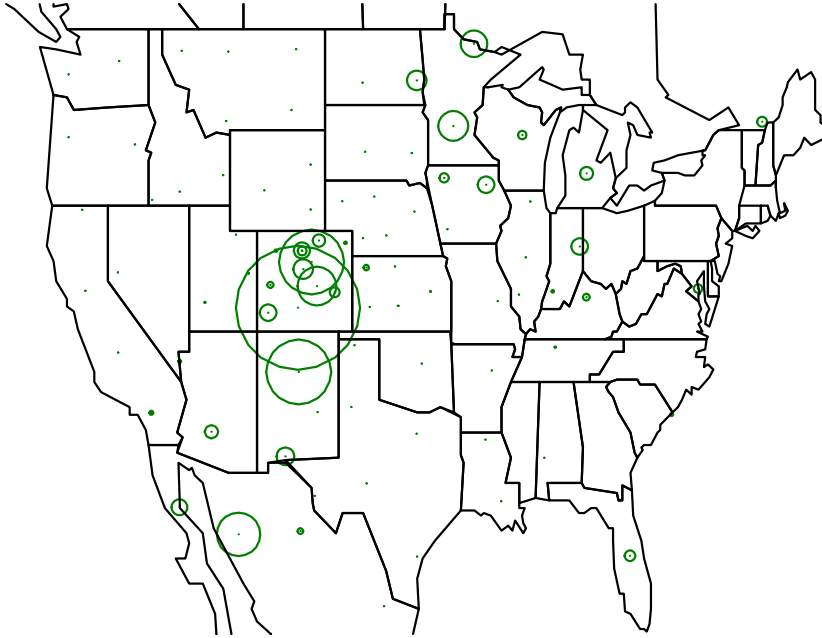


Figure 5.117. Spring  $\text{NH}_3$  source areas for Region 6.

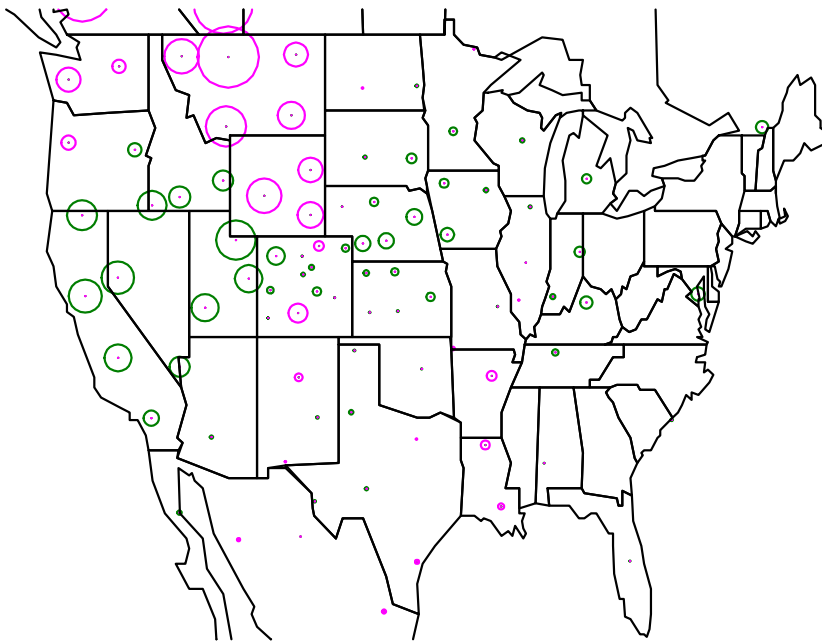


Figure 5.118. Regions 7 and 14 are source areas for spring  $\text{NH}_4$ , and Region 14 is a source area for spring  $\text{NH}_3$  and  $\text{NH}_4$ . Region 7 is shown in magenta, while Region 14 is shown in green.

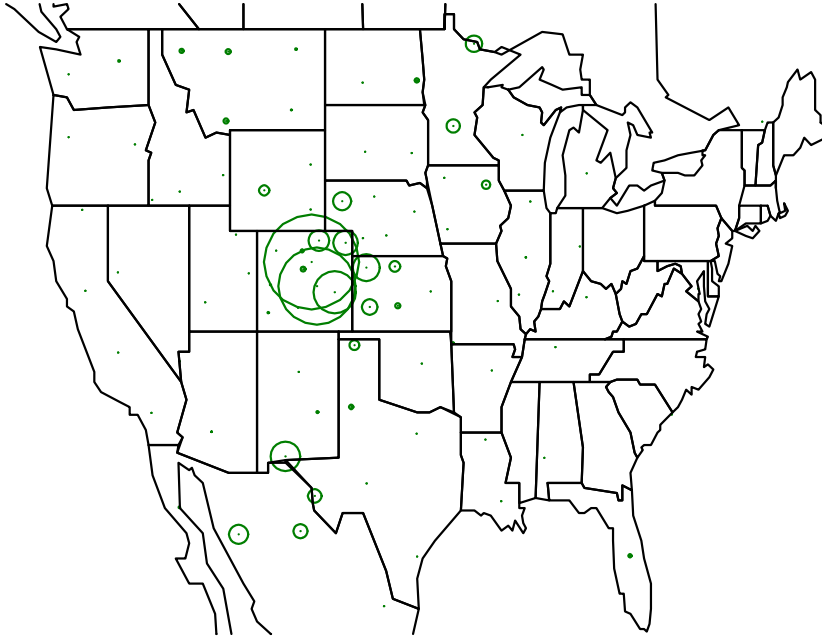


Figure 5.119. Spring  $\text{NH}_3$  and  $\text{NH}_4$  source areas for Region 15.

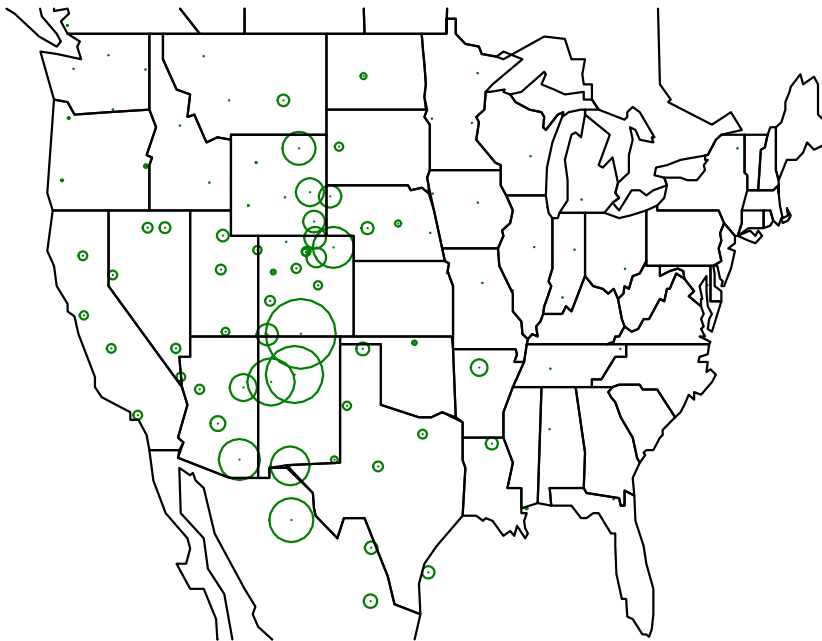


Figure 5.120. Spring  $\text{NO}_x$  and  $\text{HNO}_3$  source areas for Region 3.

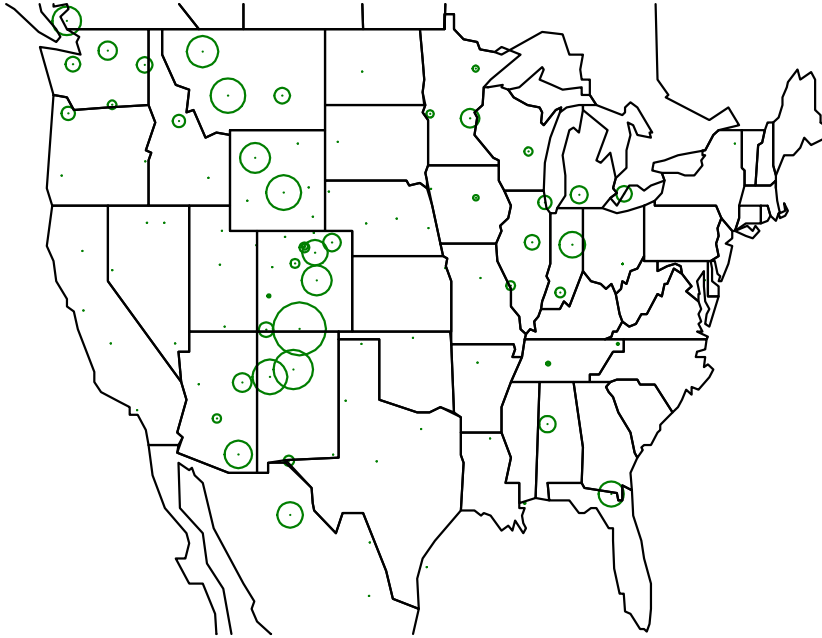


Figure 5.121. Spring  $\text{NO}_x$ ,  $\text{HNO}_3$ , and  $\text{NO}_3$  source areas for Region 5.

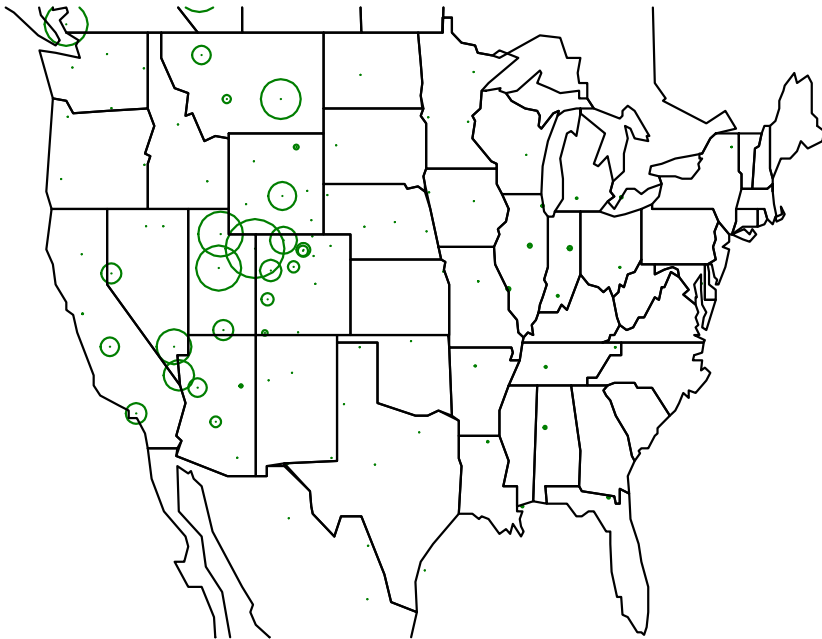


Figure 5.122. Spring  $\text{NO}_x$ ,  $\text{HNO}_3$ , and  $\text{NO}_3$  source areas for Region 6.

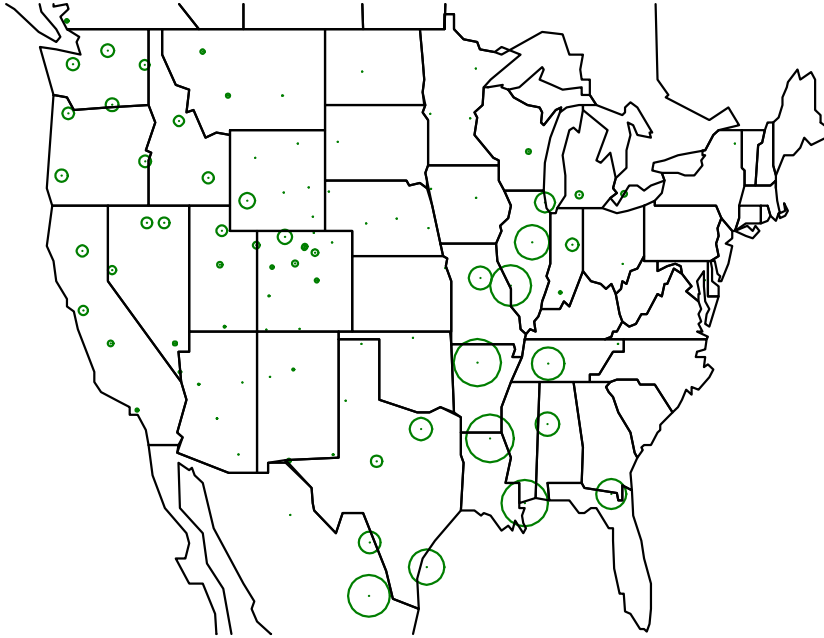


Figure 5.123. Spring NO<sub>x</sub> source areas for Region 10.

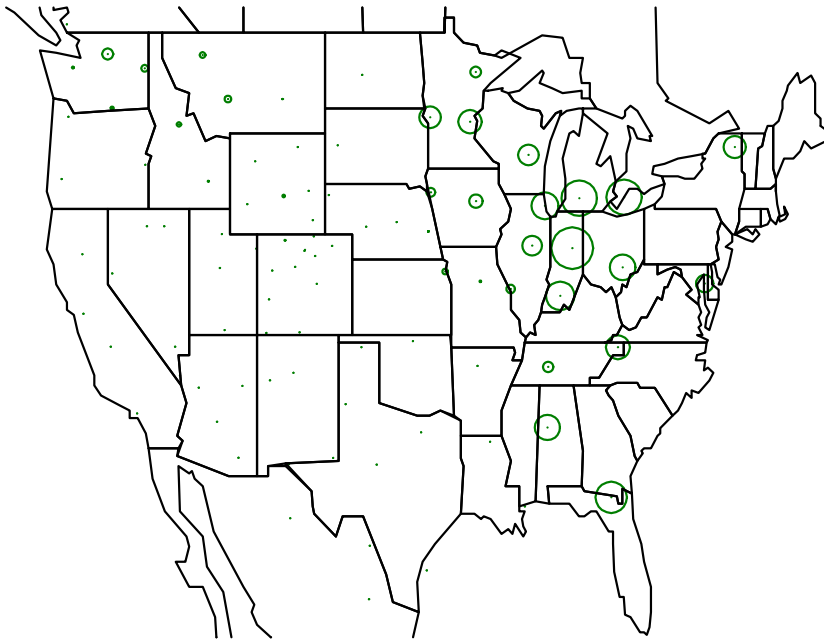


Figure 5.124. Spring NO<sub>x</sub> and NO<sub>3</sub> source areas for Region 11.

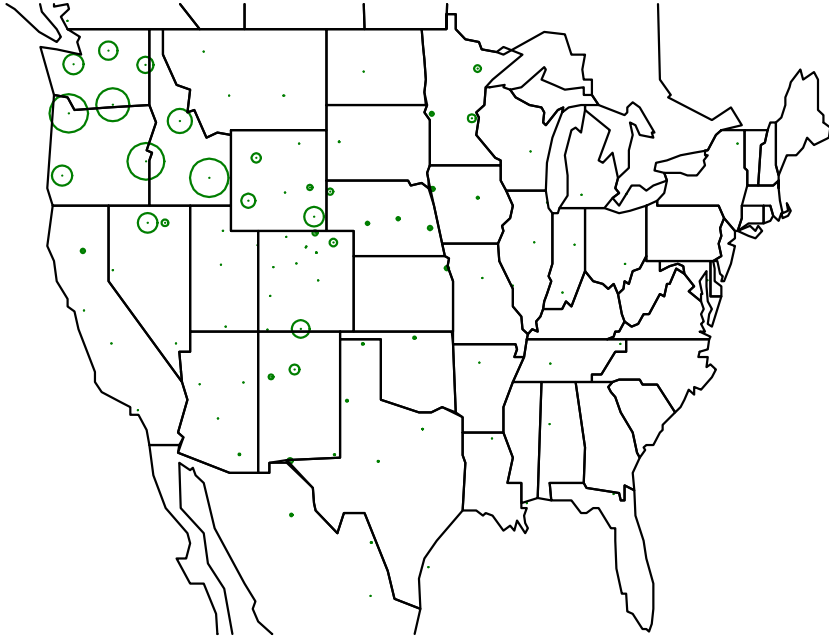


Figure 5.125. Spring NO<sub>x</sub> and HNO<sub>3</sub> source areas for Region 14.

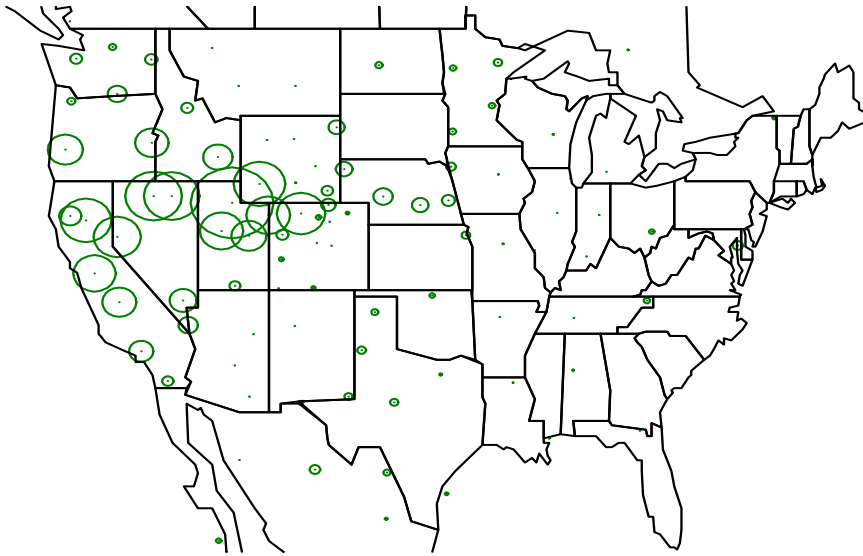


Figure 5.126. Spring SO<sub>2</sub> and SO<sub>4</sub> source areas for Region 3.

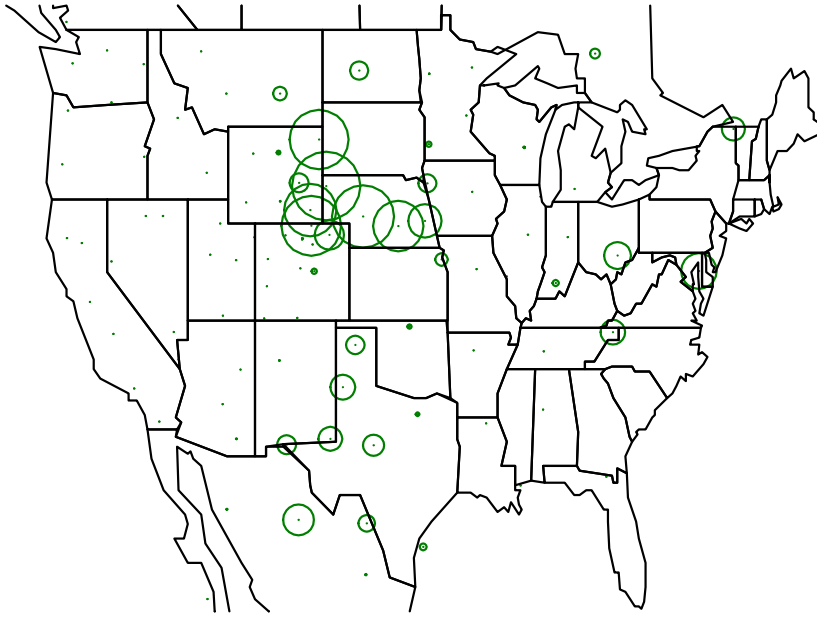


Figure 5.127. Spring SO<sub>4</sub> source areas for Region 4.

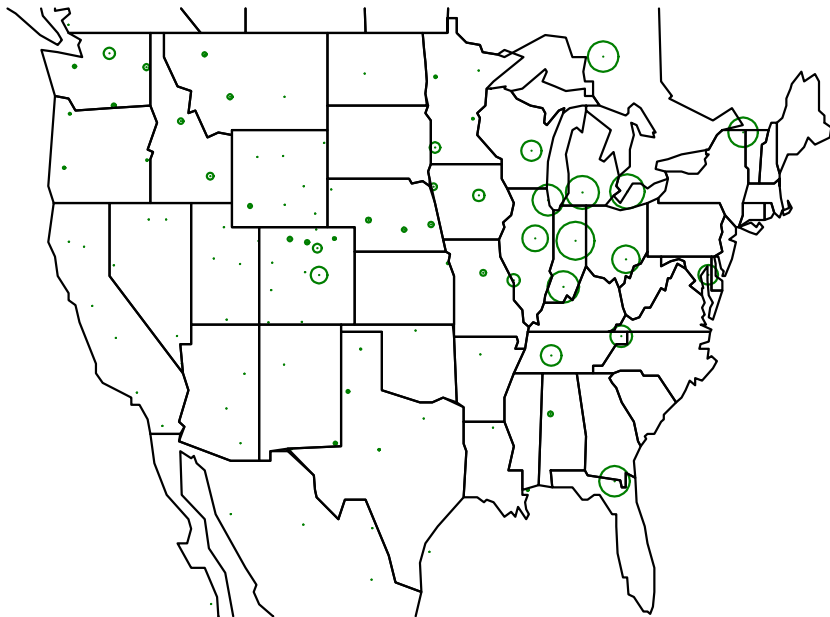


Figure 5.128. Spring SO<sub>2</sub> source areas for Region 6.

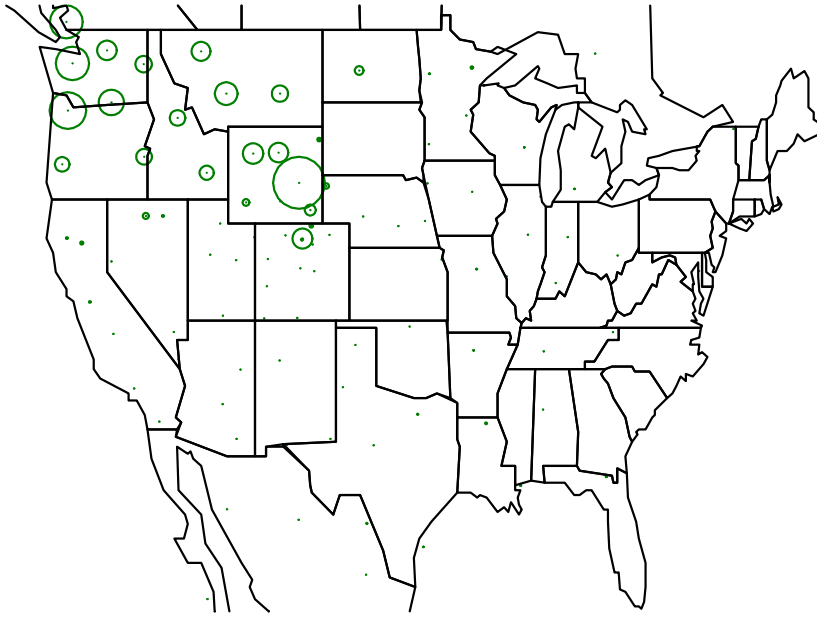


Figure 5.129. Spring SO<sub>4</sub> source areas for Region 7.

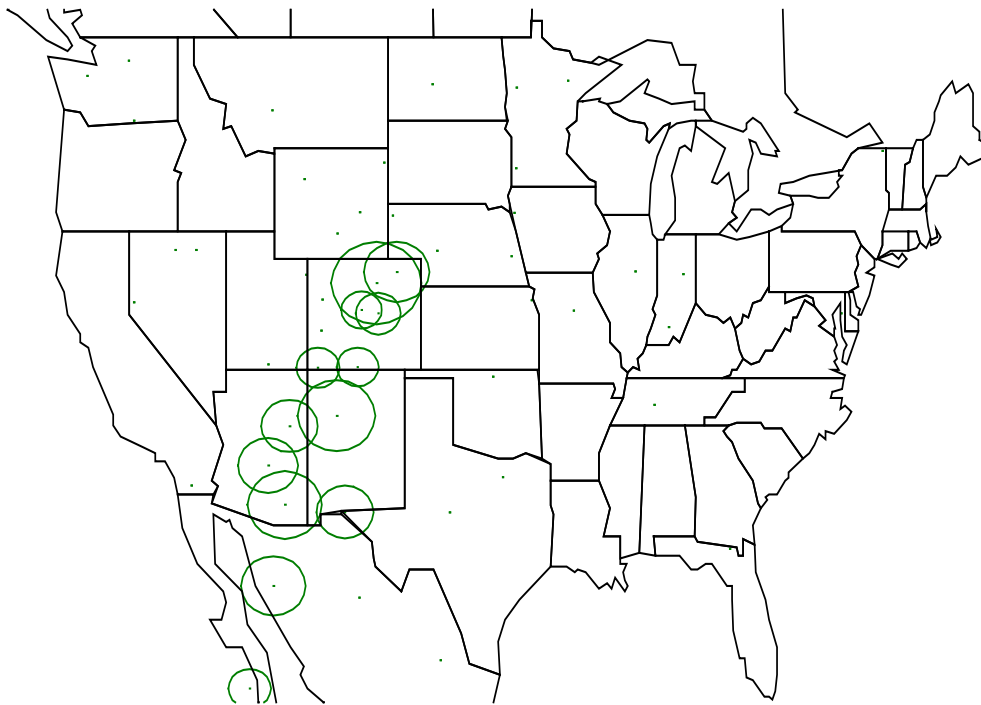


Figure 5.130. Summer SO<sub>2</sub> and SO<sub>4</sub> source areas for Region 8.

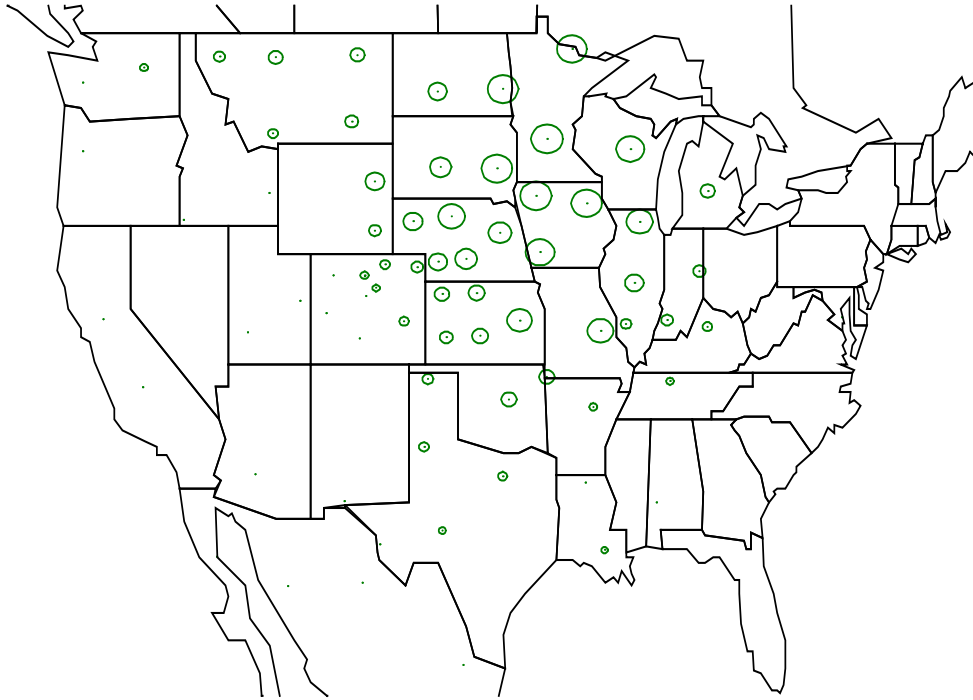


Figure 5.131. Summer NH<sub>3</sub> and NH<sub>4</sub> source areas for Region 1.

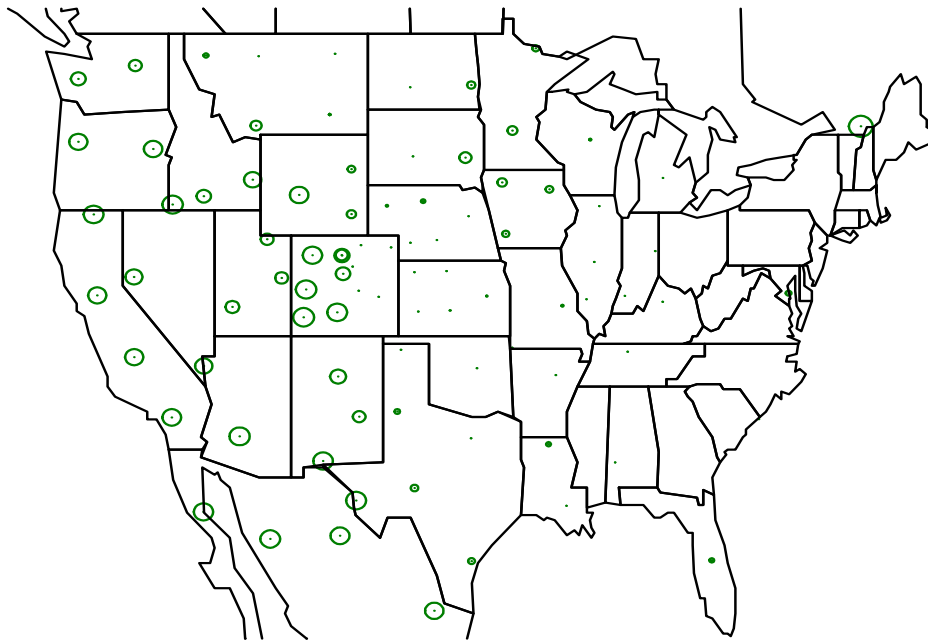


Figure 5.132. Summer NH<sub>3</sub> source areas for Region 5.

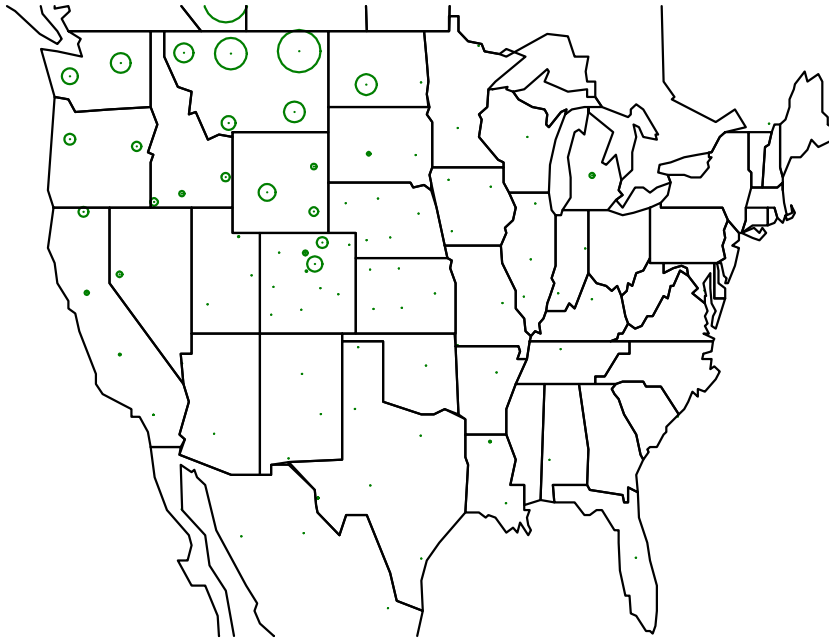


Figure 5.133. Summer NH<sub>4</sub> source areas for Region 13.

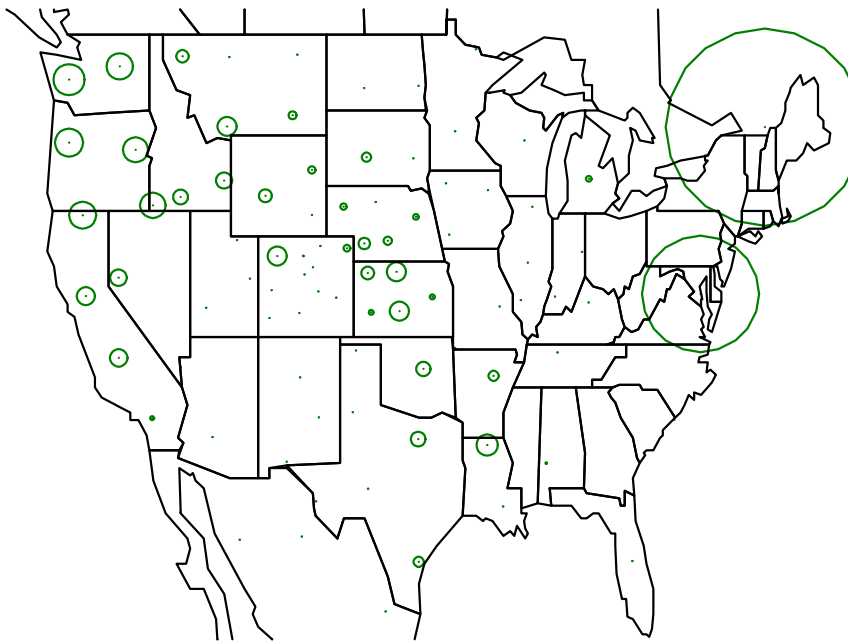


Figure 5.134. Summer NH<sub>3</sub> source areas for Region 16.

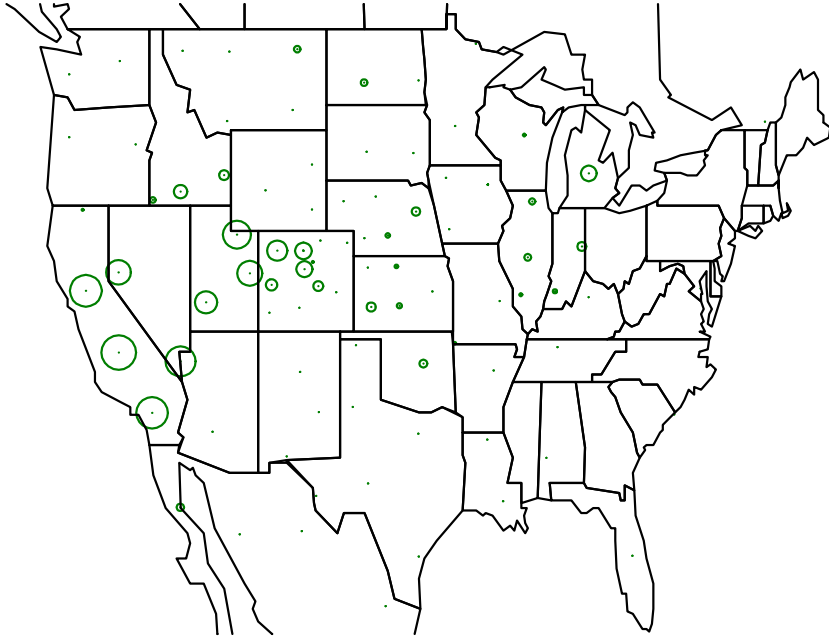


Figure 5.135. Summer  $\text{NH}_3$  and  $\text{NH}_4$  source areas for Region 18.

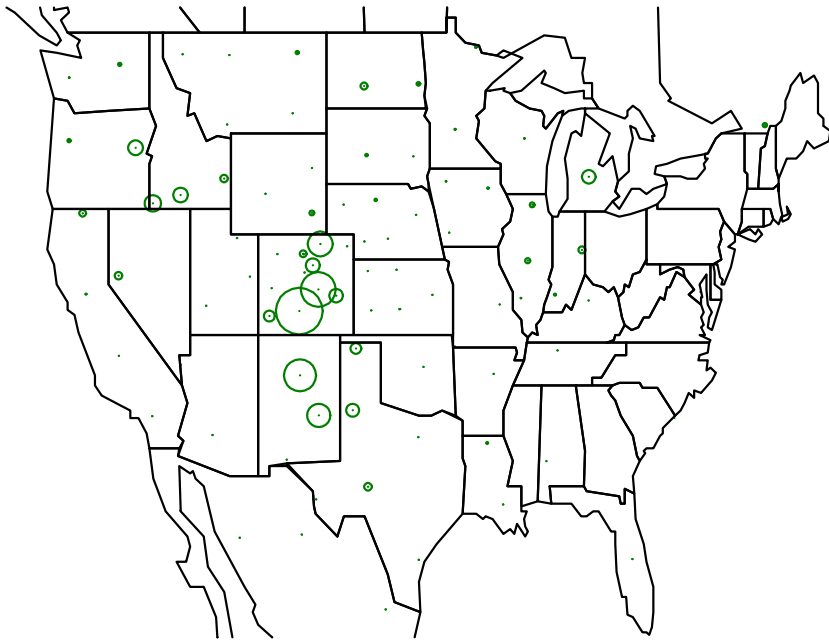


Figure 5.136. Summer  $\text{NH}_4$  source areas for Region 19.

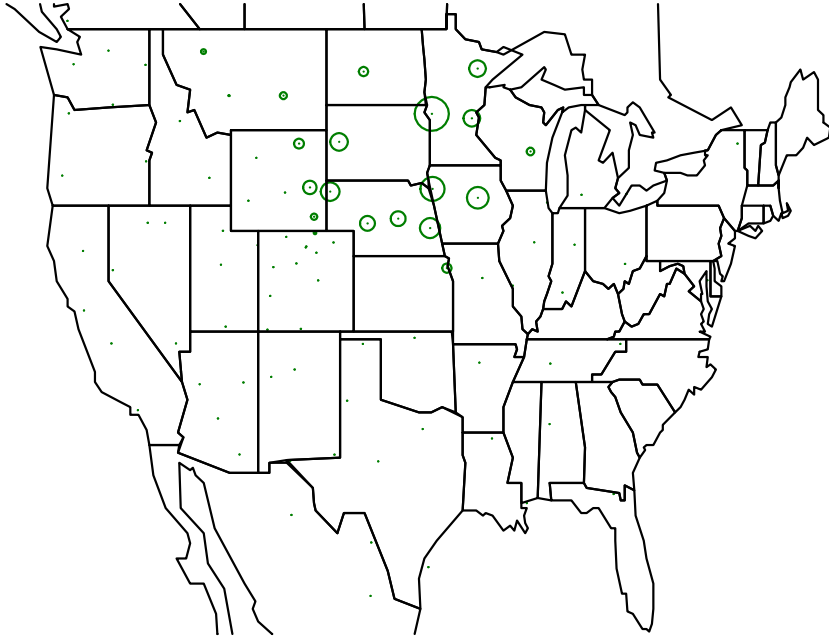


Figure 5.137. Summer  $\text{NO}_3$  source areas for Region 2.

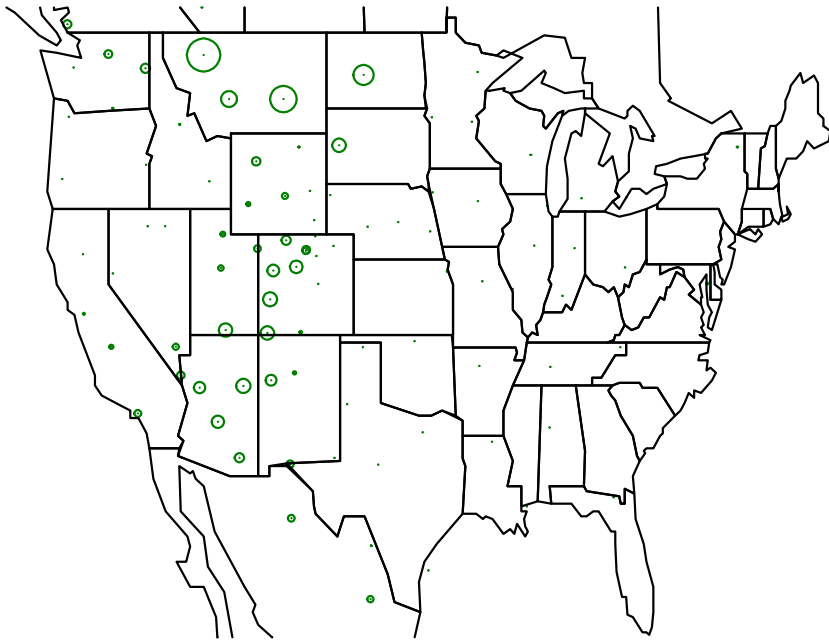


Figure 5.138. Summer  $\text{NO}_x$  and  $\text{NO}_3$  source areas for Region 5.

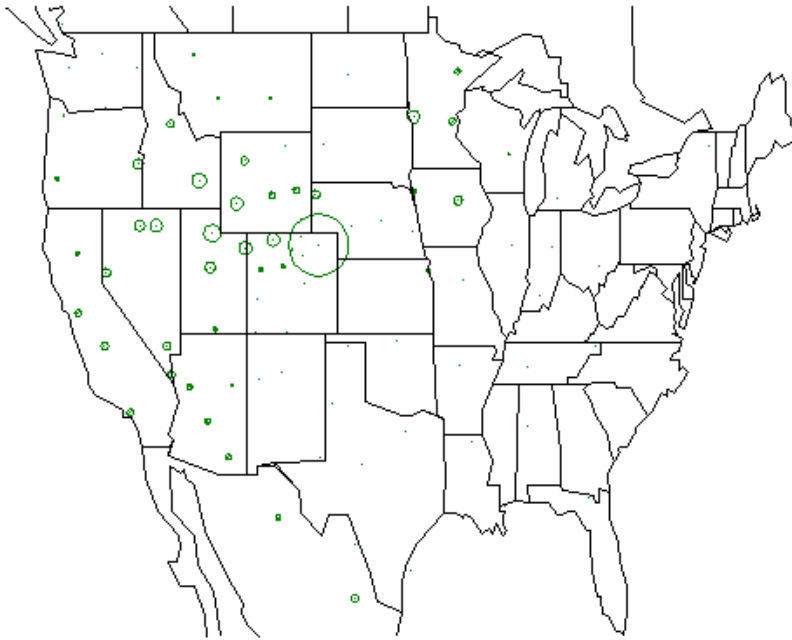


Figure 5.139. Summer  $\text{NO}_x$  and  $\text{HNO}_3$  source areas for Region 6.

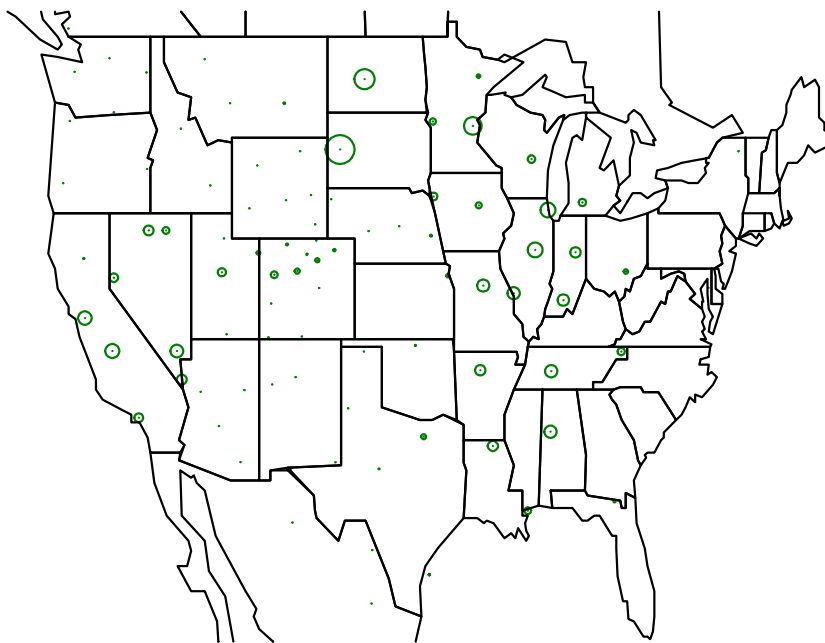


Figure 5.140. Summer  $\text{HNO}_3$  and  $\text{NO}_3$  source areas for Region 8.

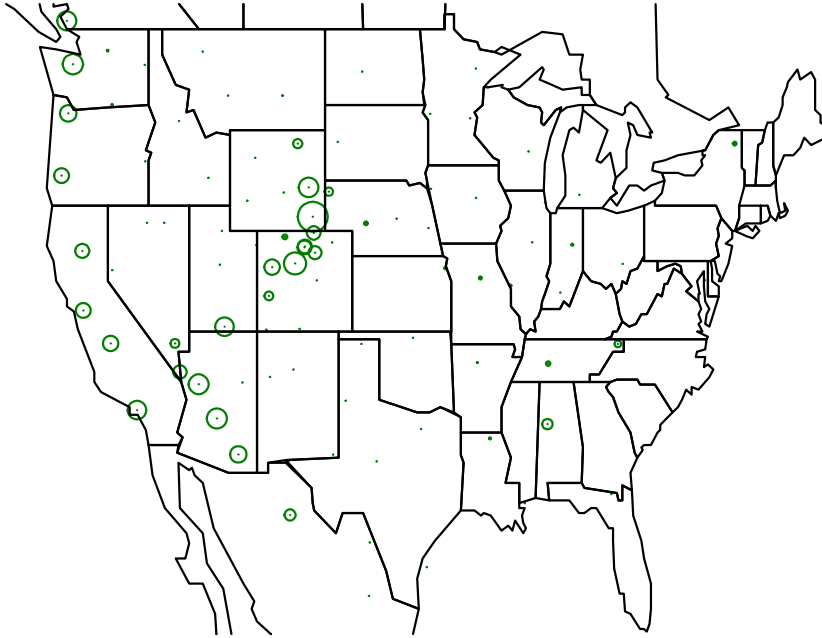


Figure 5.141. Summer  $\text{NO}_x$ ,  $\text{HNO}_3$ , and  $\text{NO}_3$  source areas for Region 9.

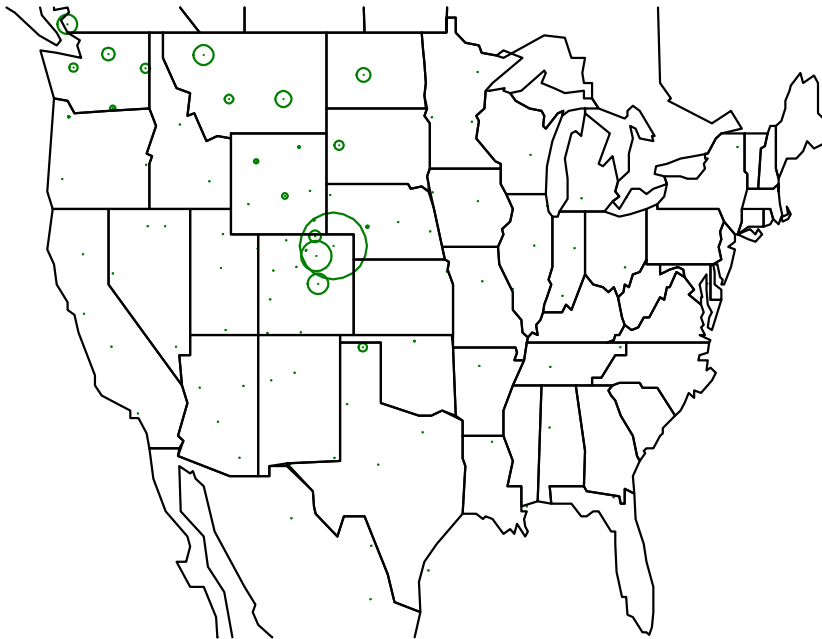


Figure 5.142. Summer  $\text{HNO}_3$  source areas for Region 13.

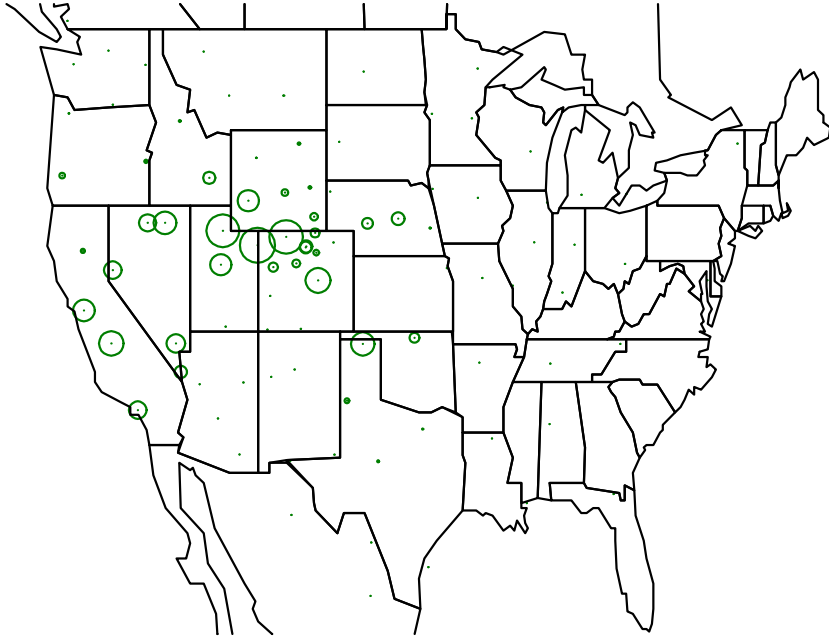


Figure 5.143. Summer HNO<sub>3</sub> source areas for Region 16.

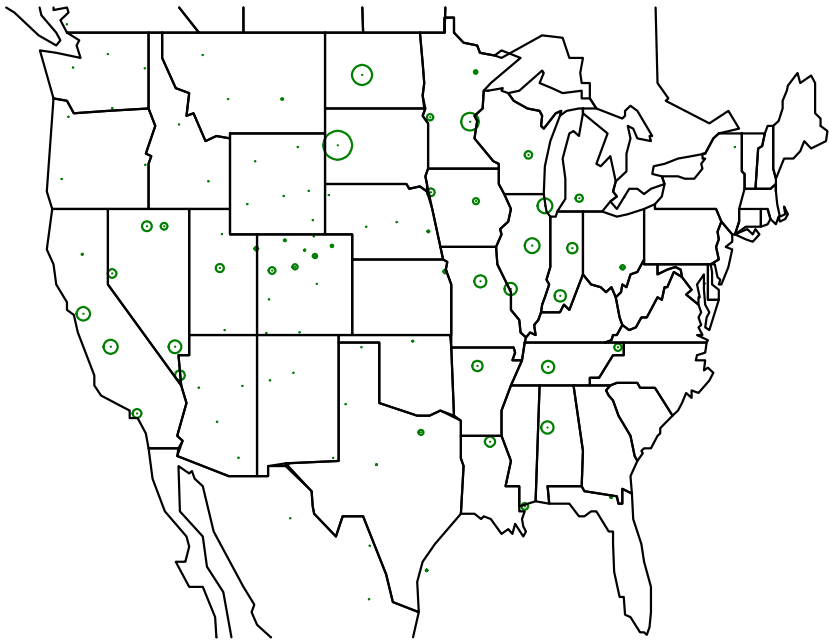


Figure 5.144. Summer NO<sub>x</sub> source areas for Region 17.

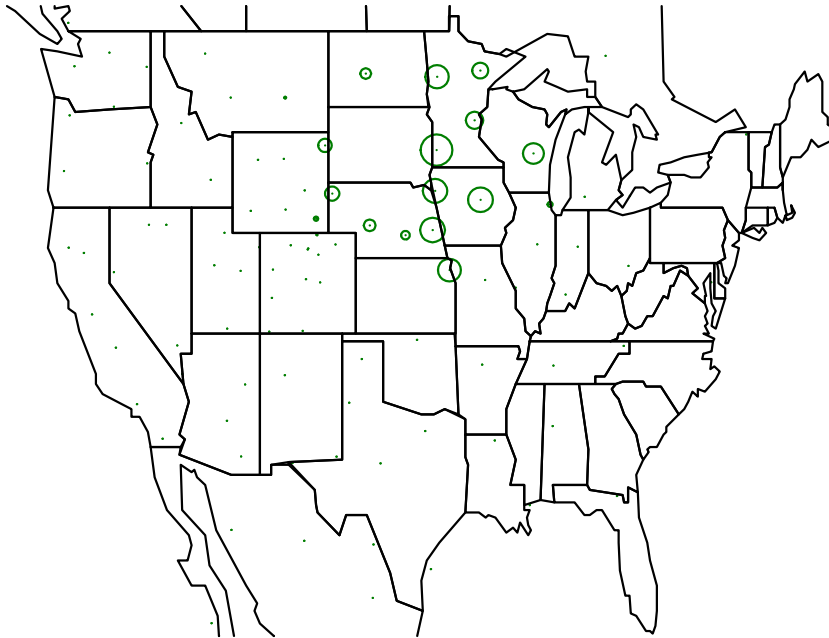


Figure 5.145. Summer SO<sub>4</sub> source areas for Region 2.

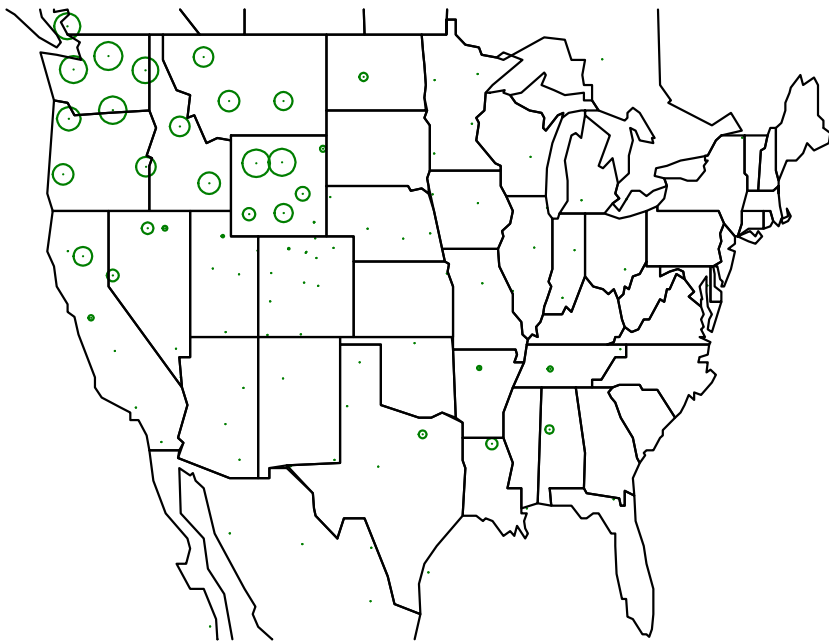


Figure 5.146. Summer SO<sub>2</sub> source areas for Region 4.

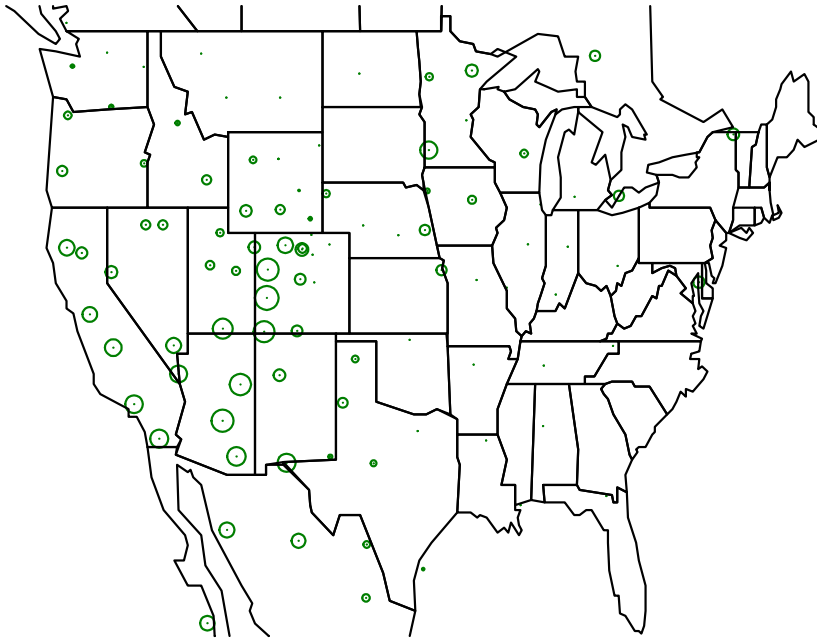


Figure 5.147. Summer SO<sub>2</sub> source areas for Region 5.

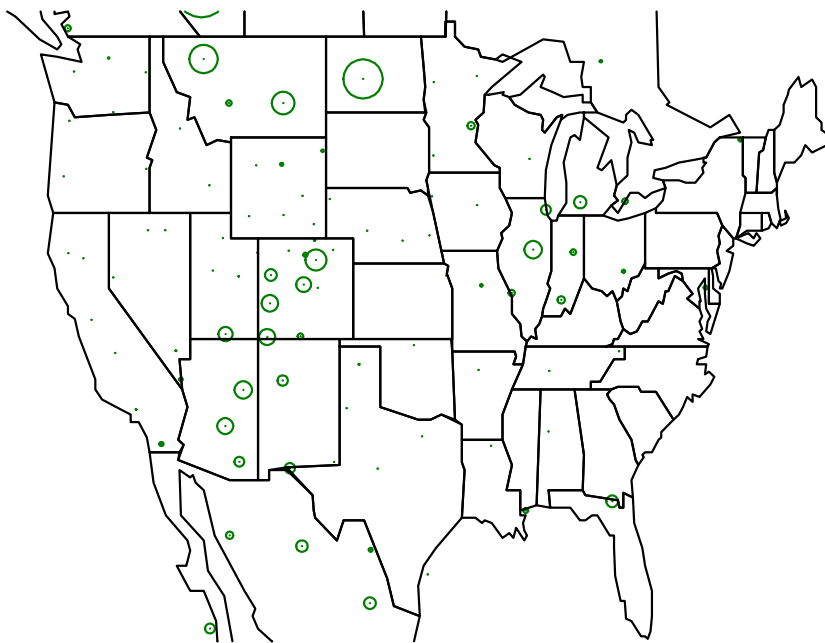


Figure 5.148. Summer SO<sub>4</sub> source areas for Region 6.

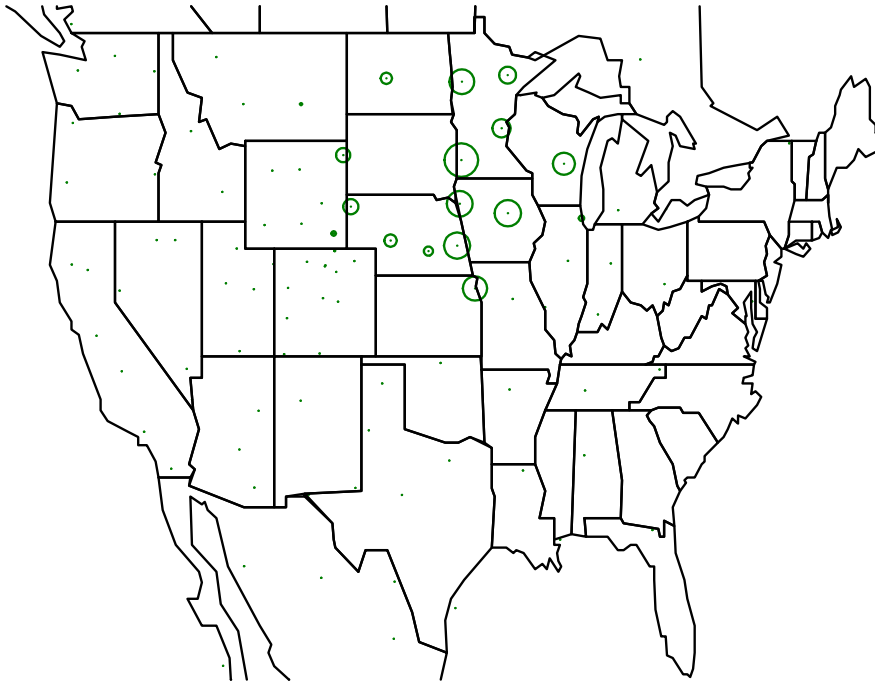


Figure 5.149. Summer SO<sub>2</sub> and SO<sub>4</sub> source areas for Region 11.

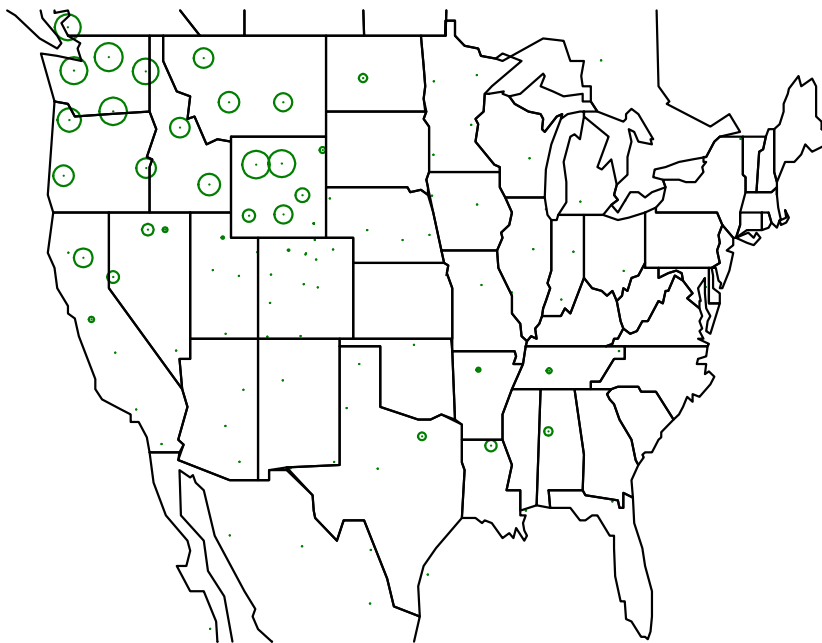


Figure 5.150. Summer SO<sub>2</sub> source areas for Region 13.

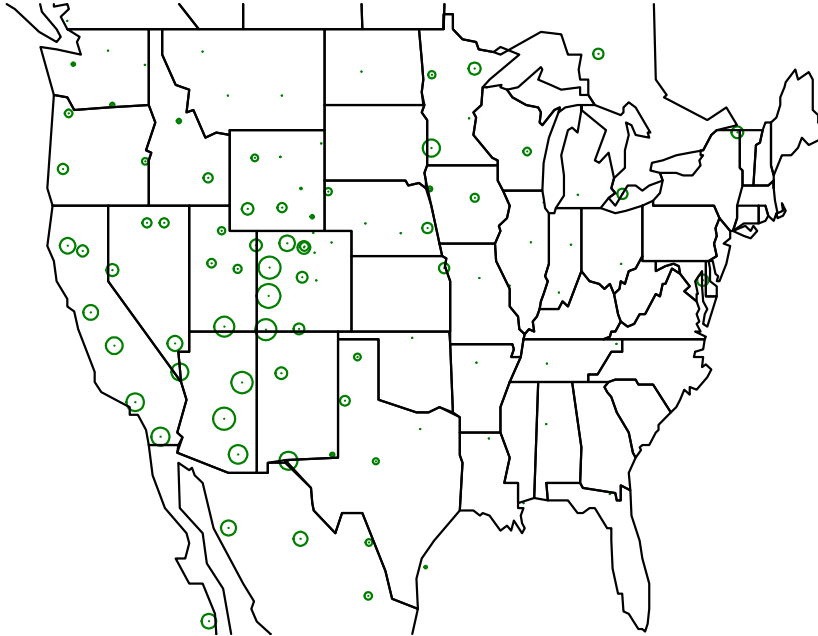


Figure 5.151. Summer SO<sub>2</sub> source areas for Region 14.

After weighting the TM concentrations for deposition, the contribution from source regions represented in Figures 5.117–5.151 were summed to form the independent variables in the regression model represented by Equation 5.23. Results of the regressions for all variables for both spring and summer are summarized in Tables 5.23 and 5.24, respectively, and the average regression model apportionment for each source region is listed under “Fraction.”

**Table 5.23.** Statistical summary of spring source area apportionment, stepwise regression analysis showing which source areas are statistically significantly related to measurements of various aerosol species at the RMNP receptor site.

	Source Area	Estimate	Std Error	t-value	Prob> t	Fraction
NH <sub>3</sub>	Region 6	1.27	0.15	8.31	0.00	0.32
	Region 14	1.66	0.24	6.93	0.00	0.22
	Region 15	1.58	0.10	16.51	0.00	0.47
NH <sub>4</sub>	Region 7	1.67	0.13	12.45	0.00	0.34
	Region 14	1.17	0.14	8.58	0.00	0.25
	Region 15	2.14	0.12	18.48	0.00	0.41
NO <sub>x</sub>	Region 3	2.11	0.69	3.05	0.00	0.11
	Region 5	2.09	0.17	12.59	0.00	0.44
	Region 6	1.06	0.21	4.99	0.00	0.16
	Region 10	6.65	1.82	3.65	0.00	0.08
	Region 11	11.48	1.72	6.69	0.00	0.17
HNO <sub>3</sub>	Region 14	2.22	1.38	1.61	0.11	0.04
	Region 3	1.48	0.21	7.10	0.00	0.31
	Region 5	0.24	0.03	8.47	0.00	0.34
	Region 6	0.27	0.04	6.08	0.00	0.23

	Source Area	Estimate	Std Error	t-value	Prob> t	Fraction
	Region 14	2.69	0.80	3.34	0.00	0.12
NO <sub>3</sub>	Region 5	0.60	0.05	12.71	0.00	0.60
	Region 6	0.12	0.06	1.89	0.06	0.09
	Region 11	4.45	0.48	9.29	0.00	0.31
SO <sub>2</sub>	Region 3	0.36	0.11	3.30	0.00	0.18
	Region 6	10.75	2.29	4.70	0.00	0.21
	Region 8	1.50	0.13	11.60	0.00	0.60
SO <sub>4</sub>	Region 3	0.78	0.16	4.73	0.00	0.14
	Region 4	2.94	0.66	4.42	0.00	0.11
	Region 7	7.33	0.58	12.58	0.00	0.41
	Region 8	2.24	0.21	10.86	0.00	0.33

**Table 5.24.** Statistical summary of summer source area apportionment, stepwise regression analysis showing which source areas are statistically significantly related to measurements of various aerosol species at the RMNP receptor site.

	Source Area	Estimate	Std Error	t-value	Prob> t	Fraction
NH <sub>3</sub>	Region 1	1.00	0.05	21.50	0.00	0.37
	Region 16	1.51	0.20	7.41	0.00	0.26
	Region 18	0.26	0.03	9.87	0.00	0.37
NH <sub>4</sub>	Region 1	0.61	0.05	12.06	0.00	0.08
	Region 5	0.81	0.04	20.47	0.00	0.60
	Region 13	0.22	0.09	2.43	0.02	0.05
	Region 18	0.08	0.01	5.84	0.00	0.16
	Region 19	0.22	0.04	5.20	0.00	0.11
NO <sub>x</sub>	Region 5	1.96	0.17	11.78	0.00	0.38
	Region 6	0.65	0.14	4.59	0.00	0.12
	Region 9	0.69	0.04	16.29	0.00	0.44
	Region 17	0.72	0.25	2.89	0.00	0.06
HNO <sub>3</sub>	Region 6	0.43	0.08	5.55	0.00	0.12
	Region 8	59.27	4.94	12.00	0.00	0.39
	Region 9	0.19	0.01	14.93	0.00	0.28
	Region 13	2.53	0.80	3.15	0.00	0.11
	Region 16	16.50	5.41	3.05	0.00	0.10
NO <sub>3</sub>	Region 2	0.53	0.08	6.97	0.00	0.18
	Region 5	0.07	0.03	2.13	0.03	0.15
	Region 8	0.97	0.12	7.82	0.00	0.55
	Region 9	0.02	0.01	2.03	0.04	0.13
SO <sub>2</sub>	Region 3	2.08	0.32	6.41	0.00	0.21
	Region 4	2.06	0.21	9.87	0.00	0.40
	Region 10	2.23	0.41	5.48	0.00	0.13
	Region 12	0.37	0.06	6.73	0.00	0.14
	Region 13	1.23	0.36	3.41	0.00	0.11
SO <sub>4</sub>	Region 2	6.07	0.43	14.05	0.00	0.13
	Region 6	0.30	0.05	6.08	0.00	0.08
	Region 11	1.98	0.06	33.72	0.00	0.79

	<b>Source Area</b>	<b>Estimate</b>	<b>Std Error</b>	<b>t-value</b>	<b>Prob&gt; t </b>	<b>Fraction</b>
NH <sub>3</sub>	Region 1	1.00	0.05	21.50	0.00	0.37
	Region 16	1.51	0.20	7.41	0.00	0.26
	Region 18	0.26	0.03	9.87	0.00	0.37
NH <sub>4</sub>	Region 1	0.61	0.05	12.06	0.00	0.08
	Region 5	0.81	0.04	20.47	0.00	0.60
	Region 13	0.22	0.09	2.43	0.02	0.05
	Region 18	0.08	0.01	5.84	0.00	0.16
	Region 19	0.22	0.04	5.20	0.00	0.11

This fraction is the fractional contribution of the sum of all sources in a given region. It is arrived at by multiplying the respective regression coefficient by the sum of the deposition-weighted TM estimations that went into the regression model. The fractional contribution of each source within the region is calculated by taking the concentration each source contributes to the region and dividing by the total regional contribution. The concentration apportionment and fractional contribution for selected source areas, on an hour-by-hour basis, are shown in Figures 5.152–5.165, a and b. Figures 5.152c–5.165c show the average relative fractional contribution of all source regions, for the species of interest, that were used in the regression model. Figures 5.166a–b and 5.167a–b summarize the average apportionments of selected regions and to inside and outside Colorado for spring and summer, respectively. It should be noted that the data gap on April 23 and 24 is a rain event with significant amounts of missing data and was not used in the analysis.

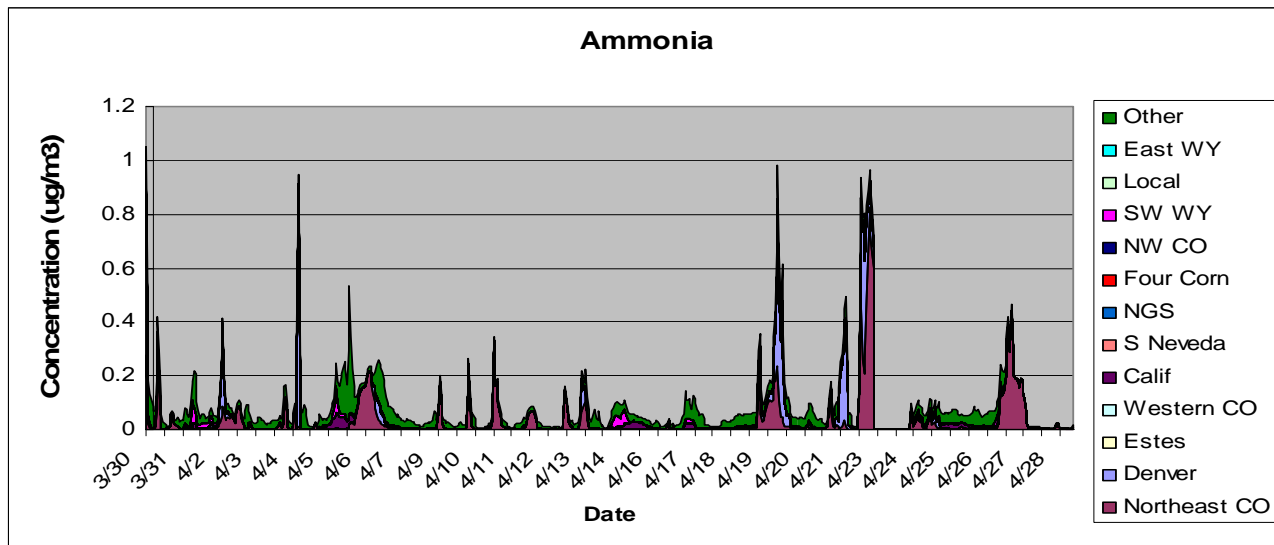


Figure 5.152a. Time series of source area contributions to NH<sub>3</sub> concentration for the spring time period.

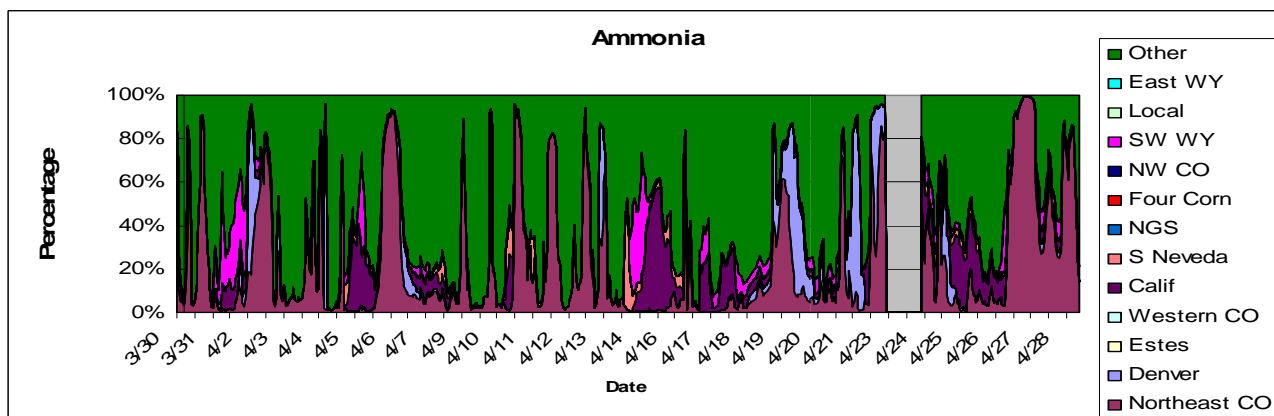


Figure 5.152b. Fraction each source contributes to NH<sub>3</sub> for the spring time period.

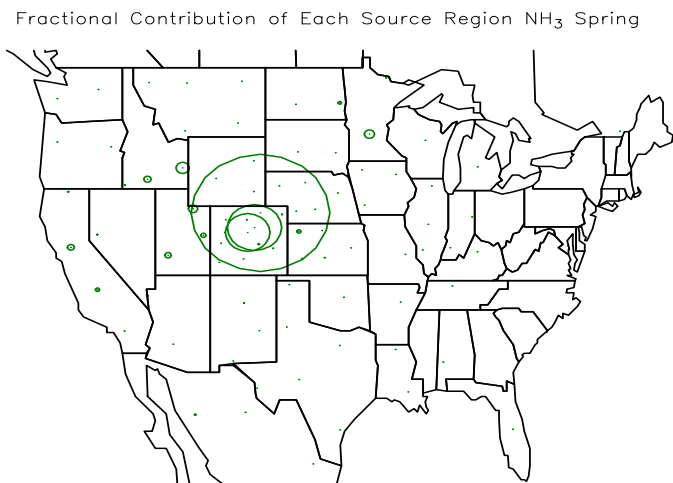


Figure 5.152c. Relative fractional contribution of each NH<sub>3</sub> source region.

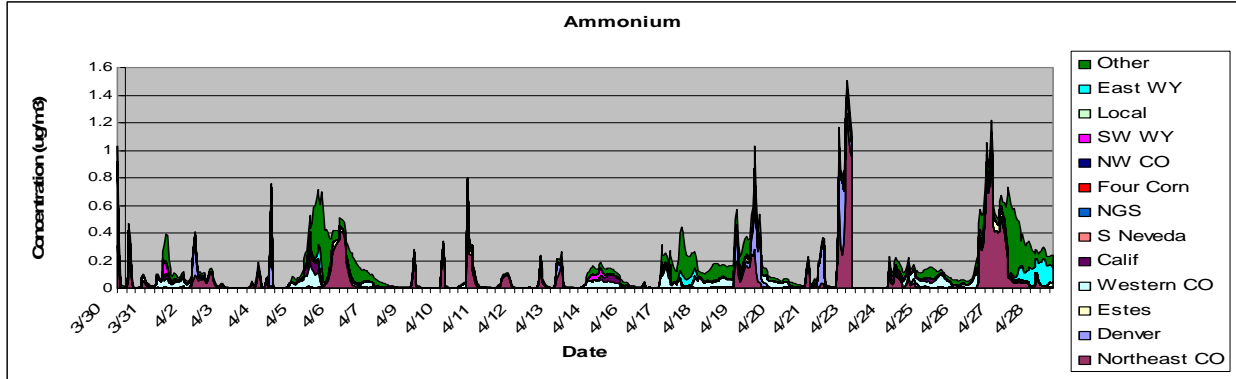


Figure 5.153a. Time series of source area contributions to NH<sub>4</sub> concentration for the spring time period.

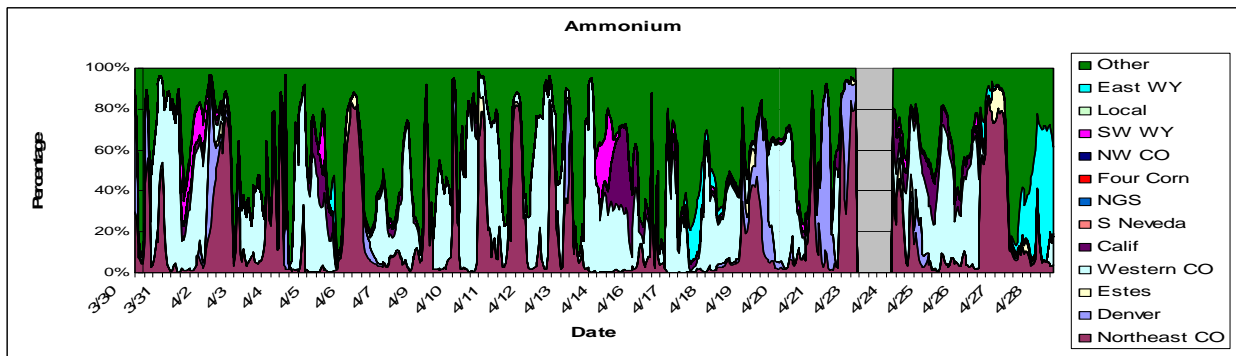


Figure 5.153b. Fraction each source contributes to NH<sub>4</sub> for the spring time period.

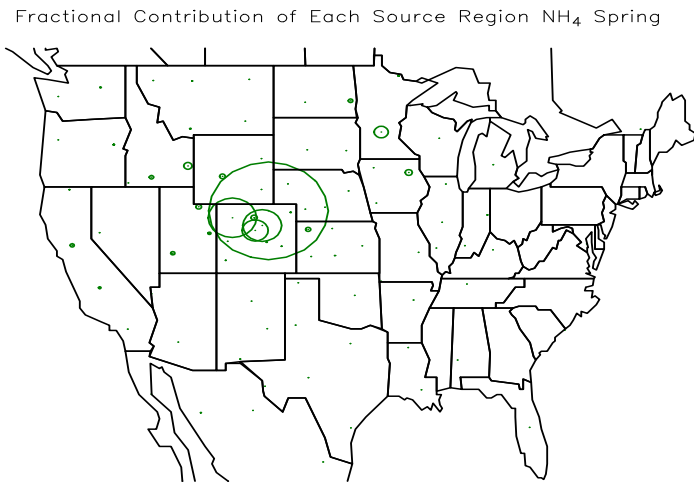


Figure 5.153c. Relative fractional contribution of each NH<sub>4</sub> source region.

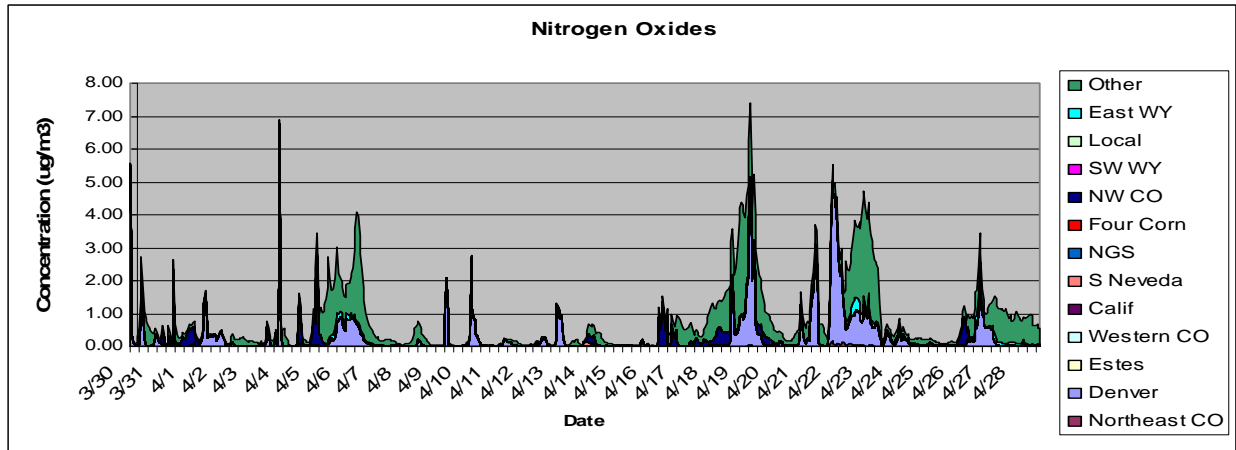


Figure 5.154a. Time series of source area contributions to NO<sub>x</sub> concentration for the spring time period.

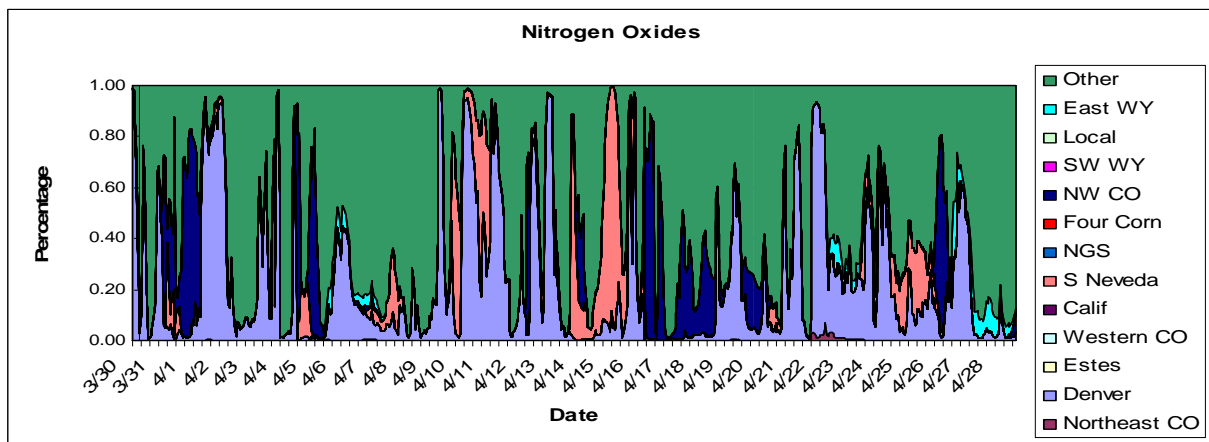


Figure 5.154b. Fraction each source contributes to NO<sub>x</sub> for the spring time period.

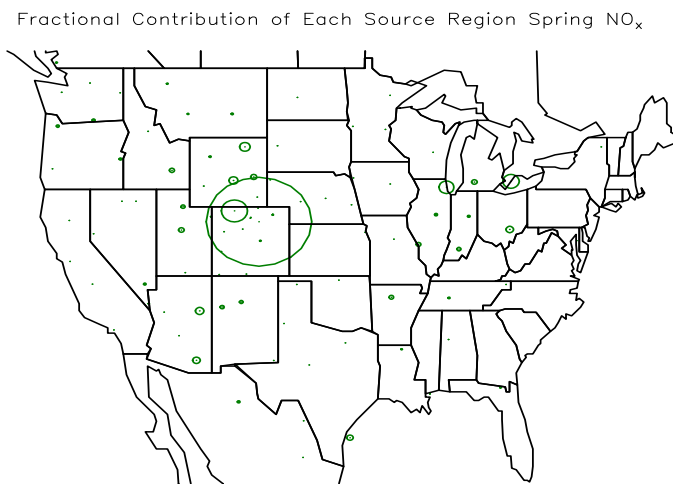


Figure 5.154c. Relative fractional contribution of each NO<sub>x</sub> source region.

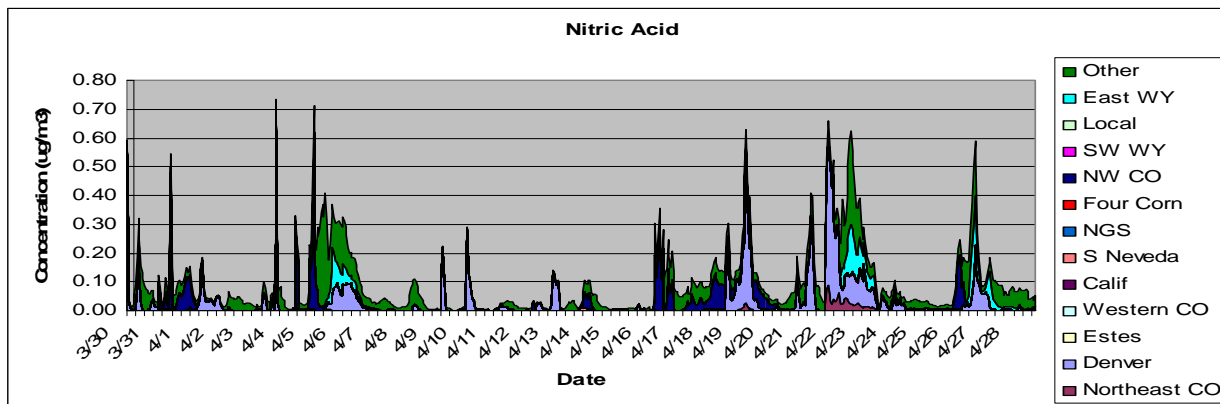


Figure 5.155a. Time series of source area contributions to HNO<sub>3</sub> concentration for the spring time period.

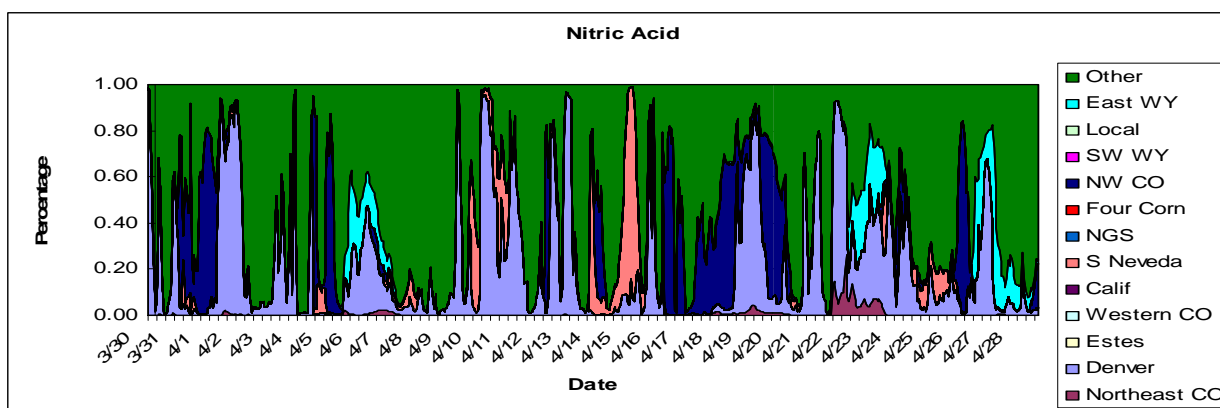


Figure 5.155b. Fraction each source contributes to HNO<sub>3</sub> for the spring time period.

Fractional Contribution of Each Source Region Spring HNO<sub>3</sub>

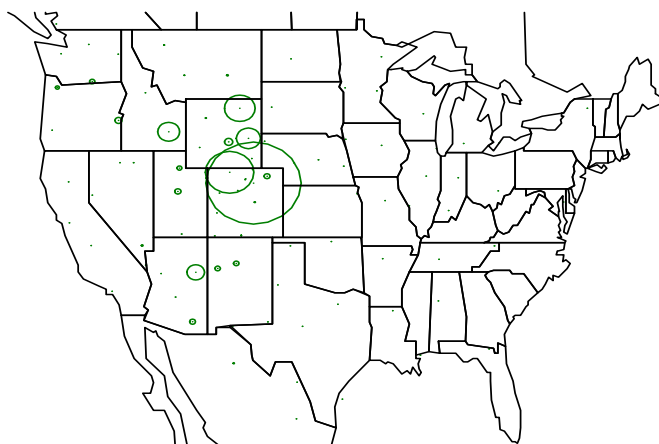


Figure 5.155c. Relative fractional contribution of each HNO<sub>3</sub> source region.

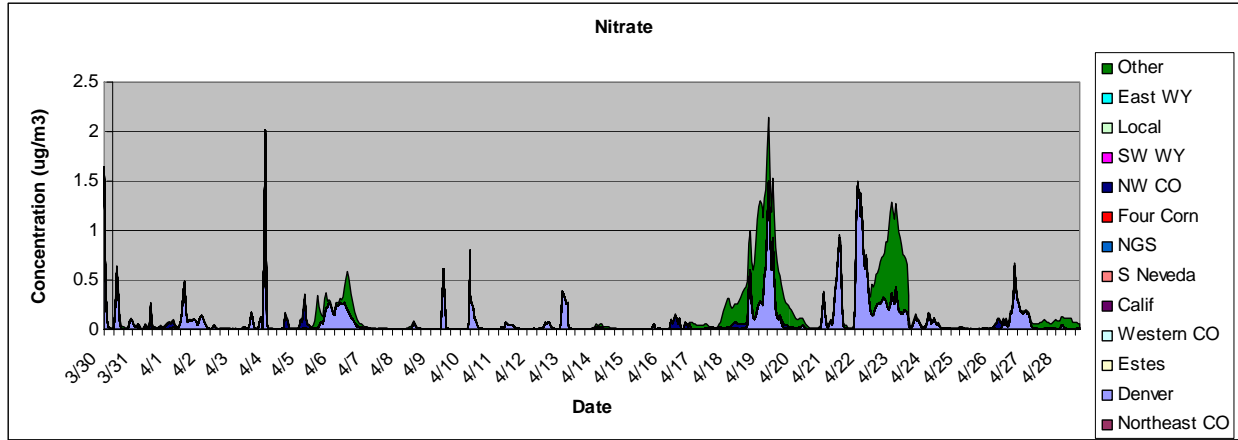


Figure 5.156a. Time series of source area contributions to NO<sub>3</sub> concentration for the spring time period.

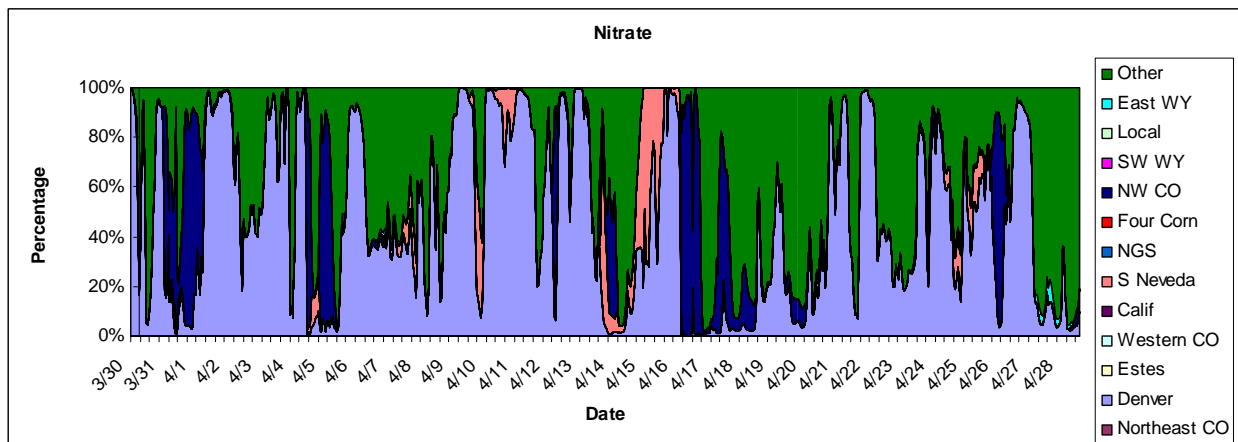


Figure 5.156b. Fraction each source contributes to NO<sub>3</sub> for the spring time period.

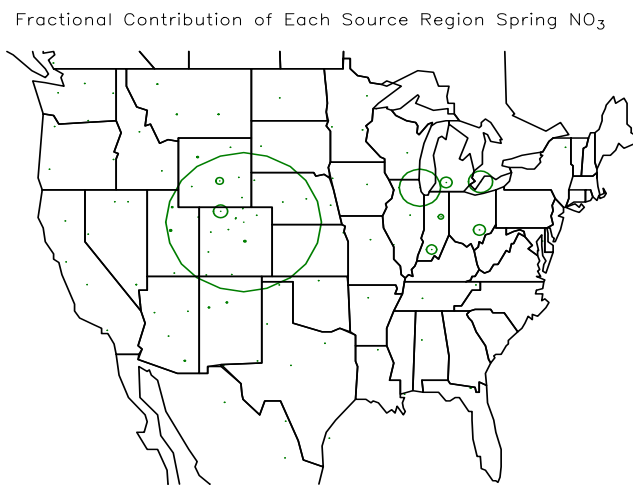


Figure 5.156c. Relative fractional contribution of each NO<sub>3</sub> source region.

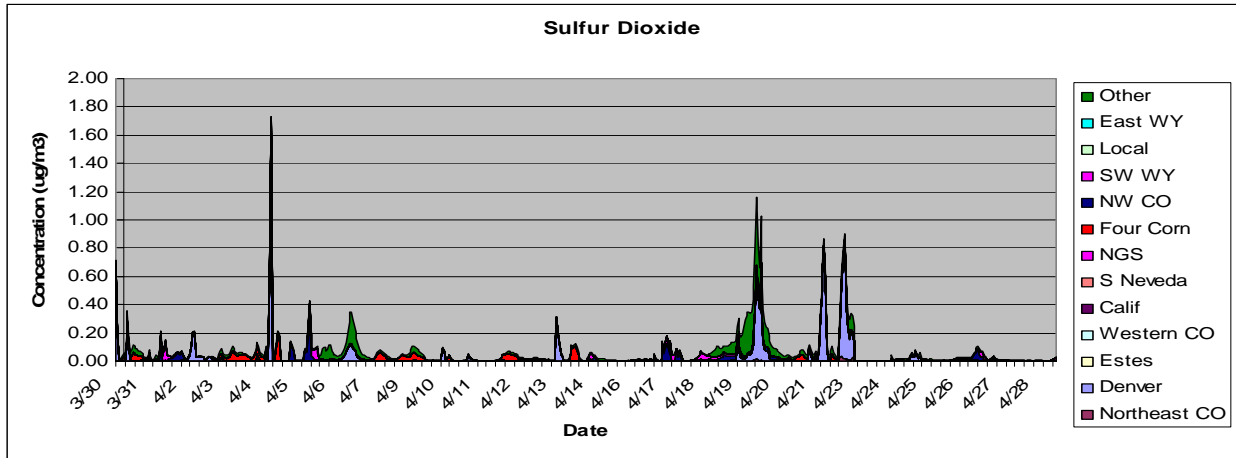


Figure 5.157a. Time series of source area contributions to SO<sub>2</sub> concentration for the spring time period.

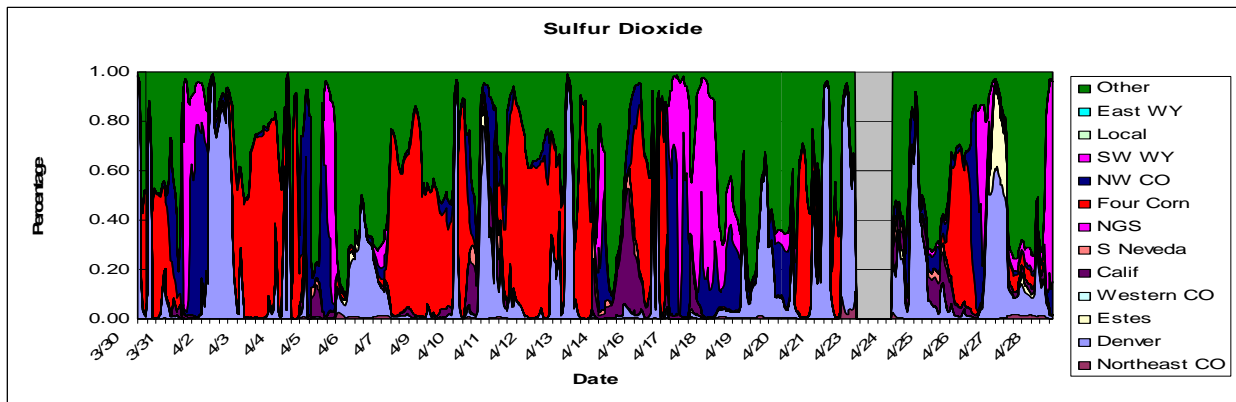


Figure 5.157b. Fraction each source contributes to SO<sub>2</sub> for the spring time period.

Fractional Contribution of Each Source Region Spring SO<sub>2</sub>

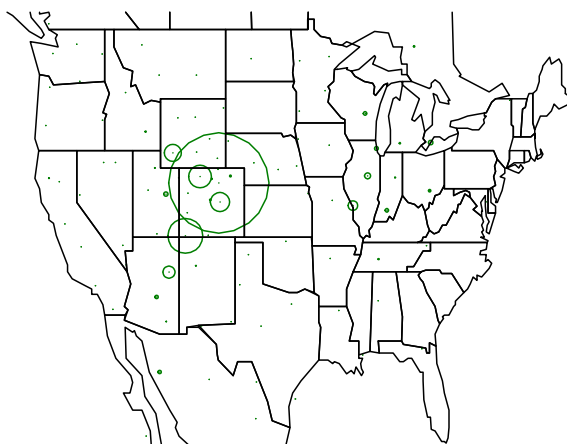


Figure 5.157c. Relative fractional contribution of each SO<sub>2</sub> source region.

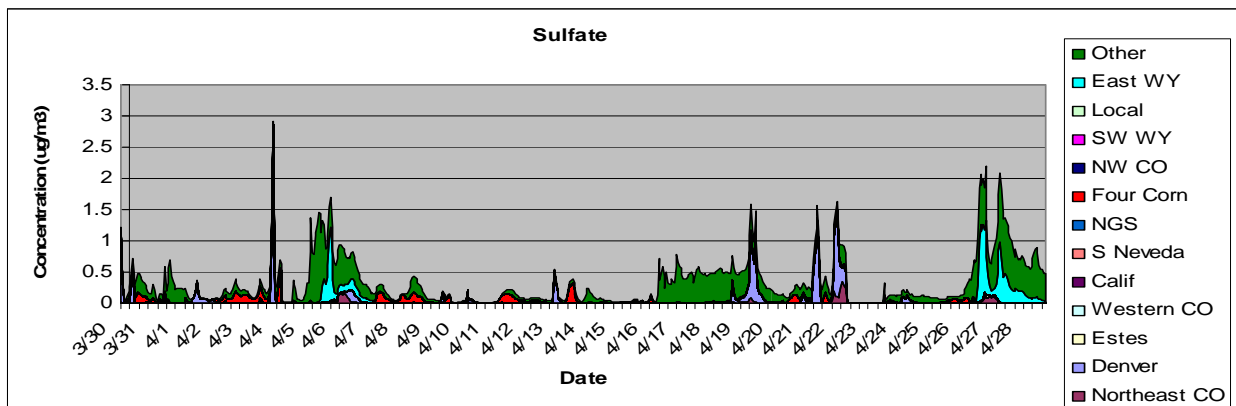


Figure 5.158a. Time series of source area contributions to SO<sub>4</sub> concentration for the spring time period.

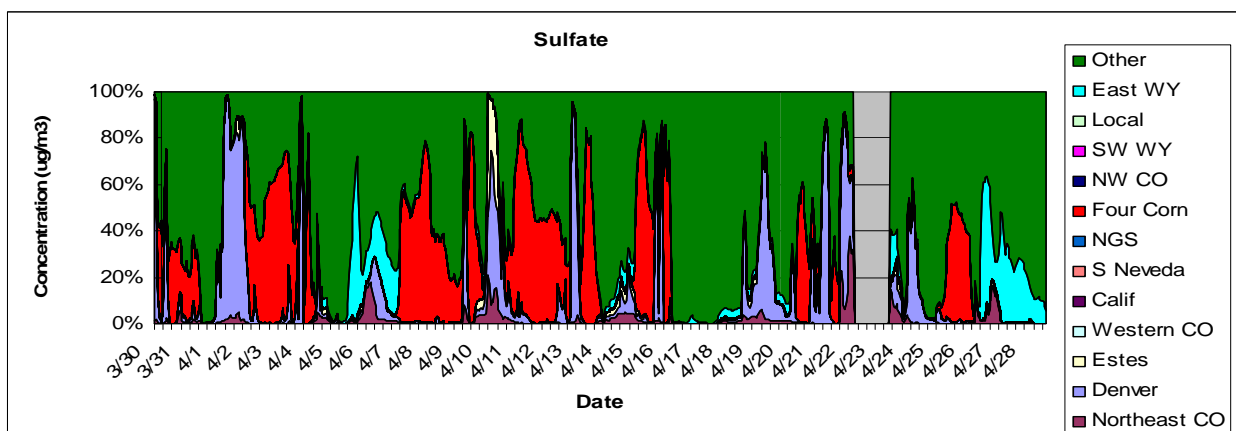


Figure 5.158b. Fraction each source contributes to SO<sub>4</sub> for the spring time period.

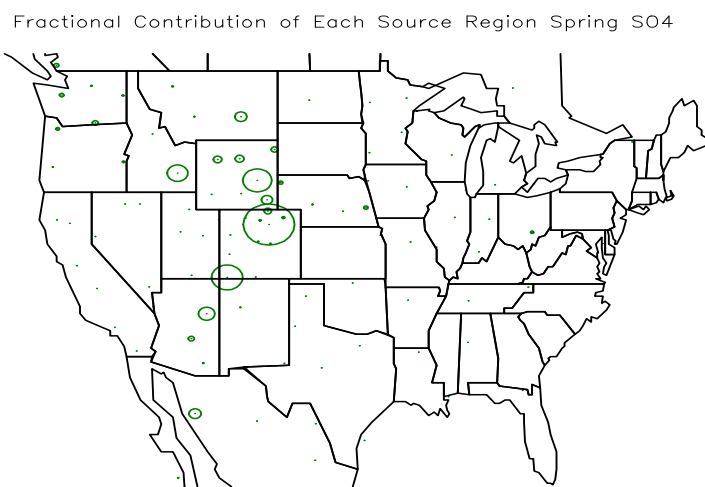


Figure 5.158c. Relative fractional contribution of each SO<sub>4</sub> source region.

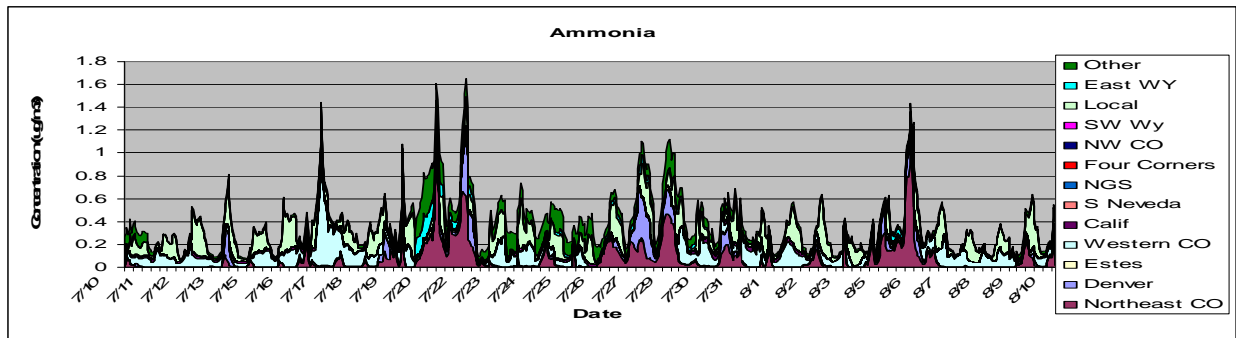


Figure 5.159a. Time series of source area contributions to NH<sub>3</sub> concentration for the summer time period.

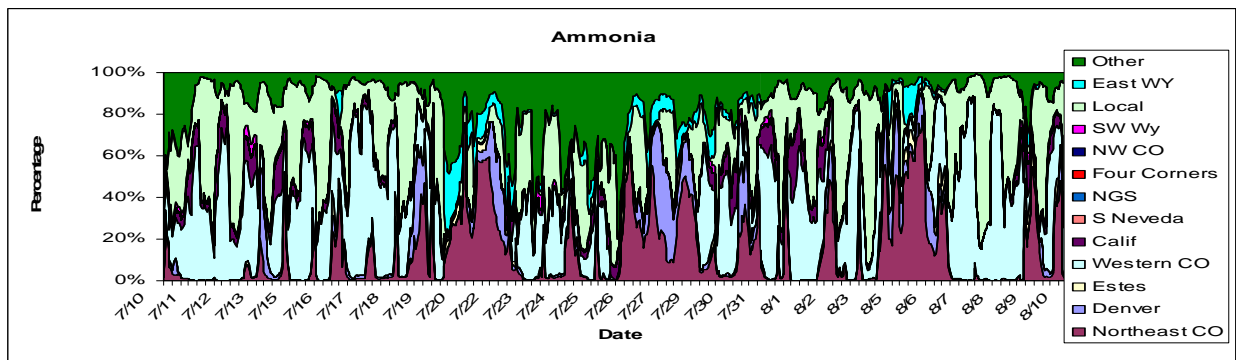


Figure 5.159b. Fraction each source contributes to NH<sub>3</sub> for the summer time period.

Fractional Contribution of Each Source Region NH<sub>3</sub> Summer

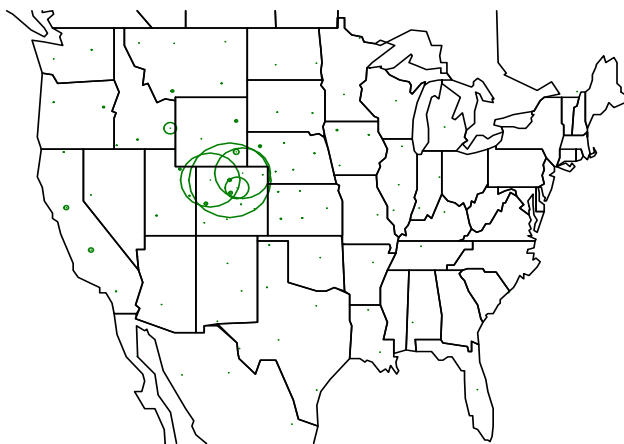


Figure 5.159c. Relative fractional contribution of each NH<sub>3</sub> source region.

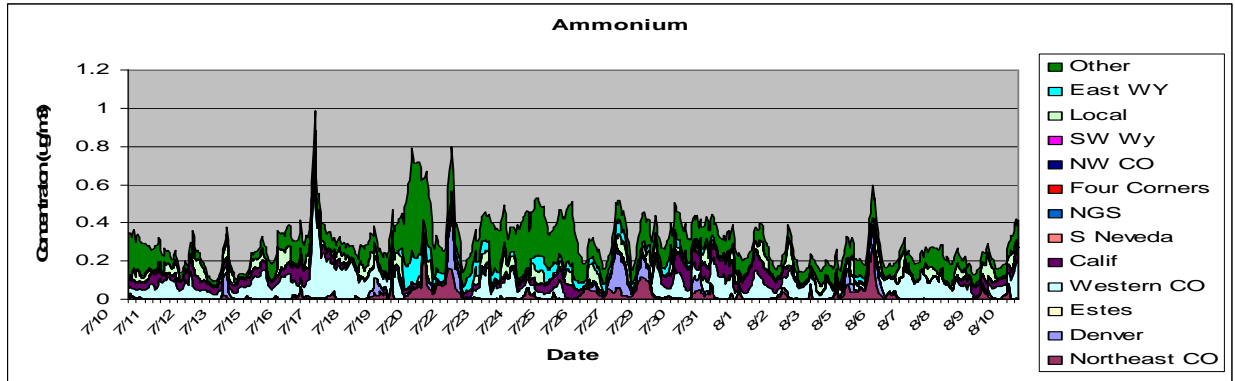


Figure 5.160a. Time series of source area contributions to NH<sub>4</sub> concentration for the summer time period.

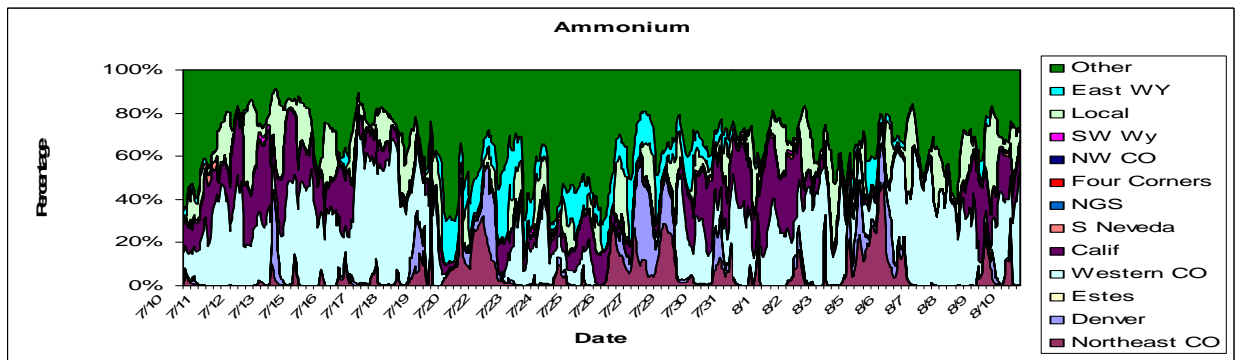


Figure 5.160b. Fraction each source contributes to NH<sub>4</sub> for the summer time period.

Fractional Contribution of Each Source Region NH<sub>4</sub> Summer

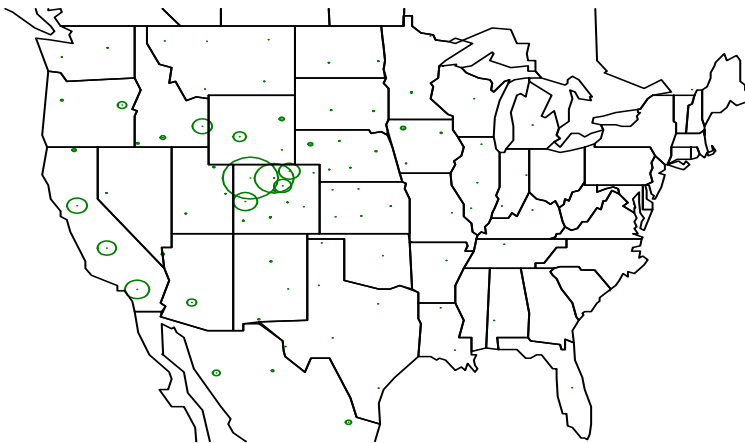


Figure 5.160c. Relative fractional contribution of each NH<sub>4</sub> source region.

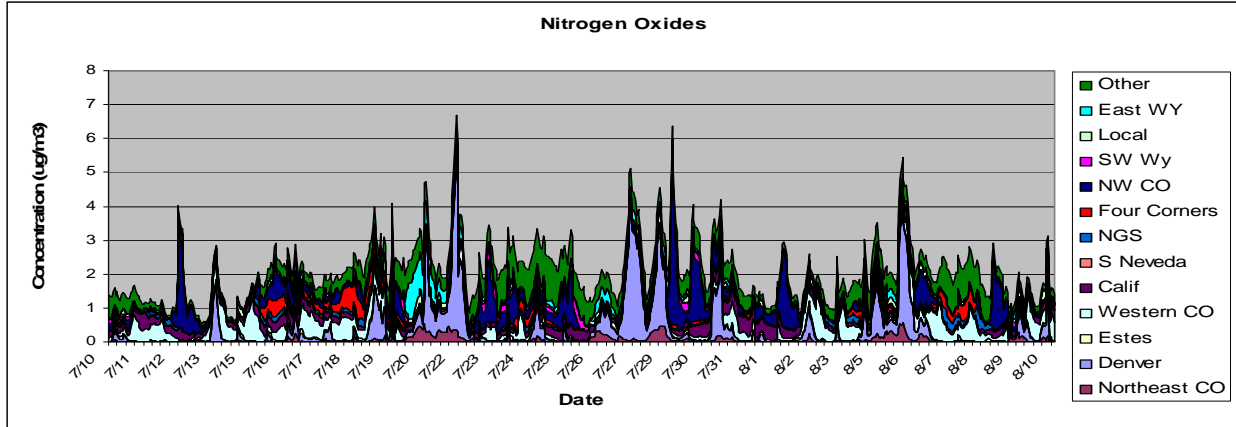


Figure 5.161a. Time series of source area contributions to NO<sub>x</sub> concentration for the summer time period.

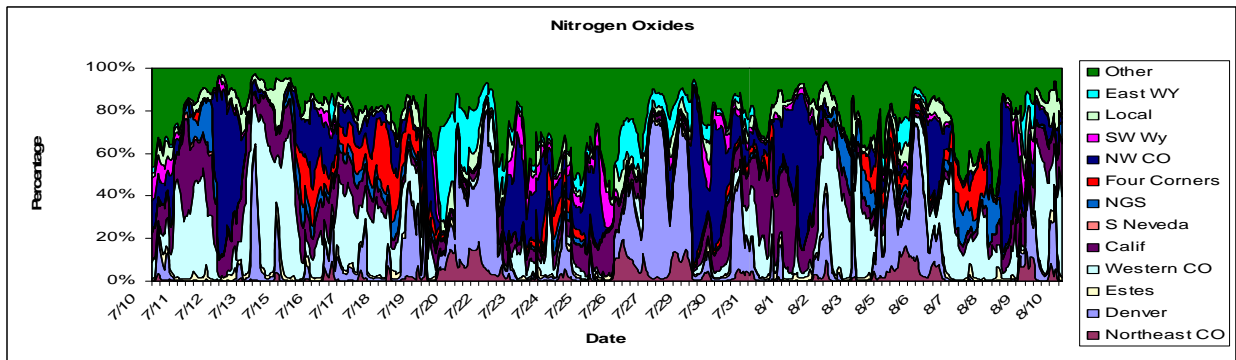


Figure 5.161b. Fraction each source contributes to NO<sub>x</sub> for the summer time period.

Fractional Contribution of Each Source Region NO<sub>x</sub> Summer

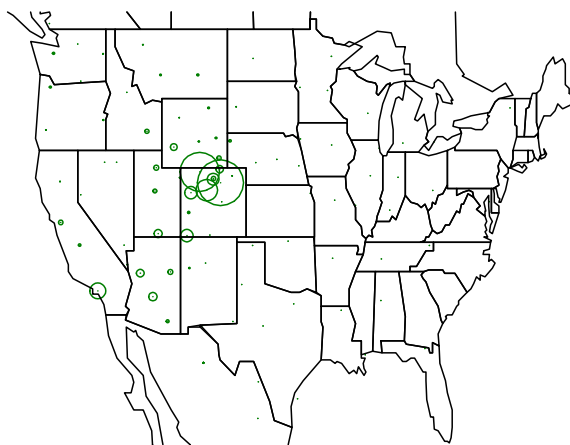


Figure 5.161c. Relative fractional contribution of each NO<sub>x</sub> source region.

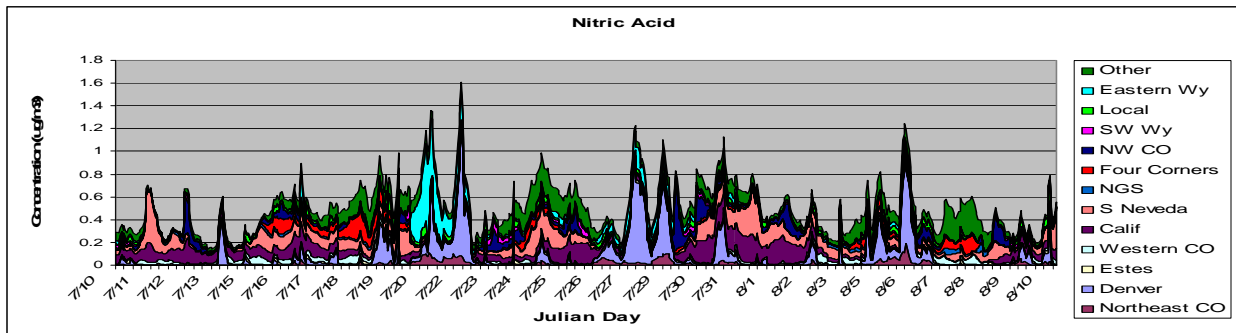


Figure 5.162a. Time series of source area contributions to HNO<sub>3</sub> concentration for the summer time period.

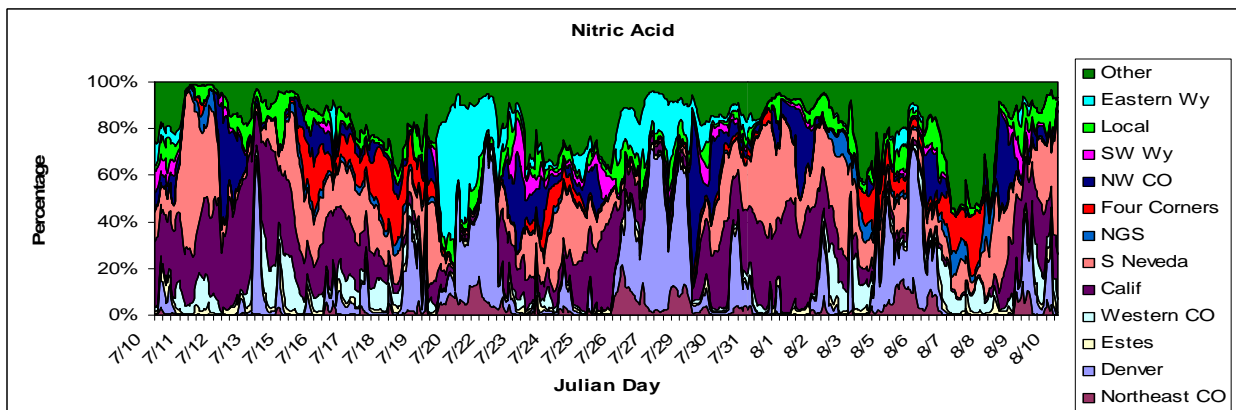


Figure 5.162b. Fraction each source contributes to HNO<sub>3</sub> for the summer time period.

Fractional Contribution of Each Source Region HNO<sub>3</sub> Summer

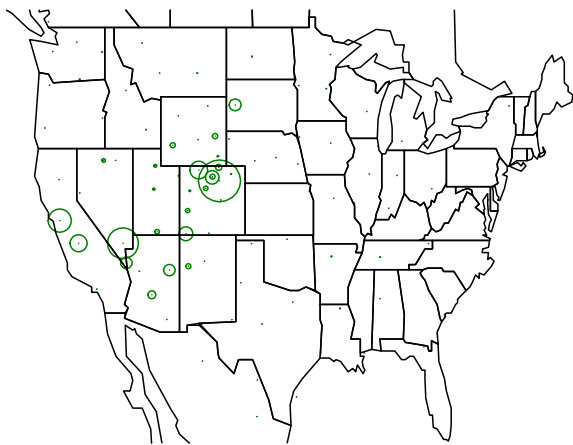


Figure 5.162c. Relative fractional contribution of each HNO<sub>3</sub> source region.

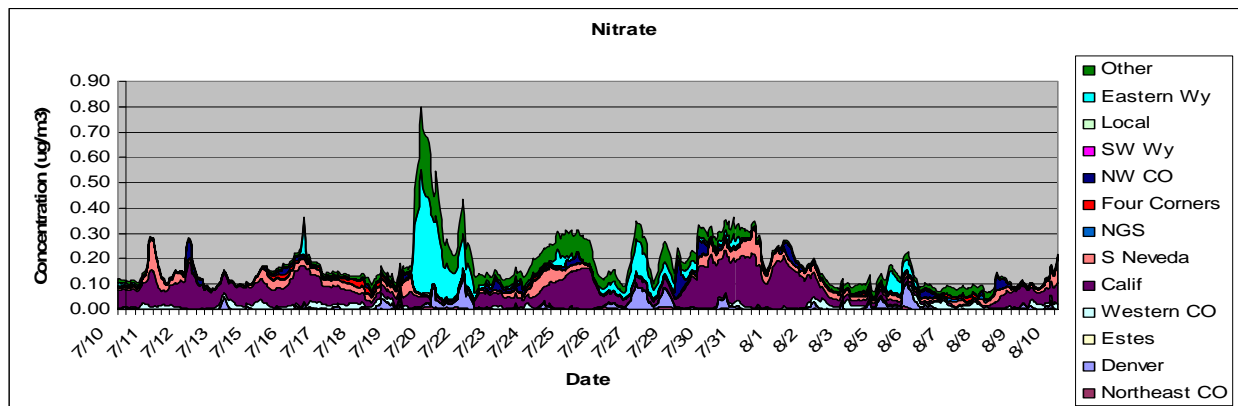


Figure 5.163a. Time series of source area contributions to NO<sub>3</sub> concentration for the summer time period.

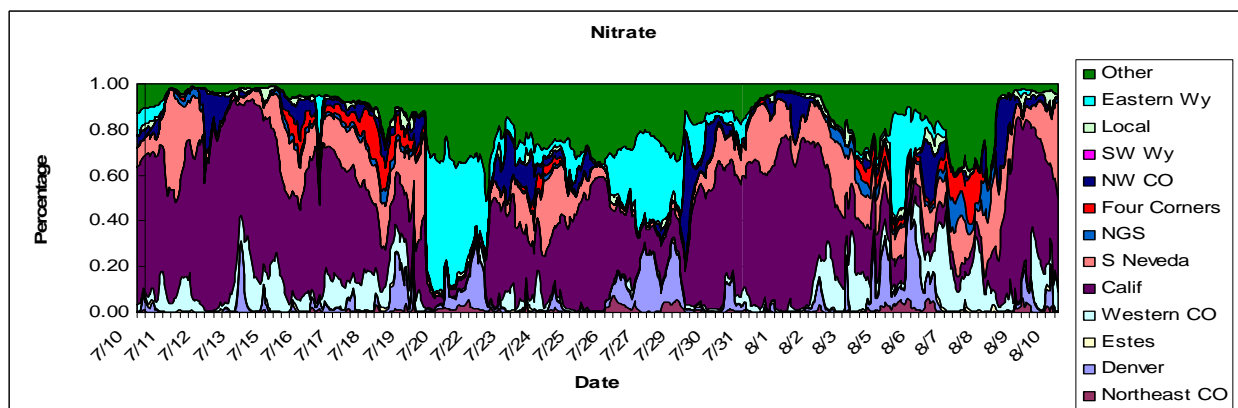


Figure 5.163b. Fraction each source contributes to NO<sub>3</sub> for the summer time period.

Fractional Contribution of Each Source Region N03 Summer

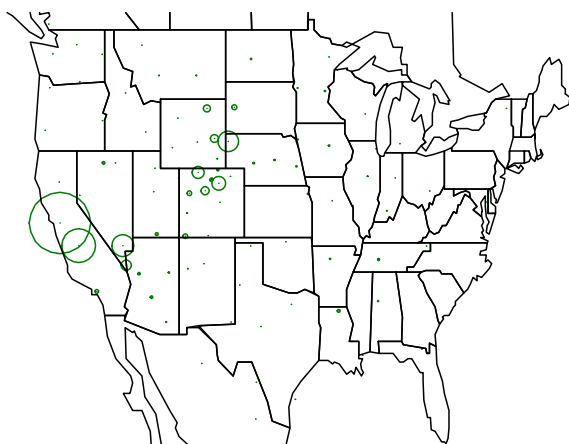


Figure 5.163c. Relative fractional contribution of each NO<sub>3</sub> source region.

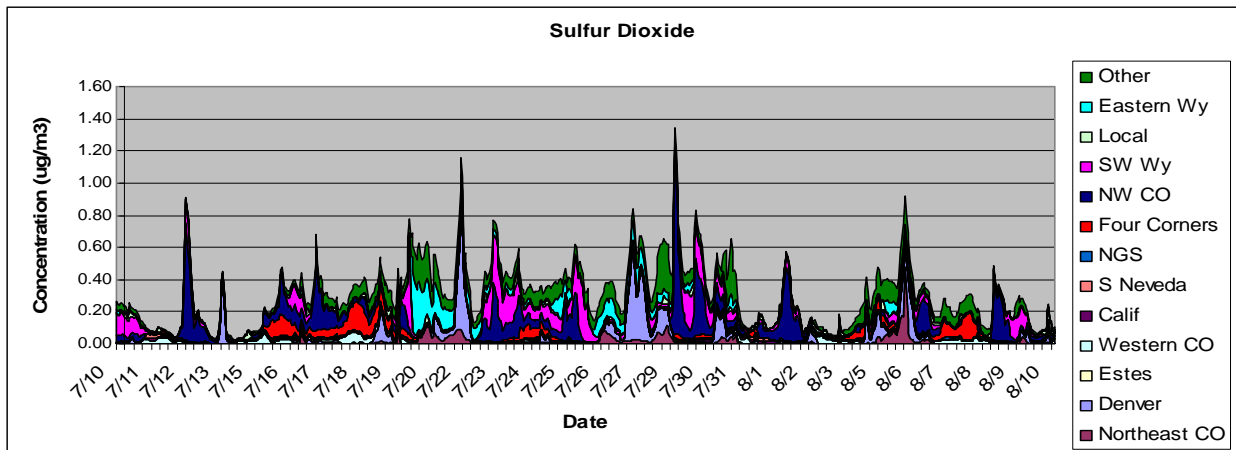


Figure 5.164a. Time series of source area contributions to SO<sub>2</sub> concentration for the summer time period.

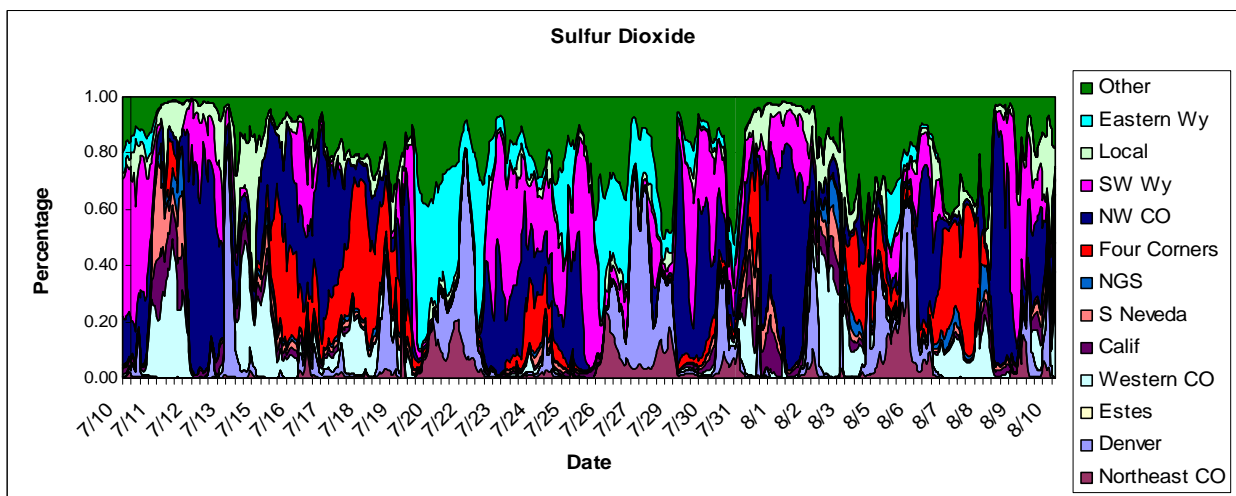


Figure 5.164b. Fraction each source contributes to SO<sub>2</sub> for the summer time period.

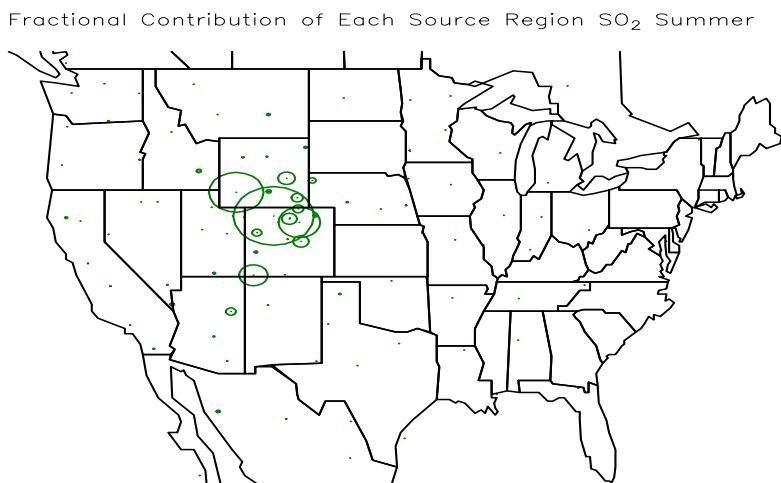


Figure 5.164c. Relative fractional contribution of each SO<sub>2</sub> source region.

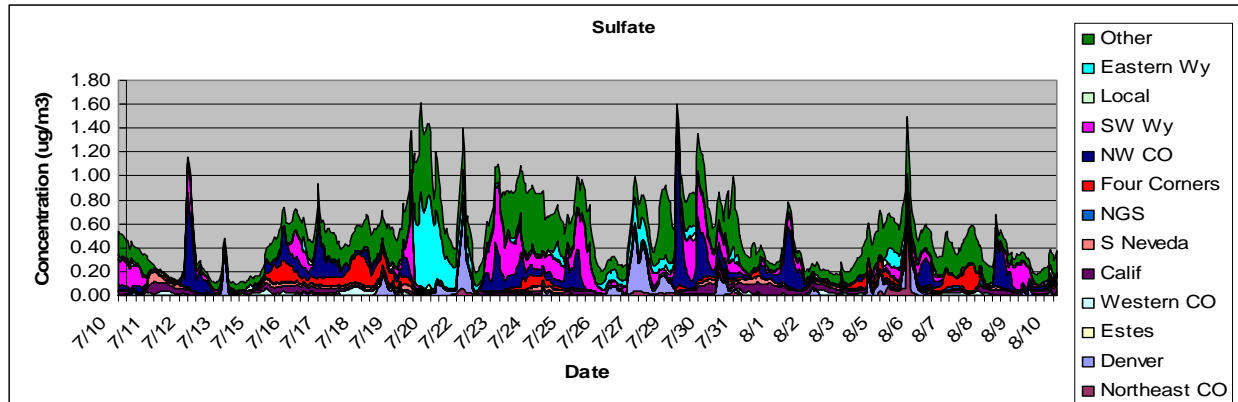


Figure 5.165a. Time series of source area contributions to SO<sub>4</sub> concentration for the summer time period.

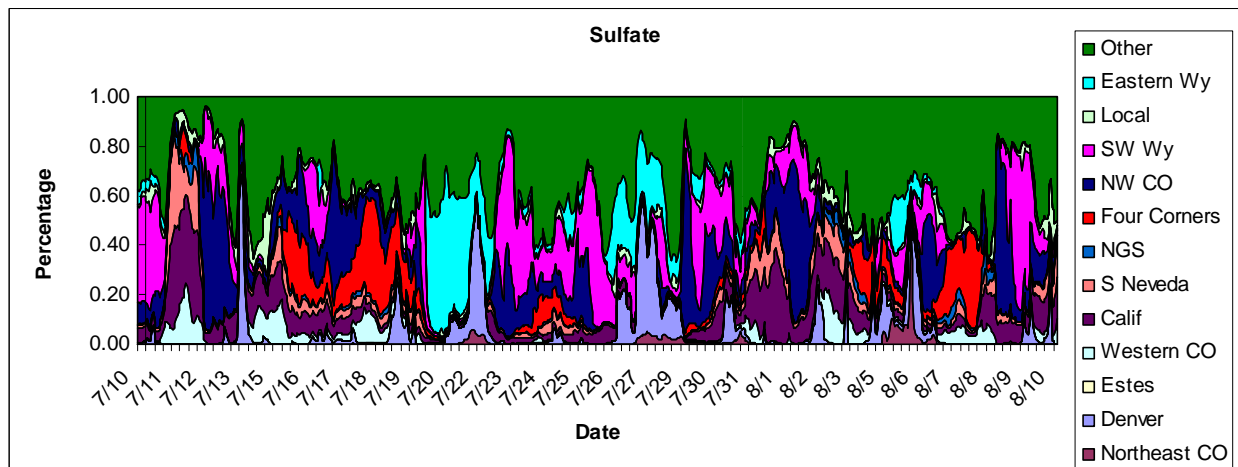


Figure 5.165b. Fraction each source contributes to SO<sub>4</sub> for the summer time period.

Fractional Contribution of Each Source Region SO<sub>4</sub> Summer

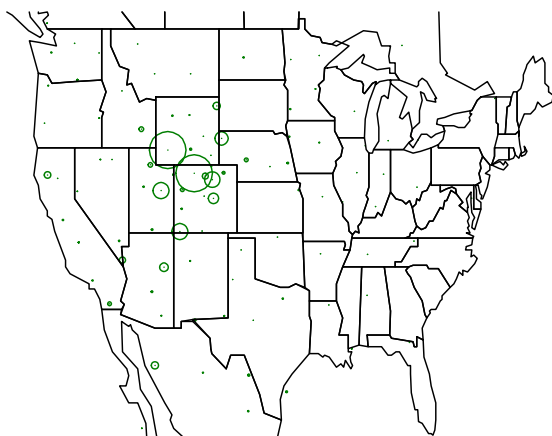


Figure 5.165c. Relative fractional contribution of each SO<sub>4</sub> source region.

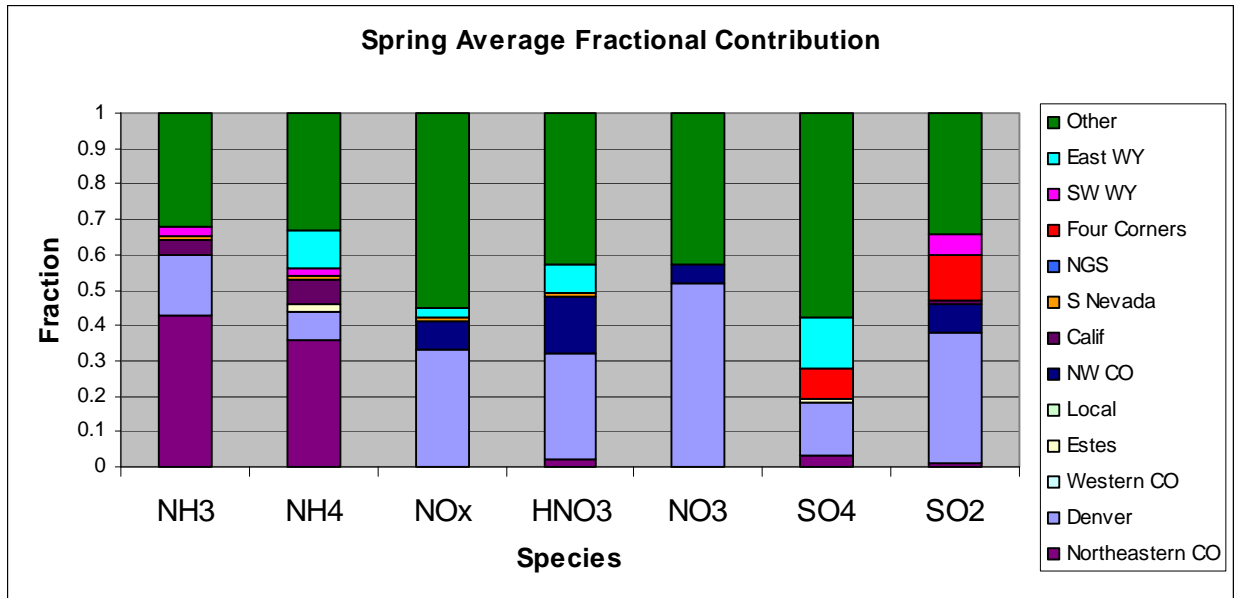


Figure 5.166a. Spring receptor modeled NH<sub>3</sub>/NH<sub>4</sub>, NO<sub>x</sub>/HNO<sub>3</sub>/NO<sub>3</sub>, and SO<sub>2</sub>/SO<sub>4</sub> average fractional contribution for selected source areas.

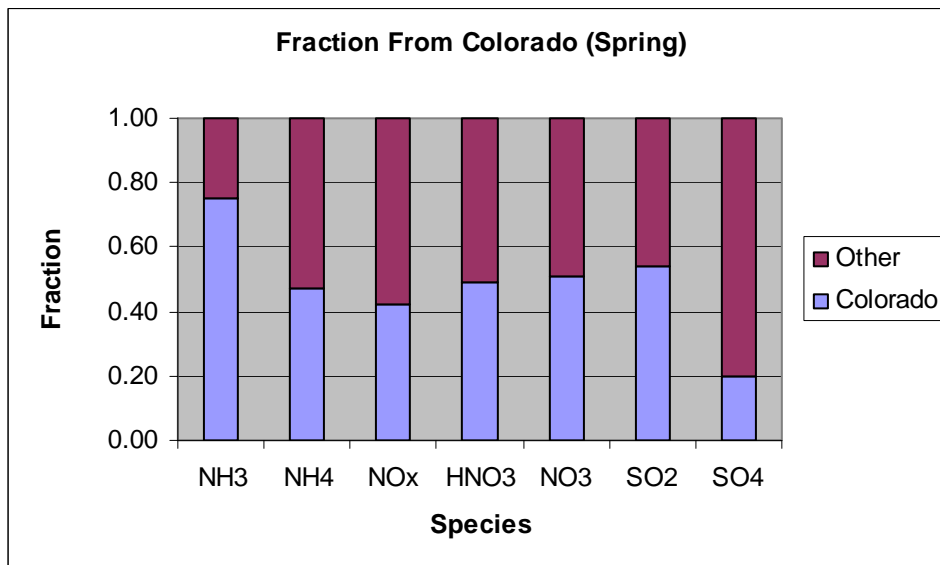


Figure 5.166b. Spring receptor modeled NH<sub>3</sub>/NH<sub>4</sub>, NO<sub>x</sub>/HNO<sub>3</sub>/NO<sub>3</sub>, and SO<sub>2</sub>/SO<sub>4</sub> average fractional contribution from within and outside the state of Colorado.

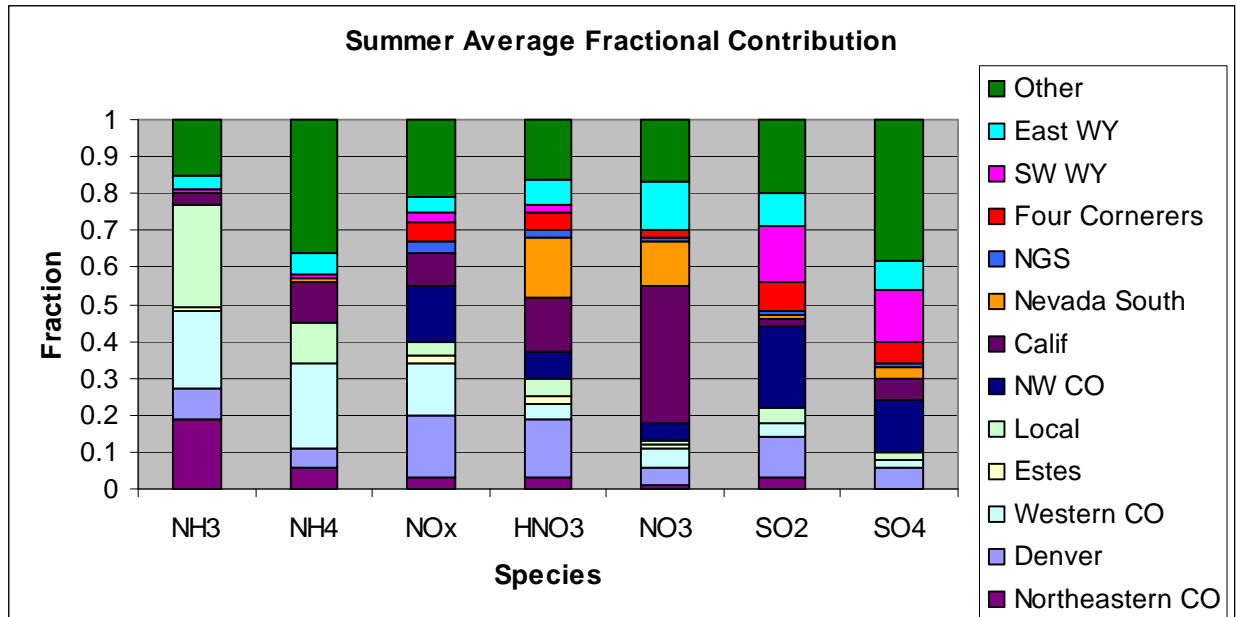


Figure 5.167a. Summer receptor modeled NH<sub>3</sub>/NH<sub>4</sub>, NO<sub>x</sub>/HNO<sub>3</sub>/NO<sub>3</sub>, and SO<sub>2</sub>/SO<sub>4</sub> average fractional contribution for selected source areas.

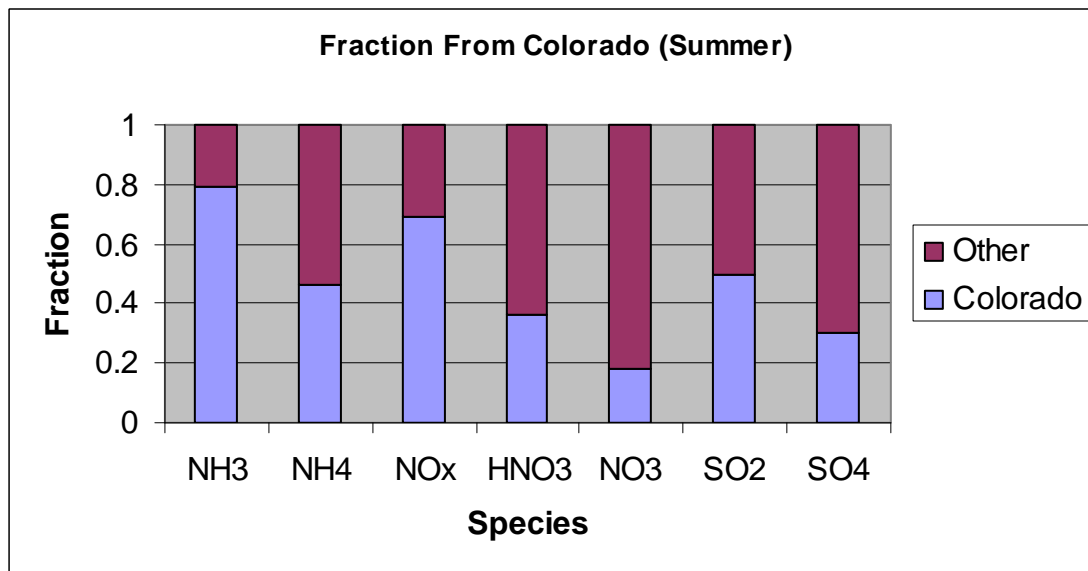


Figure 5.167b. Summer receptor modeled NH<sub>3</sub>/NH<sub>4</sub>, NO<sub>x</sub>/HNO<sub>3</sub>/NO<sub>3</sub>, and SO<sub>2</sub>/SO<sub>4</sub> average fractional contribution from within and outside the state of Colorado.

The regression coefficient is an average correction or estimation for all the chemical/physical processes not accounted for in the TM computations and for errors in estimated dispersion and emissions. If model predictions included accurate emission information, deposition estimates, transport, dispersion, and chemical conversion, the regression coefficients (estimates) would equal 1. Because the TM calculation was only for conservative tracers weighted to estimated emissions with a first-order estimation of deposition, the regression coefficients should generally be less than 1; however, referring to Tables 5.23 and 5.24, one sees that many coefficients are greater than 1, with some species/source region combinations substantially greater than 1.

For spring,  $\text{NH}_3$  in the groups of source regions listed as 6, 14, and 15 was found to have significant regression coefficients, while for the summer dataset, three similar but different groups of source regions contributed in a statistically significant way. Referring to Figures 5.117–5.119, one can see that during the spring the three groups of source regions correspond to some upslope transport, with Regions 6 and 15 showing more local transport. Regions 6 and 15 accounted for 79% of predicted ammonia, while Region 14 accounted for 21%. Summer source regions for ammonia had a more regional and westerly transport pattern associated with them. Tables 5.23 and 5.24 can be compared with Figures 5.117–5.161 to see the transport patterns that contributed to the fractional apportionment estimates of each species.

As shown in Figure 5.166a, during the spring the northeastern Colorado source regions accounted for over about 35% of ammonia, while during the summer (Figure 5.167a) they accounted for about 20%. The second largest contributor to ammonia during the spring was Denver at 17%. During summer more sources contributed, with the local source being 28%, followed by western Colorado at 21% and northeastern Colorado at 19%. Denver and other sources contributed, but at less than 10%. The large local contribution is associated with emissions of ammonia from the terrestrial and aquatic ecosystems around and in the park itself. About 75–80% of  $\text{NH}_3$  was predicted to originate from within the state of Colorado during both spring and summer time periods.

The hour-by-hour apportionments for selected source regions for spring and summer ammonia are shown in Figures 5.151a and 5.159a, while the fractional apportionments are presented in 5.151b and 5.159b. Figures 5.151c and 5.159c show the average relative fractional contributions for every source region within the United States. Referring to Figure 5.151a, one sees that the episodes with the elevated ammonia concentrations are associated with upslope conditions and transport from northeastern Colorado. The largest episode starting on April 23 (JD = 113.5), which preceded the largest wet deposition episode on April 24, had about 80% of its ammonia associated with northeastern Colorado emission sources. Both the episode starting on April 20 (JD = 110.5) and the April 23 episode had significant Denver contributions, consistent with upslope conditions. On the days when ammonia was at near background levels, many sources were predicted to contribute.

Referring to Figures 5.159a–c, which show the summer  $\text{NH}_3$  apportionment, one can see that more sources were predicted to contribute to ammonia concentrations than during the spring time period. Northeastern Colorado contributed significantly on July 21–22, July 28–30, and August 6–7. On the same days the Denver source region contributed as well. It is evident that sources west of RMNP contributed to ammonia more frequently during the summer than spring and that local ammonia emissions contributed significantly on most days. Locally emitted ammonia had a strong diurnal pattern, peaking during the daylight hours and approaching 0 during the evening. Even though a statistical relationship was not established with local emissions during the spring time period, one would expect, as in the summer that these emissions have some fractional contribution.

To further examine the contribution on specific days, the relative source contributions for each source region and 5-day back trajectories were plotted together. The same trajectories as discussed in section 5.3 were used in the analysis. Figures 5.168 and 5.169 present the results for the two spring episodes occurring on April 20 (JD = 110.6) and April 23 (JD = 113.5). As

shown, for both episodes the trajectories extend into the central and southwestern United States but terminate with upslope flow to RMNP, causing northeastern Colorado and the Denver region to have the largest contribution to measured ammonia. More distant source regions had little to no contributions to RMNP.

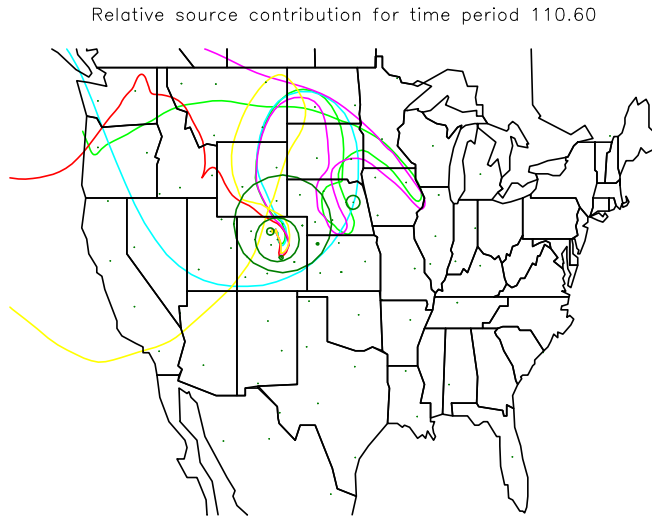


Figure 5.168. Plot showing the receptor modeled relative contribution, as open circles, of each source area to ammonia at RMNP for the episode starting on April 20 (JD = 110.6). Also shown are 5-day back trajectories corresponding to the episode.

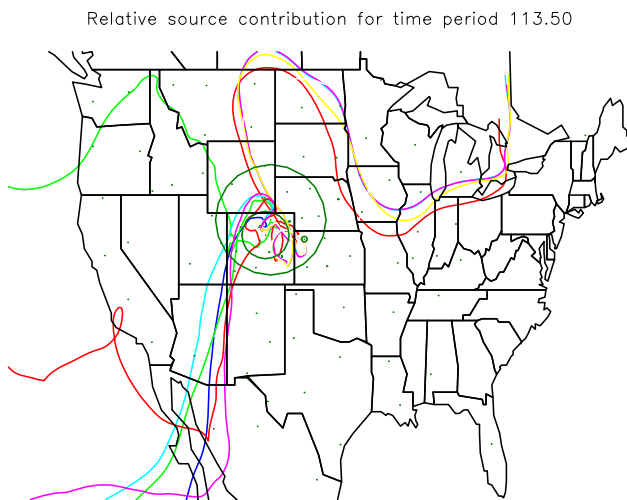


Figure 5.169. Plot showing the receptor modeled relative contribution, as open circles, of each source area to ammonia at RMNP for the episode starting on April 23 (JD = 113.5). Also shown are 5-day back trajectories corresponding to the episode.

Figures 5.170–5.173 show relative contributions of various source areas along with trajectories for the summer episodes on July 21, 22, 30, and August 1 (JD = 202.42, 203.25, 211.46, and 213.13). Notice that sources as far away as Iowa contributed on July 21; however, the single largest contributor to measured ammonia at RMNP was again northeastern Colorado. On July

22 flow was generally from the north but with upslope conditions, resulting in northeastern Colorado and Denver having the largest contribution. On July 30 and August 1 the flow was from the west with California and western Colorado contributing significantly. On July 30, even though the general flow was from the west, the final flow into RMNP is associated with upslope conditions, again causing northeastern Colorado and Denver to contribute to measured ammonia.

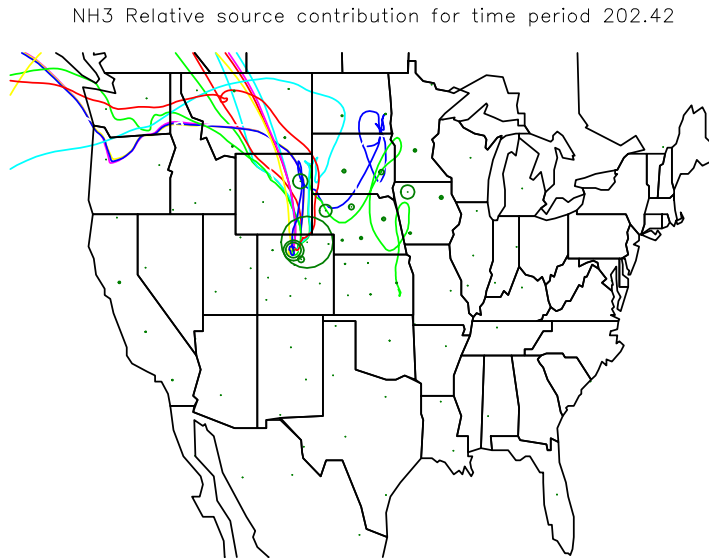


Figure 5.170. Plot showing the receptor modeled relative contribution, as open circles, of each source area to ammonia at RMNP for the episode starting on JD = 202.42 (July 21). Also shown are 5-day back trajectories corresponding to the episode.

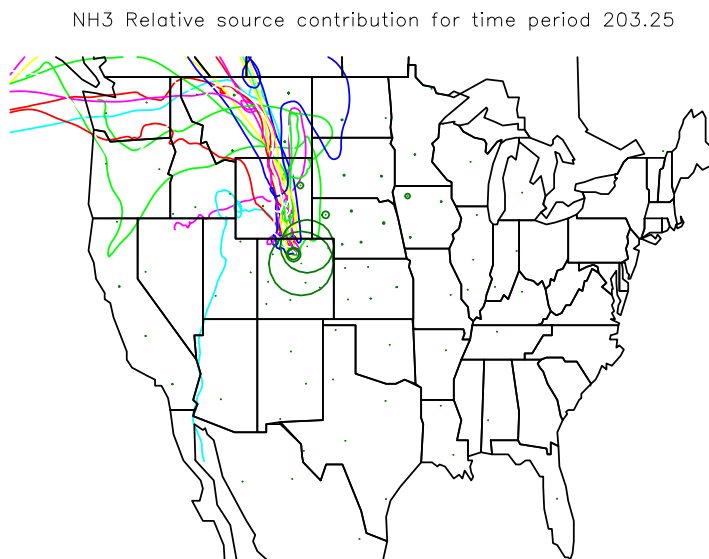


Figure 5.171. Plot showing the receptor modeled relative contribution, as open circles, of each source area to ammonia at RMNP for the episode starting on JD = 203.25 (July 22). Also shown are 5-day back trajectories corresponding to the episode.

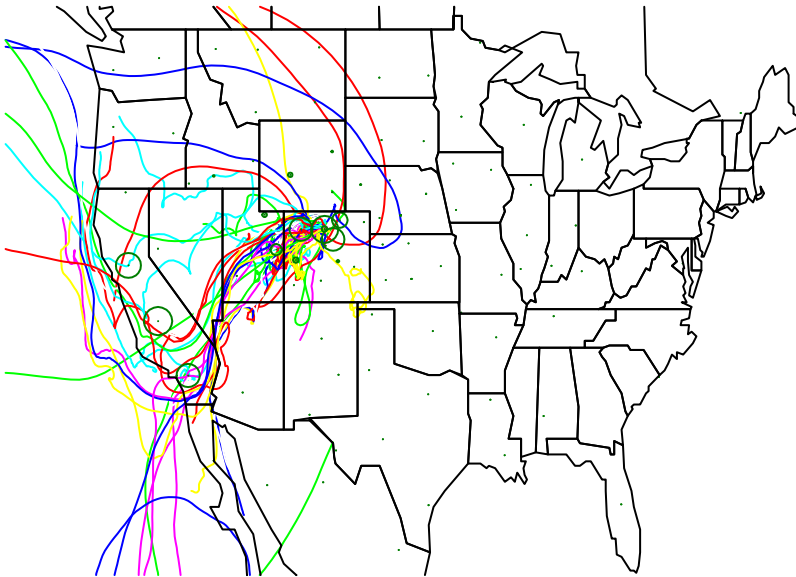
NH<sub>3</sub> Relative source contribution for time period 211.46

Figure 5.172. Plot showing the receptor modeled relative contribution, as open circles, of each source area to ammonia at RMNP for the episode starting on JD = 211.46 (July 30). Also shown are 5-day back trajectories corresponding to the episode.

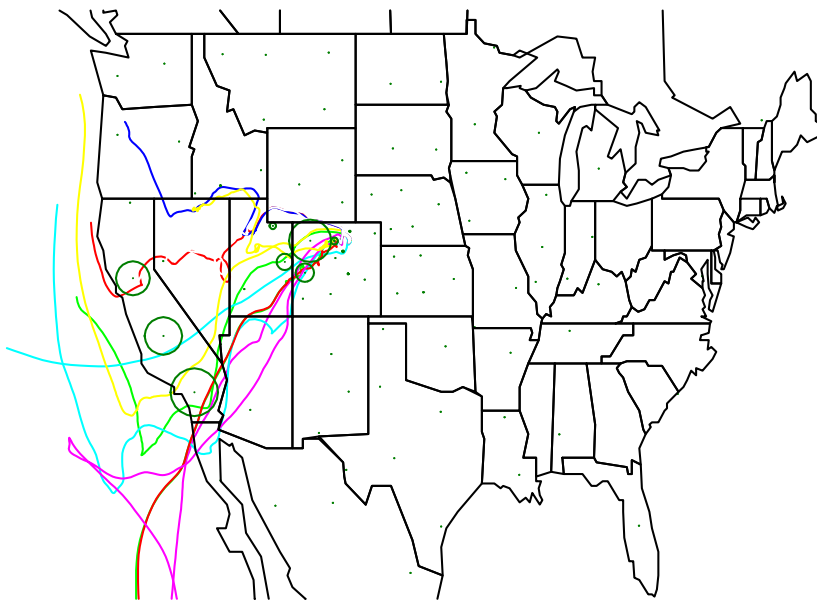
NH<sub>3</sub> Relative source contribution for time period 213.13

Figure 5.173. Plot showing the receptor modeled relative contribution, as open circles, of each source area to ammonia at RMNP for the episode starting on JD = 213.13 (August 1). Also shown are 5-day back trajectories corresponding to the episode.

An analysis similar to  $\text{NH}_3$  was carried out for  $\text{NH}_4$ ,  $\text{NO}_x/\text{HNO}_3/\text{NO}_3$ , and  $\text{SO}_2/\text{SO}_4$ . As might be expected, results of the  $\text{NH}_4$  analysis are similar but not the same as for  $\text{NH}_3$ . It is worth noting here that source regions for a secondary species will not necessarily be the same as for the primary gaseous precursor. For instance, because ammonium is a secondary product formed from ammonia reacting with molecules like nitric acid or an acidic sulfate aerosol, the correlation between ammonium and source regions could be with source areas that are rich in sulfur dioxide or nitrogen oxide emissions. However, all of the major spring episodes of  $\text{NH}_4$  are, as with  $\text{NH}_3$ , associated with upslope conditions, with the largest contributions to  $\text{NH}_4$  concentrations again coming from northeastern Colorado, with some contribution from the Denver source region. However, unlike  $\text{NH}_3$ , western Colorado also routinely contributed to  $\text{NH}_4$  during the spring time period. Figure 5.153c shows that sources as far away as California and the Midwest can at times contribute to ammonium concentrations.

During the summer period there was generally a larger contribution from sources “other” than those explicitly identified in Figures 5.152–5.165, which is consistent with longer-range transport of  $\text{NH}_3$  and  $\text{NH}_4$  species as might be expected of transport with deeper mixing heights. This was also evident in the residence time analysis (section 5.3.3), which showed a longer scale of transport for the summertime episodes compared to spring episodes. The July 21–22 (JD = 202–203) episode for  $\text{NH}_4$  is associated with upslope conditions and contributions from northeastern Colorado and Denver, but also with contributions from eastern Wyoming and other areas. The elevated  $\text{NH}_4$  levels from July 30 through August 4 (JD = 211–216) are interesting because of an apparent significant contribution from California as well as an elevated western Colorado contribution. Contributions from these source regions are consistent with westerly transport. About 30–40% of the  $\text{NH}_4$  during this time period is associated with the “other” category. This same pattern of westerly transport also occurred on July 11–19 (JD = 192–200) and August 9–12 (JD = 221–224). Close to 50% of  $\text{NH}_4$  was estimated to be associated with Colorado emissions during the spring, while about 45% was linked to Colorado emissions during the summer.

The  $\text{NO}_x$  apportionment results are shown in Figures 5.154 and 5.161. The spring and summer apportionments are similar in that upslope conditions are primarily associated with the Denver source region with little contribution from northeastern Colorado. However, many more sources contributed to  $\text{NO}_x$  concentrations during the summer than spring. At times during the summer, sources in northwestern Colorado contributed significantly as well as sources in the Four Corners region of the western United States. The source region in northwestern Colorado was estimated to be the second largest contributor to  $\text{NO}_x$  during the summer time frame.

During the spring time frame, both  $\text{HNO}_3$  and  $\text{NO}_3$  were primarily associated with transport from emissions in the Denver source region. Thirty per cent of  $\text{HNO}_3$  and 50% of  $\text{NO}_3$  was estimated to be from Denver emissions.  $\text{HNO}_3$  also had significant contributions from northwestern Colorado and sources in northeastern Wyoming, consistent with transport pathways across northern California, southern Idaho, Wyoming, and into Colorado.

The summer apportionment of  $\text{HNO}_3$  and  $\text{NO}_3$  shows a somewhat different picture. In general, during the summer westerly transport is responsible for most of the  $\text{HNO}_3$  and  $\text{NO}_3$  species. On the average, a small to negligible fraction of these species was predicted to come from northeastern Colorado, with about 15% of the  $\text{HNO}_3$  and 5% of the  $\text{NO}_3$  coming from Denver.

The July 21–23 (JD = 202–204) episode shows some contribution coming from Denver, but with eastern Wyoming being the most significant contributor. The California and southern Nevada source areas contributed significantly during much of the remaining time frame. California was estimated to contribute 37% of the  $\text{NO}_3$  and was the largest overall contributor. During the summer study period, about 40% of the  $\text{HNO}_3$  and over 22% of the particle nitrate was estimated to arrive within Colorado's borders, while for the spring time period the fractions were about 50% for both species.

For the spring dataset, shown in Figures 5.157 and 5.158,  $\text{SO}_2$  and  $\text{SO}_4$ , as with other species, are associated with transport from northeastern Colorado and Denver during the two episodes starting on April 20 and April 23 (JD = 110.6 and 113.5). Other significant contributors were southwestern Wyoming, northwestern Colorado, and the Four Corners region. On the order of 50% of the  $\text{SO}_2$  and 20% of the  $\text{SO}_4$  were predicted to originate from outside the state.

As with other species, summer meteorological conditions transport aerosols over greater distances, and contributions from more varied sources contribute. As shown in Figures 5.164 and 5.165, during the upslope condition of July 21–23 (JD = 202–204), Denver, northeastern Colorado, and eastern Wyoming contributed about 70% of the  $\text{SO}_2$  and  $\text{SO}_4$ . Denver was also a significant contributor of  $\text{SO}_2$  during July 28–30 (JD = 209–211). The single largest contributor to  $\text{SO}_2$  was northwestern Colorado and southwestern Wyoming at about 20% and 15%, respectively. These same two source areas were each predicted to contribute about 15% of the sulfate. About 50% of  $\text{SO}_2$  and 70% of  $\text{SO}_4$  were estimated to originate from outside Colorado.

As pointed out previously, the above apportionments relied on grouping together of source regions whose contributions to concentrations at RMNP were temporally collinear with each other. The apportionments to individual source areas within the larger source regions shown in Figures 5.117–5.151 necessarily rely on the emission and dispersion estimates of the TM model calculations. A potential bias in the individual source area apportionments would occur if the emission estimates from source regions within the different groups were biased in some unknown way. Potential for this kind of bias was investigated to some degree by further separating some of the source regions shown in Figures 5.117–5.151 into smaller source regions. Some interesting features become apparent from this analysis.

The source regions of Estes Park and “local” were entered into the regressions as individual independent variables. The Estes Park source region did not show a statistically significant relationship with any of the variables except  $\text{NO}_x$ ,  $\text{HNO}_3$ , and  $\text{NO}_3$  during the spring time period. The average apportionment of these three variables to Estes Park was on the order of 50%, which given the best estimate of  $\text{NO}_x$  emissions associated with Estes Park is unreasonably high. However, there is an underlying correlation between the predicted transport of Estes Park emissions and measured concentrations of these three variables. It seems evident that the Estes Park source region was making some contribution to measured  $\text{NO}_x$ ,  $\text{HNO}_3$ , and  $\text{NO}_3$  at the core monitoring site. However, the above analysis does not allow for a quantitative determination.

The other source region that contributed more significantly to a species when entered into the regression as a single independent variable is California. Transport from California is always collinear with transport from other source areas between California and RMNP. When the California, southern Nevada/Four Corners, and western Colorado source regions are used as

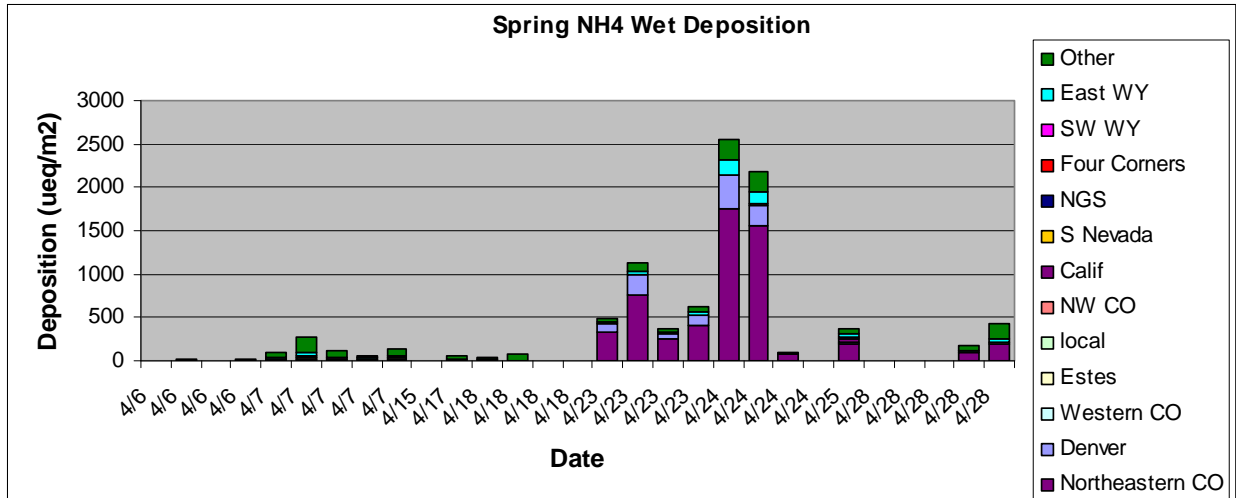
separate independent variables, the summer sulfate apportionment to California is increased from 6% to 45%, more akin to the apportionment for nitrates. The reason for the low sulfate apportionment is the relatively low estimated SO<sub>2</sub> emissions from California compared to other collinear source regions. The implication of these results is that SO<sub>2</sub> emissions from the California source region were underestimated. This could possibly be due to a poor assessment of SO<sub>2</sub> emissions from shipping lanes on the coast of California or SO<sub>2</sub> emissions from wild and prescribed fire. Another possibility is sulfate transport from Asia is collinear with transport from California.

### 5.5.5. Apportionment of Wet Deposition to Source Areas

Wet deposition refers to processes by which gases and particles are scavenged by rain, snow, and clouds/fog and deposited to terrestrial or aquatic surfaces. The scavenging process is complex, including equilibrium conditions between cloud droplets and aerosols and below cloud wash out through intersection of precipitation and ambient aerosol concentrations. Simulating wet deposition requires approximating these processes as well as the occurrence and rate of precipitation. As shown in Figures 5.174–5.176, the highest concentrations of gases and aerosols occurred starting on April 23 (JD = 113.5), followed by 2 days of precipitation. Notice that at the beginning of the precipitation episode concentrations of NH<sub>4</sub>, NO<sub>3</sub>, and SO<sub>4</sub> are high at about 500 µeq/L, 150 µeq/L, and 140 µeq/L, respectively. Within in a few hours, the concentrations drop to less than 30 µeq/L, and concentrations of ambient aerosols also drop to background levels. Ambient aerosols apparently were almost entirely scavenged from the atmosphere.

The strategy taken here to apportion source areas to wet-deposited ions is to assign the fractional contribution of various sources contributing to ambient aerosols just before and during the precipitation episode to the respective measured wet ion concentrations. For instance, it is assumed that wet concentrations of NH<sub>4</sub> are proportional to the weighted fractional source apportionments of ambient NH<sub>3</sub> and NH<sub>4</sub> concentrations. Similarly, wet NO<sub>3</sub> apportionment was linked to HNO<sub>3</sub> and particle NO<sub>3</sub> apportionments and wet SO<sub>4</sub> to SO<sub>2</sub> and particle SO<sub>4</sub> apportionments.

Results of this analysis are presented for spring in Figures 5.174–5.176 and for summer in 5.177–5.179. Data are presented as apportionments for each of the sampling periods shown in Figures 5.174–5.179. Note that the length of time over which samplers were collected varied from sampling period to sampling period. Furthermore, the data is presented as total deposition for the each sampling period in units of µeq/m<sup>2</sup> as opposed to deposition per unit time. The second half of each figure shows the average apportionment over all sampling periods.



Spring Average Wet NH4 Fractional Contribution

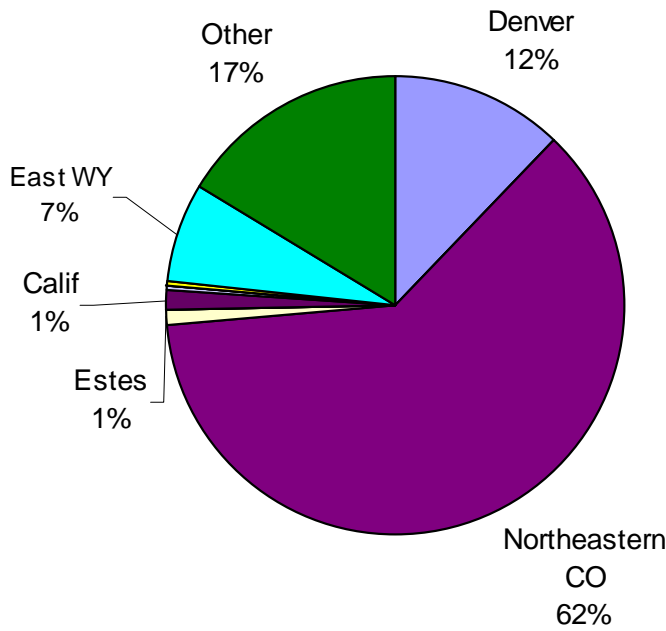
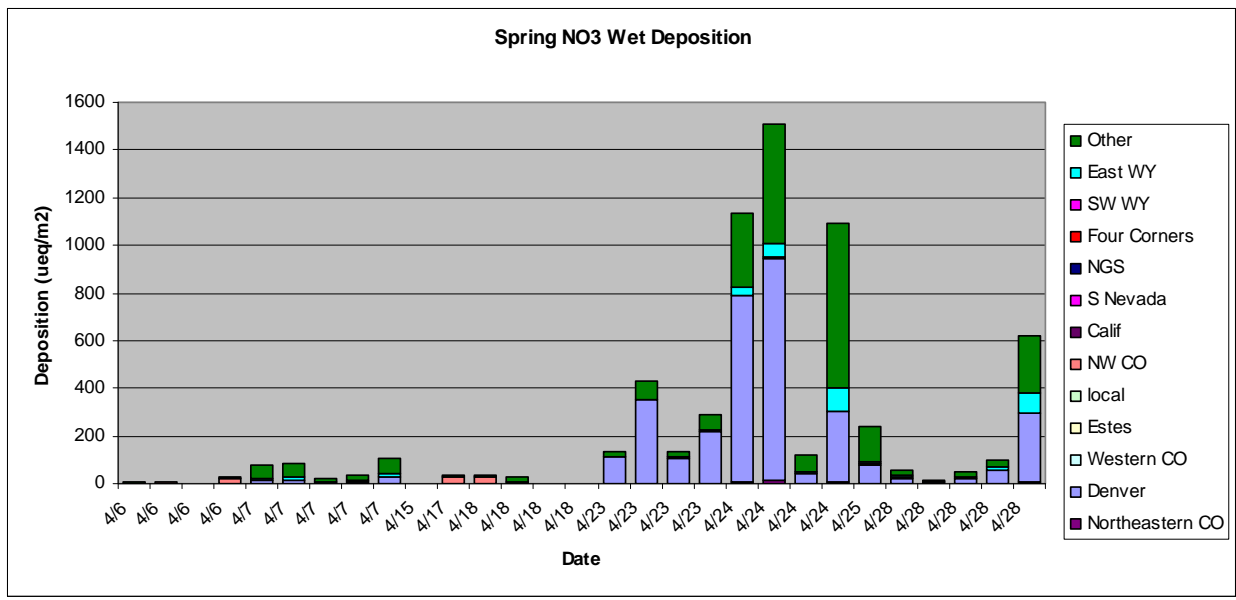


Figure 5.174. Area source apportionment of wet-deposited NH<sub>4</sub> for each sample collection period as well as the overall average during the spring time period.



**Spring Average Wet NO3 Fractional Deposition**

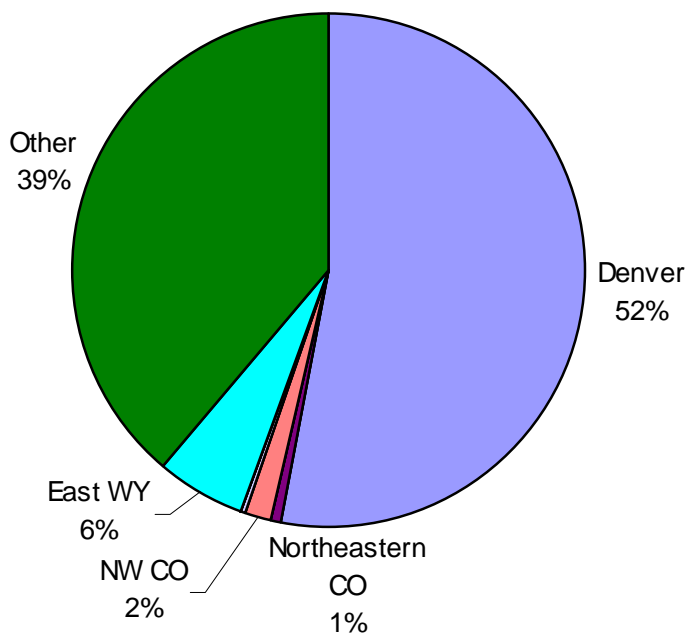
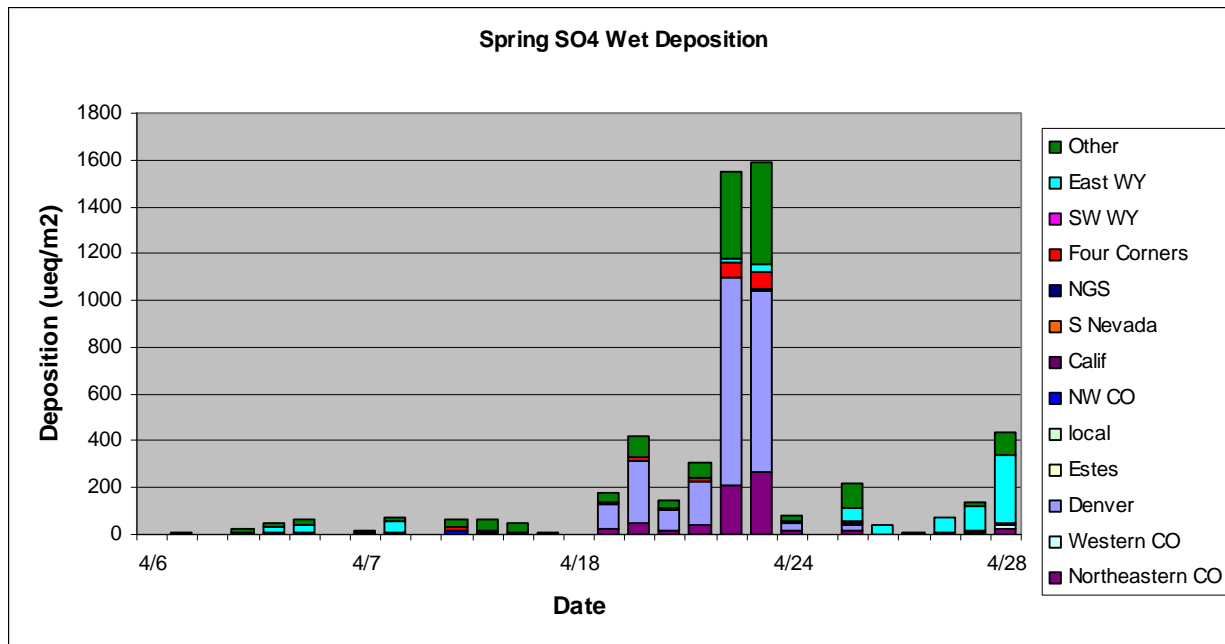


Figure 5.175. Area source apportionment of wet-deposited NO<sub>3</sub> for each sample collection period as well as the overall average during the spring time period.



Spring Average Wet SO4 Fractional Deposition

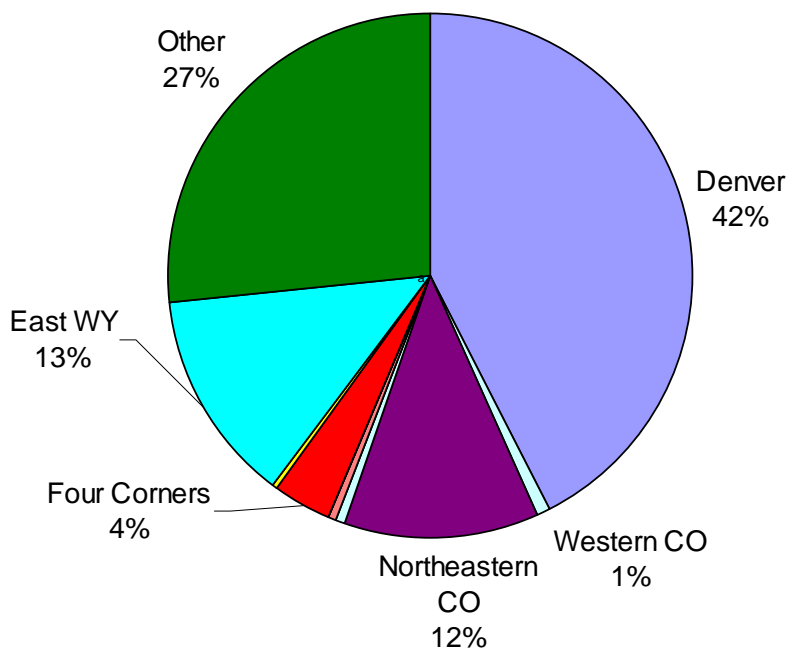
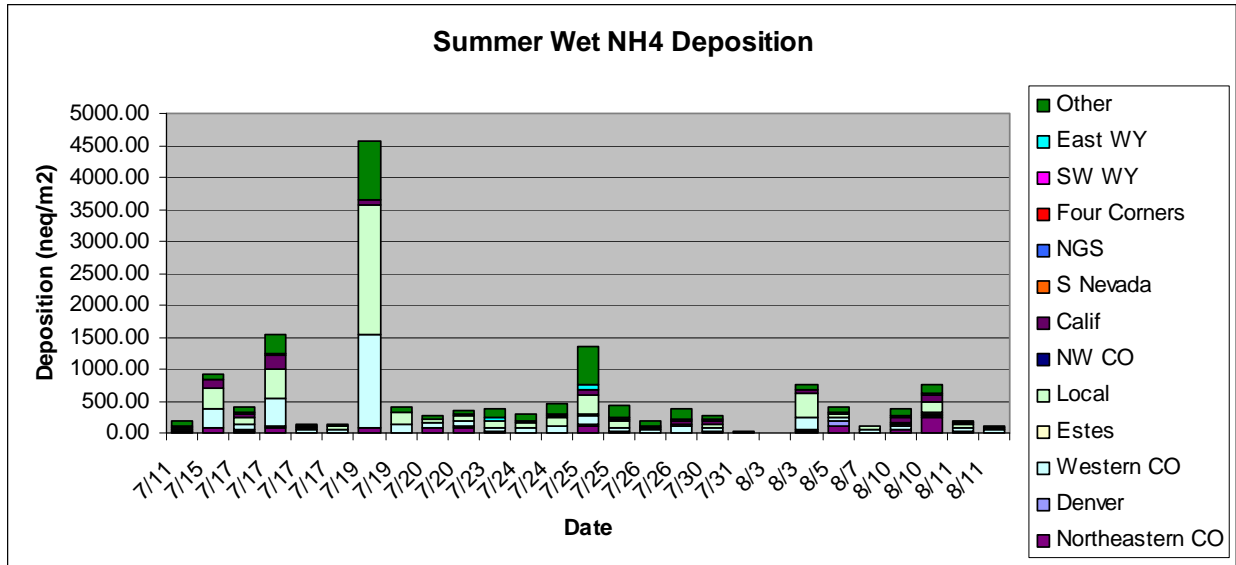


Figure 5.176. Area source apportionment of wet-deposited SO<sub>4</sub> for each sample collection period as well as the overall average during the spring time period.



### Summer Average NH4 Wet Dep

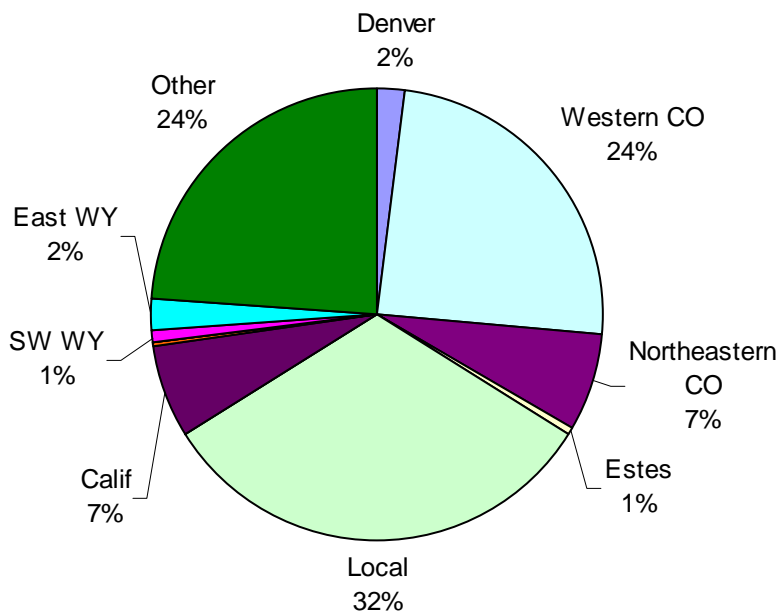


Figure 5.177. Area source apportionment of wet-deposited NH<sub>4</sub> for each sample collection period as well as the overall average during the summer time period.

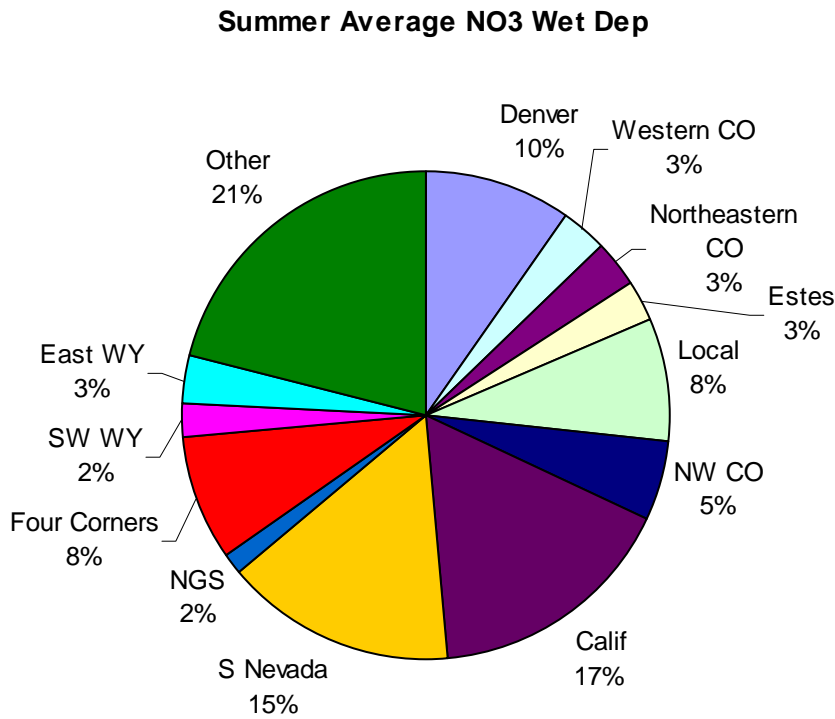
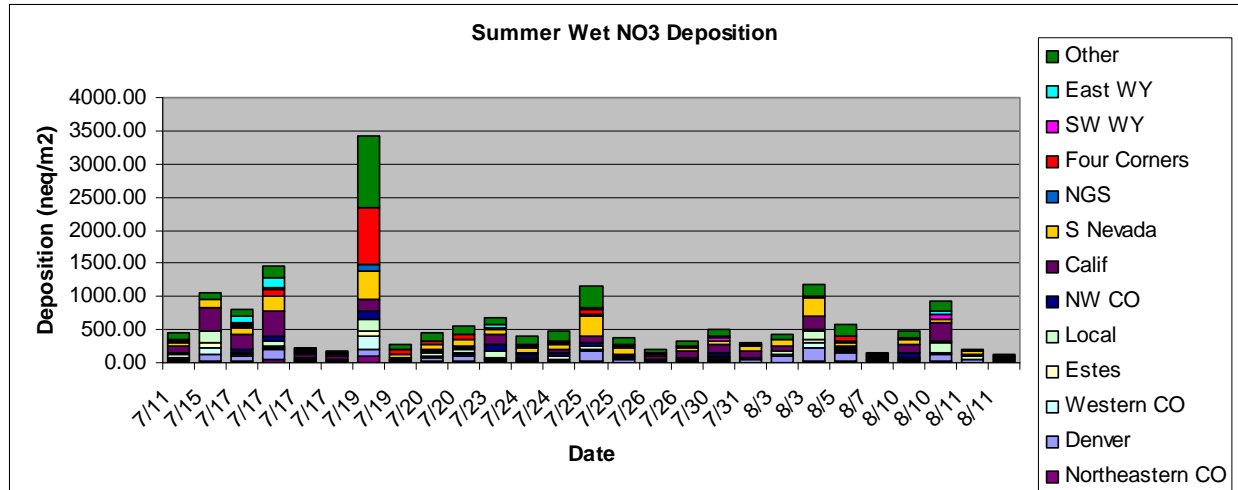


Figure 5.178. Area source apportionment of wet-deposited NO<sub>3</sub> for each sample collection period as well as the overall average during the summer time period.

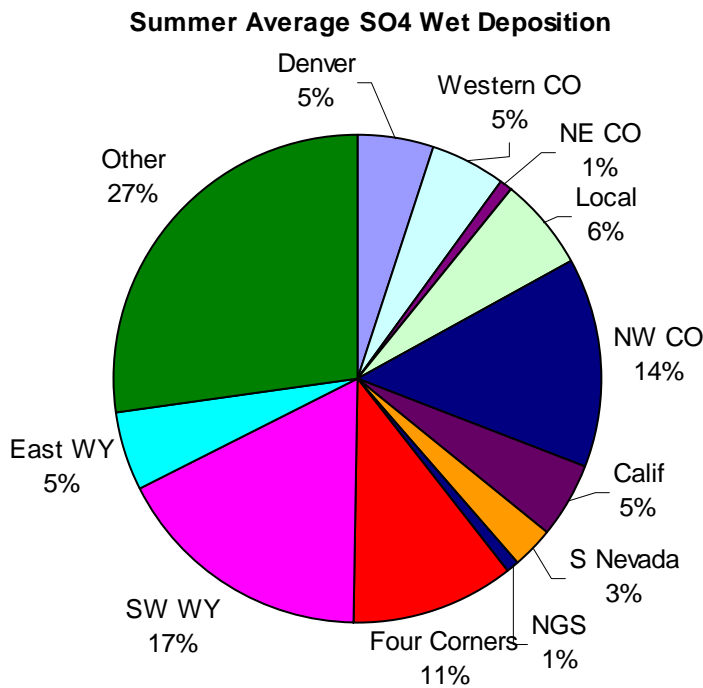
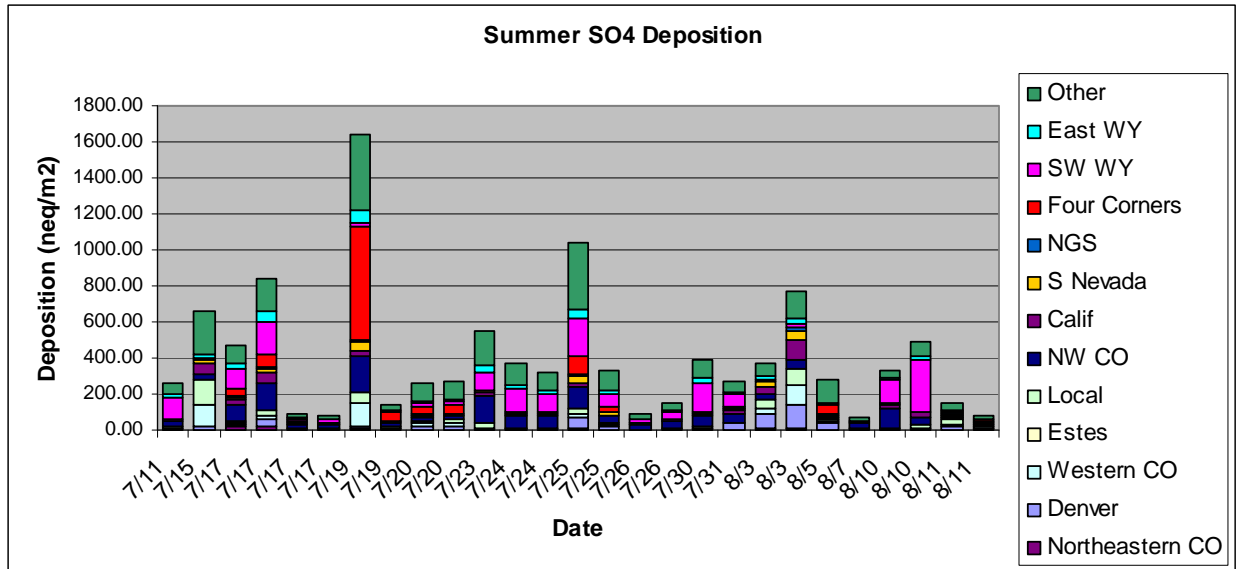


Figure 5.179. Area source apportionment of wet-deposited SO<sub>4</sub> for each sample collection period as well as the overall average during the summer time period.

From Figure 5.174 it is evident that the northeastern Colorado ammonia sources contributed, on the average, most of the reduced nitrogen deposition at about 67%. The largest wet deposition episode, which commenced on April 24 (JD = 114), had about 70% of reduced ammonia associated with northeastern Colorado and another 15% associated with the Denver source area. About 90% of the wet deposition of reduced nitrogen was predicted to be from within the borders of Colorado.

The transport pathways and source areas were the same for oxidized nitrogen; however, the sources themselves are different. Whereas reduced nitrogen is primarily associated with agriculture and feedlot activities, oxidized nitrogen is linked to NO<sub>x</sub> emissions from mobile and point sources, primarily electricity-generating facilities. As with reduced nitrogen deposition, the biggest oxidized nitrogen wet deposition event occurred starting on April 23 (JD = 114) and was primarily associated with the Denver source region, with only a small contribution from northeastern Colorado. Northwestern and western Colorado, eastern Wyoming, and California all contributed significantly to other wet deposition events, although because most of the rain/deposition occurred on April 24–25, their contribution to total NH<sub>4</sub> wet deposition was small.

Source areas for sulfur are primarily associated with coal-fired power plants. For the deposition period starting on April 24 (JD = 114), sulfur from the Denver source area contributed about 40% of the deposition, while the northeastern Colorado and eastern Wyoming source regions contributed another 25%.

Figures 5.177–5.179 show the source area apportionment for summer rain events. Whereas the spring time period was marked by one significant upslope event, the summer time period had a number of rainy periods. During the summer the source apportionment was more varied than during the spring, with more distant sources contributing to wet deposition at RMNP. On the average, western Colorado and the local source regions contributed 24% and 32% of the reduced nitrogen deposition, respectively, while northeastern Colorado and California each contributed about 7%. The source apportionment during the largest summer time episode starting on July 19 (JD = 200) was about the same as the average apportionment.

Sources contributing to wet nitrate deposition were the most varied. California and southern Nevada were estimated to have contributed the largest fraction of wet-deposited nitrate at 17% and 15%, respectively, while the Four Corners region and “local” each contributed another 8%. Western and northeastern Colorado and eastern and southwestern Wyoming each contributed 2–3% of wet nitrate deposition. On the largest deposition event on July 19, the Four Corners region contributed a little over 20% of wet-deposited nitrate. At times, sources in northwestern Colorado contributed between 15–20% wet-deposited nitrate. On the average, about 40% of wet-deposited nitrate came from within the state of Colorado.

Sources contributing to sulfate wet deposition were also quite varied. It is estimated that southwestern Wyoming and northwestern Colorado made up 17% and 14%, respectively, of wet-deposited sulfate. The Four Corners area contributed another 11%, while eastern Wyoming, California, western Colorado, and the local source area all added about 5–6% each. Episodically, the Four Corners region contributed about 40% on July 19 (JD = 200) and southwestern Wyoming contributed up to 60% at times. It is estimated that about 25% of wet-deposited sulfate was from within the state of Colorado.

Figure 5.180 summarizes estimates of how much ammonium, nitrate, and sulfate wet deposition came from within and outside the state of Colorado. More than 80% of ammonium and 60% of the nitrate and sulfate was associated with Colorado sources during the spring. During the summer about 65% of wet-deposited ammonium was from Colorado sources and Colorado sources contributed about 40% of the nitrate and sulfate.

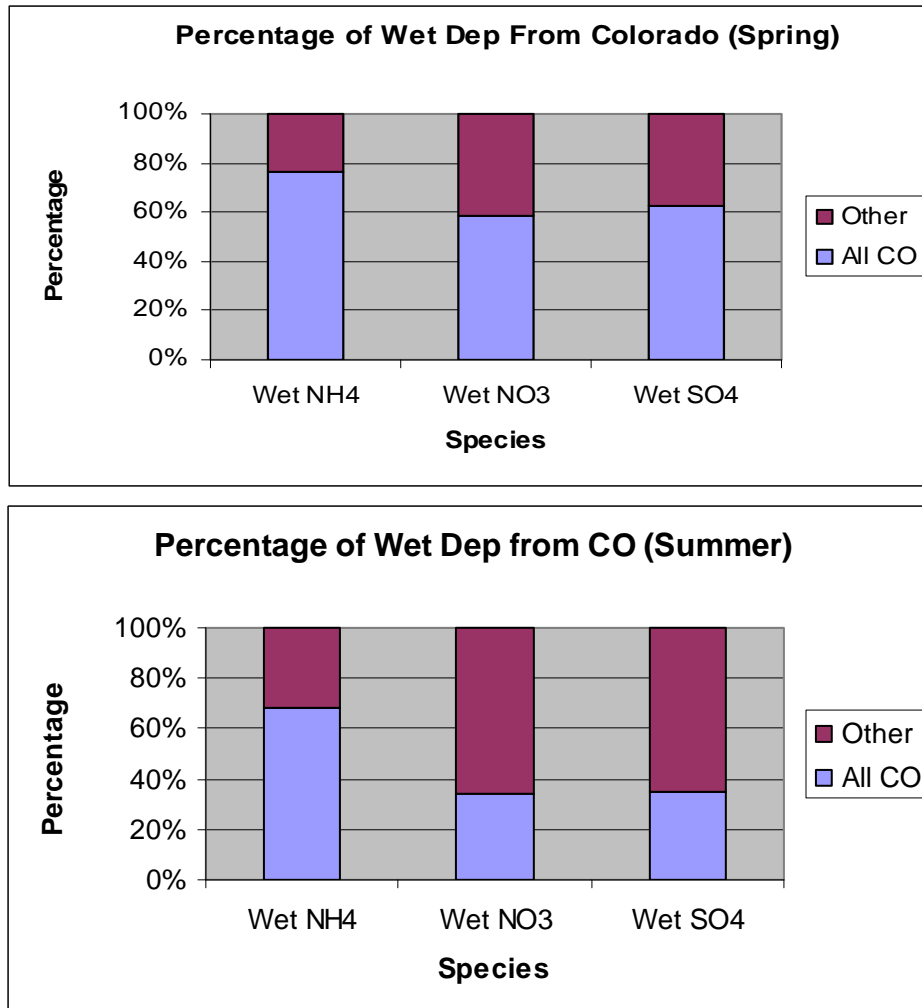


Figure 5.180. Average apportionment of wet-deposited  $\text{NH}_4$ ,  $\text{NO}_3$ , and  $\text{SO}_4$  to sources inside and outside Colorado.

Tables 5.25 and 5.26 summarize the average apportionment to source regions for dry deposition of ammonia, ammonium, nitric acid, particle nitrate, wet ammonium, and nitrate and the totals of dry and wet for the spring and summer time periods. Average dry deposition velocities of 1, 2, and 0.2 cm/sec were used for ammonia, nitric acid, and particulate species, respectively. Units are in  $\mu\text{g}/\text{m}^2/\text{sampling period}$  for the elemental nitrogen associated with each species. Table 5.27 is a similar table but for the sum of spring and summer monitoring time periods.

Figures 5.181–5.183 are graphical summaries of the data presented in these three tables. First, notice as discussed previously, that deposition during the summer time frame was about 2.5 times greater than the spring time frame, wet deposition of total nitrogen was about 2.5–3 times greater than dry deposition, and ammonia was the largest contributor to dry deposition, while wet ammonium and nitrate deposition were about the same. During the spring time period, the two source areas contributing most of the nitrogen deposition were northeastern Colorado at 40% and the Denver source region at about 25%. Eastern Wyoming and northwestern Colorado were the third and fourth largest contributors to total nitrogen deposition.

During the summer, nitrogen deposition is associated with a diverse group of sources as can be seen in Figure 5.182. The local source area was predicted to be the largest contributor at about 18% and western Colorado contributed another 13%. Southern Nevada, California, northeastern Colorado, and the Denver sources regions each contributed 8–11%. Next highest contributors were the Four Corners area, eastern Wyoming, and northwestern Colorado, all at 3–4%. Sources other than those specified in Figure 5.182 contributed on the order of 20%. Figure 5.183 is the deposition-weighted sum of the previous two figures. The five largest source areas contributing to nitrogen deposition for both time periods were northeastern Colorado, Denver, the local source region, western Colorado, and California. Sources outside those specified contributed on the order of 20%.

**Table 5.25.** Summary of wet and dry deposition for all Colorado and outside-Colorado sources and selected source regions within and outside Colorado for the spring time period.

Elemental N $\mu\text{g}/\text{m}^2$	Dry				Wet			Total	
Species	NH <sub>3</sub>	NH <sub>4</sub>	HNO <sub>3</sub>	NO <sub>3</sub>	Total Dry	NH <sub>4</sub>	NO <sub>3</sub>	Total Wet	Wet+Dry
<b>Totals</b>	1961.5	661.7	1126.4	207.5	3957.0	9313.3	6383.2	15696.5	19653.5
<b>Colorado</b>	1409.3	283.0	552.6	105.2	2350.2	7094.0	3714.4	10808.4	13158.6
<b>Outside Colorado</b>	552.2	378.6	573.8	102.3	1606.8	2219.3	2668.8	4888.1	6494.9
<b>Denver</b>	386.7	60.9	343.2	94.3	885.1	1138.5	3379.5	4518.1	5403.2
<b>Western Colorado</b>	0.0	0.0	0.0	0.0	0.0	0.0	0.0	0.0	0.0
<b>Northeastern Colorado</b>	674.0	200.0	21.6	0.0	895.6	5723.4	152.5	5876.0	6771.5
<b>Estes Park</b>	0.0	18.5	0.0	0.0	18.5	100.2	0.0	100.2	118.7
<b>Local</b>	0.0	0.0	0.0	0.0	0.0	0.0	0.0	0.0	0.0
<b>Northwestern Colorado</b>	0.0	0.0	175.3	9.0	184.3	0.0	109.3	109.3	293.6
<b>California</b>	88.4	59.0	0.0	0.0	147.4	138.2	0.0	138.2	285.7
<b>Southern Nevada</b>	14.0	6.4	9.2	1.4	31.0	9.1	4.8	13.9	44.9
<b>Navajo Generation Facility</b>	0.0	0.0	0.0	0.0	0.0	0.0	0.0	0.0	0.0
<b>Four Corners</b>	0.0	0.0	0.0	0.0	0.0	0.0	0.0	0.0	0.0
<b>Southwestern Wyoming</b>	69.0	15.7	0.0	0.0	84.7	26.6	0.0	26.6	111.3
<b>Eastern Wyoming</b>	0.0	55.5	93.9	0.8	150.3	644.5	368.6	1013.1	1163.4
<b>Other</b>	729.5	245.5	483.2	102.0	1560.1	1532.8	2368.5	3901.2	5461.4

**Table 5.26.** Summary of wet and dry deposition for all Colorado and outside-Colorado sources and selected source regions within and outside Colorado for the summer time period.

Elemental N $\mu\text{g}/\text{m}^2$	Dry				Wet			Total	
Species	NH <sub>3</sub>	NH <sub>4</sub>	HNO <sub>3</sub>	NO <sub>3</sub>	Total Dry	NH <sub>4</sub>	NO <sub>3</sub>	Total Wet	Wet+Dry
<b>Totals</b>	8691.1	1302.0	6203.9	224.9	16421.9	15422.2	17332.0	32754.2	49176.1
<b>Colorado</b>	6825.1	594.8	2261.9	39.7	9721.5	10492.9	5912.8	16405.7	26127.2
<b>Outside Colorado</b>	1866.0	707.2	3942.0	185.2	6700.3	4929.3	11419.3	16348.6	23048.9
<b>Denver</b>	699.1	63.7	969.1	11.6	1743.4	285.7	1672.6	1958.3	3701.7
<b>Western Colorado</b>	1847.2	294.7	251.2	11.8	2404.8	3764.7	549.8	4314.5	6719.3
<b>Northeastern Colorado</b>	1639.1	77.8	168.8	1.9	1887.6	1092.4	518.8	1611.2	3498.8
<b>Estes Park</b>	100.0	0.0	117.8	1.2	218.9	85.7	506.3	592.0	810.9
<b>Local</b>	2408.8	143.3	310.3	3.0	2865.4	4982.0	1376.4	6358.4	9223.9
<b>Northwestern Colorado</b>	0.0	0.0	408.8	10.3	419.1	0.0	907.5	907.5	1326.5
<b>California</b>	311.1	233.8	940.0	82.9	1567.7	1008.5	2905.4	3913.9	5481.6
<b>Southern Nevada</b>	4.7	10.5	981.5	27.2	1023.9	57.1	2621.5	2678.6	3702.5

<b>Navajo Generation Facility</b>	0.0	0.0	109.2	2.5	111.7	0.0	265.8	265.8	377.4
<b>Four Corners</b>	0.0	0.0	323.5	4.1	327.6	0.0	1427.8	1427.8	1755.3
<b>Southwestern Wyoming</b>	71.9	7.3	116.9	0.0	196.0	113.5	393.6	507.1	703.1
<b>Eastern Wyoming</b>	339.1	82.3	432.0	29.6	882.9	363.6	514.2	877.8	1760.7
<b>Other</b>	1270.2	388.5	1075.1	39.0	2772.8	3669.0	3672.5	7341.5	10114.3

**Table 5.27.** Summary of wet and dry deposition for all Colorado and outside-Colorado sources and selected source regions within and outside Colorado for the spring plus summer time periods.

Elemental N $\mu\text{g}/\text{m}^2$	Dry					Wet			Total
Species	NH <sub>3</sub>	NH <sub>4</sub>	HNO <sub>3</sub>	NO <sub>3</sub>	Total Dry	NH <sub>4</sub>	NO <sub>3</sub>	TotalWet	Wet+Dry
<b>Totals</b>	10652.6	1963.6	7330.2	432.4	20378.9	24735.5	23715.2	48450.7	68829.6
<b>Colorado</b>	8234.5	877.8	2814.5	145.0	12071.7	17586.9	9627.2	27214.1	39285.8
<b>Outside Colorado</b>	2418.2	1085.8	4515.7	287.5	8307.2	7148.6	14088.0	21236.6	29543.8
<b>Denver</b>	1085.8	124.6	1312.2	105.9	2628.5	1424.2	5052.1	6476.3	9104.8
<b>Western Colorado</b>	1847.2	294.7	251.2	11.8	2404.8	3764.7	549.8	4314.5	6719.3
<b>Northeastern Colorado</b>	2313.1	277.8	190.3	1.9	2783.1	6815.8	671.3	7487.2	10270.3
<b>Estes Park</b>	100.0	18.5	117.8	1.2	237.4	185.8	506.3	692.2	929.6
<b>Local</b>	2408.8	143.3	310.3	3.0	2865.4	4982.0	1376.4	6358.4	9223.9
<b>Northwestern Colorado</b>	0.0	0.0	584.1	19.3	603.4	0.0	1016.8	1016.8	1620.2
<b>California</b>	399.5	292.8	940.0	82.9	1715.1	1146.7	2905.4	4052.1	5767.2
<b>Southern Nevada</b>	18.7	17.0	990.7	28.6	1054.9	66.2	2626.3	2692.5	3747.4
<b>Navajo Generation Facility</b>	0.0	0.0	109.2	2.5	111.7	0.0	265.8	265.8	377.4
<b>Four Corners</b>	0.0	0.0	323.5	4.1	327.6	0.0	1427.8	1427.8	1755.3
<b>Southwestern Wyoming</b>	140.8	23.0	116.9	0.0	280.7	140.1	393.6	533.7	814.4
<b>Eastern Wyoming</b>	339.1	137.9	525.8	30.4	1033.2	1008.1	882.8	1890.9	2924.1
<b>Other</b>	1999.6	634.0	1558.3	141.0	4333.0	5201.8	6040.9	11242.7	15575.7

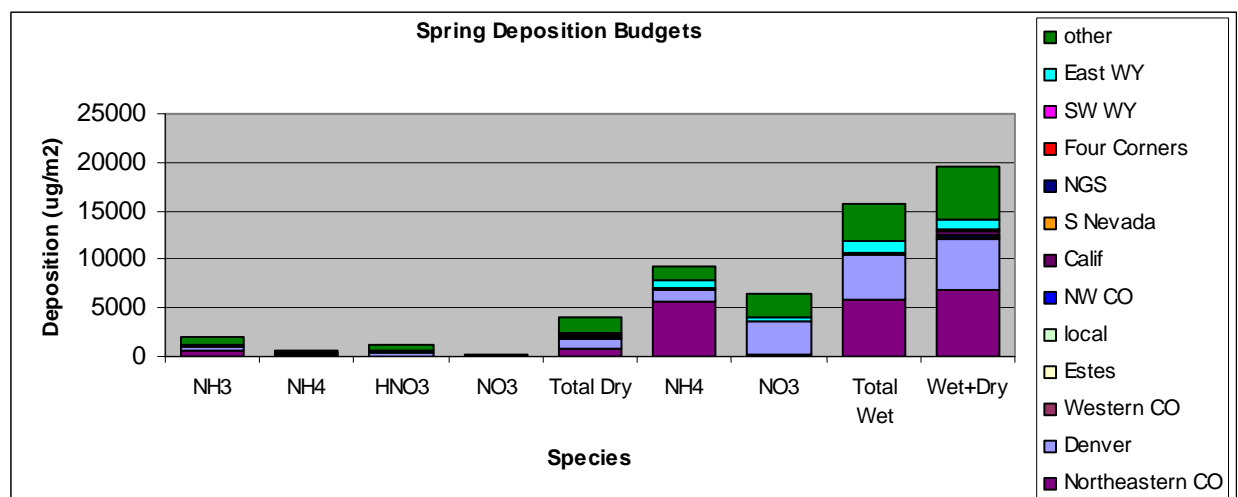


Figure 5.181. Graphical display of wet and dry source area deposition budgets for each species, total dry, total wet, and total wet plus dry deposition for the spring time period.

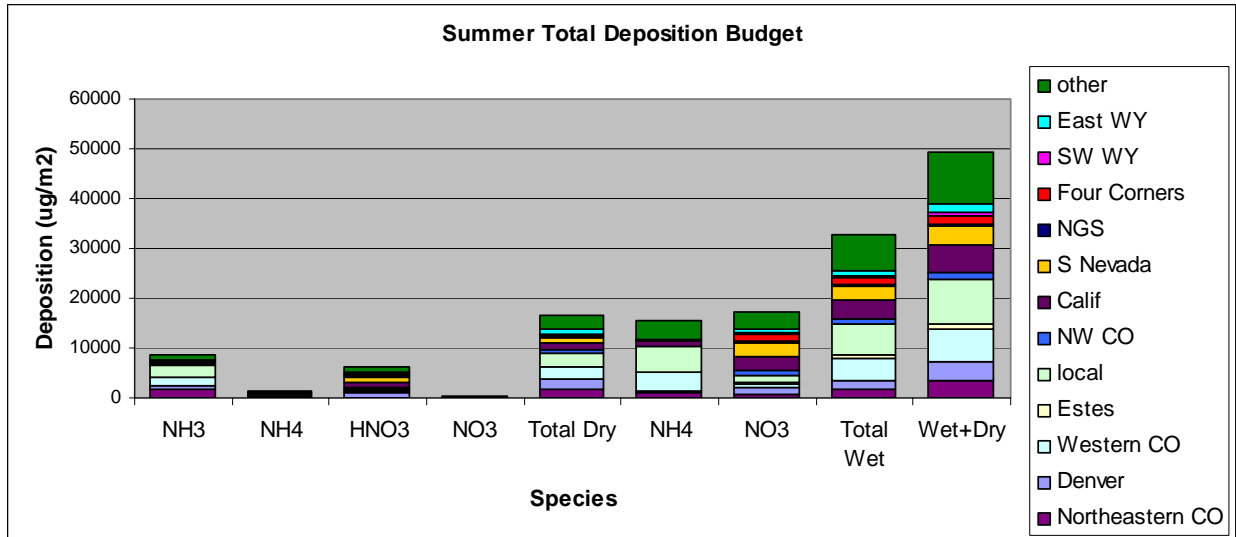


Figure 5.182. Graphical display of wet and dry source area deposition budgets for each species, total dry, total wet, and total wet plus dry deposition for the summer time period.

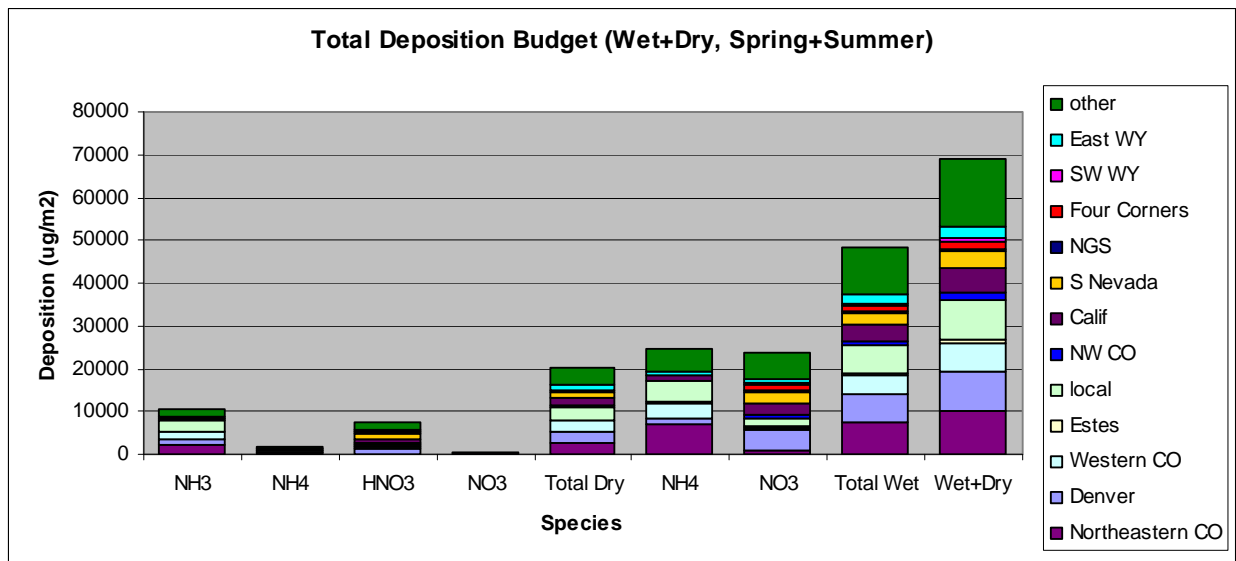


Figure 5.183. Graphical display of wet and dry source area deposition budgets for each species, total dry, total wet, and total wet plus dry deposition for the summer plus spring time periods.

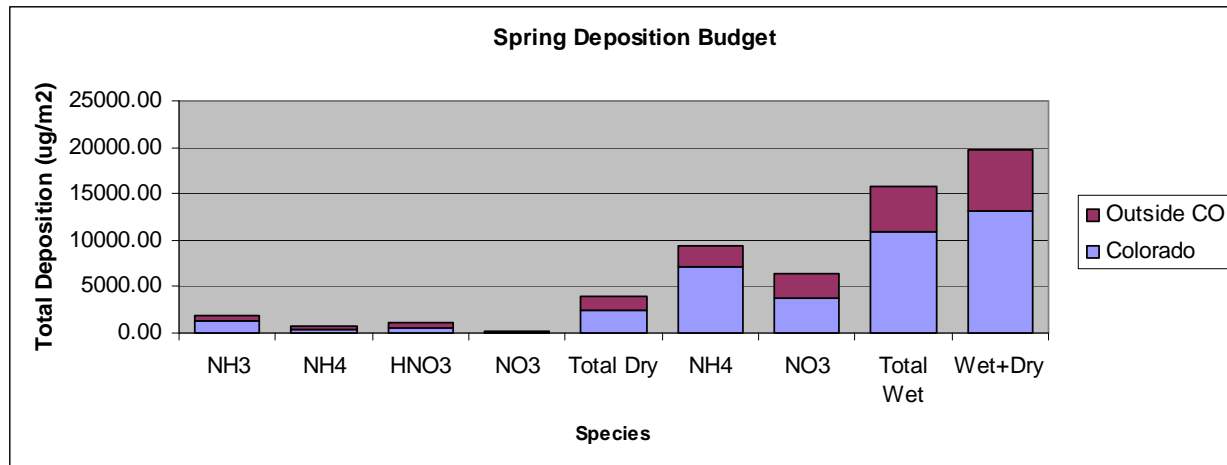


Figure 5.184. Graphical display of wet and dry, Colorado versus outside Colorado source area deposition budgets for each species, and total dry, total wet, and total wet plus dry deposition for the summer plus spring time periods.

### 5.5.6. Summary

The role of emissions in forming secondary particulates that contribute to visibility impairment and their contributions to reactive nitrogen wet and dry deposition to aquatic and terrestrial ecosystems are important and emerging issues. Ammonia and nitrogen oxides are not typically emitted from the same sources or even from the same source regions. Ammonia may be emitted from agricultural activity, while nitrogen oxides originate from mobile sources (urban areas) and large point sources such as electricity-generating facilities. Without ammonia, nitrogen oxide emissions would most likely be deposited out as nitric acid, and without nitrogen and sulfur oxide emissions, ammonia would most likely deposit as ammonia. Both gaseous nitric acid and ammonia have higher deposition rates than their particulate counterparts and are deposited closer to their sources. Therefore it is the combination of these two source types that is responsible for the resulting haze formed from their emissions and transport and deposition to more distant and sensitive receptors.

Nitrogen deposition in RMNP is above the critical load and changes are occurring in the ecosystem. One goal of the RoMANS study was to determine the sources contributing to the excess deposition. This requires separating the contributions from nearby local sources, sources along the Front Range, and other source regions east and west of the Continental Divide to reactive nitrogen in RMNP. One method of apportioning nitrogen species to these source regions is to integrate modeled transport and dispersion of a conservative tracer released in proportion to emissions with receptor-oriented models to statistically account for removal and chemical processes. From these statistical relationships, the contributions of source regions to the receptor concentrations are estimated.

#### 5.5.6.1. Spring

During the spring season, about 80% of ammonia and ammonium originated from within the state of Colorado, and 40–50% of the oxidized nitrogen species were from within state sources. It was estimated that about 50% of the  $\text{SO}_2$  came from within the state but only about 20% of the

sulfate. During two of the events with the highest concentrations of trace gases and particulates, April 20 and 23 (JD = 110.6 and 113.5), upslope conditions were present and northeastern Colorado and Denver were the largest contributors to almost all species. Northeastern Colorado contributions to ammonia were as high as 80%, and Denver contributions were as high as 65% but more typically in the 10–20% range. Apportionment of ammonium during the spring time period was similar but with more contributions from western Colorado.

During the time periods mentioned above, the relative contributions of northeastern Colorado and Denver to nitric acid and nitrates were approximately reversed from that of ammonia, with the Denver area contributing most of the oxidized nitrogen and northeastern Colorado contributing significantly. At other times, northwestern Colorado was estimated to have contributed significantly to HNO<sub>3</sub> at as high as 50–70% and on the average about 20%.

During the upslope events, as might be expected, both sulfur dioxide and sulfate were associated with sources in Denver and northeastern Colorado. However, during other time periods sources in the Southwest and eastern Wyoming made a large fractional contribution.

On the average it is estimated that about 67% of the wet-deposited ammonium was from northeastern Colorado and about 16% was from Denver source region. The largest rain/snow event started on April 23 (JD = 113.8). As with the average attribution, during this time period, on the order of 70–80% of the wet-deposited ammonium came from northeastern Colorado and about 10–20% from Denver.

Wet-deposited nitrate on the average is mostly associated with Denver emissions at over 50% with eastern Wyoming contributing another 6%.

Sources associated with wet-deposited sulfate were more varied than for ammonium or nitrate. Denver on the average was the largest contributor at 42%, with northeastern Colorado and eastern Wyoming each contributing 12–13%. The Four Corners, southern Nevada, and eastern Wyoming regions were also estimated to have made a contribution to wet sulfate deposition.

#### **5.5.6.2. Summer**

During the summer time period, sources contributing to gases and particles in RMNP were more diverse. About 70% of ammonia originated from within the state, but ammonium, nitric acid and sulfur dioxide were estimated to be at about 40–50%. Only about 20–30% of nitrate and sulfate were due to Colorado emissions.

On the average, the local source was estimated to contribute most of the ammonia at more than 25% while northeastern and western Colorado each contributed about 20% of the ammonia. These three source areas plus California were the largest contributors to ammonium as well. About 35% of the ammonium was estimated to be from sources labeled as “other,” indicating they were spread out across the United States and not explicitly identified above. Much of the nitric acid apparently was associated with NO<sub>x</sub> emissions in Denver, northwestern Colorado, the Southwest, and California. Most of the nitrate was estimated to be from California at about 35%, with contributions from the Southwest and Wyoming. Both sulfur dioxide and sulfate were estimated to have significant contributions from northwestern Colorado and southwestern Wyoming, as well as the southwest United States in general.

During the summer there were two interesting episodic time periods, one from July 21–22 (JD = 202 to 203), which corresponded to upslope conditions with contributions from Denver and northeastern Colorado contributing to all species, and another from July 30 to August 4 (JD = 211 to 216) when sources in southern Nevada, and California were the major contributors to most species.

Whereas the spring time period was marked by one significant upslope rain event, the summer time period had a number of rainy periods. During the summer the source apportionment was more varied than during the spring, with more distant sources contributing to wet deposition at RMNP. On the average, the local and western Colorado source regions contributed most of the ammonium at 32% and 24%, respectively, while northeastern Colorado and California contributed another 7% each. The source apportionment during the largest summer time episode starting on July 19 was about the same as the average apportionment. Sources contributing to wet nitrate deposition were the most varied. California and southern Nevada were estimated to have contributed the largest fraction of wet-deposited nitrate at about 15% each, while the Denver, Four Corners, and local regions each add another 8–10%. Northeastern and western Colorado, Estes Park, southwestern and eastern Wyoming all made contributions to wet nitrate deposition in the 2–5% range.

Sources for wet sulfate deposition were as varied as for nitrate but with less of a California and southern Nevada influence. Northwestern Colorado and southwestern Wyoming were predicted to be the largest contributors to wet sulfate deposition.

### **5.5.6.3. Deposition Budgets**

Wet plus dry deposition was about 2.5 times greater during the summer monitoring time frame, with wet deposition being about 2.5–3 times greater than dry deposition during both seasons. The most significant contributor to dry deposition was ammonia, and during the spring time frame it was estimated that northeastern Colorado contributed to most of this deposition at about 40%, with the Denver area contributing another 20%. These two sources were estimated to contribute 40% and 35% of the total spring time frame deposition, respectively.

During the summer, nitrogen deposition was associated with a more diverse group of sources. The local and western Colorado regions were the two source areas predicted to contribute the largest fractions of nitrogen at 18% and 13%, respectively. Southern Nevada, California, northeastern Colorado, and the Denver source regions each contributed 8–11%.

The five largest source areas contributing to nitrogen deposition for both time periods combined were northeastern Colorado, Denver, the local source region, western Colorado, and California. Sources outside the specified regions contributed on the order of 20%.

Nearly 80% of the ammonia was predicted to originate from within Colorado and about 60% of the dry-deposited nitrogen came from within the state. While most of the wet-deposited ammonium was predicted to come from within the state, less than half of wet-deposited nitrate came from within its borders. The split for total deposition, wet plus dry, between in state versus out of state was predicted to be about 55:45.

## 5.6. APPLICABILITY OF THE ROMANS RESULTS TO OTHER YEARS AND OTHER TIMES OF THE YEAR

The source attribution and nitrogen deposition results from the RoMANS study are based on about 10 weeks during 2006, and there is a question as to how representative these results are for the average nitrogen deposition source attribution at RMNP over the entire year. In other words, are the RoMANS source attribution results similar to or dramatically different from those expected for other years and other times of the year? In order to address this question, the measured ambient and wet deposition data, precipitation rates, and air parcel transport patterns during the RoMANS field campaigns were compared to historical values.

As shown in Figure 5.185, the nitrogen deposition rates of typically measured species can vary by an order of magnitude, depending on the month of the year. The two RoMANS field campaigns were selected to occur during the high-nitrogen-deposition, spring and summer periods, and the measured inorganic nitrogen deposition during these 10 weeks accounts for about a third of the total measured nitrogen deposition in a typical year. At Loch Vale, Colorado, the lower-bound average, wet-deposited inorganic nitrogen during the same weeks of the year as the RoMANS study from 2000 to 2005 is  $\sim 0.95$  kg N/ha/yr, which is almost two-thirds of the recently established critical load for inorganic nitrogen wet deposition in RMNP of 1.5 kg N/ha/yr. Consequently, a significant portion of annual nitrogen deposition occurs during the same weeks of the year as the RoMANS study periods and this deposition represents a significant portion of the critical load.

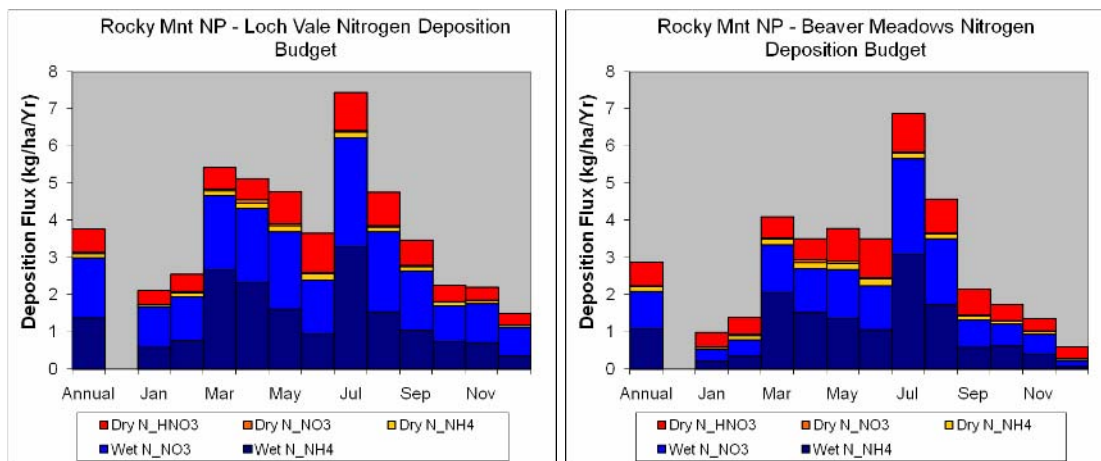


Figure 5.185. The average monthly total nitrogen deposition budgets at Loch Vale and Beaver Meadows in RMNP. The NADP wet deposition data at Loch Vale and Beaver Meadows and RMNP CASTNet data from 2000 through 2005 were used. Note, 7% and 20% of the measured precipitation at Beaver Meadows and Loch Vale, respectively, had invalid wet deposition samples and the deposition rates represent lower bounds of measured species at these sites.

Air parcel transport is one of the most influential meteorological processes affecting the nitrogen species concentrations and deposition because it determines which potential source regions are upwind of RMNP. The transport patterns were examined using the hourly, 5-day EDAS back trajectories from 2000 through 2007 in a residence time analysis. All other things being the same, a source region's potential to contribute to nitrogen deposition at a receptor site, e.g., RMNP, increases for time periods when air parcels frequently pass over and spend more time,

i.e., higher residence time, over the source region prior to transport to RMNP. Therefore, if the trajectory residence times for the study period are similar to other years and other time periods, it can be expected that sources contributing to nitrogen deposition during the study are representative or typical of other years.

Residence time analysis aggregates hourly back trajectories together. In the aggregation process, each hourly trajectory was weighted by the total nitrogen deposition rates. The hourly dry and wet nitrogen deposition rates were estimated from the weekly CASTNet and NADP data, respectively. The variation in dry deposition within a weekly CASTNet sample was due only to variations in the deposition velocities and did not capture the hourly variations in the ambient concentrations. The weekly NADP wet deposition data were apportioned to rain events by multiplying the week's wet deposition concentration by the precipitation rate each hour. Consequently, only hours with precipitation are given a non-zero wet deposition rate. The nitrogen-deposition-weighted residence time plots then show transport pathways associated with high nitrogen deposition. These residence time plots are strongly influenced by the transport during precipitation events, since hours with precipitation tend to have the highest deposition rates.

The nitrogen-deposition-weighted residence time plot for all days of the year from 2000 to 2007 is presented in Figure 5.186. On average, transport to RMNP was predominantly from the west. However, as shown in Figure 5.186, over the course of a typical year, nitrogen deposition at RMNP was associated with air parcel transport both from the west and the east. To the west of RMNP the nitrogen deposition was associated with air parcel transport from the southwest from southern Utah to northwestern Colorado to RMNP, and from the northwest from southern Idaho through northern Utah and southwestern Wyoming to RMNP. To the east of RMNP, the nitrogen deposition was associated with transport from the northeast from the Dakotas through Nebraska and northeastern Colorado and from the southeast from Kansas. The nitrogen-deposition-weighted transport patterns for only those spring and summer days included in the RoMANS study for all years from 2000 to 2007 is also presented in Figure 5.186. This transport pattern was very similar to the all-days-of-the-year pattern, though there appeared to be somewhat more transport from the east during this spring and summer period compared to an average year.

The nitrogen-deposition-weighted residence time for only the 2006 RoMANS study period shows similar transport patterns as the historical averages, with high residence times both east and west of RMNP. The common transport pathways from the southwest and northeast are well represented during RoMANS. Transport over southern Idaho and Kansas also occurred, though less frequently than on average. One important difference is that it appears that the 2006 RoMANS period had less transport from northeastern Colorado than seen on average, an indication the contribution from this region may have been underestimated compared to other years.

As discussed in section 4.3 and this chapter, during the RoMANS study period, a number of the important transport pathways, precipitation events, and nitrogen species ambient concentration and wet deposition events were captured within the field campaigns. The RoMANS source attribution results imply that sources to the east of RMNP in the Denver-Front Range and northeastern Colorado regions are important contributors, as well as sources in western Colorado

and from the southwest, including California, southern Nevada, and the Four Corners region. Although the mix of sources impacting RMNP over a typical year will most likely be different than those during the RoMANS study period, the analysis of air quality data and air parcel transport supports the notion that there will likely be broad similarities in the most important contributing source regions, and the general source attribution results from the RoMANS study are applicable to other years and other times of the years beyond RoMANS.

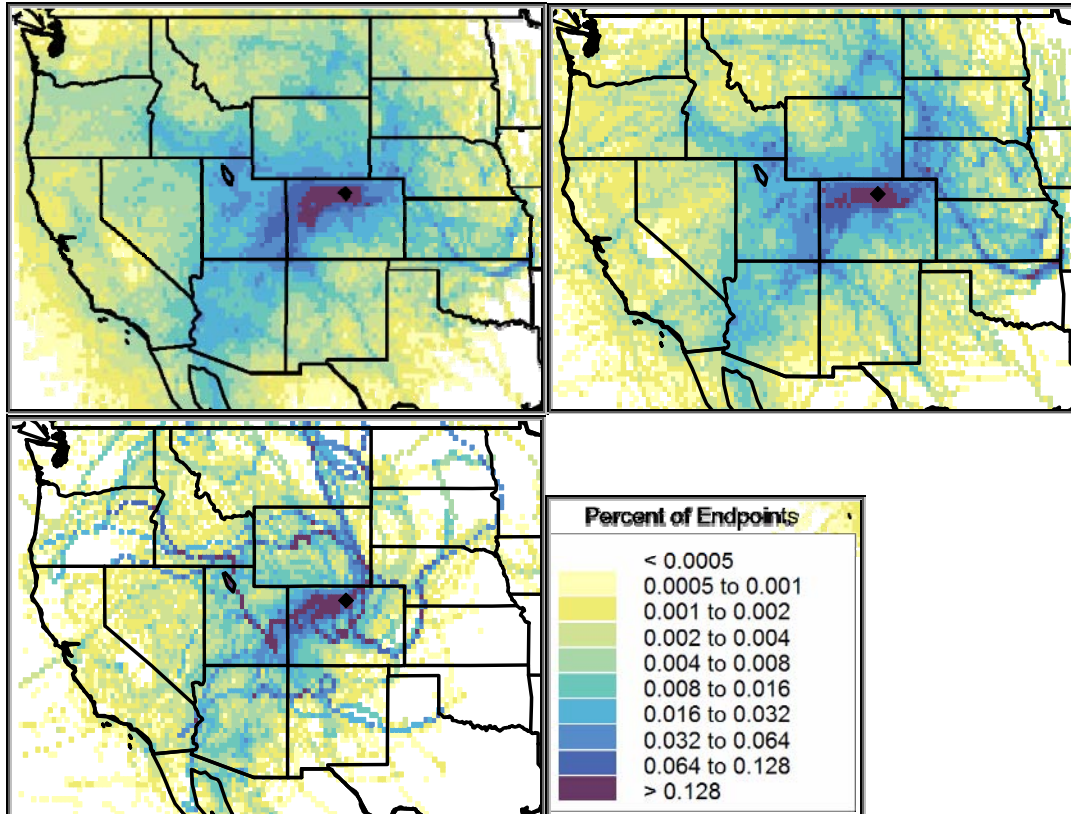


Figure 5.186. Total measured nitrogen-deposition-rate-weighted residence time analysis for a) all days of the year in 2000 to 2007, b) all days of the year during the RoMANS study period for years 2000 to 2007, and c) all days during the 2006 RoMANS study period.

## 5.7. CAMX BASE CASE SIMULATION

### 5.7.1. Methodology

CAMx (Comprehensive Air Quality Model with extensions; Environ Corp., 2005), an advanced Eulerian chemical transport model (CTM), was used to simulate nitrogen and sulfur species as well as ozone during the two RoMANS field campaigns. CAMx simulates the emissions, dispersion, chemical reactions, and removal of pollutants in the troposphere by solving the pollutant continuity equation for each chemical species on a three-dimensional grid.

Although CAMx has been used extensively in the past to simulate regional sulfate and ozone (Yarwood et al., 2003; Morris et al., 2004), and to a lesser degree nitrate and nitric acid (Baker and Scheff, 2007), its application to nitrogen species such as ammonia and organic nitrates is less common. Simulating oxidized and reduced nitrogen is a demanding problem for a CTM, given that it compounds the complexity and uncertainty of processes such as photochemistry, gas-particle partitioning of nitrate and nitric acid, rapid dry deposition velocities of ammonia and nitric acid, and variable fluxes of ammonia, to name a few. In spite of these inherent uncertainties within the model, this type of simulation is the only approach that attempts to explicitly account for the complex physical and chemical processes that govern the fate of pollutants. Example CAMx predictions of selected nitrogen species for an annual 2002 simulation are shown in Figure 5.187.

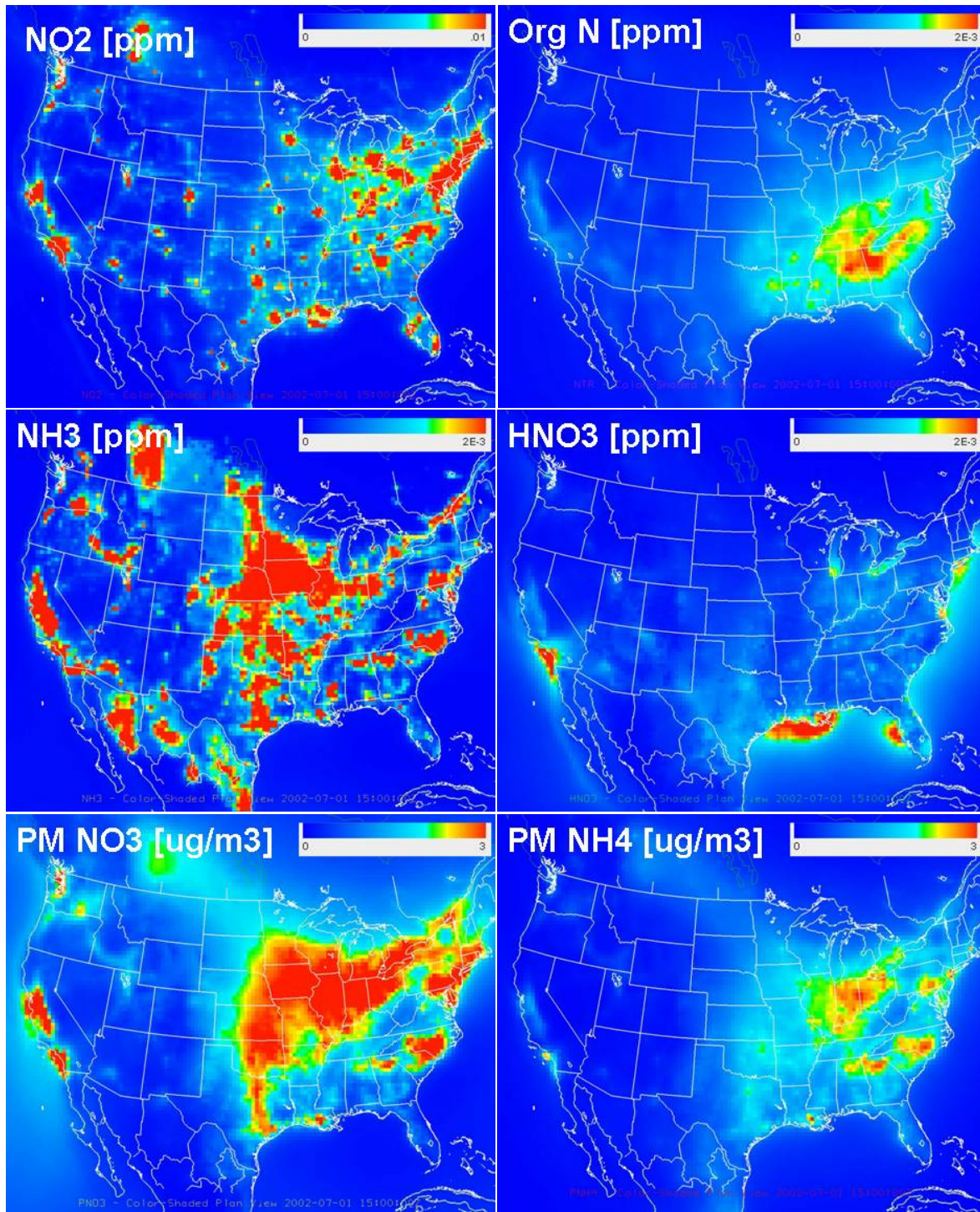


Figure 5.187. Predicted annual average mass concentrations from the 2002 CAMx simulation for (a) nitrogen dioxide, (b) organic nitrate (excluding peroxyacetyl nitrate), (c) ammonia, (d) nitric acid, (e) particulate nitrate, and (f) particulate ammonium.

For this study, CAMx was configured with three nested domains with grid sizes of 36 km, 12 km and 4 km (shown previously in Figure 5.98). The 36-km outer domain covers the contiguous United States, southern Canada, and northern Mexico. The 4-km inner domain extends over

most of Colorado. Model domains are specified using an ‘Arakawa C’ grid, and sigma pressure levels are used in the vertical dimension (Environ Corp., 2006). Horizontal advection is treated with the piecewise-parabolic method (PPM) area preserving flux-form advection solver with explicit horizontal diffusion (Odman and Ingram, 1996). Gas-phase chemistry is based on the Carbon Bond IV mechanism (Whitten et al., 1996). ISORROPIA, a thermodynamic equilibrium model (Nenes et al., 1999), is used to predict the partitioning of inorganic aerosol constituents (sulfate, nitrate, and ammonium) between the gas and particle phases. The model outputs hourly average concentrations for gas and particulate species that can be compared with available ambient monitoring data.

### 5.7.2. Model Performance Evaluation

Boylan and Russell (2006) discuss several standard performance metrics commonly applied to the evaluation of air quality models. In this section we focus on the mean fractional error (MFE) and mean fractional bias (MFB). Model error quantifies the extent to which the modeled concentrations differ from the observations and is always positive. The equation for MFE is given as 5.25:

$$\text{Equation 5.25. } \frac{2}{N} \sum_{i=1}^N \left| \frac{C_m - C_o}{C_m + C_o} \right|$$

where  $C_m$  and  $C_o$  are the modeled and observed concentrations, respectively, at station  $i$ , and  $N$  is the number of pairs of data during the time period of interest (Boylan and Russell, 2006). MFE ranges from 0 to 200%. The mean fractional bias (MFB) is given by Equation 5.26.

$$\text{Equation 5.26. } \frac{2}{N} \sum_{i=1}^N \left( \frac{C_m - C_o}{C_m + C_o} \right)$$

MFB ranges from -200% to 200%. The advantage of normalizing the concentration difference with the sum of the observed and predicted concentrations, as opposed to normalizing with only the observed concentration, is that it restricts the MFE and MFB from growing too large when very small observed concentrations are considered. These metrics bound the maximum and minimum bias and error and do not allow a few data points to dominate the metrics. These metrics are symmetric because they give equal weight, on a relative basis, to concentrations simulated higher as well as those simulated lower than observations.

The model evaluation was performed using observations from the IMPROVE network (Malm et al., 1994) across the United States, as well as observations from the RoMANS campaign. We focus on key aerosol and gas species pertinent to the RoMANS study (e.g., nitrogen and sulfur species), and use model performance metrics that are statistical measures used to identify the model performance relative to the observed data in terms of bias and error.

The results presented in the following sections are a summary of the model performance evaluation; a full description of the model performance is presented in Appendix 3.

### 5.7.2.1. Model Performance Evaluation Using IMPROVE Data for the United States

The CAMx model simulations were performed for the two periods that spanned both the spring (March 25 to April 30) and summer (July 7 to August 12) RoMANS campaigns for 2006. We used available observational data (one-in-three-day sampling frequency) from the IMPROVE monitoring network during these same time periods to evaluate the 36-km domain model results. We focused specifically on sulfate and nitrate concentration comparisons.

#### 5.7.2.1.1. Sulfate ( $\text{SO}_4^{-2}$ )

In this section we evaluate the model performance statistics for particulate sulfate concentrations. Figure 5.188(a,b) shows the estimated MFB and MFE, respectively, for sulfate concentrations, using all the available data for the whole 36-km domain and just those sites in the western United States (i.e., Arizona, California, Colorado, Idaho, Montana, New Mexico, North Dakota, Oregon, South Dakota, Utah, Washington, and Wyoming, as determined by the WRAP region). The model underpredicted sulfate concentrations both in spring and summer, but the negative biases were higher during the summer (Figure 5.188a). The values presented in this study, however, are comparable to other regional modeling studies. For instance, this study found that the MFB in the western states in April 2006 was close to -23% (MFB multiplied by 100%), while the WRAP-RMC (Regional Modeling Center) simulations done for 2002 set the MFB at approximately -40% (Tonnesen et al., 2006). For the month of July 2006 the estimated MFB was -46%, while the WRAP-RMC was close to -20%. The estimated MFEs (Figure 5.188b) show that the model errors were close to 60% (MFE multiplied by 100%), with summer errors slightly larger than spring errors. In addition to the MFE and MFB, Table 5.28 presents the mean concentrations and standard deviations for the modeled and observed concentrations for the entire 36-km domain and just the western U.S. states for spring and summer.

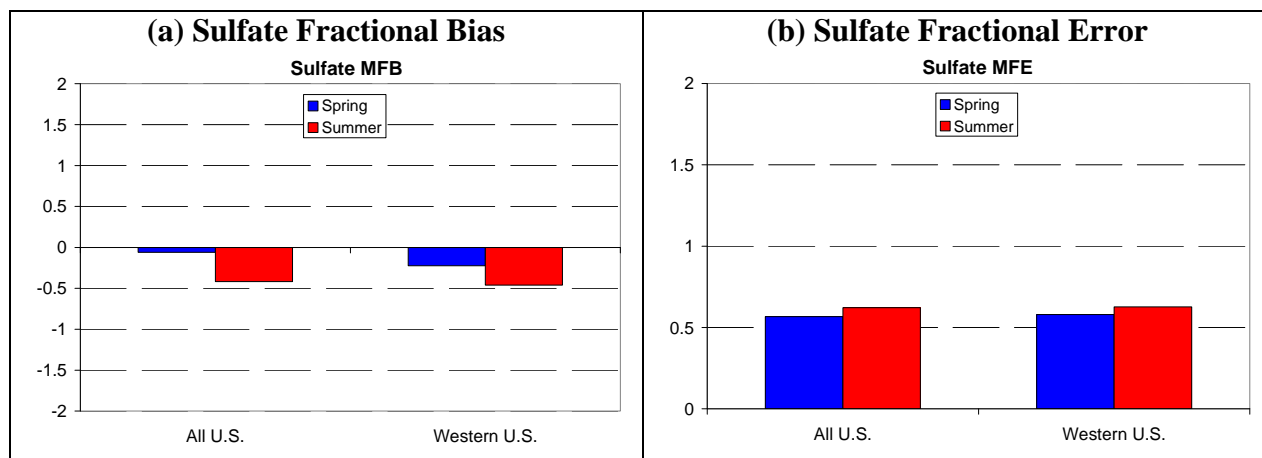


Figure 5.188. (a) Mean fractional bias and (b) mean fractional error for sulfate concentrations from the 36-km domain CAMx model predictions compared to observations from the IMPROVE network, using monitoring stations for the whole U.S. domain and monitoring stations that only fall within the western United States. Blue and red bars correspond to the spring and summer campaigns, respectively.

**Table 5.28.** Model performance statistics for sulfate concentrations during both the spring and summer RoMANS campaigns, using available IMPROVE monitoring stations for the entire 36-km U.S. domain and with sites that fall within the western United States alone.

Metric	Spring		Summer	
	36-km U.S. Domain	Western U.S.	36-km U.S. Domain	Western U.S.
Mean observation ( $\mu\text{g}/\text{m}^3$ )	1.50	0.67	2.47	1.01
Mean estimation ( $\mu\text{g}/\text{m}^3$ )	1.77	0.54	1.85	0.64
STD <sup>a</sup> obs. ( $\mu\text{g}/\text{m}^3$ )	1.57	0.47	2.9	0.68
STD est. ( $\mu\text{g}/\text{m}^3$ )	2.28	0.53	2.7	0.57
MFE <sup>b</sup> (%)	56.7%	58.0%	62.2%	62.7%
MFB <sup>c</sup> (%)	-6.0%	-22.5%	-41.8%	-46.0%

<sup>a</sup>Standard Deviation

<sup>b</sup>Mean Fractional Error (%)

<sup>c</sup>Mean Fractional Bias (%)

### 5.7.2.1.2. Nitrate ( $\text{NO}_3^-$ )

A comparison of nitrate concentrations was performed by evaluating the MFB and MFE, using available IMPROVE monitoring data for the periods that span both the spring and summer field campaigns. Figures 5.189a and Figure 5.189b show the estimated MFB and MFE for nitrate concentrations, respectively, using all the available data for the entire 36-km domain and data for just those states in the western United States. The model underpredicted nitrate concentrations both in spring and summer, but the negative biases were greater during the summer. The values presented in this study, however, were comparable to other regional modeling studies. For instance, this study finds that the MFB in the western states in April 2006 was close to -10% while the WRAP–RMC simulations done for 2002 set the MFB at approximately -50%. For the month of July 2006 the estimated MFB was -129% while the 2002 WRAP–RMC was approximately -150% (Tonnesen et al., 2006). The estimated MFE shows that the model errors varied between 120% in the spring to 160% in the summer. Table 5.29 presents the MFE, MFB, mean concentrations and standard deviations for the modeled and observed concentrations for the entire 36-km domain and just the western U.S. states for spring and summer. Not surprisingly, the model errors presented for nitrate concentrations were far larger than those for sulfate concentrations; these discrepancies point to the difficulty regional models have in adequately representing the complex thermodynamics of nitrate formation.

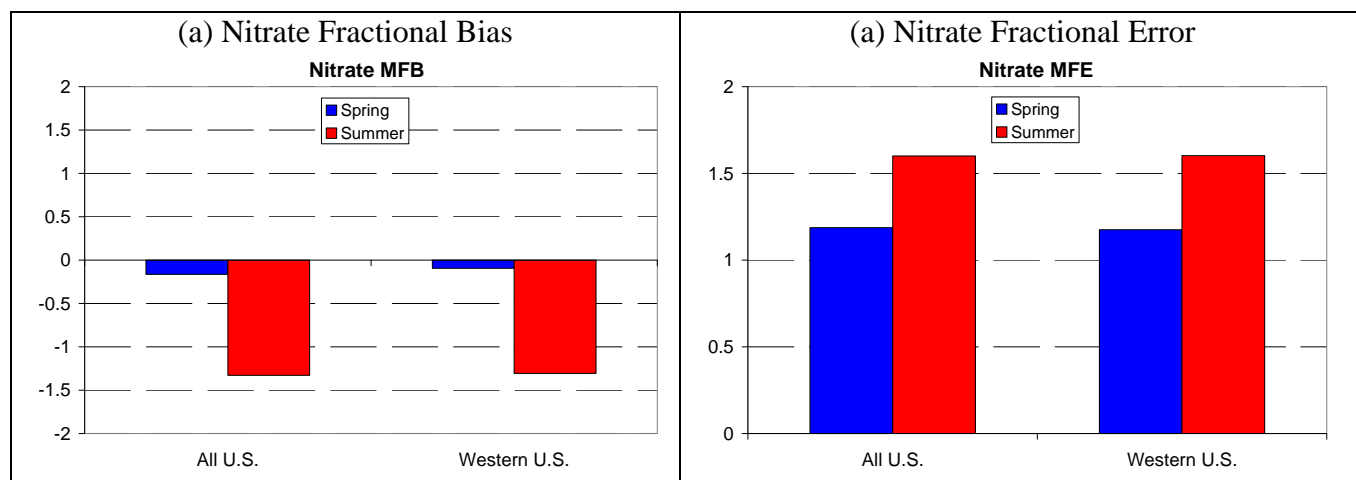


Figure 5.189. (a) Mean fractional bias and (b) mean fractional error for nitrate concentrations from the 36-km domain CAMx model predictions compared to observations from IMPROVE network, using monitoring stations for the whole U.S. domain and monitoring stations that only fall within the western United States. Blue and red bars correspond to the spring and summer campaigns, respectively.

**Table 5.29.** Model performance statistics for nitrate concentrations during both the spring and summer RoMANS campaigns, using available IMPROVE monitoring stations for the entire 36-km U.S. domain and with sites that fall within the western United States alone.

Metric	Spring		Summer	
	36-km U.S. Domain	Western U.S.	36-km U.S. Domain	Western U.S.
Mean observation ( $\mu\text{g}/\text{m}^3$ )	0.45	0.27	0.21	0.19
Mean estimation ( $\mu\text{g}/\text{m}^3$ )	0.67	0.47	0.10	0.10
STD <sup>a</sup> obs. ( $\mu\text{g}/\text{m}^3$ )	0.70	0.47	0.27	0.28
STD est. ( $\mu\text{g}/\text{m}^3$ )	1.04	0.75	0.33	0.35
MFE <sup>b</sup> (%)	118.7%	117.5%	160.1%	159.5%
MFB <sup>c</sup> (%)	-16.6%	-9.4%	-132.8%	-129.3%

<sup>a</sup>Standard Deviation

<sup>b</sup>Mean Fractional Error (%)

<sup>c</sup>Mean Fractional Bias (%)

### 5.7.2.2. Model Performance Evaluation at the RoMANS Satellite Sites.

Comparisons of measured and modeled aerosol and gas concentrations were performed at the nine satellite sites during the spring campaign (36 days, March 25 to April 19, 2006) and the seven satellite sites during the summer campaign (36 days, July 7 to August 11, 2006).

Compared to the IMPROVE data evaluations presented above, these comparisons have the added advantage of higher time (daily) and spatial resolution, as well as additional measured species other than just sulfate and nitrate. Three gas-phase species ( $\text{NH}_3$ ,  $\text{HNO}_3$ , and  $\text{SO}_2$ ) and three particle-phase species ( $\text{NH}_4^+$ ,  $\text{NO}_3^-$ , and  $\text{SO}_4^{2-}$ ) were compared, along with total reduced (N(-III) =  $\text{NH}_3 + \text{NH}_4^+$ ) and oxidized nitrogen (N(V) =  $\text{HNO}_3 + \text{NO}_3^-$ ) and total sulfur species (S =  $\text{SO}_4^{2-} + \text{SO}_2$ ). Seasonal means and performance statistics were computed for the modeled and measured concentrations for each species at each of the sites and for each study period. The comparisons were performed for the model results at 4-km, 12-km and 36-km domain grid spacing. The performance for all of the domains was similar, so only 4-km results will be

presented here. The results from the larger grid spacing can be found in Appendix 3. A more detailed discussion of the model evaluation for the satellite sites, including time series and scatter plot comparisons, can be found in this appendix also.

The mean predicted and observed concentrations for all the particulate and gas-phase nitrogen and sulfur species as a function of site location during the spring and summer campaigns are presented in Figure 5.190 and Figure 5.191, respectively. These figures provide an overview of the level of agreement between modeled and observed concentrations. A detailed discussion of the model evaluation for each species at each of these sites will be presented in the following sections. Time series and scatter plot comparisons for each site and season are provided in Appendix 3.

RoMANS 2006 Spring Average URG and 4km CAMx 24hr Concentration

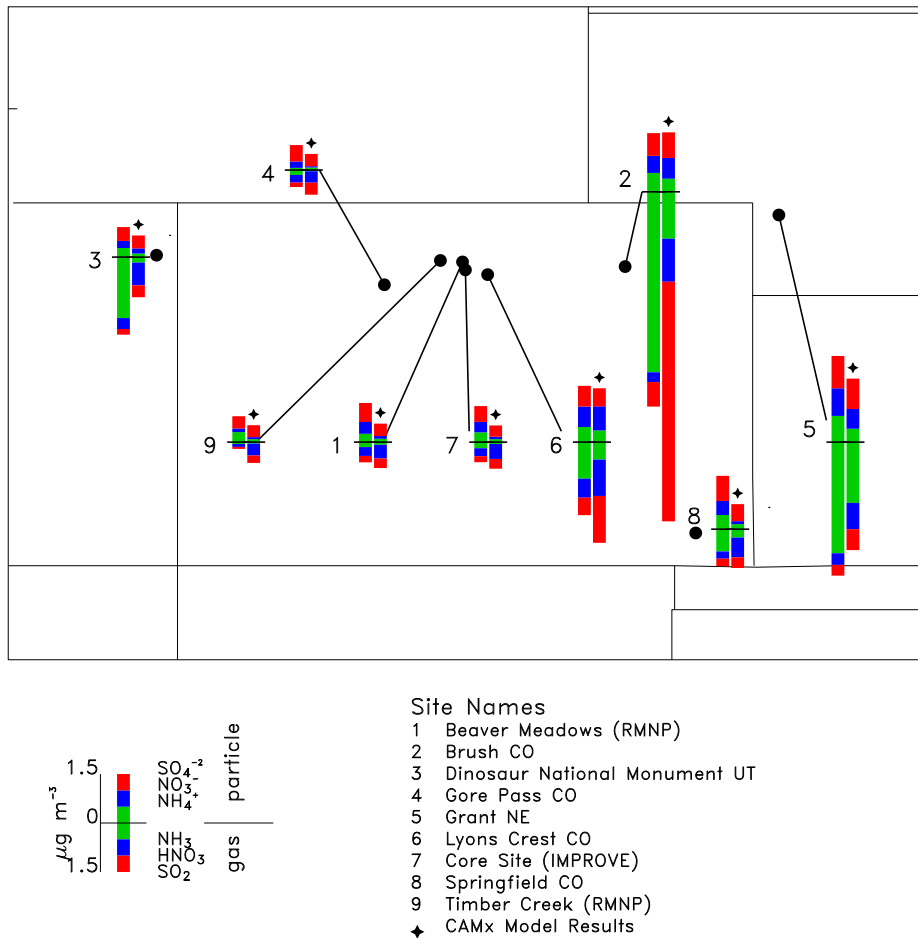


Figure 5.190. Spring study mean predicted and observed 24-hr particulate and gas-phase species concentrations ( $\mu\text{g}/\text{m}^3$ ). Particulate species are shown as the upper bar charts and gas-phase species are shown as the lower bar charts (see legend for scale). The predicted concentrations are shown with a “\*” over the bar chart. Site locations correspond to the numbers listed next to the bar chart.

RoMANS 2006 Summer Average URG and CAMx 4km 24hr Concentration

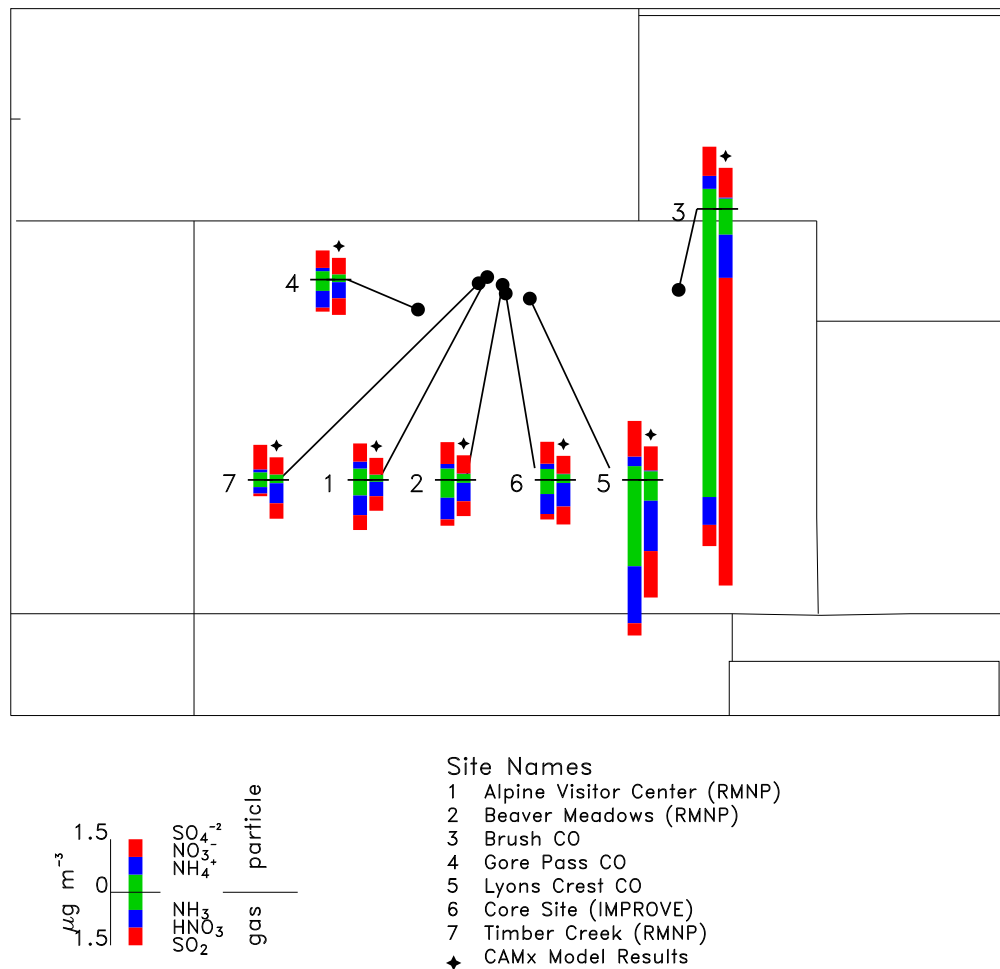


Figure 5.191. Summer study mean predicted and observed 24-hr particulate and gas-phase species concentrations ( $\mu\text{g}/\text{m}^3$ ). Particulate species are shown as the upper bar charts and gas-phase species are shown as the lower bar charts (see legend for scale). The predicted concentrations are shown with a “\*” over the bar chart. Site locations correspond to the numbers listed next to the bar chart.

#### 5.7.2.2.1. Ammonium ( $\text{NH}_4^+$ )

The model performance statistics for particulate ammonium during the spring study are reported in Table 5.30. For  $\text{NH}_4^+$  in the spring the highest correlation coefficient ( $R = 0.71$ ) occurred at the eastern site of Lyons Crest. The lowest MFE corresponded to Gore Pass (54%) while the largest corresponded to the core site (109%, see Figure 5.192a). All of the MFBs were negative, with the exception of Gore Pass, which also corresponded to the lowest fractional bias (16%). The highest fractional bias corresponded to the core site (-109%, see Figure 5.192b). The

underprediction of  $\text{NH}_4^+$  by the model for all the sites is clear from the mean concentrations presented in Figure 5.190.

**Table 5.30.** Spring campaign  $\text{NH}_4^+$  model performance statistics. The column headings refer to the site ID and site name, study mean of the estimated concentrations (ME,  $\mu\text{g m}^{-3}$ ), study mean of the observed concentrations (MO,  $\mu\text{g m}^{-3}$ ), standard deviation of the estimated and observed mean concentration (SDE and SDO, respectively,  $\mu\text{g m}^{-3}$ ), and the mean fractional error (MFE, %) and the mean fractional bias (MFB, %). The rows of the table correspond to the site locations.

Site ID	Site Name	ME ( $\mu\text{g m}^{-3}$ )	MO ( $\mu\text{g m}^{-3}$ )	SDE ( $\mu\text{g m}^{-3}$ )	SDO ( $\mu\text{g m}^{-3}$ )	MFE (%)	MFB (%)
BEME	Beaver Meadows	0.104	0.254	0.085	0.272	84.4	-66.1
BRUS	Brush CO	0.398	0.579	0.401	0.743	66.4	-25.8
DINO	Dinosaur NM UT	0.111	0.279	0.109	0.161	101.2	-85.4
GOPA	Gore Pass CO	0.077	0.066	0.04	0.042	53.9	16.3
GRAN	Grant NE	0.398	0.802	0.496	0.623	89.5	-72.6
LYCR	Lyons Crest CO	0.346	0.463	0.434	0.474	85.3	-46.0
ROMO	Core Site	0.089	0.3	0.067	0.148	108.7	-108.7
SPRI	Springfield CO	0.146	0.434	0.164	0.463	104.9	-90.6
TICR	Timber Creek	0.089	0.306	0.046	0.237	96.1	-91.4

**Table 5.31.** Summer campaign  $\text{NH}_4^+$  model performance statistics. The column headings refer to the site ID and site name, study mean of the estimated concentrations (ME,  $\mu\text{g m}^{-3}$ ), study mean of the observed concentrations (MO,  $\mu\text{g m}^{-3}$ ), standard deviation of the estimated and observed mean concentration (SDE and SDO, respectively,  $\mu\text{g m}^{-3}$ ), and the mean fractional error (MFE, %) and the mean fractional bias (MFB, %). The rows of the table correspond to the site locations.

Site ID	Site Name	ME ( $\mu\text{g m}^{-3}$ )	MO ( $\mu\text{g m}^{-3}$ )	SDE ( $\mu\text{g m}^{-3}$ )	SDO ( $\mu\text{g m}^{-3}$ )	MFE	MFB
ALVC	Alpine Visitor Cent.	0.138	0.321	0.054	0.093	78.2	-78.2
BEME	Beaver Meadows	0.171	0.324	0.07	0.157	59.0	-57.3
BRUS	Brush CO	0.301	0.568	0.096	0.239	64.0	-55.2
GOPA	Gore Pass CO	0.151	0.239	0.059	0.078	47.4	-44.9
LYCR	Lyons Crest CO	0.253	0.39	0.083	0.216	51.2	-33.0
ROMO	Core Site	0.165	0.31	0.068	0.153	64.9	-52.4
TICR	Timber Creek	0.154	0.216	0.064	0.093	53.6	-28.7

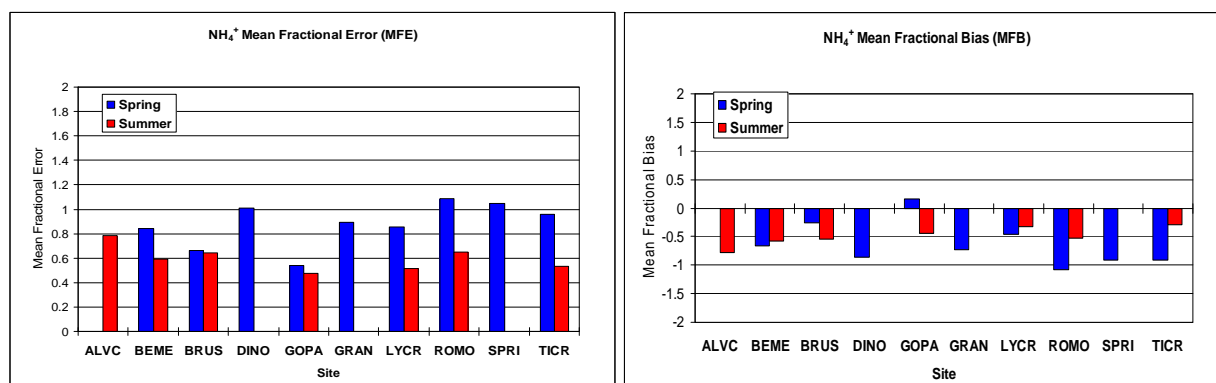


Figure 5.192. (a)  $\text{NH}_4^+$  mean fractional error and (b) mean fractional bias as a function of site for spring and summer.

The highest correlation coefficient between predicted and observed concentrations during the summer campaign for all the sites corresponded to Gore Pass and the core site ( $R = 0.36$ ), which was considerably lower than during the spring campaign. The lowest MFE also occurred at Gore Pass (47%) and the highest occurred at the Alpine Visitor Center (78%, see Figure 5.192a). The MFBs were negative for all sites, with the lowest occurring at Timber Creek (-29%) and the highest occurring at the Alpine Visitor Center (-78%, see Figure 5.192b). A summary of performance statistics for each site during the summer campaign are presented in Table 5.31.

The model appeared to perform more realistically for  $\text{NH}_4^+$  in the summer. Comparisons of MFE and MFB as a function of season for all the sites can be seen in Figures 5.192a and 5.192b. The Alpine Visitor Center site was not operated during the spring campaign and the Dinosaur National Monument, Grant, and Springfield sites were not operated during the summer campaign so data for those sites do not exist for both campaigns. In general for most sites, the MFE was higher during the spring campaign. In general the MFBs are negative, with the exception of Gore Pass in the spring. Generally, the MFBs are larger during spring with the exception of the Brush site.

#### 5.7.2.2.2. Nitrate ( $\text{NO}_3^-$ )

The performance statistics for comparisons of predicted and observed particulate nitrate ( $\text{NO}_3^-$ ) are presented in Table 5.32. The highest correlation corresponded to Springfield ( $R = 0.72$ ). The lowest MFE corresponded to Timber Creek (97%), while the highest MFE corresponded to Springfield (148%, see Figure 5.193a). The MFBs were negative for all sites, with the lowest corresponding to Brush (-62%) and the highest at Springfield (-145%, see Figure 5.193b).

**Table 5.32.** Spring campaign  $\text{NO}_3^-$  model performance statistics. The column headings refer to the site ID and site name, study mean of the estimated concentrations (ME,  $\mu\text{g m}^{-3}$ ), study mean of the observed concentrations (MO,  $\mu\text{g m}^{-3}$ ), standard deviation of the estimated and observed mean concentration (SDE and SDO, respectively,  $\mu\text{g m}^{-3}$ ), and the mean fractional error (MFE, %) and the mean fractional bias (MFB, %). The rows of the table correspond to the site locations.

Site ID	Site Name	ME ( $\mu\text{g m}^{-3}$ )	MO ( $\mu\text{g m}^{-3}$ )	SDE ( $\mu\text{g m}^{-3}$ )	SDO ( $\mu\text{g m}^{-3}$ )	MFE(%)	MFB (%)
BEME	Beaver Meadows	0.091	0.36	0.153	0.457	139	-128.6
BRUS	Brush CO	0.651	0.524	1.199	0.349	111	-61.9
DINO	Dinosaur NM UT	0.168	0.218	0.322	0.145	137.4	-102
GOPA	Gore Pass CO	0.041	0.195	0.056	0.099	139	-132.3
GRAN	Grant NE	0.623	0.848	1.293	0.833	107.8	-84.8
LYCR	Lyons Crest CO	0.721	0.626	1.15	0.654	117.6	-65.0
ROMO	Core Site	0.076	0.32	0.105	0.353	134.2	-123.1
SPRI	Springfield CO	0.069	0.43	0.139	0.986	147.8	-144.7
TICR	Timber Creek	0.063	0.113	0.068	0.048	97.1	-78.2

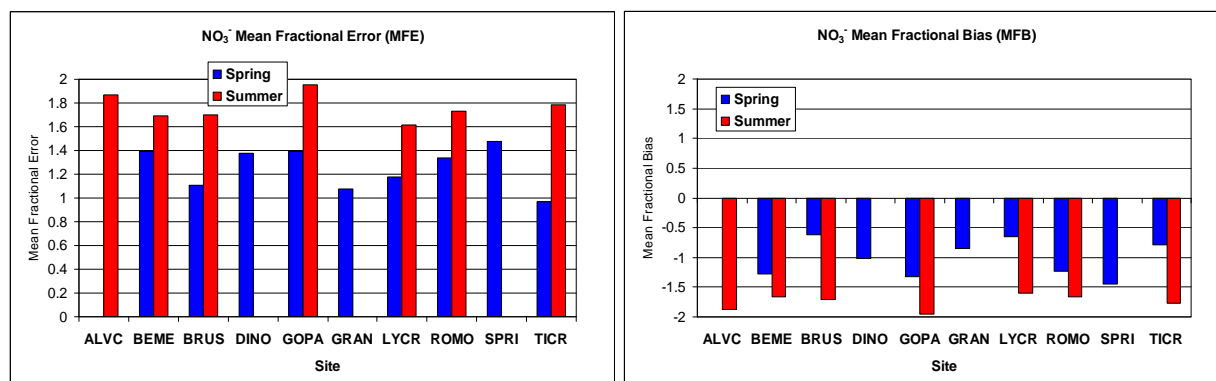


Figure 5.193. (a) NO<sub>3</sub><sup>-</sup> mean fractional error and (b) mean fractional bias as a function of site location for spring and summer.

The performance statistics for comparisons of predicted and observed particulate NO<sub>3</sub><sup>-</sup> during the summer campaign are presented in Table 5.33. The highest correlation corresponded to Lyons Crest ( $R = 0.38$ ), considerably lower than the highest correlation computed during the spring campaign. The lowest MFE occurred at Lyons Crest (161%) and the highest at Gore Pass (196%). The lowest and highest MFBs also occurred at Lyons Crest (-161%) and Gore Pass (-196%), respectively (Figure 5.193b). All sites corresponded to negative MFBs. Comparisons between spring and summer MFEs (Figure 5.193a) and MFBs (Figure 5.193b) show better model performance for nitrate during the spring campaign compared to the summer campaign. Seasonal mean observed and modeled concentrations can be compared in Figures 5.190 and 5.191 for spring and summer, respectively.

**Table 5.33.** Summer campaign NO<sub>3</sub><sup>-</sup> model performance statistics. See text for description of column headings. The column headings refer to the site ID and site name, study mean of the estimated concentrations (ME,  $\mu\text{g m}^{-3}$ ), study mean of the observed concentrations (MO,  $\mu\text{g m}^{-3}$ ), standard deviation of the estimated and observed mean concentration (SDE and SDO, respectively,  $\mu\text{g m}^{-3}$ ), and the mean fractional error (MFE, %) and the mean fractional bias (MFB, %). The rows of the table correspond to the site locations.

Site ID	Site Name	ME ( $\mu\text{g m}^{-3}$ )	MO ( $\mu\text{g m}^{-3}$ )	SDE ( $\mu\text{g m}^{-3}$ )	SDO ( $\mu\text{g m}^{-3}$ )	MFE(%)	MFB(%)
ALVC	AlpineVisitorCent.	0.006	0.197	0.009	0.165	187.3	-187.3
BEME	Beaver Meadows	0.011	0.128	0.024	0.096	169.2	-166.4
BRUS	Brush CO	0.031	0.368	0.049	0.227	170.2	-170.2
GOPA	Gore Pass CO	0.001	0.093	0.002	0.032	195.5	-195.5
LYCR	Lyons Crest CO	0.026	0.27	0.048	0.275	161.2	-160.9
ROMO	Core Site	0.012	0.148	0.027	0.136	173.2	-166.7
TICR	Timber Creek	0.004	0.082	0.006	0.055	178.8	-176.3

### 5.7.2.2.3. Sulfate (SO<sub>4</sub><sup>-2</sup>)

The highest correlation between predicted and observed concentrations corresponded to Lyons Crest ( $R = 0.75$ ). The lowest MFE occurred at Brush (42%) and the highest corresponded to Beaver Meadows (67%, see Figure 5.194a). The lowest MFB occurred at Dinosaur NM (+3%) and the highest occurred at Springfield (-48%, see Figure 5.194b). All of the biases were negative except for Brush and Dinosaur NM. The performance statistics can be found in Table 5.34.

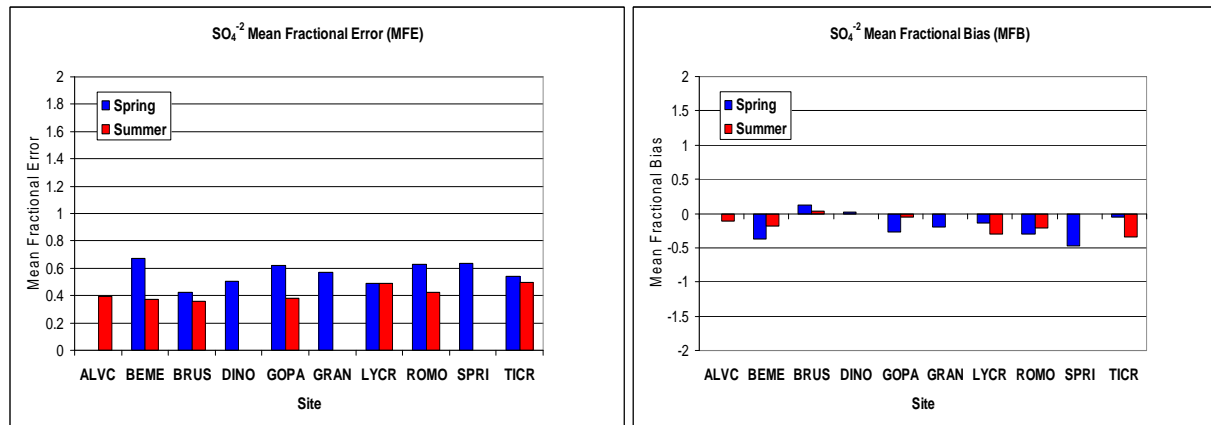


Figure 5.194. Spring and summer SO<sub>4</sub><sup>-2</sup> (a) mean fractional error and (b) mean fractional bias as a function of site location.

**Table 5.34.** Spring campaign SO<sub>4</sub><sup>-2</sup> model performance statistics. See text for a description of column headings. The column headings refer to the site ID and site name, study mean of the estimated concentrations (ME, μg m<sup>-3</sup>), study mean of the observed concentrations (MO, μg m<sup>-3</sup>), standard deviation of the estimated and observed mean concentration (SDE and SDO, respectively, μg m<sup>-3</sup>), and the mean fractional error (MFE, %) and the mean fractional bias (MFB, %). The rows of the table correspond to the site locations.

Site ID	Site Name	ME (μg m <sup>-3</sup> )	MO (μg m <sup>-3</sup> )	SDE (μg m <sup>-3</sup> )	SDO (μg m <sup>-3</sup> )	MFE (%)	MFB (%)
BEME	Beaver Meadows	0.379	0.583	0.204	0.369	66.8	-36.5
BRUS	Brush CO	0.758	0.695	0.336	0.355	42.0	11.8
DINO	Dinosaur NM UT	0.379	0.423	0.167	0.308	50.2	2.8
GOPA	Gore Pass CO	0.371	0.504	0.185	0.258	62.3	-26.5
GRAN	Grant NE	0.88	0.99	0.647	0.498	56.7	-19.1
LYCR	Lyons Crest CO	0.552	0.634	0.421	0.423	49.0	-13.2
ROMO	Core Site	0.347	0.484	0.174	0.262	62.5	-29.8
SPRI	Springfield CO	0.487	0.769	0.412	0.478	63.3	-47.8
TICR	Timber Creek	0.365	0.375	0.196	0.177	53.7	-5.7

During the summer campaign the highest correlation corresponded to Gore Pass (R = 0.37), lower than during spring. The lowest and highest MFEs corresponded to Brush (36%) and Timber Creek (50%), respectively (see Figure 5.194a). The lowest and highest MFBs also corresponded to Brush (+4%) and Timber Creek (-34%, Figure 5.194b). During summer all of the MFBs were negative with the exception of Brush (see Table 5.35). The MFEs were typically lower in the summer than the spring, and the MFBs were lower in summer for all sites but two (Lyons Crest and Timber Creek). Mean observed and modeled concentrations are depicted in Figures 5.191 and 5.191 for spring and summer, respectively.

**Table 5.35.** Summer campaign  $\text{SO}_4^{-2}$  model performance statistics. See text for a description of column headings. The column headings refer to the site ID and site name, study mean of the estimated concentrations (ME,  $\mu\text{g m}^{-3}$ ), study mean of the observed concentrations (MO,  $\mu\text{g m}^{-3}$ ), standard deviation of the estimated and observed mean concentration (SDE and SDO, respectively,  $\mu\text{g m}^{-3}$ ), and the mean fractional error (MFE, %) and the mean fractional bias (MFB, %). The rows of the table correspond to the site locations.

Site ID	Site Name	ME ( $\mu\text{g m}^{-3}$ )	MO ( $\mu\text{g m}^{-3}$ )	SDE ( $\mu\text{g m}^{-3}$ )	SDO ( $\mu\text{g m}^{-3}$ )	MFE (%)	MFB (%)
ALVC	Alpine Visitor Cent.	0.498	0.512	0.294	0.108	39.5	-11.6
BEME	Beaver Meadows	0.515	0.617	0.208	0.331	37.0	-18.5
BRUS	Brush CO	0.864	0.824	0.275	0.253	35.6	3.9
GOPA	Gore Pass CO	0.471	0.493	0.188	0.169	38.2	-4.8
LYCR	Lyons Crest CO	0.703	1.009	0.219	0.423	48.6	-30.0
ROMO	Core Site	0.51	0.621	0.227	0.189	42.4	-21.8
TICR	Timber Creek	0.482	0.694	0.228	0.254	50.0	-34.2

#### 5.7.2.2.4. Ammonia ( $\text{NH}_3$ )

During the spring campaign the highest correlation between predicted and observed concentrations was computed for data at Dinosaur NM ( $R = 0.61$ ). The lowest MFE occurred for Grant (67%) and the highest for Dinosaur NM (165%, see Figure 5.195a). The MFBs were negative for all sites, with the lowest bias occurring at Beaver Meadows (-41%) and the highest at Dinosaur NM (-165%, see Figure 5.195b). The performance statistics for  $\text{NH}_3$  comparisons can be found in Table 5.36.

During the summer campaign the highest correlation between the modeled and observed concentrations corresponded to the Alpine Visitor Center ( $R = 0.50$ ). The lowest and highest MFEs corresponded to Timber Creek (90%) and Brush (163%), respectively (see Figure 5.195a). The lowest and highest MFBs also occurred at Timber Creek (-83%) and Brush (-163%). The MFB estimates were negative for all sites (see Figure 5.195b). A summary of the performance statistics can be found in Table 5.37. The MFEs and MFBs typically were lower during the spring campaign compared to summer. The underprediction of  $\text{NH}_3$  concentrations by the model is evident in Figures 5.190 and 5.191.

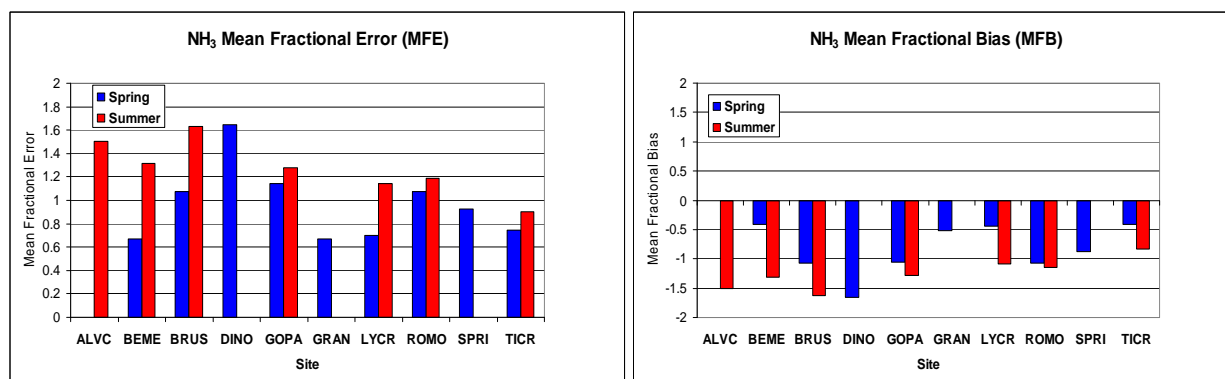


Figure 5.195. Spring and summer campaign  $\text{NH}_3$  (a) mean fractional error and (b) mean fractional bias as a function of site location.

**Table 5.36.** Spring campaign NH<sub>3</sub> model performance statistics. See text for a description of column headings. The column headings refer to the site ID and site name, study mean of the estimated concentrations (ME,  $\mu\text{g m}^{-3}$ ), study mean of the observed concentrations (MO,  $\mu\text{g m}^{-3}$ ), standard deviation of the estimated and observed mean concentration (SDE and SDO, respectively,  $\mu\text{g m}^{-3}$ ), and the mean fractional error (MFE, %) and the mean fractional bias (MFB, %). The rows of the table correspond to the site locations.

Site ID	Site Name	ME ( $\mu\text{g m}^{-3}$ )	MO ( $\mu\text{g m}^{-3}$ )	SDE ( $\mu\text{g m}^{-3}$ )	SDO ( $\mu\text{g m}^{-3}$ )	MFE (%)	MFB (%)
BEME	Beaver Meadows	0.082	0.152	0.045	0.163	67.0	-41.3
BRUS	Brush CO	1.4	5.527	0.971	4.473	107.2	-107.2
DINO	Dinosaur NM UT	0.163	1.867	0.069	0.831	164.8	-164.8
GOPA	Gore Pass	0.042	0.15	0.029	0.063	114.4	-105.2
GRAN	Grant NE	1.861	3.404	1.143	1.982	66.8	-51.4
LYCR	Lyons Crest CO	0.533	1.12	0.284	0.878	69.6	-44.7
ROMO	Core Site	0.059	0.189	0.034	0.063	107.6	-107.6
SPRI	Springfield CO	0.25	0.682	0.175	0.36	92.4	-87.4
TICR	Timber Creek	0.047	0.057	0.038	0.023	74.5	-41.6

**Table 5.37.** Summer campaign NH<sub>3</sub> model performance statistics. See text for a description of column headings. The column headings refer to the site ID and site name, study mean of the estimated concentrations (ME,  $\mu\text{g m}^{-3}$ ), study mean of the observed concentrations (MO,  $\mu\text{g m}^{-3}$ ), standard deviation of the estimated and observed mean concentration (SDE and SDO, respectively,  $\mu\text{g m}^{-3}$ ), and the mean fractional error (MFE, %) and the mean fractional bias (MFB, %). The rows of the table correspond to the site locations.

Site ID	Site Name	ME ( $\mu\text{g m}^{-3}$ )	MO ( $\mu\text{g m}^{-3}$ )	SDE ( $\mu\text{g m}^{-3}$ )	SDO ( $\mu\text{g m}^{-3}$ )	MFE (%)	MFB(%)
ALVC	AlpineVisitorCent.	0.046	0.442	0.036	0.244	150.5	-150.5
BEME	Beaver Meadows	0.084	0.505	0.035	0.305	131.7	-131.7
BRUS	Brush CO	0.737	8.151	0.322	3.685	163.1	-163.1
GOPA	Gore Pass CO	0.073	0.319	0.055	0.093	127.5	-127.5
LYCR	Lyons Crest CO	0.59	2.442	0.235	1.244	114.0	-107.9
ROMO	Core Site	0.088	0.401	0.063	0.28	118.8	-115.0
TICR	Timber Creek	0.097	0.204	0.088	0.068	90.3	-83.0

#### 5.7.2.2.5. Nitric Acid (HNO<sub>3</sub>)

During the spring campaign the highest correlation occurred for comparisons at Brush ( $R = 0.81$ ). The lowest MFE occurred for Beaver Meadows (53%) and the highest at Timber Creek (120%, see Figure 5.196a). The MFBs were positive at all sites and the lowest occurred at Gore Pass (+42%) and the highest at Timber Creek (+120%, see Figure 5.196b). The performance statistics for HNO<sub>3</sub> can be found in Table 5.38.

During the summer campaign the highest correlation between predicted and measured concentrations occurred at the core site ( $R = 0.51$ ). The lowest and highest MFEs corresponded to Gore Pass (36%) and Timber Creek (87%), respectively (see Figure 5.196a). The lowest and highest MFBs occurred at Lyons Crest (+2) and Timber Creek (+87%), respectively. Of the seven sites, three corresponded to negative biases and four sites had positive biases (see Figure 5.196b). See Table 5.39 for a summary of the performance statistics corresponding to the summer campaign. Both the MFEs and the MFBs were higher during spring than compared to

summer. Comparisons of mean modeled and observed concentrations of  $\text{HNO}_3$  are shown in Figures 5.190 and 5.191 for spring and summer, respectively.

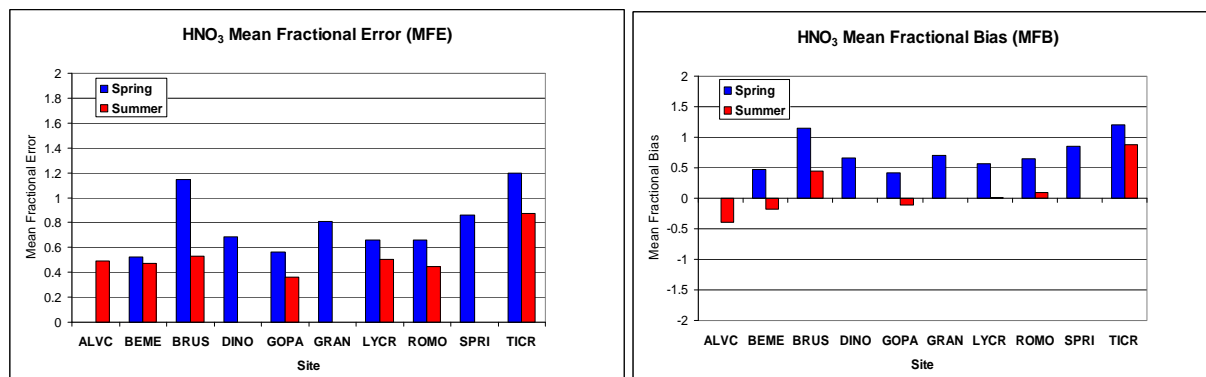


Figure 5.196. Spring and summer campaign  $\text{HNO}_3$  (a) mean fractional error and (b) mean fractional bias as a function of site location.

**Table 5.38.** Spring campaign  $\text{HNO}_3$  model performance statistics. See text for a description of column headings. The column headings refer to the site ID and site name, study mean of the estimated concentrations (ME,  $\mu\text{g m}^{-3}$ ), study mean of the observed concentrations (MO,  $\mu\text{g m}^{-3}$ ), standard deviation of the estimated and observed mean concentration (SDE and SDO, respectively,  $\mu\text{g m}^{-3}$ ), and the mean fractional error (MFE, %) and the mean fractional bias (MFB, %). The rows of the table correspond to the site locations.

Site ID	Site Name	ME ( $\mu\text{g m}^{-3}$ )	MO ( $\mu\text{g m}^{-3}$ )	SDE ( $\mu\text{g m}^{-3}$ )	SDO ( $\mu\text{g m}^{-3}$ )	MFE (%)	MFB (%)
BEME	Beaver Meadows	0.43	0.271	0.196	0.151	52.7	47.1
BRUS	Brush CO	1.261	0.301	0.779	0.156	114.4	114.4
DINO	Dinosaur NM UT	0.685	0.335	0.332	0.157	68.7	65.7
GOPA	Gore Pass	0.357	0.235	0.173	0.123	56.2	42.3
GRAN	Grant NE	0.79	0.356	0.452	0.303	81.1	70.4
LYCR	Lyons Crest CO	1.119	0.582	0.696	0.34	66.3	57.2
ROMO	Core Site	0.457	0.244	0.201	0.139	66.3	64.3
SPRI	Springfield CO	0.582	0.221	0.29	0.109	85.8	84.8
TICR	Timber Creek	0.367	0.089	0.157	0.051	119.8	119.8

**Table 5.39.** Summer campaign  $\text{HNO}_3$  model performance statistics. See text for a description of column headings. The column headings refer to the site ID and site name, study mean of the estimated concentrations (ME,  $\mu\text{g m}^{-3}$ ), study mean of the observed concentrations (MO,  $\mu\text{g m}^{-3}$ ), standard deviation of the estimated and observed mean concentration (SDE and SDO, respectively,  $\mu\text{g m}^{-3}$ ), and the mean fractional error (MFE, %) and the mean fractional bias (MFB, %). The rows of the table correspond to the site locations.

Site ID	Site Name	ME ( $\mu\text{g m}^{-3}$ )	MO ( $\mu\text{g m}^{-3}$ )	SDE ( $\mu\text{g m}^{-3}$ )	SDO ( $\mu\text{g m}^{-3}$ )	MFE (%)	MFB (%)
ALVC	Alpine Visitor Cent.	0.395	0.554	0.191	0.123	49.1	-39.2
BEME	Beaver Meadows	0.519	0.612	0.274	0.281	47.1	-17.1
BRUS	Brush CO	1.242	0.788	0.41	0.33	53.3	44.6
GOPA	Gore Pass CO	0.461	0.474	0.297	0.195	36.3	-10.6
LYCR	Lyons Crest CO	1.455	1.613	0.651	1.079	50.6	1.7
ROMO	Core Site	0.671	0.565	0.44	0.273	44.5	10.1
TICR	Timber Creek	0.577	0.182	0.383	0.068	87.4	87.4

### 5.7.2.2.6. Sulfur Dioxide (SO<sub>2</sub>)

During the spring campaign the highest correlation occurred at the core site (R = 0.80). The lowest MFE occurred at Springfield (54%) and the highest MFE occurred at Brush (161%, see Figure 5.197a). The MFBs were positive for all sites during the spring, with the lowest at Springfield (+31%) and the highest at Brush (+161%, see Figure 5.197b). The summary of performance statistics for SO<sub>2</sub> during the spring campaign is provided in Table 5.40.

During the summer campaign the highest correlation corresponded to comparisons at Timber Creek (R = 0.61). The lowest and highest MFEs corresponded to the Alpine Visitor Center (42%) and Brush (175%), respectively (see Figure 5.197a). The lowest and highest MFBs also occurred at the Alpine Visitor Center (-33%) and Brush (+175%), respectively (Figure 197b). The biases at all the sites were positive with the exception of the Alpine Visitor Center. A summary of SO<sub>2</sub> performance statistics during the summer campaign are reported in Table 5.41. The biases and errors generally were lower during the spring than the summer. Comparisons of mean concentrations are shown in Figure 5.190 and 5.191 for spring and summer, respectively.

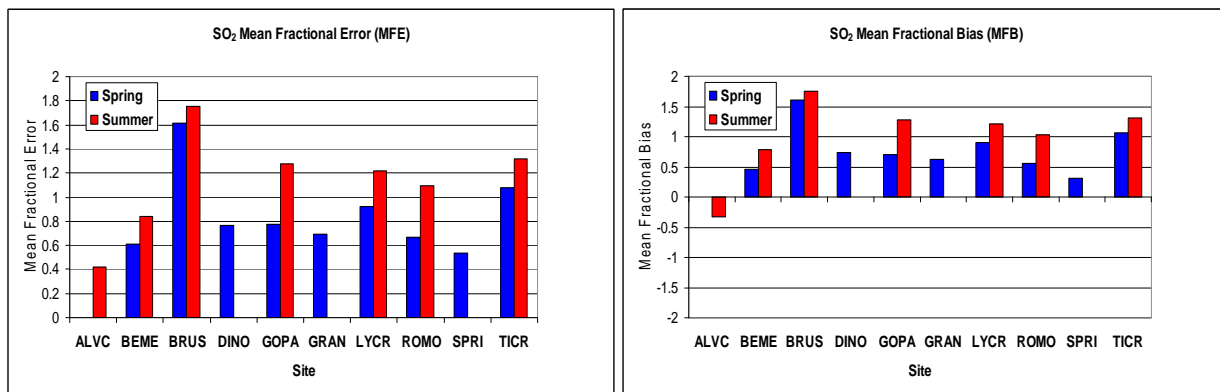


Figure 5.197. Spring and summer campaign SO<sub>2</sub> (a) mean fractional error and (b) mean fractional bias as a function of site location.

**Table 5.40.** Spring campaign SO<sub>2</sub> model performance statistics. See text for a description of column headings. The column headings refer to the site ID and site name, study mean of the estimated concentrations (ME, μg m<sup>-3</sup>), study mean of the observed concentrations (MO, μg m<sup>-3</sup>), standard deviation of the estimated and observed mean concentration (SDE and SDO, respectively, μg m<sup>-3</sup>), and the mean fractional error (MFE, %) and the mean fractional bias (MFB, %). The rows of the table correspond to the site locations.

Site ID	Site Name	ME (μg m <sup>-3</sup> )	MO (μg m <sup>-3</sup> )	SDE (μg m <sup>-3</sup> )	SDO (μg m <sup>-3</sup> )	MFE (%)	MFB (%)
BEME	Beaver Meadows	0.304	0.196	0.2	0.152	61.1	46.7
BRUS	Brush CO	7.165	0.751	4.225	0.744	161.1	161.1
DINO	Dinosaur NM UT	0.362	0.172	0.196	0.116	76.5	73.4
GOPA	Gore Pass	0.36	0.135	0.316	0.089	77.5	70.2
GRAN	Grant NE	0.649	0.331	0.532	0.23	69.2	63.0
LYCR	Lyons Crest CO	1.415	0.535	1.073	0.425	92.2	90.4
ROMO	Core Site	0.295	0.184	0.217	0.18	66.7	56.5
SPRI	Springfield CO	0.319	0.23	0.192	0.17	53.7	31.0
TICR	Timber Creek	0.216	0.061	0.11	0.039	107.5	105.9

**Table 5.41.** Summer campaign SO<sub>2</sub> model performance statistics. See text for a description of column headings. The column headings refer to the site ID and site name, study mean of the estimated concentrations (ME,  $\mu\text{g m}^{-3}$ ), study mean of the observed concentrations (MO,  $\mu\text{g m}^{-3}$ ), standard deviation of the estimated and observed mean concentration (SDE and SDO, respectively,  $\mu\text{g m}^{-3}$ ), and the mean fractional error (MFE, %) and the mean fractional bias (MFB, %). The rows of the table correspond to the site locations.

Site ID	Site Name	ME ( $\mu\text{g m}^{-3}$ )	MO ( $\mu\text{g m}^{-3}$ )	SDE ( $\mu\text{g m}^{-3}$ )	SDO ( $\mu\text{g m}^{-3}$ )	MFE (%)	MFB(%)
ALVC	Alpine Visitor Cent.	0.296	0.421	0.114	0.153	42.1	-33.4
BEME	Beaver Meadows	0.421	0.178	0.278	0.132	84.0	78.3
BRUS	Brush CO	9.045	0.598	3.422	0.616	174.9	174.9
GOPA	Gore Pass CO	0.513	0.111	0.383	0.095	127.6	127.6
LYCR	Lyons Crest CO	1.347	0.347	0.63	0.286	122.0	120.7
ROMO	Core Site	0.513	0.154	0.416	0.127	109.5	102.5
TICR	Timber Creek	0.44	0.075	0.323	0.049	131.5	131.5

#### 5.7.2.2.7. Total Reduced Nitrogen (N(-III) = NH<sub>3</sub> + NH<sub>4</sub><sup>+</sup>)

Total reduced nitrogen concentrations were evaluated to investigate whether the model performs reasonably well without regard to phase partitioning, as well as to investigate differences between reduced and oxidized nitrogen. During the spring campaign the highest correlation was computed for Dinosaur NM ( $R = 0.70$ ). The lowest MFE occurred at Lyons Crest (60%) and the highest at Dinosaur NM (154%, see Figure 5.198a). The MFBs were negative for all the sites, with the lowest at Lyons Crest (-40%) and the highest at Dinosaur NM (-154%, see Figure 5.198b). The summary of performance evaluations for N(-III) are reported in Table 5.42.

During the summer campaign the highest correlation between predicted and observed concentrations occurred at Gore Pass ( $R = 0.39$ ). The lowest and highest MFEs occurred at Timber Creek (59%) and Brush (153%), respectively (see Figure 5.198a). The lowest and highest MFBs also occurred at Timber Creek (-54%) and Brush (-153%, see Figure 5.198b). The biases at all of the sites were negative. For most of the sites the MFEs in N(-III) were lower during the spring than the summer (with the exception of two sites: the core site and Timber Creek). The pattern is similar for the MFB, and the comparisons for all of the sites for spring and summer had negative biases. A summary of performance statistics for the summer campaign is listed in Table 5.43.

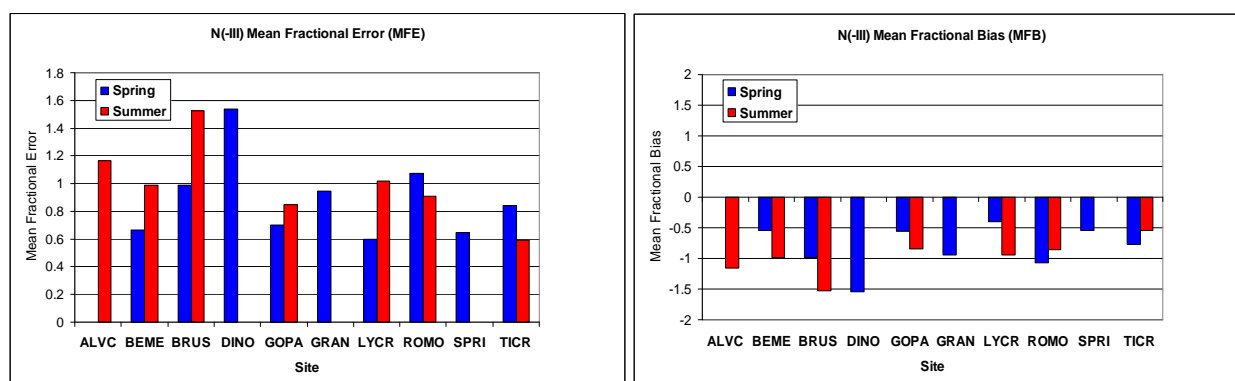


Figure 5.198. Spring and summer campaign N(-III) (a) mean fractional error and (b) mean fractional bias as a function of site location.

**Table 5.42.** Spring campaign N(-III) model performance statistics. See text for a description of column headings. The column headings refer to the site ID and site name, study mean of the estimated concentrations (ME,  $\mu\text{g m}^{-3}$ ), study mean of the observed concentrations (MO,  $\mu\text{g m}^{-3}$ ), standard deviation of the estimated and observed mean concentration (SDE and SDO, respectively,  $\mu\text{g m}^{-3}$ ), and the mean fractional error (MFE, %) and the mean fractional bias (MFB, %). The rows of the table correspond to the site locations.

Site ID	Site Name	ME ( $\mu\text{g m}^{-3}$ )	MO ( $\mu\text{g m}^{-3}$ )	SDE ( $\mu\text{g m}^{-3}$ )	SDO ( $\mu\text{g m}^{-3}$ )	MFE (%)	MFB(%)
BEME	Beaver Meadows	0.186	0.407	0.106	0.381	66.3	-54.9
BRUS	Brush CO	1.798	6.105	1.193	4.582	99.1	-98.8
DINO	Dinosaur NM UT	0.278	2.178	0.146	0.828	154.0	-154.0
GOPA	Gore Pass	0.118	0.222	0.042	0.086	70.3	-55.1
GRAN	Grant NE	0.392	1.143	0.239	0.639	94.6	-94.2
LYCR	Lyons Crest CO	0.887	1.576	0.561	1.2	59.7	-39.5
ROMO	Core Site	0.149	0.491	0.075	0.194	107.6	-107.6
SPRI	Springfield CO	2.259	4.205	1.21	2.127	64.8	-53.8
TICR	Timber Creek	0.136	0.367	0.055	0.246	84.0	-77.8

**Table 5.43.** Summer campaign N(-III) model performance statistics. See text for a description of column headings. The column headings refer to the site ID and site name, study mean of the estimated concentrations (ME,  $\mu\text{g m}^{-3}$ ), study mean of the observed concentrations (MO,  $\mu\text{g m}^{-3}$ ), standard deviation of the estimated and observed mean concentration (SDE and SDO, respectively,  $\mu\text{g m}^{-3}$ ), and the mean fractional error (MFE, %) and the mean fractional bias (MFB, %). The rows of the table correspond to the site locations.

Site ID	Site Name	ME ( $\mu\text{g m}^{-3}$ )	MO ( $\mu\text{g m}^{-3}$ )	SDE ( $\mu\text{g m}^{-3}$ )	SDO ( $\mu\text{g m}^{-3}$ )	MFE (%)	MFB(%)
ALVC	AlpineVisitorCent.	0.184	0.763	0.067	0.284	116.4	-116.4
BEME	Beaver Meadows	0.255	0.829	0.081	0.377	98.7	-98.7
BRUS	Brush CO	1.038	8.719	0.32	3.82	152.7	-152.7
GOPA	Gore Pass CO	0.224	0.558	0.082	0.149	84.8	-84.8
LYCR	Lyons Crest CO	0.846	2.833	0.281	1.412	101.9	-94.9
ROMO	Core Site	0.253	0.711	0.104	0.373	91.0	-85.4
TICR	Timber Creek	0.246	0.416	0.113	0.12	59.1	-54.1

#### 5.7.2.2.8. Total Oxidized Nitrogen (N(V) = $\text{NO}_3^- + \text{HNO}_3$ )

Comparisons of total oxidized nitrogen were performed on modeled and observed concentrations. During the spring campaign the highest correlation occurred at the core site ( $R = 0.74$ ). The lowest MFE occurred at Gore Pass (37%) while the highest occurred at Timber Creek (68%, see Figure 5.199a). The MFBs were positive at all but two sites (Beaver Meadows and Gore Pass), with the lowest occurring at Beaver Meadows (-6%) and the highest occurring at Timber Creek (+68%, see Figure 5.199b). Model performance statistics for total oxidized nitrogen are reported in Table 5.44.

During the summer campaign the highest correlation between predicted and measured concentrations occurred at the core site ( $R = 0.49$ ). The lowest and highest MFEs occurred at Brush (37%) and the Alpine Visitor Center (71%), respectively (see Figure 5.199a). The lowest (+10%) and highest (-64%) MFBs also occurred at those sites, respectively (Figure 5.199b). All but two of the sites had negative biases (with the exception of Brush and Timber Creek). A

summary of the model performance statistics for the summer campaign can be found in Table 5.45. MFEs in spring and summer were similar for most sites but MFBs generally were positive during spring and negative during summer.

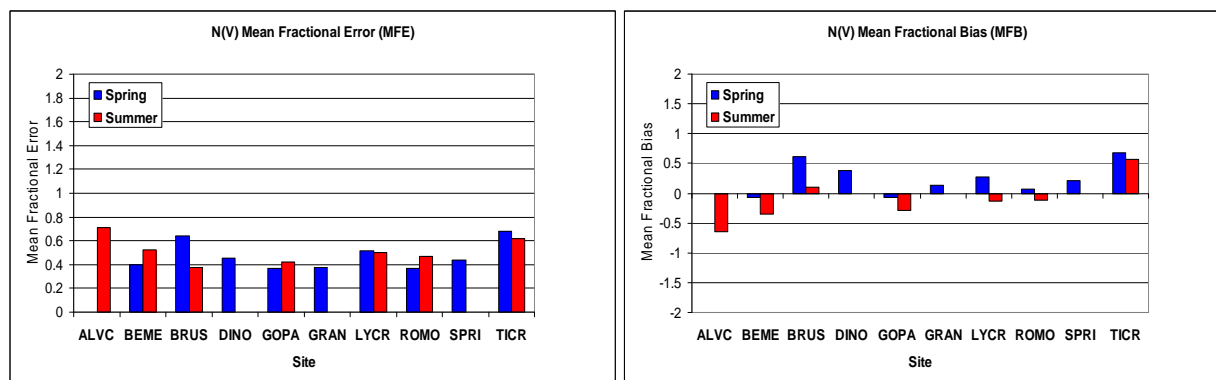


Figure 5.199. Spring and summer campaign N(V) (a) mean fractional error and (b) mean fractional bias as a function of site location.

**Table 5.44.** Spring campaign N(V) model performance statistics. See text for a description of column headings. The column headings refer to the site ID and site name, study mean of the estimated concentrations (ME,  $\mu\text{g m}^{-3}$ ), study mean of the observed concentrations (MO,  $\mu\text{g m}^{-3}$ ), standard deviation of the estimated and observed mean concentration (SDE and SDO, respectively,  $\mu\text{g m}^{-3}$ ), and the mean fractional error (MFE, %) and the mean fractional bias (MFB, %). The rows of the table correspond to the site locations.

Site ID	Site Name	ME ( $\mu\text{g m}^{-3}$ )	MO ( $\mu\text{g m}^{-3}$ )	SDE ( $\mu\text{g m}^{-3}$ )	SDO ( $\mu\text{g m}^{-3}$ )	MFE (%)	MFB (%)
BEME	Beaver Meadows	0.54	0.646	0.283	0.366	39.7	-06.4
BRUS	Brush CO	1.911	0.825	1.593	0.42	63.8	60.9
DINO	Dinosaur NM UT	0.858	0.556	0.441	0.24	45.1	37.5
GOPA	Gore Pass	0.405	0.438	0.18	0.183	36.6	-7.0
GRAN	Grant NE	1.413	1.204	1.245	0.843	37.7	13.7
LYCR	Lyons Crest CO	1.867	1.221	1.619	0.744	51.6	28.0
ROMO	Core Site	0.533	0.563	0.265	0.261	36.9	7.6
SPRI	Springfield CO	0.652	0.653	0.367	0.98	43.6	21.3
TICR	Timber Creek	0.432	0.204	0.165	0.078	68.3	67.8

**Table 5.45.** Summer campaign N(V) model performance statistics. See text for a description of column headings. The column headings refer to the site ID and site name, study mean of the estimated concentrations (ME,  $\mu\text{g m}^{-3}$ ), study mean of the observed concentrations (MO,  $\mu\text{g m}^{-3}$ ), standard deviation of the estimated and observed mean concentration (SDE and SDO, respectively,  $\mu\text{g m}^{-3}$ ), and the mean fractional error (MFE, %) and the mean fractional bias (MFB, %). The rows of the table correspond to the site locations.

Site ID	Site Name	ME ( $\mu\text{g m}^{-3}$ )	MO ( $\mu\text{g m}^{-3}$ )	SDE ( $\mu\text{g m}^{-3}$ )	SDO ( $\mu\text{g m}^{-3}$ )	MFE (%)	MFB (%)
ALVC	Alpine Visitor Cent.	0.4	0.751	0.192	0.193	71.1	-64.4
BEME	Beaver Meadows	0.531	0.74	0.282	0.308	52.6	-34.9
BRUS	Brush CO	1.273	1.157	0.432	0.419	37.2	9.6
GOPA	Gore Pass CO	0.462	0.568	0.298	0.208	42.3	-29.3
LYCR	Lyons Crest CO	1.483	1.887	0.664	1.155	49.8	-13.0
ROMO	Core Site	0.683	0.713	0.445	0.33	47.0	-11.0
TICR	Timber Creek	0.581	0.267	0.384	0.101	61.7	56.8

#### 5.7.2.2.9. Total Sulfur ( $S = \text{SO}_2 + \text{SO}_4^{-2}$ )

Comparisons of total sulfur were performed on modeled and observed concentrations. During the spring campaign the highest correlation occurred at Lyons Crest ( $R = 0.59$ ). The lowest MFE occurred at Grant (41%) and the highest occurred at Brush (130%, see Figure 5.200a). All but three sites had positive MFBs, with the lowest at the core site (-3%) and the highest at Brush (+130%, see Table 5.46 and Figure 5.200b).

During the summer campaign the highest correlation occurred at both Timber Creek and Lyons Crest ( $R = 0.44$ ). The lowest MFE corresponded to Beaver Meadows (35%) and the highest corresponded to Brush (147%, see Figure 5.200a). Beaver Meadows and Brush also corresponded to the lowest (+14%) and highest (+147%) MFBs, respectively (see Figure 5.200b). The biases were positive at all the sites except the Alpine Visitor Center.

The MFEs during summer were generally somewhat lower compared to the spring campaign with the exception of Brush (see Figure 5.200a and Table 5.47). MFBs of total S species during summer varied, with values during summer generally being larger, however not consistently at every site (see Figure 5.200b). For example, at Beaver Meadows and the core site the MFB was positive in summer and negative in spring.

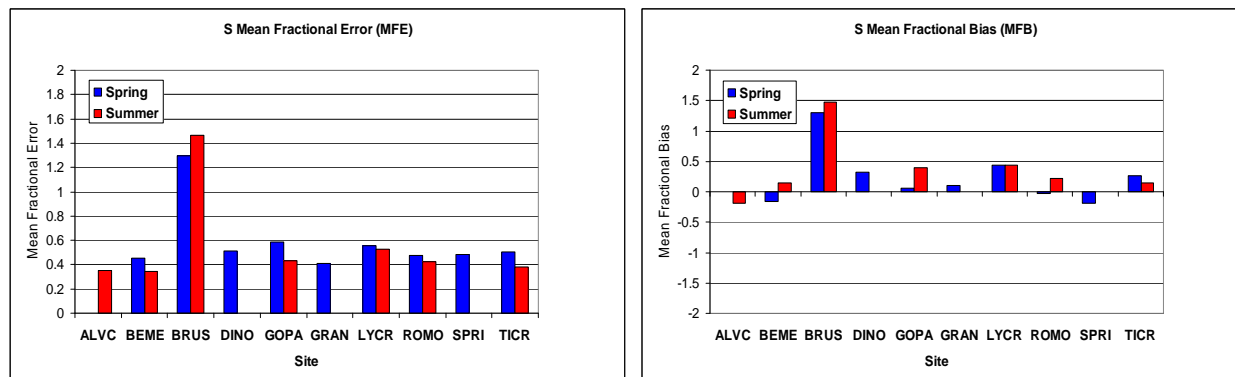


Figure 5.200. Spring and summer campaign S ( $= \text{SO}_2 + \text{SO}_4^{-2}$ ) (a) mean fractional error and (b) mean fractional bias as a function of site location.

**Table 5.46.** Spring campaign S model performance statistics. See text for a description of column headings. The column headings refer to the site ID and site name, study mean of the estimated concentrations (ME,  $\mu\text{g m}^{-3}$ ), study mean of the observed concentrations (MO,  $\mu\text{g m}^{-3}$ ), standard deviation of the estimated and observed mean concentration (SDE and SDO, respectively,  $\mu\text{g m}^{-3}$ ), and the mean fractional error (MFE, %) and the mean fractional bias (MFB, %). The rows of the table correspond to the site locations.

Site ID	Site Name	ME ( $\mu\text{g m}^{-3}$ )	MO ( $\mu\text{g m}^{-3}$ )	SDE ( $\mu\text{g m}^{-3}$ )	SDO ( $\mu\text{g m}^{-3}$ )	MFE (%)	MFB (%)
BEME	Beaver Meadows	0.643	0.774	0.297	0.389	45.7	-15.5
BRUS	Brush CO	7.924	1.446	4.379	0.786	129.6	129.6
DINO	Dinosaur NM UT	0.748	0.598	0.289	0.411	51.3	32.2
GOPA	Gore Pass	0.731	0.647	0.419	0.786	58.8	5.5
GRAN	Grant NE	1.528	1.321	1.006	0.579	41.3	9.9
LYCR	Lyons Crest CO	1.966	1.168	1.284	0.61	55.6	43.9
ROMO	Core Site	0.642	0.668	0.3	0.322	47.9	-2.7
SPRI	Springfield CO	0.805	0.999	0.443	0.55	48.1	-19.5
TICR	Timber Creek	0.581	0.436	0.255	0.196	50.2	26.4

**Table 5.47.** Summer campaign S model performance statistics. See text for description of column headings. The column headings refer to the site ID and site name, study mean of the estimated concentrations (ME,  $\mu\text{g m}^{-3}$ ), study mean of the observed concentrations (MO,  $\mu\text{g m}^{-3}$ ), standard deviation of the estimated and observed mean concentration (SDE and SDO, respectively,  $\mu\text{g m}^{-3}$ ), and the mean fractional error (MFE, %) and the mean fractional bias (MFB, %). The rows of the table correspond to the site locations.

Site ID	Site Name	ME ( $\mu\text{g m}^{-3}$ )	MO ( $\mu\text{g m}^{-3}$ )	SDE ( $\mu\text{g m}^{-3}$ )	SDO ( $\mu\text{g m}^{-3}$ )	MFE (%)	MFB (%)
ALVC	Alpine Visitor Cent.	0.794	0.933	0.317	0.214	35.3	-19.7
BEME	Beaver Meadows	0.935	0.795	0.391	0.281	34.7	14.0
BRUS	Brush CO	9.908	1.423	3.589	0.744	146.8	146.8
GOPA	Gore Pass CO	1	0.629	0.475	0.204	43.3	38.7
LYCR	Lyons Crest CO	2.056	1.354	0.716	0.658	53.0	44.5
ROMO	Core Site	1.023	0.775	0.534	0.265	42.5	21.4
TICR	Timber Creek	0.924	0.765	0.443	0.278	38.4	14.5

### 5.7.2.3. Model Performance Evaluation for High Time Resolution Observations at the Core Site

High time resolution data measured only at the core site are used to evaluate the 4-km domain model results in this section. The data include hourly concentrations of  $\text{NH}_3$ ,  $\text{NH}_4^+$ ,  $\text{NO}_3^-$ ,  $\text{SO}_4^{2-}$ , and  $\text{SO}_2$ ,  $\text{NO}_x$ , and ozone ( $\text{O}_3$ ). A discussion of the measurements was presented in section 3.5. We use the same statistical measures in this section as were discussed previously, i.e., mean fractional error and mean fractional bias. In Appendix 3 we present a more detailed comparison of the predicted and observed hourly concentrations by investigating scatter plots and time series of concentrations.

Figure 5.201 compares these statistical parameters for total oxidized nitrogen, and  $\text{NO}_3^-$  (top panel), total reduced nitrogen,  $\text{NH}_3$  and  $\text{NH}_4^+$  (second panel), sulfur species,  $\text{SO}_2$  and  $\text{SO}_4^{2-}$  (third panel), and  $\text{NO}_x$  and  $\text{O}_3$  (bottom panel). Performance evaluation statistics are reported in Table 5.48 for all the species and the two study periods (with the exception of  $\text{NO}_x$  and  $\text{O}_3$ ).

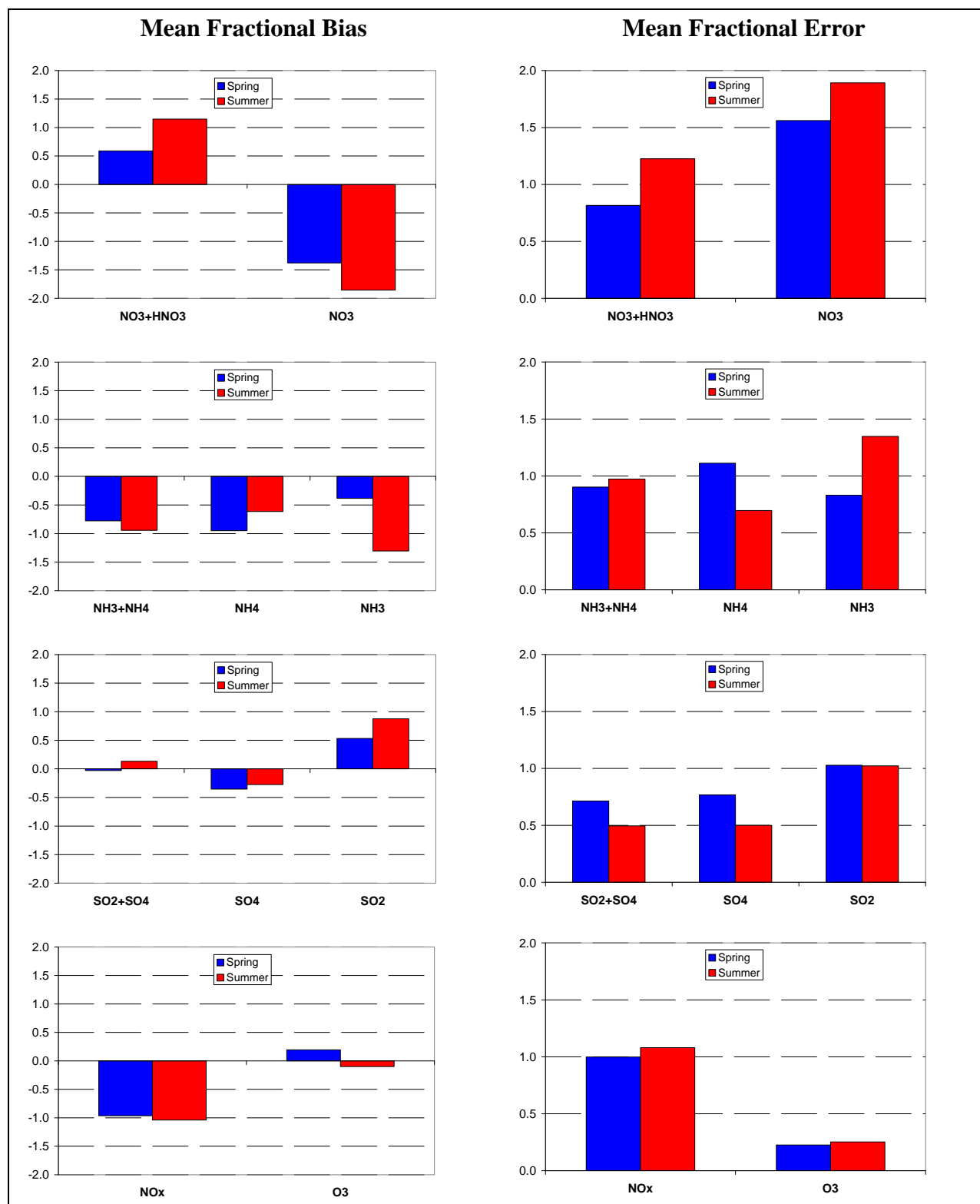


Figure 5.201. Mean fractional bias (left column) and mean fractional error (right column) for the spring (blue) and summer (red) campaigns at the core site. Total oxidized nitrogen and  $\text{NO}_3^-$  (top panel), total reduced nitrogen,  $\text{NH}_3$  and  $\text{NH}_4^+$  (second panel), sulfur species,  $\text{SO}_2$  and  $\text{SO}_4^{2-}$  (third panel), and  $\text{NO}_x$  and  $\text{O}_3$  (bottom panel).

**Table 5.48.** Model performance statistics during both spring and summer RoMANS campaigns, using hourly ambient data from the core site.

	Spring							
	N(V) ( $\mu\text{g}/\text{m}^3$ )	$\text{NO}_3^-$ ( $\mu\text{g}/\text{m}^3$ )	N(-III) ( $\mu\text{g}/\text{m}^3$ )	$\text{NH}_3$ ( $\mu\text{g}/\text{m}^3$ )	$\text{NH}_4^+$ ( $\mu\text{g}/\text{m}^3$ )	Total S ( $\mu\text{g}/\text{m}^3$ )	$\text{SO}_4^{-2}$ ( $\mu\text{g}/\text{m}^3$ )	$\text{SO}_2$ ( $\mu\text{g}/\text{m}^3$ )
Mean obs.	0.48	0.48	0.51	0.10	0.38	0.63	0.53	0.14
Mean model	0.67	0.11	0.19	0.07	0.10	0.61	0.35	0.28
STD <sup>a</sup> obs.	0.67	0.67	0.41	0.10	0.31	0.43	0.37	0.20
STD model	0.59	0.25	0.13	0.07	0.10	0.54	0.25	0.48
MFE <sup>b</sup> (%)	81.7%	156.1%	90.3%	83.0%	111.2%	71.3%	76.7%	102.8%
MFB <sup>c</sup> (%)	58.8%	-138.0%	-77.8%	-38.3%	-95.0%	-3.0%	-35.4%	53.3%
	Summer							
	N(V) ( $\mu\text{g}/\text{m}^3$ )	$\text{NO}_3^-$ ( $\mu\text{g}/\text{m}^3$ )	N(-III) ( $\mu\text{g}/\text{m}^3$ )	$\text{NH}_3$ ( $\mu\text{g}/\text{m}^3$ )	$\text{NH}_4^+$ ( $\mu\text{g}/\text{m}^3$ )	Total S ( $\mu\text{g}/\text{m}^3$ )	$\text{SO}_4^{-2}$ ( $\mu\text{g}/\text{m}^3$ )	$\text{SO}_2$ ( $\mu\text{g}/\text{m}^3$ )
Mean obs.	0.18	0.18	0.78	0.43	0.34	0.83	0.66	0.16
Mean model	0.75	0.01	0.27	0.09	0.17	1.11	0.53	0.53
STD <sup>a</sup> obs.	0.29	0.29	0.45	0.32	0.21	0.33	0.23	0.17
STD model	0.69	0.07	0.17	0.13	0.09	0.96	0.32	0.75
MFE <sup>b</sup> (%)	122.5%	189.2%	97.3%	134.7%	69.6%	49.6%	50.0%	102.3%
MFB <sup>c</sup> (%)	114.9%	-185.6%	-94.4%	-130.5%	-61.4%	13.3%	-27.5%	87.7%

<sup>a</sup>Standard Deviation<sup>b</sup>Mean Fractional Error (%)<sup>c</sup>Mean Fractional Bias (%)

The MFEs for total oxidized nitrogen were lower than when comparing particulate nitrate only, during both the spring and summer campaigns. The model performed better during spring than during the summer campaign for both N(V) and particulate  $\text{NO}_3^-$ . The MFBs for N(V) were positive and smaller in magnitude compared to negative MFBs for particulate  $\text{NO}_3^-$  during both spring and summer. MFBs for both N(V) and particulate  $\text{NO}_3^-$  were lower during the spring campaign compared to summer.

Model performance during the spring for reduced nitrogen species had MFEs for N(-III),  $\text{NH}_3$ , and  $\text{NH}_4^+$  ranging from 83% to 111%, with  $\text{NH}_4^+$  estimates highest and  $\text{NH}_3$  estimates lowest. During summer the MFE was lowest for  $\text{NH}_4^+$  (70%) and highest for  $\text{NH}_3$  (135%). The MFE for the spring campaign was higher than during summer for  $\text{NH}_4^+$  only. MFB estimates were negative for all species and for both study campaigns. During spring  $\text{NH}_3$  had the lowest MFB (-38%) and  $\text{NH}_4^+$  had the highest MFB (-95%), compared to summer when  $\text{NH}_4^+$  was lowest (-61%) and  $\text{NH}_3$  was highest (-131%).

During the spring campaign the MFE was lowest for total sulfur (71%) compared to individual comparisons of  $\text{SO}_4^{-2}$  (77%) and  $\text{SO}_2$  (103%). During the summer the MFEs for total S and  $\text{SO}_4^{-2}$  were comparable (~50%) while the MFE for  $\text{SO}_2$  was highest (102%). During spring the MFBs were negative for  $\text{SO}_4^{-2}$  (-35%) and total S (-3%) and positive for  $\text{SO}_2$  (+53%). During summer the MFBs were lowest for total S (+13%) and highest for  $\text{SO}_2$  (88%). The MFB for  $\text{SO}_4^{-2}$  was negative in the summer (-28%).

The MFEs for  $\text{NO}_x$  were lower than for  $\text{O}_3$  during both the spring and summer campaigns, and the model performed similarly for these species during both spring and summer. The MFBs for

NO<sub>x</sub> were negative and values for spring and summer were similar. MFBs for O<sub>3</sub> were lower than those for NO<sub>x</sub> and positive in the spring and negative in the summer.

The evaluation suggests that the model performed the most realistically for sulfur species and for ozone. It also appeared to perform better in the springtime for most species.

#### 5.7.2.4. Bugle Plots

Model performance evaluation of particulate matter (PM) and most gas-phase species (other than ozone) has only been minimally guided by the EPA to date. To address some of the issues inherent in evaluations and comparisons of modeled concentrations with observations, Boylan and Russell (2006) proposed model performance goals and criteria by which to examine various error and bias metrics. They define performance goals as the level of accuracy that is considered closest to the best a model can be expected to achieve, and performance criteria as the level of accuracy considered acceptable for model performance. These goals and criteria vary as a function of concentration for particulate and gas-phase species, and their recommendations are based on the analysis of many modeling studies performed around the United States.

As discussed earlier, fractional error and bias are the least biased and most robust of the possible performance metrics typically applied to model results. Boylan and Russell (2006) incorporated these metrics into their definitions of goals and criteria for model performance. Species with lower concentrations (< 2.25 µg/m<sup>3</sup>) have less strict performance goals and criteria, due to the fact that they typically contribute less to total particulate mass and because their normalized performance is often poor. Therefore, according to Boylan and Russell (2006) the performance goals of low-concentration species MFE (MFB) can extend to +200% (±200%) at zero concentrations, to +50% (±30%) at higher concentrations. Similarly, performance criteria can range from 200% (MFE) or ±200% (MFB) to +75% (MFE) or ±60% (MFB). Smoothly interpolated curves for performance goals take the forms of Equations 5.27a and 5.27b for MFE and MFB, respectively. Performance criteria curves take the form of Equations 5.28a and 5.28b for MFE and MFB, respectively:

$$\text{Equation 5.27a. } MFB \leq \pm 170e^{\frac{-0.5(C_o + C_m)}{0.5 \mu\text{g} / \text{m}^3}} + 30$$

$$\text{Equation 5.27b. } MFE \leq \pm 150e^{\frac{-0.5(C_o + C_m)}{0.75 \mu\text{g} / \text{m}^3}} + 50$$

$$\text{Equation 5.28a. } MFB \leq \pm 140e^{\frac{-0.5(C_o + C_m)}{0.5 \mu\text{g} / \text{m}^3}} + 60$$

$$\text{Equation 5.28b. } MFE \leq \pm 125e^{\frac{-0.5(C_o + C_m)}{0.75 \mu\text{g} / \text{m}^3}} + 75$$

where  $C_o$  is the average observation concentration and  $C_m$  is the model-predicted concentration.

The shape of these curves is similar to a bugle, hence the name “bugle plots.” The performance goal and criteria curves are somewhat arbitrarily defined and may represent an unreasonable goal for PM performance. These performance goals and criteria may not be adopted for regulation or

may not be the most appropriate to use for particulate matter modeling. However, these metrics have been applied during other modeling exercises performed by Regional Planning Organizations (RPOs) to evaluate intercomparisons of model performance for different episodes, species, and models (e.g., Tonnesen et al., 2006).

The goal and criteria curves computed with Equations 5.27–5.28 are plotted along with the model evaluation metrics from the previous section. MFE estimates that fall below both curves suggest good model performance, while results that fall between the curves correspond to average model performance. The area above and outside of the criteria curve is considered poor model performance. Similarly, for model results to be considered good the MFBs must fall between the positive and negative goal curves, while for average performance the MFBs fall within the criteria curves, and poor performance results fall outside of the positive and negative criteria curves. The very low concentrations (typically  $< 1 \mu\text{g}/\text{m}^3$ ) for most of the species presented in this section call into question the applicability of this type of evaluation. We present it here as a guidance tool for model performance and so that the model performance evaluation can be easily compared with other model studies performed to date (e.g., by RPOs).

Bugle plots for particulate sulfate are presented in Figure 5.202. Comparisons of modeled concentrations and (one-in-three-day) observations at IMPROVE locations for western states discussed in the previous sections are separated here by state. Also plotted are the results from the RoMANS satellite sites (24-hr concentrations) and the hourly core site data. Figures 5.202a and 5.202b are MFE bugle plots during spring and summer, respectively, and Figures 5.202c and 5.202d are the MFB bugle plots for spring and summer, respectively. For both spring and summer, the model performance for sulfate is quite good, with the MFBs and MFEs of almost all of the IMPROVE sites in the western states falling within the model performance goals. Only one site in California during the summer falls outside the performance criteria values. The IMPROVE sites within Colorado for both summer and spring fall within the performance goals but also show that sulfate was systematically underpredicted by the model for both seasons. The model performance for RoMANS 24-hr satellite and core site hourly concentrations was similar to that for the lower time resolution IMPROVE results.

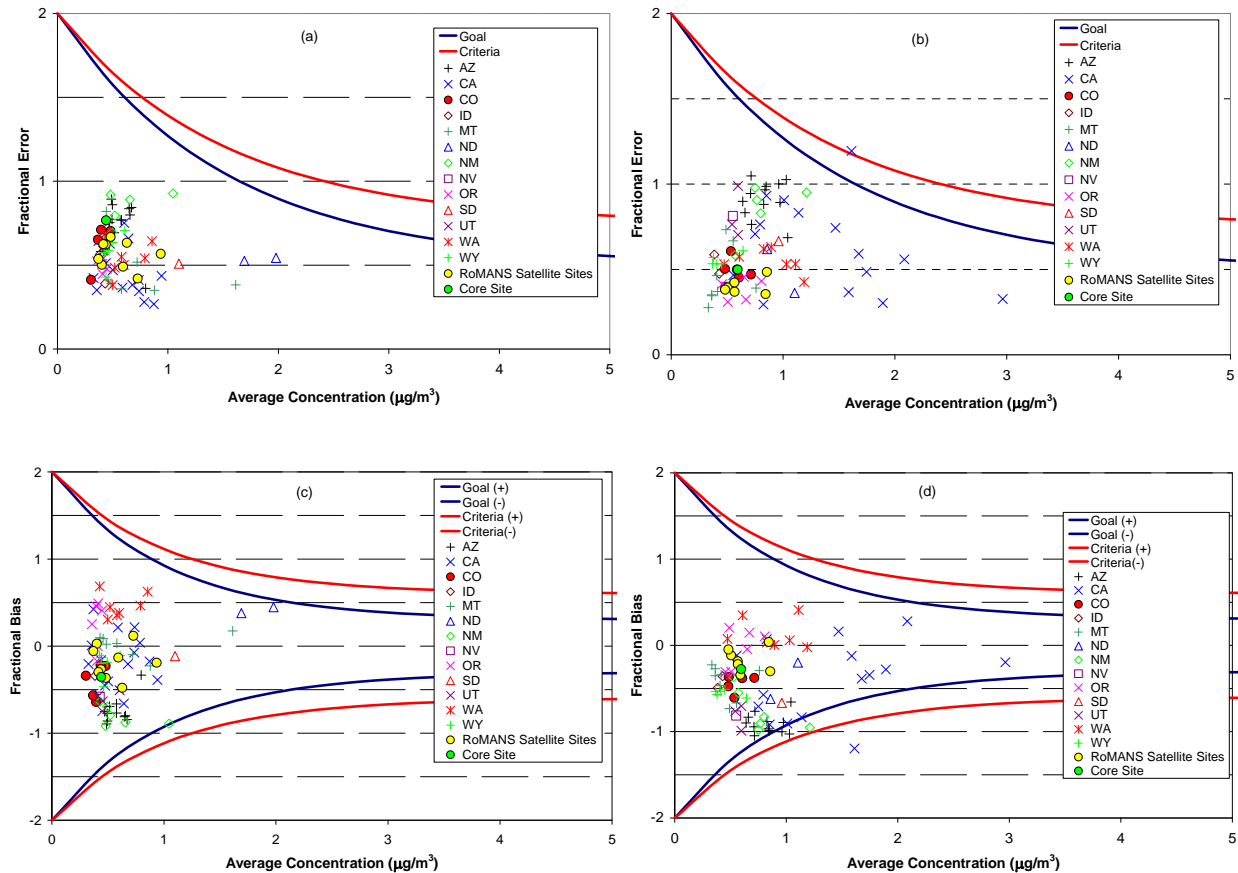


Figure 5.202. Bugle plots of sulfate (a) spring mean fractional error, (b) summer mean fractional error, (c) spring mean fractional bias, and (d) summer mean fractional bias. MFE or MFB is plotted on the y-axis and the average of the observed and modeled concentration is plotted on the x-axis ( $\mu\text{g}/\text{m}^3$ ).

The model evaluation for nitrate in spring, although not as good as sulfate, suggests that with the exception of some sites in California the MFE performance goals were met (Figure 5.203a); however, the performance in summer is worse, with several of the sites having MFEs falling outside the criteria (5.203b). Nitrate concentrations at most of the sites were underpredicted, especially during summer (see Figures 5.203c and 5.203d for spring and summer, respectively). The performance for the higher time resolution sites during RoMANS was similar to the IMPROVE sites in Colorado during spring and summer and meet performance goals. Notice the very low concentrations of nitrate, especially in summer.

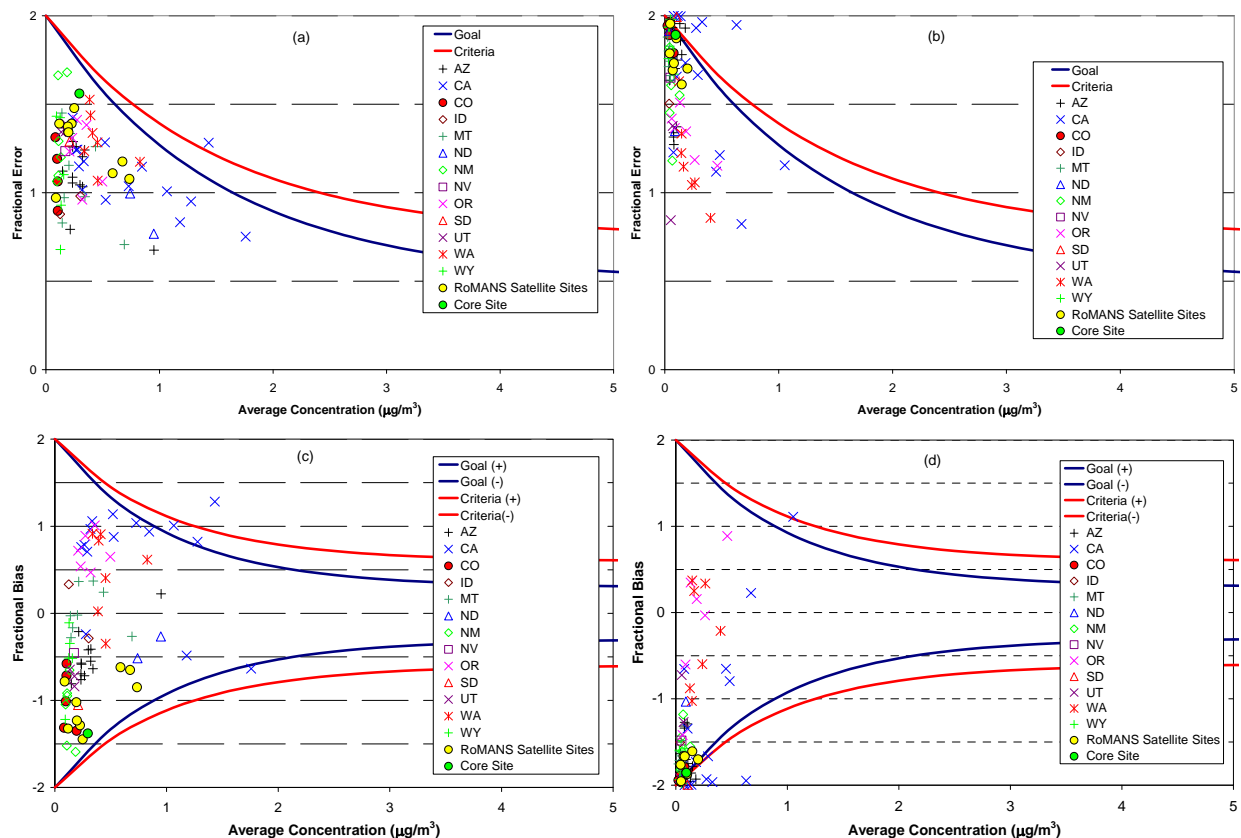


Figure 5.203. Bugle plots of nitrate (a) spring mean fractional error, (b) summer mean fractional error, (c) spring mean fractional bias, and (d) summer mean fractional bias. MFE or MFB is plotted on the y-axis and the average of the observed and modeled concentration is plotted on the x-axis ( $\mu\text{g}/\text{m}^3$ ).

Bugle plots of gas-phase species include only the results from the 24-hr satellite and hourly core site data, when available. Model evaluation of ammonium concentrations (Figures 5.204a and 5.204b) suggests that the model met the performance goals for both MFE (Figure 5.204a) and MFB (Figure 5.204b) during both spring and summer. Although the ammonium concentrations were very low ( $< 1 \mu\text{g}/\text{m}^3$ ), the MFEs were well within the goal curves. For both spring and summer ammonium concentrations were underpredicted by the model. The MFEs and MFBs for the higher time resolution estimates at the core site were comparable to the 24-hour estimates.

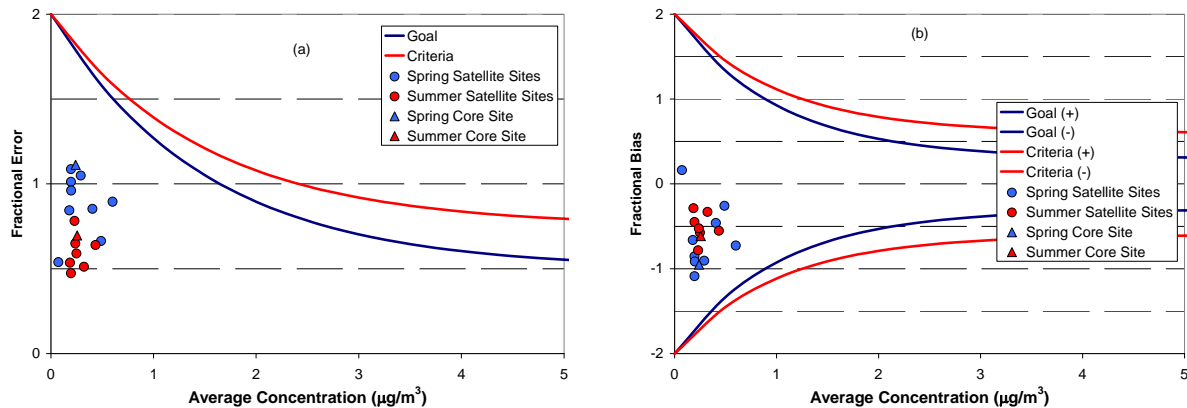


Figure 5.204. Bugle plots of ammonium (a) mean fractional error and (b) mean fractional bias. MFE or MFB is plotted on the y-axis and the average of the observed and modeled concentration is plotted on the x-axis ( $\mu\text{g}/\text{m}^3$ ).

In contrast to ammonium, the model evaluation of ammonia gas suggests much poorer performance. The bugle plots of MFE and MFB are presented in Figures 5.205a and 5.205b, respectively. MFEs tended to be larger for ammonia compared to ammonium and ammonia concentrations were more highly underpredicted by the model for all the sites for both seasons. The performance at a few sites fell outside the criteria during both spring and summer.

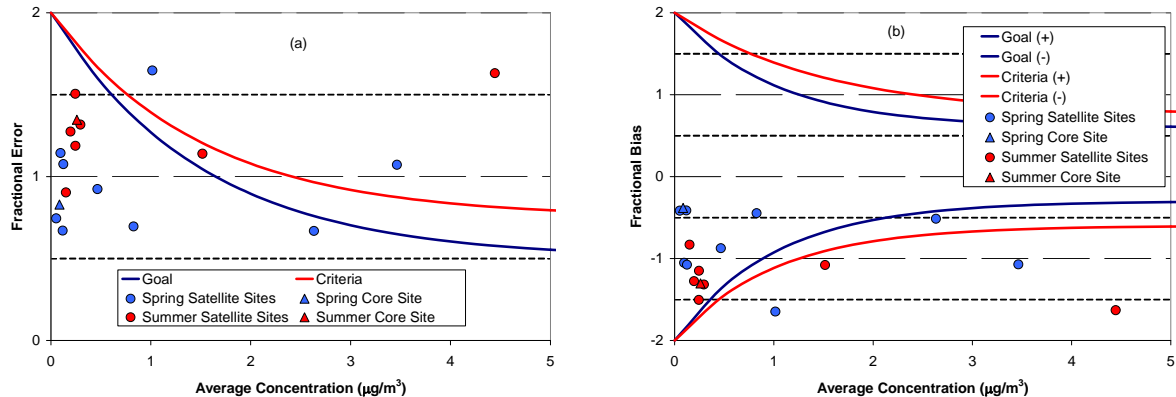


Figure 5.205. Bugle plots of ammonia (a) mean fractional error and (b) mean fractional bias. MFE or MFB is plotted on the y-axis and the average of the observed and modeled concentration is plotted on the x-axis ( $\mu\text{g}/\text{m}^3$ ).

The performance evaluation of nitric acid is shown in Figure 5.206. The model met performance goals for MFE (Figure 5.206a) during both spring and summer. The model overpredicted nitric acid during spring (Figure 5.206b), with one site falling outside of the performance goal. MFBs during summer were fairly low. Hourly core site estimates are not plotted because high time resolution nitric acid concentrations were not measured at the core site.

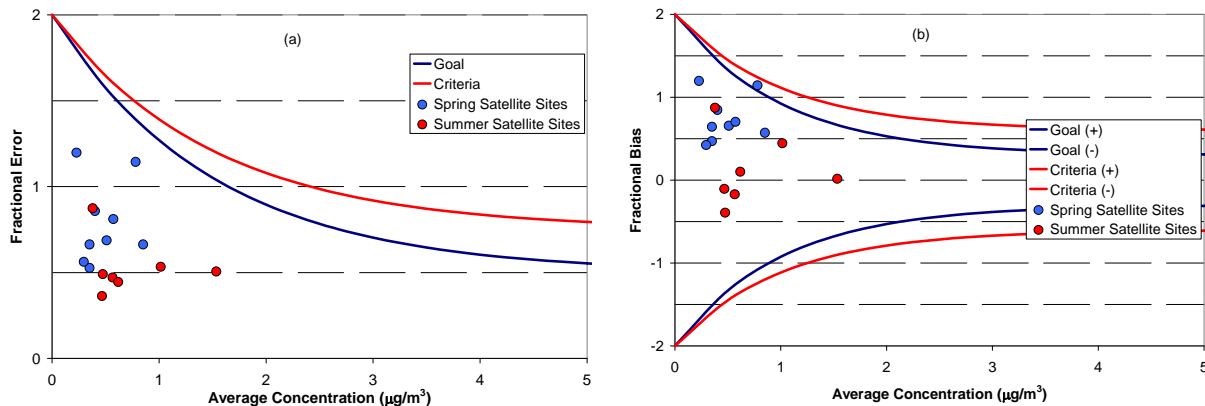


Figure 5.206. Bugle plots of nitric acid (a) mean fractional error and (b) mean fractional bias. MFE or MFB is plotted on the y-axis and the average of the observed and modeled concentration is plotted on the x-axis ( $\mu\text{g}/\text{m}^3$ ).

Evaluation of sulfur dioxide concentrations suggests that the model performance met its goals for MFE for all but one site (Brush) during both spring and summer (Figure 5.207a). The model overpredicted sulfur dioxide for almost all sites during spring and summer, with poor performance for two sites that did not meet goals or criteria for MFBs (Figure 5.207b). The concentrations of  $\text{SO}_2$  were quite low for the majority of sites ( $< 1 \mu\text{g}/\text{m}^3$ ). The model did not perform any better for the high time resolution core site data.

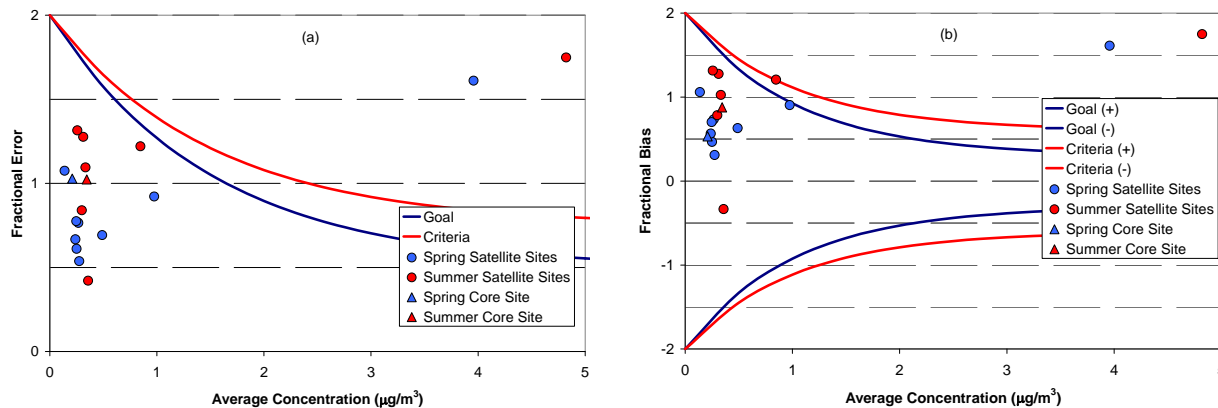


Figure 5.207. Bugle plots of sulfur dioxide (a) mean fractional error and (b) mean fractional bias. MFE or MFB is plotted on the y-axis and the average of the observed and modeled concentration is plotted on the x-axis ( $\mu\text{g}/\text{m}^3$ ).

The bugle plots of total reduced nitrogen are shown in Figures 5.208a and 5.208b. Although the model performed fairly well for ammonium, the reduced nitrogen was clearly impacted by the performance of model for ammonia (see Figures 5.205a and 5.205b). The model underpredicted reduced nitrogen species (Figure 5.208b) during both spring and summer to the same extent.

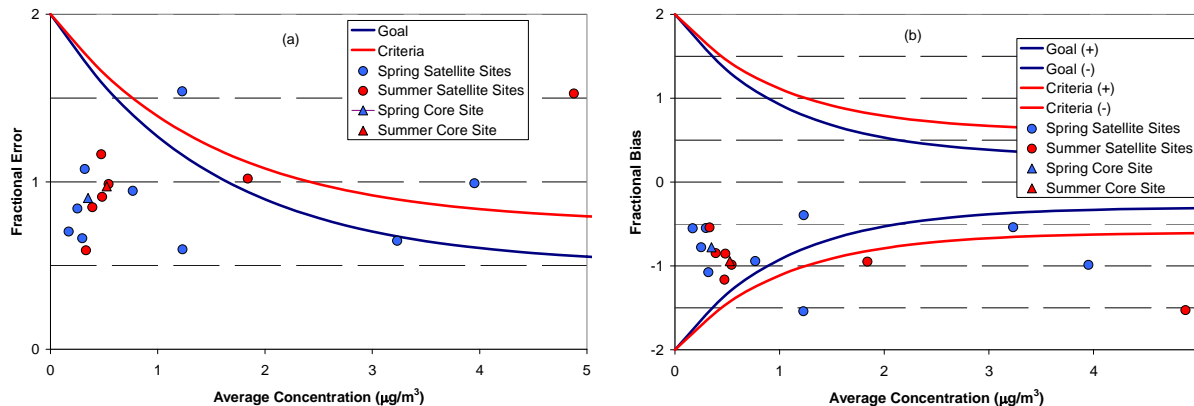


Figure 5.208. Bugle plots of N(-III) (a) mean fractional error and (b) mean fractional bias. MFE or MFB is plotted on the y-axis and the average of the observed and modeled concentration is plotted on the x-axis ( $\mu\text{g}/\text{m}^3$ ).

The model performance of total oxidized nitrogen is shown in Figures 5.209a and 5.209b. The model met performance goals for MFE and MFB for both spring and summer. Concentrations tended to be overpredicted in spring and underpredicted in summer.

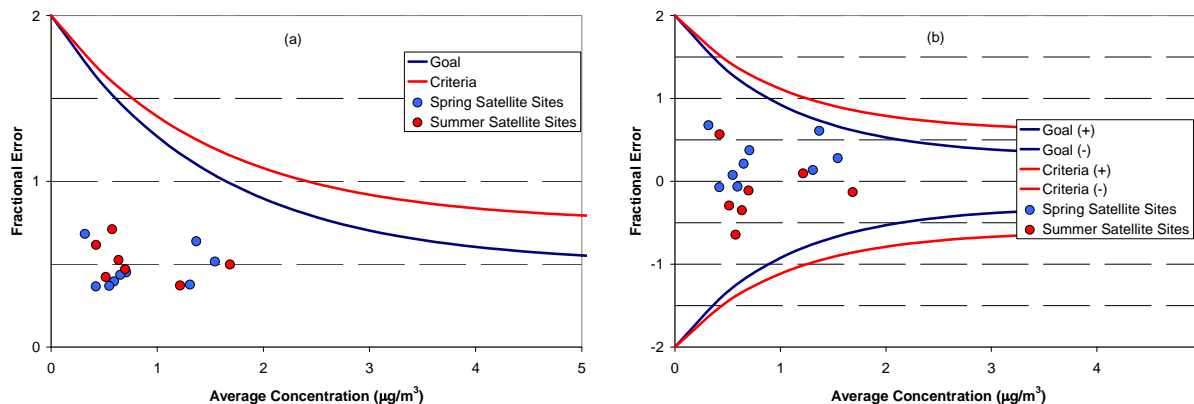


Figure 5.209. Bugle plots of N(V) (a) mean fractional error and (b) mean fractional bias. MFE or MFB is plotted on the y-axis and the average of the observed and modeled concentration is plotted on the x-axis ( $\mu\text{g}/\text{m}^3$ ).

The evaluation of model performance for total sulfur suggests the model met its performance goals for both MFE and MFB (Figure 5.210a and 5.210b, respectively). One site fell outside its criteria for both MFE and MFB due to the performance of sulfur dioxide at Brush, as discussed previously. The model tended to overpredict concentrations but not strongly.

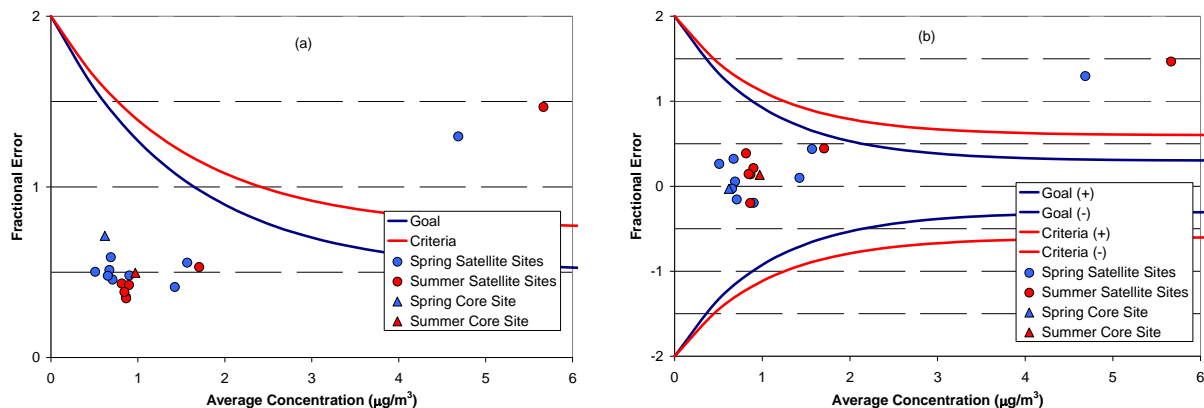


Figure 5.210. Bugle plots of total sulfur (a) mean fractional error and (b) mean fractional bias. MFE or MFB is plotted on the y-axis and the average of the observed and modeled concentration is plotted on the x-axis ( $\mu\text{g}/\text{m}^3$ ).

### 5.7.2.5. Summary and Recommendations

The comparisons of predicted and observed concentrations of particulate species ( $\text{NH}_4^+$ ,  $\text{NO}_3^-$ , and  $\text{SO}_4^{2-}$ ) demonstrate that the model captured the observed concentration spatial gradient in that modeled concentrations of particulate species were higher east of RMNP compared to within or west of the park. However, in general the model underpredicted mean particulate concentrations (see Figures 5.190 and 5.191). The model generally had the highest performance for sulfate and ammonium and poorest for nitrate. The largest biases and errors typically corresponded to nitrate.

The observed spatial gradient in gas-phase species ( $\text{NH}_3$ ,  $\text{HNO}_3$ , and  $\text{SO}_2$ ) concentrations generally was also captured by the model, in that the highest mean modeled concentrations occurred at sites east of the park. Concentrations of gas-phase species were also typically larger than those of particle-phase species at most satellite sites. Ammonia concentrations were underpredicted at all sites and for both seasons, while nitric acid and sulfur dioxide concentrations tended to be overpredicted. The model performance for nitric acid and sulfur dioxide was comparable, while model performance for ammonia at a couple of sites fell outside the MFB criteria.

With the exception of one site, model performance of total sulfur appeared to be the best, followed closely by N(V). Poor performance of the model for N(-III) was driven by the poor performance of ammonia. In general the model performed comparably for these species for both spring and summer.

The model performance evaluation presented in the previous sections leads us to the following recommendations. Because of the poor performance by the model for ammonia and total reduced nitrogen we do not recommend any further model analysis using modeled ammonia concentrations. While the model performance for other species varied during season and site, ranging from good to poor, the performance for these species was comparable to other model evaluations performed by WRAP-RMC and will be considered acceptable for further model evaluation and analysis as applicable for RoMANS.

## Chapter 6. Summary and Conceptual Model

Assessing changes in ambient concentrations of aerosol species and wet and dry deposition as a function of changing ammonia, nitrogen oxides, and sulfur dioxide emissions is dependent on a number of chemical and physical mechanisms, all of which are dependent on meteorological conditions. For example, ammonia will increase particle mass by reacting with acidic sulfate aerosols, nitric acid, and organic acids. With respect to the reaction of ammonia with nitric acid, the equilibrium between these species and the reaction product, ammonium nitrate, is temperature dependent and can go from predominantly gases to particles with the diurnal shifts in temperature. The condensation of ammonia onto particles is also dependent on the acidity of the particles and ambient relative humidity. These reactions do not necessarily take place at or near the source of ammonia, nitrogen oxides, or sulfur dioxide but over the transport pathways from source to receptor.

If chemical transport models were perfect, all apportionment problems could be addressed by modeling changing emission characteristics and observing how concentrations of species of interest at some predetermined receptor sites respond. A defensible prediction of an aerosol species' concentration and deposition relies on accurately knowing emissions, wind, cloud and precipitation fields, transport and dispersion characteristics, and chemical conversion and removal mechanisms along all transport pathways. However, many of these defining features are not known, especially for aerosols other than sulfates and ozone.

Therefore the strategy taken for apportioning various aerosol species concentrations and deposition to source emissions was a weight-of-evidence approach that included comparing and contrasting results from multiple analyses. The analyses involved examining spatial concentration gradients; simple wind direction as a function of aerosol concentration and wet deposition; and back trajectories for a number of high-concentration and wet-deposition episodes. Statistical analyses of trajectories were conducted in the form of residence time analysis and establishing quantitative statistical relationships between back trajectories and measured concentrations via the trajectory mass balance (TrMB) approach. Finally, modeled transport and dispersion of conserved tracer emissions into RMNP was used in a receptor-type framework to develop apportionment estimates of measured aerosol species concentrations as well as wet-deposition measurements.

### 6.1. MEASUREMENTS (THE DATA)

Fine and coarse mass concentrations are about a factor of 2 higher in the summer than spring. During the spring season, sulfates, organic mass, and soil made up about equal fractions of  $PM_{2.5}$  mass concentrations while during the summer time period organic mass accounted for 60% of the  $PM_{2.5}$ . The most striking feature of both fine and coarse mass was the extremely short time scale variability of aerosol concentrations. Short time scale variability suggests varying transport from regions with significantly different emission rates.

### 6.2. DEPOSITION

Historically, wet deposition contributes much more to nitrogen deposition fluxes than dry deposition in RMNP. During both the spring and summer RoMANS campaigns, wet deposition

contributed approximately three-fourths of the total nitrogen deposition measured at the study core site. Wet plus dry deposition fluxes of nitrogen were about a factor of 2 higher in the summer than spring campaign periods.

Peak wet deposition amounts usually occur during late July through early August, and summer precipitation is often due to convective storms. There is a secondary peak in wet deposition amounts in March and April, which is more often due to large-scale weather systems. The total number of hours of wet deposition is highest during April. Diurnally, both the number of hours of wet deposition and wet deposition amounts peak during the afternoon, especially about from 11:00 am through 5:00 pm.

Measurements of precipitation composition and amount, key  $PM_{2.5}$  nitrogen and sulfur species concentrations, and key nitrogen and sulfur trace gas concentrations allow construction of deposition flux budgets for RMNP during spring and summer. Daily changes in dry deposition of nitrogen and sulfur species in RMNP are driven mainly by changes in species concentrations and less by changes in dry deposition velocities.

Wet deposition reflects local cloud and precipitation scavenging of particulate and gas-phase nitrogen compounds. Wet deposition in spring was dominated by a single, upslope snowstorm; the combination of pollutant transport from the east and heavy precipitation associated with lifting of air up the east slope of the Rockies created ideal conditions for large wet deposition fluxes of both reduced and oxidized nitrogen. During the summer, the wet deposition in summer was divided more evenly across several precipitation events.

The largest deposition flux of nitrogen at the RoMANS core site on the east slope of RMNP was caused by wet deposition of ammonium, followed by wet deposition of nitrate. Ammonium wet deposition contributed 34% of total measured nitrogen deposition in both spring and summer while nitrate wet deposition contributed 24% to spring and 28% to summer totals. The third and fourth most important inputs were from dry deposition of gaseous ammonia (14% of the spring total, 16% of the summer total) and wet deposition of organic nitrogen (17% of the spring total, 12% of the summer total). Dry deposition of gaseous nitric acid was fifth in importance (8% in both seasons). Dry deposition fluxes of  $PM_{2.5}$  nitrate and ammonium each contributed 3% or less during each season. Dry deposition of organic nitrogen was not quantified.

### **6.3. WIND FLOW PATTERNS**

The predominant wind flow at RMNP is westerly. However, nearly all episodes of high concentrations of nitrogen- and sulfur-containing particulates and gases occurred during easterly flow. Upslope easterly flow on the east side of RMNP occurred during about 20% of all hours at the RoMANS core measurement site. Easterly flow is slightly more common during the warmer months of the year and occurred about twice as often during midday as at night. Easterly flow is much more common during wet deposition events than during nonprecipitating hours.

#### **6.4. CONCENTRATION GRADIENTS OF AEROSOL AND TRACE GAS SPECIES SUGGEST SOURCE REGIONS AND TRANSPORT PATHWAYS**

Typically, concentrations of most species were highest in northeastern Colorado, with a sharply decreasing east-to-west gradient. Ammonia concentrations in northeastern Colorado were 10–100 times greater than in RMNP.

Lowest concentrations of nearly all major nitrogen and sulfur species were west of the Continental Divide at Gore pass and Timber Creek. Concentrations of reduced nitrogen (ammonia + ammonium) at monitoring sites on the eastern side of the park were similar to concentrations on the western slope on many days but substantially higher on days with significant transport from the east.

The spatial gradients observed across the RoMANS network and the relationship between upslope/downslope transport and species concentrations at the RoMANS core site suggest an important link between pollutant emissions east of the park and nitrogen concentrations and deposition inside RMNP.

The relative contribution of ammonium to wet deposition of nitrogen increases moving from western Colorado, east across the Continental Divide, reflecting the higher concentrations of reduced nitrogen in the eastern part of the state.

#### **6.5. BACK TRAJECTORY RESIDENCE TIME ANALYSIS**

Back trajectory residence time analysis shows that the source areas contributing to the highest concentration time periods (90<sup>th</sup> percentile) are associated, for the most part, with easterly transport. Most species were associated with source areas in northeastern Colorado. The Front Range was highlighted as a potentially significant NO<sub>x</sub> and NH<sub>3</sub> source area, while a region to the east of the Front Range was a potentially significant NH<sub>3</sub> source area. The summertime analysis identifies a larger and more distant area potentially contributing to RMNP compared to the springtime, indicating possible contributions from a more diverse and distant set of sources. The secondary nitrate and sulfate species also show potential contributions from more distant sources than their precursors, NO<sub>2</sub> and SO<sub>2</sub>, for both the spring and summer periods.

#### **6.6. STATISTICAL APPORTIONMENT MODELS**

Apportionment regression models are based on the association of source signatures with measured concentrations. In the case of back trajectory regression analysis (TrMB), it is the number of back trajectory endpoints over source regions that contributes to elevated levels of an aerosol species, while in the hybrid approach it is the concentration of modeled conservative tracers released from various source regions that correlates with measured concentrations.

In TrMB the model establishes a “scaling” factor between the number of endpoints over a source region and the measured concentrations at the receptor site. Emissions, dispersion, all chemical transformations, and deposition are incorporated into this one scaling factor. Therefore, the apportionments derived from this technique are more accurate on the average than on an hourly or episodic basis. Furthermore, a statistical apportionment approach will inherently tend to overestimate those source regions where endpoints over the region are correlated with measured

concentrations while underestimating those source regions where endpoints over that source regions show weak to little correlation with measured concentrations.

In the hybrid modeling approach, the apportionment analysis is more robust in that emissions and dispersion are explicitly modeled, and only chemistry and deposition, as well as possible errors in the transport model, are incorporated into a “scaling” factor. However, like TrMB, the apportionment estimates are more accurate on the average than for an incrementally small time period, and apportionment of source regions whose modeled tracer concentrations are weakly correlated with measured concentrations may be underestimated.

Because measurement uncertainties are known and standard errors of the regression coefficients are reported, it would be possible to report apportionment estimates with propagated uncertainties associated with these two variables. However, the underlying model uncertainties associated with various assumptions are not known and are probably larger than measurement and statistical uncertainty. Therefore fractional apportionment estimates are not reported with an attached uncertainty. On the other hand, it is emphasized that the inherent limitations of statistical apportionment models should be kept in mind when referring to reported apportionment estimates.

#### **6.6.1. Back Trajectory Regression Analysis (TrMB)**

In both spring and summer more than 70% of measured ammonia was estimated to be from sources within the state of Colorado, while ~50% of ammonium and 15–25% of particulate nitrate were from Colorado sources. In addition, about 50–60% of sulfur dioxide is estimated to originate from within Colorado’s borders. Colorado sources both east and west of RMNP were significant contributors to ammonia and ammonium, though the eastern sources generally had a larger contribution. The Front Range was the dominant Colorado source region contributing to RMNP for particulate nitrate. Source contributions tend to be somewhat more regional in the summer versus spring time periods.

#### **6.6.2. Hybrid Receptor Modeling**

To better delineate source areas and apportion source areas to measured wet and dry deposition, transport and dispersion of a conservative tracer released in proportion to emissions were used in a receptor-oriented model to statistically account for removal and chemical processes.

##### **6.6.2.1. Reduced Nitrogen (Ammonia/Ammonium)**

During the spring season about 75% of ammonia and ammonium was estimated to originate from within the state of Colorado, while during the summer 80% of ammonia and less than 50% of the ammonium were linked to in-state emissions. On the average the source region within the state of Colorado contributing the largest fraction of ammonia at the core site during the spring was northeastern Colorado at over 40%, while the second largest contributor was the Denver source region contributing at 17%. During the summer it is estimated that on the average about 30% of measured ammonia was linked to local, naturally occurring emissions and 20% of measured ammonia was from northeastern Colorado, with western Colorado contributing another 20%.

Consistent with upslope flow during the spring time period of highest ammonia concentrations, it is estimated that over 80% of the ammonia came from northeastern Colorado, with Denver also contributing. During the summer time frame, episodically, northeastern and western Colorado are the most significant contributors. The local source region contributed almost every day on a diurnal basis.

All of the major spring episodes of  $\text{NH}_4$  are associated with upslope conditions, with the largest contributions to  $\text{NH}_4$  concentrations coming from northeastern and western Colorado, with some contribution from the Denver source area. The summer episodes of ammonium correspond to a more diversified set of source regions, with western Colorado and sources west of the Continental Divide all the way to California making significant contributions. During clear, upslope conditions, northeastern Colorado again contributed much of the measured ammonium.

#### **6.6.2.2. Oxidized Nitrogen (Nitric Acid/Nitrate)**

On the average, about 40–50% of measured nitric acid was estimated to have its origins within the state of Colorado in both spring and summer, while during the spring ~50% of the nitrate was linked to in-state emissions but only 20% during the summer measurement period. In both seasons, particulate nitrate was a minor contributor to nitrogen deposition.

On the average during the spring time period, Denver was estimated to have contributed most of the nitric acid and nitrate, while northwestern Colorado was the second largest contributor. The summer apportionment of  $\text{HNO}_3$  and  $\text{NO}_3^-$  showed a somewhat different picture. In general, during the summer westerly transport was responsible for most of the  $\text{HNO}_3$  and  $\text{NO}_3^-$  species. On the average, a small to negligible fraction of these species was predicted to come from northeastern Colorado, with about 15% of the  $\text{HNO}_3$  and 5% of the  $\text{NO}_3^-$  coming from Denver. California was the overall largest contributor to nitrate at 37%. Southern Nevada was predicted to contribute significantly to both nitric acid and nitrate during the summer time period.

Episodically, during the spring time period, the Denver source region was predicted to be the largest contributor to nitric acid and nitrate at over 80%. During the summer the major upslope event contributing to elevated nitric acid and nitrate was associated with emissions from eastern Wyoming. During most of the remaining time periods, California and southern Wyoming sources were predicted to be the most significant contributors to nitric acid and nitrate.

#### **6.6.2.3. Sulfur Dioxide and Sulfate**

In both the spring and summer time periods, about 50% of sulfur dioxide and 25% of sulfates were predicted to originate from within the state of Colorado. During the spring, most of that 50% was linked to the Denver source region, while during the summer season, northwestern Colorado was the biggest contributor. The Denver, Four Corners, and eastern Wyoming source regions were the largest contributors to sulfate during the spring, while northwestern Colorado and southwestern Wyoming source regions contributed most of the sulfate during the summer season.

At times during the spring, the Denver and Four Corners source areas individually contributed over 80% of measured sulfur dioxide or sulfate. During the summer time frame, contribution

from sources to sulfur dioxide and sulfate were more diverse; however, at times eastern Wyoming and northwestern Colorado could contribute 60–70% of these species.

#### **6.6.2.4. Apportionment of Wet-Deposited Ammonium, Nitrate, and Sulfate.**

Wet deposition of nitrogen contributes significantly more to total deposition than dry-deposited species. Average source apportionment budgets for wet-deposited species can be quite different than those for dry deposition because the transport pathways are limited to those days when precipitation occurred.

##### **6.6.2.4.1 Ammonium**

During the spring time period, wet deposition was dominated by one synoptic-scale precipitation event that occurred over a period of a few days. This precipitation event corresponded to an upslope condition with transport from northeastern Colorado. Therefore northeastern Colorado ammonia sources were predicted to contribute most of the wet-deposited ammonium at about 67%, with the Denver region contributing another 16%.

The sources contributing to ammonium wet deposition during the summer time period were significantly more varied, with the local source area being the largest contributor at 32% and western Colorado being the second largest contributor at 24%. Northeastern Colorado was predicted to only contribute 7% during this time frame.

##### **6.6.2.4.2 Nitrate**

In the spring, during the single large upslope event, the majority of the nitrate deposition occurred. The principal source area was Denver at 52%, with 39% coming from sources outside Colorado.

As with ammonium, the sources contributing to wet nitrate deposition during the summer were highly varied, with sources associated with southwesterly transport contributing over 40%. These included California, southern Nevada, and the Four Corners region. Denver was the largest Colorado source region at 10%, with another 22% coming from other in-state sources.

##### **6.6.2.4.3 Sulfate**

As with ammonium and nitrate, sulfate wet deposition was dominated by the one large precipitation event that corresponded to transport from northeastern Colorado and the Front Range. It is estimated that 42% and 12% of wet-deposited sulfate was associated with the Denver and northeastern Colorado source regions, respectively. Eastern Wyoming also was a large contributor at 13%.

Summer wet sulfate deposition was linked to many source areas, with southwestern Wyoming and northwestern Colorado being the biggest contributors and 17% and 14%, respectively. The largest single wet-deposition event was associated with southwesterly transport and a significant contribution from the Four Corners region at nearly 40%. On the average southwesterly transport contributed about 20% of wet-deposited sulfate.

### 6.6.3. Total Deposition

During the spring time period, source areas responsible for the most deposition of nitrogen were northeastern Colorado and the Denver region at about 40% and 25%, respectively. During the summer, the source regions were considerably more varied, with 25% of deposition associated with southwesterly transport and the associated source regions. Twenty per cent of nitrogen deposition was linked to local source areas, with western Colorado contributing about 13%. The Denver area contributed another 8%.

The average source apportionment budget for total deposition, wet + dry and spring + summer, between in-state versus out-of-state was predicted to be about 60:40. The source area deposition budget for total (wet + dry and summer + spring) deposition is shown in Figure 6.1. The total deposition was spread pretty much evenly between Denver, western and northeastern Colorado, the local area, and transport from the southwest, which included California plus southern Nevada and the Four Corners region.

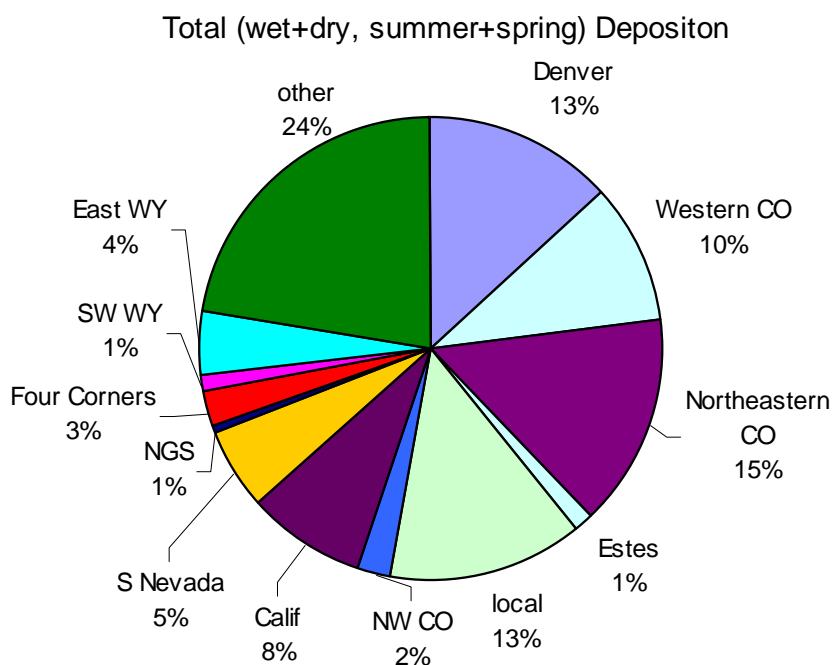


Figure 6.1. Area source apportionment to total nitrogen deposition.

## 6.7. CONCEPTUAL MODEL

Figure 6.2 is a simplified schematic diagram of chemical processes involved in atmospheric processing of nitrogen and sulfur emissions into molecules affecting ecosystems, visibility, materials, and/or human health. Primary emissions of reduced nitrogen, primarily from fertilizer application and feedlot activity, nitrogen oxides from mobile sources and power plants, and

volatile hydrocarbon emissions, both natural and anthropogenic, react in the atmosphere during transport to form secondary gases and particles such as ammonium nitrate and sulfate and oxidizing agents such as ozone.

Particles affect visibility, while dry and wet deposition of these species in all their chemical forms affects the ecosystem either through acidification or fertilization. After deposition of many of these species, natural biological processes result in remission of the primary gases such as ammonia and various oxidized forms of nitrogen that cycle back through the system. An interactive multimedia presentation of these concepts can be accessed at <http://vista.cira.colostate.edu/improve/Education/ReactiveN/NitrogenCycling.swf>.

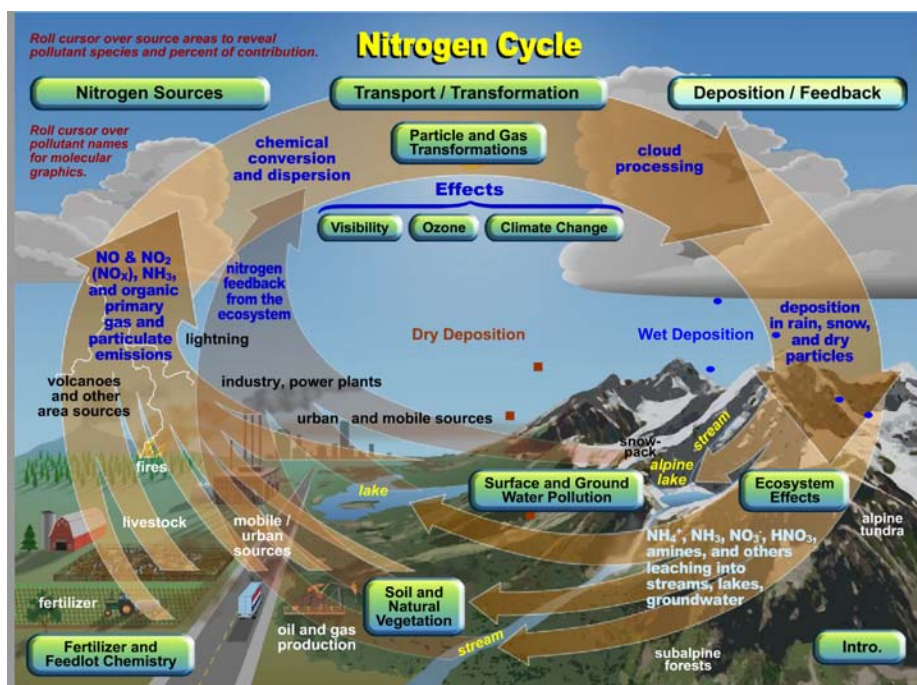


Figure 6.2. Schematic of chemical processes associated with nitrogen and sulfur species that lead to aerosol formation and deposition.

### 6.7.1. Ammonia

Ammonia emissions are primarily associated with fertilizer application and feedlots but also with mobile source emissions from catalytic converters and other human activities. Background levels of ammonia concentrations tend to vary diurnally from near 0 to about  $1 \mu\text{g}/\text{m}^3$ . The deposition rate of ammonia is high on the one hand and on the other hand it readily reacts in the atmosphere to neutralize acidic aerosol species, forming ammonium nitrate and sulfate. Therefore sources contributing to ambient levels of ammonia at RMNP were thought to be more local in nature (within state sources) as opposed to transport from sources many hundreds of kilometers distant.

Northeastern Colorado and sources farther east of Colorado are rich in ammonia emissions primarily associated with agriculture-related emissions. Measurements of ambient ammonia concentrations reflected the spatial variability of the emissions inventory in that on almost every

day the concentrations of ammonia at the Brush, Colorado, monitoring site were a factor of 10 or more than any other site in Colorado. Therefore during transport conditions that are conducive to moving emissions from eastern Colorado and beyond into RMNP, one might expect to see elevated levels of ammonia in RMNP. Two types of meteorological conditions are conducive to transporting emissions from east of RMNP into the park itself. During spring, synoptic-scale upslope events can transport emissions east of the Continental Divide into the eastern side of RMNP, while during the summer, afternoon convective conditions and mountain/valley circulations tend to transport emissions from the Front Range into the park but on smaller spatial scales.

Consistent with this conceptual model it was shown in section 4.4 that when winds blew from the east, concentrations of ammonia, and for that matter almost all gases and particles, tended to increase, in some cases dramatically. Back trajectory analysis also showed that when air masses passed over eastern Colorado, they tended to arrive at RMNP with high concentrations of ammonia. This was especially true during the spring time frame when one large event corresponded to transport from eastern Colorado and the Denver area.

Another significant source of ammonia at RMNP was western Colorado during summer conditions, when mixing depths were deep and transport could take place over the Continental Divide. Surprisingly, a large fraction of measured ammonia apparently was associated with the natural respiration of the terrestrial ecosystem. During the summer time period, background ammonia concentrations tended to cycle between near 0 at night to approximately 0.5–1.0  $\mu\text{g}/\text{m}^3$  during daylight hours.

Multiple qualitative and quantitative source attribution analyses were conducted. All analyses indicated that during spring upslope conditions northeastern Colorado was the single largest contributor to measured ammonia at RMNP. Transport from northeastern Colorado into RMNP requires air masses to pass over other source areas of ammonia such as the Denver region. Consistent with this, source apportionment results showed this region to be the second largest contributor to measured  $\text{NH}_3$  concentrations. Source emissions farther to the east and north of northeastern Colorado were sufficiently dispersed such that they contributed little to measured values.

### **6.7.2. Ammonium**

Ammonia is the precursor to ammonium and therefore has the same source regions. However, whereas ammonia is transported without undergoing chemical change, ammonium is a secondary species usually associated with particulate sulfate or nitrate or in solution as a cloud droplet. The spatial scale of the source-receptor relationship for ammonium could be substantially more than ammonia, depending on where the ammonia reacts with sulfur and oxidized nitrogen species. Northeastern Colorado is a source of ammonia and the location of coal-fired power plants that emit about 15000 tons/yr of  $\text{SO}_2$  and 5000 tons/year of  $\text{NO}_x$ . Transport pathways from northeastern Colorado also pass over Denver/Greeley/Boulder, which are large source areas of  $\text{NO}_x$  and  $\text{SO}_2$ , emitting about 200,000 and 160,000 ton/yr of  $\text{NO}_x$  and  $\text{SO}_2$ , respectively.

Not surprisingly, during the spring time period most of the measured ammonium in wet and dry deposition episodes apparently was a result of reactions of ammonia with oxidized sulfur and

nitrogen species or as a result of equilibrium processes with cloud droplets as it was transported from northeastern Colorado and Denver into RMNP. Ammonia emitted in western Colorado was also captured as ammonium and transported into RMNP and deposited as dry species, although ammonium contribution to dry deposition was relatively unimportant.

During the summer, sources of ammonia as far away as California and other areas west of RMNP make their way to RMNP. Apparently, during the summer most dry-deposited ammonium, although small, was associated with ammonia sources outside Colorado, but most wet-deposited ammonium was from ammonia sources inside Colorado.

It also seems that locally emitted ammonia reacted with acidic sulfate particles or gaseous nitric acid or was dissolved in cloud or fog droplets such that a substantial fraction of ammonium in both wet and dry form was associated with locally emitted ammonia.

### **6.7.3. Nitrogen Oxides and Nitric Acid**

Nitrogen oxides react to form nitric acid in a matter of minutes to hours. Given the considerable  $\text{NO}_x$  emission rate of the Denver area source region, it is not surprising that during spring or summer upslope conditions most  $\text{NO}_x$  and  $\text{HNO}_3$  at RMNP were linked to this region. The Denver source region was the single largest contributor of these measured species. The Craig and Hayden coal-fired power plants emit approximately 27,000 tons of  $\text{NO}_x$ /year and transport of emissions from these plants was the second largest contributor to  $\text{NO}_x$  and  $\text{HNO}_3$  at RMNP. During the summer season, emissions from oil-, gas-, and coal-fired power plants in the Four Corners area, coal-fired power plants in southern Nevada, and the large  $\text{NO}_x$  population centers in California all contributed to  $\text{NO}_x$  and  $\text{HNO}_3$  in RMNP.

### **6.7.4. Nitrate**

Particulate nitrate is typically formed from the reaction of ammonia with nitric acid and its formation is highly dependent on temperature and relative humidity. At temperatures near 80 F, little particulate nitrate is formed, while near 35 F almost all available ammonia or nitric acid will react to form ammonium nitrate, depending on the relative concentration of one species to the other. Consequently, during the summer one tends to find little particulate nitrate while during winter conditions particulate nitrate, and hence dry particle nitrate deposition, will be at its maximum.

Even though ambient levels of particulate nitrate are low in the warm summer seasons, significant amounts of nitrate are found in rainwater because nitric acid is very water soluble. Furthermore, it is possible for particle ammonium nitrate to be transported over distances of many hundreds of kilometers, even in the summer months when it is trapped aloft where temperatures are low and relative humidity high. Once transported, it can dissociate and the dissociation products are free to form equilibrium solutions with cloud droplets.

Because of dominant upslope conditions during the spring time frame, most particulate and wet-deposited nitrate was estimated to have its origins in  $\text{NO}_x$  emissions in the Denver source region, with some contribution from the Craig and Hayden coal-fired power plants. During the summer time frame, most wet and dry nitrate was predicted to come from outside Colorado, primarily from the California source regions. More than 80% of nitrate during summer conditions was

estimated to come from outside Colorado. However, because of limited-time-resolution nitric acid measurements, Front Range contributions of either wet- or dry-deposited nitrate associated with summer convective conditions may be underestimated.

#### **6.7.5. Sulfate/Sulfur Dioxide**

Sulfate formation and transport, while not having the same ecological effects as nitrogen, are key to understanding sources of ammonium that contribute to both wet and dry deposition. Sulfur dioxide is oxidized to sulfuric acid, which reacts with ammonia to form an ammoniated sulfate aerosol that can be transported of many hundreds of kilometers. Ambient levels of sulfur dioxide and ammonia are also key to understanding cloud water chemistry and therefore the concentration of ammonium in wet deposition. Most sulfate originated from sulfur dioxide sources outside the borders of Colorado, while sulfur dioxide sources inside and outside Colorado contributed about evenly during the spring time period; during the summer season most sulfur dioxide was from southwestern transport conditions.

### **6.8. POLICY-RELEVANT QUESTIONS AND ANSWERS**

- 1) What are the important species and their sources that cause the nitrogen deposition?
- 2) Is this a Colorado issue or regional issue?

The ecosystem effects of deposited nitrogen are for the most part dependent on the total deposition load. Therefore even though there are time periods when one source area contributes most of the deposition, it is the integrated deposition, both over source regions of reduced and oxidized nitrogen and over time, that is most relevant.

Referring to Figures 4.19 and 4.20, one can see that of the species that were measured, inorganic, reduced nitrogen resulting from ammonia emissions was the single largest contributor to nitrogen deposition (40–50%). Ammonia emissions are primarily associated with agricultural activity contributing about 60%, with about 40% coming from livestock production and 20% from fertilizer application. Of this 60% about 20–30% was estimated to originate in northeastern Colorado.

Agricultural emissions were the largest contributor to nitrogen deposition at RMNP, and northeastern Colorado agricultural activity (livestock feeding and fertilizer application) was the single largest source.

Inorganic, oxidized nitrogen accounted for 30–35% of total measured deposition and was primarily associated with NO<sub>x</sub> emissions. On the average, about equal amounts, 25%, came from motor vehicles and electricity-generating facilities. It is estimated that agriculture produced another 25% of NO<sub>x</sub> emissions. The Denver source region was the largest source area contributing to oxidized nitrogen deposition, and within that source region mobile sources were responsible for about 75% of NO<sub>x</sub> emissions.

About 15% of wet deposition of nitrogen was in an organic form, and because it was not speciated, it is unknown with which emission sources it is associated. Furthermore, because there were significant amounts of wet-deposited organic nitrogen, there likely were significant

concentrations of organic nitrogen gas and/or particulate matter. It is known that significant amounts of amines (organic nitrogen) can be generated in feedlots. However, gaseous and particulate organic nitrogen was not quantified during the RoMANS study.

With regard to in-state versus out-of-state contributions to total nitrogen deposition, as stated above, there was about a 60:40 split, with most nitrogen associated with in-state emissions. However, it is estimated that 13% of in-state contributions to nitrogen deposition was linked to local or natural sources. After discounting in-state emissions due to “local” sources, the split between in-state and out-of-state contributions is about equal. So, the state of Colorado contributed as much nitrogen to deposition as all other states combined. The northeastern Colorado and the Denver source regions contributed about 70% of all Colorado-associated deposition. As stated above, northeastern Colorado was primarily linked to reduced nitrogen deposition (feedlots/fertilizer), while Denver was primarily linked to oxidized nitrogen deposition (mobile sources and power plants).

## **6.9. HAZE CONSIDERATIONS**

Whereas ecosystem effects, for the most part, depend on the total deposition occurring over all time, visibility effects from changing particulate concentrations are instantaneous and directly dependent on aerosol concentrations at the time of viewing a landscape feature. Therefore the temporal characteristics of atmospheric extinction are of interest.

The most striking feature of the semicontinuous particulate data, from which extinction and visibility are derived, was the extremely short time scale variability. The average contribution of each species to visibility impairment can be quite misleading in that averages can be made of up of extreme events. Large excursions in extinction can take place in time periods as short as hours. On the average, ammonium nitrate only contributed about 5% of the extinction; however, at 8:00 pm on April 23 the ammonium nitrate scattering coefficient was near  $20 \text{ Mm}^{-1}$ , which is more than 25% of total particle extinction. On the highest extinction hours, the corresponding visual ranges were approximately 25 km and 40 km for the summer and spring time periods, respectively.

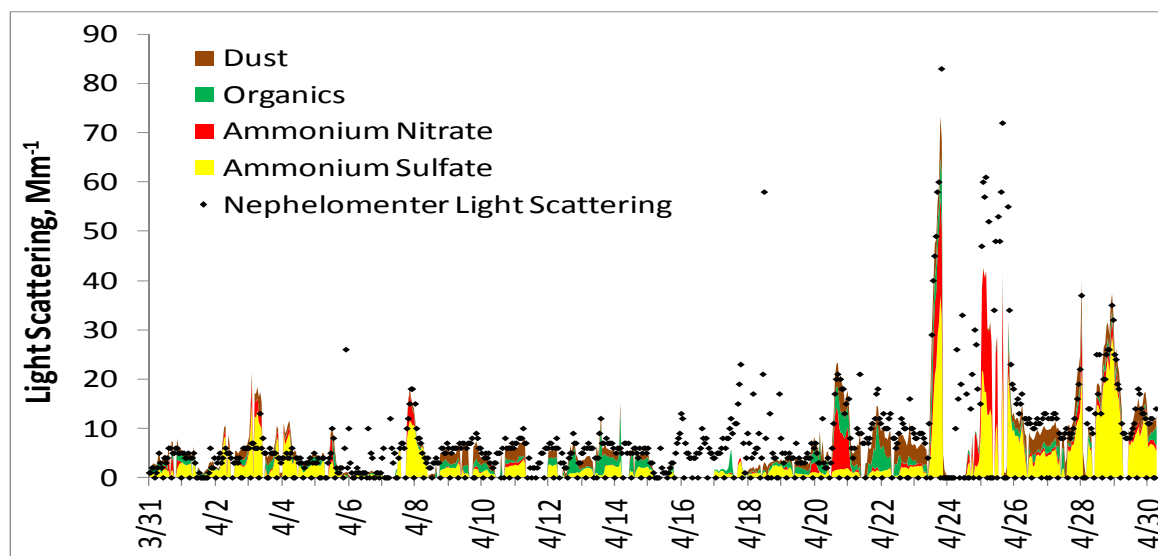


Figure 6.3. Temporal plot of measured and estimated atmospheric scattering ( $\text{Mm}^{-1}$ ) of major aerosol species during the spring RoMANS time period and the approximate extinction budgets for the spring and summer RoMANS time periods.

Referring to Figures 5.106 and 5.109, one can see that there are a number of short-term nitrate excursions that were only a few hours in duration. The receptor model estimations of nitrate concentrations were unable to reproduce these short-time-frame episodes. As discussed above, the receptor modeling approach may apportion measured concentrations quite accurately on the average; they are less accurate for episodic analysis. The short-term nitrate excursions are an example of when modeled concentrations were a substantial underestimation of actual measured concentrations.

Because winds and associated transport were modeled with reasonable accuracy, the inability of the receptor models to reproduce short-time-scale nitrate concentrations variability was likely due to nonlinear aerosol chemical processes. Every short-term nitrate excursion is accompanied by a commensurate short-time-scale ammonia fluctuation. It is likely that the increase in ammonia resulted in a shift in the ammonia/nitric acid equilibrium to particulate nitrate. These short-term ammonia/nitric acid equilibrium concentrations were not accounted for by the constant chemistry “adjustment” factor derived from the statistical averaging inherent in the receptor models. It should be pointed out that all short-time-frame nitrate excursions were accompanied by similar changes in ammonia concentrations; however, the converse is not true. There were many other ammonia excursions that were not accompanied by changes in nitrate concentrations.

During the spring, ammonium sulfate was the largest contributor to extinction at about 40%, with ammonium nitrate and POM contributing about 15% of overall extinction. Coarse mass scattering contributed another 22%, and particle absorption as the sum of fine and coarse absorption contributed another 5%. During the summer the average extinction budget was quite different. POM contributed 50% of the aerosol extinction, while ammonium sulfate contributed another 18%. Coarse particle scattering was only 8%, and total fine plus coarse absorption was 10%.

## REFERENCES

- Adelman, Z., Emissions modeling final report - RoMANS study phase I, Institute for the Environment, University of North Carolina, Chapel Hill, 2007.
- Allen, A. G. and A. H. Miguel, Biomass burning in the Amazon: Characterization of the ionic component of aerosols generated from flaming and smoldering rainforest and savannah, *Environmental Science & Technology*, 29, 486-493, 1995.
- Andersen, H. V., M. F. Hovmand, P. Hummelshoj and N. O. Jensen, Measurements of ammonia flux to a spruce stand in Denmark, *Atmospheric Environment Part A-General Topics*, 27, 189-202, 1993.
- Andersen, H. V. and M. F. Hovmand, Ammonia and nitric acid dry deposition and throughfall, *Water and Soil Pollution*, 85, 2211-2216, 1995.
- Andersen, H. V., M. F. Hovmand, P. Hummelshoj and N. O. Jensen, Measurements of ammonia concentrations, fluxes, and dry deposition velocities to a spruce forest 1991-1995, *Atmospheric Environment*, 33, 1367-1383, 1999.
- Andersen, H. V. and M. F. Hovmand, Review of dry deposition measurements of ammonia and nitric acid to forest, *Forest Ecology and Management*, 114, 5-18, 1999.
- Ashbaugh, L. L., W. C. Malm and W. Z. Sadeh, A residence timed probability analysis of sulfur concentrations at Grand Canyon National Park, *Atmos. Environ.*, 19(8), 1263-1270, 1985.
- Ayers, R. U., W. H. Schlesinger and R. H. Socolow, Human impacts on the carbon and nitrogen cycles, in *Industrial Ecology and Global Change*, edited by R. H. Socolow, C. Andrews, R. Berkhout and V. Thomas, pp. 121-155, Cambridge University Press, New York, 1994.
- Baker, K. and P. Scheff, Photochemical model performance for PM<sub>2.5</sub> sulfate, nitrate, ammonium, and precursor species SO<sub>2</sub>, HNO<sub>3</sub>, and NH<sub>3</sub> at background monitor locations in the central and eastern United States, *Atmospheric Environment*, 41(29), 6185-6195, 2007.
- Baron, J. S., H. M. Rueth, A. N. Wolfe, K. R. Nydick, E. J. Allstott, J. T. Minear and B. Moraska, Ecosystem responses to nitrogen deposition in the Colorado Front Range, *Ecosystems*, 3, 352-368, 2000.
- Baron, P. A. and K. Willeke, *Aerosol Measurement: Principles, techniques, and applications*, Wiley-Interscience, New York, 2001.
- Bashurova, V. S., V. Dreiling, T. V. Hodger, R. Jaenicke, K. P. Koutsenogii, P. K. Koutsenogii, M. Kraemer, V. I. Markarov, V. A. Obolkin, V. L. Potjomkin and A. Y. Pusep, Measurements of atmospheric condensation nuclei size distributions in Siberia, *Journal of Aerosol Science*, 23(2), 191-199, 1992.
- Belsley, D. A., E. Kuh and R. E. Welsch, *Regression Diagnostics - Identifying Influential Data and Sources of Collinearity*, John Wiley & Sons, New York, 1980.

- Blett, T. and K. Morris, Nitrogen Deposition: Issues and effects in Rocky Mountain National Park, in Technical Background Document, available at <http://www.cdphe.state.co.us/ap/rmnp/noxtech.pdf>, 2004.
- Boylan, J. W. and A. G. Russell, PM and light extinction model performance metrics, goals, and criteria for three-dimensional air quality models, *Atmospheric Environment*, *40*, 4946-4959, 2006.
- Bresch, J. F., E. R. Reiter, M. A. Klitch, H. K. Iyer, W. C. Malm and K. A. Gebhart, Origins of sulfur-laden air at national parks in the continental United States, Bhardwaja, P. S. Transactions of the APCA Specialty Conference "Visibility Protection: Research & Policy Aspects", Pittsburgh, PA, 1986.
- Burns, D. A., Atmospheric nitrogen deposition in the Rocky Mountains of Colorado and southern Wyoming - A review and new analysis of past study results, *Atmospheric Environment*, *37*, 921-932, 2003.
- Campbell, D. H., J. S. Baron, K. A. Tonnessen, P. D. Brooks and P. F. Schuster, Controls on nitrogen flux in alpine/subalpine watersheds of Colorado, *Water Resources Research*, *36*(1), 37-47, 2000.
- Campbell, D. H., C. Kendall, C. C. Y. Chang, S. R. Silva and K. A. Tonnessen, Pathways for nitrate release from an alpine watershed: Determination using delta N-15 and delta O-18, *Water Resources Research*, *38*(5), art. no.-10.1029/2001WR00294, 2002.
- Clegg, S. L., P. Brimblecombe and A. S. Wexler, A thermodynamic model of the system  $H^+-NH_4^+-Na^+-SO_4^{2-}-NO_3^- -Cl^- -H_2O$  at 298.15 K, *Journal of Physical Chemistry*, *102A*, 2155-2171, 1998.
- Colle, B. A., C. F. Mass and K. J. Westrick, Evaluation of MM5 and Eta-10 precipitation forecasts over the Pacific Northwest during the cool season, *Weather and Forecasting*, *14*, 137-154, 1999.
- Colle, B. A., C. F. Mass and K. J. Westrick, Precipitation verification over the Pacific Northwest during the 1997-99 cool seasons, *Weather and Forecasting*, *15*, 730-744, 2000.
- Colorado State Climatologist, Climate of Colorado, <http://www.wrcc.dri.edu/narratives/COLORADO.htm>, National Climatic Data Center.
- Dillon, P. J., L. A. Molot and W. A. Scheider, Phosphorus and nitrogen export from forested stream catchments in central Ontario, *Journal of Environmental Quality*, *20*, 857-864, 1991.
- Doesken, N. J., R. A. Pielke and O. A. P. Bliss, Climate of Colorado, Colorado Climate Center, Colorado State University, <http://ccc.atmos.colostate.edu/pdfs/climateofcoloradoNo.60.pdf>, Fort Collins, 2003.

- Draxler, R. R. and G. D. Hess, An overview of the HYSPLIT\_4 modeling system for trajectories, dispersion, and deposition, *Australian Meteorological Magazine*, 47, 295-308, 1998.
- Duyzer, J. H., H. L. M. Verhagen, A. S. Wexler and F. C. Bosveld, Measurement of the dry deposition flux of NH<sub>3</sub> on to coniferous forest, *Environmental Pollution*, 75, 3-13, 1992.
- Duyzer, J. H., H. L. M. Verhagen, J. H. Weststrate, F. C. Bosveld and A. W. M. Vermetten, The dry deposition of ammonia onto a Douglas fir forest in the Netherlands, *Atmospheric Environment*, 28, 1241-1253, 1994.
- Duyzer, J. H., Dry deposition of ammonia and ammonium aerosols over heathland, *Journal of Geophysical Research-Atmospheres*, 99, 18757-18763, 1994.
- Ek, M. B., K. E. Mitchell, Y. Lin, E. Rogers, P. Grunmann, V. Koren, G. Gayno and J. D. Tarpley, Implementation of Noah land surface model advances in the National Centers for Environmental Prediction operation mesoscale Eta model, *Journal of Geophysical Research*, 108, 8851-doi:10.1029/2002JD003296, 2003.
- Environ Corp., CAMx (Comprehensive Air Quality Model with Extensions) 4.20 User Guide, Environ International Corporation, Novato, California, 2005.
- Environ Corp., CAMx v.4.40 User's Guide, Environ International Corporation, Novato, CA, 2006.
- Erisman, J. W., R. Otjes, A. Hensen, P. Jongejan, P. van den Bulk, A. Khlystov, H. Mols and S. Slanina, Instrument development and application in studies and monitoring of ambient ammonia, *Atmospheric Environment*, 35, 1913-1922, 2001.
- Fernandez, J., J. P. Montavez, J. Saenz, J. F. Gonzalez-Rouco and E. Zorita, Sensitivity of the MM5 mesoscale model to physical parameterizations for regional climate studies: Annual cycle, *Journal of Geophysical Research*, 112(D04101), doi:10.1029/2005JD006649, 2007.
- Finkelstein, P. L., T. G. Ellestad, J. F. Clarke, T. P. Meyers, D. B. Schwede, E. O. Heber and J. A. Neal, Ozone and sulfur dioxide dry deposition to forests: Observations and model evaluation, *Journal of Geophysical Research*, 105, 15365-15377, 2000.
- Galloway, J. N., Likens, G.E., W. C. Keene and J. M. Miller, The composition of precipitation in remote areas of the world, *Journal of Geophysical Research*, 87, 8771-8776, 1982.
- Galloway, J. N., W. H. Schlesinger, H. Levy, A. Michaels and J. L. Schnoor, Nitrogen fixation: Atmospheric enhancement---environmental response, *Global Biogeochemical Cycles*, 9, 235-252, 1995.
- Gebhart, K. A., R. A. Ahlbrandt, W. C. Malm and H. K. Iyer, Estimating the fractional contribution of secondary aerosols from different source areas on a regional scale, Proceedings of the 81st Annual Meeting of the APCA, paper #88-54.6, Dallas, 1988.
- Gebhart, K. A. and W. C. Malm, Source apportionment of particulate sulfate concentrations at three national parks in the Eastern United States, Mathai, C. V.

- Transactions of the Air & Waste Management Association/Environmental Protection Agency Specialty Conference: Visibility and Fine Particles, Estes Park, October 15-19, 898-913, Pittsburgh, 1989.
- Gebhart, K. A. and W. C. Malm, Examination of source regions and transport pathways of organic and light absorbing carbon into remote areas of the United States, presented at the 84th Annual Meeting of the Air & Waste Management Association, paper #91-82.04, Vancouver, 1991.
- Gebhart, K. A., W. C. Malm and H. K. Iyer, Comparison of two back trajectory techniques for source apportionment, presented at the 86th Annual Mtg of the Air & Waste Management Assoc, paper #93-MP-4.05, Denver, 1993.
- Gebhart, K. A. and W. C. Malm, Source attribution & statistical summary of data measured at Grand Canyon National Park during 1989-1991, Proc of the International Specialty Conf Aerosols & Atmospheric Optics: Radiative Balance & Visual Air Quality, Snowbird, 1098-1124. Pittsburgh, 1994.
- Gebhart, K. A., B. A. Schichtel and M. G. Barna, Directional biases in back-trajectories due to model and input data, *Journal of the Air & Waste Management Association*, 55, 1649-1662, 2005.
- Gebhart, K. A., B. A. Schichtel, M. G. Barna and W. C. Malm, Quantitative back-trajectory apportionment of sources of particulate sulfate at Big Bend National Park, TX, *Atmospheric Environment*, 40, 2823-2834, 2006.
- Gorzelska, K., J. N. Galloway, K. Watterson and W. C. Keene, Water-soluble primary amine compounds in rural continental precipitation, *Atmospheric Environment Part A-General Topics*, 26, 1005-1018, 1992.
- Goulding, K. W. T., N. J. Bailey, N. J. Bradbury, P. Hargreaves, M. Howe, D. V. Murphy, P. R. Poulton and T. W. Willison, Nitrogen deposition and its contribution to nitrogen cycling and associated soil processes, *New Phytologist*, 139, 49-58, 1998.
- Green, M., J. Xu, D. DuBois and D. L. Freeman, Causes of Haze (on line), <http://www.coha.dri.edu>, 2005.
- Grell, G. A., J. Dudhia and D. R. Stauffer, A description of the fifth generation Penn State/NCAR mesoscale model (MM5), NCAR Technical Note (TN-398-STR), Boulder, 1994.
- Gronberg, L., P. Lovkvist and J. A. Jonsson, Measurement of aliphatic amines in ambient air and rainwater, *Chemosphere*, 24, 1533-1540, 1992.
- Grubisic, V., R. K. Vellore and A. W. Huggins, Quantitative precipitations forecasting of wintertime storms in the Sierra Nevada: Sensitivity to the microphysical and horizontal resolution, *Monthly Weather Review*, 133, 2834-2859, 2005.
- Hand, J. L., A New Technique for Obtaining Aerosol Size Distributions with Applications to Estimates of Aerosol Properties, PhD Dissertation, Colorado State University, 2001.

- Hand, J. L. and S. M. Kreidenweis, A New Method for Retrieving Particle Refractive Index and Effective Density from Aerosol Size Distribution Data, *Aerosol Science and Technology*, 36(10), 1012-1026, 2002.
- Harrison, R. M. and A. G. Allen, Scavenging ratios and deposition of sulfur, nitrogen, and chlorine species in eastern England, *Atmospheric Environment Part A-General Topics*, 25 , 1719-1723, 1991.
- Hedin, L. O., J. J. Armesto and A. H. Johnson, Patterns of nutrient loss from unpolluted, old-growth temperate forests: Evaluation of biogeochemical theory, *Ecology*, 76, 493-509, 1995.
- Heuer, K., K. A. Tonnessen and G. P. Ingersoll, Comparison of precipitation chemistry in the central Rocky Mountains, *Atmospheric Environment*, 34, 1713-1722, 2000.
- Higgins, R. W., J. E. Janowiak and Y.-P. Yao, A grided hourly precipitation database for the United States (1963-1993) (on line), [http://www.cpc.ncep.noaa.gov/research\\_papers/ncep\\_cpc\\_atlas/1/index.html](http://www.cpc.ncep.noaa.gov/research_papers/ncep_cpc_atlas/1/index.html), 1996.
- Hinds, W. C., *Aerosol Technology: Properties, Behavior, and Measurement of Airborne Particles*, Wiley, New York, 1999.
- Hong, S. Y. and H. L. Pan, Nonlocal boundary layer vertical diffusion in a medium-range forecast model, *Monthly Weather Review*, 124, 2322-2339, 1996.
- IE, SMOKE version 2.2 Users Manual, Institute for the Environment, University of North Carolina, Chapel Hill, NC, <http://www.ie.unc.edu/cempd/products/smoke/version2.2/html/>, 2006.
- IE, Emissions Modeling Final Report: Developing 2006 Emissions for the NPS-ARD RoMANS Study-Phase I, Institute for the Environment, University of North Carolina, Chapel Hill, NC, 2007.
- Ivens, W., G. P. J. Draaijers, W. Bleuten and M. M. Bos, The impact of air-borne ammonia from agricultural sources on fluxes of nitrogen and sulfur toward forest soils, *Catena*, 16, 535-544, 1989.
- Iyer, H. K., W. C. Malm and R. A. Ahlbrandt, A mass balance method for estimating the fractional contribution from various sources to a receptor, Bhardwaja, P. S. Transactions: Visibility Protection: Research & Policy Aspects, APCA conference, Grand Teton National Park, September 1986, 861-871, Pittsburgh, PA, 1987.
- Janson, R. and L. Granat, A foliar rinse study of the dry deposition of nitric acid to a coniferous forest, *Agricultural and Forest Meteorology*, 98(9), 683-696, 1999.
- Jones, B. L. and J. T. Cookson, Natural atmospheric microbial conditions in a typical suburban area, *Applied and Environmental Microbiology*, 45, 919-934, 1983.
- Kahl, J. D., J. M. Harris and G. A. Herbert, Intercomparison of three long-range trajectory models applied to arctic haze, *Tellus*, 41B, 524-536, 1989.
- Kahl, J. W. and P. J. Samson, Uncertainty in trajectory calculations due to low resolution meteorological data, *Journal of Climate & Applied Meteorology*, 25, 1816-1831, 1986.

- Kain, J. S. and J. M. Fritsch, Convective parameterization for mesoscale models: The Kain-Fritsch scheme, in *The Representation of Cumulus Convection in Numerical Models*, edited by K. A. Emanuel and D. J. Raymond, p. -246 pp, American Meteorological Society, 1993.
- Kain, J. S., The Kain-Fritsch convective parameterization: An update, *Journal of Applied Meteorology*, 43, 170-181, 2004.
- Koutsenogii, P. K., N. S. Bufetov, V. I. Drozdova, V. L. Golobkova, T. V. Khodger, K. P. Koutsenogii, V. I. Makarov, V. A. Obolkin and V. L. Potemkin, Ion composition of atmospheric aerosol near Lake Baikal, *Atmospheric Environment*, 27(11), 1629-1633, 1993.
- Langford, A. O. and F. C. Fehsenfeld, Natural vegetation as a source or sink for atmospheric ammonia - A case study, *Science*, 255, 581-583, 1992.
- Lehmann, C. M. B., V. C. Bowersox and S. M. Larson, Spatial and temporal trends of precipitation chemistry in the United States, *Environmental Pollution*, 135, 347-361, 2005.
- Littman, T., Atmospheric input of dust and nitrogen into the Nizzana sand dune ecosystem, northwestern Negev, Israel, *Journal of Arid Environments*, 36, 433-457, 1997.
- Losleben, M., N. Pepin and S. Moore, Air flow over complex terrain in the Colorado Front Range, 2000.
- Mace, K. A., N. Kubilay and R. A. Duce, Organic nitrogen in rain and aerosol in the eastern Mediterranean atmosphere: An association with atmospheric dust, *Journal of Geophysical Research-Atmospheres*, 108(D10), Art. no.-4320, 2003.
- Malm, W. C., H. K. Iyer, J. Watson and D. A. Latimer, Survey of a variety of receptor modeling techniques, Mathai, C. V. Transactions of the Air & Waste Management Association/Environmental Protection Agency Specialty Conference: Visibility and Fine Particles, Estes Park, October 15-19, 781-805, Pittsburgh, PA, 1989.
- Malm, W. C., K. A. Gebhart and R. C. Henry, An investigation of the dominant source regions of fine sulfur in the western United States and their areas of influence, *Atmos. Environ.*, 24A(12), 3047-3060, 1990.
- Malm, W. C., Characteristics and origins of haze in the continental United States, *Earth Science Reviews*, 33, 1-36, 1992.
- Malm, W. C., J. F. Sisler, D. Huffman, R. A. Eldred and T. A. Cahill, Spatial and seasonal trends in particle concentration and optical extinction in the United States, *Journal of Geophysical Research*, 99(D1), 1347-1370, 1994.
- Mansell, G., An Improved Inventory for the WRAP Domain, Final Report Volume I; prepared for the Western Governors' Association. Novato, California, Environ International Corporation, 2005.
- Markowski, G. R., Improving Twomey algorithm for inversion of aerosol measurement data, *Aerosol Science & Technology*, 7(2), 127-141, 1987.

- McMeeking, G. R., Size distribution measurements of wildfire smoke-influenced aerosol at Yosemite National Park, MS Thesis, Colorado State University, 2004.
- McMeeking, G. R., S. M. Kreidenweis, C. M. Carrico, T. Lee, J. L. Collett and W. C. Malm, Observations of smoke-influenced aerosol during the Yosemite Aerosol Characterization Study: 1. Size distributions and chemical composition, *Journal of Geophysical Research-Atmospheres*, 110(D9), doi:10.1029/2004JD005389, 2005.
- Mesinger, F., G. DiMego, E. Kalnay, K. Mitchell, P. C. Shafran, W. Ebisuzaki, D. Jovic, J. Woollen, E. Rogers, E. H. Berberry, M. B. Ek, Y. Fan, R. Grumbine, W. Higgins, H. Li, Y. Lin, G. Manikin, D. D. Parrish and W. Shi, North American regional reanalysis, *Bulletin of the American Meteorological Society*, 87(3), 343-360, 2006.
- Meyers, T. P., B. Huebert and B. B. Hicks, HNO<sub>3</sub> deposition to a deciduous forest, *Boundary-layer Meteorology*, 49, 395-410, 1989.
- Meyers, T. P., P. L. Finkelstein, J. Clarke, T. G. Ellestad and P. F. Sims, A multilayer model for inferring dry deposition using standard meteorological measurements, *Journal of Geophysical Research-Atmospheres*, 103, 22645-22661, 1998.
- Morris, R. E., G. Yarwood, C. Emery and B. Koo, Development and application of the CAMx regional one-atmosphere model to treat ozone, particulate matter, visibility, air toxics, and mercury, presented at the Air & Waste Management Association's 97th Annual Conference and Exhibition, Indianapolis, June 2004.
- Morris, R. E., C. Emery, D. McNally and J. Wilkinson, Revised draft: Modeling protocol for the Colombia River Gorge National Scenic Area Air Quality Study, prepared for Paul Mairose (on line), <http://www.swcleanair.org/pdf/GorgeModelingProtocolRev090706.pdf>, 2006.
- Muller, H., G. Kramm, F. Meixner, G. J. Dollard, D. Fowler and M. Possanzini, Determination of HNO<sub>3</sub> dry deposition by modified bowen ratio and aerodynamic profile techniques, *Tellus Series B-Chemical and Physical Meteorology*, 45, 346-367, 1993.
- Namiesnik, J., A. Jastrzebska and B. Zygmont, Determination of volatile aliphatic amines in air by solid-phase microextraction coupled with gas chromatography with flame ionization detection, *Journal of Chromatography A*, 1016(1), 1-9, 2003.
- Nemitz, E., M. A. Sutton, G. P. Wyers and P. A. C. and Jongejan, Gas-particle interactions above a Dutch heathland: I. Surface exchange fluxes of NH<sub>3</sub>, SO<sub>2</sub>, HNO<sub>3</sub>, and HCl, *Atmospheric Chemistry and Physics*, 4, 989-1005, 2004.
- Nenes, A., S. N. Pandis and C. Pilinis, Continued development and testing of a new thermodynamic aerosol module for urban and regional air quality models., *Atmospheric Environment*, 33(10), 1553-1560, 1999.
- North American Regional Reanalysis home page. accessed 2007.  
<http://www.emc.ncep.noaa.gov/mmb/rreanl/index.html>.
- Odman, M. T. and C. Ingram, Multiscale Air Quality Simulation Platform (MAQSiP): Source Code Documentation and Validation, Technical Report

- ENV-96TR002MCNC (Microelectronics Center of North Carolina), Research Triangle Park, NC, 1996.
- Orsini, D. A., Y. L. Ma, A. Sullivan, B. Sierau, K. Baumann and R. J. Weber, Refinements to the particle-into-liquid sampler (PILS) for ground and airborne measurements of water soluble aerosol composition, *Atmospheric Environment*, 37(9-10), 1243-1259, 2003.
- Petersen, W. A., L. D. Carey, S. A. Rutledge, J. C. Knievel, N. J. Doesken, R. H. Johnson, T. B. McKee, T. H. Vonder Haar and J. F. Weaver, Mesoscale and radar observations of the Fort Collins flash flood of 28 July 1997, *Bulletin of the American Meteorological Society*, 80, 191-216, 1999.
- Pitchford, M. L. and A. Pitchford, Analysis of regional visibility in the Southwest using principal component and back trajectory techniques, *Atmospheric Environment*, 19(8), 1301-1316, 1985.
- Poirot, R. L. and P. R. Wishinski, Visibility, sulfate and air mass history associated with the summertime aerosol in northern Vermont, *Atmospheric Environment*, 20(7), 1457-1469, 1986.
- Poirot, R. L., P. R. Wishinski, P. K. Hopke and A. V. Polissar, Comparative application of multiple receptor methods to identify aerosol sources in northern Vermont, *Environmental Science & Technology*, 35(23), 4622-4636, 2001.
- Pryor, S. C., R. J. Barthelmie, L. L. Sorensen and B. Jensen, Ammonia concentrations and fluxes over a forest in the Midwestern USA, *Atmospheric Environment*, 35, 5645-5656, 2001.
- Pryor, S. C., R. J. Barthelmie, B. Jensen, N. O. Jensen and L. L. Sorensen, HNO<sub>3</sub> fluxes to a deciduous forest derived using gradient and REA methods, *Atmospheric Environment*, 36, 5993-5999, 2002.
- Pryor, S. C. and O. Klemm, Experimentally derived estimates of nitric acid dry deposition velocity and viscous sub-layer resistance at a conifer forest, *Atmospheric Environment*, 38, 2769-2777, 2004.
- Reisner, J. R., J. Rasmussen and R. T. Bruintjes, Explicit forecasting of supercooled liquid water in winter storms using the MM5 mesoscale model, *Quarterly Journal of the Royal Meteorological Society*, 124B, 1071-1107, 1998.
- Roberts, J. M., The atmospheric chemistry of organic nitrates, *Atmospheric Environment*, 24, 243-287, 1990.
- Rolph, G. D. and R. R. Draxler, Sensitivity of three-dimensional trajectories to the spatial and temporal densities of the wind field, *Journal Applied Meteorology*, 29, 1043-1054, 1990.
- Rueth, H. M. and J. S. Baron, Differences in Englemann spruce forest biogeochemistry east and west of the Continental Divide, *Ecosystems*, 5, 45-57, 2002.
- Saxena, P. and T. W. Peterson, Thermodynamics of multicomponent electrolytic aerosols, *Journal of Colloid and Interface Science*, 79, 496-510, 1981.

- Schade, G. W. and P. J. Crutzen, Emission of aliphatic amines from animal husbandry and their reactions - Potential source of N<sub>2</sub>O and HCN, *Journal of Atmospheric Chemistry*, 22, 319-346, 1995.
- Schichtel, B. A., K. A. Gebhart, M. G. Barna and W. C. Malm, Association of air mass transport patterns and particulate sulfur concentrations at Big Bend National Park, Texas, *Atmospheric Environment*, 40(5), 992-1006, 2006.
- Seinfeld, J. H. and S. N. Pandis, *Atmospheric Chemistry and Physics: From air pollution to climate change*, John Wiley & Sons, New York, 2006.
- Sickman, J. O., A. Leydecker and J. M. Melack, Nitrogen mass balances and abiotic controls on N retention and yield in high-elevation catchments of the Sierra Nevada, California, United States, *Water Resources Research*, 37, 1445-1461, 2001.
- Sievering, H., G. Enders, L. Kins, G. Kramm, K. Ruoss, G. Roider, M. Zelger, L. Anderson and R. Dlugi, Nitric acid, particulate nitrate and ammonium profiles at the Bayerischer Wald - Evidence for large deposition rates of total nitrate, *Atmospheric Environment*, 28, 311-315, 1994.
- Sievering, H., D. Rusch and L. Marquez, Nitric acid, particulate nitrate and ammonium in the continental free troposphere: Nitrogen deposition to an alpine tundra ecosystem, *Atmospheric Environment*, 30, 2527-2537, 1996.
- Sievering, H., T. M. G. Kelly, C. Seibold and A. Turnipseed, Nitric acid dry deposition to conifer forests: Niwot Ridge spruce-fir-pine study, *Atmospheric Environment*, 35, 3851-3859, 2001.
- Smil, V., Nitrogen and phosphorus, in *The Earth as Transformed by Human Action*, edited by B. L. I. Turner, W. C. Clark, R. W. Kates, J. F. Richards, J. T. Mathews and W. B. Meyer, pp. 423-436, Cambridge University Press, Cambridge, England, 1990.
- Sorooshian, A., F. J. Brechtel, Y. L. Ma, R. J. Weber, A. Corless, R. C. Flagan and J. H. Seinfeld, Modeling and characterization of a particle-into-liquid sampler (PILS), *Aerosol Science & Technology*, 40(6), 396-409, 2006.
- Stohl, A., Computation, accuracy and applications of trajectories - a review and bibliography, *Atmospheric Environment*, 32, 947-966, 1998.
- Sutton, M. A., W. A. H. Asman and J. K. Schjorring, Dry deposition of reduced nitrogen, *Tellus B*, 46, 255-273, 1994.
- Tonnesen, G., Z. Wang, M. Omary, C.-J. Chien, Y. Wang, R. Morris, S. Kembball-Cook, Y. Jia, S. Lau, B. Koo, Z. Adelman, A. C. Holland and J. Wallace, Final Report for the Western Regional Air Partnership (WRAP) 2002 Visibility Model Performance Evaluation, WGA Contract Number 30203, Western Governors' Association, 2006.
- Twomey, S., Comparison of constrained linear inversion and an iterative nonlinear algorithm applied to indirect estimation of particle-size distributions, *Journal of Computational Physics*, 18(2), 188-200, 1975.
- U.S.EPA, User's Guide to MOBILE6.1 and MOBILE6.2: Mobile Source Emission Factor Model, , <http://www.epa.gov/otaq/models/mobile6/420r03010.pdf>, 2003.

- U.S.EPA, Biogenic Emissions Sources (on line), *Emissions Modeling Clearinghouse*, <http://www.epa.gov/ttn/chief/emch/biogenic/index.html>, 2007.
- Vitousek, P. M. and P. A. Matson, Agriculture, the global nitrogen cycle, and trace gas flux, in *The Biogeochemistry of Global Change: Radiative Trace Gases*, edited by R. S. Oremland, pp. 193-208, Chapman & Hall, New York, 1993.
- Wang, J. X. L. and J. K. Angell, Air Stagnation Climatology for the United States (1948-1998), Atlas No. I, available at <http://www.arl.noaa.gov/pubs/online/atlas.pdf>, Air Resources Laboratory, Environmental Research Laboratories, Office of Oceanic and Atmospheric Research, Silver Spring, Maryland 20910, 1999.
- Weber, R. J., D. Orsini, Y. Daun, Y. N. Lee, P. J. Klotz and F. Brechtel, A particle-into-liquid collector for rapid measurement of aerosol bulk chemical composition, *Aerosol Science & Technology*, 35(3), 718-727, 2001.
- WRAP-RMC (Western Regional Air Partnership), Final Report for the WRAP 2002 Visibility Model Performan Evaluation, Appendix A: Emissions Modeling and Quality Assurance, WRAP Regional Modeling Center, Riverside, CA, 2005.
- Whitten, G., H. P. Deuel, C. S. Burton and J. L. Haney, Memorandum to OTAG participants: Overview of the implementation of an updated isoprene chemistry mechanism in CB4/UAM-V, 1996.
- Wiedinmyer, C., B. Quayle, C. Geron, A. Belote, D. McKenzie, X. Zhang, S. O'Neill and K. K. Wynne, Estimating emissions from fires in North America for air quality modeling, *Atmospheric Environment*, 40, 3419-3432, 2006.
- Williams, M. W., E. Hood and N. Caine, The role of organic nitrogen in the nitrogen cycle of a high-elevation catchment, Colorado Front Range, *Water Resources Research*, 37, 2569-2582, 2001.
- Winklmayr, W., H. C. Wang and W. John, Adaptation of the Twomey algorithm to the inversion of cascade impactor data, *Aerosol Science & Technology*, 13(3), 322-331, 1990.
- Wyers, G. P., A. T. Vermeulen and J. Slanina, Measurement of dry deposition of ammonia on a forest, *Environmental Pollution*, 75, 25-28, 1992.
- Wyers, G. P. and J. W. Erisman, Ammonia exchange over coniferous forest, *Atmospheric Environment*, 32, 441-451, 1998.
- Yamulki, S., R. M. Harrison and K. W. T. Goulding, Ammonia surface-exchange above an agricultural field in southeast England, *Atmospheric Environment*, 30, 109-118, 1996.
- Yarwood, G., T. E. Stoeckenius, J. G. Heiken and A. M. Dunker, Modeling weekday/weekend ozone differences in the Los Angeles region for 1997, *Journal of the Air & Waste Management Association*, 53, 864, 2003.
- Yu, X. Y., T. Lee, B. Ayres, S. M. Kreidenweis, J. L. Collett Jr. and W. C. Malm, Particulate nitrate measurement using nylon filters, *Journal of the Air & Waste Management Association*, 55, 1100-1110, 2005.

- Zhang, Q. and C. Anastasio, Chemistry of fog waters in California's Central Valley - Part 3: Concentrations and speciation of organic and inorganic nitrogen, *Atmospheric Environment*, 35, 5629-5643, 2001.
- Zimmerling, R., U. Dammggen, L. Grunhage, H. D. Haenel, A. Kusters, W. Max and H. J. Jager, The classifying ratiometric method for the continuous determination of atmospheric flux densities of reactive N- and S- species with denuder filter systems, *Journal of Applied Botany-Angewandte Botanik*, 71, 38-49, 1997.
- Zimmerman, F., K. Plessow, R. Queck, C. Bernofer and J. Matschullat, Atmospheric N- and S-fluxes to a spruce forest - Comparison of inferential modeling and the throughfall method, *Atmospheric Environment*, 40, 4782-4796, 2006.